# GLYCOCALYX IN PHYSIOLOGY AND VASCULAR RELATED DISEASES

EDITED BY: Ye Zeng and Bingmei M. Fu
PUBLISHED IN: Frontiers in Cell and Developmental Biology

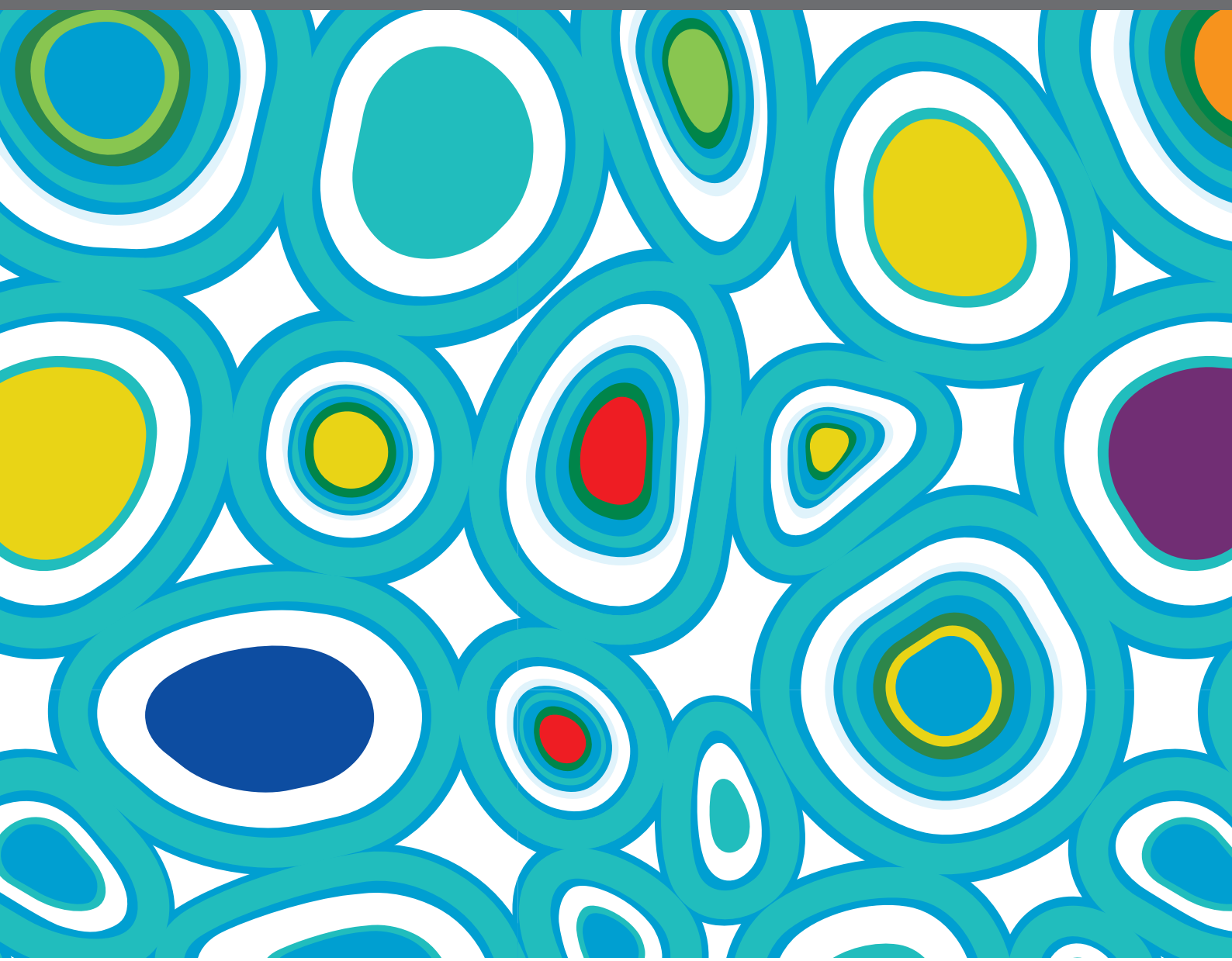

frontiers Research Topics

# frontiers



ISSN 1664-8714
ISBN 978-2-88974-367-4
DOI 10.3389/978-2-88974-367-4

## About Frontiers

Frontiers is more than just an open-access publisher of scholarly articles: it is a pioneering approach to the world of academia, radically improving the way scholarly research is managed. The grand vision of Frontiers is a world where all people have an equal opportunity to seek, share and generate knowledge. Frontiers provides immediate and permanent online open access to all its publications, but this alone is not enough to realize our grand goals.

## Frontiers Journal Series

The Frontiers Journal Series is a multi-tier and interdisciplinary set of open-access, online journals, promising a paradigm shift from the current review, selection and dissemination processes in academic publishing. All Frontiers journals are driven by researchers for researchers; therefore, they constitute a service to the scholarly community. At the same time, the Frontiers Journal Series operates on a revolutionary invention, the tiered publishing system, initially addressing specific communities of scholars, and gradually climbing up to broader public understanding, thus serving the interests of the lay society, too.

## Dedication to Quality

Each Frontiers article is a landmark of the highest quality, thanks to genuinely collaborative interactions between authors and review editors, who include some of the world's best academicians. Research must be certified by peers before entering a stream of knowledge that may eventually reach the public - and shape society; therefore, Frontiers only applies the most rigorous and unbiased reviews.
Frontiers revolutionizes research publishing by freely delivering the most outstanding research, evaluated with no bias from both the academic and social point of view. By applying the most advanced information technologies, Frontiers is catapulting scholarly publishing into a new generation.

## What are Frontiers Research Topics?

Frontiers Research Topics are very popular trademarks of the Frontiers Journals Series: they are collections of at least ten articles, all centered on a particular subject. With their unique mix of varied contributions from Original Research to Review Articles, Frontiers Research Topics unify the most influential researchers, the latest key findings and historical advances in a hot research area! Find out more on how to host your own Frontiers Research Topic or contribute to one as an author by contacting the Frontiers Editorial Office: frontiersin.org/about/contact

# GLYCOCALYX IN PHYSIOLOGY AND VASCULAR RELATED DISEASES

Topic Editors:
**Ye Zeng,** Sichuan University, China
**Bingmei M. Fu,** City College of New York (CUNY), United States

**Citation:** Zeng, Y., Fu, B. M., eds. (2022). Glycocalyx in Physiology and Vascular Related Diseases. Lausanne: Frontiers Media SA. doi: 10.3389/978-2-88974-367-4

# Table of Contents

frontiers in Cell and Developmental Biology

EDITORIAL
published: 04 January 2022
doi: 10.3389/fcell.2021.834280

# Editorial: Glycocalyx in Physiology and Vascular Related Diseases

*Ye Zeng*[1*†] *and Bingmei M. Fu*[2*†]

[1]*Institute of Biomedical Engineering, West China School of Basic Medical Sciences and Forensic Medicine, Sichuan University, Chengdu, China,* [2]*Department of Biomedical Engineering, The City College of the City University of New York, New York, NY, United States*

**Keywords: glycocalyx, homeostasis, endothelial cell, vascular related diseases, permeability, mechanotransduction, angiogenesis, inflammation**

**Editorial on the Research Topic**

**Glycocalyx in Physiology and Vascular Related Diseases**

## INTRODUCTION

Glycocalyx (GCX) covers the surface of every mammalian cell. It is closely associated with various physiological and pathophysiological events, including cytoskeleton remodeling, vascular leakage, angiogenesis, and tumor growth and metastasis. Components of GCX are promising biomarkers for many vascular-related diseases, such as sepsis, shock, coronary artery disease, COVID-19, hypertension, diabetes, ischemia-reperfusion injury, and pre-eclampsia. They are also the critical elements involved in the cell-cell and cell-external environment crosstalk in these diseases. The structure of GCX can be modified by bioactive serum constituents, drugs, mechanical forces, and other factors. As an essential signaling mediator, GCX governs the transduction of the extracellular signals into cellular responses. GCX mediated signaling is involved in the cell proliferation, apoptosis, migration, adhesion, autophagy, oxidative stress, angiogenesis, and metastasis.

The mechanisms underlying vascular-related diseases are multifactorial. For example, the interaction between endothelial GCX and the microenvironment may determine the fate of cells and regulate coagulation, permeability, migration, adhesion, and inflammation. Up to date, the research in GCX has focused on elucidating the mechanisms by which the structure and composition of the GCX are disrupted by the pathological factors, with increasing interests in the synthesis and restoration from the disruption. Nevertheless, the composition of GCX is likely to be dynamically altered to maintain the microvascular homeostasis. Enzymatic degradation, *de novo* biosynthesis of new molecules, as well as recruitment of circulating molecules from the blood, all modify the integrity of GCX and its associated functions.

This Research Topic about GCX in physiology and vascular related diseases comprises 15 articles, eight original research and seven review articles, presenting the role of GCX in vascular mechanotransduction, permeability, angiogenesis, as well as the disruption of GCX in various diseases.

## Mechanotransduction

GCX plays a key role in protecting against vascular diseases. Reduced GCX was found in aging vessels and possibly due to stiffness. Mahmoud et al. investigated the stiffness of cell culture substrates on the GCX of various endothelial cells (ECs). They found that heparan sulfate and glypican-1 of GCX in cultured human umbilical vein endothelial cells, rat fat pad endothelial cells, mouse aortic endothelial cell and mouse brain endothelial cells growing on glass were reduced compared to those growing on either soft (stiffness of 2.5 kPa) or stiff (10 kPa) gels. Their study indicates that the glass/stiff substrate



***Edited and reviewed by:***
*Ana Cuenda,*
*Spanish National Research Council (CSIC), Spain*

***Correspondence:**
*Ye Zeng*
*ye@scu.edu.cn*
*Bingmei M. Fu*
*fu@ccny.cuny.edu*

**†ORCID:**
*Bingmei M. Fu*
*orcid.org/0000-0001-9343-5895*
*Ye Zeng*
*orcid.org/0000-0001-5440-6194*

***Specialty section:***
*This article was submitted to Signaling, a section of the journal Frontiers in Cell and Developmental Biology*

***Received:*** *13 December 2021*
***Accepted:*** *15 December 2021*
***Published:*** *04 January 2022*

***Citation:***
*Zeng Y and Fu BM (2022) Editorial: Glycocalyx in Physiology and Vascular Related Diseases. Front. Cell Dev. Biol. 9:834280. doi: 10.3389/fcell.2021.834280*

could not reflect the true mechanical microenvironment *in vivo*. Numerical methods including macroscopic (continuum-based), mesoscopic [e.g., lattice Boltzmann method (LBM) and dissipative particle dynamics (DPD)] and microscopic [e.g., molecular dynamics (MD) and Monte Carlo (MC) methods] have been used to investigate the complex response of GCX to mechanical stimuli from blood flow. Jiang et al. summarized recent developments in numerical simulation of mechanotransduction of GCX to shear stress, and mechanotransduction initiated biochemical processes such as activation of endothelial nitric oxide synthase (eNOS), and release of $Ca^{2+}$.

## Permeability

The GCX is the primary molecular filter of the blood vessel to macromolecules between blood and surrounding tissues. Direct current stimulation (DCS) has been used to treat a variety of brain disorders, but the mechanism is not clear. Xia et al. demonstrated that DCS increases the blood-brain barrier (BBB) permeability by disrupting the GCX (including heparan sulfate and hyaluronic acid) and tight junction ZO-1 of the BBB and the disruption is NO dependent. The disruption is transient *in vivo* and thus backups the safety of DCS in the clinical application.

It is well established that in the steady state, reabsorption of fluid into microvessels does not occur in tissues such as skeletal muscle due to the balance of hydrostatic and colloid osmotic forces across the GCX. Curry and Michel extended this idea to demonstrate that transient changes in vascular pressure favoring initial reabsorption from the interstitial fluid of skeletal muscle result in much less fluid exchange than is commonly assumed. It is hard to explain the GCX as a filter to macromolecules if the pore size (inter-fiber spacing) is 19.5 nm measured by transmission electron microscopy (TEM). Arkill re-interpretated this pore size as the spacing between proteoglycan core proteins with the collapsed glycosaminoglycan (GAG) side chains during sample preparation in TEM. A new model consisting of the core proteins with surrounding GAGs was proposed to explain the measured reflection coefficient of albumin for the sieving function of EC GCX.

## Angiogenesis, Inflammation, and Vascular Related Diseases

GCX plays a critical role in vessel formation and maturation. Dysfunctional GCX was found in a variety of diseases. Cano et al. revealed that galectin-3 promotes angiogenesis via activation of vascular endothelial growth factor receptor 2 (VEGFR2) in the presence of exogenous VEGF but VEGF-induced VEGFR2 activation is not dependent on galectin-3. The defined pathway of GCX in angiogenesis could aid the anti-VEGF therapies for aberrant angiogenesis and associated vascular permeability and tissue dysfunction. Hu et al. further reviewed the role of GCX in angiogenesis, inflammation, diabetes and COVID-19. Puchwein-schwepcke et al. specifically summarized the role of GCX in physiology and pathology in neonates, infants, and children. Qu et al. reviewed the key role of the GCX in the inflammatory process, highlighted the interaction between inflammatory cytokines release and GCX disruption, and discussed the role of GCX in regulating inflammasomes in inflammation-related diseases such as atherosclerosis and diabetes.

Villalba et al. reviewed the structure and function of GCX across the microvasculature in different organs and the GCX disruption in pathological conditions. New pharmacological interventions attenuating GCX degradation and integrity dysfunction have been summarized. Bush et al. specifically described characteristics of EC GCX breakdown in malaria and discuss how these relate to vascular dysfunction and adverse outcomes. Schenck et al. reviewed the potential role of the GCX damage in the delayed cerebral ischemia (DCI) following an aneurysmal subarachnoid hemorrhage. It was proposed that a damaged GCX could be a potential catalysator of oxidative stress and reduced NO availability in DCI. They also highlighted the potential and limitations of methods currently used to evaluate the glycocalyx, and strategies to restore or prevent glycocalyx shedding. Koch et al. provided evidence of dermal GCX loss (ulex europaeus agglutinin-1) and endothelial dysfunction in patients with chronic kidney disease (CKD). Volume overload rather than inflammation is closely associated with dermal GCX loss, arguing for strict volume control in CKD.

Regarding the GCX in diabetes, Sampei et al. investigated the disruption of GCX in extended inflammation during endotoxemia in a diabetic mouse model. They found a lower expression of GCX synthesis-related genes including *Ext1*, *Csgalnact1*, and *Vcan* in C57BLKS/J $Iar^{-}$ +$lepr^{db}$/$lepr^{db}$ mice than in C57BLKS/J $Iar^{-}m^{+}$/+$lepr^{db}$ mice, which is associated with the delayed migration of inflammatory cells in the presence of lipopolysaccharide. Reduced circulating and retinal $H_2S$ levels are closely associated with microvascular dysfunction in diabetes. Allen et al. found that $H_2S$ donors prevented high glucose-induced loss of GCX, and increased monocyte adhesion. They also showed that the pretreatment by donors of $H_2S$ prevented vascular permeability increase in retina in the streptozotocin-induced diabetic rats.

## CONCLUDING REMARKS

GCX plays critical roles in EC mechanotransduction, permeability, angiogenesis, and progression of various vascular-related diseases. The reduction in specific components of GCX is closely associated with EC dysfunction and tissue injury, whereas the increased circulating GCX degradation components serve as biomarkers. These findings also suggest that preservation or restoration of GCX is a promising therapeutic strategy for vascular-related diseases. Since the GCX from specific cells is sensitive to mechanical microenvironment, a better substrate should be employed for exploring the endothelial cell biology. Nevertheless, challenges remain in intrinsic complexity, detection technique, *in vitro*/*in vivo* visualization, and drugs or interventions for persevering and restoring GCX. In addition, the details of GCX signaling cascades in the vascular physiology and pathology are yet to be elucidated.

## AUTHOR CONTRIBUTIONS

All authors listed have made a substantial, direct, and intellectual contribution to the work and approved it for publication.

## FUNDING

The authors would like to thank the funding support from the National Institutes of Health 1UG3UH3TR002151, and the Key Research and Development Projects in Sichuan Province in China 2021YFS0188.

**Conflict of Interest:** The authors declare that the research was conducted in the absence of any commercial or financial relationships that could be construed as a potential conflict of interest.

**Publisher's Note:** All claims expressed in this article are solely those of the authors and do not necessarily represent those of their affiliated organizations, or those of the publisher, the editors and the reviewers. Any product that may be evaluated in this article, or claim that may be made by its manufacturer, is not guaranteed or endorsed by the publisher.

frontiers in Cell and Developmental Biology

ORIGINAL RESEARCH
published: 01 April 2021
doi: 10.3389/fcell.2021.623582

# Endothelial Glycocalyx Disorders May Be Associated With Extended Inflammation During Endotoxemia in a Diabetic Mouse Model

*So Sampei[1,2], Hideshi Okada[1]*, Hiroyuki Tomita[3], Chihiro Takada[1], Kodai Suzuki[1], Takamasa Kinoshita[3,4], Ryo Kobayashi[5], Hirotsugu Fukuda[1], Yuki Kawasaki[1], Ayane Nishio[1], Hirohisa Yano[1], Isamu Muraki[1], Yohei Fukuda[1], Keiko Suzuki[5], Nagisa Miyazaki[6], Takatomo Watanabe[7], Tomoaki Doi[1], Takahiro Yoshida[1], Akio Suzuki[5], Shozo Yoshida[1], Shigeki Kushimoto[2] and Shinji Ogura[1]*

[1] Department of Emergency and Disaster Medicine, Gifu University Graduate School of Medicine, Gifu, Japan, [2] Division of Emergency and Critical Care Medicine, Tohoku University Graduate School of Medicine, Sendai, Japan, [3] Department of Tumor Pathology, Gifu University Graduate School of Medicine, Gifu, Japan, [4] Department of Neurosurgery, Gifu University Graduate School of Medicine, Gifu, Japan, [5] Department of Pharmacy, Gifu University Hospital, Gifu, Japan, [6] Department of Internal Medicine, Asahi University School of Dentistry, Mizuho, Japan, [7] Department of Clinical Laboratory, Gifu University Hospital, Gifu, Japan

OPEN ACCESS

**Edited by:**
*Ye Zeng,*
*Sichuan University, China*

**Reviewed by:**
*Arif Malik,*
*The University of Lahore, Pakistan*
*Qiulun Lu,*
*Nanjing Medical University, China*

***Correspondence:**
*Hideshi Okada*
*hideshi@gifu-u.ac.jp*

**Specialty section:**
*This article was submitted to Signaling, a section of the journal Frontiers in Cell and Developmental Biology*

**Received:** *30 October 2020*
**Accepted:** *03 February 2021*
**Published:** *01 April 2021*

**Citation:**
*Sampei S, Okada H, Tomita H, Takada C, Suzuki K, Kinoshita T, Kobayashi R, Fukuda H, Kawasaki Y, Nishio A, Yano H, Muraki I, Fukuda Y, Suzuki K, Miyazaki N, Watanabe T, Doi T, Yoshida T, Suzuki A, Yoshida S, Kushimoto S and Ogura S (2021) Endothelial Glycocalyx Disorders May Be Associated With Extended Inflammation During Endotoxemia in a Diabetic Mouse Model. Front. Cell Dev. Biol. 9:623582. doi: 10.3389/fcell.2021.623582*

In diabetes mellitus (DM) patients, the morbidity of infectious disease is increased, and these infections can easily progress from local to systemic infection. Sepsis is a characteristic of organ failure related to microcirculation disorders resulting from endothelial cell injury, whose most frequent comorbidity in patients is DM. The aim of the present study was to evaluate the influence of infection on DM-induced microvascular damage on inflammation and pulmonary endothelial structure using an experimental endotoxemia model. Lipopolysaccharide (LPS; 15 mg/kg) was injected intraperitoneally into 10-week-old male C57BLKS/J lar$^{-}$ $^{+}$ *lepr*$^{db}$/*lepr*$^{db}$ (db/db) mice and into C57BLKS/J lar$^{-}$m $^{+}$ / + *lepr*$^{db}$ (db/ +) mice, which served as the littermate non-diabetic control. At 48 h after LPS administration, the survival rate of db/db mice (0%, 0/10) was markedly lower ($P < 0.05$) than that of the db/ + mice (75%, 18/24), whereas the survival rate was 100% in both groups 24 h after LPS administration. In control mice, CD11b-positive cells increased at 6 h after LPS administration; by comparison, the number of CD11b-positive cells increased gradually in db/db mice until 12 h after LPS injection. In the control group, the number of Iba-1-positive cells did not significantly increase before and at 6, 12, and 24 h after LPS injection. Conversely, Iba-1-positive cells continued to increase until 24 h after LPS administration, and this increase was significantly greater than that in the control mice. Expression of *Ext1*, *Csgalnact1*, and *Vcan* related to endothelial glycocalyx synthesis was significantly lower in db/db mice than in the control mice before LPS administration, indicating that endothelial glycocalyx synthesis is attenuated in db/db/mice. In addition, ultrastructural analysis revealed that endothelial glycocalyx was thinner in db/db mice before LPS injection.

In conclusion, in db/db mice, the endothelial glycocalyx is already injured before LPS administration, and migration of inflammatory cells is both delayed and expanded. This extended inflammation may be involved in endothelial glycocalyx damage due to the attenuation of endothelial glycocalyx synthesis.

**Keywords: glycocalyx, diabetes, endothelium, inflammation, lipopolysaccharide**

## INTRODUCTION

Endothelial disorder in patients with non-insulin-dependent diabetes mellitus (type 2 DM), which accounts for 90–95% of DM cases, is caused by chronic micro-inflammation from the early stages of diabetes (Ross, 1999). Systemic microcirculation disorder by endothelial cell injury is deeply involved in organ failure and other diseases, such as cardiovascular disease, nephropathy, retinopathy, and neuropathy (Solinas et al., 2007). In patients with type 2 DM, the morbidity of infectious disease is increased, and these infections can easily progress from local infection to systemic infection (Muller et al., 2005). Additionally, poor glycemic control in patients with type 2 DM can complicate the infection (Koh et al., 2012). Likewise, glycemic control is aggravated by infection, further increasing the severity of infection. One factor accounting for the easy contraction of infectious diseases by DM patients is endothelial disorder (Koh et al., 2012). Moreover, the most frequent comorbidity in patients with sepsis is DM (Abe et al., 2018; Kushimoto et al., 2020).

Diabetes mellitus patients account for approximately 20% of patients with sepsis (Investigators et al., 2009; Koh et al., 2012). The diagnostic criteria for sepsis include organ failure caused by several factors, including blood distribution abnormalities, heart contractility disorder, vascular hyper-permeability, endothelial injury, and decreased glomerular filtration (Singer et al., 2016). These factors are related to endothelial injury.

Vascular endothelial glycocalyx, which comprises a glycoprotein complex including syndecans, heparin sulfate, hyarulonan, and chondroitin sulfate, coats the surface of the vascular endothelium and maintains vascular homeostasis (Salmon and Satchell, 2012; Chelazzi et al., 2015). Versican, one of the core proteins of the glycocalyx, is encoded by *VCAN*. *Ext1*, *Has1*, *Has2*, and *Csgalnact1* are essential genes in the synthesis of heparan sulfate, hyaluronan, and chondroitin sulfate, respectively. Since syndecan-1 is released from the endothelium upon injury to the glycocalyx, causing its concentration in circulation to increase, syndecan-1 is useful as an endothelial glycocalyx injury marker. For instance, albumin-urea, which is a reliable marker of endothelial barrier alteration, is associated with the endothelial glycocalyx structure. Since the endothelial glycocalyx has a negative charge, the barrier of endothelial cells is destroyed and albumin flows out when the endothelial glycocalyx is injured (Adembri et al., 2011). Several previous reports have suggested associations of endothelial glycocalyx injury with severe diseases, such as acute kidney injury, chronic kidney disease, sepsis, and cardiovascular disease (Steppan et al., 2011; Padberg et al., 2014; Liborio et al., 2015; Neves et al., 2015). In addition, chronic conditions, such as diabetes (Nieuwdorp et al., 2006a,b; Broekhuizen et al., 2010), aging (Machin et al., 2018), and hypertriglyceridemia (Oda et al., 2019), injure the structure of the endothelial glycocalyx and cause degradation.

Sepsis alters neutrophil deformity in lung capillaries and subsequently causes permeability alterations and edema. In ARDS, a histologic hallmark secondary to sepsis is the recruitment of neutrophils to the lung. It has been reported that the mortality rate of granulocyte macrophage-CSFKO mice, which have only a few neutrophils and macrophages, was reduced (Spight et al., 2008). In addition, vascular endothelial glycocalyx injury was attenuated in an experimental sepsis model with a few neutrophils (Fukuta et al., 2019; Suzuki et al., 2019). In type 2 diabetes, the gene expression and phenotypic profiles of monocytes and neutrophils are altered in response to glucose (Gupta et al., 2017).

The endothelial glycocalyx regulates adhesion and migration of leukocytes, and likewise prevents the adhesion of leukocytes to endothelial cells. Therefore, it is presumed that leukocytes adhere easily to endothelial cells in injured endothelial glycocalyx in DM. However, a morphological analysis of DM-induced damage in endothelial glycocalyx has not yet been performed. In addition, it is also unknown if injured endothelial glycocalyx under DM is altered by an endotoxemic condition.

Therefore, the aim of the present study is to evaluate the influence of infection in DM-induced microvascular damage on inflammation and pulmonary endothelial structure using an experimental endotoxemia model.

## MATERIALS AND METHODS

### *In vivo* Animal Studies

This study conformed to the Guide for the Care and Use of Laboratory Animals and was approved by the Institutional Animal Research Committee of Gifu University (Gifu, Japan).

C57BLKS/J Iar$^{-}$m$^{+}$/$+$ *lepr*$^{db}$ (db/ $+$) mice were purchased from SLC Japan Inc. (Hamamatsu, Japan). They were mated, and male C57BLKS/J Iar$^{-+}$ *lepr*$^{db}$/*lepr*$^{db}$ (db/db) mice served as a model for type 2 DM in this study. As the littermate non-diabetic control, male C57BLKS/J Iar$^{-}$m$^{+}$/$+$ *lepr*$^{db}$ (db/ $+$) mice were used.

After 16 h of starvation as described in previous studies (Fukuta et al., 2019; Suzuki et al., 2019), 10-week-old db/db and db/ $+$ mice were intraperitoneally administered LPS (15 mg/kg; MilliporeSigma, Burlington, MA). Survival rates were determined at 12, 24, 36, and 48 h after LPS administration, and surviving mice were sacrificed and lung specimens collected.

## Serum Preparation and Enzyme-Linked Immunosorbent Assay

Blood samples were collected from the maxillary artery, allowed to clot at 25°C for 2 h, and centrifuged at 2,000 × *g* for 20 min at 4°C. The supernatant was collected as the serum and used for measuring IL-1β and syndecan-1 levels by enzyme-linked immunosorbent assay quantitation kits for mouse IL-1β (MLB00C; R&D Systems, Minneapolis, MN, United States) and mouse syndecan-1 (860.090.192; Diaclone, Besancon Cedex, France).

## Histopathologic Scoring

After deparaffinization, lung sections were cut (4 μm thick), counterstained with hematoxylin and eosin, and scored by a certified pathologist as follows for neutrophilic infiltration: (1) absent to rare solitary neutrophils; (2) detectable extravasated neutrophils observed as small loose cellular accumulates in one to a few airways and/or alveoli; (3) detectable extravasated neutrophils observed as loose to compact cellular accumulates in multiple to coalescing airway and/or alveoli with some effacement of lung architecture; and (4) detectable extravasated neutrophils observed as compact cellular accumulates effacing most adjacent pulmonary structures. Pulmonary edema was scored as 1, absent; 2, detectable seroproteinaceous fluid in one to a few alveoli; and 3, seroproteinaceous fluid filling alveoli in a multifocal to coalescing pattern in the lung (Suzuki et al., 2019).

## Immunohistochemistry

Lung sections were incubated with primary antibodies against the neutrophil and macrophage surface marker CD11b (ab133357; Abcam, Cambridge, United Kingdom), the vascular endothelial cell marker CD31 (DIO-310; Dianova GmbH, Hamburg, Germany), and the activated macrophage surface marker Iba-1 (019-19741; Wako Pure Chemical, Osaka, Japan). Sections were immunostained with the Vectastain Elite ABC system (Vector Laboratories, Burlingame, CA, United States) as previously described (Suzuki et al., 2019). To diminish autofluorescence, the TrueVIEW Autofluorescence Quenching Kit (Vector Laboratories, Burlingame, CA, United States) was used according to the manufacturer's protocol. Cell counting was performed on five randomly selected high-power fields (HPF) in each section ($n = 6$).

## RNA Extraction, cDNA Synthesis, and Quantitative Real-Time PCR

RNA was extracted and purified from the lung tissues of six individual mice in each group using RNA-Bee (Tel-Test, Inc., Friendswood, TX) according to the manufacturer's protocol. RNA concentration and integrity were assessed spectrophotometrically. RNA was reverse-transcribed using the High-Capacity cDNA Reverse Transcription Kit (Applied Biosystems, Carlsbad, CA). cDNA was a template for qRT-PCR. qRT-PCR was performed using TB Green Premix Ex Taq II (TAKARA BIO, Kusatsu, Japan) following the manufacturer's protocol on a Thermal Cycler Dice TP 990 machine (TAKARA BIO, Kusatsu Japan). The PCR reaction conditions were 50°C for 2 min, 95°C for 10 min, and 40 cycles of 95°C for 15 s and 60°C for 1 min. The relative quantification of each transcript (*SDC1*, *Has1, Has2, Csgalnact1, Ext1*, and *VCAN*) was determined by setting the threshold cycle (Ct) for each sample to reflect the cycle number at which the fluorescence generated within the reaction crossed the threshold level chosen as a point when the amplification was in an exponential phase. *GAPDH* was the loading control. The function $2\Delta Ct$ was used to determine relative abundance differences, where $\Delta Ct$ is the difference in Ct values between the compared samples. Primers used in the PCR reactions are provided in **Supplementary Table 1**.

## Scoring of Lectin Staining Intensity

For quantitative analysis of glycocalyx injury, scoring of *Lycopersicon esculentum* lectin (tomato lectin, B-1025-5; Vector Laboratories, Burlingame, CA, United States) staining intensity was performed using a confocal fluorescence microscope (BZ-X810, Keyence, Osaka, Japan) and ImageJ software (Olympus Corp, Tokyo, Japan). A preferred sugar of tomato lectin is N-acetylgalactosamine, which is one of the components of glycosaminoglycan, and vascular labeling by tomato lectin is a useful method to reveal vascular patterns (Robertson et al., 2015). Tomato lectin (100 μL) was injected into the jugular vein 10 min before sacrifice. The lung of each mouse was embedded in OCT compound and frozen with liquid nitrogen. The frozen blocks were stored at −80°C. Sections of frozen tissues (5–7 μm thick) were prepared with a cryostat. The intensity of tomato lectin was scored manually in 10 HPF per sample ($n = 6$ per sample) in the focal plane.

## Electron Microscopy

Electron microscopy analysis of the endothelial glycocalyx was performed as previously described (Okada et al., 2017; Ando et al., 2018; Inagawa et al., 2018). Briefly, mice were anesthetized and then perfused with a solution comprising 2% glutaraldehyde, 2% sucrose, 0.1 mol/L sodium cacodylate buffer (pH 7.3), and 2% lanthanum nitrate, at a steady flow rate of 1 ml/min, through a cannula placed in the left ventricle. After the mice were sacrificed, lung samples were fixed in a solution without glutaraldehyde and then washed in 2% alkaline (0.03 mol/L NaOH) sucrose solution. The freeze-fracture method was used to prepare samples for scanning electron microscopy (S-4800; Hitachi High-Technologies Global, Tokyo, Japan). To prepare samples for transmission electron microscopy (TEM), specimens were embedded in epoxy resin, and then ultrathin (90 nm) sections were generated, stained with uranyl acetate and lead citrate, and subjected to TEM analysis (HT-7700, Hitachi High-Technologies Global, Tokyo, Japan). To prepare samples for conventional electron microscopy, a fixative with 2.5% glutaraldehyde in 0.1 mol/L phosphate buffer (pH 7.4) was used, without lanthanum nitrate.

## Data Analysis

Data are presented as the mean ± SEM. A paired-samples *t*-test was used to compare the two groups, and survival data were analyzed using the log-rank test; $P < 0.05$ was considered significant. All calculations were performed using Prism software version 7.02 (GraphPad, La Jolla, CA).

# RESULTS

## Profiles of Diabetic Mice

The db/db mice had significantly greater body weight and higher plasma glucose and hemoglobin alpha1c levels than did non-diabetic db/ + mice (**Figures 1A,B**). Blood urea nitrogen and alanine aminotransferase levels were also higher in db/db mice than in db/ + mice, whereas creatinine and aspartate aminotransferase levels were not significantly different between the two groups (**Figures 1C–F**).

## Proinflammatory Cytokine Concentrations in db/db Mice Upon Lipopolysaccharide Administration

To produce LPS-induced experimental endotoxemia model mice, we intraperitoneally injected 15 mg/kg LPS into 10-week-old

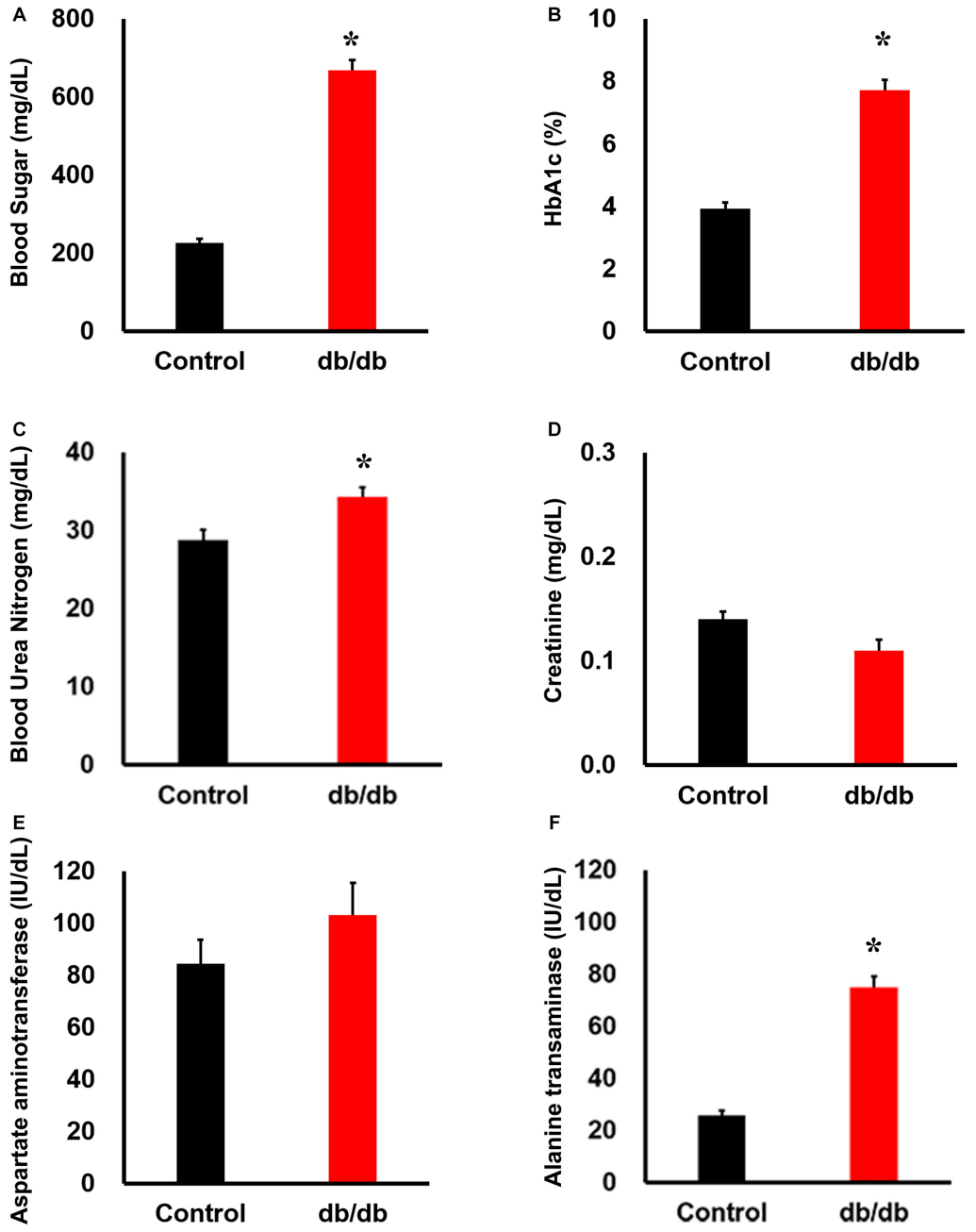


**FIGURE 1 |** Phenotype of db/db mice under normal conditions. Serum **(A)** blood sugar, **(B)** HbA1c, **(C)** blood urea nitrogen, **(D)** creatinine, **(E)** aspartate aminotransferase, and **(F)** alanine transferase concentration: blood sugar, HbA1c, blood urea nitrogen, and alanine transferase concentrations were significantly higher in db/db mice ($n = 6$) than in the wild-type mice ($n = 6$). *, $P < 0.05$ vs. wild type.

db/db mice and littermate db/ + male mice. At 48 h after LPS administration, the survival rate of db/db mice (0%, 0/10) was markedly lower ($P < 0.05$) than the db/ + mice (75%, 18/24) (**Figure 2A**).

Before LPS injection, the body weight was 40.5 ± 2.4 g in db/db mice whereas it was 22.4 ± 0.6 g in the control mice. Twenty-four hours after LPS administration, the body weight was 39.2 ± 2.4 g in db/db mice whereas it was 20.5 ± 0.6 g in the control mice.

In the control mice, the serum proinflammatory cytokine IL-1β reached 266.5 ± 18.9 ng/ml at 6 h after LPS injection and 200.7 ± 42.8 ng/ml at 12 h after injection. Thereafter, the serum IL-1β levels decreased to 30.3 ± 6.7 ng/ml within 24 h after LPS injection (**Figure 2B**). In db/db mice, IL-1β concentration was not significantly different at 6 and 12 h after LPS administration compared with the control mice (357.0 ± 49.8 ng/ml and 337.7 ± 63.7 ng/ml, respectively). However, 24 h after LPS injection, it was 248.7 ± 85.7 ng/ml, which was significantly higher than that in control mice. However, before LPS injection, there was no significant difference between the db/db mice and control mice. This result indicated that inflammation was prolonged in db/db mice compared with the control mice.

## Lung Injury in db/db Mice Under Lipopolysaccharide Administration

To determine pulmonary injury 24 h after LPS injection, we used a scoring system (**Figures 2C–G**). After LPS administration, the levels of neutrophil infiltration and pulmonary edema increased compared with pre-LPS injection levels. db/db mice showed a significant increase in neutrophil infiltration and pulmonary edema compared with the control mice. These results suggest that inflammation was aggravated in db/db mice compared with the control mice.

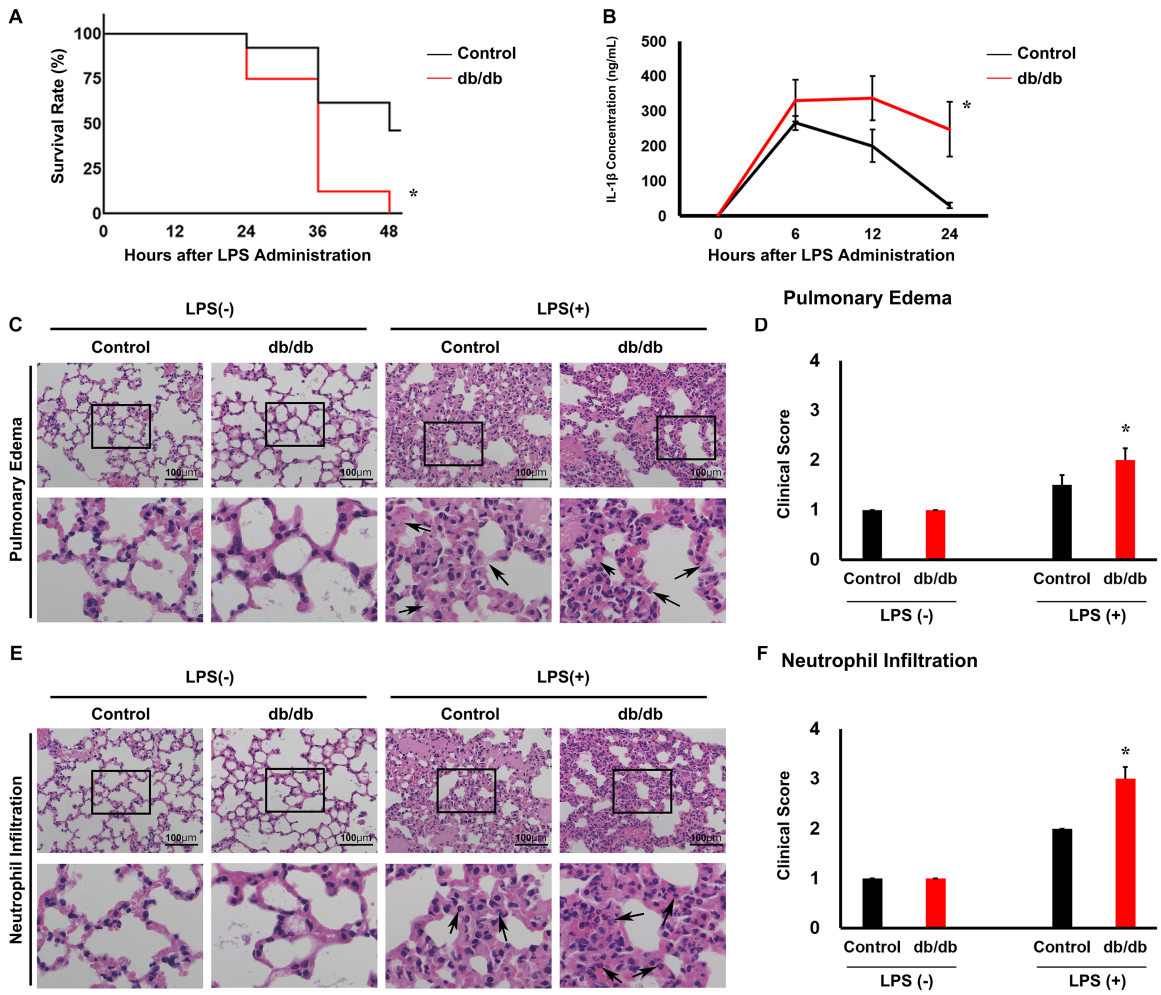


**FIGURE 2 |** Lipopolysaccharide (LPS)-induced lung injury is accelerated in db/db mice compared with in control mice. **(A)** Kaplan–Meier survival curves for control mice ($n = 24$) and LPS-treated mice ($n = 10$). **(B)** Serum interleukin 1β (IL-1β) was measured in mice using an enzyme-linked immunosorbent assay. **(C)** Hematoxylin and eosin-stained lung tissues. Arrows indicate neutrophil infiltration. **(D)** Graphs of the histologic scoring of lung injury around the pulmonary edema. **(E)** Hematoxylin and eosin-stained lung tissues. **(F)** Arrows indicate edema. Graphs of the histologic scoring of lung injury around neutrophil filtration. $n = 6$ mice per group. *, $P < 0.05$.

## Inflammation Duration in db/db Mice

To examine the infiltration of inflammatory cells after LPS administration, immunohistochemistry analysis of CD11b was performed. Before LPS administration, the number of CD11b-positive cells in db/db mice is larger than in control mice. In control mice, the proportion of CD11b-positive cells increased at 6 h after LPS administration (404 ± 18 cells/HPF), and then decreased gradually. By comparison, in db/db mice, the number of CD11b-positive cells increased gradually until 12 h after LPS injection (211 ± 9 cells/HPF at 6 h, 350 ± 9 cells/HPF at 12 h after LPS administration) and gradually decreased at 24 h after LPS administration (316 ± 8 cells/HPF) (**Figures 3A,B**).

Furthermore, to assess activated macrophages, immunohistochemical analysis of Iba-1 was performed (**Figures 3C,D**). Before LPS injection, there were fewer Iba-1-positive cells in db/db mice than in control mice. In the control group, the number of Iba-1 positive cells did not significantly increase before or at 6, 12, and 24 h after LPS injection (22 ± 2, 26 ± 1, 29 ± 1, and 34 ± 3 cells/HPF, respectively). However, Iba-1-positive cells continued to increase until 24 h after LPS administration, increasing to a significantly greater extent than that in the control mice.

## Pulmonary Endothelial Glycocalyx Injury in db/db Mice

To investigate pulmonary endothelial glycocalyx injury, serum syndecan-1 concentration was measured.

Serum syndecan-1 concentration in db/db mice was not significantly different from that in control mice before LPS administration (**Figure 4A**). In the control group, serum syndecan-1 levels reached 7.7 ± 0.8 ng/ml at 6 h after LPS injection and 11.2 ± 0.9 ng/ml at 12 h after injection. At later time points, serum syndecan-1 levels gradually decreased to 7.2 ± 1.4 ng/ml at 24 h after LPS administration. Conversely, serum syndecan-1 concentration in db/db mice continued to increase up to 24 h after LPS injection and was significantly higher than that in control mice at 12 and 24 h after LPS administration (16.5 ± 1.1 and 20.0 ± 1.9 ng/ml, respectively, vs. control mice, $P < 0.01$) (**Figure 4A**).

To quantitatively assess endothelial glycocalyx injury, we measured the intensity of tomato lectin staining because lectin binds to glycoproteins within the endothelial glycocalyx. Injected tomato lectin co-localize on pulmonary capillary endothelial cells (**Supplementary Figure 1**). In db/db mice, tomato lectin intensity was lower than in the control mice before LPS administration (**Figure 4B** and **Supplementary Figure 2**). After LPS injection, intensity score is lower in both the control and db/db mice compared with before LPS injection, and especially, it was also lower in db/db mice than in the control mice. These results suggest that injury to endothelial glycocalyx in pulmonary capillaries was aggravated in db/db mice.

## Pulmonary Endothelial Glycocalyx Synthesis in db/db Mice

To confirm endothelial glycocalyx synthesis before LPS administration, qRT-PCR was performed for syndecan-1 (*SDC1*, **Figure 4C**), hyaluronan synthase 1 (*HAS1*, **Figure 4D**), hyaluronan synthase 2 (*HAS2*, **Figure 4E**), chondroitin sulfate

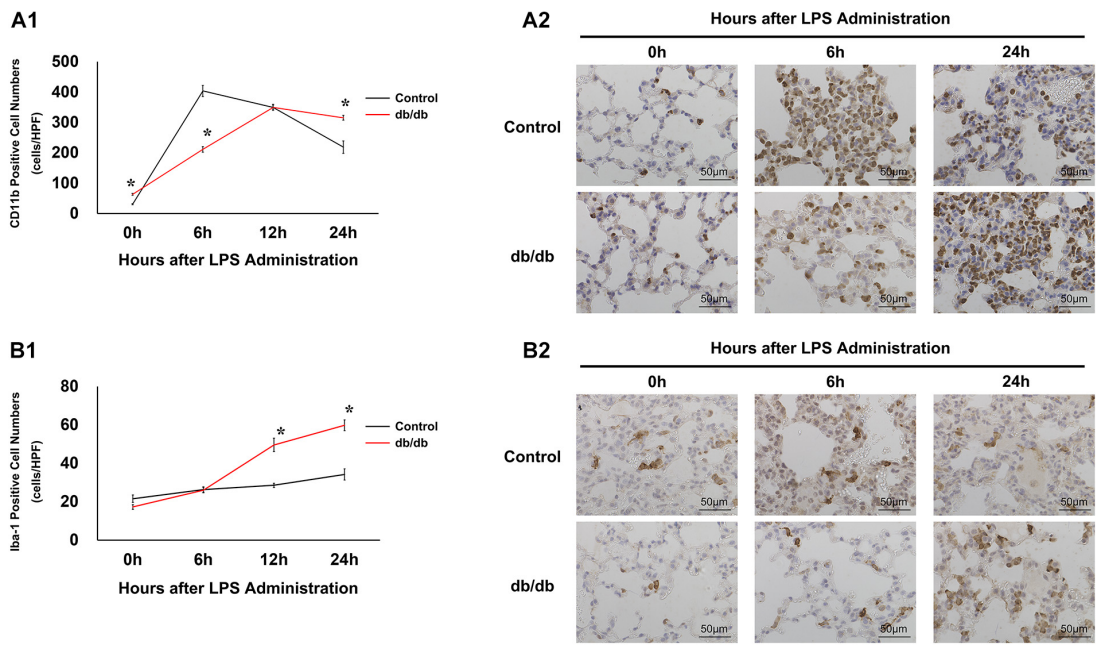


**FIGURE 3 |** Modulation of inflammatory cells under endotoxemic conditions. **(A1)** CD11b-positive cells were quantified as numbers of cells per high-power field. **(A2)** Representative images of CD11b cells in immunostained lung specimens. **(B1)** Iba-1 positive cells were quantified as the number of cells per high-power field. **(B2)** Representative images of Iba-1 in immunostained lung samples. *, $P < 0.05$.

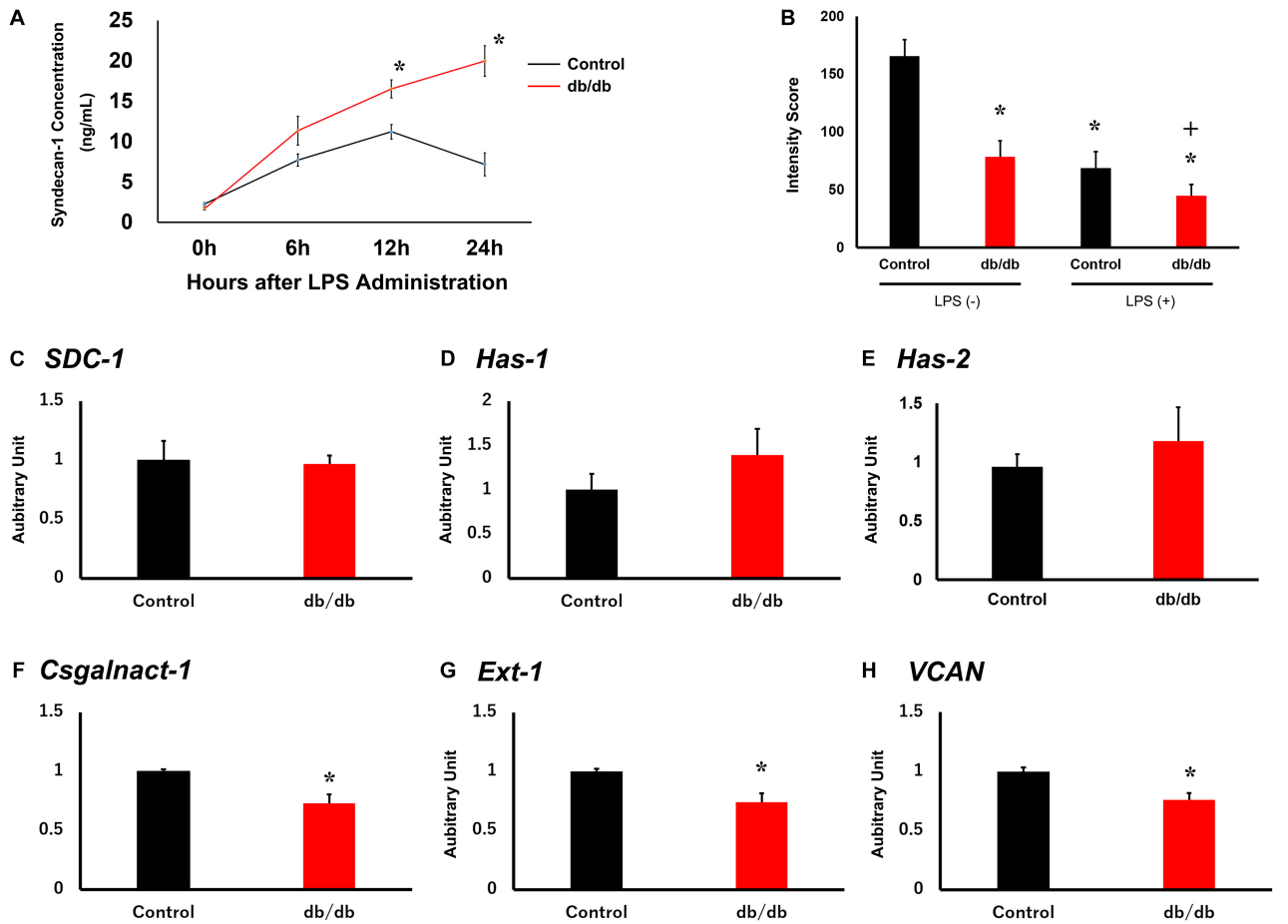


**FIGURE 4 |** Pulmonary endothelial glycocalyx is injured in db/db mice. **(A)** Serum syndecan-1 was measured in mice using an enzyme-linked immunosorbent assay. **(B)** Tomato lectin intensity of control and db/db mouse lungs with and without LPS administration. *, $P < 0.05$ vs. non-LPS-injected control mice; +, $P < 0.05$ vs. LPS-injected control mice. **(C–H)** qRT-PCR for **(C)** *SDC1*, **(D)** *Has1*, **(E)** *Has2*, **(F)** *Csgalnact1*, **(G)** *Ext1*, and **(H)** *Vcan* in control and db/db mice under normal conditions. *, $P < 0.05$.

N-acetylgalactosaminyltransferase 1 (*Csgalnact1*, **Figure 4F**), exostosin-1 (*EXT1*, **Figure 4G**), and versican (*Vcan*, **Figure 4H**) in the control and db/db mouse groups. Results showed that the expression of *EXT1*, *Csgalnact1*, and *Vcan* in db/db mice was significantly decreased compared with that in the control mice before LPS administration.

The ultrastructure of the endothelium and endothelial glycocalyx was analyzed using electron microscopy. Conventional SEM results showed that pulmonary capillaries were of the continuous type, characterized by an uninterrupted endothelium and a continuous basal lamina, in control group mice before LPS administration (**Figure 5A**). To determine the endothelial glycocalyx structure, SEM with lanthanum staining was performed (**Figure 5B**). The endothelium-like structure of endothelial glycocalyx covered the surface of the vascular endothelium in the control group, under normal conditions, whereas the endothelial glycocalyx structure was thinner in db/db mice. After LPS injection, the endothelial glycocalyx was degraded completely in db/db mice, whereas its injury was attenuated in the control mice (**Figure 5B**).

Conventional TEM also revealed that the endothelium was thin and smooth in control mice before LPS injection. However, in the control mice after LPS injection, the endothelial wall became edematous, and the extent of this was greater in db/db mice than in the control mice with or without LPS (**Figure 6A**).

The endothelial glycocalyx structure showed greater degradation in db/db mice than in control mice, even in the absence of LPS (**Figure 6B**). After LPS injection, the endothelial glycocalyx caused a skip lesion in control mice, and a part of the endothelium was exposed to the vascular lumen. In db/db mice, the endothelial glycocalyx was significantly degraded than that in the control group (**Figure 6B**).

## DISCUSSION

The current study showed that extended inflammation occurs in db/db mice after LPS administration. Specifically, we showed that (a) the endothelial glycocalyx layer in db/db mice was thinner than in the control mice before LPS injection, (b) the survival

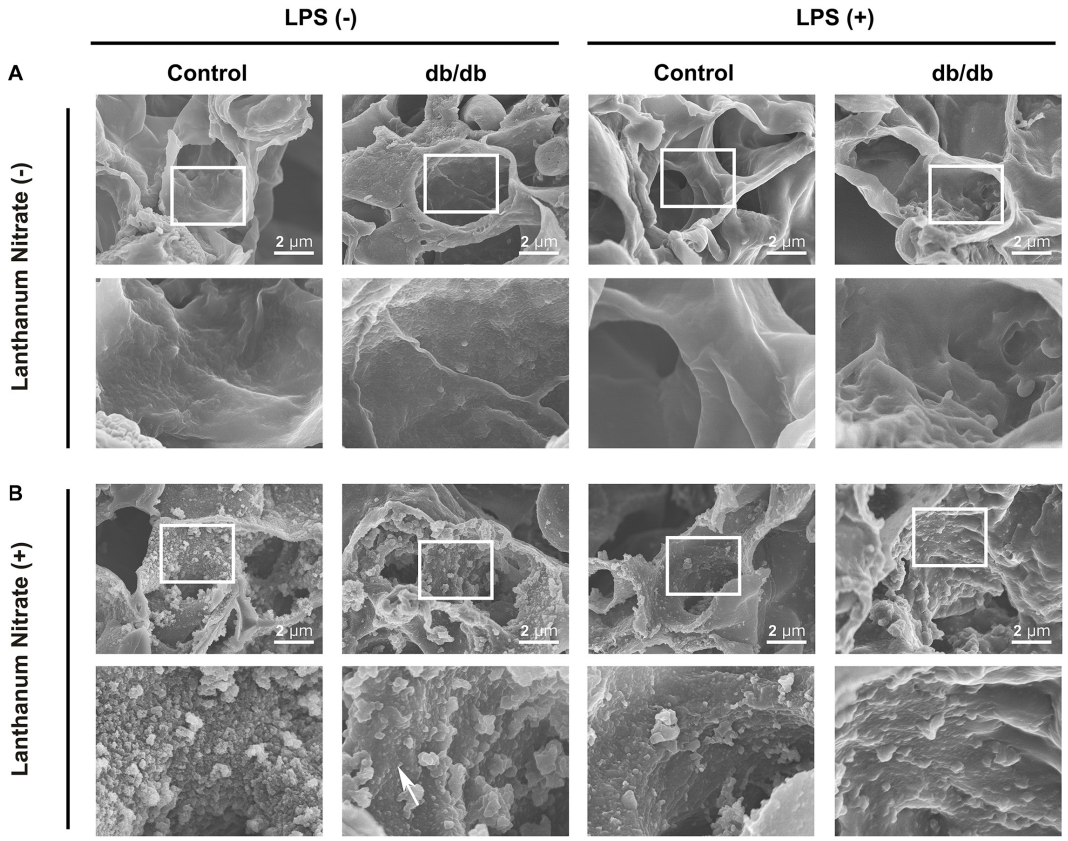


**FIGURE 5 |** Ultrastructural imaging of pulmonary endothelial injury by SEM. **(A)** Images for samples not stained with lanthanum nitrate; the endothelial glycocalyx was not detected**. (B)** The endothelial glycocalyx was detected using lanthanum nitrate staining. Although the moss-like structure of the endothelial glycocalyx covered the surface of the vascular endothelium in the control group mice under normal conditions, the endothelial glycocalyx structure was already degraded and dispersed (white arrow) in db/db mice. After LPS injection, the endothelial glycocalyx was degraded completely in db/db mice, whereas its injury was attenuated in control mice.

rate was significantly decreased in db/db mice compared with in the control group, and (c) the migration of inflammatory cells was delayed and extended in db/db mice compared with in control mice.

## Endothelial Glycocalyx Layer in db/db Mice

The endothelial glycocalyx is injured under hyperglycemic conditions (Nieuwdorp et al., 2006a,b; Hirota et al., 2020). One mechanism responsible for this may involve attenuation of glycocalyx synthesis. We found that *Ext1*, *Csgalnact1,* and *Vcan* gene expression decreased in db/db mice before LPS injection. These results suggested the possibility that endothelial glycocalyx synthesis decreased in db/db mice, although the synthesis of glycocalyx is complicated by multiple enzymatic pathways, and factors regulating its shedding include local pH and mechanical stimuli (Reitsma et al., 2007).

Previous reports have shown that endothelial glycocalyx is synthesized on endothelial cells (Mensah et al., 2017), and it was also found that endothelial cell dysregulation is involved in DM (McVeigh et al., 1992; De Vriese et al., 2000). Under hyperglycemia, glucose intake into endothelial cells is promoted via glucose transporter 1 (Mann et al., 2003), and endothelial disorder results from intracellular metabolic disorders (Wautier et al., 2001; Quagliaro et al., 2003). Likewise, insulin resistance and inflammatory cytokines can also impair the function of endothelial cells (Groop et al., 2005; Razavi Nematollahi et al., 2009; Taegtmeyer et al., 2015).

The endothelial glycocalyx is injured directly by hyperglycemia; and its synthesis may be damaged because endothelial cells under DM are exposed to hyperglycemic conditions for an extended time.

## Migration of Inflammatory Cells Is Delayed and Expanded in db/db Mice

In db/db mice, the number of CD11b-positive cells, including neutrophils and macrophages, delayed in reaching the peak compared with that in the control mouse group. After reaching the peak, the number of cells did not decrease in db/db mice, whereas cell number was significantly decreased in the lungs of control mice. This result is also supported by the result of analysis of serum proinflammatory cytokine IL-1β, which did

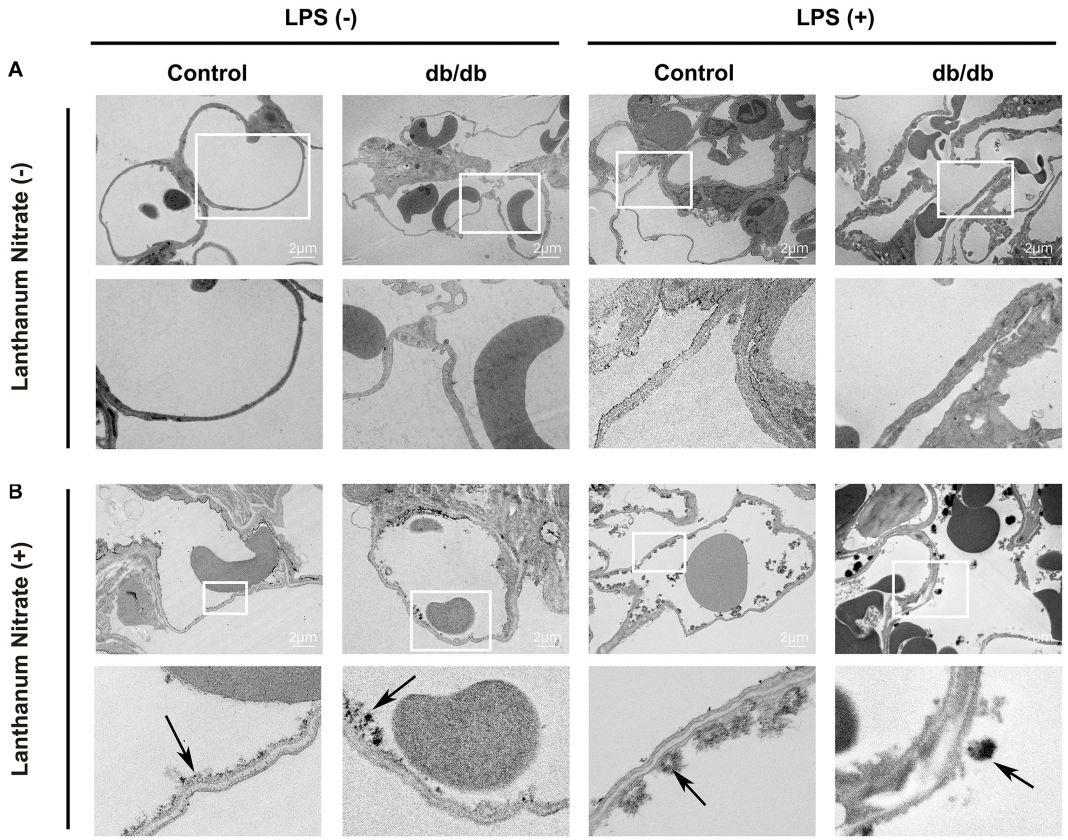


**FIGURE 6 |** Ultrastructural imaging of pulmonary endothelial injury by transmission electron microscopy (TEM). **(A)** Images taken from samples not stained with lanthanum nitrate; the endothelial glycocalyx was not detected. The pulmonary endothelium was thin and smooth in control mice before LPS injection. In control mice after LPS injection, the endothelial wall became edematous, but the extent of this was greater in db/db mice than in control mice treated with or without LPS. **(B)** The endothelial glycocalyx was detected using lanthanum nitrate staining. The endothelial glycocalyx structure showed greater degradation in db/db mice than in control mice under normal conditions. After LPS injection, the endothelial glycocalyx formed a skip lesion in control mice, whereas the endothelial glycocalyx was more degraded in db/db mice. Black arrows indicate the endothelial glycocalyx.

not decrease in db/db mice compared to the control group. Meanwhile, tissue-resident macrophages, as indicated by Iba-1-positive migration to lung tissue, continued to increase in db/db mice after LPS injection, whereas there was no significant change in the control mice.

Consistent with our findings showing a delayed peak in neutrophil numbers, it was reported that neutrophil migration capability is attenuated in DM (Delamaire et al., 1997; Koh et al., 2012). However, tissue-resident macrophages may increase compensatory mechanisms, instead of neutrophils with low migration capability. Consequently, in db/db mice, extended inflammation may occur. In addition, the alteration of serum syndecan-1 concentration, serving as a marker of endothelial glycocalyx injury, was also similar to the modulation of inflammatory cells after LPS injection.

## Endothelial Glycocalyx Injury Influences Extended Inflammation

The intact glycocalyx prevents the inadvertent adhesion of platelets and leukocytes to the vascular wall (Mulivor and Lipowsky, 2002; Reitsma et al., 2007; Becker et al., 2010a,b). Specifically, the glycocalyx thickness (approximately 0.5 μm) exceeds the dimension of cellular adhesion molecules expressed on endothelial cells, such as integrins, selectins, and ICAMs, thus attenuating the interactions of these molecules with circulating blood cells (Becker et al., 2010a,b). Injury of the endothelial glycocalyx leaves the endothelial cells vulnerable to injury, and it is easy to expose the cell surface receptors to the vascular lumen, and granulocytes and platelets enable them to adhere to endothelial cells.

In db/db mice, the endothelial glycocalyx was thinner than that in the control mice before LPS administration. In addition, hyperglycemia itself stimulates ICAM expression on endothelial cells (Jafar et al., 2016). Therefore, it is thought that endothelial cells are easily injured. This phenomenon may have led to extended inflammation in the lungs of db/db mice.

Lipopolysaccharide administration causes endothelial glycocalyx injury; subsequently, the endothelial cells are damaged by pathogens and damage associated molecular patterns. It was recently reported that endothelial cells cause pyroptosis under stress (Cheng et al., 2017; Jia et al., 2019) and

secrete proinflammatory cytokines, such as IL-1β. Pyroptosis is a highly inflammatory form of programed cell death that occurs most frequently upon infection with intracellular pathogens and is likely to form part of the antimicrobial response (Jorgensen and Miao, 2015). This process promotes the rapid clearance of various bacterial, viral, fungal, and protozoan infections by removing intracellular replication niches and enhancing the host's defensive responses (Jorgensen and Miao, 2015). Although this reaction promotes inflammatory responses for host defense, excessive promotion of the inflammatory response leads to injury in the host itself. Since it is possible that pyroptosis contributes to extended inflammation in db/db mice, further study is required.

Recently, the novel coronavirus disease 2019 (COVID-19) caused by SARS-CoV-2 has become a serious concern. It is suggested that DM plays a pivotal role in COVID-19 progression. In particular, endothelial disorders, including loss of endothelial glycocalyx, may be involved in increased morbidity and mortality in diabetic patients with COVID-19 (Hayden, 2020). This phenomenon may also be explained by the extended inflammation that occurs in diabetic patients.

Notably, a limitation of this study is that it is descriptive, and further research is required to clarify the implicated mechanisms. In addition, sepsis is an exceedingly complicated disease and analysis with a simple experimental endotoxemia model may not suffice. Therefore, additional studies using a bacteremia model are required. As lanthanum binds to not only endothelial glycocalyx but also calcium-binding sites, it has been used as a calcium probe in several organs (Shaklai and Tavassoli, 1982). Therefore, lanthanum staining is not specific to glycocalyx.

## CONCLUSION

In conclusion, this study provided the ultrastructure of endothelial glycocalyx injury under diabetic conditions. In db/db mice, endothelial glycocalyx is already injured before LPS administration, and the migration of inflammatory cells is both delayed and expanded. This extended inflammation may be involved in endothelial glycocalyx damage due to the attenuation of endothelial glycocalyx synthesis.

## DATA AVAILABILITY STATEMENT

The original contributions presented in the study are included in the article/**Supplementary Material**, further inquiries can be directed to the corresponding author/s.

## ETHICS STATEMENT

The animal study was reviewed and approved by the Institutional Animal Research Committee of Gifu University (Gifu, Japan). Written informed consent was obtained from the owners for the participation of their animals in this study.

## AUTHOR CONTRIBUTIONS

SS and HO wrote the manuscript. CT, and NM performed the TEM imaging. SS, HO, KoS, HF, and YK performed the SEM imaging. CT prepared the samples for TEM imaging. SS, HO, HY, and IM prepared the samples for SEM imaging. SS, TK, and HT performed the histological assessment. SS, YF, TK, and HT performed the immunohistochemical analysis. SS, KeS, and TW performed the ELISA. SS, HY, IM, TD, TY, and SY conducted the animal studies. RK and AS performed the FACS analysis. SK and SO supervised the animal studies. HO and HT revised and edited the manuscript. All authors have read and approved the final manuscript.

## FUNDING

This study was supported in part by grants-in-aid for scientific research Nos. 20K09281, 19H03756, 19K18347, 19K09410, 18K08914, 18K08884, 18K16511, 17K11569, 16H05497, 16K09509, and 16K20381 from the Ministry of Education, Science and Culture of Japan.

## ACKNOWLEDGMENTS

The authors want to express their deepest gratitude to Genzou Takemura, Professor of Internal Medicine, Asahi University of Dentistry, for his help in interpreting the significance of the results.

## SUPPLEMENTARY MATERIAL

The Supplementary Material for this article can be found online at: https://www.frontiersin.org/articles/10.3389/fcell.2021.623582/full#supplementary-material

## REFERENCES

Abe, T., Ogura, H., Shiraishi, A., Kushimoto, S., Saitoh, D., Fujishima, S., et al. (2018). Characteristics, management, and in-hospital mortality among patients with severe sepsis in intensive care units in Japan: the forecast study. *Crit. Care* 22:322. doi: 10.1186/s13054-018-2186-7

Adembri, C., Sgambati, E., Vitali, L., Selmi, V., Margheri, M., Tani, A., et al. (2011). Sepsis induces albuminuria and alterations in the glomerular filtration barrier: a morphofunctional study in the rat. *Crit. Care* 15:R277. doi: 10.1186/cc10559

Ando, Y., Okada, H., Takemura, G., Suzuki, K., Takada, C., Tomita, H., et al. (2018). Brain-specific ultrastructure of capillary endothelial glycocalyx and its possible contribution for blood brain barrier. *Sci. Rep*. 8:17523. doi: 10.1038/s41598-018-35976-2

Becker, B. F., Chappell, D., Bruegger, D., Annecke, T., and Jacob, M. (2010a). Therapeutic strategies targeting the endothelial glycocalyx: acute deficits, but great potential. *Cardiovasc. Res*. 87, 300–310. doi: 10.1093/cvr/cvq137

Becker, B. F., Chappell, D., and Jacob, M. (2010b). Endothelial glycocalyx and coronary vascular permeability: the fringe benefit. *Basic Res. Cardiol*. 105, 687–701. doi: 10.1007/s00395-010-0118-z

Broekhuizen, L. N., Lemkes, B. A., Mooij, H. L., Meuwese, M. C., Verberne, H., Holleman, F., et al. (2010). Effect of sulodexide on endothelial glycocalyx and vascular permeability in patients with type 2 diabetes mellitus. *Diabetologia* 53, 2646–2655. doi: 10.1007/s00125-010-1910-x

Chelazzi, C., Villa, G., Mancinelli, P., De Gaudio, A. R., and Adembri, C. (2015). Glycocalyx and sepsis-induced alterations in vascular permeability. *Crit. Care* 19:26. doi: 10.1186/s13054-015-0741-z

Cheng, K. T., Xiong, S., Ye, Z., Hong, Z., Di, A., Tsang, K. M., et al. (2017). Caspase-11-mediated endothelial pyroptosis underlies endotoxemia-induced lung injury. *J. Clin. Invest.* 127, 4124–4135. doi: 10.1172/JCI94495

De Vriese, A. S., Verbeuren, T. J., Van de Voorde, J., Lameire, N. H., and Vanhoutte, P. M. (2000). Endothelial dysfunction in diabetes. *Br. J. Pharmacol.* 130, 963–974. doi: 10.1038/sj.bjp.0703393

Delamaire, M., Maugendre, D., Moreno, M., Le Goff, M. C., Allannic, H., and Genetet, B. (1997). Impaired leucocyte functions in diabetic patients. *Diabet. Med.* 14, 29–34. doi: 10.1002/(SICI)1096-9136(199701)14:1<29::AID-DIA300<3.0.CO;2-V

Fukuta, T., Okada, H., Takemura, G., Suzuki, K., Takada, C., Tomita, H., et al. (2019). Neutrophil elastase inhibition ameliorates endotoxin-induced myocardial injury accompanying degradation of cardiac capillary glycocalyx. *Shock* 54, 386–393. doi: 10.1097/SHK.0000000000001482

Groop, P. H., Forsblom, C., and Thomas, M. C. (2005). Mechanisms of disease: pathway-selective insulin resistance and microvascular complications of diabetes. *Nat. Clin. Pract. Endocrinol. Metab.* 1, 100–110. doi: 10.1038/ncpendmet0046

Gupta, S., Maratha, A., Siednienko, J., Natarajan, A., Gajanayake, T., Hoashi, S., et al. (2017). Analysis of inflammatory cytokine and TLR expression levels in Type 2 diabetes with complications. *Sci. Rep.* 7:7633. doi: 10.1038/s41598-017-07230-8

Hayden, M. R. (2020). Endothelial activation and dysfunction in metabolic syndrome, type 2 diabetes and coronavirus disease 2019. *J. Int. Med. Res.* 48:300060520939746. doi: 10.1177/0300060520939746

Hirota, T., Levy, J. H., and Iba, T. (2020). The influence of hyperglycemia on neutrophil extracellular trap formation and endothelial glycocalyx damage in a mouse model of type 2 diabetes. *Microcirculation* 27:e12617. doi: 10.1111/micc.12617

Inagawa, R., Okada, H., Takemura, G., Suzuki, K., Takada, C., Yano, H., et al. (2018). Ultrastructural alteration of pulmonary capillary endothelial glycocalyx during endotoxemia. *Chest* 154, 317–325. doi: 10.1016/j.chest.2018.03.003

Investigators, N.-S. S., Finfer, S., Chittock, D. R., Su, S. Y., Blair, D., Foster, D., et al. (2009). Intensive versus conventional glucose control in critically ill patients. *N. Engl. J. Med.* 360, 1283–1297. doi: 10.1056/NEJMoa0810625

Jafar, N., Edriss, H., and Nugent, K. (2016). The effect of short-term hyperglycemia on the innate immune system. *Am. J. Med. Sci.* 351, 201–211. doi: 10.1016/j.amjms.2015.11.011

Jia, C., Zhang, J., Chen, H., Zhuge, Y., Chen, H., Qian, F., et al. (2019). Endothelial cell pyroptosis plays an important role in Kawasaki disease via HMGB1/RAGE/cathespin B signaling pathway and NLRP3 inflammasome activation. *Cell Death Dis.* 10:778. doi: 10.1038/s41419-019-2021-3

Jorgensen, I., and Miao, E. A. (2015). Pyroptotic cell death defends against intracellular pathogens. *Immunol. Rev.* 265, 130–142. doi: 10.1111/imr.12287

Koh, G. C., Peacock, S. J., van der Poll, T., and Wiersinga, W. J. (2012). The impact of diabetes on the pathogenesis of sepsis. *Eur. J. Clin. Microbiol. Infect. Dis.* 31, 379–388. doi: 10.1007/s10096-011-1337-4

Kushimoto, S., Abe, T., Ogura, H., Shiraishi, A., Saitoh, D., Fujishima, S., et al. (2020). Impact of blood glucose abnormalities on outcomes and disease severity in patients with severe sepsis: an analysis from a multicenter, prospective survey of severe sepsis. *PLoS One* 15:e0229919. doi: 10.1371/journal.pone.0229919

Liborio, A. B., Braz, M. B., Seguro, A. C., Meneses, G. C., Neves, F. M., Pedrosa, D. C., et al. (2015). Endothelial glycocalyx damage is associated with leptospirosis acute kidney injury. *Am. J. Trop. Med. Hyg.* 92, 611–616. doi: 10.4269/ajtmh.14-0232

Machin, D. R., Bloom, S. I., Campbell, R. A., Phuong, T. T. T., Gates, P. E., Lesniewski, L. A., et al. (2018). Advanced age results in a diminished endothelial glycocalyx. *Am. J. Physiol. Heart Circ. Physiol.* 315, H531–H539. doi: 10.1152/ajpheart.00104.2018

Mann, G. E., Yudilevich, D. L., and Sobrevia, L. (2003). Regulation of amino acid and glucose transporters in endothelial and smooth muscle cells. *Physiol. Rev.* 83, 183–252. doi: 10.1152/physrev.00022.2002

McVeigh, G. E., Brennan, G. M., Johnston, G. D., McDermott, B. J., McGrath, L. T., Henry, W. R., et al. (1992). Impaired endothelium-dependent and independent vasodilation in patients with type 2 (non-insulin-dependent) diabetes mellitus. *Diabetologia* 35, 771–776. doi: 10.1007/BF00429099

Mensah, S. A., Cheng, M. J., Homayoni, H., Plouffe, B. D., Coury, A. J., and Ebong, E. E. (2017). Regeneration of glycocalyx by heparan sulfate and sphingosine 1-phosphate restores inter-endothelial communication. *PLoS One* 12:e0186116. doi: 10.1371/journal.pone.0186116

Mulivor, A. W., and Lipowsky, H. H. (2002). Role of glycocalyx in leukocyte-endothelial cell adhesion. *Am. J. Physiol. Heart Circ. Physiol.* 283, H1282–H1291. doi: 10.1152/ajpheart.00117.2002

Muller, L. M., Gorter, K. J., Hak, E., Goudzwaard, W. L., Schellevis, F. G., Hoepelman, A. I., et al. (2005). Increased risk of common infections in patients with type 1 and type 2 diabetes mellitus. *Clin. Infect. Dis.* 41, 281–288. doi: 10.1086/431587

Neves, F. M., Meneses, G. C., Sousa, N. E., Menezes, R. R., Parahyba, M. C., Martins, A. M., et al. (2015). Syndecan-1 in acute decompensated heart failure–association with renal function and mortality. *Circ. J.* 79, 1511–1519. doi: 10.1253/circj.CJ-14-1195

Nieuwdorp, M., Mooij, H. L., Kroon, J., Atasever, B., Spaan, J. A., Ince, C., et al. (2006a). Endothelial glycocalyx damage coincides with microalbuminuria in type 1 diabetes. *Diabetes* 55, 1127–1132. doi: 10.2337/diabetes.55.04.06.db05-1619

Nieuwdorp, M., van Haeften, T. W., Gouverneur, M. C., Mooij, H. L., van Lieshout, M. H., Levi, M., et al. (2006b). Loss of endothelial glycocalyx during acute hyperglycemia coincides with endothelial dysfunction and coagulation activation in vivo. *Diabetes* 55, 480–486. doi: 10.2337/diabetes.55.02.06.db05-1103

Oda, K., Okada, H., Suzuki, A., Tomita, H., Kobayashi, R., Sumi, K., et al. (2019). Factors enhancing serum syndecan-1 concentrations: a large-scale comprehensive medical examination. *J. Clin. Med.* 8:1320. doi: 10.3390/jcm8091320

Okada, H., Takemura, G., Suzuki, K., Oda, K., Takada, C., Hotta, Y., et al. (2017). Three-dimensional ultrastructure of capillary endothelial glycocalyx under normal and experimental endotoxemic conditions. *Crit. Care* 21:261. doi: 10.1186/s13054-017-1841-8

Padberg, J. S., Wiesinger, A., di Marco, G. S., Reuter, S., Grabner, A., Kentrup, D., et al. (2014). Damage of the endothelial glycocalyx in chronic kidney disease. *Atherosclerosis* 234, 335–343. doi: 10.1016/j.atherosclerosis.2014.03.016

Quagliaro, L., Piconi, L., Assaloni, R., Martinelli, L., Motz, E., and Ceriello, A. (2003). Intermittent high glucose enhances apoptosis related to oxidative stress in human umbilical vein endothelial cells: the role of protein kinase C and NAD(P)H-oxidase activation. *Diabetes* 52, 2795–2804. doi: 10.2337/diabetes.52.11.2795

Razavi Nematollahi, L., Kitabchi, A. E., Stentz, F. B., Wan, J. Y., Larijani, B. A., Tehrani, M. M., et al. (2009). Proinflammatory cytokines in response to insulin-induced hypoglycemic stress in healthy subjects. *Metabolism* 58, 443–448. doi: 10.1016/j.metabol.2008.10.018

Reitsma, S., Slaaf, D. W., Vink, H., van Zandvoort, M. A., and Oude Egbrink, M. G. (2007). The endothelial glycocalyx: composition, functions, and visualization. *Pflugers Arch.* 454, 345–359. doi: 10.1007/s00424-007-0212-8

Robertson, R. T., Levine, S. T., Haynes, S. M., Gutierrez, P., Baratta, J. L., Tan, Z., et al. (2015). Use of labeled tomato lectin for imaging vasculature structures. *Histochem. Cell Biol.* 143, 225–234. doi: 10.1007/s00418-014-1301-3

Ross, R. (1999). Atherosclerosis–an inflammatory disease. *N. Engl. J. Med.* 340, 115–126. doi: 10.1056/NEJM199901143400207

Salmon, A. H., and Satchell, S. C. (2012). Endothelial glycocalyx dysfunction in disease: albuminuria and increased microvascular permeability. *J. Pathol.* 226, 562–574. doi: 10.1002/path.3964

Shaklai, M., and Tavassoli, M. (1982). Lanthanum as an electron microscopic stain. *J. Histochem. Cytochem.* 30, 1325–1330. doi: 10.1177/30.12.6185564

Singer, M., Deutschman, C. S., Seymour, C. W., Shankar-Hari, M., Annane, D., Bauer, M., et al. (2016). The third international consensus definitions for sepsis and septic shock (sepsis-3). *JAMA* 315, 801–810. doi: 10.1001/jama.2016.0287

Solinas, G., Vilcu, C., Neels, J. G., Bandyopadhyay, G. K., Luo, J. L., Naugler, W., et al. (2007). JNK1 in hematopoietically derived cells contributes to diet-induced inflammation and insulin resistance without affecting obesity. *Cell Metab*. 6, 386–397. doi: 10.1016/j.cmet.2007.09.011

Spight, D., Trapnell, B., Zhao, B., Berclaz, P., and Shanley, T. P. (2008). Granulocyte-macrophage-colony-stimulating factor-dependent peritoneal macrophage responses determine survival in experimentally induced peritonitis and sepsis in mice. *Shock* 30, 434–442. doi: 10.1097/SHK.0b013e3181673543

Steppan, J., Hofer, S., Funke, B., Brenner, T., Henrich, M., Martin, E., et al. (2011). Sepsis and major abdominal surgery lead to flaking of the endothelial glycocalix. *J. Surg. Res*. 165, 136–141. doi: 10.1016/j.jss.2009.04.034

Suzuki, K., Okada, H., Takemura, G., Takada, C., Kuroda, A., Yano, H., et al. (2019). Neutrophil elastase damages the pulmonary endothelial glycocalyx in lipopolysaccharide-induced experimental endotoxemia. *Am. J. Pathol*. 189, 1526–1535. doi: 10.1016/j.ajpath.2019.05.002

Taegtmeyer, H., Beauloye, C., Harmancey, R., and Hue, L. (2015). Comment on Nolan et al. insulin resistance as a physiological defense against metabolic stress: implications for the management of subsets of type 2 diabetes. diabetes 2015;64:673-686. *Diabetes* 64:e37. doi: 10.2337/db15-0655

Wautier, M. P., Chappey, O., Corda, S., Stern, D. M., Schmidt, A. M., and Wautier, J. L. (2001). Activation of NADPH oxidase by AGE links oxidant stress to altered gene expression via RAGE. *Am. J. Physiol. Endocrinol. Metab*. 280, E685–E694. doi: 10.1152/ajpendo.2001.280.5.E685

**Conflict of Interest:** The authors declare that the research was conducted in the absence of any commercial or financial relationships that could be construed as a potential conflict of interest.

frontiers in Cell and Developmental Biology

MINI REVIEW
published: 14 July 2021
doi: 10.3389/fcell.2021.711003

# The Endothelial Glycocalyx as a Double-Edged Sword in Microvascular Homeostasis and Pathogenesis

*Nuria Villalba[1], Sheon Baby[1] and Sarah Y. Yuan[1,2]**

*[1] Department of Molecular Pharmacology and Physiology, Morsani College of Medicine, University of South Florida, Tampa, FL, United States, [2] Department of Surgery, Morsani College of Medicine, University of South Florida, Tampa, FL, United States*

Expressed on the endothelial cell (EC) surface of blood vessels, the glycocalyx (GCX), a mixture of carbohydrates attached to proteins, regulates the access of cells and molecules in the blood to the endothelium. Besides protecting endothelial barrier integrity, the dynamic microstructure of the GCX confers remarkable functions including mechanotransduction and control of vascular tone. Recently, a novel perspective has emerged supporting the pleiotropic roles of the endothelial GCX (eGCX) in cardiovascular health and disease. Because eGCX degradation occurs in certain pathological states, the circulating levels of eGCX degradation products have been recognized to have diagnostic or prognostic values. Beyond their biomarker roles, certain eGCX fragments serve as pathogenic factors in disease progression. Pharmacological interventions that attenuate eGCX degradation or restore its integrity have been sought. This review provides our current understanding of eGCX structure and function across the microvasculature in different organs. We also discuss disease or injury states, such as infection, sepsis and trauma, where eGCX dysfunction contributes to severe inflammatory vasculopathy.

**Keywords: inflammation, microvascular homeostasis, permeability, endothelium, glycocalyx**

OPEN ACCESS

***Edited by:***
*Ye Zeng,*
*Sichuan University, China*

***Reviewed by:***
*D. Neil Granger,*
*Louisiana State University Health Shreveport, United States*
*Eric Schmidt,*
*University of Colorado, Denver, United States*

****Correspondence:***
*Sarah Y. Yuan*
*syuan@usf.edu*

***Specialty section:***
*This article was submitted to Signaling, a section of the journal Frontiers in Cell and Developmental Biology*

***Received:*** *17 May 2021*
***Accepted:*** *22 June 2021*
***Published:*** *14 July 2021*

***Citation:***
*Villalba N, Baby S and Yuan SY (2021) The Endothelial Glycocalyx as a Double-Edged Sword in Microvascular Homeostasis and Pathogenesis. Front. Cell Dev. Biol. 9:711003. doi: 10.3389/fcell.2021.711003*

## INTRODUCTION

The vascular endothelial surface is coated by the GCX matrix that confers important functions in circulatory homeostasis (Weinbaum et al., 2007). The endothelial GCX (eGCX), first visualized in the late 1960s after the invention of transmission electron microscope (Luft, 1966), is mainly formed by proteoglycans and glycoproteins, core proteins anchored to the EC membrane that serve as a foundation for the rest of the glycocalyx constituents. Proteoglycans, principally syndecans and glypicans, are decorated by glycosaminoglycan (GAG) chains such as heparan sulfate and chondroitin sulfate (Li et al., 2012). GAGs are characterized by long linear polysaccharides of repeating disaccharide units with a hexosamine and either an uronic acid or a galactose

**Abbreviations:** BBB, blood–brain barrier; DAMP, danger-associated molecular pattern; EC, endothelial cell; eNOS, endothelial nitric oxide synthase; eSOD, endothelial superoxide dismutase; GAG, glycosaminoglycan; eGCX, endothelial glycocalyx; LPS, lipopolysaccharide; NO, nitric oxide; ROS, reactive oxygen species; SAE, sepsis–associated encephalopathy; TRPs, transient receptor potential channels.

(Esko et al., 2009). The amount of GAG chains, length and molecular modifications by sulfation and/or (de)acetylation provide the eGCX an extensive source of structural rearrangements. Notably, heparan sulfate proteoglycans are the most prominent members expressed on the surface of the endothelial cells, accounting for 50–90% of the total endothelial proteoglycans (Ihrcke et al., 1993). The majority of the interactions between syndecans and extracellular matrix molecules, growth factors and cell adhesion molecules seem to be mediated by their heparan sulfate chains through electrostatic interaction (Bernfield et al., 1992; Stringer and Gallagher, 1997). Unlike other eGCX constituents, hyaluronic acid is a linear, non-sulfated GAG that interacts with the cell surface receptor CD44, a glycoprotein (Aruffo et al., 1990). The glycoproteins are highly branched short carbohydrate chains (2–15 sugar residues) capped with sialic acid or a fucose, which mainly function as either endothelial adhesion molecules or components of the coagulation system (e.g., selectins, immunoglobulins, and integrins) (**Figure 1**). Further detailed structure and specific components of the eGCX are reviewed elsewhere (Pries and Kuebler, 2006; Tarbell and Pahakis, 2006; Reitsma et al., 2007; Weinbaum et al., 2007; Esko et al., 2009). It is worth noting that the eGCX composition is subject to a highly dynamic regulation and constant replacement or re-arrangement of molecules, ranging from enzymatic degradation ("shedding") to *de novo* biosynthesis of new molecules and to recruitment of circulating molecules from the blood.

In the following sections, we will focus our discussion on the eGCX as an active component of the EC barrier, its functions, and structural variations within the vascular tree and across organs. Furthermore, we will also summarize the new findings from eGCX research with respect to how eGCX degradation leads to certain vascular pathologies.

## The eGCX: An Active Layer Without a Passive Role

The eGCX matrix is an integral component of the vascular wall. Apart from being a physical barrier, the eGCX also plays an effective role in modulating vascular homeostasis. Historically, the eGCX was considered to function as an additional physical barrier between the vessel lumen and the EC membrane (Curry and Adamson, 2012); however, solid experimental evidence has shown an important physiological role for the eGCX in performing a variety of microvascular functions such as regulating vascular permeability, mechanotransduction and leukocyte transmigration (Ihrcke et al., 1993; Davies, 1995; Baldwin and Thurston, 2001; Constantinescu et al., 2003; Curry, 2005; Tarbell and Ebong, 2008; Lopez-Quintero et al., 2009; Lennon and Singleton, 2011; Curry and Adamson, 2012).

The eGCX is one of the major determinants in maintaining endothelial barrier function by acting as an additional molecular filter for the endothelium. The eGCX modulates vascular permeability and hydraulic conductivity by limiting the flux of water and macromolecules (Curry and Michel, 1980; Adamson, 1990; Curry, 2005; Lennon and Singleton, 2011; Curry and Adamson, 2012). It also acts as a vascular barrier through modulation of molecular binding to the EC surface due to the high density of anionic charges on its GAGs side chains. The net negative charge of the eGCX carried by sulfate residues along the GAG chains favors the docking (adsorption) of positively charged molecules (Schnitzer, 1988; Lieleg et al., 2009). Thus, the eGCX regulates vascular permeability by restricting circulating molecules from strongly attaching to the endothelium based on their net charge. Importantly, the molecular size (70–kDa cutoff) is also relevant in determining the penetration of molecules into the eGCX layer, as much as chemical binding (Henry and Duling, 1999; Vink and Duling, 2000; Curry and Adamson, 2012).

Previous studies using perfusion models or intravital microscopy techniques found that eGCX damage by heparinase causes microvascular leakage (Rehm et al., 2004; Jacob et al., 2006). Similar results were found using genetic knock down of a specific eGCX component (Voyvodic et al., 2014). In this regard, increased hydraulic conductivity (*Lp*) of microvessels after removal of the eGCX or plasma proteins has also been shown (Huxley and Curry, 1985; Adamson and Clough, 1992; Weinbaum et al., 2007).

The eGCX plays a pivotal role in mechanotransduction together with other sensors in the endothelium, including G–protein–coupled receptors (Zou et al., 2004; Mederos y Schnitzler et al., 2008), Piezo and transient receptor potential (TRP) channels (Martinac, 2004; Coste et al., 2010; Dragovich et al., 2016), caveolar structures (Rizzo et al., 1998), and integrins and focal adhesions (Ringer et al., 2017). Blood flow exerts mechanical tangential forces to the endothelial surface such as shear stress, which is sensed by the eGCX and triggers the production of nitric oxide (NO), an important modulator of vascular tone (Davies, 1995; Dimmeler et al., 1999; Tarbell and Ebong, 2008; Fu and Tarbell, 2013; Zeng et al., 2018). The ability of the eGCX to reorganize the actin cytoskeleton under shear forces has been demonstrated in studies using EC monolayers as well as *in vivo* approaches. The eGCX core protein syndecan-1 interacts with cytoskeletal proteins through a highly conserved tyrosine residue in the syndecan family (Carey et al., 1996). Also, syndecan-4 acts synergistically with integrins to assemble and rearrange actin stress fibers to orchestrate cell adhesion and focal contact formation (Echtermeyer et al., 1999; Bass et al., 2007; Multhaupt et al., 2009). Interestingly, while syndecans are the main effector in cell adhesion or shape changes via their interaction with the cytoskeleton, glypicans mediate flow–induced endothelial NO synthase (eNOS) activation, based on their location at the endothelial membrane microdomains where caveolae reside (Ebong et al., 2014; Zeng and Liu, 2016; Bartosch et al., 2017). Prior studies with cultured ECs have shown that breakdown of heparan sulfate alters shear stress and impairs NO production (Florian et al., 2003); similar responses were also observed *in vivo* on canine femoral and rabbit mesenteric arteries, where infusion of hyaluronidase (to degrade hyaluronic acid GAGs) or neuraminidase (to remove sialic acid residues), respectively, reduced flow–dependent vasodilation, which is mediated by NO release (as in the majority of vascular beds) (Pohl et al., 1991; Mochizuki et al., 2003).

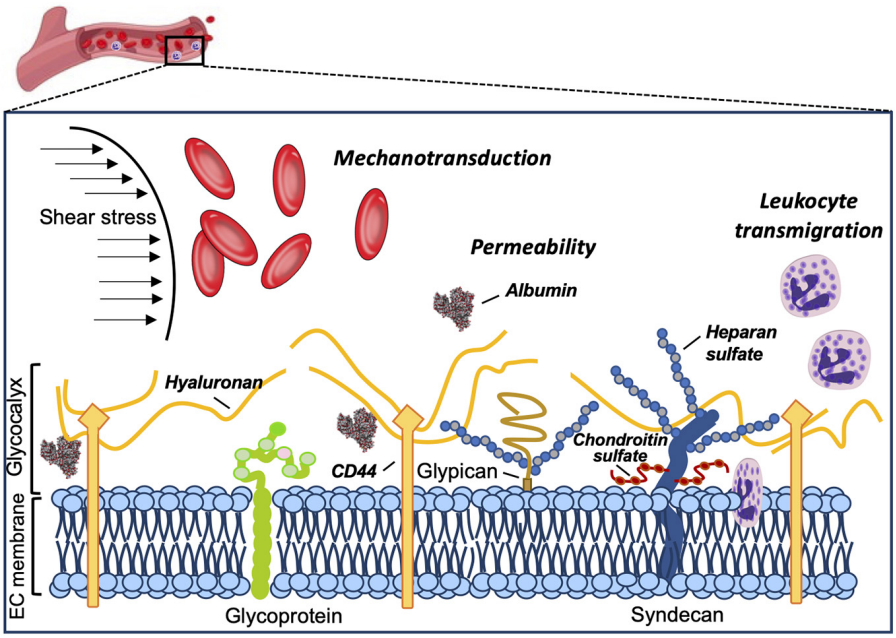


**FIGURE 1 |** Structure and functions of the eGCX. Schematic representation of the main components and functions of the endothelial glycocalyx. The eGCX is composed of proteoglycans, with long glycosaminoglycan side-chains (GAG-chain) and glycoproteins, with short branched carbohydrate side-chains. The eGCX modulates coagulation, inflammation and mechanotransduction processes.

Additionally, the eGCX also controls the interaction between the endothelium and circulating cells by preventing the latter from approaching the endothelium under basal conditions. Upon inflammatory stimulation, the glycans are shed from the EC surface allowing slow rolling and adhesion of leukocytes (Constantinescu et al., 2003; Lipowsky et al., 2011). Similarly, breakdown of the eGCX increases platelet–vessel wall interactions, further demonstrating an anti-coagulant effect by the eGCX layer (Vink et al., 2000).

## The Endothelium Is Heterogenous, So Is the eGCX

The morphology of the microvascular endothelium and associated gene expression vary across different vascular beds in different tissues, therefore showing a remarkable heterogeneity (Aird, 2007; Jambusaria et al., 2020). Likewise, different GAG chain arrangements and eGCX compositions result in great biochemical or structural variations, further contributing to the eGCX heterogeneity. With reference to the thickness and microstructure of the eGCX, it is now well established that both vary across different species, vascular beds, organs and shear stress rates.

The estimation of the eGCX thickness extends from 0.2 to 0.5 μm in capillaries (van den Berg et al., 2003) and venules (Yoon et al., 2017), to 2–3 μm in small arteries (van Haaren et al., 2003; Yen et al., 2015), and 4.5 μm in conductance arteries (Megens et al., 2007). These studies used different methods of eGCX visualization and measurements, including alcian blue staining for transmission electron microscopy, dye–exclusion of different sized tracers, and fluorescently labeled lectins for microscopic imaging (Roth, 1983; Vink and Duling, 2000; van den Berg et al., 2003). Still, there is a large discrepancy when it comes to reporting eGCX thickness, making experimental observations particularly difficult to be reconciled. The reason for this variability, which might not be entirely attributed to differences in the microstructure and composition of the eGCX, might rather be due to a poor preservation of such a fragile structure during fixation and tissue handling (de Mesy Bentley, 2011; Ebong et al., 2011). Comparatively, direct *in vivo* measurements using bright-field microscopy also embody challenges. The close optical refractive index of the eGCX to the surrounding blood makes it very difficult to visualize the eGCX limits, also contributing to bias in the results. *In vitro*, ECs in culture exhibit slightly different eGCX in comparison to the complex structure found in *in vivo* vessels (Potter and Damiano, 2008; Potter et al., 2009). Recently, super resolution fluorescence microscopy (STORM) has been applied to identify the spatio-chemical organization of the eGCX *in vitro* (Fan et al., 2019). Also, glycomic analysis by liquid chromatography coupled to mass spectrometry has emerged as a novel method providing a more detailed and comprehensive characterization of eGCX in cells and tissues (Li et al., 2019, 2020; Riley et al., 2020).

A close view of the eGCX using both scanning and transmission electron microscopy has revealed different eGCX thickness among continuous, fenestrated and sinusoidal capillaries in the heart, kidney, and liver, respectively (Okada et al., 2017). The eGCX layer in both continuous and fenestrated capillaries is thicker than in the sinusoids. In the heart, the eGCX covers the entire luminal endothelial surface. In the kidney, the eGCX appears to occlude the endothelial pores of the fenestrated capillaries. In the hepatic sinusoids, however, the eGCX covers

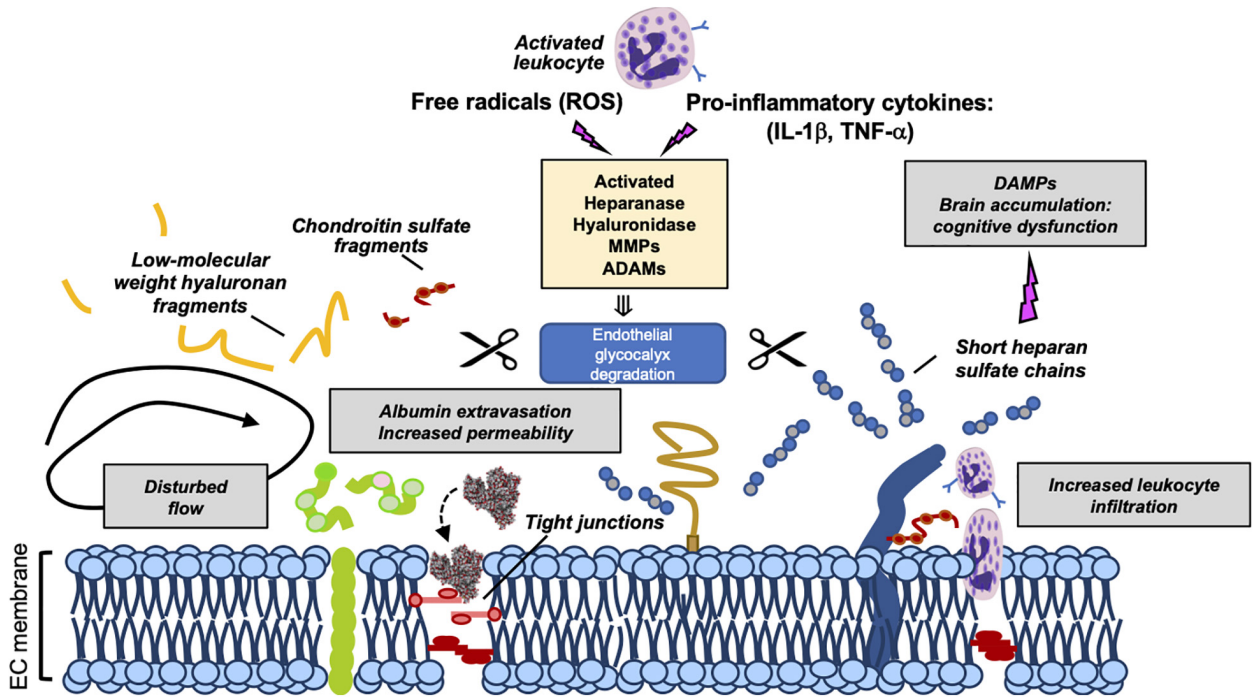


**FIGURE 2 |** Mechanisms of eGCX degradation and pathogenic consequences of released GCX fragments. Representation of enzymatic degradation of GCX components. The structure of the eGC is the result of a balance between the enzymatic degradation and *de novo* biosynthesis of new molecules and adsorption of circulating components from blood. Several enzymes mediate this degradation. Heparinase, hyaluronidase, MMPs and ADAMs are activated by pro-inflammatory cytokines and ROS promoting the damage and shedding of one or more of its components. This degradation releases eGCX components (such as short heparan sulfate chains, low-molecular weight hyaluronan fragments, and chondroitin sulfate fragments) into the circulation. As a result of its degradation, the eGC becomes thinner allowing the extravasation of albumin, leukocyte adhesion and dysregulated vasodilation. Once in circulation, eGCX components such as heparan sulfate fragments can act as DAMPs leading to cognitive impairment (Hippensteel et al., 2019a). Gray box areas summarize major pathophysiologic features of eGCX degradation. DAMPs, danger-associated molecular patterns; MMP, metalloproteinase; IL-1β, interleukin-1β; TNF-α, tumor necrosis factor-α. Scissors symbol means "degradation".

both the luminal side and opposite side facing the perisinusoidal space (Okada et al., 2017).

In organs like the brain and heart, where the capillary endothelium is categorized as continuous (non-fenestrated), the endothelial eGCX appears to be denser compared to that in the lung, whose capillaries are also covered by continuous endothelium (Ando et al., 2018). These differences might be explained by the mechanotransduction properties of the eGCX in sensing fluid shear stress, which alters GAGs synthesis (Arisaka et al., 1995; Gouverneur et al., 2006; Zeng and Tarbell, 2014). Since the pulmonary circulation is a low fluid shear stress system (because of its low resistance), a lower rate of GAGs synthesis renders a thinner eGCX on the pulmonary capillaries compared to other organs like the heart or the kidney. However, experimental evidence shows discrepancies in eGCX depth between pulmonary eGC (>1.5 micrometers) exceeding that of systemic vessels such as the eGCX in cremaster muscle capillaries (Schmidt et al., 2012; Han et al., 2016). The same principle can be applied to the macro vs. microvascular network, where arteries receiving higher shear stress exhibit greater eGCX depths compared to venules and capillaries with lower shear stress (Lipowsky et al., 1978, 1980; van den Berg et al., 2003). In light of recent discoveries, differences in capillary EC structure and shear stress might not be sufficient to explain eGCX heterogeneity. Gene expression profiling and single–cell RNA-sequencing might yield a more comprehensive picture of the distinct EC subsets and associated eGCX structures (Jambusaria et al., 2020; Gao and Galis, 2021).

## Severe Inflammation as a Cause of eGCX Dysfunction

Recently, the eGCX integrity has emerged as an important determinant of cardiovascular health and disease. Given the fundamental role of the eGCX in maintaining vascular homeostasis, one would predict that when components of the eGCX are lost or degraded, the endothelial function could be impaired, which has indeed been demonstrated. eGCX degradation is triggered by inflammatory mechanisms through the activation of specific enzymes such as metalloproteinases, heparanase, and hyaluronidase. These enzymes are activated by reactive oxygen species (ROS) and pro-inflammatory cytokines such as tumor necrosis factor alpha (TNF-α) and interleukin-1 beta (IL-1β) (**Figure 2**) (Chappell et al., 2008; Schmidt et al., 2012; Lipowsky and Lescanic, 2013; Manon-Jensen et al., 2013; Becker et al., 2015).

The lack of an intact eGCX has been observed in several pathological conditions, the best characterized being sepsis. In the broad scheme of sepsis, systemic inflammatory injury of the eGCX leads to capillary leak, adverse immune response, and impaired vasodilation. Following septic challenge, enzymes such as ADAM15 (a disintegrin and metalloproteinase 15) and heparanase can shed glycoproteins (CD44) and heparan sulfate, respectively, leading to eGCX disruption (Schmidt et al., 2012; Yang et al., 2018). As a result of eGCX damage, the eGCX layer becomes thinner and more sparse while its degradation products are released into the bloodstream, a phenomenon that has been observed in animal models of sepsis as well as in human patients with sepsis, trauma or shock (Nelson et al., 2008; Haywood-Watson et al., 2011; Sallisalmi et al., 2012; Luker et al., 2018; Uchimido et al., 2019).

Similar to sepsis, sterile inflammation following trauma or tissue injury also causes shedding of proteoglycans, hyaluronan and heparan sulfate chains. The eGCX fragments function as Danger-Associated Molecules Patterns (DAMPs) that activate toll–like receptor or/and RAGE receptor-dependent pathways (Johnson et al., 2002) RAGE (Xu et al., 2011, 2013). High levels of circulating eGCX elements, which propagate sterile inflammation and drive trauma induced coagulopathy (TIC), are highly correlated with the severity of injury and clinical outcomes (Johansson et al., 2011a,b).

Oxidative stress also plays an important role in eGCX degradation during inflammation. The eGCX along with vascular ECs are vulnerable to circulating ROS produced during oxidative stress. *In vitro* exposure of ROS (superoxide and hydroxyl radicals) to the eGCX promotes fragmentation of GAGs and loss of some of its components. Previous studies have demonstrated that hyaluronan and chondroitin sulfate are the most susceptible to depolymerization and chemical modifications by ROS (Halliwell, 1978; Greenwald and Moy, 1980; Bartold et al., 1984; Moseley et al., 1995, 1997; Lipowsky and Lescanic, 2013; Singh et al., 2013). Intact eGCX has the capability to quench free radicals by having binding sites for anti-oxidant enzymes like xanthine oxidoreductase (Adachi et al., 1993) and endothelial superoxide dismutase (eSOD) (Becker et al., 1994).

Viral infections, such as those caused by dengue, hanta and the novel severe acute respiratory syndrome (SARS)-CoV-2 (COVID-19), are also accompanied by eGCX disruption. In the case of the dengue virus, in particular, the secreted dengue virus (DENV) non-structural protein 1 (NS1) disrupts the eGCX on human pulmonary capillaries by increasing the expression of sialidases, heparanase and metalloproteinases. All these events cause systemic microvascular leakage leading to hypovolemic shock and potentially fatal complications in severe dengue infections (Luplertlop and Misse, 2008; Puerta-Guardo et al., 2016; Glasner et al., 2017; Suwarto et al., 2017; Tang et al., 2017; Chen et al., 2018; Wang et al., 2019). Hantavirus infection is also associated with endothelial dysfunction and elevated circulating levels of syndecan-1, allowing a clinical association of disease severity with eGCX damage (Marsac et al., 2011; Connolly-Andersen et al., 2014). In contrast, other viruses do not seem to cause eGCX shedding, but they exploit eGCX components on the host cell surface as a binding site to infect target cells. For example, Influenza A uses sialic acid as a receptor (Weis et al., 1988; Matrosovich et al., 1993; Suzuki, 2003; Russell et al., 2008) while HIV lentivirus (Saphire et al., 2001; Bobardt et al., 2003; Gallay, 2004) and SARS-CoV-2 (Clausen et al., 2020) interact with heparan sulfate. Also, several recent studies have emphasized the implications of eGCX damage and endothelial dysfunction in the pathogenesis of COVID-19 (Jung et al., 2020; Kaur et al., 2020; Libby and Luscher, 2020; Teuwen et al., 2020; Yamaoka-Tojo, 2020).

Previous research on fluid resuscitation for critical illness management has shown mixed results, some show attenuating eGCX degradation while others show inducing eGCX disruption (Hippensteel et al., 2019b). However, there is consensus that colloids (e.g., albumin), or fresh frozen plasma, reduce eGCX damage following sepsis, hemorrhagic shock and traumatic brain injury (Zehtabchi and Nishijima, 2009; Haywood-Watson et al., 2011; Kozar et al., 2011; Peng et al., 2013; Mica et al., 2016; Nikolian et al., 2018).

## Endothelial GCX in Blood–Brain Barrier (BBB) Injury

The diagnostic utility of eGCX degradation products as a biomarker of disease is supported by the correlation between circulating eGCX fragments and clinical outcomes [reviewed by Uchimido et al. (2019)]. Compared to the cardiac and pulmonary capillaries, cerebral capillaries have a thicker eGCX layer which is better preserved following lipopolysaccharide (LPS) administration (Ando et al., 2018). Additionally, the eGCX joins astrocyte endfeet and basement membrane in reinforcing BBB properties as a part of a newly defined "tripartite" BBB layered structure (Kutuzov et al., 2018). During sepsis, heparan sulfate fragments released from the injured eGCX can circulate in the bloodstream for days and penetrate into the hippocampal area, interfering with long-term potentiation (LTP) and contributing to sepsis–associated encephalopathy (SAE), a common neurological complication of sepsis in the absence of direct brain infection (Hippensteel et al., 2019a). Circulating eGCX fragments predicted cognitive impairment in septic patients, however, whether they have potential diagnostic utility as biomarkers to predict cognitive dysfunction in sepsis survivors, still remains to be confirmed.

## CONCLUSION

The eGCX, a complex and fragile structure that protects endothelial barrier integrity, plays a crucial role in maintaining microcirculatory homeostasis and blood-tissue exchange. Disruption of eGCX is a consequence as well as cause of microvascular injury, as eGCX degradation products act as pathogenic factors capable of inducing endothelial hyperpermeability and microvascular leakage during inflammation. Further studies are required to understand eGCX structure and function in order to maximize its protective

contribution to endothelial cell stability while minimizing its pathological role in vascular disease and injury.

## AUTHOR CONTRIBUTIONS

NV performed literature search, drafted the manuscript, and prepared the figures. SB and SY participated in manuscript editing. SY initiated, directed, and sponsored the work throughout all levels of development. All authors approved the final version for publication.

## FUNDING

This work was supported by the National Institutes of Health grants R35 HL1150732 and GM097270 (to SY).

## REFERENCES

Adachi, T., Fukushima, T., Usami, Y., and Hirano, K. (1993). Binding of human xanthine oxidase to sulphated glycosaminoglycans on the endothelial-cell surface. *Biochem. J.* 289, 523–527. doi: 10.1042/bj2890523

Adamson, R. H. (1990). Permeability of frog mesenteric capillaries after partial pronase digestion of the endothelial glycocalyx. *J. Physiol.* 428, 1–13. doi: 10.1113/jphysiol.1990.sp018197

Adamson, R. H., and Clough, G. (1992). Plasma proteins modify the endothelial cell glycocalyx of frog mesenteric microvessels. *J. Physiol.* 445, 473–486. doi: 10.1113/jphysiol.1992.sp018934

Aird, W. C. (2007). Phenotypic heterogeneity of the endothelium: i. structure, function, and mechanisms. *Circ. Res.* 100, 158–173. doi: 10.1161/01.RES.0000255691.76142.4a

Ando, Y., Okada, H., Takemura, G., Suzuki, K., Takada, C., Tomita, H., et al. (2018). Brain-specific ultrastructure of capillary endothelial Glycocalyx and its possible contribution for blood brain barrier. *Sci. Rep.* 8:17523. doi: 10.1038/s41598-018-35976-2

Arisaka, T., Mitsumata, M., Kawasumi, M., Tohjima, T., Hirose, S., and Yoshida, Y. (1995). Effects of shear stress on glycosaminoglycan synthesis in vascular endothelial cells. *Ann. N. Y. Acad. Sci.* 748, 543–554. doi: 10.1111/j.1749-6632.1994.tb17359.x

Aruffo, A., Stamenkovic, I., Melnick, M., Underhill, C. B., and Seed, B. (1990). CD44 is the principal cell surface receptor for hyaluronate. *Cell* 61, 1303–1313. doi: 10.1016/0092-8674(90)90694-A

Baldwin, A. L., and Thurston, G. (2001). Mechanics of endothelial cell architecture and vascular permeability. *Crit. Rev. Biomed. Eng.* 29, 247–278. doi: 10.1615/CritRevBiomedEng.v29.i2.20

Bartold, P. M., Wiebkin, O. W., and Thonard, J. C. (1984). The effect of oxygen-derived free radicals on gingival proteoglycans and hyaluronic acid. *J. Periodontal. Res.* 19, 390–400. doi: 10.1111/j.1600-0765.1984.tb01012.x

Bartosch, A. M. W., Mathews, R., and Tarbell, J. M. (2017). Endothelial glycocalyx-mediated nitric oxide production in response to selective AFM pulling. *Biophys. J.* 113, 101–108. doi: 10.1016/j.bpj.2017.05.033

Bass, M. D., Morgan, M. R., and Humphries, M. J. (2007). Integrins and syndecan-4 make distinct, but critical, contributions to adhesion contact formation. *Soft Matter.* 3, 372–376. doi: 10.1039/b614610d

Becker, B. F., Jacob, M., Leipert, S., Salmon, A. H., and Chappell, D. (2015). Degradation of the endothelial glycocalyx in clinical settings: searching for the sheddases. *Br. J. Clin. Pharmacol.* 80, 389–402. doi: 10.1111/bcp.12629

Becker, M., Menger, M. D., and Lehr, H. A. (1994). Heparin-released superoxide dismutase inhibits postischemic leukocyte adhesion to venular endothelium. *Am. J. Physiol.* 267, H925–H930. doi: 10.1152/ajpheart.1994.267.3.H925

Bernfield, M., Kokenyesi, R., Kato, M., Hinkes, M. T., Spring, J., Gallo, R. L., et al. (1992). Biology of the syndecans: a family of transmembrane heparan sulfate proteoglycans. *Annu. Rev. Cell Biol.* 8, 365–393. doi: 10.1146/annurev.cb.08.110192.002053

Bobardt, M. D., Saphire, A. C., Hung, H. C., Yu, X., Van Der Schueren, B., Zhang, Z., et al. (2003). Syndecan captures, protects, and transmits HIV to T lymphocytes. *Immunity* 18, 27–39. doi: 10.1016/S1074-7613(02)00504-6

Carey, D. J., Bendt, K. M., and Stahl, R. C. (1996). The cytoplasmic domain of syndecan-1 is required for cytoskeleton association but not detergent insolubility. identification of essential cytoplasmic domain residues. *J. Biol. Chem.* 271, 15253–15260. doi: 10.1074/jbc.271.25.15253

Chappell, D., Jacob, M., Rehm, M., Stoeckelhuber, M., Welsch, U., Conzen, P., et al. (2008). Heparinase selectively sheds heparan sulphate from the endothelial glycocalyx. *Biol. Chem.* 389, 79–82. doi: 10.1515/BC.2008.005

Chen, H. R., Chao, C. H., Liu, C. C., Ho, T. S., Tsai, H. P., Perng, G. C., et al. (2018). Macrophage migration inhibitory factor is critical for dengue NS1-induced endothelial glycocalyx degradation and hyperpermeability. *PLoS Pathog.* 14:e1007033. doi: 10.1371/journal.ppat.1007033

Clausen, T. M., Sandoval, D. R., Spliid, C. B., Pihl, J., Perrett, H. R., Painter, C. D., et al. (2020). SARS-CoV-2 infection depends on cellular heparan sulfate and ACE2. *Cell* 183, 1043–1057 e1015.

Connolly-Andersen, A. M., Thunberg, T., and Ahlm, C. (2014). Endothelial activation and repair during hantavirus infection: association with disease outcome. *Open Forum Infect. Dis.* 1:ofu027. doi: 10.1093/ofid/ofu027

Constantinescu, A. A., Vink, H., and Spaan, J. A. (2003). Endothelial cell glycocalyx modulates immobilization of leukocytes at the endothelial surface. *Arterioscler. Thromb. Vasc. Biol.* 23, 1541–1547. doi: 10.1161/01.ATV.0000085630.24353.3D

Coste, B., Mathur, J., Schmidt, M., Earley, T. J., Ranade, S., Petrus, M. J., et al. (2010). Piezo1 and Piezo2 are essential components of distinct mechanically activated cation channels. *Science* 330, 55–60. doi: 10.1126/science.1193270

Curry, F. E., and Adamson, R. H. (2012). Endothelial glycocalyx: permeability barrier and mechanosensor. *Ann. Biomed. Eng.* 40, 828–839. doi: 10.1007/s10439-011-0429-8

Curry, F. E., and Michel, C. C. (1980). A fiber matrix model of capillary permeability. *Microvasc. Res.* 20, 96–99. doi: 10.1016/0026-2862(80)90024-2

Curry, F. R. (2005). Microvascular solute and water transport. *Microcirculation* 12, 17–31. doi: 10.1080/10739680590894993

Davies, P. F. (1995). Flow-mediated endothelial mechanotransduction. *Physiol. Rev.* 75, 519–560. doi: 10.1152/physrev.1995.75.3.519

de Mesy Bentley, K. L. (2011). An 11-mum-thick glycocalyx?: it's all in the technique! *Arterioscler. Thromb. Vasc. Biol.* 31, 1712–1713. doi: 10.1161/ATVBAHA.111.229849

Dimmeler, S., Fleming, I., Fisslthaler, B., Hermann, C., Busse, R., and Zeiher, A. M. (1999). Activation of nitric oxide synthase in endothelial cells by Akt-dependent phosphorylation. *Nature* 399, 601–605. doi: 10.1038/21224

Dragovich, M. A., Chester, D., Fu, B. M., Wu, C., Xu, Y., Goligorsky, M. S., et al. (2016). Mechanotransduction of the endothelial glycocalyx mediates nitric oxide production through activation of TRP channels. *Am. J. Physiol. Cell Physiol.* 311, C846–C853. doi: 10.1152/ajpcell.00288.2015

Ebong, E. E., Lopez-Quintero, S. V., Rizzo, V., Spray, D. C., and Tarbell, J. M. (2014). Shear-induced endothelial NOS activation and remodeling via heparan sulfate, glypican-1, and syndecan-1. *Integr. Biol.* 6, 338–347. doi: 10.1039/C3IB40199E

Ebong, E. E., Macaluso, F. P., Spray, D. C., and Tarbell, J. M. (2011). Imaging the endothelial glycocalyx in vitro by rapid freezing/freeze substitution transmission electron microscopy. *Arterioscler. Thromb. Vasc. Biol.* 31, 1908–1915. doi: 10.1161/ATVBAHA.111.225268

Echtermeyer, F., Baciu, P. C., Saoncella, S., Ge, Y., and Goetinck, P. F. (1999). Syndecan-4 core protein is sufficient for the assembly of focal adhesions and actin stress fibers. *J. Cell Sci.* 112(Pt 20), 3433–3441. doi: 10.1242/jcs.112.20.3433

Esko, J. D., Kimata, K., and Lindahl, U. (2009). "Proteoglycans and sulfated glycosaminoglycans," in *Essentials of Glycobiology*, eds A. Nd, R. D. Varki, J. D. Cummings, H. H. Esko, and P. Freeze. (New York: Cold Spring Harbor).

Fan, J., Sun, Y., Xia, Y., Tarbell, J. M., and Fu, B. M. (2019). Endothelial surface glycocalyx (ESG) components and ultra-structure revealed by stochastic optical

reconstruction microscopy (STORM). *Biorheology* 56, 77–88. doi: 10.3233/BIR-180204

Florian, J. A., Kosky, J. R., Ainslie, K., Pang, Z., Dull, R. O., and Tarbell, J. M. (2003). Heparan sulfate proteoglycan is a mechanosensor on endothelial cells. *Circ. Res.* 93, e136–e142. doi: 10.1161/01.RES.0000101744.47866.D5

Fu, B. M., and Tarbell, J. M. (2013). Mechano-sensing and transduction by endothelial surface glycocalyx: composition, structure, and function. *Wiley Interdiscip. Rev. Syst. Biol. Med.* 5, 381–390. doi: 10.1002/wsbm.1211

Gallay, P. (2004). Syndecans and HIV-1 pathogenesis. *Microbes Infect.* 6, 617–622. doi: 10.1016/j.micinf.2004.02.004

Gao, Y., and Galis, Z. S. (2021). Exploring the role of endothelial cell resilience in cardiovascular health and disease. *Arterioscler. Thromb. Vasc. Biol.* 41, 179–185. doi: 10.1161/ATVBAHA.120.314346

Glasner, D. R., Ratnasiri, K., Puerta-Guardo, H., Espinosa, D. A., Beatty, P. R., and Harris, E. (2017). Dengue virus NS1 cytokine-independent vascular leak is dependent on endothelial glycocalyx components. *PLoS Pathog.* 13:e1006673. doi: 10.1371/journal.ppat.1006673

Gouverneur, M., Spaan, J. A., Pannekoek, H., Fontijn, R. D., and Vink, H. (2006). Fluid shear stress stimulates incorporation of hyaluronan into endothelial cell glycocalyx. *Am. J. Physiol. Heart Circ. Physiol.* 290, H458–H452. doi: 10.1152/ajpheart.00592.2005

Greenwald, R. A., and Moy, W. W. (1980). Effect of oxygen-derived free radicals on hyaluronic acid. *Arthritis Rheum.* 23, 455–463. doi: 10.1002/art.1780230408

Halliwell, B. (1978). Superoxide-dependent formation of hydroxyl radicals in the presence of iron salts. its role in degradation of hyaluronic acid by a superoxide-generating system. *FEBS Lett.* 96, 238–242. doi: 10.1016/0014-5793(78)80409-8

Han, S., Lee, S. J., Kim, K. E., Lee, H. S., Oh, N., Park, I., et al. (2016). Amelioration of sepsis by TIE2 activation-induced vascular protection. *Sci. Transl. Med.* 8:335ra55. doi: 10.1126/scitranslmed.aad9260

Haywood-Watson, R. J., Holcomb, J. B., Gonzalez, E. A., Peng, Z., Pati, S., Park, P. W., et al. (2011). Modulation of syndecan-1 shedding after hemorrhagic shock and resuscitation. *PLoS One* 6:e23530. doi: 10.1371/journal.pone.0023530

Henry, C. B., and Duling, B. R. (1999). Permeation of the luminal capillary glycocalyx is determined by hyaluronan. *Am. J. Physiol.* 277, H508–H514. doi: 10.1152/ajpheart.1999.277.2.H508

Hippensteel, J. A., Anderson, B. J., Orfila, J. E., Mcmurtry, S. A., Dietz, R. M., Su, G., et al. (2019a). Circulating heparan sulfate fragments mediate septic cognitive dysfunction. *J. Clin. Invest.* 129, 1779–1784. doi: 10.1172/JCI124485

Hippensteel, J. A., Uchimido, R., Tyler, P. D., Burke, R. C., Han, X., Zhang, F., et al. (2019b). Intravenous fluid resuscitation is associated with septic endothelial glycocalyx degradation. *Crit. Care* 23:259. doi: 10.1186/s13054-019-2534-2

Huxley, V. H., and Curry, F. E. (1985). Albumin modulation of capillary permeability: test of an adsorption mechanism. *Am. J. Physiol.* 248, H264–H273. doi: 10.1152/ajpheart.1985.248.2.H264

Ihrcke, N. S., Wrenshall, L. E., Lindman, B. J., and Platt, J. L. (1993). Role of heparan sulfate in immune system-blood vessel interactions. *Immunol. Today* 14, 500–505. doi: 10.1016/0167-5699(93)90265-M

Jacob, M., Bruegger, D., Rehm, M., Welsch, U., Conzen, P., and Becker, B. F. (2006). Contrasting effects of colloid and crystalloid resuscitation fluids on cardiac vascular permeability. *Anesthesiology* 104, 1223–1231. doi: 10.1097/00000542-200606000-00018

Jambusaria, A., Hong, Z., Zhang, L., Srivastava, S., Jana, A., Toth, P. T., et al. (2020). Endothelial heterogeneity across distinct vascular beds during homeostasis and inflammation. *Elife* 9:e51413. doi: 10.7554/eLife.51413

Johansson, P. I., Sorensen, A. M., Perner, A., Welling, K. L., Wanscher, M., Larsen, C. F., et al. (2011a). Disseminated intravascular coagulation or acute coagulopathy of trauma shock early after trauma? an observational study. *Crit. Care* 15:R272. doi: 10.1186/cc10553

Johansson, P. I., Stensballe, J., Rasmussen, L. S., and Ostrowski, S. R. (2011b). A high admission syndecan-1 level, a marker of endothelial glycocalyx degradation, is associated with inflammation, protein C depletion, fibrinolysis, and increased mortality in trauma patients. *Ann. Surg.* 254, 194–200. doi: 10.1097/SLA.0b013e318226113d

Johnson, G. B., Brunn, G. J., Kodaira, Y., and Platt, J. L. (2002). Receptor-mediated monitoring of tissue well-being via detection of soluble heparan sulfate by Toll-like receptor 4. *J. Immunol.* 168, 5233–5239. doi: 10.4049/jimmunol.168.10.5233

Jung, F., Kruger-Genge, A., Franke, R. P., Hufert, F., and Kupper, J. H. (2020). COVID-19 and the endothelium. *Clin. Hemorheol. Microcirc.* 75, 7–11. doi: 10.3233/CH-209007

Kaur, S., Tripathi, D. M., and Yadav, A. (2020). The enigma of endothelium in COVID-19. *Front. Physiol.* 11:989. doi: 10.3389/fphys.2020.00989

Kozar, R. A., Peng, Z., Zhang, R., Holcomb, J. B., Pati, S., Park, P., et al. (2011). Plasma restoration of endothelial glycocalyx in a rodent model of hemorrhagic shock. *Anesth. Analg.* 112, 1289–1295. doi: 10.1213/ANE.0b013e318210385c

Kutuzov, N., Flyvbjerg, H., and Lauritzen, M. (2018). Contributions of the glycocalyx, endothelium, and extravascular compartment to the blood-brain barrier. *Proc. Natl. Acad. Sci. U. S. A.* 115, E9429–E9438. doi: 10.1073/pnas.1802155115

Lennon, F. E., and Singleton, P. A. (2011). Hyaluronan regulation of vascular integrity. *Am. J. Cardiovasc. Dis.* 1, 200–213.

Li, L., Ly, M., and Linhardt, R. J. (2012). Proteoglycan sequence. *Mol. Biosyst.* 8, 1613–1625. doi: 10.1039/c2mb25021g

Li, Q., Xie, Y., Wong, M., and Lebrilla, C. B. (2019). Characterization of cell Glycocalyx with mass spectrometry methods. *Cells* 8:882. doi: 10.3390/cells8080882

Li, Q., Xie, Y., Wong, M., Barboza, M., and Lebrilla, C. B. (2020). Comprehensive structural glycomic characterization of the glycocalyxes of cells and tissues. *Nat. Protoc.* 15, 2668–2704. doi: 10.1038/s41596-020-0350-4

Libby, P., and Luscher, T. (2020). COVID-19 is, in the end, an endothelial disease. *Eur. Heart J.* 41, 3038–3044. doi: 10.1093/eurheartj/ehaa623

Lieleg, O., Baumgartel, R. M., and Bausch, A. R. (2009). Selective filtering of particles by the extracellular matrix: an electrostatic bandpass. *Biophys. J.* 97, 1569–1577. doi: 10.1016/j.bpj.2009.07.009

Lipowsky, H. H., and Lescanic, A. (2013). The effect of doxycycline on shedding of the glycocalyx due to reactive oxygen species. *Microvasc. Res.* 90, 80–85. doi: 10.1016/j.mvr.2013.07.004

Lipowsky, H. H., Kovalcheck, S., and Zweifach, B. W. (1978). The distribution of blood rheological parameters in the microvasculature of cat mesentery. *Circ. Res.* 43, 738–749. doi: 10.1161/01.RES.43.5.738

Lipowsky, H. H., Sah, R., and Lescanic, A. (2011). Relative roles of doxycycline and cation chelation in endothelial glycan shedding and adhesion of leukocytes. *Am. J. Physiol. Heart Circ. Physiol.* 300, H415–H422. doi: 10.1152/ajpheart.00923.2010

Lipowsky, H. H., Usami, S., and Chien, S. (1980). In vivo measurements of "apparent viscosity" and microvessel hematocrit in the mesentery of the cat. *Microvasc. Res.* 19, 297–319. doi: 10.1016/0026-2862(80)90050-3

Lopez-Quintero, S. V., Amaya, R., Pahakis, M., and Tarbell, J. M. (2009). The endothelial glycocalyx mediates shear-induced changes in hydraulic conductivity. *Am. J. Physiol. Heart Circ. Physiol.* 296, H1451–H1456. doi: 10.1152/ajpheart.00894.2008

Luft, J. H. (1966). Fine structures of capillary and endocapillary layer as revealed by ruthenium red. *Fed. Proc.* 25, 1773–1783.

Luker, J. N., Vigiola Cruz, M., Carney, B. C., Day, A., Moffatt, L. T., Johnson, L. S., et al. (2018). Shedding of the endothelial glycocalyx is quantitatively proportional to burn injury severity. *Ann. Burns Fire Disasters* 31, 17–22.

Luplertlop, N., and Misse, D. (2008). MMP cellular responses to dengue virus infection-induced vascular leakage. *Jpn. J. Infect. Dis.* 61, 298–301.

Manon-Jensen, T., Multhaupt, H. A., and Couchman, J. R. (2013). Mapping of matrix metalloproteinase cleavage sites on syndecan-1 and syndecan-4 ectodomains. *FEBS J.* 280, 2320–2331. doi: 10.1111/febs.12174

Marsac, D., Garcia, S., Fournet, A., Aguirre, A., Pino, K., Ferres, M., et al. (2011). Infection of human monocyte-derived dendritic cells by ANDES Hantavirus enhances pro-inflammatory state, the secretion of active MMP-9 and indirectly enhances endothelial permeability. *Virol. J.* 8:223. doi: 10.1186/1743-422X-8-223

Martinac, B. (2004). Mechanosensitive ion channels: molecules of mechanotransduction. *J. Cell Sci.* 117, 2449–2460. doi: 10.1242/jcs.01232

Matrosovich, M. N., Gambaryan, A. S., Tuzikov, A. B., Byramova, N. E., Mochalova, L. V., Golbraikh, A. A., et al. (1993). Probing of the receptor-binding sites of the

H1 and H3 influenza A and influenza B virus hemagglutinins by synthetic and natural sialosides. *Virology* 196, 111–121. doi: 10.1006/viro.1993.1459

Mederos y Schnitzler, M., Storch, U., Meibers, S., Nurwakagari, P., Breit, A., Essin, K., et al. (2008). Gq-coupled receptors as mechanosensors mediating myogenic vasoconstriction. *EMBO J.* 27, 3092–3103. doi: 10.1038/emboj.2008.233

Megens, R. T., Reitsma, S., Schiffers, P. H., Hilgers, R. H., De Mey, J. G., Slaaf, D. W., et al. (2007). Two-photon microscopy of vital murine elastic and muscular arteries. combined structural and functional imaging with subcellular resolution. *J. Vasc. Res.* 44, 87–98. doi: 10.1159/000098259

Mica, L., Simmen, H., Werner, C. M., Plecko, M., Keller, C., Wirth, S. H., et al. (2016). Fresh frozen plasma is permissive for systemic inflammatory response syndrome, infection, and sepsis in multiple-injured patients. *Am. J. Emerg. Med.* 34, 1480–1485. doi: 10.1016/j.ajem.2016.04.041

Mochizuki, S., Vink, H., Hiramatsu, O., Kajita, T., Shigeto, F., Spaan, J. A., et al. (2003). Role of hyaluronic acid glycosaminoglycans in shear-induced endothelium-derived nitric oxide release. *Am. J. Physiol. Heart Circ. Physiol.* 285, H722–H726. doi: 10.1152/ajpheart.00691.2002

Moseley, R., Waddington, R. J., and Embery, G. (1997). Degradation of glycosaminoglycans by reactive oxygen species derived from stimulated polymorphonuclear leukocytes. *Biochim. Biophys. Acta* 1362, 221–231. doi: 10.1016/S0925-4439(97)00083-5

Moseley, R., Waddington, R., Evans, P., Halliwell, B., and Embery, G. (1995). The chemical modification of glycosaminoglycan structure by oxygen-derived species in vitro. *Biochim. Biophys. Acta* 1244, 245–252. doi: 10.1016/0304-4165(95)00010-9

Multhaupt, H. A., Yoneda, A., Whiteford, J. R., Oh, E. S., Lee, W., and Couchman, J. R. (2009). Syndecan signaling: when, where and why? *J. Physiol. Pharmacol.* 60, 31–38.

Nelson, A., Berkestedt, I., Schmidtchen, A., Ljunggren, L., and Bodelsson, M. (2008). Increased levels of glycosaminoglycans during septic shock: relation to mortality and the antibacterial actions of plasma. *Shock* 30, 623–627. doi: 10.1097/SHK.0b013e3181777da3

Nikolian, V. C., Dekker, S. E., Bambakidis, T., Higgins, G. A., Dennahy, I. S., Georgoff, P. E., et al. (2018). Improvement of blood-brain barrier integrity in traumatic brain injury and hemorrhagic shock following treatment with valproic acid and fresh Frozen Plasma. *Crit. Care Med.* 46, e59–e66. doi: 10.1097/CCM.0000000000002800

Okada, H., Takemura, G., Suzuki, K., Oda, K., Takada, C., Hotta, Y., et al. (2017). Three-dimensional ultrastructure of capillary endothelial glycocalyx under normal and experimental endotoxemic conditions. *Crit. Care* 21:261. doi: 10.1186/s13054-017-1841-8

Peng, Z., Pati, S., Potter, D., Brown, R., Holcomb, J. B., Grill, R., et al. (2013). Fresh frozen plasma lessens pulmonary endothelial inflammation and hyperpermeability after hemorrhagic shock and is associated with loss of syndecan 1. *Shock* 40, 195–202. doi: 10.1097/SHK.0b013e31829f91fc

Pohl, U., Herlan, K., Huang, A., and Bassenge, E. (1991). EDRF-mediated shear-induced dilation opposes myogenic vasoconstriction in small rabbit arteries. *Am. J. Physiol.* 261, H2016–H2023. doi: 10.1152/ajpheart.1991.261.6.H2016

Potter, D. R., and Damiano, E. R. (2008). The hydrodynamically relevant endothelial cell glycocalyx observed in vivo is absent in vitro. *Circ. Res.* 102, 770–776. doi: 10.1161/CIRCRESAHA.107.160226

Potter, D. R., Jiang, J., and Damiano, E. R. (2009). The recovery time course of the endothelial cell glycocalyx in vivo and its implications in vitro. *Circ. Res.* 104, 1318–1325. doi: 10.1161/CIRCRESAHA.108.191585

Pries, A. R., and Kuebler, W. M. (2006). Normal endothelium. in: moncasa, S., higgs, A. the vascular endothelium I. *Handb. Exp. Pharmacol.* 176, 1–40. doi: 10.1007/3-540-32967-6_1

Puerta-Guardo, H., Glasner, D. R., and Harris, E. (2016). Dengue virus NS1 disrupts the endothelial glycocalyx, leading to hyperpermeability. *PLoS Pathog.* 12:e1005738. doi: 10.1371/journal.ppat.1005738

Rehm, M., Zahler, S., Lotsch, M., Welsch, U., Conzen, P., Jacob, M., et al. (2004). Endothelial glycocalyx as an additional barrier determining extravasation of 6% hydroxyethyl starch or 5% albumin solutions in the coronary vascular bed. *Anesthesiology* 100, 1211–1223. doi: 10.1097/00000542-200405000-00025

Reitsma, S., Slaaf, D. W., Vink, H., Van Zandvoort, M. A., and Oude Egbrink, M. G. (2007). The endothelial glycocalyx: composition, functions, and visualization. *Pflugers Arch.* 454, 345–359. doi: 10.1007/s00424-007-0212-8

Riley, N. M., Bertozzi, C. R., and Pitteri, S. J. (2020). A pragmatic guide to enrichment strategies for mass spectrometry-based glycoproteomics. *Mol. Cell. Proteomics* 20:100029. doi: 10.1074/mcp.R120.002277

Ringer, P., Colo, G., Fassler, R., and Grashoff, C. (2017). Sensing the mechano-chemical properties of the extracellular matrix. *Matrix Biol.* 64, 6–16. doi: 10.1016/j.matbio.2017.03.004

Rizzo, V., Mcintosh, D. P., Oh, P., and Schnitzer, J. E. (1998). In situ flow activates endothelial nitric oxide synthase in luminal caveolae of endothelium with rapid caveolin dissociation and calmodulin association. *J. Biol. Chem.* 273, 34724–34729. doi: 10.1074/jbc.273.52.34724

Roth, J. (1983). Application of lectin–gold complexes for electron microscopic localization of glycoconjugates on thin sections. *J. Histochem. Cytochem.* 31, 987–999. doi: 10.1177/31.8.6190857

Russell, R. J., Kerry, P. S., Stevens, D. J., Steinhauer, D. A., Martin, S. R., Gamblin, S. J., et al. (2008). Structure of influenza hemagglutinin in complex with an inhibitor of membrane fusion. *Proc. Natl. Acad. Sci. U. S. A.* 105, 17736–17741. doi: 10.1073/pnas.0807142105

Sallisalmi, M., Tenhunen, J., Yang, R., Oksala, N., and Pettila, V. (2012). Vascular adhesion protein-1 and syndecan-1 in septic shock. *Acta Anaesthesiol. Scand.* 56, 316–322. doi: 10.1111/j.1399-6576.2011.02578.x

Saphire, A. C., Bobardt, M. D., Zhang, Z., David, G., and Gallay, P. A. (2001). Syndecans serve as attachment receptors for human immunodeficiency virus type 1 on macrophages. *J. Virol.* 75, 9187–9200. doi: 10.1128/JVI.75.19.9187-9200.2001

Schmidt, E. P., Yang, Y., Janssen, W. J., Gandjeva, A., Perez, M. J., Barthel, L., et al. (2012). The pulmonary endothelial glycocalyx regulates neutrophil adhesion and lung injury during experimental sepsis. *Nat. Med.* 18, 1217–1223. doi: 10.1038/nm.2843

Schnitzer, J. E. (1988). Glycocalyx electrostatic potential profile analysis: ion, pH, steric, and charge effects. *Yale J. Biol. Med.* 61, 427–446.

Singh, A., Ramnath, R. D., Foster, R. R., Wylie, E. C., Friden, V., Dasgupta, I., et al. (2013). Reactive oxygen species modulate the barrier function of the human glomerular endothelial glycocalyx. *PLoS One* 8:e55852. doi: 10.1371/journal.pone.0055852

Stringer, S. E., and Gallagher, J. T. (1997). Heparan sulphate. *Int. J. Biochem. Cell Biol.* 29, 709–714. doi: 10.1016/S1357-2725(96)00170-7

Suwarto, S., Sasmono, R. T., Sinto, R., Ibrahim, E., and Suryamin, M. (2017). Association of endothelial glycocalyx and tight and adherens junctions with severity of plasma leakage in dengue infection. *J. Infect. Dis.* 215, 992–999. doi: 10.1093/infdis/jix041

Suzuki, Y. (2003). [Receptor binding specificity of influenza virus and its budding from the host cells]. *Tanpakushitsu Kakusan Koso* 48, 1141–1146.

Tang, T. H., Alonso, S., Ng, L. F., Thein, T. L., Pang, V. J., Leo, Y. S., et al. (2017). Increased serum hyaluronic acid and heparan sulfate in dengue fever: association with plasma leakage and disease severity. *Sci. Rep.* 7:46191. doi: 10.1038/srep46191

Tarbell, J. M., and Ebong, E. E. (2008). The endothelial glycocalyx: a mechano-sensor and -transducer. *Sci. Signal.* 1:t8. doi: 10.1126/scisignal.140pt8

Tarbell, J. M., and Pahakis, M. Y. (2006). Mechanotransduction and the glycocalyx. *J. Intern. Med.* 259, 339–350. doi: 10.1111/j.1365-2796.2006.01620.x

Teuwen, L. A., Geldhof, V., Pasut, A., and Carmeliet, P. (2020). COVID-19: the vasculature unleashed. *Nat. Rev. Immunol.* 20, 389–391. doi: 10.1038/s41577-020-0343-0

Uchimido, R., Schmidt, E. P., and Shapiro, N. I. (2019). The glycocalyx: a novel diagnostic and therapeutic target in sepsis. *Crit. Care* 23:16. doi: 10.1186/s13054-018-2292-6

van den Berg, B. M., Vink, H., and Spaan, J. A. (2003). The endothelial glycocalyx protects against myocardial edema. *Circ. Res.* 92, 592–594. doi: 10.1161/01.RES.0000065917.53950.75

van Haaren, P. M., Vanbavel, E., Vink, H., and Spaan, J. A. (2003). Localization of the permeability barrier to solutes in isolated arteries by confocal microscopy. *Am. J. Physiol. Heart Circ. Physiol.* 285, H2848–H2856. doi: 10.1152/ajpheart.00117.2003

Vink, H., and Duling, B. R. (2000). Capillary endothelial surface layer selectively reduces plasma solute distribution volume. *Am. J. Physiol. Heart Circ. Physiol.* 278, H285–H289. doi: 10.1152/ajpheart.2000.278.1.H285

Vink, H., Constantinescu, A. A., and Spaan, J. A. (2000). Oxidized lipoproteins degrade the endothelial surface layer : implications for platelet-endothelial

cell adhesion. *Circulation* 101, 1500–1502. doi: 10.1161/01.CIR.101.13.1500

Voyvodic, P. L., Min, D., Liu, R., Williams, E., Chitalia, V., Dunn, A. K., et al. (2014). Loss of syndecan-1 induces a pro-inflammatory phenotype in endothelial cells with a dysregulated response to atheroprotective flow. *J. Biol. Chem.* 289, 9547–9559. doi: 10.1074/jbc.M113.541573

Wang, C., Puerta-Guardo, H., Biering, S. B., Glasner, D. R., Tran, E. B., Patana, M., et al. (2019). Endocytosis of flavivirus NS1 is required for NS1-mediated endothelial hyperpermeability and is abolished by a single N-glycosylation site mutation. *PLoS Pathog.* 15:e1007938. doi: 10.1371/journal.ppat.1007938

Weinbaum, S., Tarbell, J. M., and Damiano, E. R. (2007). The structure and function of the endothelial glycocalyx layer. *Annu. Rev. Biomed. Eng.* 9, 121–167. doi: 10.1146/annurev.bioeng.9.060906.151959

Weis, W., Brown, J. H., Cusack, S., Paulson, J. C., Skehel, J. J., and Wiley, D. C. (1988). Structure of the influenza virus haemagglutinin complexed with its receptor, sialic acid. *Nature* 333, 426–431. doi: 10.1038/333426a0

Xu, D., Young, J. H., Krahn, J. M., Song, D., Corbett, K. D., Chazin, W. J., et al. (2013). Stable RAGE-heparan sulfate complexes are essential for signal transduction. *ACS Chem. Biol.* 8, 1611–1620. doi: 10.1021/cb4001553

Xu, D., Young, J., Song, D., and Esko, J. D. (2011). Heparan sulfate is essential for high mobility group protein 1 (HMGB1) signaling by the receptor for advanced glycation end products (RAGE). *J. Biol. Chem.* 286, 41736–41744. doi: 10.1074/jbc.M111.299685

Yamaoka-Tojo, M. (2020). Endothelial glycocalyx damage as a systemic inflammatory microvascular endotheliopathy in COVID-19. *Biomed. J.* 43, 399–413. doi: 10.1016/j.bj.2020.08.007

Yang, X., Meegan, J. E., Jannaway, M., Coleman, D. C., and Yuan, S. Y. (2018). A disintegrin and metalloproteinase 15-mediated glycocalyx shedding contributes to vascular leakage during inflammation. *Cardiovasc. Res.* 114, 1752–1763. doi: 10.1093/cvr/cvy167

Yen, W., Cai, B., Yang, J., Zhang, L., Zeng, M., Tarbell, J. M., et al. (2015). Endothelial surface glycocalyx can regulate flow-induced nitric oxide production in microvessels in vivo. *PLoS One* 10:e0117133. doi: 10.1371/journal.pone.0117133

Yoon, J. H., Lee, E. S., and Jeong, Y. (2017). In vivo imaging of the cerebral endothelial Glycocalyx in mice. *J. Vasc. Res.* 54, 59–67. doi: 10.1159/000457799

Zehtabchi, S., and Nishijima, D. K. (2009). Impact of transfusion of fresh-frozen plasma and packed red blood cells in a 1:1 ratio on survival of emergency department patients with severe trauma. *Acad. Emerg. Med.* 16, 371–378. doi: 10.1111/j.1553-2712.2009.00386.x

Zeng, Y., and Liu, J. (2016). Role of glypican-1 in endothelial NOS activation under various steady shear stress magnitudes. *Exp. Cell Res.* 348, 184–189. doi: 10.1016/j.yexcr.2016.09.017

Zeng, Y., and Tarbell, J. M. (2014). The adaptive remodeling of endothelial glycocalyx in response to fluid shear stress. *PLoS One* 9:e86249. doi: 10.1371/journal.pone.0086249

Zeng, Y., Zhang, X. F., Fu, B. M., and Tarbell, J. M. (2018). The role of endothelial surface Glycocalyx in mechanosensing and transduction. *Adv. Exp. Med. Biol.* 1097, 1–27. doi: 10.1007/978-3-319-96445-4_1

Zou, Y., Akazawa, H., Qin, Y., Sano, M., Takano, H., Minamino, T., et al. (2004). Mechanical stress activates angiotensin II type 1 receptor without the involvement of angiotensin II. *Nat. Cell Biol.* 6, 499–506. doi: 10.1038/ncb1137

**Conflict of Interest:** The authors declare that the research was conducted in the absence of any commercial or financial relationships that could be construed as a potential conflict of interest.

frontiers in Cell and Developmental Biology

ORIGINAL RESEARCH
published: 12 August 2021
doi: 10.3389/fcell.2021.729873

# The Colloid Osmotic Pressure Across the Glycocalyx: Role of Interstitial Fluid Sub-Compartments in Trans-Vascular Fluid Exchange in Skeletal Muscle

*Fitzroy E. Curry*[1]* *and C. Charles Michel*[2]

[1] Department of Physiology and Membrane Biology, School of Medicine, University of California, Davis, Davis, CA, United States, [2] Department of Bioengineering, Imperial College London, London, United Kingdom

The primary purpose of these investigations is to integrate our growing knowledge about the endothelial glycocalyx as a permeability and osmotic barrier into models of trans-vascular fluid exchange in whole organs. We describe changes in the colloid osmotic pressure (COP) difference for plasma proteins across the glycocalyx after an increase or decrease in capillary pressure. The composition of the fluid under the glycocalyx changes in step with capillary pressure whereas the composition of the interstitial fluid takes many hours to adjust to a change in vascular pressure. We use models where the fluid under the glycocalyx mixes with sub-compartments of the interstitial fluid (ISF) whose volumes are defined from the ultrastructure of the inter-endothelial cleft and the histology of the tissue surrounding the capillaries. The initial protein composition in the sub-compartments is that during steady state filtration in the presence of a large pore pathway in parallel with the "small pore" glycocalyx pathway. Changes in the composition depend on the volume of the sub-compartment and the balance of convective and diffusive transport into and out of each sub-compartment. In skeletal muscle the simplest model assumes that the fluid under the glycocalyx mixes directly with a tissue sub-compartment with a volume less than 20% of the total skeletal muscle interstitial fluid volume. The model places limits on trans-vascular flows during transient filtration and reabsorption over periods of 30–60 min. The key assumption in this model is compromised when the resistance to diffusion between the base of the glycocalyx and the tissue sub-compartment accounts for more than 1% of the total resistance to diffusion across the endothelial barrier. It is well established that, in the steady state, there can be no reabsorption in tissue such as skeletal muscle. Our approach extends this idea to demonstrate that transient changes in vascular pressure favoring initial reabsorption from the interstitial fluid of skeletal muscle result in much less fluid exchange than is commonly assumed. Our approach should enable critical evaluations of the empirical models of trans-vascular fluid exchange being used in the clinic that do not account for the hydrostatic and COPs across the glycocalyx.

**Keywords: endothelial glycocalyx, colloid osmotic pressure, capillary permeability, Starling principle, reabsorption, filtration, plasma proteins**

OPEN ACCESS

***Edited by:***
*Bingmei M. Fu,*
*City College of New York (CUNY), United States*

***Reviewed by:***
*John Tarbell,*
*City College of New York (CUNY), United States*
*Michael S. Goligorsky,*
*New York Medical College, United States*

***Correspondence:**
*Fitzroy E. Curry*
*fecurry@ucdavis.edu*

***Specialty section:***
*This article was submitted to Signaling, a section of the journal Frontiers in Cell and Developmental Biology*

***Received:*** *23 June 2021*
***Accepted:*** *22 July 2021*
***Published:*** *12 August 2021*

***Citation:***
*Curry FE and Michel CC (2021) The Colloid Osmotic Pressure Across the Glycocalyx: Role of Interstitial Fluid Sub-Compartments in Trans-Vascular Fluid Exchange in Skeletal Muscle. Front. Cell Dev. Biol. 9:729873. doi: 10.3389/fcell.2021.729873*

## INTRODUCTION

The glycocalyx is the primary barrier to the movement of plasma proteins between the circulating blood and the tissue fluids. The colloid osmotic pressure (COP) differences across the glycocalyx balances the hydrostatic pressure difference across microvascular walls and holds the blood within the circulation (Levick and Michel, 2010; Michel, 1997; Weinbaum, 1998; Michel et al., 2020). The aim of this paper is to investigate the factors determining this difference in oncotic pressure. Since the plasma lies on one side of the glycocalyx and its value can be estimated under most circumstances, our investigation concerns the factors determining the protein composition of the fluid on the tissue side of the glycocalyx both under steady state conditions and during transients of fluid filtration and reabsorption. The rates of fluid exchange may vary considerably from tissue to tissue with different permeability coefficients of the microvessels and differences in the partitioning of their interstitial fluid (ISF). In this paper, we have used values for permeability coefficients and ISF partitioning for skeletal muscle.

Here, microvascular permeability has been treated in terms of its traditional model where fluid exchange is described in terms of two parallel pathways through microvascular walls: the "small pore" and the "large pore" systems. The "small pores" are the main pathways for exchange of fluid and small hydrophilic solutes and ions. We identify the glycocalyx together with the intercellular clefts of continuous endothelia that act as hydraulic resistances in series as the small pore system (Levick and Michel, 2010; Curry, 2018; Curry et al., 2020; Michel et al., 2020). The large pore system is the separate parallel route that is taken by macromolecules to enter the ISF. While its morphological identity remains uncertain, over-whelming experimental evidence accumulated over the past 65 years supports its existence (e.g., Grotte, 1956; Renkin, 1978; Taylor and Granger, 1984; Rippe and Haraldsson, 1994). Not included at this stage of our analysis is an exclusive water (aquaporin) channel.

The traditional model of microvascular permeability assumed that the effluent of the small and large pores mixed freely in the tissues and the oncotic pressure difference determining transcapillary fluid exchange was that between the plasma oncotic pressure and the average oncotic pressure of the interstitial fluid. Simultaneous measurements of plasma oncotic pressure, average interstitial oncotic pressure and venous or venular interstitial hydrostatic pressures in a range of tissues predicted high levels of fluid filtration inconsistent with measurements of lymph flow (Levick, 1991). In nearly all the tissues showing these discrepancies, the endothelia of the microvessels were continuous (like those of skeletal muscle).

To account for these discrepancies, it was suggested that differences in oncotic pressure across the glycocalyx could differ considerably from the difference estimated from the mean oncotic pressure of the interstitial fluid, particularly in those microvessels with continuous endothelia (Michel, 1997; Weinbaum, 1998; Michel and Curry, 1999). The glycocalyx lies on the luminal side of the endothelia, and in those vessels with continuous endothelia, the fluid filtered through the glycocalyx has to traverse the intercellular cleft including the short breaks in the strand forming the tight intercellular junctions before it reaches the ISF. Previously, steady state fluid exchange across the glycocalyx was modeled in three dimensions to include flow through the intercellular clefts (Hu et al., 2000; Adamson et al., 2004).This model demonstrated that large differences of protein concentration can occur between the general ISF and the sub-glycocalyx space in microvessels with continuous endothelia. This prediction was subsequently supported by experiments in rat mesenteric venules (Adamson et al., 2004).

The sub-glycocalyx space may be considered to be a sub-compartment of the ISF. Small compartments of ISF surrounding pulmonary capillaries had previously been suggested to account for rapid transient fluid exchange following small changes in pulmonary capillary pressures (Hughes et al., 1958; Lunde and Waaler, 1969). Step reductions of hydrostatic pressure in mesenteric capillaries are also followed by very rapid transient absorption of fluid from the tissue. Although these transients are short lived, the volume of the sub-glycocalyx space appears too small to account for them. It has been proposed that a volume of the interstitial fluid, beyond and continuous with, the intercellular clefts of mesenteric capillaries and venules lies between the endothelium and the sleeve of pericytes encasing the vessels. Zhang et al. (2006, 2008) used a simplified 1D form of their 3D model based on the ultrastructure of rat mesenteric venules to account for the time course of transients of fluid exchange following a step change in hydrostatic pressure in these vessels.

Here, we extend the 1D model to describe the transient exchange of water and solutes across the glycocalyx in skeletal muscle, where the transients of fluid exchange are much slower, continuing for more than 30–60 min. We use vascular permeability characteristics and anatomical features of the ISF of muscle to guide our model development.

## MATERIALS AND METHODS

### Model Development

Two models are shown in **Figure 1**. The simplest model (**Figure 1A**, the tissue sub-compartment model) assumes the fluid leaving the glycocalyx mixes with a single tissue sub-compartment (volume Vt) formed from a portion of the ISF in close proximity to microvessels. We describe the anatomical equivalent of this tissue sub-compartment for muscle as part of the development of this model. The second model (**Figure 1B**, the series compartment model) extends this approach to include two additional sub-compartments, *Vf* directly under the glycocalyx (the glycocalyx sub-compartment), and Vg created by the arrangement of the junctional strands in the intercellular cleft.

Previously, steady state fluid exchange across the glycocalyx on the luminal surface of the endothelium and the intercellular cleft was modelled using estimates of (i) the average distance between the base of the glycocalyx and the barrier formed by the tight junctions within the cleft *Lf* and (ii) the distance from infrequent breaks in this barrier and the exit from the intercellular cleft to the tissue sub compartment

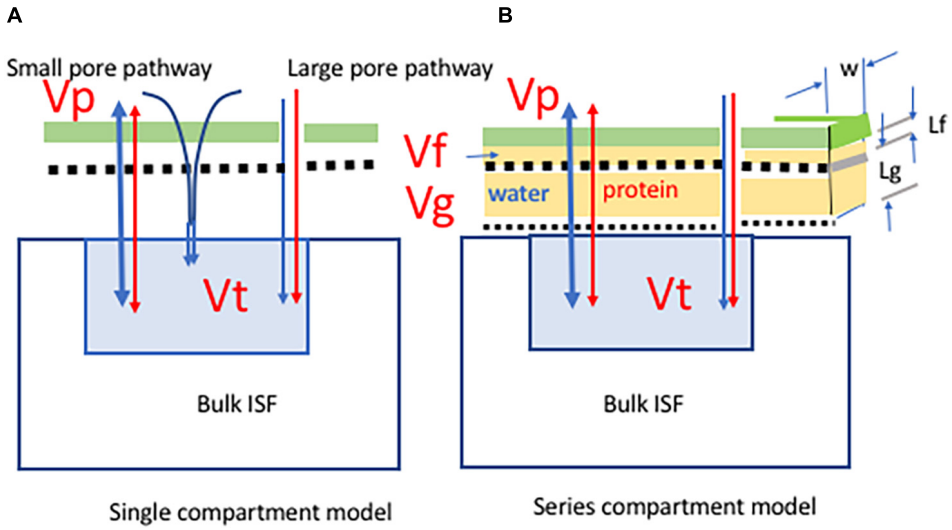


**FIGURE 1 |** Two models of water (blue) and protein (red) exchange from the plasma *Vp* to a sub-compartment of the interstitial fluid space *Vt*. In both models the restriction to movement of plasma proteins is determined by the fiber size and fiber spacing in the glycocalyx (green) and the glycocalyx is the primary barrier to the movement of protein from circulating plasma to the interstitial fluid. The fluid leaving the glycocalyx is funneled through breaks in the junction strands in the inter-endothelial cell junctions. A small number of large pores are in parallel with the glycocalyx-junction pathway. The colloid osmotic pressure difference determining water exchange is between the plasma and the fluid under the glycocalyx. The model on the panel **(A)** (single tissue compartment model) assumes the fluid leaving the glycocalyx mixes with a single tissue sub-compartment (volume *Vt*) formed from a portion of the ISF that is in close proximity to microvessels. The model on the panel **(B)** (series compartment model) has two additional sub-compartments. *Vf* is within the inter-endothelial cell cleft and directly under the glycocalyx. *Vg* lies within the inter-endothelial junction and between the breaks in the junctional strands and the tissue sub-compartment. The volumes of these sub-compartments are determined from published details of the ultrastructure of the intercellular junctions and the position of the junction strand as indicated in panel **(B)**. In both models the PS product of the glycocalyx barrier is PdS1 and of the large pore pathway is PdS4. In the series compartment model PdS2 accounts for the barrier between *Vf* and *Vg* and PdS3 accounts for the barrier between *Vg* and *Vt*. **Tables 1**, **2** describe the model parameters in detail.

*Lg* (Hu et al., 2000; Adamson et al., 2004). Here, we estimate the volumes of sub-compartment that lie directly beneath the glycocalyx and proximal to the array of junctional strands within the intercellular cleft as $Lf.W \times Lj/2$ and the volume of the second sub-compartment between breaks in the junction stand and the cleft exit as $Lg.W.Lj/2$ where $W$ is the mean width of the intercellular cleft taking into account that the cleft tends to be wider at the cleft entrance and exit and $Lj$ is the endothelial cleft length per unit area taking into account that on average two endothelial cells share a common line of contact (**Figure 1B**).

**Table 1** lists the parameters in the models and **Table 2** their assigned values. Because we describe transvascular exchange representative of skeletal muscle, we have scaled all parameters to a mass of 40 kg of muscle in a lean 70 kg human subject.

## The Volume of Tissue Sub-Compartment

Clues to interstitial fluid distribution in skeletal muscle are provided by the arrangement of three layers of its connective tissue. The muscle cells (or fibers) are long thin cylinders and each is surrounded by a thin layer of connective tissue called the endomysium. The cells are collected into bundles, the number of cells per bundle varying with the function of the muscle: small number of fibers – for fine movements as in external eye muscles; large numbers of fibers per bundle in muscles contributing to strength. The bundles are surrounded by a layer of connective tissue called the perimysium. Bundles making up the entire muscle are surrounded by an outer layer of connective tissue called the epimysium (Csapo et al., 2020; Wang et al., 2020).

The endomysium surrounding each multi-nuclear muscle cell carries three or more capillaries supplying the adjacent muscle cells. Arterioles and venules are found in the perimysium with occasional branches running perpendicular and usually together to supply and drain the capillaries of the endomysium. If we assume the large pores responsible for macromolecular exchange between blood and interstitial fluid are located in the venules, the ISF in the endomysium would form a sub-compartment adjacent to the capillaries. To estimate the volume of this sub-compartment, we assume it surrounds each muscle cell with a thickness of 0.5 μm. If the average diameter of the muscle cell is 80 μm, the endomysial fluid would represent just less than 2.5% of the cross-section area of cell plus ISF sub-compartment. If the total volume of ISF is 15% of the muscle mass, the endomysial fluid is one sixth of the total ISF. In a lean 70 kg man, 40 kg of which is skeletal muscle, this would represent one liter of fluid. It is possible that this volume is split into short stretches of 100–300 μm along the length of the muscle cells by the transverse branches of arterioles and venules as they run to and from the capillaries. But the endomysial fluid surrounding one cell is continuous with fluid surrounding adjacent cells increasing the volume of the compartment as a whole. In all the calculations below, we used 1,000 ml for the tissue sub-compartment. **Figure 2** shows a model for muscle.

**TABLE 1 |** Symbols, abbreviations, and subscripts.

| |
|---|
| *C*, concentration mg/ml |
| COP, colloid osmotic pressure mmHg millimeters of mercury |
| ISF, interstitial fluid mls |
| *Js*, solute flux in mg/min |
| *Jv*, water flux in ml/min |
| *L*, distances within the intercellular cleft |
| LpS, capillary filtration coefficient ml/min/mmHg |
| *P*, pressure in mmHg |
| *Pd*, is solute permeability coefficient cm/s |
| *PS*, is permeability surface area product ml/min |
| Pe, Peclet number dimensionless |
| *S*, surface in $cm^2$ |
| *T*, time in seconds or minutes |
| *V*, is volume mls |
| *w*, width of inter cellular cleft |
| *Z*, dimensionless term = Pe/(exp(Pe) − 1) |
| Π, colloid osmotic pressure (COP) mmHg |
| σ, osmotic reflection coefficient |
| Subscripts |
| *p*, *f*, *g*, *t* in plasma, subglycocalyx, cleft, and tissue |
| 1, 2, 3, 4 permeability coefficients in the barriers across glycocalyx, glycocalyx to cleft, cleft to tissue, and large pore, respectively |

**TABLE 2 |** Model parameters.

| |
|---|
| $C_p$, plasma protein concentration 69 mg/ml, COP = 25 mmHg |
| $L_f$, 100 nm (Hu et al., 2000; Adamson et al., 2004) |
| $L_g$, 600 nm (Hu et al., 2000; Adamson et al., 2004) |
| $L_j$, 1,000 cm/$cm^2$ (Adamson, 1993) |
| $LpS_1$, 2 ml/(min mmHg) from Michel and Moyses (1985) |
| $LpS_4$, 0.02 ml/(min mmHg) calculated using Taylor and Granger (1984)* |
| $P_dS_1$, 0.4 ml/min (Renkin and Tucker, 1998) |
| $P_dS_2$, is 5.6 ml/min Estimated from Zhang et al. (2006)* |
| $P_dS_3$, 50 ml/min Estimated for albumin diffusion in ISF* |
| *S*, surface 7,000 $cm^2$/100 g (Pappenheimer et al., 1951) |
| $V_f$, 0.05 ml Calculated as *Lf.w.Lj*/2 |
| $V_g$, 0.3 ml Calculated as *Lg.w.Lj*/2 |
| $V_t$, 1,000 ml Estimated as 1/6 of ISF volume* |
| *w*, 20 nm (Adamson and Michel, 1993; Adamson et al., 2004) |
| $\sigma_1$, 0.95 (Michel, 1984) |
| $\sigma_2$, $\sigma_4$, 0.2 estimated for albumin in slit, width 20 nm (Curry, 1984) |
| $\sigma_3$, 0 estimated for albumin in ISF |

**See text for further details.*

One form of the model assumes the large pores mix with the smaller endomysium compartment, the other assumes large pores mix only with the large perimysium compartment. The steady state relations do not require a distinction between exchange into the tissue sub-compartments. However, for modeling of transient exchange we examined only the limiting case where all large pore exchange occurs into the endomysial sub-compartment.

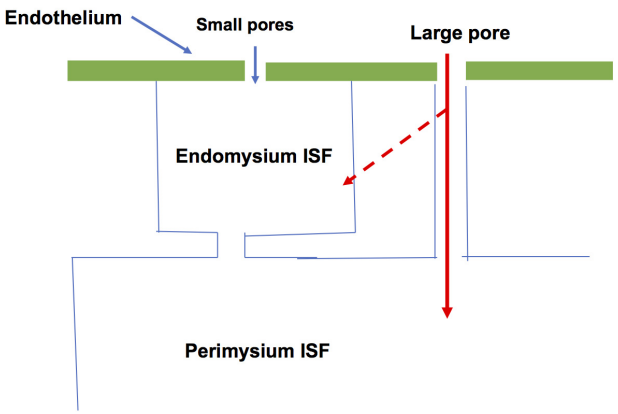


**FIGURE 2 |** A specific form of Model in **Figure 1A** used to describe water and solute exchange in skeletal muscle is shown. The endomysium is adjacent to the capillaries and is estimated to occupy one sixth of the interstitial fluid space. The bulk of the ISF is in the perimysium. During the transient exchanges investigated in this paper it is assumed that exchange across both the glycocalyx and large pore pathways mixes into the endomysium ISF (broken arrow).

## Volume of the Sub-Compartment Under the Glycocalyx and in the Endothelial Cleft Between the Glycocalyx and the Tissue Compartment

To scale the length of the line of junction (*Lj*) 1,000 cm/$cm^2$ for a 40 kg muscle mass we used 7,000 $cm^2$/100 gm as an estimate of surface area (Pappenheimer et al., 1951). This value is for fully dilated cat and dog hindlimb. The corresponding volume for a region within the intercellular cleft 100 nm deep, 20 nm wide under the glycocalyx is 0.056 mls. On one hand this estimate would be lower when the microvasculature was not fully dilated. On the other hand, the cleft is often seen to be wider than 20 nm directly under the glycocalyx at the cleft entrance. We used 0.05 mls for *Vf*. The cleft volume was set at 0.3 mls based on a ratio of *Lg*/*Lf* of close to 6 (**Figure 1B**; Adamson et al., 2004).

## Permeability Parameters

The published clearances of albumin in rodent skeletal muscle, 0.1–0.12 μL/min per gram of dry tissue weight, scale to 0.48–0.72 ml/min for the 40 kg muscle mass assuming a wet to dry weight ratio of 5 (Renkin and Tucker, 1998). We used the value of 0.5 ml/min corresponding to an albumin permeability coefficient of $1 \times 10^{-8}$ cm/s. A PS product of 0.5 ml/min accounts for both large pore and small pore diffusive pathways. We partitioned the PS product as 0.4 ml/min for the small pore pathway glycocalyx and 0.1 ml/min for large pores based on estimates of their size and frequency in skeletal muscle (Taylor and Granger, 1984).

We used the results from the 1D model of Zhang et al. (2006) to assign a preliminary PS product to the barrier beneath the glycocalyx sub-compartment. Under conditions where there was no net flow across the glycocalyx in the 1D model, the glycocalyx

accounted for 93% of the concentration difference between plasma and tissue. This corresponded to a ratio of diffusion resistance in the glycocalyx to the diffusion resistance beneath the glycocalyx of 14:1. With a glycocalyx PS of 0.4 ml/min, a similar distribution of diffusion resistances for muscle gives a PS product of 14 × 0.4 ml/min or 5.6 ml/min for the barrier between the glycocalyx and the cleft. This estimate takes into account the extra resistance as solute flows are funneled into infrequent breaks in the junction strand. It is also assumes that the PS product for albumin in muscle is fivefold to 10 fold less than values in mesentery because the more complex arrangement of the junction strand in the endothelial barrier muscle reduces the effective size and frequency of breaks (Wissig and Williams, 1978; Bundgaard, 1984). We also tested other values of PS that accounted for more resistance in the junction strands (PS = 3 ml/min where the strands accounted for 10% of the resistance as well as PS = 12 and 24 ml/min where the strands accounted for resistances of 4 and 1% the resistance to solute diffusion, respectively.

We set the PS product for diffusion from the cleft into the issue compartment as 50 ml/min corresponding to a mean diffusion distance as high as 150 μm based on diffusion distances that could range from a minimum of 12 μm for direct mixing with a 1,000 ml volume, to mixing with isolated segments 300 μm apart. All model results were relatively insensitive to the value of this parameter.

## Capillary Filtration Coefficient LpS

Michel and Moyses (1985) measured the swelling of human forearm with increments of venous pressure in healthy human subjects as 3.2–4 × $10^{-3}$ ml/(min mmHg 100 g) after allowances had been made for bone content of the forearm. This value was close to earlier estimates by Landis and Gibbon (1933). The value increased to the order of 5 × $10^{-3}$ ml/(min mmHg 100 g) as a reasonable approximation to the swelling due to changes in capillary pressure (rather than venous pressure) based on values of the ratio of arteriolar to venular resistance to blood flow in animal and human experiments (Pappenheimer and Soto-Rivera, 1948; Levick and Michel, 1978). The value 5 × $10^{-3}$ ml/(min mmHg 100 g) leads to a figure of 2 ml/(min mmHg) for 40 kg muscle.

The reflection coefficient of the glycocalyx was set at 0.95 (Michel, 1984). The solvent drag reflection coefficient in the large pore and lateral cleft was 0.2 based on a cleft width of 20 nm (Curry, 1984). Hydrostatic pressures below the glycocalyx, in the intercellular cleft and tissue are assumed close to zero but a finite pressure gradient is required to drive flow from the tissue toward the glycocalyx sub-compartment.

## Steady State Relations for the Single Tissue Compartment Model

The relations for the single tissue model are given below, followed by relations for the series-compartment model. To calculate the concentration difference of protein across the glycocalyx, the small pore pathway is treated as membranes in series. For each membrane, the diffusive permeability-surface area product is PS and the solvent drag reflection coefficient is σ. For the protein flux from plasma to a tissue sub-compartment, the solvent drag component of the protein flux is $Jv\ (1-\sigma)\ Cp$ where $Jv$ is the water flux and $Cp$ is the plasma protein concentration. The diffusive component of the protein flux between the plasma and a tissue sub-compartment (protein concentration $Ct$) is PS $(Cp-Ct).z$ where $z$ is Pe/(exp(Pe) − 1) with Pe, the Peclet number, given by $(Jv(1-\sigma)/PS)$ (Curry, 1984). In the following, subscripts 1 and 4 refer to the membrane barriers in the glycocalyx and the large pores, respectively. Subscripts2 and 3 are used in the series model to refer to the additional membrane barriers in the intercellular cleft.

For Steady state exchange across the glycocalyx and large pores in the single tissue compartment,

$$Jv\text{Total}\ Ct\ =\ Js1 + Jv4 \tag{1}$$

$Jv_{total}$ is the water flow across both pathways in ml/min, $Jv_{total} = Jv1 + Jv4$. $Ct$ is the concentration in the tissue sub-compartment $Js1$ is small pore flux and $Jv4$ is large pore flux.

$$Js1\ =\ Jv1 \cdot (1-\sigma 1) \cdot Cp + PdS1 \cdot \left(Cp - Ct\right) z1 \tag{2}$$

and

$$Js4\ =\ Jv4 \cdot (1-\sigma 2) \cdot Cp + PdS4 \cdot \left(Cp - Ct\right) z4 \tag{3}$$

Substituting in Eq. 1:

$$Ct\ =\ Cp \cdot \frac{\left\{Jv1\,(1-\sigma 1) + PdS1z1 + Jv4\,(1-\sigma 4) + PdS4z4\right\}}{\left\{(Jv1 + Jv4) + PdS4z4 + Pds1z1\right\}} \tag{4}$$

The fluid exchange across the glycocalyx is described by the Starling principle,

$$Jv1\ =\ LpS1 \cdot \left\{\left(Pp - Pt\right) - \sigma 1\left(\pi p - \pi t\right)\right\} \tag{5}$$

where $Pp$ and $Pt$ are the pressures in the capillary and the tissue sub-compartment and $\pi p$ and $\pi t$ are the corresponding COPs calculated from the plasma protein concentrations at 37°C by the relation,

$$\pi\ =\ 2.1C\ +\ 0.16C^2\ +\ 0.009C^3 \ldots . \tag{6}$$

(Landis and Pappenheimer, 1963)

$C$ is mg/ml. The relation is used to calculate COP in all compartments. The relation is strictly valid only for fluid with the protein concentrations of circulating plasma. In this paper the same relation is used to convert tissue protein concentrations to COPs. This ignores the fact that COP for ISF fluid should be calculated from a relation closer to that expected for albumin. The composition of the fluid under the glycocalyx and tissue differs from the plasma because larger plasma proteins such as IgG are retained in the plasma and the unit mass of tissue protein contains more albumin than a corresponding mass of plasma protein. This difference is ignored in the present calculations because the relation corresponding to Eq. 6 for ISF fluid has not been reported.

The fluid exchange across the large pores is:

$$Jv4 \;=\; LpS4 \cdot \{(Pp - Pt) - \sigma 4\,(\pi p - \pi t)\} \tag{7}$$

It is assumed that tissue pressure is zero.

The key assumption in the single tissue model is that the effluent leaving the base of the glycocalyx mixes instantly with the tissue compartment contents. To enable comparison of this model with the series compartment model where there are barriers to the exchanges between the effluent behind the glycocalyx and the tissue sub-compartment, it is useful to note that a well-mixed volume is one where diffusion gradients do not exist. With this assumption for the single compartment model, the flux of protein carried away from the base of the glycocalyx and equal to the flux across the glycocalyx is written as,

$$Js1 \;=\; Jv1 \cdot Cf \tag{8}$$

where $Cf$ is equal to $Js1/Jv1$ in Eq. 2.

$$Cf \;=\; Cp \cdot (1 - \sigma 1)/\{1 - \sigma \cdot exp\,(-Pe)\} \tag{9}$$

$Cf$ can be understood as the concentration of effluent from beneath the glycocalyx fluid that would be measured if this effluent did not mix directly and immediately with the contents of the ISF. Furthermore, it is noted that Eq. 8 has the form of a convection dominated equation, not because $Jv1$ is high but because the well mixed assumption is equivalent to the assumption that convection dominates at all values of $Jv$.

The steady state relation between $Jv_{total}$ and pressure was constructed by substituting $Jv.Cf$ for $Js1$ in Eq. 2, so that,

$$Ct \;=\; Cf \cdot \left(\frac{Jv1}{\{Jv1 + (Jv4)\}}\right) + \{Jv4\,(1 - \sigma 2) \cdot Cp$$

$$+ PdS4z4(Cp - Ct)\}/(Jv1 + Jv4) \tag{10}$$

The following iterative steps were used to construct the steady state relation between $Jv$ and pressure. We note that for a given value of $Jv1$, the values of $Pe1$ and $z1$ in Eqs. 2 and 3 are known for assigned values of PS and σ .

Step 1: For a given $Jv1$, a first approximation for tissue concentration is calculated from Eq. 10 neglecting the large pore contribution.

Step 2: A capillary pressure is then calculated from Eq. 5. This capillary pressure acts across both small pores and large pores.

Step 3: $Jv4$ was calculated from Eq. 7 using the estimated Pc in step 2 and the COP for the initial estimate of $Ct$.

Step 4: The new $Jv4$ and $Pc$ are used to calculate a new $Ct$ from Eq. 10. Successive iterations quickly converged to consistent estimates of $Ct$, and $Jv1$, and $Jv4$ at each capillary pressure. All calculations are carried out in Excel worksheets.

## Transient Changes in Fluid Exchange

The time course of changes in protein concentration in the tissue sub-compartment is calculated by numerical solution of the differential equation describing the mass balance relation:

$Vt(T)\mathrm{d}Ct/\mathrm{d}T = Js1(T) + Js4(T)$

The calculation of the concentration $Ct$ as a function of time $T$ was carried out with time steps ($\Delta T$) of 1 min in an Excel worksheet: $Ct$ at time $T + 1$ relative to $Ct$ at time $T$:

$$Ct\,(T{+}1) \;=\; \{Vt\,(T) \cdot Ct\,(T) + Js1\,(T) + Js4\,(T)\}/Vt(T) \tag{11}$$

Here, $Js1$ and $Js4$ are calculated from Eqs. 3 and 8 with the values of $Cp$ and $Ct$ at time $T$.

## Series Compartment Model

The same approach as for the single compartment is used. The overall steady state relation is the same as text Eq. 1 but $Js1$ is the flux from the sub-compartment in the cleft ($Cg$) into the tissue compartment.

$$Jv1Cg\,(1 - \sigma 3)\,Cg + PdS3z3\,(Cg - Ct)$$
$$+ Jv4\,(1 - \sigma 4)\,Cp + PdS4z4\,(Cp - Ct) \;=\; Ct\,(Jv1 + Jv4) \tag{12}$$

Equation 12 can be written as

$$Ct \;=\; A.Cg + B \tag{13}$$

Where

$$A \;=\; Cp\left[Jv1\,(1 - \sigma 1) + PdS3z3\right]/\{(Jv1 + Jv4) + PdS3z3 + PdS4z4\} \tag{14}$$

and

$$B \;=\; Cp\left[Jv4\,(1 - \sigma 4) + PdS4z4\right]/\{(Jv1 + Jv4) + Pds3z3 + Pds4z4\} \tag{15}$$

Continuity requires the flux into the cleft compartment from the sub-compartment under the glycocalyx to equal the flux out of the cleft compartment into the tissue,

$$Jv1\,(1 - \sigma 2)\,Cf + PdS2z2\,(Cf - Cg) \;=\; Jv1 \cdot Cg\,(1 - \sigma 3) + PdS3z3\,(Cg - Ct) \tag{16}$$

Substitute for $Ct$ from equation,

$$Cg \;=\; C.Cf + D \tag{17}$$

Where

$$C \;=\; \left[Jv1\,(1 - \sigma 2) + PdS2z2\right]/\{Jv1 + PdS2z2 + PdS3\,(1 - A)\} \tag{18}$$

And

$$D \;=\; PdS3z3B/\{Jv1 + Pds2z2 + Pds3z3\,(1 - A)\} \tag{19}$$

Similarly, the flux from plasma compartment across the glycocalyx equals flux out of the sub-compartment under the glycocalyx.

$$Jv1\,(1 - \sigma 1)\,Cp + PdS1z1\,(Cp - Cf) \;=\; Jv1Cg\,(1 - \sigma 2) + PdS3z3\,(Cg - Ct) \tag{20}$$

Substitution for *Cg* gives *Cf* as a function of *Cp*.

The steady state relation between $Jv_{total}$ and capillary pressure is calculated from an iterative process as described for the single compartment model. The transient equations are calculated from mass balances over each compartment as in Eq. 11. Values of *Cf*, *Cg*, and *Ct* were calculated using the same numerical method as used for the single tissue compartment model. As explained in the section "Discussion," time steps were reduced to 0.1 s to account for rapid changes in concentration in the very small volumes of the glycocalyx and cleft sub-compartments.

# RESULTS

## Steady State Relation Between $Jv_{total}$ and Pressure With and Without Large Pore

**Figure 3** shows steady state relations for $Jv_{total}$ ($Jv1$ + $Jv4$) versus Pressure (Top Panels) with and without large pores as a function of presssure. The hockey stick shaped relation between total water flux and capillary pressure is raised up and moved slightly to the left by the presence of the large pores. The LpS of the large pore is 1% of the small pore, glycocalyx pathway, but at a pressure of 13 mmHg large pores carry 40% of the protein flux as solvent drag. As pressure increases the fraction of total flow through the large pores reduces to 10% or less above $P = 25$ mmHg.

The lower panel of **Figure 3** shows the concentration of plasma protein below the glycocalyx (*Cf*) and in the tissue (*Ct*) as a function of pressure. When there are no large pores, the steady state tissue concentration is determined solely by the transport across the glycocalyx. In the presence of large pores, **Figure 3D** shows the difference between the concentration in the tissue and that leaving the glycocalyx before mixing with the tissue. At 20 mmHg capillary pressure, the concentration of plasma protein in the tissue is 27 mg/ml (COP = 7.3 mmHg when Eq. 6 is used). This concentration is 7 mg/ml greater than that fluid leaving the glycocalyx 20 mg/mg (COP 4.9 mmHg), which in this model mixes instantly with the tissue. A key part of the Revised Starling principle is demonstrated by these observations. The effective osmotic pressure difference that opposes filtration across the glycocalyx is larger than that predicted from the difference between plasma and the average interstitial plasma protein concentration. Specifically, with a glycocalyx reflection coefficient of 0.95 and plasma COPs of the effective COP opposing filtration across the glycocalyx (19 mm Hg) is 2.1 mmHg larger than would be calculated from the plasma to average interstitial protein concentration difference. This difference is small but an important general observation is that for capillary pressures in the range 13–25 mmHg, steady state fluid exchange between plasma and tissue is determined by small differences in hydrostatic pressure and osmotic pressures, because COP and capillary pressure are closely balanced. The following examples demonstrate the importance of understanding this balance across the glycocalyx after a change in pressure from a well-established steady state.

## Transient Filtration and Reabsorption for the Single Tissue Compartment Model With Large Pore and Endomysial Compartment

Because the model with mixing of the effluent below the glycocalyx directly into a tissue compartment describes the limiting case where there are no additional diffusion barriers between the glycocalyx and the tissue sub-compartment, the results are presented first. To enable comparison with the series compartment model where diffusion barriers are present, the single tissue compartment model is used to evaluate the filtration transient when pressure is reduced from 20 to 17 mmHg and the reabsorption transient when pressure is reduced from 20 to 13 mmHg. These two examples cover the same range of pressure examined in the series-compartment model ($P$ = 20–13 mmHg).

### Transient Filtration

The concentration of plasma protein in the tissue during steady state filtration at $P = 20$ is 27 mg/ml; COP = 7.3 mmHg) as in **Figure 3D**. When the pressure is suddenly reduced to 17 mmHg and this tissue protein concentration is used as a measure of the protein concentration under the glycocalyx, the effective COP opposing filtration is 16.8 mmHg, calculated as 0.95(25–7.3) mmHg. The corresponding initial filtration rate across the glycocalyx is 0.4 ml/min (Eq. 5). This value is much lower than the filtration rate at a steady state with pressure of 17 mmHg. At steady state the tissue concentration is 37 mg/ml and the colloid pressure opposing filtration is reduced to 12.8 mm Hg, however, this low filtration rate right after pressure is reduced to 17 mmHg would continue for some time because tissue concentration will increase slowly toward the steady state because protein is added to the tissue volume only by exchange through large pores.

One estimate of the half time for fluid filtered through both the large pore and the glycocalyx is the ratio of the large pore filtration rate to tissue volume. The initial large pore filtration rate is 0.38 ml/min (Eq. 7 with reflection coefficient as 0.2). For a tissue volume of 1,000 ml, the corresponding time constant is $0.78 \times 10^{-3}$ $min^{-1}$ and the half time for exchange exceeds 1,000 min. It follows that over a 30-min period early in the transient, the model predicts a loss of less than 25 mls from the plasma volume.

### Reabsorption With Single Tissue Compartment

During reabsorption tissue fluid enters the junction clefts behind the glycocalyx when reabsorption begins across the glycocalyx. The rate plasma protein accumulates in the intercellular cleft beneath the glycocalyx is a race between convective transport carrying solute into the cleft and diffusion of the accumulated solute back toward the tissue. The assumption that the fluid under the glycocalyx mixes with the tissue fluid means that the concentration under the glycocalyx cannot exceed the

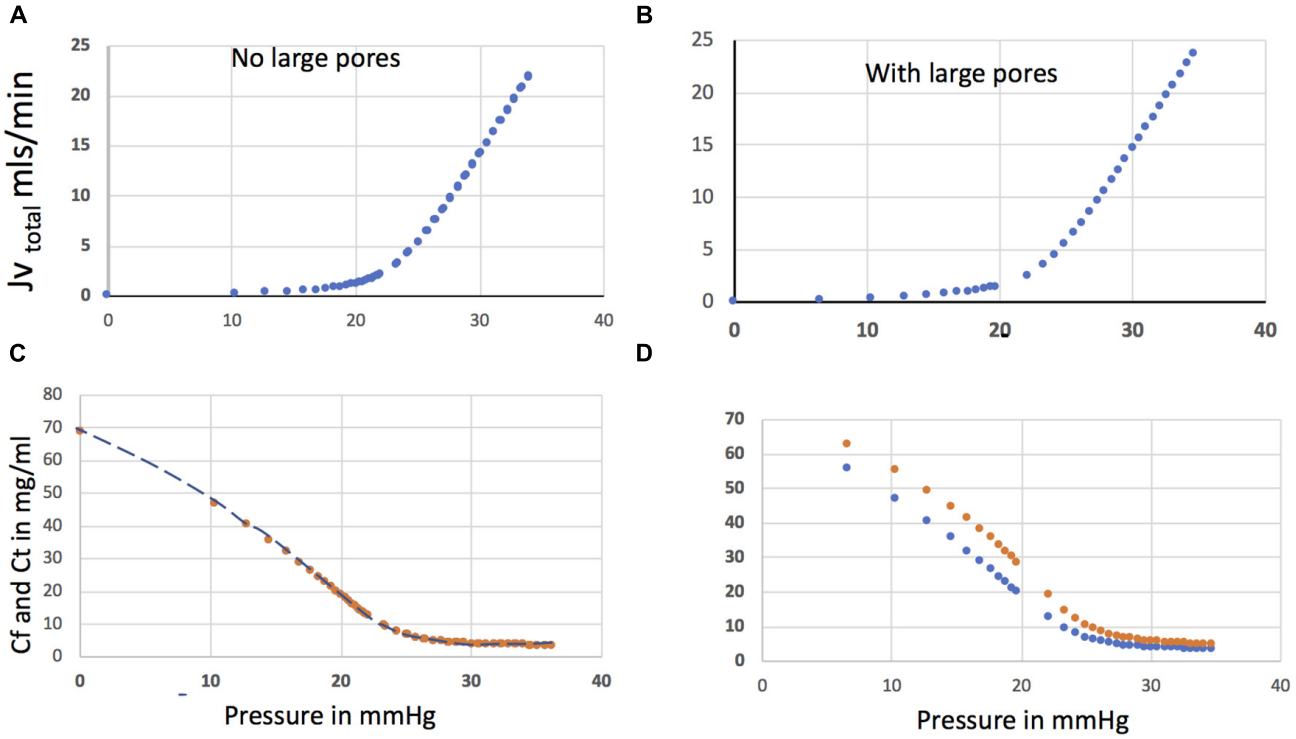


**FIGURE 3 |** Steady state relations between *Jv*Total (*Jv*1 + *Jv*4) and Pressure [top panels **(A)** and **(B)**] with and without large pores. The lower panels of **Figure 3** show the concentration of plasma protein below the glycocalyx (*Cf*) (blue) and in the interstitial fluid (*Ct*) (red) as a function of capillary pressure with and without the presence of large pores. These relations are independent of the size of the ISF as the steady state ISF concentration is determined only by the relation *Ct* = *Js Total*/*Jv Total*. Many hours are required to establish steady state. Panel **(C)** shows that in the absence of large pores the ISF fluid has the composition of the fluid leaving the base of the glycocalyx. When the flux through large pores also mixes with the ISF (**D**) there is a difference in concentration between the fluid leaving the base of the glycocalyx and the tissue fluid.

tissue concentration. This is equivalent to assuming that back diffusion from the base of the glycocalyx to the tissue sub-compartment ensures that the solute concentration at the back of the glycocalyx has a value equal to the tissue concentration. The model therefore describes the maximum COP difference between plasma and the tissue under the glycocalyx and the corresponding maximum rate of reabsorption after pressure is reduced from a steady state.

The initial effective COP across the glycocalyx at a pressure of 20 mmHg, determined by steady state filtration into the tissue sub-compartment, is the same as at the beginning of the filtration transient described above. But when pressure is reduced to 13 mmHg, the balance of hydrostatic and COP is −3.8 mmHg and favors reabsorption. The reabsorption rate across the glycocalyx is −7.5 ml/min. This rate slows as plasma proteins are diluted and solute accumulates in the tissue by exchange through large pores. These reabsorption rates differ significantly from the steady states at $P = 13$ mmHg which is slow filtration at a rate of less than 0.5 ml/min (**Figure 3B**).

**Figure 4A** shows the reabsorption transient using the single tissue compartment model of **Figure 2**. Tissue concentrations calculated from a mass balance over the tissue compartment (Eq. 11) are in **Figure 4B**. Protein concentration in the tissue sub-compartment slowly approaches the steady state value of 47 mg/ml (Broken line) corresponding to a condition of steady state filtration at a pressure of 13 in **Figure 3D**. Plasma protein concentration falls with dilution by reabsorbed fluid.

From **Figure 4A**, 180 ml are reabsorbed after 30 min and a maximum of 270 ml reabsorbed after 60 min. For the assigned model parameters, this rate of reabsorption is the largest expected for a tissue mass of 40 kg of muscle in a human subject.

Two conclusions follow from investigations using the single tissue compartment. First, a more precise quantification of the convective and diffusive components of the solute flux leaving the base of the glycocalyx is required. During filtration and reabsorption transients, protein accumulation below the glycocalyx is determined by both convection and diffusion between the base of the glycocalyx and the tissue compartment. Second, the volume of 180 ml predicted to be reabsorbed after 30 min of reabsorption in **Figure 4** is much lower than the commonly quoted figure of close to 500 ml in 60 min after a reduction in microvessel pressure (Lanne and Lundvall, 1992). This preliminary result suggests that reabsorption rates greater than 180 ml over 30 min would be difficult to account for if muscle tissue was the primary source of reabsorbed fluid. The series compartment model enables further evaluation of all three observations.

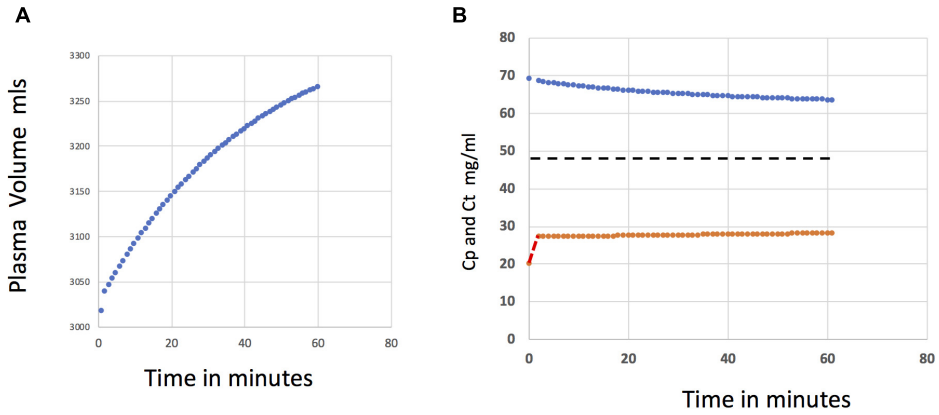


**FIGURE 4 | (A)** Plasma volume is shown as a function of time during reabsorption after capillary pressure reduced from 20 to 13 mmHg. The rate of reabsorption predicted using models Model 1a scaled for skeletal muscle (**Figure 2**) is a maximum because protein accumulation in the fluid behind the glycocalyx cannot exceed with concentration of the ISF in the tissue sub-compartment (volume 1,000 ml). **(B)** The protein concentrations in in vascular space (*Cp*) (blue) is reduced as reabsorbed fluid is added to the vascular volume. The tissue protein concentration *Ct* increases slowly as protein flux through large pores accumulates in the tissue sub-compartment. It takes many hours for the protein concentration in the tissue compartment to reach the steady state concentration for pressure of 13 mmHg (broken black line).

## The Series Compartment Model. Fluid Exchange During a Change in Pressure Over the Same Range (*P* = 20–13) as in the Single Compartment Model

**Figure 5A** show the steady state plasma protein concentrations in the sub-compartments under the glycocalyx, in the cleft, and in the tissue compartment from the series compartment model when the PS product for diffusion between the sub-glycocalyx and the cleft is 5.6 ml/min. **Figure 5B** shows the transient changes in the concentrations in the sub-glycocalyx compartment, cleft, and tissue compartments as pressure is reduced in steps of 0.1 mmHg each 0.1 s from steady *P* = 20–13. The initial concentration of plasma proteins in each sub-compartment is the steady state at *P* = 20 mmHg (**Figure 5A**). The concentration under the glycocalyx *Cf* is 21.56 mg/ml (COP 5.4 mmHg); in the cleft (*Cg*), 26 mg/ml, COP 6.7 mmHg) and in the tissue (*Ct*) 28 mg/ml (COP 7.3 mmHg). The tissue steady state concentrations are, as expected, close to those in the single compartment model. However, in contrast to conditions in the single compartment model where gradients between the base of the glycocalyx and the tissue were neglected and the kinetics of fluid exchange is determined only by slowly changing tissue sub-compartment concentrations, the series compartment model demonstrates the significant changes in the concentration in the compartment under the glycocalyx as pressure changes. The example in **Figure 5B** enables a direct comparison of the osmotic pressure determining the magnitude and direction of water and solute flux in each compartment model with the single tissue compartment model as described below.

### Filtration *P* = 20–17 mmHg

The key observation is that the protein concentration under the glycocalyx from the moment pressure is first reduced tracks directly with pressure. If pressure had been changed more rapidly, the concentration under the glycocalyx would also have changed more rapidly. *Cf* increases with each 0.1 mmHg pressure reduction because the filtration rate falls below that sufficient to offset back diffusion from cleft compartment (26 mg/ml) versus the glycocalyx sub-compartment (21.6 mg/ml). Solute continues to accumulate by this mechanism as pressure falls. Each step reduction in pressure causes solute to accumulate by reducing the water velocity opposing diffusion toward the glycocalyx.

**Figure 5B** shows that when pressure reaches 17 mmHg after 3 s, protein concentration in the glycocalyx compartment is very close to that in the cleft compartment and both are very close to the mean ISF concentration, all 28 mg/ml (COP = 7.3). The filtration rate is the same as predicted from the single compartment model. This demonstrates that the assumption in the single tissue model that *Cf* can be set equal to the tissue immediately after a step reduction in pressure is a very reasonable approximation.

### Reabsorption in the Series Compartment Model: Pressure Reduced From 17 to 13 mmHg

At a pressure of 16.4 mmHg filtration ceases when the net filtration pressure is zero. Reabsorption begins as pressure is reduced further and protein, carried into the cleft from the tissue sub-compartment by solvent drag, accumulates there. The direction of the diffusion gradient (glycocalyx to cleft) reverses (red line crosses the gray line in **Figure 5B**).When pressure stabilizes at *P* = 13 mmHg, the solute concentration beneath the glycocalyx is 36.8 mg/ml (COP of 10.4 mmHg). This concentration determines the net driving force for reabsorption the moment *P* is 13 mmHg. In contrast to the case during filtration, accumulation causes the concentration of protein under the glycocalyx to be significantly higher than the tissue concentration (36.8 mg/ml vs. 28 mg/ml; COPs 10.4 vs. 7.33 mmHg, respectively). The tissue concentration is not a useful substitute for the protein concentration under the glycocalyx.

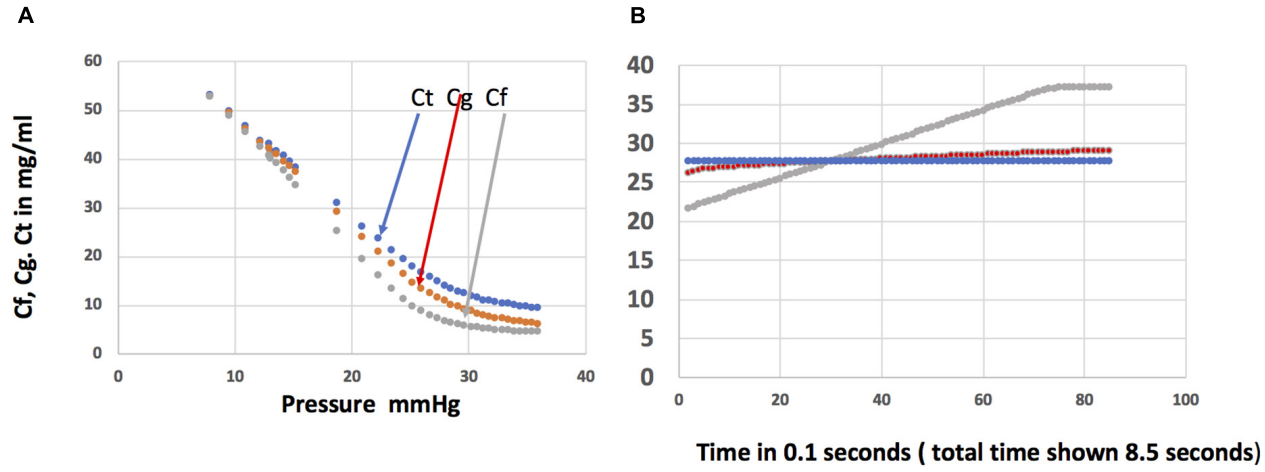


**FIGURE 5 |** Panel **(A)** shows the steady state concentrations in the fluid in the sub-compartment *Cf* (gray), the sub-compartment between the base of the glycocalyx and the tissue sub-compartment *Cg* (red), and in the tissue sub-compartment *Ct* (blue) as a function of pressure when the barriers behind the glycocalyx account for 7% of the total resistance to exchange across the glycocalyx-endothelial cleft pathway (PdS2 = 5.6 ml/min; PdS1 = 0.4 ml/min). Panel **(B)** shows the time course of changes in the concentrations in each of the three sub-compartments as pressure is reduced in steps of 0.1 mmHg each 0.1 s from a steady state at *P* = 20 mmHg to a pressure of 13 mmHg after 7 seconds. A detailed analysis of the magnitude and direction of diffusion and convective transport of protein fluxes as pressure is reduced is in the text.

This is why the single tissue model overestimates the rate of reabsorption.

Our model demonstrates that convective transport of protein into the cleft dominates over back diffusion until the sub-glycocalyx reaches 37.1 mg/ml. At this point back diffusion limits further build-up of protein under the glycocalyx. Thereafter a slow readjustment of the rate of back diffusion determines the time course of reabsorption along with changes in plasma protein concentration. We analyse this example further in the section "Discussion."

The conclusion from the reabsorption case is that the average ISF concentration can significantly underestimate the concentration under the glycocalyx in the presence of a diffusion barrier between the glycocalyx compartment and the tissue compartment. The volume reabsorbed for a range of values for the PS product for the barrier between the glycocalyx and cleft compartment is shown in **Figure 6**.

The value of PS of 5.6 ml/min assigned to the barrier between the glycocalyx compartment and the cleft In **Figure 5** corresponds to diffusion barriers that accounted for 7% of the total transvascular resistance. The blue curve in **Figure 6** is the corresponding time course of reabsorption over 60 min. After 30 min, 36 ml are reabsorbed. This is less than 20% of the 180 ml predicted using the single tissue sub-compartment in **Figure 4**.The lowest curve in **Figure 6** shows that the volume is further reduced when these diffusion barriers account for 10% of the resistance (PS = 3 ml/min). On the other hand, decreased resistance increases the volume reabsorbed after 30 min to 117 ml (PS = 12 ml/min, 4% of total resistance). Only a further increase in PS to 24 ml/min (1% of diffusion resistance) predicts a volume reabsorbed of 150 ml in 30 min, approaching that in the single tissue compartment. The increased reabsorption reflects more rapid dissipation of solute accumulation under the glycocalyx. Taken together, **Figures 5, 6** provide the first examination of the range of permeability characteristic for barriers between the glycocalyx and the tissue sub-compartment that would support reabsorption when the glycocalyx is present and both the ultrastructure of the junction in a continuous capillary and the anatomy of muscle tissue are considered. They are consistent with the tentative conclusion from the single compartment model that, for the skeletal muscle parameters selected, reabsorption from muscle is unlikely to account for volume up to 500 ml over 60 min.

# DISCUSSION

## Overview

Our results demonstrate the importance of recognizing the small pore glycocalyx as part of a barrier to fluid exchange between blood and the body tissues that includes additional series and parallel pathways for exchange. Barriers to water and solute exchange within the endothelial cleft in series with the glycocalyx determine the extent to which the plasma protein concentration beneath the glycocalyx differs from the protein concentration in the ISF. Furthermore, both steady state and transient exchange across the glycocalyx is modified by the presence of large pores that carry a large proportion of total transvascular solute flux at low capillary pressures. In their simplest form large pores can be understood as regions when the glycocalyx is degraded in microvessels where the inter-endothelial junctions are less tight (e.g., in venular microvessels). While the functions of this combined barrier during steady state filtration are reasonably well understood (Levick and Michel, 2010; Curry, 2018; Michel et al., 2020), our analysis demonstrates a fundamental difference between filtration and reabsorption across the endothelial barrier

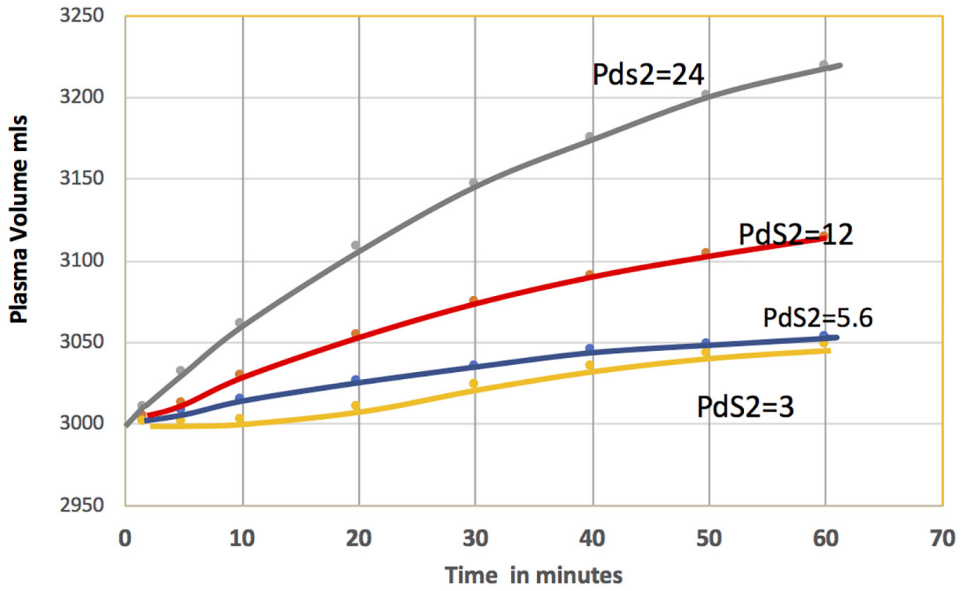


**FIGURE 6 |** The plasma volume as a function of time is shown for a range of values the PS product for the barrier between the glycocalyx sub-compartment and the sub-compartment in the cleft. The highest resistance to diffusion (10% of total corresponds, PdS2 = 3 ml/min) results in the least volume reabsorbed (orange curve). Reduced resistance increases the volume reabsorbed: 7% of resistance, PdS2 = 5.6 ml/min, blue; 4% of resistance, PdS2 = 12 ml/min, red) and 1% of resistance, PdS2 = 24 ml/min, blue).These results can be compared with **Figure 4A** where the resistance in the cleft was effectively zero.

in the presence of the glycocalyx. As illustrated by transient filtration, new filtration rates after a small change in capillary pressure can be predicted quite accurately from the steady state conditions that exist just prior to the change in pressure. However, as illustrated by examples in **Figures 5, 6**, prediction of the magnitude and time course of reabsorption rates requires detailed understanding of diffusive and convective transport in the cleft beneath the glycocalyx. Following a pressure drop that results in a change from filtration to reabsorption, there is rapid accumulation of plasma proteins from the ISF beneath the glycocalyx that reduces the reabsorption rate well below that expected from the initial conditions. There is then a prolonged period of gradually reducing reabsorption rates as plasma protein concentrations below the glycocalyx and in tissue approach to a new steady state.

Our modeling is at best a first step toward a more detailed analysis of such reabsorption transients. This is important because the results showing reabsorption of volumes of the order 50–250 mls of ISF from 40 kg of muscle ISF over a period of 30 min would not account for reports in human subjects that up to one half-liter of interstitial fluid can be returned to the plasma volume after a significant fall in capillary pressure. At this time we do not know whether it is valid to use predictions from the model in their present form to make detailed comparisons with observations in human subjects. However, some clinical investigators are currently using models of transvascular flow that fail to consider any of the mechanisms that our approach describes (Hahn, 2020). Additional studies with the models in this paper can help to bridge this gap between purely empirical data fitting models and more mechanistic analyses. To guide such future investigations the section "Discussion" below provides a detailed analysis of the strengths and weakness of the models to identify areas for further investigation.

## Comparison With Previous Models

Within the endothelial glycocalyx and barriers in the intercellular cleft there are significant differences in the solute concentration over length scales of tens to hundreds of nanometers. On the other hand, the diffusion distances in the ISF beyond the cleft exit are tens to hundreds of microns and the corresponding concentration gradients can be much smaller than that in the cleft. This makes numerical calculations that accurately account for the wide range of length scales difficult to use. Previously the 3D model used a combination of analytical and numerical methods for a detailed hydrodynamic analysis that accounted for convective-diffusion exchange across the glycocalyx and through an idealized arrangement of the junction strands (Hu et al., 2000; Adamson et al., 2004). Despite the success of this model to account for measured transvascular flows in individually perfused microvessels in the mesentery, it was far too complex to be used for further experimental investigation. A 1D equivalent model was developed to describe convection and diffusion through successive layers of glycocalyx and the junction cleft by choosing transport coefficients for barriers in the cleft so that the transvascular fluxes of water and solute in the 1D model were equivalent to those in the 3D model (Zhang et al., 2006). The modified model was extended to account for the observation that reabsorption transients in individually perfused mesenteric microvessels approaches a new steady state after 2 min, instead of an expected time greater than 1 h (Michel and Phillips, 1987; Zhang et al., 2008).

The series compartment model evaluated in this paper extends this approach, but it is important to stress that this model is far less sophisticated than even the 1D. The simplifying step was to lump the resistance with each successive layer of the 1D model as a membrane with permeability characteristic of the resistance expected to transport into and across that layer. Water and solute flux are assumed to exchange across this membrane into a well-mixed volume with dimensions characteristic of each layer. When reasonable volume estimates are assigned, transient changes are described in terms of the composition of plasma protein within each compartment determined by a simple mass balance over each sub-compartment.

## Series Compartment Model

The most important result from this lumped parameter-series compartment model is the quantitative evaluation of solute accumulation under the glycocalyx during reabsorption. **Figure 5** demonstrates one example as pressure was reduced in steps on 0.1 mmHg every 0.1 s. Small time steps were necessary because modeling at a time scale of seconds is incompatible with the length scales in this model. For example a sudden pressure drop from 20 to 13 mmHg with no change in the concentration difference across the glycocalyx would cause such a large reabsorption rate (>10 ml/min) that convective transport of plasma proteins into the cleft opening to the tissue compartment would exceed 300 mg/min (5 mg/s) and the protein concentration in the glycocalyx sub-compartment would exceed plasma protein concentration. This is an example of the problem Weinbaum and colleagues anticipated when setting up the 3D model.

## Convection vs. Diffusion in the Sub-Glycocalyx Compartments

The relative contributions of diffusion and convective transport are determined by the Peclet number when used in the Hertzian equation for transport across a membrane. For exchange between the sub-compartment under the glycocalyx concentration *Cf* and the cleft compartment *Cg*:

$$Js = Jv1\,(1-\sigma)\,[\frac{Cf - Cgexp\,(-Pe)}{1-\exp\,(-Pe)}\}\qquad(21)$$

*Pe* is the ratio of the velocity of the solute due to solvent drag to the diffusive velocity over the barrier between the compartments. The convective solute velocity is measured as $Jv\,(1-\sigma)$ and the diffusive velocity as *Pd*. This relation can be used to evaluate the relative contribution of convective and diffusive transport at any stage of a transient. For example, at $P$ = 13 mm Hg, $Cf$ = 36.8 mg/ml and $Cg$ is 28.8 mg/ml. Setting the direction $Cf$ to $Cg$ as positive, the question is whether $Js1$ is directed away from the glycocalyx sub-compartment due to diffusion or into the sub-compartment due to convection.

Equation 21 shows that the magnitude and direction of $Js$ depends on the difference between the value of $Cf$ and $Cg\exp(-Pe)$. For $P$ = 13 mmHg, the Peclet Number corresponding to the calculated reabsorption rate (1.95 ml/min) is −0.279. The value of $Cf - Cg\exp(-Pe)$ calculated as 36.8–38 mg/ml, is negative. Protein flux is into the sub-glycocalyx space. Thus when pressure is first set at 13 mmHg, convective flux adds solute from the cleft compartment below the glycocalyx. Specifically the convective flux from the cleft is 0.75 mg/0.1 s and the diffusion back into the cleft is 0.057 mg/0.1 s. Our calculations show that solute accumulation continues to a peak value beneath the glycocalyx of 37.17 mg/ml. The reabsorption rate is then 1.71 ml/min and Pe = −0.244. Now $Cf - Cg\exp(-Pe)$ is positive, and net diffusion is directed away from the glycocalyx. The fine balance between the convective transport into the sub-compartment and diffusion determines the subsequent time course of the reabsorption until reabsorption stops and eventually $Cg$ rises as the tissue concentration approaches a new steady state.

It might be argued that the fine balance between back diffusion and convective transport into the sub-compartment below the glycocalyx during reabsorption can be compromised because water velocity increases as the reabsorbed fluid is funneled into the breaks in the junction strand. Although water velocity would indeed increase due to such funneling, this does not mean that convective transport necessarily dominates diffusion at the breaks. This is because the geometry of the break is such that the diffusion distances ($\Delta X$ strand) corresponding to the region near the breaks where the funneling of reabsorbed fluid occurs are less than 100 nm, relative to total diffusion distances in the cleft (up to 1 μ or 1,000 nm). Thus if breaks in the junction strand (representing 10% of the length of junction strand available to flow) increased local water velocity 10-fold, the local diffusion velocity measured as $D/\Delta X$ strand would also be increased, independently, by a similar order of magnitude (where $D$ = diffusion coefficient of protein). The ratio of water velocity to diffusion velocity would remain close to that estimated for the lumped parameters.

## Comparing the Series Compartment Model With the Simple Compartment Model

The assumption used in the single tissue compartment (**Figures 1A, 2**) is that the concentration in the tissue compartment can be substituted for the sub-glycocalyx concentration during both filtration and reabsorption. As shown by **Figure 5**, during filtration the tissue concentration is a good approximation to sub-glycocalyx concentration because of the rapid readjustment of concentration gradient under the glycocalyx. A similar rapid adjustment would take place when pressure was increased. This assumption enables a reasonable prediction of volume shifts that occur over periods of tens of minutes because change in tissue concentration toward a true new tissue concentration take place over time periods of 100s of minutes. One example of a practical use of the single compartment model to describe changes in filtration after plasma proteins are diluted by saline infusion has been published (Michel et al., 2020).

On the other hand during reabsorption, the use of the prior steady state tissue concentration as an estimate of the sub-glycocalyx significantly overestimates the driving forces for reabsorption and overestimates the volume reabsorbed. Prior knowledge of the barriers to solute exchange between the

base of the glycocalyx and the tissue is required for more accurate evaluation of such fluid exchange. One version of this observation has been recognized for one and a quarter centuries. Transvascular exchange described by the Starling principle is self-limiting. Reabsorption concentrates the plasma protein concentration in the ISF and the corresponding increase in tissue COP limits further reabsorption. This action is amplified many times when reabsorption leads to accumulation of plasma proteins in the much more limited space under the glycocalyx.

## The Composition of the Tissue Compartment

There are many limitations to the treatment of sub-compartments in the ISF. We estimated the time for protein concentration in the smaller endomysial ISF compartment to reach a new steady after a change in pressure to be over 1,000 min when all the protein flux mixed with this compartment. However, as **Figure 2** shows, a significant fraction of the large pore flux from venular vessels may exchange directly into the larger perimysium and the time to reach steady state would be corresponding longer. Two additional issues related to tissue composition. One is that the use of an average tissue composition to estimate effective transvascular COP differences ignores the fact that in the steady state the filtration rate and the COP opposing filtration vary as pressure falls from the arterial to the venular side of the microvascular bed. Thus as Levick (1991) demonstrated, the use of average tissue composition predicts filtration rates far in excess of measured lymph flows. A subtler but important second issue is that the composition of the ultrafiltrate from the glycocalyx contains fewer proteins than the plasma and more albumin per unit volume. For a given protein concentration the COP of an ISF sample is expected to be larger than that calculated from Eq. 8 for a plasma sample. The analysis of these interactions requires a far more sophisticated model than considered here.

## Transient vs. Sustained Reabsorption

Zhang et al. (2006) noted that there could be sustained reabsorption in microvessels when capillary pressures were reduced below 17 mmHg when the COP in blood was set to 25 mmHg and the tissue plasma protein concentrations were set at 40% of plasma concentration some distance from the microvessel wall. It is important to emphasize that this result does not contradict the "no steady state reabsorption" rule established by the Revised Starling principle in tissues where the ISF is generated initially as a capillary ultrafiltrate as in **Figure 3**.The reason these investigators described sustained reabsorption is that the ISF concentration of protein was held constant at 40% of plasma concentrations at all capillary pressures, including those at 17 mmHg and below. In contrast, true steady state tissue concentration increases significantly above 40% plasma concentration at pressures below 17 mmHg when the steady state rule that $Ct = Js/Jv$ summed over all pathways is applied. This observation focuses attention on the rate of change of tissue concentrations after a reabsorption transient as a determinant of the reabsorption transient. We show (e.g., **Figure 4**) that the time course of reabsorption can be very long in muscle, even when the volume of the sub-compartment of ISF is less than 20% of the total ISF (1,000 ml vs. 6–8,000 ml). When reabsorption begins after steady state filtration at a pressure of 20 mmHg, the tissue plasma concentration is in the range of 30–40% blood concentration as in **Figure 3D**. After a rapid re-adjustment of concentration beneath the glycocalyx as pressure falls there is slow reabsorption for more than an hour because tissue concentration increases slowly. This is similar to that described by Zhang et al. (2006) with a fixed tissue concentration.

It is also noted that there can be a clear exception to "no sustained reabsorption" rule. In the kidney, lymph nodes, and absorbing GI tissues there are additional mechanisms to limit the extent of plasma protein concentration in the tissue and a compartment beneath the glycocalyx (especially in fenestrated capillaries as described elsewhere; Michel et al., 2020). These mechanisms to maintain steady state reabsorption are not present in muscle.

## Other Junction Configurations and the Sensitivity of the Models to Uncertainty in the Parameters

Our calculations emphasize the need to understand the resistance to water and solute transport between the base of the glycocalyx and ISF in a local tissue compartment. Freeze fracture images of the intercellular cleft reveal multiple junction strands within the junction of capillaries of diaphragm and heart muscle (Wissig and Williams, 1978; Bundgaard, 1984). In contrast to the simple geometry for strands used in the present analysis, the tortuous pathway though the junction complex suggests a resistance to both water and plasma protein higher than in the present analysis. When setting up the 3D model, Hu et al. (2000) argued that the distributed resistance of multi strand patterns in mesenteric microvessel to diffusion could be replaced by the single equivalent barrier, but the validity of this argument for more complex multi-layer arrays for both solute and water flows remains to be evaluated. This is important because the predictions of protein concentrations across the glycocalyx are most sensitive to uncertainties in the volumes of the sub-compartments *Vf* and *Vg* within the cleft, and to the diffusion resistance to exchange between *Vf* and *Vg* as illustrated in **Figure 6**. Furthermore, a notable omission in the present analysis is consideration of resistance to water flow in the space under the glycocalyx. A better description of the pressure differences between the space under the glycocalyx and the tissue compartment is needed.

## Other Model Parameters

We have considered only the limiting case where the large pore pathway mixed with the endomysial compartment. If exchange occurred between the endomysial and the perimysium the effective volume regulating tissue concentration would increase. Further we have previously estimated that there is, on average, only one to two large pores per microvessel in tissues such as muscle (Michel and Curry, 1999). It is not unreasonable to suggest that some regions of the microvascular bed have no large pores. There is limited understanding of the extent that

fluid and solute exchange into and between the endomysial and the perimysial compartments over time periods of 30–60 min. Our estimates of the total volume of ISF fluid reabsorbed after reduction in capillary pressure would be underestimated if the volume used for the tissue compartment was too small or tissue plasma protein concentrations were lower than the steady state concentrations we used. At the same time it should be noted that clinical and experimental measurement of changes in plasma volume based on small changes in hematocrit are prone to much larger errors than are commonly recognized (Michel and Curry, 2009). Progress toward better understanding of the way sub compartments of the ISF modulate transvascular fluid exchange in whole organs such as the skeletal muscle mass in human subjects requires refinements in both the models described in this paper and the measurement of changes in plasma volume in human subjects during filtration and reabsorption.

## Summary

The primary purpose of these investigations is to integrate our growing knowledge about the endothelial glycocalyx as a permeability and osmotic barrier into models of trans-vascular exchange in whole organs. For plasma proteins we describe changes in their COP difference across the glycocalyx after an increase or decrease in capillary pressure. The composition of the fluid under the glycocalyx can change in step with capillary pressure, whereas the average composition of the interstitial fluid takes many hours to adjust to the same change in vascular pressure. We used models where the fluid under the glycocalyx mixes with sub-compartments of the ISF whose volumes could be reasonably well defined from the ultrastructure of the inter-endothelial cleft and the histology of the tissue surrounding the capillaries. The initial protein composition in the sub-compartment is set as that during steady state filtration in the presence of a large pore pathway in parallel with the "small pore" glycocalyx pathway. Changes in the composition of the sub-compartments depend on their volume and the balance of convective and diffusive transport into and out of each compartment. We used skeletal muscle as an example. The simplest model assumes the fluid under the glycocalyx mixes directly with a tissue sub-compartment with a volume less than 20% of the total skeletal muscle ISF volume. This model places limits on transvascular flows during transient filtration and reabsorption over periods up to 60 min. The key assumption in this model is compromised when the resistance to diffusion between the base of the glycocalyx and the tissue volume accounts for more than 1% of the total resistance to diffusion across the endothelial barrier formed by the glycocalyx and intercellular cleft. It is well established that in steady state, the balance of hydrostatic and colloid osmotic forces across the glycocalyx requires that reabsorption does not occur in tissue such as skeletal muscle. Our approach extends this idea to demonstrate that the change in vascular pressure favoring transient reabsorption from the skeletal muscle interstitial fluid result in much less fluid exchange than is commonly assumed.

We envision at least two further extensions of the approach used in the present analysis. One is to apply a similar analysis to other organs where reasonable estimates of capillary ultrastructure and ISF histology is available. The lung would be of particular interest as would the G-I tract because, with its large fraction of resing cardiac output and permeable capillaries, it could have large and rapid effects on plasma composition. The second is to enable critical evaluation of the empirical models of trans-vascular fluid exchange being used for in some clinical applications. While there is an understandable desire to describe fluid exchange between plasma and tissue as simply as possible, the balance of hydrostatic and COPs across the glycocalyx cannot be ignored. This is the case in the approach known as "volume kinetic analysis" which describes fluid exchange between the plasma compartment and an arbitrarily defined tissue sub-compartment assuming fluid exchange is proportional to the changes in the volume of fluid in these compartments from an initial state (Hahn, 2020). The failure of these models to account for the fine balance of hydrostatic and COPs across the glycocalyx that our model describes must compromise their utility.

## DATA AVAILABILITY STATEMENT

The original contributions presented in the study are included in the article/supplementary material, further inquiries can be directed to the corresponding author.

## AUTHOR CONTRIBUTIONS

FC drafted the manuscript. Both authors discussed the changes that lead to the final version.

## REFERENCES


Adamson, R. H. (1993). Microvascular endothelial cell shape and size in situ. *Microvasc. Res.* 46, 77–88. doi: 10.1006/mvre.1993.1036

Adamson, R. H., Lenz, J. F., Zhang, X., Adamson, G. N., Weinbaum, S., and Curry, F. E. (2004). Oncotic pressures opposing filtration across non-fenestrated rat microvessels. *J. Physiol. (London)* 557, 889–907. doi: 10.1113/jphysiol.2003.058255

Adamson, R. H., and Michel, C. C. (1993). Pathways through the intercellular clefts of frog mesenteric capillaries. *J. Physiol.* 466, 303–327.

Bundgaard, M. (1984). The three-dimensional organization of tight junctions in a capillary endothelium revealed by serial-section electron microscopy. *J. Ultrastruct. Res.* 88, 1–17. doi: 10.1016/s0022-5320(84)90177-1

Csapo, R., Gumpenberger, M., and Wessner, B. (2020). Skeletal muscle extracellualr matrix. A narrative review. *Front. Physiol.* 11:253.

Curry, F. E. (1984). "Mechanics and thermodynamics of transcapillary exchange," in *Handbook of Physiology: Microcirculation*, Vol. IV, eds E. M. Renkin and C. C. Michel (Rockville MD: American Physiological Society), 309–374.

Curry, F. E. (2018). The molecular structure of the endothelial glycocalyx layer (EGL)and surface layers (ESL). Modulation of transvascular exchange. *Adv. Exp. Med. Biol.* 1097, 29–49. doi: 10.1007/978-3-319-96445-4_2

Curry, F. E., Arkill, K. P., and Michel, C. C. (2020). "Chapter 3 the functions of endothelial glycocalyx and their effects on patient's outcomes during the

perioperative period. A review of current methods to evaluate structure-function relations in the glycocalyx in both basic research and clinical settings," in *Perioperative Fluid Management*, 2nd Edn, eds E. Frag, A. Kunz, and C. Troianas (Cham: Springer).

Grotte, G. (1956). Passage of dextran molecules across the blood- lymph barrier. *Acta Chir. Scand. Suppl.* 211, 1–84.

Hahn, R. G. (2020). kinetics. *Acta Anaesthesia Scand.* 64, 570–578.

Hu, X., Adamson, R. H., Liu, B., Curry, F. E., and Weinbaum, S. (2000). Starling forces that oppose filtration after tissue oncotic pressure is increased. *Am. J. Physiol.* 279, H1724–H1736.

Hughes, R., May, A. J., and Widdicombe, J. G. (1958). Mechanical factors in the formation of oedema in perfused rabbits' lungs. *J. Physiol.* 142, 292–305. doi: 10.1113/jphysiol.1958.sp006016

Landis, E. M., and Gibbon, J. H. (1933). The effects of temperature and of tissue pressure on the movement of fluid through the human capillary wall. *J. Clin. Invest.* 12, 105–138. doi: 10.1172/jci100482

Landis, E. M., and Pappenheimer, J. R. (1963). "Chap. 29 exchange of substances through the capillary walls," in *Handbook of Physiology, Circulation. Sect. 2*, Vol. 2, eds W. F. Hamilton and P. Dow (Washington, DC: American Physiological Society), 961–1034.

Lanne, T., and Lundvall, J. (1992). Mechanisms in man for rapid refill of the circulatory system in hypovolaemia. *Acta Physiol. Scand.* 146, 299–306. doi: 10.1111/j.1748-1716.1992.tb09423.x

Levick, J. R. (1991). Capillary filtration-absorption balance reconsidered in light of dynamic extravascular factors. *Exp. Physiol.* 76, 825–857. doi: 10.1113/expphysiol.1991.sp003549

Levick, J. R., and Michel, C. C. (1978). The effects of position and skin temperature on the capillary pressure of the fingers and toes. *J. Physiol.* 274, 97–109. doi: 10.1113/jphysiol.1978.sp012136

Levick, J. R., and Michel, C. C. (2010). Microvascular fluid exchange and the revised Starling principle. *Cardiovasc. Res.* 87, 198–210. doi: 10.1093/cvr/cvq062

Lunde, P. K. M., and Waaler, B. A. (1969). Transvascular fluid balance in the lungs. *J. Physiol.* 1969, 1–18. doi: 10.1097/00004311-198308000-00003

Michel, C. C. (1984). "Fluid movements through capillary walls," in *Handbook of Physiology. The Cardiovascular System, Microcirculation, Part 1*, Vol. 4, eds E. M. Renkin and C. C. Michel (Rockville, MD: American Physiological Society), 375–409.

Michel, C. C. (1997). Starling: the formulation of his hypothesis of microvascular fluid exchange and its significance after 100 years. *Exp Physiol.* 82, 1–30. doi: 10.1113/expphysiol.1997.sp004000

Michel, C. C., Arkill, K. P., and Curry, F. E. (2020). "Chapter 3 the revised Starling principle and its relevance to peri-operative fluid management," in *Perioperative Fluid Management*, 2nd Edn, eds E. Farag, A. Kunz, and C. Troianas (Cham: Springer).

Michel, C. C., and Curry, F. E. (1999). Microvascular Permeability. *Physiol. Rev.* 79, 703–761.

Michel, C. C., and Curry, F. R. (2009). Glycocalyx volume: a critical review of tracer dilution methods for its measurement. *Microcirculation* 16, 213–219. doi: 10.1080/10739680802527404

Michel, C. C., and Moyses, C. (1985). "The measurement of fluid filtration in human limbs," in *Clinical Investigation of the Microcirculation*, eds J. E. Tooke and L. H. Smaje (Lancaster: Martinus Nijhoff Publishing), 1985.

Michel, C. C., and Phillips, M. E. (1987). Steady-state fluid filtration at different capillary pressures in perfused frog mesenteric capillaries. *J. Physiol.* 388, 421–435. doi: 10.1113/jphysiol.1987.sp016622

Pappenheimer, J. R., Renkin, E. M., and Borrero, L. M. (1951). Filtration, diffusion and molecular sieving through peripheral capillary membranes. *Am. J. Physiol.* 167, 13–46. doi: 10.1152/ajplegacy.1951.167.1.13

Pappenheimer, J. R., and Soto-Rivera, A. (1948). Effective osmotic pressure of the plasma proteins and other quantities associated with the capillary circulation in the hind limbs of cats and dogs. *Am. J. Physiol.* 152, 471–491. doi: 10.1152/ajplegacy.1948.152.3.471

Renkin, E. M. (1978). Transport pathways through capillary endothelium. *Microvasc. Res.* 15, 123–135.

Renkin, E. M., and Tucker, V. L. (1998). Measurement of microvascular transport parameters of macromolecules in tissues and organs of intact animals. *Microcirculation* 5, 139–152. doi: 10.1080/713773856

Rippe, B., and Haraldsson, B. (1994). Transport of macromolecules across capillary walls: the two pore theory. *Physiol. Rev.* 74, 163–213. doi: 10.1152/physrev.1994.74.1.163

Taylor, A. E., and Granger, D. N. (1984). "Exchange of macromolecules across the microcirculation," in *Handbook of Physiology, Section 2. Volume 4, Micrcirculation Part 1*, Vol. 4, eds E. M. Renkin and C. C. Michel (Bethesda, MY: American Physiological Society), 467–520.

Wang, Q., Pei, S., Lu, X. L., Wang, L., and Wu, Q. (2020). On the characterization of interstitial fluid flow in skeletal muscle endomysium. *J. Mech. Behav. Biomed. Mater.* 102:103504. doi: 10.1016/j.jmbbm.2019.103504

Weinbaum, S. (1998). 1997 Whitaker Distinguished Lecture: models to solve mysteries in biomechanics at the cellular level; a new view of fiber matrix layers. *Ann. Biomed. Eng.* 26, 627–643. doi: 10.1114/1.134

Wissig, S. L., and Williams, M. C. (1978). Permeability of muscle capillaries to microperoxidase. *J. Cell Biol.* 76, 341–359. doi: 10.1083/jcb.76.2.341

Zhang, X., Adamson, R. H., Curry, F. E., and Weinbaum, S. (2006). A 1-D model to explore the effects of tissue loading and tissue concentration gradients in the revised Starling Principle. *Am. J. Physiol. Heart Circ.* 291, H2950–H2964.

Zhang, X., Adamson, R. H., Curry, F. E., and Weinbaum, S. (2008). Transient regulation of transport by pericytes in venular microvessels via trapped microdomains. *Proc. Natl. Acad. Sci. U.S.A.* 105, 1374–1379. doi: 10.1073/pnas.0710986105

**Conflict of Interest:** The authors declare that the research was conducted in the absence of any commercial or financial relationships that could be construed as a potential conflict of interest.

**Publisher's Note:** All claims expressed in this article are solely those of the authors and do not necessarily represent those of their affiliated organizations, or those of the publisher, the editors and the reviewers. Any product that may be evaluated in this article, or claim that may be made by its manufacturer, is not guaranteed or endorsed by the publisher.

frontiers in Cell and Developmental Biology

MINI REVIEW
published: 17 August 2021
doi: 10.3389/fcell.2021.732815

# Understanding the Role of Endothelial Glycocalyx in Mechanotransduction via Computational Simulation: A Mini Review

*Xi Zhuo Jiang[1]*, Kai H. Luo[2]* and Yiannis Ventikos[2]**

[1] School of Mechanical Engineering and Automation, Northeastern University, Shenyang, China, [2] Department of Mechanical Engineering, University College London, London, United Kingdom

OPEN ACCESS

**Edited by:**
*Bingmei M. Fu,*
*City College of New York,*
*United States*

**Reviewed by:**
*Yang Liu,*
*Hong Kong Polytechnic University,*
*China*
*Miguel Vicente-Manzanares,*
*Consejo Superior de Investigaciones Científicas, Spain*

***Correspondence:**
*Xi Zhuo Jiang*
*jiangxz@mail.neu.edu.cn*
*Kai H. Luo*
*k.luo@ucl.ac.uk*
*Yiannis Ventikos*
*y.ventikos@ucl.ac.uk*

**Specialty section:**
*This article was submitted to Signaling, a section of the journal Frontiers in Cell and Developmental Biology*

**Received:** *29 June 2021*
**Accepted:** *27 July 2021*
**Published:** *17 August 2021*

**Citation:**
*Jiang XZ, Luo KH and Ventikos Y (2021) Understanding the Role of Endothelial Glycocalyx in Mechanotransduction via Computational Simulation: A Mini Review. Front. Cell Dev. Biol. 9:732815. doi: 10.3389/fcell.2021.732815*

Endothelial glycocalyx (EG) is a forest-like structure, covering the lumen side of blood vessel walls. EG is exposed to the mechanical forces of blood flow, mainly shear, and closely associated with vascular regulation, health, diseases, and therapies. One hallmark function of the EG is mechanotransduction, which means the EG senses the mechanical signals from the blood flow and then transmits the signals into the cells. Using numerical modelling methods or *in silico* experiments to investigate EG-related topics has gained increasing momentum in recent years, thanks to tremendous progress in supercomputing. Numerical modelling and simulation allows certain very specific or even extreme conditions to be fulfilled, which provides new insights and complements experimental observations. This mini review examines the application of numerical methods in EG-related studies, focusing on how computer simulation contributes to the understanding of EG as a mechanotransducer. The numerical methods covered in this review include macroscopic (i.e., continuum-based), mesoscopic [e.g., lattice Boltzmann method (LBM) and dissipative particle dynamics (DPD)] and microscopic [e.g., molecular dynamics (MD) and Monte Carlo (MC) methods]. Accounting for the emerging trends in artificial intelligence and the advent of exascale computing, the future of numerical simulation for EG-related problems is also contemplated.

**Keywords: microscale, mesoscale, macroscale, computational simulation, mechanotransduction, endothelial glycocalyx, numerical modelling**

## INTRODUCTION

The inner surface of blood vessel walls is covered by a layer of dendritic structures termed endothelial glycocalyx (EG). A typical glycocalyx unit consists of a few glycosaminoglycan (GAG) chains and a core protein which anchors the GAGs to cell membrane. The EG is exposed to the blood flow and is the first barrier in direct contact with blood. Such a unique location allows EG to coordinate microvascular mass transport (Kang et al., 2021), regulate cell adhesion (Robert et al., 2006) and participate in mechanotransduction (Tarbell and Pahakis, 2006). Mechanotransduction describes a process of bio-structures perceiving and transferring their ambient mechanical signals.

Specifically for EG, mechanotransduction means the EG senses the mechanical stimuli from blood flow and transmits such signals to the cytoplasm. The response of EG to the haemodynamic forces is critical to maintaining vascular health and function (Goligorsky and Sun, 2020; Weinbaum et al., 2021). Malfunction of the EG in sensing and transmitting mechanical signals can cause severe vascular diseases such as atherosclerosis, hypertension, stroke, and sepsis (Tarbell and Cancel, 2016; Goligorsky and Sun, 2020), just to name a few.

Using wet-lab experiments, especially enzymatic degradation, is an effective way to explore the role of EG and its components in regulating mechanotransduction. Experiments have probed the glycocalyx as a mechanotrasnducer, revealed the potential manner in which the shear (mechanical stimuli) is felt and uncovered the activities involved in the message delivery after sensing the mechanical signal. Experimental evidences supporting the relationship between EG and the mechanotransduction are reviewed in Tarbell and Pahakis (2006).

Complementary to wet-lab experimental methods, *in silico* experiments, also named numerical simulations or computational modelling, approach the problems of EG mechanotransduction from a different angle. As the name itself indicates, *in silico* experiments are implemented on computers, which allow precise control of EG properties in order to delineate how EG and its components play their roles in mechanotransduction. Initially, numerical studies of EG adopted simple models only with a limited number of glycocalyx features, and the aim was mainly to reproduce wet-lab results by simulations. The recent progresses in advanced numerical methods and supercomputers empower *in silico* experiments to tackle far more challenging EG-related problems with high spatial and temporal resolutions. Breakthroughs in crystallographic structure determination lend numerical simulations the possibility to offer accurate results with a resolution at the atomic/molecular level.

The aim of this mini review is to critically summarise recent developments in numerical methods and their applications in the study of the EG mechanotransduction, demonstrating knowledge generation through *in silico* experiments. Principles of the relevant numerical methods are individually described briefly, together with their contributions to the understanding of the EG functionality as a mechanotransducer. The future of numerical studies in EG functionality is also considered, accounting for trends in artificial intelligence, big data and the advent of exascale computing.

## NUMERICAL METHODS

Numerical methods can be classified into macroscopic, mesoscopic, and microscopic approaches in terms of length and time scales resolved, as illustrated in **Figure 1**. Macroscopic simulations have the longest history in solving EG-related problems and are still a popular and powerful tool. Macroscopic simulations deal with problems at cell- or tissue-scales, like endothelial cell deformation, force distribution on glycocalyx ultrastructures and flow shear stress over the EG layer (Tarbell and Shi, 2013; Dabagh et al., 2014). Mesoscopic methods can further explore detailed fluid-structure interactions (O'connor and Revell, 2019) between blood flow and endothelium surface structures but at slightly higher computational cost. Microscopic *in silico* experiments have been successfully applied to capture the atomic/molecular interactions in a single proteoglycan unit (Jiang et al., 2017). Such microscopic simulations, however, confined to a computation domain measured in nanometers and a physical time in nanoseconds, due to high computational cost.

In this section, the basic principles of these methods are described, and their applications are demonstrated. It should be noted that the main purpose of this mini review is to show advances in using numerical methods to understand the EG mechanotransduction while the algorithmic details of individual simulation methods are described in the relevant references.

### Macroscopic Simulations

In macroscopic methods, the EG is generally treated as a continuum layer with a limited number of bio-features, and the simulation outcomes are the macroscopic properties of the endothelial dendritic structures. Computational fluid dynamics (CFD; Tu et al., 2019) and the finite element method (FEM; Zienkiewicz et al., 2005) are two commonly used techniques in macroscopic simulations, which originated from the fluid mechanics and solid mechanics communities, respectively. Generally, continuum-based conservation laws and macroscopic physical models for bio-features are solved to obtain flow profile over and/or through the EG layer (Wang, 2007; Lee et al., 2016, 2020), deformation/force of the anchoring cells or membranes (Tarbell and Shi, 2013; Dabagh et al., 2014), order of magnitude of force transmitted via the glycocalyx (Saez et al., 2019).

In numerical modelling, simplifications of the problems under concern are inevitable due to the complexity of EG structures. With a focus on different aspects of the EG features, mechanotransduction can be approached from different perspectives. For example, the endothelial surface is covered by a layer of interweaving, dynamic and brush-like GAG chains. Such a layer can be simplified as an array of side chains or a layer of porous structures. By assuming the EG layer as an organised array of elastic chains, with individual chains having one end fixed to the cell membrane, Secomb et al. (2001) were able to identify the role of EG in transmitting shear stress to the endothelial cell surface and conclude that the EG layer would mediate rapid flow fluctuations and attenuate shear stress. By treating the EG layer as a porous medium, Tarbell and Shi reported that the solid stress of the endothelial cell surface is one to two orders of magnitude higher than the surface fluid stress in the presence of EG layer, suggesting that the interstitial flow shear stress can be sensed by the EG layer (Tarbell and Shi, 2013). As such, the role of EG is to strengthen the mechanical signals. Combining these results, a possible pathway for force transmission via the EG layer is proposed, i.e., flow shear stress → EG → cell membrane, as discussed in Tarbell and Pahakis (2006).

Simplification based on experimental observation is imperative for achieving numerical results of acceptable accuracy in reasonable timeframes. Take geometric periodicity

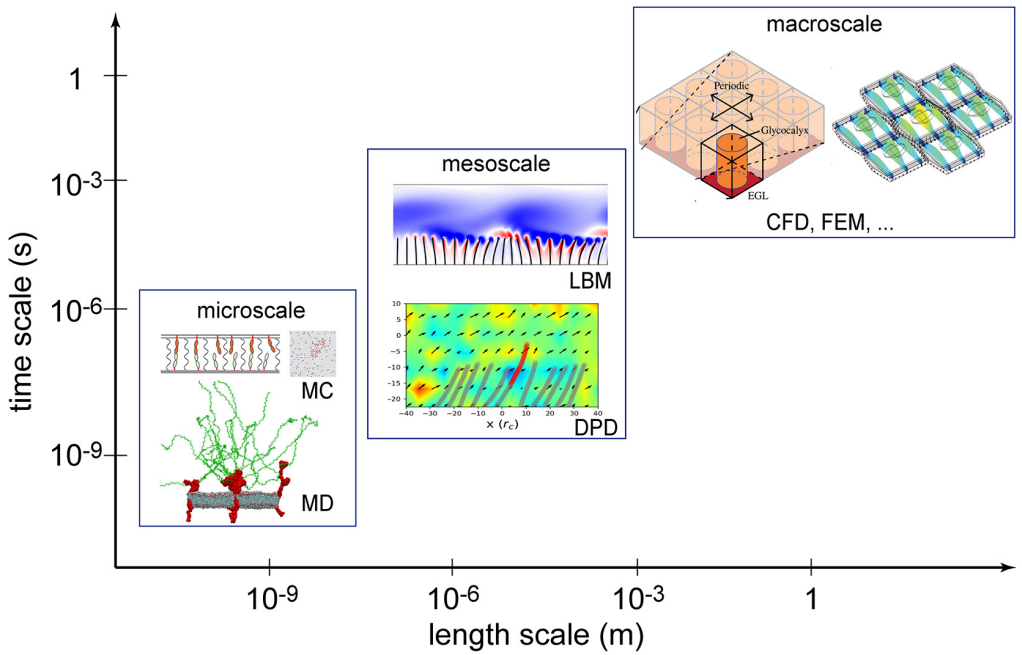


**FIGURE 1 |** Numerical methods used in the investigation of the endothelial glycocalyx (EG) mechanotransduction. Computational fluid dynamics (CFD) and the finite element method (FEM) are two established macroscopic methods; lattice Boltzmann method (LBM) and dissipative particle dynamics (DPD) are typical mesoscopic methods; molecular dynamics (MD) and Monte Carlo (MC) are deterministic and stochastic microscopic methods, respectively. Sources: MC is from Xu et al. (2016), MD from Jiang et al. (2017), LBM from O'connor and Revell (2019), DPD from Jiang et al. (2021), CFD from Lee et al. (2020), and FEM from Dabagh et al. (2014). Reuse of figures are permitted by the Cambridge University Press, Royal Society of Chemistry and the Royal Society (United Kingdom).

as an example: Researchers (Lee et al., 2020) have set up different periodic geometries for core proteins and GAGs and analysed the pressure gradient (an indicator used to quantify mechanotransduction in the research) differences among different periodic geometries. Results suggest that the periodicity type determines the pressure gradient within the EG layer: hexagonal periodicity of the core proteins leads to greater mechanotransduction, and rectangular periodicity of aggregated GAGs leads to the greatest conversion of pressure gradients to wall tractions. Indeed, a hexagonal periodicity is favoured by previous studies (Weinbaum et al., 2003; Zeng et al., 2013), and conclusion based on the hexagonal periodicity is sensible.

For macroscopic methods, a "complete" model with all the features of the system is definitely beneficial for accurate results from numerical simulations. On the other hand, the computational cost would increase as more details are involved in computational models. Such a complete model is intimately related with access to accurate structural information which in turn relies on the availability (and possibly invention) of cutting-edge microscopic observation equipment.

## Mesoscopic Simulations

The lattice Boltzmann method (LBM) and the dissipative particle dynamics (DPD) are two widely used mesoscopic methodologies in mechnotransduction studies. Both methods are based on the kinetic theory of particle dynamics.

In the framework of LBM, the fluid is modelled as a set of fictitious particles, and such particles interact with each other on a regular discrete lattice mesh through a two-stage "collision and streaming" process. A systematic review of the LBM in flow studies can be found in Chen and Doolen (1998) and Li et al. (2016). In DPD models, the system of interest is simplified to a set of interacting beads, each bead representing a cluster of constitutive molecules or atoms. The governing equation in the DPD method is Newton's Law of Motion, i.e., $F = ma$, where $F$ is the force on the bead, $m$ is the mass of the bead, and $a$ is the acceleration of motion of the bead. The force term comprises three elements: a conservative force, a random force and a dissipative force (Liu et al., 2014). A detailed review of DPD can be found in Espanol and Warren (2017). The particle-based nature of both mesoscale methods facilitates the construction of complex structures at the fluid-structure interface. Thus, recent mesoscale simulation studies are mostly about interpreting the fluid-structure interactions between the blood flow and the complex endothelium surface structures (Yin and Zhang, 2013).

At the mesoscales, more features of the glycocalyx can be included, which enables detailed comparison with experiments. By coupling the LBM with immersed boundary methods, alongside structural solvers, researchers revealed a broad range of behaviours for slender structures, from a single flap in a periodic array, to a small finite array of flaps, and finally to a large finite array (Yin and Zhang, 2013; O'connor et al., 2016; O'connor and Revell, 2019). The findings suggest that the flow instability over the slender array depends on the natural frequencies of the flow and the surface structures (O'connor and Revell, 2019). As a simple extension, one may expect that the shedding or

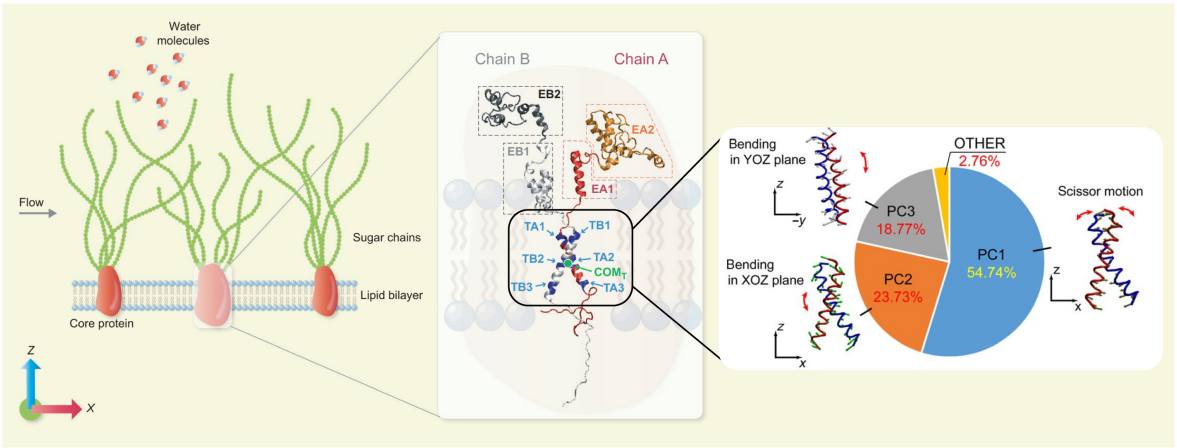


**FIGURE 2 |** Force transmission mode of Syndecan-4 revealed by MD simulations. **(Left)** An MD model for EG. **(Middle)** Secondary structure of Syndecan-4. **(Right)** Force transmission mode via the transmembrane part of Syndecan-4 (Jiang et al., 2020b; reuse of figure under CC BY 4.0 permission).

impairment of EG chains would change flow patterns, cause flow instability and further disturb mechanotransduction. The role of EG in regulating flow field was also demonstrated in a recent DPD study (Jiang et al., 2021).

Beyond the fluid-structure interactions between the blood flow and EG layer, mesoscopic methods have been applied to a wide spectrum of haemodynamic problems, like cell suspension and leukocyte adhesion over endothelium (Yan et al., 2019), the glycocalyx–endothelium–erythrocyte interaction in the microcirculation (Pontrelli et al., 2015; Jiang et al., 2021) and the formation of the cell-free layer (Deng et al., 2012).

## Microscopic Simulations

Molecular dynamics (MD) is a typical microscopic simulation method that describes how atoms and molecules move and interact during a period of time. The governing equation of MD is also Newton's Law of Motion as in the DPD method, but a wide range of interatomic and intermolecular forces can be included and often parameterised as force fields. For the theoretical and numerical details of the MD method, the readers are referred to Frenkel and Smit (2002) and Rapaport (2011). When the structural configurations of biomolecules are known and a set of force field parameters are properly chosen, the trajectories of the constitutive atoms can be calculated by MD and the behaviour of the biomolecular system is then fully characterised. In principle, all biophysical problems could be tackled by MD if the structural information at the atomic scale were known. The bottleneck preventing the broad application of MD is its high computational cost, which limits not only the number of observed individual molecules to be included but also the duration of observations (i.e., simulated physical time). Despite such constraints, MD has been increasingly employed in studying dynamics of EG and surrounding molecules, thanks to its unique ability to gain atomic level insight. In the classic vasoregulation signalling problem – *in what manner does glycocalyx transmit force to the cytoskeleton from the flowing blood?*, the glycocalyx was regarded as a rigid body and the force was transmitted by the local torque induced by the movement of the glycocalyx core protein. In recent MD simulations, Jiang et al. (2020b) elucidated the dynamics of Syndecan-4 (a typical type of transmembrane protein of the glycocalyx), and concluded that a *scissor-like* motion of the Syndecan-4 transmembrane dimer, together with its bending, is responsible for the force transmission and the force transmitted into the cytoplasm is of an order 10–100 pN. The MD model and force transmission mode is summarised in **Figure 2**. The same all-atom model for MD has also been applied to understand how the local lipid membrane around glycocalyx core proteins responds to the flow shear stress (Jiang et al., 2020a). By artificially switching off the charges of the core protein, the contributions of electrostatic and van der Waals interactions to cell membrane deformation induced by flow were quantified for the first time (Jiang et al., 2020a). The capability of isolating specific effects in MD demonstrates an important advantage of *in silico* experiments in exploring the mechanisms of mechanotransduction.

It is worthwhile to mention that fluid-structure interactions between blood flow and EG can also be interrogated by MD. When the current supercomputing platforms are employed, large-scale MD simulations are able to tackle flow problems in the proximity of the EG layer. As reported in recent studies, the blood flow changes the conformation of EG (Cruz-Chu et al., 2014; Pikoula et al., 2018), and the EG spatial configuration in turn modifies the blood flow profile (Jiang et al., 2017, 2018). This is in accordance with the clearly detrimental cycle between the endothelial dysfunction and the degradation of glycocalyx (Zhang et al., 2018).

Together with MD, the Monte Carlo (MC) method, based on the stochastic theory, is also able to capture microscopic features of bio-systems. A recent MC study has demonstrated that the glycocalyx promotes cooperative binding and clustering of adhesion receptors (Xu et al., 2016). The role of glycocalyx in nanocarrier-cell adhesion is also investigated by the MC method (Agrawal and Radhakrishnan, 2007).

## DISCUSSION

In the previous sections, the main features of macroscopic, meoscopic and microscopic simulation methods and their applications in the EG studies are reviewed. Each of these methods (i.e., CFD, FEM; LBM, DPD; MD, and MC) is designed to cover a specific range of length and time scales, and plays a different role in revealing the multiscale multiphysics nature of EG-related phenomena. These methods, however, are not mutually exclusive and can be used in combination. For example, MD, DPD, and LBM have all been used to study the fluid-structure interactions between blood flow and EG, which provide different levels of understanding. MC and LBM have been both used to explore the acceptor-receptor binding, revealing the stochastic and deterministic features, respectively. Moreover, the cell membrane deformation phenomena have been investigated by continuum models and MD, which can give interesting comparisons between macroscopic and microscopic properties of the same process. In short, a hierarchy of numerical simulations have been developed and applied to EG studies, which complement experiments and provide time-dependent and 3D information.

In this mini review, we have focused on the biophysical aspects of mechanotransduction, as the vast majority of numerical studies have been devoted to so far. The biochemical aspects of mechanotransduction, on the other hand, have been rarely studied using numerical simulations, due to the added complexity of biochemical reactions, like the generation of NO (Ignarro, 1989; Bartosch et al., 2017). In principle, the hierarchy of numerical methods can all be developed to reproduce the biochemical processes in mechanotransduction. For example, quantum mechanics/molecular mechanics (QM/MM) computations, which fall under microscopic methods (subatomic scale, to be precise) and advances in probing the electron transfer process, can be applied to find reaction mechanisms of enzymes, like the activation of eNOS (endothelial nitric oxide synthase) as reviewed in Bignon et al. (2019). Also, reactive force field MD (Senftle et al., 2016) simulations, which uses QM-trained force fields to mimic bond breaking and formation and have been extensively proved to be effective in capturing reaction pathways, can be applied to work out the chain reactions after the release of $Ca^{2+}$ initiated by mechanotransduction.

Although mechanotransduction has been investigated using a multitude of methods, in most case, these methods are applied individually or sequentially. A truly multiscale numerical method requires the dynamic coupling of different simulation methods in one simulation (Fedosov and Karniadakis, 2009). For example, a coupling between DPD and MD via a special multi-scale interface server (Wang et al., 2019) could solve the fluid problem and force transmission simultaneously. The challenge, however, is to find a suitable mapping between high- and low-resolution simulations in both spatial and temporal senses. Despite such inherent difficulties, dynamic coupling of simulations is expected to play an ever increasing role in studying multiscale phenomena such as mechanotranduction, as more powerful and cheaper computing platforms become as available.

Finally, we anticipate increasingly coupled use of artificial intelligence and numerical simulations in the coming years. Already, machine learning techniques have been used to empower MD to simulate a molecular system of 100 million atoms with *ab initio* accuracy (Jia et al., 2020), which is unprecedented. Together with the advent of exascale supercomputers, the integration of artificial intelligence and big data strategies into numerical simulations will revolutionise the way to conduct *in silico* experiments, leading to better understanding of the detailed mechanisms of mechanotransduction. Another significant development based on numerical simulations is the construction of a digital twin for a bio-system such as an EG layer, which will enable real-time diagnosis of diseases and, better still, instant repair of diseased components.

## AUTHOR CONTRIBUTIONS

XJ drafted the manuscript. KL and YV offered the direction, proposed ideas, and revised the manuscript. All authors contributed to the article and approved the submitted version.

## FUNDING

This work was in part supported by the UK Engineering and Physical Sciences Research Council under the project "UK Consortium on Mesoscale Engineering Sciences (UKCOMES)" (Grant No. EP/R029598/1). XJ acknowledges the financial support from the Starting Fund of Northeastern University, China.

## REFERENCES

Agrawal, N. J., and Radhakrishnan, R. (2007). The Role of Glycocalyx in Nanocarrier-Cell Adhesion Investigated Using a Thermodynamic Model and Monte Carlo Simulations. *J. Phys. Chem. C Nanomater Interfaces* 111, 15848–15856. doi: 10.1021/jp074514x

Bartosch, A. M. W., Mathews, R., and Tarbell, J. M. (2017). Endothelial Glycocalyx-Mediated Nitric Oxide Production in Response to Selective AFM Pulling. *Biophys. J.* 113, 101–108. doi: 10.1016/j.bpj.2017.05.033

Bignon, E., Rizza, S., Filomeni, G., and Papaleo, E. (2019). Use of Computational Biochemistry for Elucidating Molecular Mechanisms of Nitric Oxide Synthase. *Comput. Struct. Biotechnol. J.* 17, 415–429. doi: 10.1016/j.csbj.2019.03.011

Chen, S., and Doolen, G. D. (1998). Lattice Boltzmann Method for Fluid Flows. *Annu. Rev. Fluid Mech.* 30, 329–364.

Cruz-Chu, E. R., Malafeev, A., Pajarskas, T., Pivkin, I. V., and Koumoutsakos, P. (2014). Structure and response to flow of the glycocalyx layer. *Biophys. J.* 106, 232–243. doi: 10.1016/j.bpj.2013.09.060

Dabagh, M., Jalali, P., Butler, P. J., and Tarbell, J. M. (2014). Shear-induced force transmission in a multicomponent, multicell model of the endothelium. *J. R. Soc. Interface.* 11:20140431. doi: 10.1098/rsif.2014.0431

Deng, M., Li, X., Liang, H., Caswell, B., and Karniadakis, G. E. (2012). *Simulation and Modelling of Slip Flow Over Surfaces Grafted with Polymer Brushes and Glycocalyx Fibres*. United Kingdom: Cambridge University Press.

Espanol, P., and Warren, P. B. (2017). Perspective: dissipative particle dynamics. *J. Chem. Phys.* 146:150901. doi: 10.1063/1.4979514

Fedosov, D. A., and Karniadakis, G. E. (2009). Triple-decker: Interfacing atomistic–mesoscopic–continuum flow regimes. *J. Comput. Phys.* 228, 1157–1171. doi: 10.1016/j.jcp.2008.10.024

Frenkel, D., and Smit, B. (2002). *Understanding Molecular Simulation*. Netherlands: Elsevier.

Goligorsky, M. S., and Sun, D. (2020). Glycocalyx in Endotoxemia and Sepsis. *Am. J. Pathol.* 190, 791–798. doi: 10.1016/j.ajpath.2019.06.017

Ignarro, L. J. (1989). Biological actions and properties of endothelium-derived nitric oxide formed and released from artery and vein. *Circ. Res.* 65, 1–21. doi: 10.1161/01.res.65.1.1

Jia, W., Wang, H., Chen, M., Lu, D., Lin, L., Car, R., et al. (2020). "Pushing the Limit of Molecular Dynamics with Ab Initio Accuracy to 100 Million Atoms with Machine Learning" in *SC20: international Conference for High Performance Computing, Networking, Storage and Analysis*. (United States: ACM). 1–14.

Jiang, X. Z., Feng, M., Ventikos, Y., and Luo, K. H. (2018). Regimes of Flow over Complex Structures of Endothelial Glycocalyx: a Molecular Dynamics Simulation Study. *Sci. Rep.* 8:5732.

Jiang, X. Z., Goligorsky, M. S., and Luo, K. H. (2021). Cross Talk between Endothelial and Red Blood Cell Glycocalyces via Near-field Flow. *Biophys. J.* 120, 1–12. doi: 10.1016/j.bpj.2021.06.002

Jiang, X. Z., Gong, H., Luo, K. H., and Ventikos, Y. (2017). Large-scale molecular dynamics simulation of coupled dynamics of flow and glycocalyx: towards understanding atomic events on an endothelial cell surface. *J. R. Soc. Interface* 14:20170780. doi: 10.1098/rsif.2017.0780

Jiang, X. Z., Guo, L., Luo, K. H., and Ventikos, Y. (2020a). Membrane Deformation of Endothelial Surface Layer Interspersed with Syndecan-4: a Molecular Dynamics Study. *Ann. Biomed. Eng.* 48, 357–366. doi: 10.1007/s10439-019-02353-7

Jiang, X. Z., Luo, K. H., and Ventikos, Y. (2020b). Principal mode of Syndecan-4 mechanotransduction for the endothelial glycocalyx is a scissor-like dimer motion. *Acta Physiol.* 228:e13376.

Kang, H., Yang, J., Zhang, W., Lu, J., Ma, X., Sun, A., et al. (2021). Effect of endothelial glycocalyx on water and LDL transport through the rat abdominal aorta. *Am. J. Physiol. Heart Circ. Physiol.* 320, H1724–H1737.

Lee, T. C., Long, D. S., and Clarke, R. J. (2016). Effect of endothelial glycocalyx layer redistribution upon microvessel poroelastohydrodynamics. *J. Fluid Mech.* 798, 812–852. doi: 10.1017/jfm.2016.337

Lee, T. C., Suresh, V., and Clarke, R. J. (2020). *Influence of Endothelial Glycocalyx Layer Microstructure upon its Role as a Mechanotransducer*. United Kingdom: Cambridge University Press.

Li, Q., Luo, K. H., Kang, Q. J., He, Y. L., Chen, Q., and Liu, Q. (2016). Lattice Boltzmann methods for multiphase flow and phase-change heat transfer. *Prog. Energy Combust. Sci.* 52, 62–105.

Liu, M. B., Liu, G. R., Zhou, L. W., and Chang, J. Z. (2014). Dissipative Particle Dynamics (DPD): an Overview and Recent Developments. *Arch. Comput. Methods Eng.* 22, 529–556. doi: 10.1007/s11831-014-9124-x

O'connor, J., and Revell, A. (2019). Dynamic interactions of multiple wall-mounted flexible flaps. *J. Fluid Mech.* 870, 189–216. doi: 10.1017/jfm.2019.266

O'connor, J., Revell, A., Mandal, P., and Day, P. (2016). Application of a lattice Boltzmann-immersed boundary method for fluid-filament dynamics and flow sensing. *J. Biomech.* 49, 2143–2151. doi: 10.1016/j.jbiomech.2015.11.057

Pikoula, M., Tessier, M. B., Woods, R. J., and Ventikos, Y. (2018). Oligosaccharide model of the vascular endothelial glycocalyx in physiological flow. *Microfluid Nanofluidics* 22:21.

Pontrelli, G., Halliday, I., Spencer, T. J., Konig, C. S., and Collins, M. W. (2015). Modelling the glycocalyx-endothelium-erythrocyte interaction in the microcirculation: a computational study. *Comput. Methods Biomech. Biomed. Eng.* 18, 351–361. doi: 10.1080/10255842.2013.799146

Rapaport, D. C. (2011). *The Art of Molecular Dynamics Simulation*. United Kingdom: Cambridge University Press.

Robert, P., Limozin, L., Benoliel, A.-M., Pierres, A., and Bongrand, P. (2006). "7 - GYCOCALYX REGULATION OF CELL ADHESION" in *Principles of Cellular Engineering*. ed. M. R. King (Burlington: Academic Press). 143–169. doi: 10.1016/b978-012369392-1/50008-5

Saez, P., Gallo, D., and Morbiducci, U. (2019). Mechanotransmission of haemodynamic forces by the endothelial glycocalyx in a full-scale arterial model. *R. Soc. Open Sci.* 6:190607. doi: 10.1098/rsos.190607

Secomb, T. W., Hsu, R., and Pries, A. R. (2001). Effect of the endothelial surface layer on transmission of fluid shear stress to endothelial cells. *Biorheology* 38, 143–150.

Senftle, T. P., Hong, S., Islam, M. M., Kylasa, S. B., Zheng, Y., Shin, Y. K., et al. (2016). The ReaxFF reactive force-field: development, applications and future directions. *NPJ Comput. Mater.* 2:15011.

Tarbell, J. M., and Cancel, L. M. (2016). The glycocalyx and its significance in human medicine. *J. Intern. Med.* 280, 97–113. doi: 10.1111/joim.12465

Tarbell, J. M., and Pahakis, M. Y. (2006). Mechanotransduction and the glycocalyx. *J. Intern. Med.* 259, 339–350. doi: 10.1111/j.1365-2796.2006.01620.x

Tarbell, J. M., and Shi, Z. D. (2013). Effect of the glycocalyx layer on transmission of interstitial flow shear stress to embedded cells. *Biomech. Model Mechanobiol.* 12, 111–121. doi: 10.1007/s10237-012-0385-8

Tu, J., Yeoh, G.-H., and Liu, C.(2019). Computational Fluid Dynamics (Third Edition), Elsevier Butterworth Heinemann.

Wang, W. (2007). Change in properties of the glycocalyx affects the shear rate and stress distribution on endothelial cells. *J. Biomech. Eng.* 129, 324–329. doi: 10.1115/1.2720909

Wang, Y., Li, Z., Xu, J., Yang, C., and Karniadakis, G. E. (2019). Concurrent coupling of atomistic simulation and mesoscopic hydrodynamics for flows over soft multi-functional surfaces. *Soft Matter* 15, 1747–1757. doi: 10.1039/c8sm02170h

Weinbaum, S., Cancel, L. M., Fu, B. M., and Tarbell, J. M. (2021). The Glycocalyx and Its Role in Vascular Physiology and Vascular Related Diseases. *Cardiovasc. Eng. Technol.* 12, 37–71. doi: 10.1007/s13239-020-00485-9

Weinbaum, S., Zhang, X., Han, Y., Vink, H., and Cowin, S. C. (2003). Mechanotransduction and flow across the endothelial glycocalyx. *Proc. Natl. Acad. Sci. U. S. A.* 100, 7988–7995. doi: 10.1073/pnas.1332808100

Xu, G. K., Qian, J., and Hu, J. (2016). The glycocalyx promotes cooperative binding and clustering of adhesion receptors. *Soft Matter* 12, 4572–4583. doi: 10.1039/c5sm03139g

Yan, W., Liu, Y., and Fu, B. (2019). LBM simulations on the influence of endothelial SGL structure on cell adhesion in the micro-vessels. *Comput. Math. Appl.* 78, 1182–1193. doi: 10.1016/j.camwa.2016.07.005

Yin, X., and Zhang, J. (2013). Modeling the dynamic flow-fiber interaction for microscopic biofluid systems. *J. Biomech.* 46, 314–318. doi: 10.1016/j.jbiomech.2012.11.001

Zeng, Y., Waters, M., Andrews, A., Honarmandi, P., Ebong, E. E., Rizzo, V., et al. (2013). Fluid shear stress induces the clustering of heparan sulfate via mobility of glypican-1 in lipid rafts. *Am. J. Physiol. Heart Circ. Physiol.* 305, H811–H820.

Zhang, X., Sun, D., Song, J. W., Zullo, J., Lipphardt, M., Coneh-Gould, L., et al. (2018). Endothelial cell dysfunction and glycocalyx - A vicious circle. *Matrix Biol.* 7, 421–431. doi: 10.1016/j.matbio.2018.01.026

Zienkiewicz, O. C., Taylor, R. L., and Zhu, J. Z. (2005). The Finite Element Method: Its Basis and Fundamentals (Sixth Edition), Elsevier Butterworth Heinemann.

**Conflict of Interest:** The authors declare that the research was conducted in the absence of any commercial or financial relationships that could be construed as a potential conflict of interest.

frontiers in Cell and Developmental Biology

MINI REVIEW
published: 31 August 2021
doi: 10.3389/fcell.2021.734276

# Update on the Role of the Endothelial Glycocalyx in Angiogenesis and Vascular Inflammation

*Zhengping Hu[1,2], Issahy Cano[1,2] and Patricia A. D'Amore[1,2,3]**

*[1] Schepens Eye Research Institute of Massachusetts Eye and Ear, Boston, MA, United States, [2] Department of Ophthalmology, Harvard Medical School, Boston, MA, United States, [3] Department of Pathology, Harvard Medical School, Boston, MA, United States*

The endothelial glycocalyx is a negatively charged, carbohydrate-rich structure that arises from the luminal surface of the vascular endothelium and is comprised of proteoglycans, glycoproteins, and glycolipids. The glycocalyx, which sits at the interface between the endothelium and the blood, is involved in a wide array of physiological and pathophysiological processes, including as a mechanotransducer and as a regulator of inflammation. Most recently, components of the glycocalyx have been shown to play a key role in controlling angiogenesis. In this review, we briefly summarize the structure and function of the endothelial glycocalyx. We focus on its role and functions in vascular inflammation and angiogenesis and discuss the important unanswered questions in this field.

**Keywords: barrier, leukocytes, COVID-19, diabetes, endomucin**

OPEN ACCESS

***Edited by:***
*Ye Zeng,*
*Sichuan University, China*

***Reviewed by:***
*Christian Hiepen,*
*Freie Universität Berlin, Germany*
*Krishna Rajarathnam,*
*University of Texas Medical Branch at Galveston, United States*
*Xizhuo Jiang,*
*Northeastern University, China*

****Correspondence:***
*Patricia A. D'Amore*
*patricia_damore@meei.harvard.edu*

***Specialty section:***
*This article was submitted to Signaling, a section of the journal Frontiers in Cell and Developmental Biology*

***Received:*** *30 June 2021*
***Accepted:*** *12 August 2021*
***Published:*** *31 August 2021*

***Citation:***
*Hu Z, Cano I and D'Amore PA (2021) Update on the Role of the Endothelial Glycocalyx in Angiogenesis and Vascular Inflammation. Front. Cell Dev. Biol. 9:734276. doi: 10.3389/fcell.2021.734276*

## INTRODUCTION AND FUNCTION OF THE ENDOTHELIAL GLYCOCALYX

### Structure

The apical surface of the endothelium, which lines the entire vasculature, is covered by a non-uniform, but complex structure comprised of glycosaminoglycans (GAGs) (primarily heparan sulfate, chondroitin sulfate, and hyaluronan) glycoproteins, glycolipids, and proteoglycans (predominantly syndecans and glypican), along with adsorbed proteins [such as albumin, antithrombin III, superoxide dismutase, and a number of growth factors, e.g., vascular endothelial growth factor (VEGFs) and fibroblast growth factors (FGFs)]. This structure is collectively referred to as the glycocalyx (sugar coat": glykys = sweet, kalyx = husk). The thickness and composition of the negatively charged glycocalyx varies throughout the vasculature and is estimated to be between 0.5 and 5 μm thick, depending on methods used to measure the glycocalyx and at what level the vasculature it is being examined (Nieuwdorp et al., 2008). Interestingly, the glycocalyx has also been referred to as a "specialized extracellular matrix" (Moore et al., 2021), though one tends to think of an extracellular matrix as being on the basal side of a polarized cell layer such as the endothelium. In the broadest sense, one of the primary functions of the endothelial glycocalyx is to reduce access of circulating cells and plasma constituents to the vasculature (reviewed in Curry and Adamson, 2012).

As was once the case for the endothelium itself, the glycocalyx was initially considered to be a passive structure. However, an increasing body of research has revealed important roles for

the glycocalyx in a wide range of homeostatic processes, reviewed below. The role of glycocalyx components in various disease processes and the effect of pathologies on the glycocalyx is discussed in section "Modulation of Glycocalyx Under Inflammation and Other Pathological Conditions."

## Physiologic Functions

### Anti-inflammation

Net negatively charged cells such as white and red blood cells and platelets are repelled from the glycocalyx due to its negative charge. Interactions between leukocytes and endothelial cell (EC) are mediated by adhesion molecules that direct leukocyte rolling along and adhesion to the endothelial surface. Under resting (non-activated) conditions these selectins and integrins are expressed at low or non-detectable levels and are masked by the overlying glycocalyx (Reitsma et al., 2007). The specific glycocalyx constituents responsible for preventing leukocyte adhesion have not been fully elucidated. At the level of the mouse intestinal mesentery, heparinase treatment results in increased leukocyte adhesion, pointing to a role for Heparan sulfate proteoglycans (HSPGs) (Mulivor and Lipowsky, 2002). In addition, using human umbilical vein ECs in culture, our group has shown that the knockdown of endomucin (EMCN) using siRNA leads to increased leukocyte adhesion in non-activated EC and that the adhesion was mediated by constitutively expressed I-CAM (Zahr et al., 2016). In addition, using the same system, the overexpression of EMCN in tumor necrosis factor-alpha (TNF-α) (activated) EC was able to significantly suppress leukocyte adherence as did adenoviral expression of EMCN in a mouse model of ocular inflammation.

### Anti-thrombosis

A number of molecules bound to the glycocalyx account for its anti-coagulant and anti-thrombotic properties, including anti-thrombin III, tissue factor pathway inhibitor, and dermatan sulfate (reviewed in Potje et al., 2020). In addition, thrombomodulin, one of the glycocalyx proteoglycans, is another major contributor to this activity, acting via binding to thrombin (reviewed in Martin et al., 2013).

### Permeability Control

Under normal conditions, the glycocalyx forms a barrier against vascular permeability, partly by acting as a negatively charged molecular sieve (Alphonsus and Rodseth, 2014). The glycocalyx impacts vascular permeability via its three-dimensional structure—interactions among the various components generate a "mesh-like" structure that can control passage of molecules based on their size. Its tight mesh structure excludes macromolecules greater than 70 kDa (Pries et al., 2000). In addition, the glycocalyx structure is negatively charged and thus can limit the transit of molecules based on charge. For instance, the glycocalyx is the primary site for the restriction of the passage of albumin across the endothelium (Curry and Adamson, 2012), which although net negatively charged binds to the glycocalyx due its amphoteric characteristics (reviewed in Aldecoa et al., 2020).

### Mechanosensor

Heparan sulfate has been demonstrated to be a primary sensor of the directionality of shear stress. Exposure of cultured EC to heparinase increased the speed of flow-induced endothelial migration but prevented shear-stress stimulated directionality of migration and recruitment of phosphorylated focal adhesion kinase (Moon et al., 2005). The glycocalyx also transmits the effects of shear stress on endothelial nitric oxide synthase (eNOS), which is localized to caveolae on the endothelial surface. Enzymatic removal of heparan sulfate prevents sheer stress-induced NO production (Pahakis et al., 2007). Recent evidence indicates that it is heparan sulfate in the form of glypican-1 that mediates this signal, as depletion of glypican-1 using siRNA prevent the shear stress activation of eNOS (Ebong et al., 2014). Using syndecan-4 core protein as a model, a large-scale molecular dynamics computational experiment indicated the syndecan-4 core protein manifests as a scissors-like motion and transmits force as a main pathway of signal transmission. While blood flow velocity changes the shedding of proteoglycan sugar chain, its functional role is to protect the core protein from severe conformational changes (Jiang et al., 2020). More mechanistic roles of glycocalyx in mechanosensing and transduction have been thoroughly reviewed recently (Zeng et al., 2018).

### Membrane Shape Regulation

A number of the proteoglycan core proteins span the plasma membrane and associate with the endothelial cortical cytoskeleton via linker proteins such as talin and dystonin, thus communicating extracellular forces though the cell (reviewed in Cosgun et al., 2020). Conversely, the cortical cytoskeleton can alter the conformation of the glycocalyx so that polymerized actin leads to a flattened glycocalyx and actin disassembly results in a more extended glycocalyx. A recent study has demonstrated cooperation between intracellular cytoskeletal components and constituents of the glycocalyx in how cells alter their shape in response to their microenvironment. Specifically, it was shown that "polymers" formed by glycocalyx mucins and polysaccharides "generate an entropic bending force to favor formation of curved membrane structures" (Shurer et al., 2019). The authors speculate that the morphological impact of the glycocalyx would have "broad consequences on membrane processes, ranging from absorption and secretion to cellular communication, signaling, and motility."

### Regulation of Growth Factor, Cytokine, and Chemokine Signaling

With heparan sulfate comprising the largest proportion of the glycocalyx (Reitsma et al., 2007) and knowing the significant effect that heparan sulfate has on the bioavailability, activity, and stability of a wide number of growth factors (Ricard-Blum and Lisacek, 2017), it is not surprising that the glycocalyx has an essential role in vessel formation and maturation. For example, heparan sulfate containing GAGs have been shown to interact with both the angiopoietins and Tie receptors as well as serving as a ligand for Tie1, enhancing signaling and cell survival (Griffin et al., 2021). HSPGs interact with VEGF and promotes angiogenesis through increasing VEGF levels in the

extracellular microenvironment and fine-tuning the interaction of VEGF with its receptor and co-receptor (Nagarajan et al., 2018). Another membrane glycoprotein, neuropilin, is known to function as a co-receptor for VEGF receptor 2 (VEGFR2) and guide developmental angiogenesis (Gelfand et al., 2014). Using zebrafish as a model, it was demonstrated that fish lacking perlecan failed to develop primary intersegmental vessel sprouts (Zoeller et al., 2008). In addition, work from our group has identified a role for EMCN, a type 1 transmembrane glycoprotein abundantly expressed by venous and capillary endothelium, in the regulation of VEGFR2 signaling (see Part 2 below on glycocalyx and angiogenesis). Chemokines-GAG interactions mediates chemokines membrane localization and surface presentation and fine-tune the function of chemokines (Proudfoot et al., 2017). Interaction between CXCL8 and extracellular HSPGs regulates the leukocyte recruitment and transmigration (Sarris et al., 2012).

### Regulation of the Glycocalyx

One major regulator of glycocalyx thickness is flow, such that exposure of culture EC to laminar flow leads to the increased synthesis of hyaluronan (Maroski et al., 2011). Whereas disturbed flow induces an approximately 50% decrease in endothelial glycocalyx compared to uniform laminar flow *in vitro* (Mensah et al., 2020). This effect of shear stress on the glycocalyx becomes particularly relevant in the pathogenesis of atherosclerosis (see Part 3). Exposure to pro-inflammatory cytokines leads to a dramatic reduction in the glycocalyx, largely by endothelial-derived metalloproteinase-mediated shedding (Yang et al., 2020) as well as by heparinase secreted by mast cells and hyaluronidase produced by the EC (Bourguignon and Flamion, 2016).

## THE GLYCOCALYX IN ANGIOGENESIS

## Role of Glycocalyx in Angiogenesis

### Normal Angiogenesis

Angiogenesis is the formation of blood vessels from pre-existing vessels, and components of the glycocalyx mediate elements of angiogenesis in diverse and multifaceted ways. GAGs play an active role in regulating angiogenesis. In general, the gel-like composition generated by the presence GAGs, in combination with identified cytokine interactions, mainly FGFs and VEGF, facilitate growth factor signaling in ECs by influencing their bioavailability, local concentrations, and stability (Muramatsu and Muramatsu, 2008; Huynh et al., 2012).

Proteoglycans have been implicated in modulating angiogenesis more specifically by influencing cell proliferation and migration under both normal and pathologic conditions (Iozzo and Sanderson, 2011; Gubbiotti et al., 2020). Heparan sulfate is a known regulator of angiogenesis, and its 6-O-sulfation specifically has been reported to modulate VEGF165-induced angiogenesis (Stringer, 2006). VEGF, a well-studied, angiogenic factor, is produced as a number of splice variations, which differ in their ability to bind to heparan sulfate proteoglycan. Whereas VEGF120 does not contain any heparan sulfate binding domains, it is freely soluble upon its secretions from cells, VEGF188, on the other hand, binds very tightly to heparan sulfate and remains cell-associated upon release, and VEGF164 displays intermediate properties. Mice genetically engineered to express only VEGF120, that is lacking both heparan sulfate binding isoforms, are lethal perinatally due to defective lung development (Galambos et al., 2002), indicating the importance of growth factor association with the glycocalyx to their function.

Members of syndecan family of heparan sulfate proteoglycans have been studied for their diverse roles in angiogenesis regulation. Various syndecans have distinct function in promoting or inhibiting angiogenesis depending on whether they are present on the EC extracellular membrane or shed (De Rossi and Whiteford, 2013; De Rossi et al., 2014). Syndecan-1 knockdown in both *in vivo* and *in vitro* has been shown to interrupt VEGFR2 internalization by preventing clathrin-mediated endocytosis (Jing et al., 2016). A decrease in VEGFR2 expression following syndecan-1 depletion has also been reported (Lamorte et al., 2012). Syndecan-2 is necessary for angiogenesis, potentially acting as a co-receptor for VEGF signaling, giving it a critical role in promoting angiogenesis whereas the shed variant of the protein plays an active role in inhibiting cell migration (Essner et al., 2006; De Rossi et al., 2014). Similarly, syndecan-4 binds VEGF "sequestering" and preventing it from exerting its angiogenic signaling (Lambert et al., 2020).

Hyaluronan (HA), an abundant glycocalyx GAG, exerts an anti-angiogenic effect in its native form, whereas its degradation products induce angiogenesis by activating HA receptors CD44 and CD168 (West and Kumar, 1989; Slevin et al., 2007; Ghose et al., 2018). HA has also been reported to prevent the binding of VEGF to its primary signaling receptor VEGFR2 in a sulfate-dependent manner (Rother et al., 2017).

Another prominent glycocalyx component is EMCN, a membrane spanning mucin-type glycoprotein that has been shown to be involved for VEGFR2 signaling. Initial studies demonstrated that the knockdown of EMCN in the developing vasculature led to impaired vascular development and reduced tip cell activity (Park-Windhol et al., 2017). Investigation of the mechanism underlying this effect using primary human retinal capillary EC in culture revealed that siEMCN knockdown of EMCN blocked VEGF-stimulated proliferation, migration, and tube formation. Subsequent studies showed that the lack of EMCN leads to a failure of VEGF-activated VEGFR2 to internalize, thereby preventing the sustained intracellular signaling that is necessary for VEGF to stimulate endothelial function. EMCN, however, is itself not internalized with VEGFR2 during normal signaling (LeBlanc et al., 2019). Structure-function analysis using EMCN truncation mutants has revealed the minimum extracellular 21–121 amino acids of EMCN necessary for modulating VEGFR2 signaling and indicated also that the activity is dependent on N-glycosylation (Hu et al., 2020).

### Pathologic Angiogenesis

Since the first description of the animal glycocalyx by Martínez-Palomo (1970), there has been growing interest in the role of the glycocalyx, including in pathologic angiogenesis. Recent reports demonstrate that the glycocalyx is important for not only developmental angiogenesis and its maintenance, but for

cancer progression secondary to its vascularization as well. Angiogenesis is necessary for tumor growth beyond the limits of diffusion. The modification of the glycocalyx structure of cancer cells has been suggested to provide tumors with the ability to survive and overcome vascular limitations, for example by mimicking the vasculogenic nature of ECs with 3-dimentional organization, while lacking EC markers such as CD31 and CD34 (Tachi et al., 2019). FGF and VEGF contain heparan-binding domains and their signal transduction depends on its sulfation. Alteration of heparan sulfate's ability to bind FGF and VEGF has been reported to reduce angiogenic signal transduction and weaken the vascular foundation for tumors (Fuster et al., 2007). As the specific components of the glycocalyx are actively involved in aberrant angiogenesis, they may represent promising targets for therapy.

The stability of the vasculature is also dependent on the integrity of the glycocalyx layer as seen in diabetic retinopathy. Hyperglycemia has been reported induce the shedding of various components of the glycocalyx, disrupting EC function by increasing permeability in glomerular ECs (Singh et al., 2011). Loss of EMCN, for example, has been suggested to be associated with diabetic retinopathy and the overexpression of EMCN leads to the restoration of the glycocalyx and the related EC function in streptozotocin-induced diabetic rats (Niu et al., 2019). VEGF165b, a non-angiogenic isoform of VEGFA, was reported to restore the glycocalyx and ultimately the endothelium after diabetic damage in isolated diabetic human and rat glomeruli. VEGF165b shares the protective prosurvival and antiapoptotic signaling of canonical VEGF isoforms and was reported to restore the glycocalyx in short and long-term conditions (Oltean et al., 2015).

## MODULATION OF GLYCOCALYX UNDER INFLAMMATION AND OTHER PATHOLOGICAL CONDITIONS

As described above, the glycocalyx protects endothelial cells by acting as a barrier between circulating blood cells and the endothelium, regulating permeability, controlling nitric oxide production, and functioning as a mechanosensor. Systemic and local inflammatory responses, including diabetes, atherosclerosis, surgical ischemia/reperfusion injury, and sepsis, have been shown to cause rapid loss of glycocalyx and its activities, both directly and indirectly. A summary of the modulation of glycocalyx under activated conditions is shown in **Figure 1**.

### Inflammation

The vascular endothelium is the earliest site of involvement in the systemic inflammatory response syndrome (Becker et al., 2010). Proinflammatory stimuli lead to dramatic alterations in the thickness of the glycocalyx. For instance, during sepsis the thickness of the glycocalyx decreases by up to 66% *in vivo*, measured by intravital microscopy (Kennett and Davies, 2007). Shedding of the glycocalyx during inflammation has been reported in many studies and its breakdown is accompanied by shedding of one or more glycocalyx components into circulation including syndecan-1, heparan sulfate, and HA (Dogne and Flamion, 2020). Moreover, markers of endothelial glycocalyx shedding, like heparan sulfate and syndecan-1, have been found increased in both plasma and urine in sepsis patients (Schmidt et al., 2016), and shown to correlate with disease severity (Anand et al., 2016). Increased plasma levels of endothelial surface layer components in septic patients are positively correlated with increased mortality (Becker et al., 2010).

The damage to the endothelial glycocalyx noted during inflammation is initiated by the actions of TNF-α, bacterial lipopolysaccharides and other cytokines on the endothelium, which leads to the production and secretion of endothelial-derived metalloproteinases and heparinases that mediate the shedding of glycocalyx (Tarbell and Cancel, 2016). In addition, mast cells are activated by TNF-α and release cytokines, proteases, histamine, and heparinase, further degrading the glycocalyx. Concomitant with the cytokine-induced degradation of the glycocalyx exposing constitutively expressed adhesion molecules including I-CAM, the cytokines also stimulate the expression of selectins and integrins to facilitate rolling and adhesion of monocytes and polynuclear neutrophils followed by diapedesis (Nelson et al., 2008). With the altered glycocalyx no longer able to perform its normal functions, there is increased vascular permeability, tissue edema, increased leukocyte adhesion, platelet aggregation, and dysregulated vasodilation (Becker et al., 2015).

### Diabetes

Diabetes is another major pathology in which the degradation of the glycocalyx has been implicated, as demonstrated in type 1 and type 2 diabetics in both animal models as well as in humans (Broekhuizen et al., 2010; Leskova et al., 2019). Experimental evidence indicates the involvement of reactive oxygen species, advanced glycation end products (AGEs), and activation of the sheddases heparanase and hyaluronidase in glycocalyx deterioration during diabetes (Dogne et al., 2018). Overproduction of superoxide anion results in increased oxidative stress, which leads to a depolymerization of GAGs, particularly HA, as well as AGE formation (Kennett and Davies, 2009). AGE levels were significantly higher in vitreous and serum of patients with diabetic retinopathy compared to normal controls (Sebag et al., 1994) and AGEs have been shown to promote the degradation of HA *in vivo* (Katsumura et al., 2004). Heparinase, secreted by macrophages and activated podocytes, is also well documented to be involved in the process of endothelial glycocalyx degradation and diabetic nephropathy (Boels et al., 2016), and, matrix metalloproteinases (MMPs), including MMP-2 and MMP-9, have been implicated in glycocalyx changes seen during the progression of diabetic retinopathy (Eshaq et al., 2017). In immortalized human glomerular EC, IL-1β and TNF-α increased MMP-9 mediated shedding of cell surface heparan sulfate and syndecan-4, measured by western blot (Ramnath et al., 2014). In addition, there are increased levels of plasma hyaluronidase, as measured by *ex vivo* enzymatic activity, in the streptozotocin-induced mice diabetes model. Deficiency of hyaluronidase in knockout mice resulted in a thicker glycocalyx and protection from HA shedding (Dogne et al., 2016).

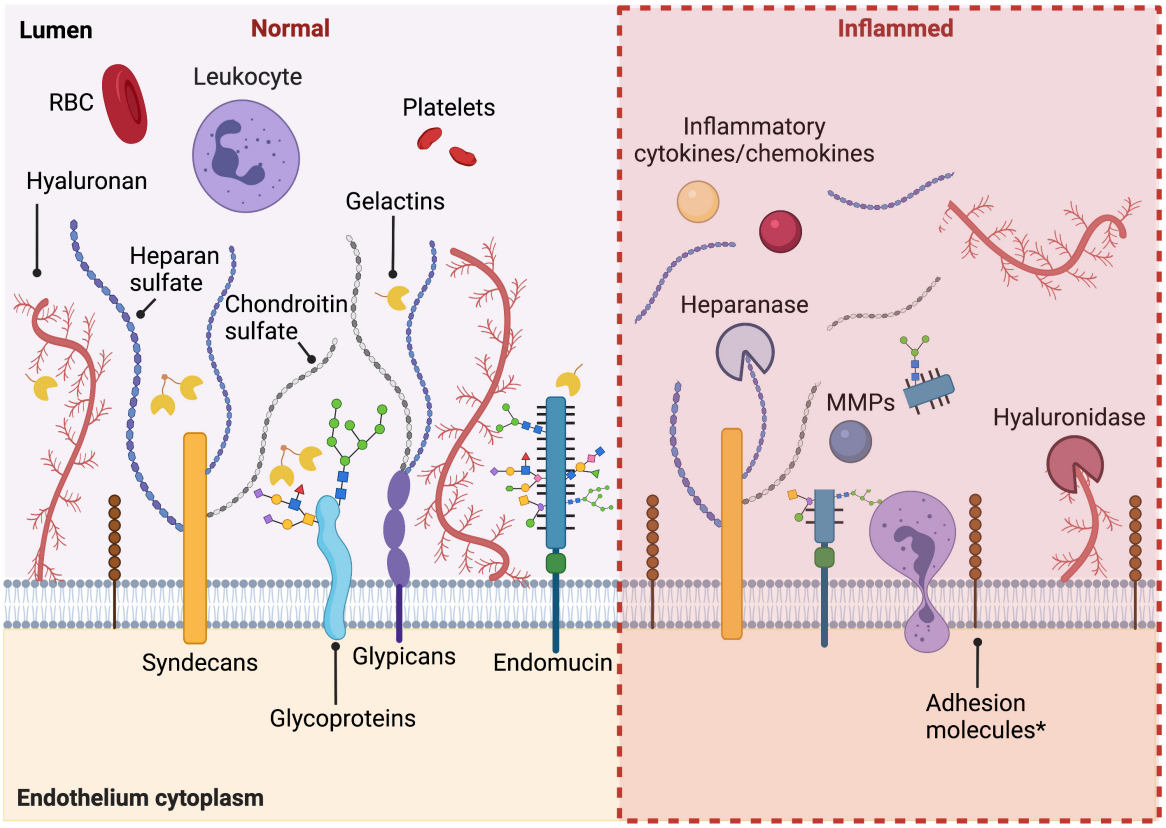


**FIGURE 1 |** Summary of the modulation of glycocalyx under activated conditions. Under healthy conditions, intact endothelial glycocalyx maintains endothelium homeostasis, regulating permeability, and plays an anti-inflammation and anti-thrombosis role. When activated in pathological conditions, during inflammation, diabetes, and other pathological conditions, there is increased shedding of the glycocalyx. An increased expression of adhesion molecules under inflammatory conditions is also observed. Figure was created with BioRender.com.

## COVID-19

Endothelial glycocalyx damage has been recently reported in COVID-19 patients (Buijsers et al., 2020; Fraser et al., 2020; Stahl et al., 2020; Rovas et al., 2021). A number of the features of COVID-19 that are not been seen in other viral infections including, asymptomatic pneumonia, acute respiratory distress syndrome (Kazory et al., 2020), disseminated intravascular coagulation (Guan et al., 2020), rapid progression, and sudden death associated with thromboembolism, all appear to be by-products of known glycocalyx functions. Thus, it has been suggested that COVID-19 is an endothelial disease, particularly in its later stages, which often involve a "cytokine storm" that shifts endothelial functions into a "defensive mode" (Libby and Luscher, 2020). In light of the role of the endothelial glycocalyx in vascular homeostasis, including vascular permeability and vessel tone as well as an anti-thrombotic and anti-inflammatory (Yang et al., 2020), it appears that levels of glycocalyx components may be employed as a biomarker for the severity of COVID-19 and as an indicator of therapeutic response. Patients on mechanical ventilation had severe damage to the glycocalyx, with the glycocalyx being thinner as measured by perfusion boundary region and higher blood levels of shed glycocalyx constituents such as hyaluronic acid (Ding et al., 2020), chondroitin sulfate (Fraser et al., 2020), and syndecan-1, a transmembrane heparan sulfate proteoglycan (Rovas et al., 2021). Levels of heparanase, known to degrade the endothelial glycocalyx, were found to be considerably higher in COVID-19 patients than healthy controls and the levels of heparanase activity are linked to the severity of COVID-19 disease (Buijsers et al., 2020).

## UNANSWERED QUESTION AND CHALLENGES

Our understanding of the structure and function of the glycocalyx has evolved tremendously over the last few decades. One challenge is obtaining proper visualization of the glycocalyx. Early imaging of the structure led to the underestimation of the thickness of the glycocalyx layer (Reitsma et al., 2007; Dane et al., 2015). The glycocalyx structure is too fragile for common sample preparation techniques, and degradation and dehydration of the layer is common. Alternatives methods for preparation, such as rapid freezing, have provided more accurate dimensions for the glycocalyx, 100-fold thicker in some regions than previously reported (Ebong et al., 2011).

Despite increasing evidence of the biological relevance of endothelial glycocalyx in various pathological conditions, detailed mechanisms of its role and regulation are difficult to dissect at the molecular level. Although new scientific techniques have allowed for a better understanding and detection of endothelial glycocalyx derangement and more components of glycocalyx are being used as markers in pathological conditions, the intrinsic complexity of the glycosylation process and the enormous diversity of glycan structures combined with the technical limitations of the current experimental tools for modulating the structure and expression of glycoproteins are among the challenges faced in the study of the endothelial glycocalyx (de Haas et al., 2020).

## AUTHOR CONTRIBUTIONS

ZH, IC, and PD'A shared equally in writing the manuscript. All authors contributed to the article and approved the submitted version.

## FUNDING

This work was supported by the NIH/NEI R01 EY026539 and NIH/NEI T32 EY007145 (to PD'A) and the Knights Templar Pediatric Ophthalmology Competitive Renewal Grant (to ZH).

## REFERENCES

Aldecoa, C., Llau, J. V., Nuvials, X., and Artigas, A. (2020). Role of albumin in the preservation of endothelial glycocalyx integrity and the microcirculation: a review. *Ann. Intensive Care* 10:85. doi: 10.1186/s13613-020-00697-1

Alphonsus, C. S., and Rodseth, R. N. (2014). The endothelial glycocalyx: a review of the vascular barrier. *Anaesthesia* 69, 777–784. doi: 10.1111/anae.12661

Anand, D., Ray, S., Srivastava, L. M., and Bhargava, S. (2016). Evolution of serum hyaluronan and syndecan levels in prognosis of sepsis patients. *Clin. Biochem.* 49, 768–776. doi: 10.1016/j.clinbiochem.2016.02.014

Becker, B. F., Chappell, D., Bruegger, D., Annecke, T., and Jacob, M. (2010). Therapeutic strategies targeting the endothelial glycocalyx: acute deficits, but great potential. *Cardiovasc. Res.* 87, 300–310. doi: 10.1093/cvr/cvq137

Becker, B. F., Jacob, M., Leipert, S., Salmon, A. H., and Chappell, D. (2015). Degradation of the endothelial glycocalyx in clinical settings: searching for the sheddases. *Br. J. Clin. Pharmacol.* 80, 389–402. doi: 10.1111/bcp.12629

Boels, M. G., Avramut, M. C., Koudijs, A., Dane, M. J., Lee, D. H., van der Vlag, J., et al. (2016). Atrasentan reduces albuminuria by restoring the glomerular endothelial glycocalyx barrier in diabetic nephropathy. *Diabetes* 65, 2429–2439. doi: 10.2337/db15-1413

Bourguignon, V., and Flamion, B. (2016). Respective roles of hyaluronidases 1 and 2 in endogenous hyaluronan turnover. *FASEB J.* 30, 2108–2114. doi: 10.1096/fj.201500178R

Broekhuizen, L. N., Lemkes, B. A., Mooij, H. L., Meuwese, M. C., Verberne, H., Holleman, F., et al. (2010). Effect of sulodexide on endothelial glycocalyx and vascular permeability in patients with type 2 diabetes mellitus. *Diabetologia* 53, 2646–2655. doi: 10.1007/s00125-010-1910-x

Buijsers, B., Yanginlar, C., de Nooijer, A., Grondman, I., Maciej-Hulme, M. L., Jonkman, I., et al. (2020). Increased plasma heparanase activity in COVID-19 patients. *Front. Immunol.* 11:575047. doi: 10.3389/fimmu.2020.575047

Cosgun, Z. C., Fels, B., and Kusche-Vihrog, K. (2020). Nanomechanics of the endothelial glycocalyx: from structure to function. *Am. J. Pathol.* 190, 732–741. doi: 10.1016/j.ajpath.2019.07.021

Curry, F. E., and Adamson, R. H. (2012). Endothelial glycocalyx: permeability barrier and mechanosensor. *Ann. Biomed. Eng.* 40, 828–839. doi: 10.1007/s10439-011-0429-8

Dane, M. J., van den Berg, B. M., Lee, D. H., Boels, M. G., Tiemeier, G. L., Avramut, M. C., et al. (2015). A microscopic view on the renal endothelial glycocalyx. *Am. J. Physiol. Renal Physiol.* 308, F956–F966. doi: 10.1152/ajprenal.00532.2014

de Haas, P., Hendriks, W., Lefeber, D. J., and Cambi, A. (2020). Biological and technical challenges in unraveling the role of N-glycans in immune receptor regulation. *Front. Chem.* 8:55. doi: 10.3389/fchem.2020.00055

De Rossi, G., and Whiteford, J. R. (2013). A novel role for syndecan-3 in angiogenesis. *F1000Res.* 2:270. doi: 10.12688/f1000research.2-270.v1

De Rossi, G., Evans, A. R., Kay, E., Woodfin, A., McKay, T. R., Nourshargh, S., et al. (2014). Shed syndecan-2 inhibits angiogenesis. *J. Cell Sci.* 127(Pt 21), 4788–4799. doi: 10.1242/jcs.153015

Ding, M., Zhang, Q., Li, Q., Wu, T., and Huang, Y. Z. (2020). Correlation analysis of the severity and clinical prognosis of 32 cases of patients with COVID-19. *Respir. Med.* 167:105981. doi: 10.1016/j.rmed.2020.105981

Dogne, S., and Flamion, B. (2020). Endothelial glycocalyx impairment in disease: focus on hyaluronan shedding. *Am. J. Pathol.* 190, 768–780. doi: 10.1016/j.ajpath.2019.11.016

Dogne, S., Flamion, B., and Caron, N. (2018). Endothelial glycocalyx as a shield against diabetic vascular complications: involvement of hyaluronan and hyaluronidases. *Arterioscler. Thromb. Vasc. Biol.* 38, 1427–1439. doi: 10.1161/ATVBAHA.118.310839

Dogne, S., Rath, G., Jouret, F., Caron, N., Dessy, C., and Flamion, B. (2016). Hyaluronidase 1 deficiency preserves endothelial function and glycocalyx integrity in early streptozotocin-induced diabetes. *Diabetes* 65, 2742–2753. doi: 10.2337/db15-1662

Ebong, E. E., Lopez-Quintero, S. V., Rizzo, V., Spray, D. C., and Tarbell, J. M. (2014). Shear-induced endothelial NOS activation and remodeling via heparan sulfate, glypican-1, and syndecan-1. *Integr. Biol.* 6, 338–347. doi: 10.1039/c3ib40199e

Ebong, E. E., Macaluso, F. P., Spray, D. C., and Tarbell, J. M. (2011). Imaging the endothelial glycocalyx in vitro by rapid freezing/freeze substitution transmission electron microscopy. *Arterioscler. Thromb. Vasc. Biol.* 31, 1908–1915. doi: 10.1161/ATVBAHA.111.225268

Eshaq, R. S., Aldalati, A. M. Z., Alexander, J. S., and Harris, N. R. (2017). Diabetic retinopathy: breaking the barrier. *Pathophysiology* 24, 229–241. doi: 10.1016/j.pathophys.2017.07.001

Essner, J. J., Chen, E., and Ekker, S. C. (2006). Syndecan-2. *Int. J. Biochem. Cell Biol.* 38, 152–156. doi: 10.1016/j.biocel.2005.08.012

Fraser, D. D., Patterson, E. K., Slessarev, M., Gill, S. E., Martin, C., Daley, M., et al. (2020). Endothelial injury and glycocalyx degradation in critically ill coronavirus disease 2019 patients: implications for microvascular platelet aggregation. *Crit. Care Explor.* 2:e0194. doi: 10.1097/CCE.0000000000000194

Fuster, M. M., Wang, L., Castagnola, J., Sikora, L., Reddi, K., Lee, P. H., et al. (2007). Genetic alteration of endothelial heparan sulfate selectively inhibits tumor angiogenesis. *J. Cell Biol.* 177, 539–549. doi: 10.1083/jcb.200610086

Galambos, C., Ng, Y. S., Ali, A., Noguchi, A., Lovejoy, S., D'Amore, P. A., et al. (2002). Defective pulmonary development in the absence of heparin-binding vascular endothelial growth factor isoforms. *Am. J. Respir. Cell Mol. Biol.* 27, 194–203. doi: 10.1165/ajrcmb.27.2.4703

Gelfand, M. V., Hagan, N., Tata, A., Oh, W. J., Lacoste, B., Kang, K. T., et al. (2014). Neuropilin-1 functions as a VEGFR2 co-receptor to guide developmental angiogenesis independent of ligand binding. *Elife* 3:e03720. doi: 10.7554/eLife.03720

Ghose, S., Biswas, S., Datta, K., and Tyagi, R. K. (2018). Dynamic hyaluronan drives liver endothelial cells towards angiogenesis. *BMC Cancer* 18:648. doi: 10.1186/s12885-018-4532-1

Griffin, M. E., Sorum, A. W., Miller, G. M., Goddard, W. A. III, and Hsieh-Wilson, L. C. (2021). Sulfated glycans engage the Ang-Tie pathway to regulate vascular development. *Nat. Chem. Biol.* 17, 178–186. doi: 10.1038/s41589-020-00657-7

Guan, W. J., Ni, Z. Y., Hu, Y., Liang, W. H., Ou, C. Q., He, J. X., et al. (2020). Clinical characteristics of coronavirus disease 2019 in China. *N. Engl. J. Med.* 382, 1708–1720. doi: 10.1056/NEJMoa2002032

Gubbiotti, M. A., Buraschi, S., Kapoor, A., and Iozzo, R. V. (2020). Proteoglycan signaling in tumor angiogenesis and endothelial cell autophagy. *Semin. Cancer Biol.* 62, 1–8. doi: 10.1016/j.semcancer.2019.05.003

Hu, Z., Cano, I., Saez-Torres, K. L., LeBlanc, M. E., Saint-Geniez, M., Ng, Y. S., et al. (2020). Elements of the endomucin extracellular domain essential for VEGF-induced VEGFR2 activity. *Cells* 9:1413. doi: 10.3390/cells9061413

Huynh, M. B., Morin, C., Carpentier, G., Garcia-Filipe, S., Talhas-Perret, S., Barbier-Chassefiere, V., et al. (2012). Age-related changes in rat myocardium involve altered capacities of glycosaminoglycans to potentiate growth factor functions and heparan sulfate-altered sulfation. *J. Biol. Chem.* 287, 11363–11373. doi: 10.1074/jbc.M111.335901

Iozzo, R. V., and Sanderson, R. D. (2011). Proteoglycans in cancer biology, tumour microenvironment and angiogenesis. *J. Cell. Mol. Med.* 15, 1013–1031. doi: 10.1111/j.1582-4934.2010.01236.x

Jiang, X. Z., Luo, K. H., and Ventikos, Y. (2020). Principal mode of Syndecan-4 mechanotransduction for the endothelial glycocalyx is a scissor-like dimer motion. *Acta Physiol.* 228:e13376. doi: 10.1111/apha.13376

Jing, Z., Wei-Jie, Y., Yi-Feng, Z. G., and Jing, H. (2016). Downregulation of Syndecan-1 induce glomerular endothelial cell dysfunction through modulating internalization of VEGFR-2. *Cell. Signal.* 28, 826–837. doi: 10.1016/j.cellsig.2016.04.001

Katsumura, C., Sugiyama, T., Nakamura, K., Obayashi, H., Hasegawa, G., Oku, H., et al. (2004). Effects of advanced glycation end products on hyaluronan photolysis: a new mechanism of diabetic vitreopathy. *Ophthalmic Res.* 36, 327–331. doi: 10.1159/000081635

Kazory, A., Ronco, C., and McCullough, P. A. (2020). SARS-CoV-2 (COVID-19) and intravascular volume management strategies in the critically ill. *Proc. (Bayl. Univ. Med. Cent.)* 33, 370–375. doi: 10.1080/08998280.2020.1754700

Kennett, E. C., and Davies, M. J. (2007). Degradation of matrix glycosaminoglycans by peroxynitrite/peroxynitrous acid: evidence for a hydroxyl-radical-like mechanism. *Free Radic. Biol. Med.* 42, 1278–1289. doi: 10.1016/j.freeradbiomed.2007.01.030

Kennett, E. C., and Davies, M. J. (2009). Glycosaminoglycans are fragmented by hydroxyl, carbonate, and nitrogen dioxide radicals in a site-selective manner: implications for peroxynitrite-mediated damage at sites of inflammation. *Free Radic. Biol. Med.* 47, 389–400. doi: 10.1016/j.freeradbiomed.2009.05.002

Lambert, J., Makin, K., Akbareian, S., Johnson, R., Alghamdi, A. A. A., Robinson, S. D., et al. (2020). ADAMTS-1 and syndecan-4 intersect in the regulation of cell migration and angiogenesis. *J. Cell Sci.* 133:jcs235762. doi: 10.1242/jcs.235762

Lamorte, S., Ferrero, S., Aschero, S., Monitillo, L., Bussolati, B., Omede, P., et al. (2012). Syndecan-1 promotes the angiogenic phenotype of multiple myeloma endothelial cells. *Leukemia* 26, 1081–1090. doi: 10.1038/leu.2011.290

LeBlanc, M. E., Saez-Torres, K. L., Cano, I., Hu, Z., Saint-Geniez, M., Ng, Y. S., et al. (2019). Glycocalyx regulation of vascular endothelial growth factor receptor 2 activity. *FASEB J.* 33, 9362–9373. doi: 10.1096/fj.201900011R

Leskova, W., Pickett, H., Eshaq, R. S., Shrestha, B., Pattillo, C. B., and Harris, N. R. (2019). Effect of diabetes and hyaluronidase on the retinal endothelial glycocalyx in mice. *Exp. Eye Res.* 179, 125–131. doi: 10.1016/j.exer.2018.11.012

Libby, P., and Luscher, T. (2020). COVID-19 is, in the end, an endothelial disease. *Eur. Heart J.* 41, 3038–3044. doi: 10.1093/eurheartj/ehaa623

Maroski, J., Vorderwulbecke, B. J., Fiedorowicz, K., Da Silva-Azevedo, L., Siegel, G., Marki, A., et al. (2011). Shear stress increases endothelial hyaluronan synthase 2 and hyaluronan synthesis especially in regard to an atheroprotective flow profile. *Exp. Physiol.* 96, 977–986. doi: 10.1113/expphysiol.2010.056051

Martin, F. A., Murphy, R. P., and Cummins, P. M. (2013). Thrombomodulin and the vascular endothelium: insights into functional, regulatory, and therapeutic aspects. *Am. J. Physiol. Heart Circ. Physiol.* 304, H1585–H1597. doi: 10.1152/ajpheart.00096.2013

Martínez-Palomo, A. (1970). *The Surface Coats of Animal Cells. International Review of Cytology-A Survey of Cell Biology*, Vol. 29, 29–75.

Mensah, S. A., Nersesyan, A. A., Harding, I. C., Lee, C. I., Tan, X., Banerjee, S., et al. (2020). Flow-regulated endothelial glycocalyx determines metastatic cancer cell activity. *FASEB J.* 34, 6166–6184. doi: 10.1096/fj.201901920R

Moon, J. J., Matsumoto, M., Patel, S., Lee, L., Guan, J. L., and Li, S. (2005). Role of cell surface heparan sulfate proteoglycans in endothelial cell migration and mechanotransduction. *J. Cell. Physiol.* 203, 166–176. doi: 10.1002/jcp.20220

Moore, K. H., Murphy, H. A., and George, E. M. (2021). The glycocalyx: a central regulator of vascular function. *Am. J. Physiol. Regul. Integr. Comp. Physiol.* 320, R508–R518. doi: 10.1152/ajpregu.00340.2020

Mulivor, A. W., and Lipowsky, H. H. (2002). Role of glycocalyx in leukocyte-endothelial cell adhesion. *Am. J. Physiol. Heart Circ. Physiol.* 283, H1282–H1291. doi: 10.1152/ajpheart.00117.2002

Muramatsu, T., and Muramatsu, H. (2008). Glycosaminoglycan-binding cytokines as tumor markers. *Proteomics* 8, 3350–3359. doi: 10.1002/pmic.200800042

Nagarajan, A., Malvi, P., and Wajapeyee, N. (2018). Heparan sulfate and heparan sulfate proteoglycans in cancer initiation and progression. *Front. Endocrinol.* 9:483. doi: 10.3389/fendo.2018.00483

Nelson, A., Berkestedt, I., Schmidtchen, A., Ljunggren, L., and Bodelsson, M. (2008). Increased levels of glycosaminoglycans during septic shock: relation to mortality and the antibacterial actions of plasma. *Shock* 30, 623–627. doi: 10.1097/SHK.0b013e3181777da3

Nieuwdorp, M., Meuwese, M. C., Mooij, H. L., Ince, C., Broekhuizen, L. N., Kastelein, J. J., et al. (2008). Measuring endothelial glycocalyx dimensions in humans: a potential novel tool to monitor vascular vulnerability. *J. Appl. Physiol.* 104, 845–852. doi: 10.1152/japplphysiol.00440.2007

Niu, T., Zhao, M., Jiang, Y., Xing, X., Shi, X., Cheng, L., et al. (2019). Endomucin restores depleted endothelial glycocalyx in the retinas of streptozotocin-induced diabetic rats. *FASEB J.* 33, 13346–13357. doi: 10.1096/fj.201901161R

Oltean, S., Qiu, Y., Ferguson, J. K., Stevens, M., Neal, C., Russell, A., et al. (2015). Vascular endothelial growth factor-A165b is protective and restores endothelial glycocalyx in diabetic nephropathy. *J. Am. Soc. Nephrol.* 26, 1889–1904. doi: 10.1681/ASN.2014040350

Pahakis, M. Y., Kosky, J. R., Dull, R. O., and Tarbell, J. M. (2007). The role of endothelial glycocalyx components in mechanotransduction of fluid shear stress. *Biochem. Biophys. Res. Commun.* 355, 228–233. doi: 10.1016/j.bbrc.2007.01.137

Park-Windhol, C., Ng, Y. S., Yang, J., Primo, V., Saint-Geniez, M., and D'Amore, P. A. (2017). Endomucin inhibits VEGF-induced endothelial cell migration, growth, and morphogenesis by modulating VEGFR2 signaling. *Sci. Rep.* 7:17138. doi: 10.1038/s41598-017-16852-x

Potje, S. R., Paula, T. D., Paulo, M., and Bendhack, L. M. (2020). The role of glycocalyx and caveolae in vascular homeostasis and diseases. *Front. Physiol.* 11:620840. doi: 10.3389/fphys.2020.620840

Pries, A. R., Secomb, T. W., and Gaehtgens, P. (2000). The endothelial surface layer. *Pflugers Arch.* 440, 653–666. doi: 10.1007/s004240000307

Proudfoot, A. E. I., Johnson, Z., Bonvin, P., and Handel, T. M. (2017). Glycosaminoglycan interactions with chemokines add complexity to a complex system. *Pharmaceuticals* 10:70. doi: 10.3390/ph10030070

Ramnath, R., Foster, R. R., Qiu, Y., Cope, G., Butler, M. J., Salmon, A. H., et al. (2014). Matrix metalloproteinase 9-mediated shedding of syndecan 4 in response to tumor necrosis factor alpha: a contributor to endothelial cell glycocalyx dysfunction. *FASEB J.* 28, 4686–4699. doi: 10.1096/fj.14-252221

Reitsma, S., Slaaf, D. W., Vink, H., van Zandvoort, M. A., and Oude Egbrink, M. G. (2007). The endothelial glycocalyx: composition, functions, and visualization. *Pflugers Arch.* 454, 345–359. doi: 10.1007/s00424-007-0212-8

Ricard-Blum, S., and Lisacek, F. (2017). Glycosaminoglycanomics: where we are. *Glycoconj. J.* 34, 339–349. doi: 10.1007/s10719-016-9747-2

Rother, S., Samsonov, S. A., Moeller, S., Schnabelrauch, M., Rademann, J., Blaszkiewicz, J., et al. (2017). Sulfated hyaluronan alters endothelial cell activation in vitro by controlling the biological activity of the angiogenic factors vascular endothelial growth factor-A and tissue inhibitor of metalloproteinase-3. *ACS Appl. Mater. Interfaces* 9, 9539–9550. doi: 10.1021/acsami.7b01300

Rovas, A., Osiaevi, I., Buscher, K., Sackarnd, J., Tepasse, P. R., Fobker, M., et al. (2021). Microvascular dysfunction in COVID-19: the MYSTIC study. *Angiogenesis* 24, 145–157. doi: 10.1007/s10456-020-09753-7

Sarris, M., Masson, J. B., Maurin, D., Van der Aa, L. M., Boudinot, P., Lortat-Jacob, H., et al. (2012). Inflammatory chemokines direct and restrict leukocyte migration within live tissues as glycan-bound gradients. *Curr. Biol.* 22, 2375–2382. doi: 10.1016/j.cub.2012.11.018

Schmidt, E. P., Overdier, K. H., Sun, X., Lin, L., Liu, X., Yang, Y., et al. (2016). Urinary glycosaminoglycans predict outcomes in septic shock and acute respiratory distress syndrome. *Am. J. Respir. Crit. Care Med.* 194, 439–449. doi: 10.1164/rccm.201511-2281OC

Sebag, J., Nie, S., Reiser, K., Charles, M. A., and Yu, N. T. (1994). Raman spectroscopy of human vitreous in proliferative diabetic retinopathy. *Invest. Ophthalmol. Vis. Sci.* 35, 2976–2980.

Shurer, C. R., Kuo, J. C., Roberts, L. M., Gandhi, J. G., Colville, M. J., Enoki, T. A., et al. (2019). Physical principles of membrane shape regulation by the glycocalyx. *Cell* 177, 1757–1770.e21. doi: 10.1016/j.cell.2019.04.017

Singh, A., Friden, V., Dasgupta, I., Foster, R. R., Welsh, G. I., Tooke, J. E., et al. (2011). High glucose causes dysfunction of the human glomerular endothelial glycocalyx. *Am. J. Physiol. Renal Physiol.* 300, F40–F48. doi: 10.1152/ajprenal.00103.2010

Slevin, M., Krupinski, J., Gaffney, J., Matou, S., West, D., Delisser, H., et al. (2007). Hyaluronan-mediated angiogenesis in vascular disease: uncovering RHAMM and CD44 receptor signaling pathways. *Matrix Biol.* 26, 58–68. doi: 10.1016/j.matbio.2006.08.261

Stahl, K., Gronski, P. A., Kiyan, Y., Seeliger, B., Bertram, A., Pape, T., et al. (2020). Injury to the endothelial glycocalyx in critically ill patients with COVID-19. *Am. J. Respir. Crit. Care Med.* 202, 1178–1181. doi: 10.1164/rccm.202007-2676LE

Stringer, S. E. (2006). The role of heparan sulphate proteoglycans in angiogenesis. *Biochem. Soc. Trans.* 34(Pt 3), 451–453. doi: 10.1042/BST0340451

Tachi, M., Okada, H., Matsuhashi, N., Takemura, G., Suzuki, K., Fukuda, H., et al. (2019). Human colorectal cancer infrastructure constructed by the glycocalyx. *J. Clin. Med.* 8:1270. doi: 10.3390/jcm8091270

Tarbell, J. M., and Cancel, L. M. (2016). The glycocalyx and its significance in human medicine. *J. Intern. Med.* 280, 97–113. doi: 10.1111/joim.12465

West, D. C., and Kumar, S. (1989). Hyaluronan and angiogenesis. *Ciba Found. Symp.* 143, 187–201; discussion 201–187, 281–185. doi: 10.1002/9780470513774.ch12

Yang, J., LeBlanc, M. E., Cano, I., Saez-Torres, K. L., Saint-Geniez, M., Ng, Y. S., et al. (2020). ADAM10 and ADAM17 proteases mediate proinflammatory cytokine-induced and constitutive cleavage of endomucin from the endothelial surface. *J. Biol. Chem.* 295, 6641–6651. doi: 10.1074/jbc.RA119.011192

Zahr, A., Alcaide, P., Yang, J., Jones, A., Gregory, M., dela Paz, N. G., et al. (2016). Endomucin prevents leukocyte-endothelial cell adhesion and has a critical role under resting and inflammatory conditions. *Nat. Commun.* 7:10363. doi: 10.1038/ncomms10363

Zeng, Y., Zhang, X. F., Fu, B. M., and Tarbell, J. M. (2018). The role of endothelial surface glycocalyx in mechanosensing and transduction. *Adv. Exp. Med. Biol.* 1097, 1–27. doi: 10.1007/978-3-319-96445-4_1

Zoeller, J. J., McQuillan, A., Whitelock, J., Ho, S. Y., and Iozzo, R. V. (2008). A central function for perlecan in skeletal muscle and cardiovascular development. *J. Cell Biol.* 181, 381–394. doi: 10.1083/jcb.200708022

**Conflict of Interest:** The authors declare that the research was conducted in the absence of any commercial or financial relationships that could be construed as a potential conflict of interest.

**Publisher's Note:** All claims expressed in this article are solely those of the authors and do not necessarily represent those of their affiliated organizations, or those of the publisher, the editors and the reviewers. Any product that may be evaluated in this article, or claim that may be made by its manufacturer, is not guaranteed or endorsed by the publisher.

frontiers in Cell and Developmental Biology

ORIGINAL RESEARCH
published: 01 September 2021
doi: 10.3389/fcell.2021.734661

# A Reinterpretation of Evidence for the Endothelial Glycocalyx Filtration Structure

*Kenton P. Arkill**

*School of Medicine, University of Nottingham Biodiscovery Institute, University Park, Nottingham, United Kingdom*

The endothelial glycocalyx (eGlx) is thought to be the primary macromolecular filter for fluid flux out of the vasculature. This filter maintains the higher protein concentration within the vessel lumen relative to the tissue. Whilst the arguments for the eGlx being the size filter are convincing the structural evidence has been limited to specialized stains of perfusion fixed tissue, which are further processed for resin embedding for transmission electron microscopy. The staining and processing of the delicate pore structure has left many researchers struggling to interpret the observed surface coat. Previous work has alluded to a 19.5 nm spacing between fibers; however, whilst repeatable it does not give an eGlx pore size consistent with known glycosaminoglycan (GAG) molecular structure due to the required fiber thickness of >10 nm. Here a new interpretation is proposed based on the likelihood that the electron micrographs of are often of collapsed eGlx. The 19.5 nm spacing measured may therefore be the core protein of the proteoglycans (PGs) with the GAGs wrapped up around them rather than in an expanded *in vivo* state. The concept is explored to determine that this is indeed consistent with experimental measurements of permeability if the syndecans are predominately dimerized. Further an alteration of core protein lattice from hexagonal packing to square packing dramatically changes the permeability which could be facilitated *via* known mechanisms such as transient actin binding.

**Keywords: Starling hypothesis, vascular permeabilty, macromolecular transport, glycosaminoglycans, proteoglycan, heparan sulfate**

OPEN ACCESS

***Edited by:***
*Bingmei M. Fu,*
*City College of New York,*
*United States*

***Reviewed by:***
*Fitzroy Curry,*
*University of California, Davis,*
*United States*
*Weiqi Li,*
*Queen Mary University of London,*
*United Kingdom*
*C. Charles Michel,*
*Imperial College London,*
*United Kingdom*

***Correspondence:**
*Kenton P. Arkill*
*kenton.arkill@nottingham.ac.uk*

***Specialty section:***
*This article was submitted to Signaling, a section of the journal Frontiers in Cell and Developmental Biology*

***Received:*** *01 July 2021*
***Accepted:*** *13 August 2021*
***Published:*** *01 September 2021*

***Citation:***
*Arkill KP (2021) A Reinterpretation of Evidence for the Endothelial Glycocalyx Filtration Structure. Front. Cell Dev. Biol. 9:734661. doi: 10.3389/fcell.2021.734661*

## INTRODUCTION

For most capillaries the primary method of fluid exchange between the plasma and the tissues is defined by the Starling Hypothesis as interpreted in 1997 by CC Michel (1997) and Weinbaum (1998) often dubbed the "revised Starling hypothesis." With this interpretation, in the steady state, the oncotic pressure (Π) difference resisting the hydrostatic pressure ($P$) is across the endothelial glycocalyx (eGlx) rather than the whole vessel wall:

$$J_v = L_p A \left[ (P_{lumen} - P_{eGlx}) - \sigma \left( \Pi_{lumen} - \Pi_{eGlx} \right) \right] \quad (1)$$

Where the $J_v$ is the volumetric fluid flux, $L_p$ the hydraulic conductivity and $A$ the capillary surface area. The osmotic reflection coefficient () (Staverman, 1951) is due to the membrane not being a perfect filter, and for albumin, the primary protein concentration in the plasma, the value is experimentally $0.9 \leq \sigma < 1$. The fluid route out of the vessel is therefore *via* the eGlx, the endothelial junctions (or fenestrations), any significant basement membrane and finally between surrounding support cells (e.g., pericyte or podocyte). The role of the eGlx is to effectively block albumin, the

primary oncotic pressure constituent, from leaving the vessel to equilibrate with the interstitum. The implication is that eGlx as a filter covers the whole intercellular junction entrance, so fluid is subsequently funneled into the junctions and further funneled through the junctional strands. The velocity becomes high enough from the funneling that albumin cannot diffuse against this, i.e., from the tissue to the vessel. If this is the case under steady flow across the vascular wall the oncotic pressure difference across the eGlx cannot be influenced by the interstitial albumin concentration. In Adamson et al. (2004) performed experiments which demonstrated this predication in single capillaries, whilst also mathematically predicting that the eGlx contribution to resistance to hydraulic flux is ≈50% in mesenteric capillaries. However; as later measured, the eGlx acts as a macromolecular filter, when chemically removed the hydraulic conductivity increased by 2.5-fold in line with an expected ≈50% increase but the albumin solute permeability increases by 20-fold (Betteridge et al., 2017). Perhaps it is fortuitous that the experimentally accessible mesenteric capillaries are relatively permeable. The cremaster muscle also accessible for such measurements has 10-fold more hydraulic resistance which may have made the signal-to-background too difficult to evaluate (Smaje et al., 1970). Of course, the different hydraulic conductivities across tissues are of physiological importance, and allow normal processes such as an immune response to manipulate the molecular size ratio of transported molecules (Owen-Woods et al., 2020).

Until this point the remaining unknown was to confirm the pore size of the eGlx. A study of electron micrographs and a limited number of Pt/C replicate micrographs from freeze-etched frog mesenteric and pulmonary vessels indicated a spacing between the eGlx fibers of 19.5 nm (Squire et al., 2001). Of note for this manuscript is that several different staining types gave the same measurement and this value also seen in follow up work on mammalian samples across stains in 2D and limited 3D quantification (Arkill et al., 2011, 2012, 2014). The space between fibers does not give us the size of the holes between the fibers and whilst some attempt a measurement was made in those works, this was clearly stain dependent and inconsistent. Fundamentally there is an issue between linking the ≈20 nm spacing repeatedly observed in perfusion fixed resin embedded electron microscopy and the expected 7–8 nm pore size to exclude albumin, as the required fiber thickness would be too large to fit with our understanding of eGlx composition. This manuscript explores a reinterpretation of what the ≈20 nm spacing represents, which whilst far from proof, leaves a hypothesis that fits links underlying biochemistry and maintains the observed physiology. Instead of the ≈20 nm spacing being the distance between fibers causing the filter, the spacing is the core protein that multiple glycosaminoglycan (GAG) side chains are attached to.

## Electron Microscopy of the Endothelial Glycocalyx

As discussed, the expected pore size to retain albumin in the lumen is around 7–8 nm diameter; therefore, the only method of visualization of this structure for the foreseeable future is transmission electron microscopy. An endothelial surface coat was first reported by Luft (1965). The difficulty in observation comes from a combination of technical challenges. Primarily, the physiological eGlx is dependent on plasma components, shear stress and other multiple cell type microenvironmental factors hencewith replication of the structure *in vitro* has been unsatisfactory. Secondly, to visualize the eGlx in resin sections one needs a counter stain.

Suitable stains include Alcian Blue 8GX (van den Berg et al., 2003; Betteridge et al., 2017) and similar cupromeronic blue (Meuwese et al., 2010), Ruthenium Red (Luft, 1966; Baldwin and Winlove, 1984), Cationised Ferritin (Clough, 1982), Tannic Acid (Qvortrup and Rostgaard, 1993), and lanthanides including lanthanum (Hjalmarsson et al., 2004; Chappell et al., 2009) terbium (Wagner and Chen, 1990), thorium (Hegermann et al., 2015), and mixtures such as LaDy (Arkill et al., 2012). Unfortunately, these electron dense stains are both non-specific and require perfusion fixation to get them to the eGlx. None of the standard stains prevent loss of the layer consistently. The favored reasoning being that there is an altered effect from shear stress when the eGlx is coated in stain. The final problem with all these stains is that they work by charge and therefore alter the structure (e.g., may collapse the layer) once it is coated, but even so the 19.5 nm spacing discussed occurs across these stains. Cryogenic immobilization techniques with freeze substitution have been attempted with various degrees of success (Ebong et al., 2011), although no direct visualization in amorphous ice has yet been observed.

## Composition of the Endothelial Glycocalyx Filter

The composition of the eGlx filter is thought to be the GAGs. All GAGs have a negative fixed charge density and the most notable for our case are heparan sulfate (HS), chondroitin sulfate (CS) bound in place by proteoglycans (PGs), and hyaluronan (HA) *via* CD44 if it is membrane bound. Of course, these GAGs have mechanistic roles and as such binding is dynamic (Smith et al., 2011; Dyer et al., 2016; Clausen et al., 2020). A GAG chain is a polysaccharide, in (very) simplistic terms a chain of carbon rings with side groups giving a diameter in the order of 1 nm. HS has been measured with molecular weights of 35–45kDa, although with overexpression of N-Deacetylase/N-Sulfotransferase-2 in HEK cells up to 160kDa (Lyon et al., 1994; Deligny et al., 2016) giving a chain length between 60 and 300 nm. The eGlx HS length has not been measured *in situ* in eGlx, but the 100–150 nm in length depicted is entirely feasible, whilst CS is a little longer than HS HA would typically be 250 nm to several mm in length (Cowman et al., 2015). Current dogma, which whilst likely has not been definitively shown, is that the eGlx filter itself is made from the sulfated GAGs and the HA forms a supportive role possibly under the sulfated GAG (Fan et al., 2019). The repeated observations of $>1$ μm thick eGlx indicate a multilayer structure and the full depth is unlikely to be the filtration mechanism. $>1$ μm

thick, with a pore size of ≈7 nm would have a very low permeability not observed *in vivo*. The consensus is that the "filtration zone" is the membrane end of the eGlx, and bilayer implications on permeability have been explored (Curry and Michel, 2019). Perhaps noteworthy at this juncture is that the filter only needs to be over the intercellular junctions (in non-fenestrated vessels) and modeling suggests that this is only required to extend ≈200 nm away from the junction (Dalwadi et al., 2020).

There are therefore a multitude of unknowns and as such the subsequent interpretation of the electron microscopy is not claimed as definitive, but instead claims to fit current understanding consistently and therefore offers a promising alternative on previous interpretations.

## MATERIALS AND METHODS

### Axioms

Here it is explored that the filter is determined from the sulfated GAGs perpendicular to the membrane extending over 100 nm into the lumen, and that the 19.5 nm spacing observed is the core protein spacing not the fiber spacing thought previously (**Figure 1**). These core proteins have the GAG chains attached

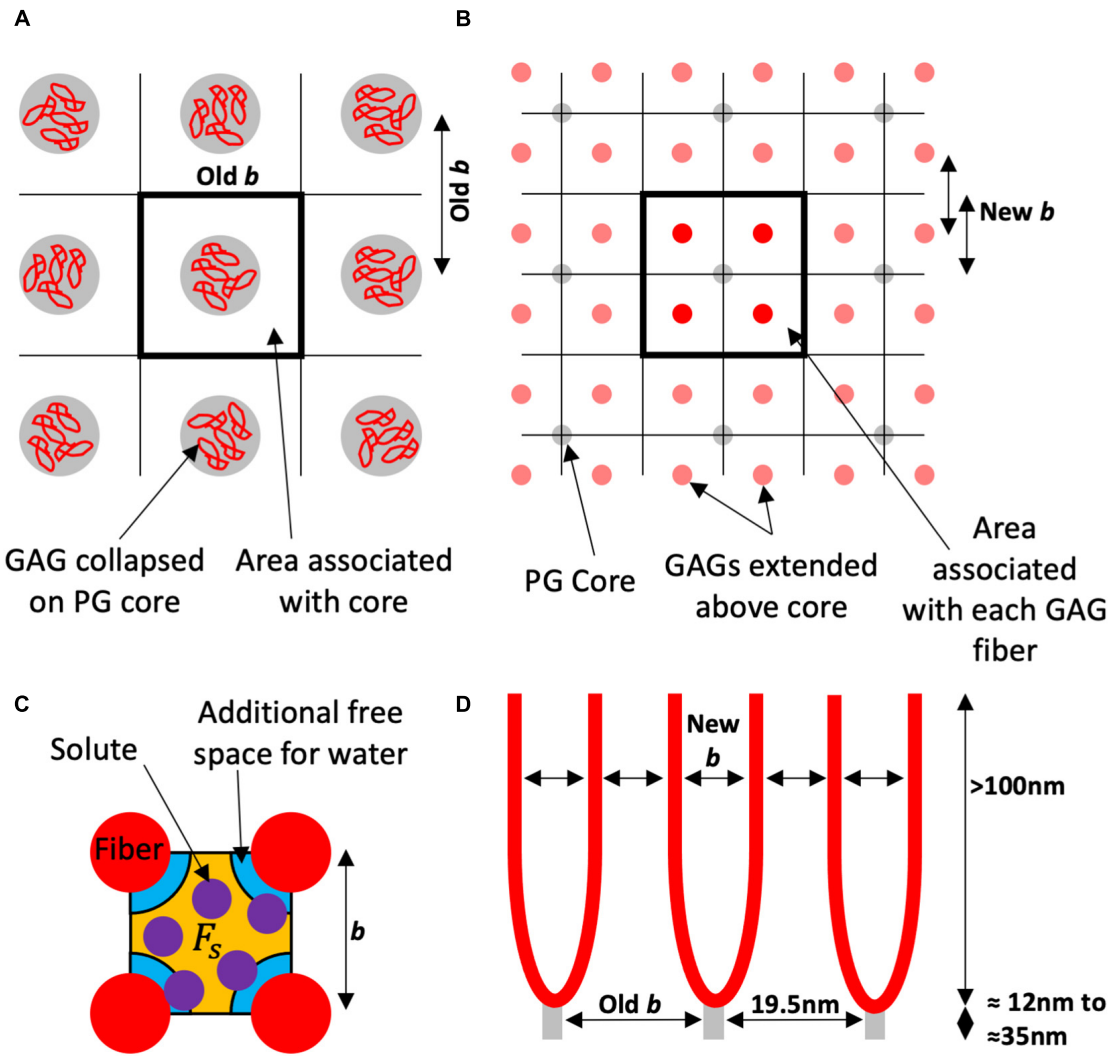


**FIGURE 1 |** Schematic of the proposed model using the square lattice example. **(A)** Looking to the wall from the lumen the electron microscopy visualizes the proteoglycan (PG) core protein with the glycosaminoglycan (GAG) fibers collapsed around them. This gives an inter-fiber spacing (Old *b*) that has been measured experimentally as 19.5 nm, and an area associated with each fiber for the solvent and solute to pass. **(B)** The red GAG fibers (in this example four per core protein), are unraveled and spaced accordingly (in this case also into square ordering). Each fiber in this example has $\frac{1}{4}$ of the associated area to the PG core protein, and a new spacing (New *b*). **(C)** The orange free space ($F_S$) for the purple solute is a proportion of the free space for water which has the orange and the additional blue space. The water is only excluded by the fiber diameter. This proportion is used to estimate the solute reflection coefficient. **(D)** Is a side view of the endothelial glycocalyx (eGlx) with the PG core protein spaced as "Old *b*" or 19.5 nm. There is now a new spacing "New *b*" between GAG fibers and a different fiber diameter to calculate the proportions of free space.

and they will therefore find an equilibrium spacing, effectively making the membrane area covered by a single core protein the area covered by the separated multiple GAG fibers attached to that protein core.

## Estimates and Variables

The reflection coefficient can be estimated or predicted from a structure. Here, the derivation of Anderson and Malone (1974) is used, which is applicable to long pores with a spherical non-binding solute:

$$\sigma = (1-\emptyset)^2 \quad (2)$$

Where $\emptyset$ is the partition coefficient defined as the relative free space between the solute ($F_s$) and the water ($F_w$):

$$\emptyset = \frac{F_s}{F_w} \quad (3)$$

The partition coefficient can be calculated by geometry (**Figure 1C**) as previously for hexagonal packing (Zhang et al., 2006) and for a square lattice (Arkill et al., 2011). In this case the supplementary material from Arkill et al. (2011) is used, as contains the derivations for both lattices. The albumin's Stoke–Einstein radius as deemed to be 3.5 nm.

Fiber Diameter has been a major problem with interpreting the spacing data with estimates from the electron dense staining ranging from 3 nm up to 18 nm. As discussed in Arkill et al. (2011) the measured sizes anecdotally tend to rise in 3 nm jumps consistent with a stain such as Alcian Blue coating a ≈1 nm fiber and then clumping together. Regardless, clearly the stains are affecting the structure, and of course adding to the size of the GAGs when bound. Here, we estimate for a range of fiber diameters ranging from 0.5 to 3 nm depicted as an error on the varied parameter. The expectation is that the true diameter is around 0.4–1 nm (Ogston and Preston, 1966); however, the Debye length (Debye and Hückel, 1923) for charge shielding is *circa* 0.5–1 nm, which therefore could effectively add up to 2 nm to the diameter of each fiber for negatively charged molecules.

Number of Fibers per core is also uncertain. Transmembrane Syndecan-2 and Syndecan-4 have three GAG attachment sites, whereas Syndecan-1 has five and Syndecan-3 has six, though the latter has limited presence in endothelium (Couchman et al., 2015). Syndecans are also expected to occur in dimers although other configurations exist (Godmann et al., 2020; Chen et al., 2021). Glypicans, likely more mobile in the outer layer only of the membrane lipid bilayer, have two GAG chains are also abundant in the endothelium (Iozzo and Schaefer, 2015).

Fiber Spacing has been measured as 19.5 nm (Squire et al., 2001; Arkill et al., 2011; **Figure 1A**), but if we factor in section shrinkage from electron flux can be 8–10% (Mantell et al., 2012) in x-y orientations and general variation between samples we have displayed from 13 to 25 nm. There is likely a periodic core structure which can be square, possibly due to interactions of transmembrane syndecans with the actin cytoskeleton or a less constrained hexagonally spaced. As the multiple GAG chains are expanded off the PG core to fill the same area they too can be square or hexagonally packed. Here we display Hexagonal core with Hexagonal GAGs (Hex-Hex), Square core with Hexagonal GAGs (SQ-Hex), and Square core with Square GAGs (SQ-SQ). The latter is intuitively unlikely unless there are other regular supports in the structure (examples could include albumin or possibly HA).

# RESULTS AND DISCUSSION

The SQ-SQ has a more open structure than Hex-Hex for equivalent fiber parameters, perhaps less intuitively the SQ-Hex is more open than SQ-SQ structures as in the latter the GAG chains' nearest neighbor is forced closer and is more constrained.

## Dependance on Number of Fibers per Core

**Figure 2A** illustrates that for 19.5 nm core spacing the proposed model is only consistent with physiological experiments ($0.9 \leq \sigma < 1$) when there are at least five, but almost certainly at least six GAG chains; therefore, the estimate that there are likely six from syndecan-2 and -4 in dimers seems to hold well. There are likely to be mixtures of syndecans present and so whilst only dimerized syndecan-1 would exclude albumin, raising the mean fiber number to seven or even eight GAGs per core is still possible. Clearly for this model to be true the syndecans must dimerise in normo-physiology.

## Dependence on the Spacing Value

**Figure 2B** illustrates that for six GAG chains per core is highly sensitive to the fiber spacing. Of note, and perhaps what spurred the dissemination of this work, is that for a 1.5 nm diameter fiber, the most justifiable from the addition of native core and Debye shielding diameter, for albumin falls in the physiological range for Hex-Hex for an inter-fiber spacing between 18.2 and 20 nm. A slightly larger spacing would require either a slightly thicker GAG fiber or more GAG chains per core, both options are likely. SQ-SQ, without further structural evidence, makes it the least likely formation, as it would need more GAG chains or the extreme end of the fiber thickness estimate to be consistent with the model. SQ-Hex formation is almost certainly not the formation in normo-physiology.

## Strengths and Weakness of the Proposed Filter Model

Here it is proposed that the filter model which previously measured inter-fiber spacing of 19.5 nm by transmission electron microscopy is false and that this spacing is instead the inter-PG core spacing with the GAG chains collapsed around them. These calculations show that the proposed model fits decades of both *in vivo* experimental measurements and our (limited) biomolecular understanding of the sulfated GAGs in the eGlx. There are two particular additional strengths for the proposed model:

Firstly, that as the GAG chains are floating above the core protein, and likely self-spacing, the system has built-in flexibility missing from the original model. One can envisage a missing core protein (or GAG chain) due to engagement in a mechanistic role or simply random chance, and the remaining GAG chains

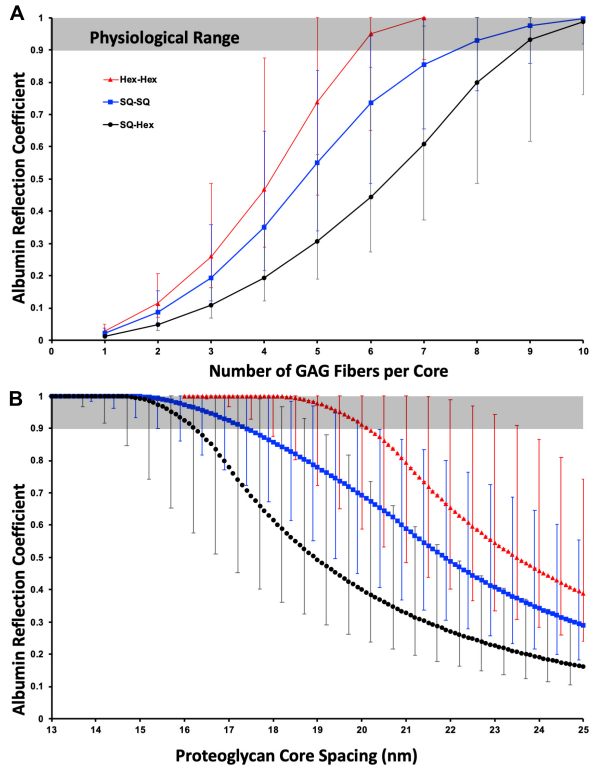


**FIGURE 2 |** The physiological albumin reflection coefficient fits well with a hexagonally packed dimerized PG core with a total of ≥6 GAG chains with a diameter of 1.5 nm (including charge effects). **(A)** Variation of reflection coefficient with the number of GAG chains per PG core structure. The data is depicted for hexagonal and square core organization (Hex- and SQ-, respectively) with the overlaying GAG chain organization hexagonal (Hex) or square (SQ). **(B)** As A but demonstrating the dependance of reflection coefficient on fiber spacing with six GAG chains per core structure. The physiological reflection coefficient is the grayed area. The error bars are for a 0.5 nm (lower reflection coefficient) and a 3 nm (higher reflection coefficient) fiber diameter.

drifting slightly further apart, but still performing their albumin excluding role. Thus, the proposed model is flexible enough to allow for physiological variation in an essential system, and hopefully pacify some valid concerns especially with ignored variables such as membrane curvature around fenestrations and intercellular junctions or the unlikely rigidity of spacings as modeled here.

The second is that a change of lattice structure, for example to a SQ core formation, would radically alter the reflection coefficient to albumin and indeed the permeability to macromolecules. Whilst speculative in the context here, this type of formational change is feasible, for example by selective binding mechanisms to the actin cytoskeleton (Yoneda and Couchman, 2003; Multhaupt et al., 2009; Li and Wang, 2019), and would allow for great functional control over what is a dynamic system. Further, there would still be direct GAG control over the filtration *via* other mechanisms, such as those hypothesized in immunology for clumping of the HS leaving short term gaps (Dyer et al., 2017; Handel and Dyer, 2021) as well as the activity of shedases [e.g., (Annecke et al., 2011)].

Weaknesses in the new filter model stem from a current lack of biomolecular knowledge, particularly *in vivo*, which limits our interpretation substantially. What is the physiological composition of the eGlx? Are components there by chance, transiently, or do they have a structural role? Perhaps the largest structural unknown is that of HA. It is abundant and tends to have a structural role, but is the HA located amongst the sulfated GAG, running underneath or looping over the top? Is the HA involved in determining the pore size and organization directly or indirectly? The model does not include the outer layer of the eGlx that seems to exist, which perhaps is the layer now dubbed "perfused boundary region" in human *in vivo* detection (Nieuwdorp et al., 2008). Certainly, the size of the eGlx has been robustly measured in the 1 μm range, and this is far too thick to account for the observed permeability if it is all "filtration zone." There also remains the question of the outer region's composition as sulfated GAGs are not expected to be that long. There are also longer spacings noted by Squire et al. (2001), Arkill et al. (2011), and Hegermann et al. (2015). These do not seem to fit a multiple of the 19.5 nm spacing, but are around 50 nm. There is no evidence on what these are, however, convenient it would be for them to be HA membrane binding. A fuller understanding of the biochemistry of the filter would inform the validity of many of the mathematical assumptions and approximations here. Perhaps the main two being the validity of Eq. 2 (that requires long pores with a spherical non-binding solute), and the distribution of fiber spacings only as a mean distance is considered not the variance in distribution around that mean.

Direct visualization of the structure, is technically very challenging. To visualize the eGlx *in situ* by cryogenic TEM may be possible with the emergence of direct electron cameras and phase plates becoming more accessible. Continuing freeze-etching techniques (Squire et al., 2001; Sun et al., 2020) on eGlx are another method worth pursuing. Both these methods would benefit from correlating with optical fluorescence to be sure of imaging location post tissue fracture, and unfortunately higher throughput. The proposed model whilst not definitive would allow for biomolecular testing that does not rely on direct visualization, such as syndecan ratios or GAG chain length, that perhaps will allude to the full eGlx structure. Once such possibility imaging mass spectrometry that can separate GAG composition (Hook et al., 2021) and can have <100 nm precision. Further the model can indirectly be compared to others by determining the reflection coefficient (along with the permeability) on the same vessel from multiple charged and sized solutes, such as organic nanodots (Mongin et al., 2008) as $\frac{F_s}{F_w}$ will vary in a unique manor.

## CONCLUSION

The model proposed here fits both the historical electron microscopy and our current understanding of the sulfated GAGs in the eGlx. It also highlights that a change in formation, for example *via* actin binding, would dramatically alter the size of macromolecule that can pass through to the junction or the membrane.

## DATA AVAILABILITY STATEMENT

The original contributions presented in the study are included in the article/supplementary material, further inquiries can be directed to the corresponding author.

## AUTHOR CONTRIBUTIONS

The author confirms being the sole contributor of this work and has approved it for publication.

## FUNDING

This work was supported by the Medical Research Council MR/ P003214/1.

## ACKNOWLEDGMENTS

The work was inspired by the late John Squire (Squire et al., 2001; Arkill et al., 2011, 2012, 2014) who sadly was one of many victims of Covid-19.

## REFERENCES

Adamson, R. H., Lenz, J. E., Zhang, X., Adamson, G. N., Weinbaum, S., and Curry, F. E. (2004). Oncotic pressures opposing filtration across non-fenestrated rat microvessels. *J. Physiol. Lond.* 557, 889–907. doi: 10.1113/jphysiol.2003.058255

Anderson, J. L., and Malone, D. M. (1974). Mechanism of osmotic flow in porous membranes. *Biophys. J.* 14, 957–982. doi: 10.1016/s0006-3495(74)85962-x

Annecke, T., Fischer, J., Hartmann, H., Tschoep, J., Rehm, M., Conzen, P., et al. (2011). Shedding of the coronary endothelial glycocalyx: effects of hypoxia/reoxygenation vs ischaemia/reperfusion. *Br. J. Anaesth.* 107, 679–686. doi: 10.1093/bja/aer269

Arkill, K. P., Knupp, C., Michel, C. C., Neal, C. R., Qvortrup, K., Rostgaard, J., et al. (2011). Similar endothelial glycocalyx structures in microvessels from a range of mammalian tissues: evidence for a common filtering mechanism? *Biophys. J.* 101, 1046–1056. doi: 10.1016/j.bpj.2011.07.036

Arkill, K. P., Neal, C. R., Mantell, J. M., Michel, C. C., Qvortrup, K., Rostgaard, J., et al. (2012). 3D reconstruction of the glycocalyx structure in mammalian capillaries using electron tomography. *Microcirculation* 19, 343–351. doi: 10.1111/j.1549-8719.2012.00168.x

Arkill, K. P., Qvortrup, K., Starborg, T., Mantell, J. M., Knupp, C., Michel, C. C., et al. (2014). Resolution of the three dimensional structure of components of the glomerular filtration barrier. *BMC Nephrol.* 15:24. doi: 10.1186/1471-2369-15-24

Baldwin, A., and Winlove, C. (1984). Effects of perfusate composition on binding of ruthenium red and gold colloid to glycocalyx of rabbit aortic endothelium. *J. Histochem. Cytochem.* 32, 259–266. doi: 10.1177/32.3.6198357

Betteridge, K. B., Arkill, K. P., Neal, C. R., Harper, S. J., Foster, R. R., Satchell, S. C., et al. (2017). Sialic acids regulate microvessel permeability, revealed by novel in vivo studies of endothelial glycocalyx structure and function. *J. Physiol.* 595, 5015–5035. doi: 10.1113/jp274167

Chappell, D., Jacob, M., Paul, O., Rehm, M., Welsch, U., Stoeckelhuber, M., et al. (2009). The glycocalyx of the human umbilical vein endothelial cell an impressive structure ex vivo but not in culture. *Circ. Res.* 104, 1313–1317. doi: 10.1161/circresaha.108.187831

Chen, J., Wang, F., He, C., and Luo, S.-Z. (2021). Multiple dimerizing motifs at different locations modulate the dimerization of the syndecan transmembrane domains. *J. Mol. Graphics Model.* 106:107938. doi: 10.1016/j.jmgm.2021.107938

Clausen, T. M., Sandoval, D. R., Spliid, C. B., Pihl, J., Perrett, H. R., Painter, C. D., et al. (2020). SARS-CoV-2 infection depends on cellular heparan sulfate and ACE2. *Cell* 183, 1043–1057.

Clough, G. (1982). The steady-state transport of cationized ferritin by endothelial cell vesicles. *J. Physiol.* 328, 389–401. doi: 10.1113/jphysiol.1982.sp014272

Couchman, J. R., Gopal, S., Lim, H. C., Nørgaard, S., and Multhaupt, H. A. (2015). Fell-Muir Lecture: syndecans: from peripheral coreceptors to mainstream regulators of cell behaviour. *Int. J. Exp. Pathol.* 96, 1–10. doi: 10.1111/iep.12112

Cowman, M. K., Lee, H.-G., Schwertfeger, K. L., McCarthy, J. B., and Turley, E. A. (2015). The content and size of hyaluronan in biological fluids and tissues. *Front. Immunol.* 6:261.

Curry, F. E., and Michel, C. C. (2019). The endothelial glycocalyx: barrier functions versus red cell hemodynamics: a model of steady state ultrafiltration through a bi-layer formed by a porous outer layer and more selective membrane-associated inner layer. *Biorheology* 56, 113–130. doi: 10.3233/bir-180198

Dalwadi, M. P., King, J. R., Dyson, R. J., and Arkill, K. P. (2020). Mathematical model to determine the effect of a sub-glycocalyx space. *Phys. Rev. Fluids* 5:043103.

Debye, P. and Hückel, E. (1923). *The Theory of Electrolytes. I. Freezing Point Depression and Related Phenomena (Translation)*, trans. M. Braus. Available online at: https://minds.wisconsin.edu/handle/1793/79225

Deligny, A., Dierker, T., Dagälv, A., Lundequist, A., Eriksson, I., Nairn, A. V., et al. (2016). NDST2 (N-Deacetylase/N-Sulfotransferase-2) enzyme regulates heparan sulfate chain length. *J. Biol. Chem.* 291, 18600–18607. doi: 10.1074/jbc.m116.744433

Dyer, D. P., Migliorini, E., Salanga, C. L., Thakar, D., Handel, T. M., and Richter, R. P. (2017). Differential structural remodelling of heparan sulfate by chemokines: the role of chemokine oligomerization. *Open Biol.* 7:160286. doi: 10.1098/rsob.160286

Dyer, D. P., Salanga, C. L., Johns, S. C., Valdambrini, E., Fuster, M. M., Milner, C. M., et al. (2016). The anti-inflammatory protein TSG-6 regulates chemokine function by inhibiting chemokine/glycosaminoglycan interactions. *J. Biol. Chem.* 291, 12627–12640. doi: 10.1074/jbc.m116.720953

Ebong, E. E., Macaluso, F. P., Spray, D. C., and Tarbell, J. M. (2011). Imaging the endothelial glycocalyx in vitro by rapid freezing/freeze substitution transmission electron microscopy. *Arterioscler. Thromb Vasc. Biol.* 31, 1908–1915. doi: 10.1161/atvbaha.111.225268

Fan, J., Sun, Y., Xia, Y., Tarbell, J. M., and Fu, B. M. (2019). Endothelial surface glycocalyx (ESG) components and ultra-structure revealed by stochastic optical reconstruction microscopy (STORM). *Biorheology* 56, 77–88. doi: 10.3233/bir-180204

Godmann, L., Bollmann, M., Korb-Pap, A., König, U., Sherwood, J., Beckmann, D., et al. (2020). Antibody-mediated inhibition of syndecan-4 dimerisation reduces interleukin (IL)-1 receptor trafficking and signalling. *Ann. Rheumatic Dis.* 79, 481–489. doi: 10.1136/annrheumdis-2019-216847

Handel, T. M., and Dyer, D. P. (2021). Perspectives on the biological role of chemokine: glycosaminoglycan interactions. *J. Histochem. Cytochem.* 69, 87–91.

Hegermann, J., Lünsdorf, H., Ochs, M., and Haller, H. (2015). Visualization of the glomerular endothelial glycocalyx by electron microscopy using cationic colloidal thorium dioxide. *Histochem. Cell Biol.* 145, 41–51. doi: 10.1007/s00418-015-1378-3

Hjalmarsson, C., Johansson, B. R., and Haraldsson, B. (2004). Electron microscopic evaluation of the endothelial surface layer of glomerular capillaries. *Microvasc. Res.* 67, 9–17. doi: 10.1016/j.mvr.2003.10.001

Hook, A. L., Hogwood, J., Gray, E., Mulloy, B., and Merry, C. L. (2021). High sensitivity analysis of nanogram quantities of glycosaminoglycans using ToF-SIMS. *Commun. Chem.* 4, 1–8.

Iozzo, R. V., and Schaefer, L. (2015). Proteoglycan form and function: a comprehensive nomenclature of proteoglycans. *Matrix Biol.* 42, 11–55. doi: 10.1016/j.matbio.2015.02.003

Li, W., and Wang, W. (2019). Membrane tension regulates syndecan-1 expression through actin remodelling. *Biochim. Biophys. Acta (BBA)* 1863:129413. doi: 10.1016/j.bbagen.2019.129413

Luft, J. H. (1965). FINE STRUCTURE OF CAPILLARIES - ENDOCAPILLARY LAYER. *Anatom. Record* 151:380.

Luft, J. H. (1966). FINE STRUCTURE OF CAPILLARY AND ENDOCAPILLARY LAYER AS REVEALED BY RUTHENIUM RED. *Fed. Proc.* 25:1773.

Lyon, M., Deakin, J. A., and Gallagher, J. T. (1994). Liver heparan sulfate structure. A novel molecular design. *J. Biol. Chem.* 269, 11208–11215. doi: 10.1016/s0021-9258(19)78112-5

Mantell, J. M., Verkade, P., and Arkill, K. P. (2012). "Iop: quantitative biological measurement in transmission electron tomography," in *Proceedings of the Electron Microscopy and Analysis Group Conference 2011*, (Birmingham: IOP Publishing Ltd).

Meuwese, M. C., Broekhuizen, L. N., Kuikhoven, M., Heeneman, S., Lutgens, E., Gijbels, M. J. J., et al. (2010). Endothelial surface layer degradation by chronic hyaluronidase infusion induces proteinuria in apolipoprotein E-deficient mice. *PLoS One* 5:e14262. doi: 10.1371/journal.pone.0014262

Michel, C. (1997). Starling: the formulation of his hypothesis of microvascular fluid exchange and its significance after 100 years. *Exp. Physiol.* 82, 1–30. doi: 10.1113/expphysiol.1997.sp004000

Mongin, O., Rouxel, C., Robin, A.-C., Pla-Quintana, A., Krishna, T. R., Recher, G., et al. (2008). "Brilliant organic nanodots: novel nano-objects for bionanophotonics," in *Proceedings of the NanoScience+ Engineering: International Society for Optics and Photonics*, (Bellingham, WA: SPIE).

Multhaupt, H., Yoneda, A., Whiteford, J., Oh, E., Lee, W., and Couchman, J. (2009). Syndecan signaling: when, where and why. *J. Physiol. Pharmacol.* 60(Suppl. 4), 31–38.

Nieuwdorp, M., Meuwese, M. C., Mooij, H. L., Ince, C., Broekhuizen, L. N., Kastelein, J. J., et al. (2008). Measuring endothelial glycocalyx dimensions in humans: a potential novel tool to monitor vascular vulnerability. *J. Appl. Physiol.* 104, 845–852. doi: 10.1152/japplphysiol.00440.2007

Ogston, A., and Preston, B. (1966). The exclusion of protein by hyaluronic acid: MEASUREMENT BY LIGHT SCATTERING. *J. Biol. Chem.* 241, 17–19. doi: 10.1016/s0021-9258(18)96951-6

Owen-Woods, C., Joulia, R., Barkaway, A., Rolas, L., Ma, B., Nottebaum, A. F., et al. (2020). Local microvascular leakage promotes trafficking of activated neutrophils to remote organs. *J. Clin. Invest.* 130, 2301–2318. doi: 10.1172/jci133661

Qvortrup, K., and Rostgaard, J. (1993). Ultrastructure of the Endolymphatic Duct in the Rat Fixation and Preservation. *Acta Oto-Laryngol.* 113, 731–740. doi: 10.3109/00016489309135893

Smaje, L., Zweifach, B., and Intaglietta, M. (1970). Micropressures and capillary filtration coefficients in single vessels of the cremaster muscle of the rat. *Microvasc. Res.* 2, 96–110. doi: 10.1016/0026-2862(70)90055-5

Smith, R. A., Meade, K., Pickford, C. E., Holley, R. J., and Merry, C. L. (2011). *Glycosaminoglycans as Regulators of Stem Cell Differentiation*. London: Portland Press Ltd.

Squire, J. M., Chew, M., Nneji, G., Neal, C., Barry, J., and Michel, C. (2001). Quasi-periodic substructure in the microvessel endothelial glycocalyx: a possible explanation for molecular filtering? *J. Struct. Biol.* 136, 239–255. doi: 10.1006/jsbi.2002.4441

Staverman, A. (1951). The theory of measurement of osmotic pressure. *Recueil des Travaux Chimiques des Pays-Bas* 70, 344–352. doi: 10.1002/recl.19510700409

Sun, W. W., Krystofiak, E. S., Leo-Macias, A., Cui, R., Sesso, A., Weigert, R., et al. (2020). Nanoarchitecture and dynamics of the mouse enteric glycocalyx examined by freeze-etching electron tomography and intravital microscopy. *Commun. Biol.* 3, 1–10.

van den Berg, B. M., Vink, H., and Spaan, J. A. E. (2003). The endothelial glycocalyx protects against myocardial edema. *Circ. Res.* 92, 592–594. doi: 10.1161/01.res.0000065917.53950.75

Wagner, R. C., and Chen, S. C. (1990). Ultrastructural distribution of terbium across capillary endothelium: detection by electron spectroscopic imaging and electron energy loss spectroscopy. *J. Histochem. Cytochem.* 38, 275–282. doi: 10.1177/38.2.2299181

Weinbaum, S. (1998). 1997 Whitaker distinguished lecture: models to solve mysteries in biomechanics at the cellular level; a new view of fiber matrix layers. *Ann. Biomed. Eng.* 26, 627–643.

Yoneda, A., and Couchman, J. R. (2003). Regulation of cytoskeletal organization by syndecan transmembrane proteoglycans. *Matrix Biol.* 22, 25–33. doi: 10.1016/s0945-053x(03)00010-6

Zhang, X. B., Curry, F. R., and Weinbaum, S. (2006). Mechanism of osmotic flow in a periodic fiber array. *Am. J. Physiol. Heart Circ. Physiol.* 290, H844–H852.

**Conflict of Interest:** The author declares that the research was conducted in the absence of any commercial or financial relationships that could be construed as a potential conflict of interest.

The reviewer FC declared a past co-authorship with the author to the handling editor.

frontiers in Cell and Developmental Biology

MINI REVIEW
published: 01 September 2021
doi: 10.3389/fcell.2021.733557

# The Endothelial Glycocalyx: Physiology and Pathology in Neonates, Infants and Children

*Alexandra Puchwein-Schwepcke[1,2], Orsolya Genzel-Boroviczény[1] and Claudia Nussbaum[1]**

*[1] Division of Neonatology, Department of Pediatrics, Dr. von Hauner Children's Hospital, University Hospital, LMU Munich, Munich, Germany, [2] Department of Pediatric Neurology and Developmental Medicine, University of Basel Children's Hospital, Basel, Switzerland*

The endothelial glycocalyx (EG) as part of the endothelial surface layer (ESL) is an important regulator of vascular function and homeostasis, including permeability, vascular tone, leukocyte recruitment and coagulation. Located at the interface between the endothelium and the blood stream, this highly fragile structure is prone to many disruptive factors such as inflammation and oxidative stress. Shedding of the EG has been described in various acute and chronic diseases characterized by endothelial dysfunction and angiopathy, such as sepsis, trauma, diabetes and cardiovascular disease. Circulating EG components including syndecan-1, hyaluronan and heparan sulfate are being evaluated in animal and clinical studies as diagnostic and prognostic markers in several pathologies, and advances in microscopic techniques have enabled *in vivo* assessment of the EG. While research regarding the EG in adult physiology and pathology has greatly advanced throughout the last decades, our knowledge of the development of the glycocalyx and its involvement in pathological conditions in the pediatric population is limited. Current evidence suggests that the EG is present early during fetal development and plays a critical role in vessel formation and maturation. Like in adults, EG shedding has been demonstrated in acute inflammatory conditions in infants and children and chronic diseases with childhood-onset. However, the underlying mechanisms and their contribution to disease manifestation and progression still need to be established. In the future, the glycocalyx might serve as a marker to identify pediatric patients at risk for vascular sequelae and as a potential target for early interventions.

**Keywords: glycocalyx, neonate, children, development, perfused boundary region, shedding**

OPEN ACCESS

***Edited by:***
*Ye Zeng,*
*Sichuan University, China*

***Reviewed by:***
*Charles Wade,*
*University of Texas Health Science Center at Houston, United States*
*Cynthia L. Bristow,*
*Alpha-1 Biologics, United States*

***Correspondence:**
*Claudia Nussbaum*
*claudia.nussbaum@med.uni-muenchen.de*

***Specialty section:***
*This article was submitted to Signaling, a section of the journal Frontiers in Cell and Developmental Biology*

***Received:*** *30 June 2021*
***Accepted:*** *12 August 2021*
***Published:*** *01 September 2021*

***Citation:***
*Puchwein-Schwepcke A, Genzel-Boroviczény O and Nussbaum C (2021) The Endothelial Glycocalyx: Physiology and Pathology in Neonates, Infants and Children. Front. Cell Dev. Biol. 9:733557. doi: 10.3389/fcell.2021.733557*

## INTRODUCTION

The endothelial glycocalyx (EG), a complex and highly versatile brush-like carbohydrate-rich layer, lines the luminal endothelial surface of the whole vasculature including blood and lymphatic vessels. The structure and composition of the glycocalyx have been described in several excellent reviews and will not be covered in detail in this paper (Reitsma et al., 2007; Weinbaum et al., 2007; Couchman and Pataki, 2012). Briefly, the EG is mainly composed of proteoglycans, consisting of a core protein with attached long unbranched glycosaminoglycans (GAGs) and glycoproteins characterized by short, branched carbohydrate side chains. Together with associated plasma

proteins, it forms the endothelial surface layer (ESL) (**Figure 1**). The core protein of proteoglycans is linked to the cell membrane (syndecans and glypicans) or secreted (e.g., versican, perlecan, agrin) (Couchman and Pataki, 2012). Among the bound GAGs, heparan sulfate is the most abundant, followed by chondroitin-/dermatansulfate, whereas hyaluronan, another structurally important GAG, is not firmly attached (Sarrazin et al., 2011). The composition and dimension of the EG varies within different types of blood and lymphatic vessels and ranges from approximately 0.3 to 0.5 μm in lymphatic collectors and blood capillaries to several micrometers in large arteries (Vink and Duling, 1996; Megens et al., 2007; Zolla et al., 2015).

Due to its central position within the vasculature, the EG is an important regulator of vessel function and homeostasis, including permeability, vascular tone, leukocyte recruitment and coagulation (Reitsma et al., 2007; Weinbaum et al., 2007). Similarly, in the lymphatic system the glycocalyx exerts an important role in limiting permeability and thereby contributes essentially to the drainage and transport of interstitial fluid and macromolecules (Zolla et al., 2015; Arokiasamy et al., 2019).

Since its first visualization more than 50 years ago by Luft (1966), the glycocalyx has gained increasing interest in cardiovascular research, especially throughout the last two decades. Numerous *in vitro* and *in vivo* studies have broadened our understanding of the EG's function and its contribution to pathophysiological processes. For further information the reader is referred to recent comprehensive reviews on the topic (Pillinger and Kam, 2017; Cosgun et al., 2020). However, almost all studies have been performed in adults, leaving a knowledge gap concerning the composition and function of the EG in the developing organism. This review aims to summarize our current understanding of the EG in the fetus, neonate and in children and its involvement in pathological processes in the pediatric population, thereby identifying open questions for future research.

## ASSESSMENT OF THE ENDOTHELIAL GLYCOCALYX IN PEDIATRIC CLINICAL STUDIES

While the scientific interest in the EG has significantly increased throughout the last decades, the assessment of the EG *in vivo* remains challenging. Using conventional intravital microscopy, Vink and Duling were the first to indirectly visualize the EG in vessels of the mouse cremaster muscle by demonstrating an exclusion zone near the vessel wall for flowing erythrocytes or a fluorescent plasma marker unable to penetrate the EG (Vink and Duling, 1996). Advanced imaging techniques such as multiphoton laser scanning microscopy may offer the potential to directly image the glycocalyx *in vivo* in animal models using fluorescent dyes or antibodies targeting EG components (Wu et al., 2017). However, none of these approaches is currently practicable for *in vivo* assessment of the EG in humans. Nieuwdorp et al. (2006b) applied a tracer dilution method to gain estimates of systemic glycocalyx volume in adult test persons, but the validity of this technique has been questioned (Michel and Curry, 2009) and ethical concerns hamper its application in the pediatric population. Currently, evaluation of the EG in clinical studies is mainly based on two principles: (i) measurement of circulating glycocalyx components such as syndecan-1, hyaluronan, heparan sulfate and chondroitin sulfate in the plasma/serum and urine as an indicator for glycocalyx shedding and (ii) videomicroscopic assessment of the EG in vessels of the microcirculation (Cerny et al., 2017). Both methods only provide indirect information on the EG, and in the pediatric population, specific challenges need to be overcome.

While measurements of circulating EG biomarkers are relatively easy to realize in adults, obtaining the necessary blood samples in children for research purposes alone is disputable. Furthermore, especially in preterm newborns, drawing the sample volumes required for accurate analyses is critical due to the low total blood volume. Newer videomicroscopy techniques, including Orthogonal Polarization Spectral (OPS), Sidestream Dark Field (SDF), and Incident Dark Field (IDF) imaging, have enabled *in vivo* visualization of the human microcirculation, including neonates and children (Genzel-Boroviczeny et al., 2002; Erdem et al., 2019). These video sequences can be used to measure the local microvascular EG based on changes in vessel diameter. One of the best established and validated parameters is the so-called perfused boundary region (PBR), resembling the luminal part of the EG partially accessible to flowing erythrocytes (Lee et al., 2014; Eickhoff et al., 2020). Changes in glycocalyx composition or shedding of the EG, allowing erythrocytes to further penetrate into the EG, are reflected by an increase in PBR. The PBR has been evaluated in various clinical studies in adults and correlated to patient outcome (Vlahu et al., 2012; Dekker et al., 2019; Rovas et al., 2019; Beurskens et al., 2020). Performing videomicroscopic studies in children and especially in infants and neonates is challenging due to the need for minimal movement during image acquisition.

## PHYSIOLOGICAL PROPERTIES OF THE EG IN THE FETUS AND NEONATE

### Role of the EG in Blood Vessel Formation

In the developing embryo, blood vessel formation and growth are necessary at an early stage to guarantee cellular supply with oxygen and nutrients. In general, two distinct processes can be distinguished in the development of vasculature. Vasculogenesis describes the *de novo* formation of vessels by differentiation, proliferation and migration of endothelial progenitor cells. In contrast, angiogenesis characterizes the generation of new vessels from existing ones by sprouting and intussusception (i.e., splitting of an existing vessel) (Conway et al., 2001; Naito et al., 2020). Components of the glycocalyx have been shown to be critically involved in both processes (Iozzo and San Antonio, 2001; Piecewicz and Sengupta, 2011). It is long known that pro-angiogenic factors critical for vasculo- and angiogenesis, including vascular endothelial growth factor (VEGF) and fibroblast growth fact-2 (FGF-2), bind to heparan sulfate proteoglycans (HSPG), the most abundant component of the EG (Yayon et al., 1991; Gitay-Goren et al., 1992; Lundin et al., 2000).

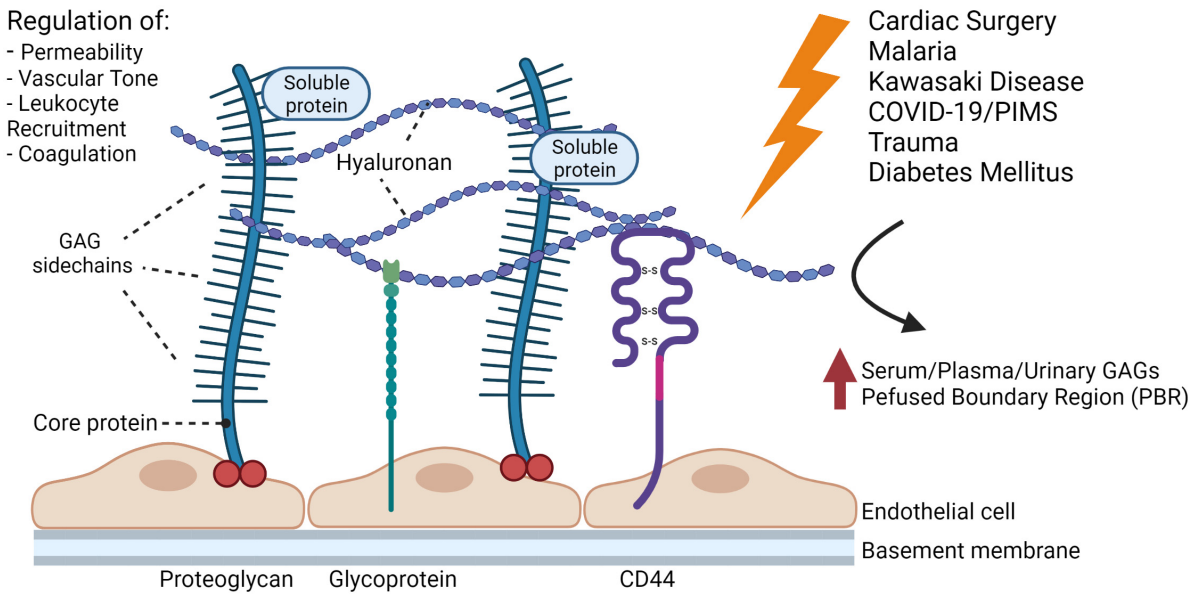


**FIGURE 1 |** Schematic representation of the glycocalyx covering the endothelial cells of a blood vessel. The main membrane bound components of the EG include proteoglycans (e.g., syndecans and glypicans) with long glycosaminoglycan side-chains (GAGs) and glycoproteins (e.g., selectins and integrins). Hyaluronan, plasma proteins and soluble proteoglycans are integrated into the glycocalyx forming the so called endothelial surface layer. The EG is an important regulator of vascular function and homeostasis, and shedding of the EG has been suggested in different conditions and disease states in the pediatric population including cardiac surgery, trauma, infectious diseases and diabetes mellitus. Note: dimensions in the figure are not drawn to scale. The figure was created with Bio.Render.com.

As demonstrated by Harfouche et al. (2009), differentiation of embryonic stem cells into endothelial cells is paralleled by an increase in the synthesis of di- and trisulfated heparan sulfate glycosaminoglycans (HSGAG). Vice versa, inhibition of HSGAG sulfation by treatment with sodium chloride or digestion of HSGAGs by heparinase led to a significantly lower expression of endothelial markers such as von Willebrand factor and angiopoetin-2 (Harfouche et al., 2009). These *in vitro* findings were validated in zebrafish embryos showing that knock-down of the enzyme N-deacetylase/N-sulfotransferase 1 (NDST1), which is critical for posttranslational sulfation of glycosaminoglycans, led to impaired vessel formation (Harfouche et al., 2009).

Syndecan-2, a plasma membrane-bound HSPG expressed on human microvascular endothelial cells (EC), is upregulated under stimulation with FGF or VEGF. Inhibition of Syndecan-2 gene transcription using antisense oligonucleotides led to impaired EC adhesion (i.e., attachment of EC to fibronectin coated culture dishes), spreading (i.e., number of attached ECs showing extended cytoplasm) and capillary tube formation *in vitro* (Noguer et al., 2009). *In vivo*, knock-down of Syndecan-2 by injection of morpholino designed against the 5′ UTR region of Syndecan-2 mRNA, led to impaired VEGF-dependent angiogenic sprouting in the zebrafish (Chen et al., 2004). These studies point at the importance of the EG, and HSPGs in particular, during vasculogenesis and angiogenesis. As reviewed by Iozzo and San Antonio, HSPGs act in concert with pro-angiogenic factors to control vascular development by providing a depot for these factors, limiting their diffusion and promoting receptor-ligand interaction and intracellular signaling (Iozzo and San Antonio, 2001).

More recent studies by the group of D'amore investigated the function of endomucin (EMCN), an integral sialoglycoprotein present in the EG of capillaries and veins, during angiogenesis (Park-Windhol et al., 2017; LeBlanc et al., 2019). Using a model of mouse retinal vascularization, it was demonstrated that silencing of EMCN resulted in a significant reduction of retinal vessel density and branching (Park-Windhol et al., 2017). Further analyses with human retinal endothelial cells lacking or overexpressing EMCN corroborated the role of EMCN in VEGF-induced signaling pathways by modulating internalization of the VEGF receptor 2 (VEGFR2), thereby regulating EC proliferation and migration (LeBlanc et al., 2019). It was recently shown that this effect of EMCN was dependent on N-glycosylation of its extracellular domain (Hu et al., 2020). Taken together, these studies highlight the essential involvement and contribution of the EG in vessel formation.

## Characterization of the EG in the Fetus and Neonate

One of the challenges in interpreting the results of studies on the EG in pediatric diseases is the lack of reference values. Recent investigations in animals and humans have provided evidence that aging is accompanied by a reduction in the EG size possibly due to increased EG shedding in combination with decreased synthesis of glycocalyx components

(Machin et al., 2018; Majerczak et al., 2019). The glycocalyx thickness in sublingual capillaries of old study participants (mean age 60 ± 2 years) compared to young (mean age 29 ± 1 years) decreased by around 30%. Interestingly, a significant reduction in glycocalyx thickness was also demonstrated in the aging lymphatic vasculature of the rat mesentery with a decrease by more than 50% in 24-month old animals versus 9 month old animals (note: 1 month of life in a rat equals about 3 years in a human) (Zolla et al., 2015). Considering the profound physiological changes occurring in the growing fetus, neonate and child, it seems very likely that the EG is also subject to age-dependent variations. At present, very limited data is available on the ontogeny of the EG. As reported by Henderson-Toth et al. (2012), the EG can be detected in the dorsal aorta of quail embryos at an early developmental stage (14 somites) as soon as blood flow commences. Immunohistochemistry confirmed the presence of functionally important EG components, including hyaluronic acid, heparan sulfate and chondroitin sulfate. Selective enzymatic digestion of these components demonstrated a role of hyaluronan (and chondroitin-/dermatan-sulfate) in maintaining blood flow as well as vascular barrier function, thereby emphasizing the functional importance of the EG at this early developmental stage. Using SDF-imaging for PBR measurements in the cutaneous microcirculation, we have recently shown that the endothelial glycocalyx in preterm and term neonates depends on gestational age at birth (Puchwein-Schwepcke et al., 2021). Intriguingly, we observed an inverse correlation of the EG dimension with gestational age, i.e., the most immature neonates exhibited the thickest EG (represented by low PBR values). Whether this finding reflects the functionally importance of the EG in vascular development remains speculative due to the observational nature of the study. Longitudinal follow-up in the group of preterm infants further demonstrated an effect of postnatal age on the EG with a gradual decrease of EG thickness (increase in PBR). This effect was most pronounced in the group of extremely preterm neonates resulting in significantly higher PBR values (smaller EG) when reaching term age compared to term born neonates. This acceleration of PBR changes over time might be due to the frequent presence of multiple EG stressors (e.g., hyperglycemia, sepsis, reactive oxygen species) and could possibly contribute to a higher vascular vulnerability in this patient group.

Interestingly, PBR values reported for neonates and infants are consistently higher than in adults. In healthy mature newborns (mean age 3 days) the PBR was 2.14 ± 0.25 μm (Puchwein-Schwepcke et al., 2021) versus a PBR of 1.88 ± 0.2 μm measured in healthy adults (mean age 20.7 years) (Astapenko et al., 2019). Likewise, infants with cardiac defects (mean age 8.9 month) had a higher baseline PBR than adult cardiac patients (median age 64–69 years) before undergoing surgery on cardiopulmonary bypass (2.5 μm [2.44–2.7 IQR] vs. 2.0 ± 0.2 μm, respectively) (Nussbaum et al., 2015; Dekker et al., 2019; Dekker et al., 2020). At present it remains unclear whether these differences in PBR magnitude are due to methodological differences (e.g., measurements obtained sublingually versus the fossa auricularis of the ear conch) or truly reflect an age-dependence in PBR values.

Further studies in various age groups and in larger cohorts are needed to better understand the natural course of EG development and establish normal values necessary for the implementation of EG measurements in the clinical routine.

# PATHOLOGY OF THE EG IN ACUTE CHILDHOOD DISEASES AND CHRONIC CONDITIONS WITH CHILDHOOD-ONSET

Shedding of the glycocalyx has been observed in many acute and chronic diseases in adults characterized by inflammation, endothelial dysfunction and microangiopathy, indicating its crucial role in the homeostasis of the microvasculature. In addition, acute events such as surgery or trauma have been shown to affect the glycocalyx, and patient outcome seems to be directly related to the extent of glycocalyx damage (Ostrowski and Johansson, 2012; Qi et al., 2021). In the pediatric population, information on disease-related EG alterations is still limited. Most data stems from studies evaluating the glycocalyx after pediatric heart surgery or pediatric trauma. **Table 1** lists the clinical trials investigating the EG with respect to different pathologies in neonates, infants and children.

## EG in Pediatric Heart Surgery

Surgery on cardiopulmonary bypass has been shown to acutely and severely affect the integrity of the EG in adults (Rehm et al., 2007). In children undergoing cardiac surgery on cardiopulmonary bypass (CPB), an increase of circulating hyaluronan and syndecan-1 was witnessed in dependence of the ischemic impact indicating acute shedding of the EG (Bruegger et al., 2015). This was further confirmed in a longitudinal cohort study investigating 40 children that underwent cardiac surgery (36 with and four without CPB) using SDF-imaging to visualize the microcirculation at the ear conch (Nussbaum et al., 2015). A significant reduction in glycocalyx thickness (indicated by an increased PBR) was observed after cardiac surgery with cardiopulmonary bypass compared to preoperative values. In contrast, no significant change in PBR was observed in control patients subjected to a different procedure requiring general anesthesia (cleft palate surgery, cardiac catheterization), indicating a direct effect of the cardiopulmonary bypass in perturbation of the microvascular glycocalyx in pediatric heart surgery (Nussbaum et al., 2015). Similar results have been obtained in adult patients undergoing coronary bypass operation on CPB, demonstrating a significant increase in PBR during surgery. However, the time course of PBR changes described in adults differs from that in infants. While PBR values were shown to further increase during the first three postoperative days in adults following surgery on cardiopulmonary bypass (Dekker et al., 2019, 2020), in infants PBR values were already decreasing 24 h after surgery (Nussbaum et al., 2015). As the studies vary largely with respect to the underlying cardiac disease (congenital heart defect vs. coronary artery disease), surgical procedures applied and presence of cardiac risk factors, it is impossible to draw a conclusion from these studies regarding possible age-dependent differences in shedding and recovery of the glycocalyx.

**TABLE 1 |** Clinical studies investigating the EG in the pediatric population.

| | Study type | EG parameters | *n* | Mean age | Major findings |
|---|---|---|---|---|---|
| **Pediatric heart surgery** | | | | | |
| Nussbaum et al. (2015) | Longitudinal cohort study | PBR (SDF imaging) | 40 patients (36 with CPB, 4 without CPB) | CPB group: 8.9 months [0.2–29] w/o CPB: 9 months [0.2–31] | Increase in PBR after surgery on CPB |
| Bruegger et al. (2015) | Prospective cohort study | Serum syndecan-1, HA | 42 | 7 months (2.9–23) | Increase of circulating HA and syndecan-1 associated with the ischemic impact |
| Pesonen et al. (2016) | 2 double blinded placebo-controlled trials | Plasma syndecan-1 | 40 (1st trial), 45 (2nd trial) | 1st trial: 7 days (1–27), 2nd trial: 0.37 years (0.15–1.36) | Lower syndecan-1 plasma levels after high-dose steroid treatment in complex heart surgery |
| de Melo Bezerra Cavalcante et al. (2016) | Prospective cohort study | Plasma syndecan-1 | 289 | 3.0 years (SD: ± 4.4) | Association of higher syndecan-1 levels with poorer outcomes and postoperative acute kidney disease |
| Ferrer et al. (2018) | Prospective cohort study | urinary syndecan-1 | 86 | < 2.0 years: 61.2% | Higher postoperative urine syndecan-1 levels in patients with acute kidney injury |
| Bangalore et al. (2021) | Prospective cohort study | Plasma HS | 27 | 4.9 months (1–22 months) | Association of circulating HS with metabolic acidosis, renal dysfunction and capillary leak after CPB |
| **Pediatric trauma** | | | | | |
| Richter et al. (2019) | Prospective cohort study | Plasma syndecan-1, angiopoetin-1 and angiopoetin-2 | 64 (52 trauma, 12 controls) | Trauma: 9.7 years (6.2–13.6), controls: 5 years (1.8–15) | Higher angiopoetin-2 levels associated with worse clinical outcome, pos. correlation of syndecan-1 and angiopoetin-2 |
| Russell et al. (2018) | Prospective cohort study | Plasma syndecan-1 and hcDNA | 211 (149 trauma, 62 controls) | Trauma: 8.3 years (4.6–12.3), controls 6.24 ±6.2 years | Highest syndecan 1 levels correspond to highest hcDNA levels and poor outcome |
| **Pediatric inflammatory and infectious diseases** | | | | | |
| *Kawasaki disease (KD)* | | | | | |
| Ohnishi et al. (2019) | Prospective cohort study | Plasma syndecan-1, HA | 103 (70 complete KD, 18 febrile controls, 15 afebrile controls) | CAL (coronary artery lesions): 27 months (3–121), CAL negative: 18.5 (1–88) | Higher syndecan-1 and HA levels in KD compared to febrile and afebrile controls |
| Luo et al. (2019) | Prospective cohort study | Plasma syndecan-1 | 203 (119 KD, 43 healthy children, 40 children with febrile disease) | 26 months (16.0–43.75) | Higher syndecan-1 levels in KD compared to matched febrile and afebrile controls |
| *COVID-19/PIMS* | | | | | |
| Fraser et al. (2021) | Case report | Plasma HA | 1 pt., 20 controls | 15 years [IQR 8] | Increased HA in a patient suffering from PIMS compared to controls |
| *Malaria* | | | | | |
| Yeo et al. (2019a) | Retrospective analysis of frozen samples of a prospective cohort study | Urinary GAGs | 85 | Uncomplicated Malaria: 3.1 years (0.5–7.8), complicated malaria: 3.6 years (0.6–7.2) | Higher urine excretion of GAGs in malaria groups compared to healthy children |

*(Continued)*

**TABLE 1 |** Continued

| | Study type | EG parameters | *n* | Mean age | Major findings |
|---|---|---|---|---|---|
| Lyimo et al. (2020) | Cross-sectional study | PBR (IDF imaging), plasma sulfated GAGs | 119 (healthy: 31, non-malaria fever NMF: 7, uncomplicated malaria UM: 12, severe malaria SM: 69) | Healthy: 2.5 years (0.8–4.3), NMF: 2.28 years (1.0–4.), UM: 5.5 years (1.1–10.1), SM: 4.1 years (0.6–10.0) | Increased PBR in patients with SM; sulfated GAGs higher in patients with complicated malaria compared to UM; positive association between HA and PBR |
| **Diabetes mellitus** | | | | | |
| Nussbaum et al. (2014) | Observational study | Glycocalyx thickness (SDF imaging) | 14 patients, 14 controls | patients: 13.6 [9.9–14.4], controls: 11.6 [9.7–14] | Reduced EG thickness in diabetic children compared to controls; inverse correlation of EG with blood glucose levels |

In two double-blinded, randomized, placebo-controlled trials, syndecan-1 plasma levels were evaluated in neonates subjected to open heart surgery (neonatal trial) and in infants undergoing correction of a ventricular septal defect (VSD trial) to determine whether high-dose steroid treatment might have a protective effect on the glycocalyx. The authors could prove that in complex heart surgery in neonates, high-dose steroid treatment resulted in lower syndecan-1 levels compared to a placebo group. However, there were no differences in syndecan-1 levels between treatment and placebo groups in older children after VSD repair (Pesonen et al., 2016).

In a prospective cohort study on 289 children undergoing cardiac surgery, higher syndecan-1 levels were associated with poor outcomes and postoperative acute kidney disease (de Melo Bezerra Cavalcante et al., 2016). Similar results were found in a prospective cohort study on 86 pediatric patients recovering from heart surgery. Postoperative urinary syndecan-1 was collected within 2 h after surgery and was higher in patients suffering from acute kidney injury in the follow-up. In addition, the prediction of acute kidney injury in a risk-stratified statistical model of clinical outcome was improved after adding urinary syndecan-1 (Ferrer et al., 2018). These data were recently confirmed and expanded by Bangalore et al. (2021), demonstrating an association of the amount of circulating heparan sulfate with metabolic acidosis, renal dysfunction and capillary leak in 27 neonates and infants following cardiopulmonary bypass surgery.

Collectively, these studies provide univocal evidence for EG alterations in pediatric cardiac surgery contributing to adverse outcomes. Thus, assessment of the EG might offer the potential to identify patients at risk for postoperative complications and serve as a monitoring parameter to evaluate treatment strategies aiming at EG restoration.

## EG in Pediatric Trauma

Multiorgan failure after pediatric trauma has been discussed to be associated with an imbalanced inflammatory reaction that may lead to endothelial disruption and impairment of the glycocalyx. An increase of endothelial-derived angiopoietins (angiopoietin-1 and angiopoietin-2) indicates a developing endotheliopathy, whereas circulating syndecan-1 can be interpreted as a sign of glycocalyx injury. In a prospective cohort study, 52 pediatric trauma patients were compared to 12 pediatric controls with respect to angiopoietin levels, syndecan-1 levels and clinical outcome. The authors could show that higher angiopoietin-2 levels were associated with worse clinical outcomes and were positively correlated to syndecan-1 levels. This may indicate that glycocalyx injury results in adverse outcome (Richter et al., 2019).

Similar findings were observed in another prospective cohort study on 149 pediatric trauma patients and 62 pediatric controls studying the role of histonic DNA (hcDNA) as a marker of damage-associated molecular patterns (DAMPs) and circulating syndecan-1 levels as a marker of EG shedding (Russell et al., 2018). Syndecan-1 levels were evaluated in relation to hcDNA levels at admission and after 24 h. Control patients had low levels of both syndecan-1 and hcDNA, whereas these parameters were significantly higher in the pediatric trauma group, with the highest hcDNA levels corresponding to the highest levels of syndecan-1 and poor outcome. This indicates a link between trauma-induced extracellular hcDNA release and endothelial glycocalyx degradation. However, the causality of the association and the underlying mechanisms still need to be established.

## EG in Pediatric Inflammatory and Infectious Disease

Similarly, infectious diseases may result in acute effects on the microvasculature and the glycocalyx. During sepsis, shedding of the endothelial glycocalyx has been well established in the adult population and linked to mortality (Puskarich et al., 2016; Rovas et al., 2019; Beurskens et al., 2020; Saoraya et al., 2021). In the pediatric population, primarily Kawasaki disease and Malaria were studied for their association with glycocalyx damage.

### Kawasaki Disease (KD)

Serum syndecan-1 and hyaluronic levels were analyzed in a prospective cohort study of 70 children with KD, 18 febrile controls and 15 afebrile controls. Patients suffering from KD had higher serum levels of syndecan-1 and hyaluronan, indicating EG damage. Moreover, patients that developed coronary artery

lesions in the follow-up had higher levels of these parameters in the blood than those who didn't, with serum hyaluronan being a highly contributive predictor of coronary involvement (Ohnishi et al., 2019).

Similar results were obtained in a prospective cohort of 120 pediatric patients with acute KD that were compared to a group of 43 matched healthy and 40 matched febrile controls. Patients suffering from KD had significantly higher levels of syndecan-1 in the plasma compared to febrile and healthy controls. Moreover, syndecan-1 levels were higher in patients suffering from coronary artery involvement than in uncomplicated Kawasaki disease (Luo et al., 2019).

### COVID-19

During the COVID-19 pandemic, a novel syndrome termed PIMS (pediatric inflammatory, multisystem syndrome) or MIS-C (multisystem inflammatory syndrome in children) has emerged in the pediatric population following infection with SARS-CoV-2 (Feldstein et al., 2020; Whittaker et al., 2020). This severe hyperinflammatory condition shares similarities with Kawasaki disease and as with KD, increased levels of glycocalyx degrading enzymes (MMP-7) and hyaluronan have been reported, suggesting shedding of the endothelial glycocalyx (Fraser et al., 2021). Interestingly, in an experimental cell model (human H1299 cells, derived from type 2 alveolar cells) it was shown that SARS-CoV-2 requires cell surface heparan sulfate to promote binding and infection of host cells via angiotensin-converting enzyme (Clausen et al., 2020). Data from post-mortem studies in adults with severe courses of COVID-19 revealed direct involvement of the endothelial cells with widespread endothelitis (Varga et al., 2020). Furthermore, shedding of syndecan-1 and heparan sulfate and an increase in the PBR (i.e., decreased glycocalyx thickness) have been demonstrated during acute COVID-19 disease in adult patients (Stahl et al., 2020; Fernández et al., 2021; Rovas et al., 2021). While PIMS is also characterized by multiorgan involvement, it typically occurs weeks after the initial infection with SARS-CoV-2, which itself may have presented only with mild symptoms or even asymptomatic. Therefore, it is currently unclear whether the supposed disturbance of the glycocalyx in PIMS results from a direct effect of the virus on the endothelium or is rather a consequence of systemic inflammation. As PIMS is a relatively rare condition with reported incidence rates of 2 in 100,000 (Dufort et al., 2020), systematic research on its pathogenesis and the role of the glycocalyx remains a challenge.

### Malaria

Urinary GAGs can be used as a marker of glycocalyx damage. Frozen urine samples of a prospective cohort study from 1994–1995 were thawed and analyzed for glycocalyx damage in three groups- healthy controls (10 children), children with uncomplicated malaria (20 children) and children suffering from cerebral malaria (55 children). Total urine excretion of GAGs was higher in pediatric malaria patients (mean age ∼ 4 years) compared to healthy children and inversely related to plasma nitrate and nitrite levels; however, no difference was seen between infants with cerebral malaria compared to those with uncomplicated disease. The authors concluded that this was a sign of glycocalyx breakdown leading to impaired endothelial nitric oxide (NO) production (Yeo et al., 2019a). By contrast, a study in adult malaria patients from the same group demonstrated significant differences in urinary GAGs between severely affected malaria patients (mean age 25 years) versus patients with a moderate course of disease (mean age 27 years) (Yeo et al., 2019b). The authors hypothesized that these differences might be due to more generalized vascular activation and dysfunction in adult malaria patients compared to children, where vascular dysfunction may possibly be limited to the cerebral microcirculation. In addition, it is conceivable that age dependent differences in glycocalyx breakdown and urinary elimination of GAGs might contribute to the observed differences (Sabir et al., 2020).

In a cross-sectional study on glycocalyx loss in pediatric malaria patients, authors assessed glycocalyx thickness *in vivo* by incident dark Field-imaging and glycocalyx degradation parameters in the plasma. As such, the PBR was increased in severe malaria patients indicating a loss of glycocalyx. Similarly, sulfated GAGs in the plasma were significantly higher in patients with severe malaria compared to those with uncomplicated malaria. There was a positive association between hyaluronic acid and PBR, suggesting that the loss of glycocalyx is related to disease severity (Lyimo et al., 2020).

### EG in Children and Adolescents With Diabetes Mellitus

Many chronic diseases with long-term vascular sequelae are well known to affect the glycocalyx and the microvasculature. Diabetes mellitus type 1 and 2 belong to best-studied conditions with respect to the impact of experimental hyperglycemia on the endothelial glycocalyx (Zuurbier et al., 2005; Nieuwdorp et al., 2006b) as well as changes of the microcirculation and the EG in adult diabetic patients (Nieuwdorp et al., 2006a; Broekhuizen et al., 2010; Dogné et al., 2018; Wadowski et al., 2020). By contrast, only limited data is available on the effect of diabetes mellitus on the EG in the pediatric population. Indirect evidence for a possible impairment of the EG in children with diabetes mellitus stems from studies investigating the hyperemic response to a heat stimulus (Shore et al., 1991; Shah et al., 2015) or following arterial occlusion (Järvisalo et al., 2004; Pillay et al., 2018; Cao et al., 2021), consistently demonstrating endothelial dysfunction with impaired flow-mediated dilation. As the EG was shown to function as a mechanosensor regulating vascular tone in response to increased shear stress (Florian et al., 2003; Curry and Adamson, 2012; Dragovich et al., 2016), the finding of endothelial dysfunction in diabetic children is suggestive of EG alterations in these patients. This notion was supported by an observational study of 14 children between 9 and 14 years of age with diabetes type 1, demonstrating reduced glycocalyx thickness in video recordings of the sublingual microcirculation compared to a control group of 14 children. Furthermore, a significant inverse correlation between serum glucose levels and glycocalyx thickness was observed, suggesting a direct harmful effect of blood sugar levels on the glycocalyx (Nussbaum et al., 2014).

## OUTLOOK AND FUTURE AREAS OF RESEARCH

In view of the importance of the EG for vascular integrity and the possible deleterious effects of EG destruction in acute and chronic diseases, methods to quickly assess the EG's condition in patients would be of high relevance for the clinician. Especially in intensive care medicine, bedside approaches yielding fast results could help to identify patients at risk for adverse outcome and guide clinical decision making. As shown in the GlycoNurse study, after theoretical and practical training, nurses were able to perform high quality PBR measurements in patients of the emergency department and the intensive care unit in less than 10 min duration using a handheld videomicroscope and automated analysis software (Rovas et al., 2018). PBR values showed a high level of inter- and intraobserver reliability and an association with clinical markers of disease severity including mean arterial blood pressure, C-reactive protein levels as a marker of inflammation and SOFA score as an assessment tool for organ failure. Despite these promising results, before EG measurements can be implemented into clinical routine, further studies on larger patient numbers are needed to establish normal values in different age groups, define cut-off values for certain disease entities and evaluate the diagnostic and prognostic usefulness in predicting patient outcome.

In the last decade, the EG has evolved as a possible target for novel treatment strategies aiming at protection or reconstitution of the EG (Becker et al., 2010). Therapeutic approaches evaluated *in vitro* and *in vivo* include reduction of glycocalyx degradation by attenuating inflammation, e.g., by administration of corticosteroids (Chappell et al., 2009a; Pesonen et al., 2016; Brettner et al., 2019) and inhibition of EG degrading enzymes such as heparinase and metallo-matrix proteinases (Chappell et al., 2009b; Mulivor and Lipowsky, 2009; Zeng et al., 2014; Mensah et al., 2017). Furthermore, administration of glycocalyx and plasma components (e.g., sulodexid and albumin) and colloids (e.g., 6% Hydroxyethyl starch) have shown potential benefit in restoring the EG (Broekhuizen et al., 2010; Margraf et al., 2018; Aldecoa et al., 2020). Several of these strategies have lately gained scientific attention during the COVID-19 pandemic due to the increasing evidence for an involvement of the EG in severely affected patients (Buijsers et al., 2020; Okada et al., 2021; Potje et al., 2021). As with most of the studies investigating the EG, almost all of trials were performed in adults. Furthermore, the treatment effect was mostly monitored by evaluating the EG directly and indirectly, whereas patient outcome was usually not considered.

In summary, the EG is recognized as a critical regulator of vascular integrity and health, and its involvement in acute and chronic diseases affecting the vasculature in adult patients has been well established. In the pediatric population, research concerning the EG is still sparse. Future studies are needed to characterize the normal evolution of the EG during infant and child development, define the contribution of the EG to childhood pathology, evaluate its potential as therapeutic target and prove the benefit of EG preservation/reconstitution on patient outcome.

## AUTHOR CONTRIBUTIONS

AP-S and CN wrote the manuscript. OG-B revised the manuscript. All authors contributed to the article and approved the submitted version.

## REFERENCES


Aldecoa, C., Llau, J. V., Nuvials, X., and Artigas, A. (2020). Role of albumin in the preservation of endothelial glycocalyx integrity and the microcirculation: a review. *Ann. Intens. Care* 10:85.

Arokiasamy, S., King, R., Boulaghrasse, H., Poston, R. N., Nourshargh, S., Wang, W., et al. (2019). Heparanase-dependent remodeling of initial lymphatic glycocalyx regulates tissue-fluid drainage during acute inflammation in vivo. *Front. Immunol.* 10:2316. doi: 10.3389/fimmu.2019.02316

Astapenko, D., Ticha, A., Tomasova, A., Hyspler, R., Zadak, Z., Lehmann, C., et al. (2019). Evaluation of endothelial glycocalyx in healthy volunteers – An observational study. *Clin. Hemorheol. Microcirc.* 75, 257–265.

Bangalore, H., Carter, M. J., Parmar, K., Austin, C., Shankar-Hari, M., Hunt, B. J., et al. (2021). Degradation of the endothelial glycocalyx contributes to metabolic acidosis in children following cardiopulmonary bypass surgery. *Pediatr. Crit. Care Med.* [Epub ahead of print].

Becker, B. F., Chappell, D., Bruegger, D., Annecke, T., and Jacob, M. (2010). Therapeutic strategies targeting the endothelial glycocalyx: acute deficits, but great potential. *Cardiovasc. Res.* 87, 300–310. doi: 10.1093/cvr/cvq137

Beurskens, D. M., Bol, M. E., Delhaas, T., van de Poll, M. C., Reutelingsperger, C. P., Nicolaes, G. A., et al. (2020). Decreased endothelial glycocalyx thickness is an early predictor of mortality in sepsis. *Anaes. Intens. Care* 48, 221–228. doi: 10.1177/0310057x20916471

Brettner, F., Chappell, D., Nebelsiek, T., Hauer, D., Schelling, G., Becker, B. F., et al. (2019). Preinterventional hydrocortisone sustains the endothelial glycocalyx in cardiac surgery. *Clin. Hemorheol. Microc.* 71, 59–70. doi: 10.3233/ch-180384

Broekhuizen, L. N., Lemkes, B. A., Mooij, H. L., Meuwese, M. C., Verberne, H., Holleman, F., et al. (2010). Effect of sulodexide on endothelial glycocalyx and vascular permeability in patients with type 2 diabetes mellitus. *Diabetologia* 53, 2646–2655. doi: 10.1007/s00125-010-1910-x

Bruegger, D., Brettner, F., Rossberg, I., Nussbaum, C., Kowalski, C., Januszewska, K., et al. (2015). Acute degradation of the endothelial glycocalyx in infants undergoing cardiac surgical procedures. *Ann. Thorac. Surg.* 99, 926–931. doi: 10.1016/j.athoracsur.2014.10.013

Buijsers, B., Yanginlar, C., de Nooijer, A., Grondman, I., Maciej-Hulme, M. L., Jonkman, I., et al. (2020). Increased plasma heparanase activity in COVID-19 patients. *Front. Immunol.* 11:575047. doi: 10.3389/fimmu.2020.575047

Cao, L., Hou, M., Zhou, W., Sun, L., Shen, J., Chen, Y., et al. (2021). Decreased flow-mediated dilatation in children with Type 1 diabetes: a systematic review and meta-analysis. *Angiology* 33197211010096. [Epub ahead of print].

Cerny, V., Astapenko, D., Burkovskiy, I., Hyspler, R., Ticha, A., Trevors, M. A., et al. (2017). Glycocalyx in vivo measurement. *Clin. Hemorheol. Microcirc.* 67, 499–503. doi: 10.3233/ch-179235

Chappell, D., Hofmann-Kiefer, K., Jacob, M., Rehm, M., Briegel, J., Welsch, U., et al. (2009a). TNF-alpha induced shedding of the endothelial glycocalyx is prevented by hydrocortisone and antithrombin. *Basic Res. Cardiol.* 104, 78–89. doi: 10.1007/s00395-008-0749-5

Chappell, D., Jacob, M., Hofmann-Kiefer, K., Rehm, M., Welsch, U., Conzen, P., et al. (2009b). Antithrombin reduces shedding of the endothelial glycocalyx following ischaemia/reperfusion. *Cardiovasc. Res.* 83, 388–396. doi: 10.1093/cvr/cvp097

Chen, E., Hermanson, S., and Ekker, S. C. (2004). Syndecan-2 is essential for angiogenic sprouting during zebrafish development. *Blood* 103, 1710–1719. doi: 10.1182/blood-2003-06-1783

Clausen, T. M., Sandoval, D. R., Spliid, C. B., Pihl, J., Perrett, H. R., Painter, C. D., et al. (2020). SARS-CoV-2 infection depends on cellular heparan sulfate and ACE2. *Cell* 183, 1043–1057.e15.

Conway, E. M., Collen, D., and Carmeliet, P. (2001). Molecular mechanisms of blood vessel growth. *Cardiovasc. Res.* 49, 507–521. doi: 10.1016/s0008-6363(00)00281-9

Cosgun, Z. C., Fels, B., and Kusche-Vihrog, K. (2020). Nanomechanics of the endothelial glycocalyx: from structure to function. *Am. J. Pathol.* 190, 732–741. doi: 10.1016/j.ajpath.2019.07.021

Couchman, J. R., and Pataki, C. A. (2012). An introduction to proteoglycans and their localization. *J Histochem. Cytochem.* 60, 885–897. doi: 10.1369/0022155412464638

Curry, F. E., and Adamson, R. H. (2012). Endothelial glycocalyx: permeability barrier and mechanosensor. *Ann. Biomed. Eng.* 40, 828–839. doi: 10.1007/s10439-011-0429-8

de Melo Bezerra Cavalcante, C. T., Castelo Branco, K. M., Pinto Júnior, V. C., Meneses, G. C., de Oliveira Neves, F. M., de Souza, N. M., et al. (2016). Syndecan-1 improves severe acute kidney injury prediction after pediatric cardiac surgery. *J. Thorac. Cardiovasc. Surg.* 152, 178–186.e2.

Dekker, N. A. M., Veerhoek, D., Koning, N. J., van Leeuwen, A. L. I., Elbers, P. W. G., van den Brom, C. E., et al. (2019). Postoperative microcirculatory perfusion and endothelial glycocalyx shedding following cardiac surgery with cardiopulmonary bypass. *Anaesthesia* 74, 609–618. doi: 10.1111/anae.14577

Dekker, N. A. M., Veerhoek, D., van Leeuwen, A. L. I., Vonk, A. B. A., van den Brom, C. E., and Boer, C. (2020). Microvascular alterations during cardiac surgery using a heparin or phosphorylcholine-coated circuit. *J. Cardiothorac. Vasc. Anesth.* 34, 912–919. doi: 10.1053/j.jvca.2019.10.012

Dogné, S., Flamion, B., and Caron, N. (2018). Endothelial glycocalyx as a shield against diabetic vascular complications: involvement of hyaluronan and hyaluronidases. *Arterioscler. Thromb. Vasc. Biol.* 38, 1427–1439. doi: 10.1161/atvbaha.118.310839

Dragovich, M. A., Chester, D., Fu, B. M., Wu, C., Xu, Y., Goligorsky, M. S., et al. (2016). Mechanotransduction of the endothelial glycocalyx mediates nitric oxide production through activation of TRP channels. *Am. J. Physiol. Cell Physiol.* 311, C846–C853.

Dufort, E. M., Koumans, E. H., Chow, E. J., Rosenthal, E. M., Muse, A., Rowlands, J., et al. (2020). Multisystem inflammatory syndrome in children in New York state. *N. Engl. J. Med.* 383, 347–358.

Eickhoff, M. K., Winther, S. A., Hansen, T. W., Diaz, L. J., Persson, F., Rossing, P., et al. (2020). Assessment of the sublingual microcirculation with the GlycoCheck system: reproducibility and examination conditions. *PLoS One* 15:e0243737. doi: 10.1371/journal.pone.0243737

Erdem, Ö, Ince, C., Tibboel, D., and Kuiper, J. W. (2019). Assessing the microcirculation with handheld vital microscopy in critically ill neonates and children: evolution of the technique and its potential for critical Care. *Front. Pediatr.* 7:273. doi: 10.3389/fped.2019.00273

Feldstein, L. R., Rose, E. B., and Randolph, A. G. (2020). Multisystem Inflammatory syndrome in children in the United States. *N. Engl. J. Med.* 383, 1794–1795.

Fernández, S., Moreno-Castaño, A. B., Palomo, M., Martinez-Sanchez, J., Torramadé-Moix, S., Téllez, A., et al. (2021). Distinctive biomarker features in the endotheliopathy of COVID-19 and septic syndromes. *Shock.* [Epub ahead of print].

Ferrer, N. M. B., de Melo Bezerra Cavalcante, C. T., Branco, K. M. C., Júnior, V. C. P., Meneses, G. C., de Oliveira Neves, F. M., et al. (2018). Urinary Syndecan-1 and acute kidney injury after pediatric cardiac surgery. *Clin. Chim. Acta* 485, 205–209. doi: 10.1016/j.cca.2018.06.033

Florian, J. A., Kosky, J. R., Ainslie, K., Pang, Z., Dull, R. O., and Tarbell, J. M. (2003). Heparan sulfate proteoglycan is a mechanosensor on endothelial cells. *Circ. Res.* 93, e136–e142.

Fraser, D. D., Patterson, E. K., Daley, M., and Cepinskas, G. (2021). Case report: inflammation and endothelial injury profiling of COVID-19 pediatric multisystem inflammatory syndrome (MIS-C). *Front. Pediatr.* 9:597926. doi: 10.3389/fped.2021.597926

Genzel-Boroviczeny, O., Strotgen, J., Harris, A. G., Messmer, K., and Christ, F. (2002). Orthogonal polarization spectral imaging (OPS): a novel method to measure the microcirculation in term and preterm infants transcutaneously. *Pediatr. Res.* 51, 386–391. doi: 10.1203/00006450-200203000-00019

Gitay-Goren, H., Soker, S., Vlodavsky, I., and Neufeld, G. (1992). The binding of vascular endothelial growth factor to its receptors is dependent on cell surface-associated heparin-like molecules. *J. Biol. Chem.* 267, 6093–6098. doi: 10.1016/s0021-9258(18)42666-x

Harfouche, R., Hentschel, D. M., Piecewicz, S., Basu, S., Print, C., Eavarone, D., et al. (2009). Glycome and transcriptome regulation of vasculogenesis. *Circulation* 120, 1883–1892. doi: 10.1161/circulationaha.108.837724

Henderson-Toth, C. E., Jahnsen, E. D., Jamarani, R., Al-Roubaie, S., and Jones, E. A. (2012). The glycocalyx is present as soon as blood flow is initiated and is required for normal vascular development. *Dev. Biol.* 369, 330–339. doi: 10.1016/j.ydbio.2012.07.009

Hu, Z., Cano, I., Saez-Torres, K. L., LeBlanc, M. E., Saint-Geniez, M., Ng, Y. S., et al. (2020). Elements of the endomucin extracellular domain essential for VEGF-induced VEGFR2 activity. *Cells* 9:1413. doi: 10.3390/cells9061413

Iozzo, R. V., and San Antonio, J. D. (2001). Heparan sulfate proteoglycans: heavy hitters in the angiogenesis arena. *J. Clin. Invest.* 108, 349–355. doi: 10.1172/jci200113738

Järvisalo, M. J., Raitakari, M., Toikka, J. O., Putto-Laurila, A., Rontu, R., Laine, S., et al. (2004). Endothelial dysfunction and increased arterial intima-media thickness in children with type 1 diabetes. *Circulation* 109, 1750–1755. doi: 10.1161/01.cir.0000124725.46165.2c

LeBlanc, M. E., Saez-Torres, K. L., Cano, I., Hu, Z., Saint-Geniez, M., Ng, Y. S., et al. (2019). Glycocalyx regulation of vascular endothelial growth factor receptor 2 activity. *FASEB J.* 33, 9362–9373. doi: 10.1096/fj.201900011r

Lee, D. H., Dane, M. J., van den Berg, B. M., Boels, M. G., van Teeffelen, J. W., de Mutsert, R., et al. (2014). Deeper penetration of erythrocytes into the endothelial glycocalyx is associated with impaired microvascular perfusion. *PLoS One* 9:e96477. doi: 10.1371/journal.pone.0096477

Luft, J. H. (1966). Fine structures of capillary and endocapillary layer as revealed by ruthenium red. *Feder. Proc.* 25, 1773–1783.

Lundin, L., Larsson, H., Kreuger, J., Kanda, S., Lindahl, U., Salmivirta, M., et al. (2000). Selectively desulfated heparin inhibits fibroblast growth factor-induced mitogenicity and angiogenesis. *J. Biol. Chem.* 275, 24653–24660. doi: 10.1074/jbc.m908930199

Luo, L., Feng, S., Wu, Y., Su, Y., Jing, F., and Yi, Q. (2019). Serum levels of Syndecan-1 in patients With Kawasaki disease. *Pediatr. Infect. Dis. J.* 38, 89–94. doi: 10.1097/inf.0000000000002047

Lyimo, E., Haslund, L. E., Ramsing, T., Wang, C. W., Efunshile, A. M., Manjurano, A., et al. (2020). In vivo imaging of the buccal mucosa shows loss of the endothelial glycocalyx and perivascular hemorrhages in pediatric plasmodium falciparum malaria. *Infect. Immun.* 88:e00679-19.

Machin, D. R., Bloom, S. I., Campbell, R. A., Phuong, T. T. T., Gates, P. E., Lesniewski, L. A., et al. (2018). Advanced age results in a diminished endothelial glycocalyx. *Am. J. Physiol. Heart Circ. Physiol.* 315, H531–H539.

Majerczak, J., Grandys, M., Frołow, M., Szkutnik, Z., Zakrzewska, A., Niñankowski, R., et al. (2019). Age-dependent impairment in endothelial function and arterial stiffness in former high class male athletes is no different to that in men with no history of physical training. *J. Am. Heart Assoc.* 8:e012670.

Margraf, A., Herter, J. M., Kühne, K., Stadtmann, A., Ermert, T., Wenk, M., et al. (2018). 6% hydroxyethyl starch (HES 130/0.4) diminishes glycocalyx degradation and decreases vascular permeability during systemic and pulmonary inflammation in mice. *Crit. Care* 22:111.

Megens, R. T., Reitsma, S., Schiffers, P. H., Hilgers, R. H., De Mey, J. G., Slaaf, D. W., et al. (2007). Two-photon microscopy of vital murine elastic and muscular arteries. Combined structural and functional imaging with subcellular resolution. *J. Vasc. Res.* 44, 87–98. doi: 10.1159/000098259

Mensah, S. A., Cheng, M. J., Homayoni, H., Plouffe, B. D., Coury, A. J., and Ebong, E. E. (2017). Regeneration of glycocalyx by heparan sulfate and sphingosine 1-phosphate restores inter-endothelial communication. *PLoS One* 12:e0186116. doi: 10.1371/journal.pone.0186116

Michel, C. C., and Curry, F. R. (2009). Glycocalyx volume: a critical review of tracer dilution methods for its measurement. *Microcirculation* 16, 213–219. doi: 10.1080/10739680802527404

Mulivor, A. W., and Lipowsky, H. H. (2009). Inhibition of glycan shedding and leukocyte-endothelial adhesion in postcapillary venules by suppression of

matrixmetalloprotease activity with doxycycline. *Microcirculation* 16, 657–666. doi: 10.3109/10739680903133714

Naito, H., Iba, T., and Takakura, N. (2020). Mechanisms of new blood-vessel formation and proliferative heterogeneity of endothelial cells. *Int. Immunol.* 32, 295–305. doi: 10.1093/intimm/dxaa008

Nieuwdorp, M., Mooij, H. L., Kroon, J., Atasever, B., Spaan, J. A., Ince, C., et al. (2006a). Endothelial glycocalyx damage coincides with microalbuminuria in type 1 diabetes. *Diabetes* 55, 1127–1132. doi: 10.2337/diabetes.55.04.06.db05-1619

Nieuwdorp, M., van Haeften, T. W., Gouverneur, M. C., Mooij, H. L., van Lieshout, M. H., Levi, M., et al. (2006b). Loss of endothelial glycocalyx during acute hyperglycemia coincides with endothelial dysfunction and coagulation activation in vivo. *Diabetes* 55, 480–486. doi: 10.2337/diabetes.55.02.06.db05-1103

Noguer, O., Villena, J., Lorita, J., Vilaró, S., and Reina, M. (2009). Syndecan-2 downregulation impairs angiogenesis in human microvascular endothelial cells. *Exp. Cell Res.* 315, 795–808. doi: 10.1016/j.yexcr.2008.11.016

Nussbaum, C., Cavalcanti Fernandes Heringa, A., Mormanova, Z., Puchwein-Schwepcke, A. F., Bechtold-Dalla Pozza, S., and Genzel-Boroviczeny, O. (2014). Early microvascular changes with loss of the glycocalyx in children with type 1 diabetes. *J. Pediatr.* 164, 584–589.e1.

Nussbaum, C., Haberer, A., Tiefenthaller, A., Januszewska, K., Chappell, D., Brettner, F., et al. (2015). Perturbation of the microvascular glycocalyx and perfusion in infants after cardiopulmonary bypass. *J. Thorac. Cardiovasc. Surg.* 150, 1474–1481.e1.

Ohnishi, Y., Yasudo, H., Suzuki, Y., Furuta, T., Matsuguma, C., Azuma, Y., et al. (2019). Circulating endothelial glycocalyx components as a predictive marker of coronary artery lesions in Kawasaki disease. *Int. J. Cardiol.* 292, 236–240. doi: 10.1016/j.ijcard.2019.05.045

Okada, H., Yoshida, S., Hara, A., Ogura, S., and Tomita, H. (2021). Vascular endothelial injury exacerbates coronavirus disease 2019: the role of endothelial glycocalyx protection. *Microcirculation* 28:e12654.

Ostrowski, S. R., and Johansson, P. I. (2012). Endothelial glycocalyx degradation induces endogenous heparinization in patients with severe injury and early traumatic coagulopathy. *J. Trauma Acute Care Surg.* 73, 60–66. doi: 10.1097/ta.0b013e31825b5c10

Park-Windhol, C., Ng, Y. S., Yang, J., Primo, V., Saint-Geniez, M., and D'Amore, P. A. (2017). Endomucin inhibits VEGF-induced endothelial cell migration, growth, and morphogenesis by modulating VEGFR2 signaling. *Sci. Rep.* 7:17138.

Pesonen, E., Keski-Nisula, J., Andersson, S., Palo, R., Salminen, J., and Suominen, P. K. (2016). High-dose methylprednisolone and endothelial glycocalyx in paediatric heart surgery. *Acta Anaesthesiol. Scand.* 60, 1386–1394. doi: 10.1111/aas.12785

Piecewicz, S., and Sengupta, S. (2011). The dynamic glycome microenvironment and stem cell differentiation into vasculature. *Stem Cells Dev.* 20, 749–758. doi: 10.1089/scd.2010.0454

Pillay, S., Anderson, J., Couper, J., Maftei, O., Gent, R., and Peña, A. S. (2018). Children with Type 1 diabetes have delayed flow-mediated dilation. *Can. J. Diabet.* 42, 276–280. doi: 10.1016/j.jcjd.2017.06.011

Pillinger, N. L., and Kam, P. (2017). Endothelial glycocalyx: basic science and clinical implications. *Anaes. Intens. Care* 45, 295–307. doi: 10.1177/0310057x1704500305

Potje, S. R., Costa, T. J., Fraga-Silva, T. F. C., Martins, R. B., Benatti, M. N., Almado, C. E. L., et al. (2021). Heparin prevents in vitro glycocalyx shedding induced by plasma from COVID-19 patients. *Life Sci.* 276, 119376. doi: 10.1016/j.lfs.2021.119376

Puchwein-Schwepcke, A., Artmann, S., Rajwich, L., Genzel-Boroviczény, O., and Nussbaum, C. (2021). Effect of gestational age and postnatal age on the endothelial glycocalyx in neonates. *Sci. Rep.* 11: 3133.

Puskarich, M. A., Cornelius, D. C., Tharp, J., Nandi, U., and Jones, A. E. (2016). Plasma syndecan-1 levels identify a cohort of patients with severe sepsis at high risk for intubation after large-volume intravenous fluid resuscitation. *J. Crit. Care* 36, 125–129. doi: 10.1016/j.jcrc.2016.06.027

Qi, F., Zhou, H., Gu, P., Tang, Z. H., Zhu, B. F., Chen, J. R., et al. (2021). Endothelial glycocalyx degradation is associated with early organ impairment in polytrauma patients. *BMC Emerg. Med.* 21:52. doi: 10.1186/s12873-021-00446-y

Rehm, M., Bruegger, D., Christ, F., Conzen, P., Thiel, M., Jacob, M., et al. (2007). Shedding of the endothelial glycocalyx in patients undergoing major vascular surgery with global and regional ischemia. *Circulation* 116, 1896–1906. doi: 10.1161/circulationaha.106.684852

Reitsma, S., Slaaf, D. W., Vink, H., van Zandvoort, M. A., and oude Egbrink, M. G. (2007). The endothelial glycocalyx: composition, functions, and visualization. *Pflugers Arch.* 454, 345–359. doi: 10.1007/s00424-007-0212-8

Richter, R. P., Russell, R. T., Hu, P. J., Uhlich, R. M., Swain, T. A., Kerby, J. D., et al. (2019). Plasma Angiopoietin-2/-1 ratio is elevated and Angiopoietin-2 levels correlate with plasma Syndecan-1 following pediatric Trauma. *Shock* 52, 340–346. doi: 10.1097/shk.0000000000001267

Rovas, A., Lukasz, A. H., Vink, H., Urban, M., Sackarnd, J., Pavenstädt, H., et al. (2018). Bedside analysis of the sublingual microvascular glycocalyx in the emergency room and intensive care unit – the GlycoNurse study. *Scand. J. Trauma Resusc. Emerg. Med.* 26:16.

Rovas, A., Osiaevi, I., Buscher, K., Sackarnd, J., Tepasse, P. R., Fobker, M., et al. (2021). Microvascular dysfunction in COVID-19: the MYSTIC study. *Angiogenesis* 24, 145–157. doi: 10.1007/s10456-020-09753-7

Rovas, A., Seidel, L. M., Vink, H., Pohlkötter, T., Pavenstädt, H., Ertmer, C., et al. (2019). Association of sublingual microcirculation parameters and endothelial glycocalyx dimensions in resuscitated sepsis. *Crit. Care* 23:260.

Russell, R. T., Christiaans, S. C., Nice, T. R., Banks, M., Mortellaro, V. E., Morgan, C., et al. (2018). Histone-complexed DNA fragments levels are associated with coagulopathy, endothelial cell damage, and increased mortality after severe pediatric Trauma. *Shock* 49, 44–52. doi: 10.1097/shk.0000000000000902

Sabir, E. S., Lafhal, K., Ezoubeiri, A., Harkati, I., Sbyea, S., Aldamiz-Echevarria, L., et al. (2020). Usefulness of urinary glycosaminoglycans assay for a mucopolysaccharidosis-specific screening. *Pediatr. Int.* 62, 1077–1085. doi: 10.1111/ped.14278

Saoraya, J., Wongsamita, L., Srisawat, N., and Musikatavorn, K. (2021). Plasma syndecan-1 is associated with fluid requirements and clinical outcomes in emergency department patients with sepsis. *Am. J. Emerg. Med.* 42, 83–89. doi: 10.1016/j.ajem.2021.01.019

Sarrazin, S., Lamanna, W. C., and Esko, J. D. (2011). Heparan sulfate proteoglycans. *Cold Spring Harb. Perspect. Biol.* 3:a004952.

Shah, A. S., Gao, Z., Dolan, L. M., Dabelea, D., D'Agostino, R. B. Jr., and Urbina, E. M. (2015). Assessing endothelial dysfunction in adolescents and young adults with type 1 diabetes mellitus using a non-invasive heat stimulus. *Pediatr. Diabet.* 16, 434–440.

Shore, A. C., Price, K. J., Sandeman, D. D., Green, E. M., Tripp, J. H., and Tooke, J. E. (1991). Impaired microvascular hyperaemic response in children with diabetes mellitus. *Diabet. Med.* 8, 619–623. doi: 10.1111/j.1464-5491.1991.tb01667.x

Stahl, K., Gronski, P. A., Kiyan, Y., Seeliger, B., Bertram, A., Pape, T., et al. (2020). Injury to the endothelial glycocalyx in critically ill patients with COVID-19. *Am. J. Respir. Crit. Care Med.* 202, 1178–1181. doi: 10.1164/rccm.202007-2676le

Varga, Z., Flammer, A. J., Steiger, P., Haberecker, M., Andermatt, R., Zinkernagel, A. S., et al. (2020). Endothelial cell infection and endotheliitis in COVID-19. *Lancet* 395, 1417–1418. doi: 10.1016/s0140-6736(20)30937-5

Vink, H., and Duling, B. R. (1996). Identification of distinct luminal domains for macromolecules, erythrocytes, and leukocytes within mammalian capillaries. *Circ. Res.* 79, 581–589. doi: 10.1161/01.res.79.3.581

Vlahu, C. A., Lemkes, B. A., Struijk, D. G., Koopman, M. G., Krediet, R. T., and Vink, H. (2012). Damage of the endothelial glycocalyx in dialysis patients. *J. Am. Soc. Nephrol.* 23, 1900–1908. doi: 10.1681/asn.2011121181

Wadowski, P. P., Kautzky-Willer, A., Gremmel, T., Koppensteiner, R., Wolf, P., Ertl, S., et al. (2020). Sublingual microvasculature in diabetic patients. *Microvasc. Res.* 129:103971. doi: 10.1016/j.mvr.2019.103971

Weinbaum, S., Tarbell, J. M., and Damiano, E. R. (2007). The structure and function of the endothelial glycocalyx layer. *Ann. Rev. Biomed. Eng.* 9, 121–167. doi: 10.1146/annurev.bioeng.9.060906.151959

Whittaker, E., Bamford, A., Kenny, J., Kaforou, M., Jones, C. E., Shah, P., et al. (2020). Clinical characteristics of 58 children with a pediatric inflammatory multisystem syndrome temporally associated with SARS-CoV-2. *JAMA* 324, 259–269.

Wu, Z., Rademakers, T., Kiessling, F., Vogt, M., Westein, E., Weber, C., et al. (2017). Multi-photon microscopy in cardiovascular research. *Methods (San Diego, Calif.)* 130, 79–89. doi: 10.1016/j.ymeth.2017.04.013

Yayon, A., Klagsbrun, M., Esko, J. D., Leder, P., and Ornitz, D. M. (1991). Cell surface, heparin-like molecules are required for binding of basic fibroblast growth factor to its high affinity receptor. *Cell* 64, 841–848. doi: 10.1016/0092-8674(91)90512-w

Yeo, T. W., Bush, P. A., Chen, Y., Young, S. P., Zhang, H., Millington, D. S., et al. (2019a). Glycocalyx breakdown is increased in African children with cerebral and uncomplicated falciparum malaria. *FASEB J.* 33, 14185–14193. doi: 10.1096/fj.201901048rr

Yeo, T. W., Weinberg, J. B., Lampah, D. A., Kenangalem, E., Bush, P., Chen, Y., et al. (2019b). Glycocalyx breakdown is associated with severe disease and fatal outcome in plasmodium falciparum Malaria. *Clin. Infect. Dis.* 69, 1712–1720. doi: 10.1093/cid/ciz038

Zeng, Y., Adamson, R. H., Curry, F. R., and Tarbell, J. M. (2014). Sphingosine-1-phosphate protects endothelial glycocalyx by inhibiting syndecan-1 shedding. *Am. J. Physiol. Heart Circ. Physiol.* 306, H363–H372.

Zolla, V., Nizamutdinova, I. T., Scharf, B., Clement, C. C., Maejima, D., Akl, T., et al. (2015). Aging-related anatomical and biochemical changes in lymphatic collectors impair lymph transport, fluid homeostasis, and pathogen clearance. *Aging Cell* 14, 582–594. doi: 10.1111/acel.12330

Zuurbier, C. J., Demirci, C., Koeman, A., Vink, H., and Ince, C. (2005). Short-term hyperglycemia increases endothelial glycocalyx permeability and acutely decreases lineal density of capillaries with flowing red blood cells. *J. Appl. Physiol. (1985)* 99, 1471–1476. doi: 10.1152/japplphysiol.00436.2005

**Conflict of Interest:** The authors declare that the research was conducted in the absence of any commercial or financial relationships that could be construed as a potential conflict of interest.

**Publisher's Note:** All claims expressed in this article are solely those of the authors and do not necessarily represent those of their affiliated organizations, or those of the publisher, the editors and the reviewers. Any product that may be evaluated in this article, or claim that may be made by its manufacturer, is not guaranteed or endorsed by the publisher.

frontiers in Cell and Developmental Biology

REVIEW
published: 03 September 2021
doi: 10.3389/fcell.2021.731641

# The Role of the Glycocalyx in the Pathophysiology of Subarachnoid Hemorrhage-Induced Delayed Cerebral Ischemia

*Hanna Schenck[1]*, Eliisa Netti[2], Onno Teernstra[1], Inger De Ridder[3], Jim Dings[1], Mika Niemelä[2], Yasin Temel[1], Govert Hoogland[1] and Roel Haeren[1,2]*

*[1] Department of Neurosurgery, Maastricht University Medical Center, Maastricht, Netherlands, [2] Department of Neurosurgery, Helsinki University Hospital, Helsinki, Finland, [3] Department of Neurology, Cardiovascular Research Institute Maastricht, Maastricht University Medical Center, Maastricht, Netherlands*

The glycocalyx is an important constituent of blood vessels located between the bloodstream and the endothelium. It plays a pivotal role in intercellular interactions in neuroinflammation, reduction of vascular oxidative stress, and provides a barrier regulating vascular permeability. In the brain, the glycocalyx is closely related to functions of the blood-brain barrier and neurovascular unit, both responsible for adequate neurovascular responses to potential threats to cerebral homeostasis. An aneurysmal subarachnoid hemorrhage (aSAH) occurs following rupture of an intracranial aneurysm and leads to immediate brain damage (early brain injury). In some cases, this can result in secondary brain damage, also known as delayed cerebral ischemia (DCI). DCI is a life-threatening condition that affects up to 30% of all aSAH patients. As such, it is associated with substantial societal and healthcare-related costs. Causes of DCI are multifactorial and thought to involve neuroinflammation, oxidative stress, neuroinflammation, thrombosis, and neurovascular uncoupling. To date, prediction of DCI is limited, and preventive and effective treatment strategies of DCI are scarce. There is increasing evidence that the glycocalyx is disrupted following an aSAH, and that glycocalyx disruption could precipitate or aggravate DCI. This review explores the potential role of the glycocalyx in the pathophysiological mechanisms contributing to DCI following aSAH. Understanding the role of the glycocalyx in DCI could advance the development of improved methods to predict DCI or identify patients at risk for DCI. This knowledge may also alter the methods and timing of preventive and treatment strategies of DCI. To this end, we review the potential and limitations of methods currently used to evaluate the glycocalyx, and strategies to restore or prevent glycocalyx shedding.

**Keywords: subarachnoid hemorrhage, aneurysm, delayed cerebral ischemia, glycocalyx, pathophysiology, review**

OPEN ACCESS

***Edited by:***
*Bingmei M. Fu,*
*City College of New York (CUNY), United States*

***Reviewed by:***
*H. E. Hinson,*
*Oregon Health and Science University, United States*
*Tahir Ali,*
*Peking University, China*

****Correspondence:***
*Hanna Schenck*
*hanna.schenck@mumc.nl*

***Specialty section:***
*This article was submitted to Signaling, a section of the journal Frontiers in Cell and Developmental Biology*

***Received:*** *27 June 2021*
***Accepted:*** *06 August 2021*
***Published:*** *03 September 2021*

***Citation:***
*Schenck H, Netti E, Teernstra O, De Ridder I, Dings J, Niemelä M, Temel Y, Hoogland G and Haeren R (2021) The Role of the Glycocalyx in the Pathophysiology of Subarachnoid Hemorrhage-Induced Delayed Cerebral Ischemia. Front. Cell Dev. Biol. 9:731641. doi: 10.3389/fcell.2021.731641*

## INTRODUCTION

Intracranial aneurysms (IAs) are a common vascular pathology affecting around 2.8% of the population (Vlak et al., 2011). Rupture of an IA leads to a subarachnoid hemorrhage (aSAH), which is associated with high morbidity and mortality rates (Vlak et al., 2011). Yearly, aSAH affect around 9 per 100,000 persons, with a median age of 55 years (Zacharia et al., 2010; Geraghty and Testai, 2017). Despite the advent of new therapies to treat aSAH, the clinical course of aSAH is prone to severe complications.

Initially, the rupture of an IA results in immediate damage to the brain, also referred to as early brain injury (EBI). A delayed response to EBI commonly presents between 4 and 10 days following ictus, and occurs in around 30% of aSAH (Geraghty and Testai, 2017; Peeyush Kumar et al., 2019). This response is called delayed cerebral ischemia (DCI), defined as the development of a new neurological deficit, or a decrease in the Glasgow Coma Scale by two or more points lasting for at least 1 h after exclusion of other complications (Vergouwen et al., 2010). DCI strongly affects the outcome of aSAH, as it increases morbidity and mortality rates among aSAH patients, and also prolongs hospital stays.

Until recently, DCI was considered a clinical manifestation of cerebral vasospasm, i.e., the narrowing of large intracranial arteries (Suzuki et al., 1983; Vergouwen et al., 2010). However, studies targeting vasospasm have failed to reduce the incidence of DCI. Moreover, DCI was observed in the absence of radiological vasospasms (Stein et al., 2006; Dhar and Diringer, 2015; Oka et al., 2020). These incongruences have resulted in a paradigm shift toward focusing on microvascular changes in the pathophysiology of DCI. Subsequently, several processes including neuro-inflammation, oxidative stress, neurovascular uncoupling, and microthrombosis have been related to endothelial dysfunction and the development of DCI (Budohoski et al., 2014). However, the complete pathophysiological process underlying DCI is poorly understood, thereby impeding early diagnosis and targeted treatment.

In this regard, disruption of the glycocalyx may be a relevant contributor to endothelial dysfunction and the associated processes in the development of DCI. The glycocalyx is a gel-like layer covering the luminal side of the endothelium, and is involved in numerous mechanisms regulating endothelial functions (Reitsma et al., 2007). Located between the bloodstream and the endothelium, the glycocalyx protects the endothelium and functions as an interface for integrating various signals involved in inflammation, nitric oxide (NO) release, and coagulation (Tarbell and Pahakis, 2006; Abassi et al., 2020). In recent years, the glycocalyx has gained wider attention for its pathophysiological role in the development of a multitude of vascular pathologies, like atherosclerosis and sepsis, as well as neurological disorders, like small vessel disease and epilepsy (Martens et al., 2013; Rovas et al., 2019; Yamaoka-Tojo, 2020a). Multiple studies have reported that molecules like TNF-alpha, atrial natriuretic peptide, and abnormal vascular shear stress can induce damage to the glycocalyx (Schött et al., 2016). Moreover, rodent model studies revealed that conditions like hyperglycemia, hemorrhagic shock, inflammation, and ischemia-reperfusion injuries are associated with glycocalyx shedding (Abassi et al., 2020). In addition, sepsis, trauma, and ischemia-reperfusion following aortic bypass surgery have been shown to induce glycocalyx disruption in humans (Rehm et al., 2007). The precise underlying mechanisms of glycocalyx disruption are not completely understood, but the release of a disintegrin and metalloproteinases (ADAMs), matrix metalloproteinases (MMPs) in response to inflammation or ischemia, and increased activity of heparinase and hyaluronidases have been associated with glycocalyx disruption (Ramnath et al., 2014, 2020; Goligorsky and Sun, 2020).

Since the glycocalyx is involved in mechanisms that also contribute to DCI, we hypothesize that the glycocalyx plays a role in the pathophysiology of DCI. In this review, we will discuss the role of the glycocalyx within different endothelial and microvascular processes, and relate this to the microvascular changes that have been associated with the pathophysiology of DCI. As such, we aim to evaluate the potential contribution of the glycocalyx to the development of DCI.

## MATERIALS AND METHODS

Our narrative review is based on multiple search strategies addressing the various aspects of the pathogenesis of DCI following aSAH. Firstly, we sought to understand the pathophysiological mechanisms occurring at a microvascular levels following aSAH in pre-clinicals models. The search terms included "subarachnoid hemorrhage"(MESH) OR "subarachnoid hemorrhage," OR "aneurysmal subarachnoid hemorrhage" OR "subarachnoid bleeding" combined with "experimental model" OR "animal model" OR "rodent" and "microvascular dysfunction" OR "endothelial cells" OR "microvasculature." Papers focusing solely on vasospasms were excluded. Delayed cerebral ischemia was excluded from this search due to the difficulty of assessing neurological deterioration in animals, a prerequisite for the diagnosis of DCI. Secondly, we performed a comparable search to identify clinical studies describing pathomechanisms at the endothelial level, including the glycocalyx, and microvascular level in DCI following aSAH. The following search terms were used: "subarachnoid hemorrhage"(MESH) OR "subarachnoid hemorrhage," OR "aneurysmal subarachnoid hemorrhage" OR "subarachnoid bleeding" combined with ("Delayed cerebral ischemia" OR "Delayed cerebral ischemia" OR "delayed ischemic neurologic deficit" OR "secondary brain ischemia" OR "secondary brain ischemia" OR "secondary cerebral deficit" OR "delayed ischemic complications") and ("glycocalyx" OR "endothelial glycocalyx" OR "endothelial surface layer" OR "pericellular matrix" OR "endothelium" OR "endothelial cell lining" OR "microvascular dysfunction" OR "endothelial cells" OR "microvasculature" OR "microcirculation." We applied the species filter "Humans" to this search. Based on the findings of these search strategies, we identified four main microvascular pathomechanisms underlying DCI, i.e., inflammation, oxidative stress, thrombosis, and neurovascular coupling.

Due to limited output from this search with regards to the glycocalyx, we subsequently applied search strategies focusing on the role of the glycocalyx in the delineated microvascular pathomechanisms: ("glycocalyx" OR "endothelial glycocalyx" OR "endothelial surface layer" OR "pericellular matrix") AND (1) ("inflammation" OR "inflammatory disease"); OR (2) ("oxidative stress" OR "oxidation"); OR (3) ("coagulation" OR "coagulative state" OR "coagulative disorder" OR "thrombus" OR "thrombosis"); OR (4) ("Neurovascular unit" OR "Neurovascular coupling" OR "neurovascular decoupling"). Following title and

abstract screening, the studies were included in the evidence pile per pathomechanisms, and subsequently classified as: pathophysiology-related or treatment-related. Finally, studies were included following reference screening. The search strategy was conducted by two authors (HS and RH).

# THE GLYCOCALYX

The glycocalyx is a gel-like layer located between the endothelium and the circulating blood (Reitsma et al., 2007; Schött et al., 2016; Cosgun et al., 2020). The main constituents of the glycocalyx are proteoglycans and glycoproteins. These form the backbone of the glycocalyx, to which glycosaminoglycans are connected (Reitsma et al., 2007). The glycocalyx is a dynamic structure under constant renewal in response to hemodynamic changes, wall shear stress, and enzymatic degradation from (or by) plasma cells (Cosgun et al., 2020). Importantly, it provides a physical, cellular and electrostatic barrier that limits the passage of most plasma constituents through the endothelium (Tarbell and Pahakis, 2006). A healthy glycocalyx prevents binding of plasma cells and proteins to endothelial receptors and glycocalyx-bound molecules, thereby regulating multiple endothelial functions. As such, the glycocalyx is considered a relevant component of the blood-brain barrier (BBB) (Ando et al., 2018; Haeren et al., 2018). When in a state of disease such as in those mentioned above, the glycocalyx is disrupted, thus exposing the endothelium and its receptors to plasma cells and proteins. This leads to inflammation, reduced endothelial synthesis of nitric oxide (NO), BBB dysfunction, neurovascular uncoupling and microthrombosis.

## Glycocalyx and Inflammation

The most important glycoproteins within the glycocalyx include selectins, integrins, and adhesion molecules (Reitsma et al., 2007; Kolářová et al., 2014). Endothelium-expressed P and E-selectins are involved in leukocyte-endothelium interaction, rolling and activation, while also promoting fibrin deposition and thrombus formation (Reitsma et al., 2007). Integrins are heterodimeric transmembrane receptors on leukocytes and platelets involved in binding these cells to the endothelium (Reitsma et al., 2007). Adhesion molecules, e.g., vascular cell adhesion molecule-1 (VCAM-1) and intercellular adhesion molecule-1 (ICAM-1), act as endothelial ligands for integrins and play a crucial role in leukocyte adhesion to the endothelium. In healthy vasculature, the glycocalyx components (thickness range: 400 – 500 nm) cover these cell-adhesion molecules (thickness range: 20 – 40 nm) on the endothelium, thereby preventing them from interacting with their ligands (Reitsma et al., 2007; Lipowsky, 2012; Choi and Lillicrap, 2020). Hence, an intact glycocalyx isolates the endothelium from circulating inflammatory cells, and limits inflammatory processes (**Figure 1**). When components of the glycocalyx are disrupted, the cell-adhesion glycoproteins become exposed and get activated, thus initiating a cascade of inflammatory mechanisms.

## Glycocalyx and Nitric Oxide

Nitric oxide (NO) is involved in essential functions such as regulation of smooth muscle cell relaxation, neutrophil adhesion to the endothelium, and platelet activation. In endothelial cells, NO is released from endothelial caveolae by glypican (Tarbell and Pahakis, 2006; Kumagai et al., 2009; Ebong et al., 2014; Yen et al., 2015), a membrane-bound proteoglycan that forms one of the backbones of the glycocalyx. Glypican is activated by biochemical reactions that are induced by heparan sulfate in response to changes in mechanical forces or blood flow conditions (Tarbell and Pahakis, 2006; Ebong et al., 2014; Zeng, 2017). Thus, the glycocalyx stimulates the synthesis of NO via heparan sulfate and glypican in response to an increase in shear stress, thereby regulating vasodilation (Tarbell and Pahakis, 2006). Conversely, shedding of the glycocalyx reduces shear stress-induced NO release (Yen et al., 2015). The availability and release of NO is highly relevant to ensure the continuous adjustment of local cerebral blood flow in response to the metabolic demands of neuronal tissue (Abbott et al., 2006; Stanimirovic and Friedman, 2012; Kaplan et al., 2020), a mechanism known as neurovascular coupling (NVC). As an orchestrator of NO synthesis, the glycocalyx plays a significant role in NVC, hence its degradation may lead to a reversed ischemic reaction (Kaplan et al., 2020). Moreover, the glycocalyx accommodates anti-oxidants like superoxide dismutase (SOD), which is bound to heparan sulfate (Tarbell and Pahakis, 2006). Reactive oxygen species (ROS) are usually produced in mitochondria as a product of aerobic cellular metabolism (He et al., 2017). Oxidative stress appears when ROS are insufficiently counterbalanced by antioxidants. At low levels, ROS contribute to cell processes, enabling communication between organelles and cells (Palma et al., 2020). However, at higher levels and when surpassing signaling thresholds, ROS contribute to the activation of apoptosis and autophagy, and induce damage to DNA and RNA (Palma et al., 2020). ROS include superoxide anion ($O_2^-$) and peroxynitrite ($ONOO^-$) (Di Wang et al., 2010). Of these, $O_2^-$ is produced by vascular cells, for example from uncoupled endothelial nitric oxide synthase (Sena et al., 2018). This $O_2^-$ is moderately reactive by itself, but it participates in reactions with NO that result in the formation of ROS such as peroxynitritre and reactive nitrogen species, from which a diversity of other highly reactive species can be produced (Wang et al., 2018; Yin et al., 2018). Moreover, it inactivates NO and uncouples endothelial nitric oxide synthase, thereby reducing NO bioavailability (Hamed et al., 2009). Antioxidants, such as SOD, counteract and neutralize $O_2^-$ by catalyzing the dismutation of $O_2^-$ into $O_2$ and $H_2O_2$, thereby preventing the formation of $ONOO^-$ (Kumagai et al., 2009; Schött et al., 2016; He et al., 2017). As such, SOD represents a first-line of defense against oxygen-derived free radicals and reduces the damaging effect of superoxide (Reitsma et al., 2007; Østergaard et al., 2013; He et al., 2017). Experiments in rodents have revealed that inhibition of SOD induces endothelial dysfunction consistent with inactivation of basal NO by $O_2^-$ (Laight et al., 1998). Conversely, experimental treatment of cells with SOD attenuates $O_2^-$ production and restores NO production (Hamed et al., 2009). To conclude, the glycocalyx plays an important role in the

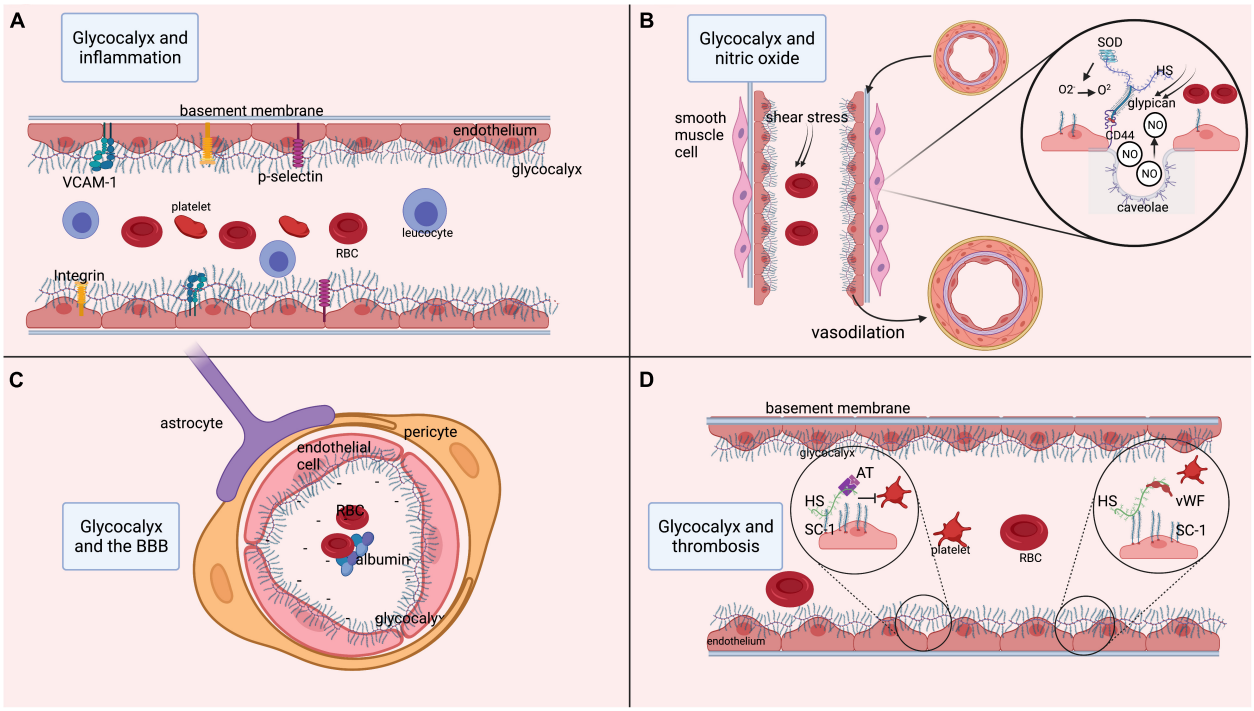


**FIGURE 1 |** Functions of the glycocalyx. **(A)** Role of the glycocalyx in adhesion of platelets and inflammatory cells such as leukocytes. Multiple endothelial glycoproteins such as selectins, integrins, and cell-adhesion molecules (VCAM-1) are docked within the glycocalyx. As such, the glycocalyx prevents their activation and thereby prevents inflammatory processes. **(B)** Process of releasing nitric oxide (NO) from the endothelium in response to shear stress. Shear stress is sensed by heparan sulfate, which is bound to glypican. Glypican then attaches to the transmembrane CD44. This mechanical signal in response to shear stress is translated into an intracellular signaling process resulting in the release of NO from endothelial caveolae. The released NO induces relaxation of vascular smooth muscle cells, resulting in vasodilatation. Moreover, superoxide dismutase is bound to heparan sulfate and can convert oxidative $O_2^-$ into $O_2$, thereby regulating the level of free radicals. **(C)** Role of the glycocalyx in maintenance of the BBB. Within cerebral microcirculation, the glycocalyx is also part of the blood-brain barrier (BBB). The BBB is further composed of tightly connected endothelial cells encapsulated by pericytes that are surrounded by astrocytic feet. At the luminal side of the endothelium, the glycocalyx layer prevents large molecules from passing the BBB. Since the glycocalyx is negatively charged, the BBB is not permeable to negatively charged cells such as platelets and red blood cells, or proteins like albumin. **(D)** Anti-coagulant function of the glycocalyx, as it docks anti-coagulant molecules like anti-thrombin, tissue factor pathway inhibitor and the von Willebrand factor (vWf). In states of increased shear stress, the vWf is elongated and able to bind platelets that in turn attach to the endothelium and initiate coagulation. AT, anti-thrombin; BBB, blood-brain barrier; ET, endothelin; GAG, glycosaminoglycan; HS, heparan sulfate; ICAM-1, inter-cellular cell-adhesion molecule 1; NO, nitric oxide; $O_2$, oxygen, $O_2^-$, PG, proteoglycan; superoxide; RBC, red blood cell; VCAM-1, SC-1, syndecan-1; SOD, superoxide dismutase; vascular-cell adhesion molecule 1; vWF, von Willebrand factor. Image is created using BioRender.com.

bioavailability of endothelial NO and its functions related to NVC and oxidative stress (**Figure 1**).

## Glycocalyx and the Blood-Brain Barrier

The BBB is composed of a single layer of endothelial cells that are interconnected by tight junctions, surrounded by the basement membrane and pericytes, and covered by astrocytic end-feet (Sharif et al., 2018; Kaplan et al., 2020). On the luminal side of the endothelium, the glycocalyx contributes to the barrier function of the BBB (**Figure 1**). Using two-photon microscopy, several studies have shown that the glycocalyx acts as a barrier for large molecules (Kutuzov et al., 2018; Khan et al., 2021). The glycocalyx also functions as an electrostatic barrier to plasma proteins due to its negative charge carried by core proteins like hyaluronan, thereby repelling negatively charged cells and preventing them from binding the endothelium (Iba, 2016). Furthermore, perturbation of the glycocalyx has been shown to increase BBB permeability (Zhu et al., 2018), leading to extravasation of plasma proteins, especially albumin, which further results in astrocytic transformation and alterations in NVC (Friedman et al., 2009).

## The Glycocalyx and Coagulation

There is growing evidence that constituents of the glycocalyx also play a role in the prevention of coagulation (**Figure 1**). Heparan sulfate and syndecan-1 within the glycocalyx bind to anticoagulant molecules like anti-thrombin, activated protein C, and tissue factor pathway inhibitors (Reitsma et al., 2007; Iba, 2016; Peeyush Kumar et al., 2019). This leads to the production of endothelial prostacyclins that prevent platelets and neutrophils from binding to the endothelium (Iba, 2016). The glycocalyx also forms an anchorage point for the von Willebrand factor (vWF) (Choi and Lillicrap, 2020). In the presence of non-physiological or increased shear stress, the vWF changes its configuration and extends into the lumen to bind platelets. Experimental degradation of heparan sulfate from

the glycocalyx has indeed revealed a decrease in vWF-induced platelet activation, underlining the role of the glycocalyx in platelet activation (Kalagara et al., 2018).

## PHASES AND PATHOMECHANISMS IN DCI

The period following an aSAH can be roughly divided into four different phases that are likely to contribute to the development of DCI, each characterized by various pathophysiological processes. Firstly, the initial hemodynamic changes following rupture of the IA induce *phase I: an acute inflammatory response and concurrent increased coagulation* (Sercombe et al., 2002). Thereafter, the products of inflammation in combination with the breakdown of the released erythrocytes contribute to *phase II: creating an environment high* in *oxidative stress,* which peaks at day 7 after the aSAH (Peeyush Kumar et al., 2019). Both early inflammation and oxidative stress potentiate further inflammation, ensuing *phase III: a breakdown of the* BBB coinciding with increased apoptosis of endothelial cells starting at day 7 after the ictus (Østergaard et al., 2013). Finally, all of the previous processes result in *phase IV: dysfunction of neurovascular coupling*, causing a mismatch between brain tissue metabolism and blood (oxygen) supply, which ultimately contributes to the development of DCI (Rowland et al., 2012). Based on the central role of the glycocalyx in modulating vascular inflammation, oxidative stress, BBB permeability and NVC, disintegration of the glycocalyx may play a role in the above-mentioned processes contributing to DCI. Below, we will discuss these four phases and their role in the pathophysiology of DCI in more detail.

## PHASE I: NEUROINFLAMMATION AND A PROCOAGULATIVE STATE

The first phase starts directly following rupture of an IA. The rupture leads to a rapid increase in intracranial pressure, causing a decrease in cerebral blood flow and perfusion. The resulting brief cerebral circulation arrest (Terpolilli et al., 2015; Peeyush Kumar et al., 2019) causes the release of damage-associated molecular patterns (DAMPs) from necrotic cells or from extracellular matrix (Chaudhry et al., 2018; Muhammad et al., 2020). DAMPs are sensed by cerebral resident immune cells, which in turn release cytokines, like TNF-alpha, IL-1 and IL-6 (Schneider et al., 2018; Mastorakos and McGavern, 2019). These pro-inflammatory cytokines affect glycocalyx integrity, causing endothelial dysfunction and further stimulating pro-inflammatory conditions (Lipowsky, 2012; Cosgun et al., 2020). For example, cytokine-induced glycocalyx degradation exposes endothelial-bound selectins and adhesion molecules, which in turn stimulate pro-inflammatory conditions (Pradilla et al., 2010; Peeyush Kumar et al., 2019). An increased number of neutrophils and VCAM-1 in post-hemorrhagic cerebrospinal fluid (CSF) supports this idea of concomitant glycocalyx disruption and increased neuroinflammation (Nissen et al., 2001; Bell et al., 2017; Schneider et al., 2018). Moreover, clinical studies have reported increased levels of ICAM-1 in the CSF and serum of DCI patients (Nissen et al., 2001), while rodent SAH models revealed an important role of p-selectin activation in the pathophysiology of SAH-induced damage to the cerebral tissue (Ishikawa et al., 2009; Friedrich et al., 2011; Sehba and Friedrich, 2011; Atangana et al., 2017).

The increased level of p-selectin is also associated with activation and adhesion of platelets to the endothelium, and subsequently promotes fibrin deposition, platelet-leucocyte aggregation and thrombus formation (Sabri et al., 2012). Indeed, damage to the endothelium and inevitably to the glycocalyx following ictus has been associated with platelet aggregations invading the brain parenchyma in experimental rodent SAH models using rodents (Ishikawa et al., 2009; Friedrich et al., 2010; Clarke et al., 2020). Furthermore, serological measurements of pro-coagulants such as platelet activating factor (PAF), thrombin anti-thrombin complex, the vWf and fibrinogen have all been found to be increased in DCI patients compared to that of non-DCI patients (Hiroshima et al., 1997; Frijns et al., 2006; Vergouwen et al., 2008; Naraoka et al., 2014). This underlines the failure of anti-coagulants within the glycocalyx to inhibit coagulation, suggesting disruption of the glycocalyx.

Following activation of adhesion molecules, inflammatory cells get activated and release a multitude of damaging enzymes. For example, neutrophils adhere to the endothelium (Sehba et al., 2011) and release myeloperoxidase and heparinase, which are reactive oxygen species (ROS) known to disrupt the glycocalyx (Changyaleket et al., 2017; Abassi et al., 2020). This further exposes the endothelium to circulating inflammatory cells and shear stress, thereby sustaining extravasation of inflammatory cells through the endothelium (Manchanda et al., 2018). Animal models of SAH in ICAM-1 knock-out mice have revealed a decrease in the accumulation of activated microglia (Atangana et al., 2017). This finding illustrates the role of adhesion molecule activation in stimulating neuroinflammatory processes following rupture of an IA. Moreover, platelets and leukocytes recruited to the site of injury release signaling molecules such as PAF, platelet derived growth factor (PDGF) and chemokine CC motif ligand 5 (CCL5). These signaling molecules activate endothelial cells and macrophages to release additional pro-inflammatory cytokines including IL-1, IL-1β, IL-6, and TNF-α. Previous studies have shown that CSF levels of these cytokines are indeed associated with DCI in aSAH patients (Osuka et al., 1998; Sercombe et al., 2002; Budohoski et al., 2014; Bell et al., 2017). As mentioned, these cytokines degrade the glycocalyx, creating a vicious pathophysiological cycle.

## PHASE II: OXIDATIVE STRESS

The aSAH is associated with an increase in oxidative stress (Sehba et al., 2011), which is inversely related to the availability of NO. This increase in oxidative stress is mostly the result of the lysis of red blood cells (RBCs) released into the subarachnoid space (Sehba et al., 2011). Under physiological conditions, the extracellular RBC-derived hemoglobin (Hb) and free heme are bound to haptoglobin (Hp) that neutralizes

the strong oxidative capacity of heme-iron and prepares it for phagocytosis (Rifkind et al., 2015). The Hb-Hp complex subsequently binds to the scavenger membrane receptor CD163 on macrophages and microglia, leading to its internalization (Fabriek et al., 2005; Blackburn et al., 2018). The heme is then degraded by hemeoxygenase into biliverdin and iron (Meguro et al., 2007). The latter is bound to ferritin and transported by transferritin, thereby preventing it from exercising its toxic effects (Wagner et al., 2003). The aim of this process is to prevent extracellular Hb from oxidizing, and free iron from inducing oxidation of surrounding tissue which causes the release of free radicals. However, following an aSAH, the available Hp is rapidly depleted by the sudden increase of RBCs in the subarachnoid space (Blackburn et al., 2018). As a result, only some of the Hb and free heme originating from RBCs is neutralized by Hp as discussed above (**Figure 2**). The remaining non-neutralized free heme and iron in the extracellular space function as highly oxidative factors, causing the formation of ROS (Macdonald and Weir, 1991; Wagner et al., 2003; Østergaard et al., 2013; Blackburn et al., 2018). Antioxidants such as NO are increasingly consumed to balance the oxidative stress in the tissue (Macdonald and Weir, 1991; Dreier et al., 2000; Sehba et al., 2011). Indeed, reduced NO synthesis has been reported following SAH in studies measuring inhibitors of nitric oxide synthesis such as Asymmetricdimethyl-l-arginine (ADMA) in cerebrospinal fluid (Jung et al., 2012; Appel et al., 2018), and in rodent SAH models measuring nitric oxide availability (Sabri et al., 2011, 2012). The final reduced NO availability is the result of unbounded extracellular Hb scavenging NO (Østergaard et al., 2013; Geraghty and Testai, 2017; Peeyush Kumar et al., 2019). This process of RBC lysis begins 2 days after the aSAH, and peaks at around day seven (Pluta et al., 1998; Østergaard et al., 2013).

Endothelial synthesis of NO is usually regulated by the ferrous dioxygen complex. However, in the presence of oxidative stress, this complex generates superoxide ($O_2^-$) which binds to NO, thereby further reducing NO availability (Sabri et al., 2011). Moreover, aSAH induces endothelial dysfunction, which limits NO synthesis and exacerbates the effects of oxidative stress (Sehba et al., 2000; Sabri et al., 2011). Finally, aSAH patients with DCI have increased levels of bilirubin oxidation products (BOXs) compared to patients without DCI (Pyne-Geithman et al., 2013). This difference is mainly dependent on levels of oxidative products in the CSF (Pyne-Geithman et al., 2013; Rapoport, 2018; Peeyush Kumar et al., 2019). Similar to free Hb, BOXs inhibit endothelial NO synthesis (Peeyush Kumar et al., 2019).

Overall, the rupture of an IA results in an excess of oxidative products that cannot be metabolized properly by the brain (Budohoski et al., 2014). This leads to a decrease in the availability of NO, which is aggravated by reduced endothelial NO synthesis. Consequently, intracellular mechanisms and metabolism are affected, leading to increased vasoconstriction with dysfunctional NVC, inflammation and lipid peroxidation. Since the glycocalyx is involved in the synthesis of endothelial NO and has additional antioxidant properties via the actions of glycocalyx-bound SOD, a damaged glycocalyx could be a potential catalysator of oxidative stress and reduced NO availability in the pathomechanisms underlying DCI (**Figure 2**).

## PHASE III: BLOOD-BRAIN BARRIER DYSFUNCTION

Delayed cerebral ischemia has been associated with increased BBB permeability, a phenomenon mirrored by a peak of apoptotic cells around day seven post-ictus (El Amki et al., 2018). Both the initial phase I (acute inflammatory response) and the breakdown of RBCs in phase II following rupture of an IA contribute to the degradation of the BBB (Sehba et al., 2011). Products of RBC lysis serve as DAMPs and bind to innate immune cells such as microglia, which are the resident macrophage-like cells of the central nervous system (Geraghty and Testai, 2017). Microglia release inflammatory cytokines and trigger the up-regulation of endothelial adhesion molecules on the endothelium, allowing macrophages, and neutrophils to bind to the endothelium and migrate into the subarachnoid space (Atangana et al., 2017; Peeyush Kumar et al., 2019). There, they phagocytize RBCs and their released components, a process that has been correlated with DCI (Ahn et al., 2019). The accumulation of neutrophils on the endothelium also results in increased lipid peroxidation, oxidative stress and the release of enzymes that degrade the extracellular matrix, which further promote damage to the endothelium and basement membrane (Sen et al., 2006; Sabri et al., 2009; Friedrich et al., 2011; Fumoto et al., 2019). For example, upregulation of enzymes like MMP-1 and MMP-9 that are involved in remodeling of the extracellular matrix and degradation of basal membrane have been found to be good predictors of DCI when measured in plasma and CSF of aSAH patients (Fischer et al., 2013; Triglia et al., 2016; Bell et al., 2017; de Oliveira Manoel and Loch Macdonald, 2018).

Lining the luminal side of the endothelium, the glycocalyx is the first barrier to overcome for all inflammatory cells that seek to migrate into the subarachnoid space. As discussed, the glycocalyx indeed limits the passage of molecules through the endothelium, both physically and electrostatically. Previous studies using aSAH models have revealed extravasation of albumin through the BBB, suggesting increased BBB permeability (Schöller et al., 2007). Extravasation of albumin into the brain parenchyma may result in cerebral edema and astrocytic transformation, further stimulating dysfunction of NVC mechanisms (Friedman et al., 2009). These findings suggest a synergistic action of the glycocalyx in combination with BBB failure to prevent large molecules from crossing the endothelium that contributes to edema formation and eventually to a reduced blood flow manifesting itself as DCI (Tarbell and Pahakis, 2006; Østergaard et al., 2013; Alphonsus and Rodseth, 2014; Schoknecht et al., 2015; Sharif et al., 2018; Nian et al., 2020).

## PHASE IV: NEUROVASCULAR UNCOUPLING

The physiological process of NVC by inducing vasodilation or vasoconstriction is essential to ensure adequate blood flow to the brain parenchyma in response to changes in tissue metabolic demands. The process of NVC is regulated by the complex interaction of endothelial cells, smooth muscle

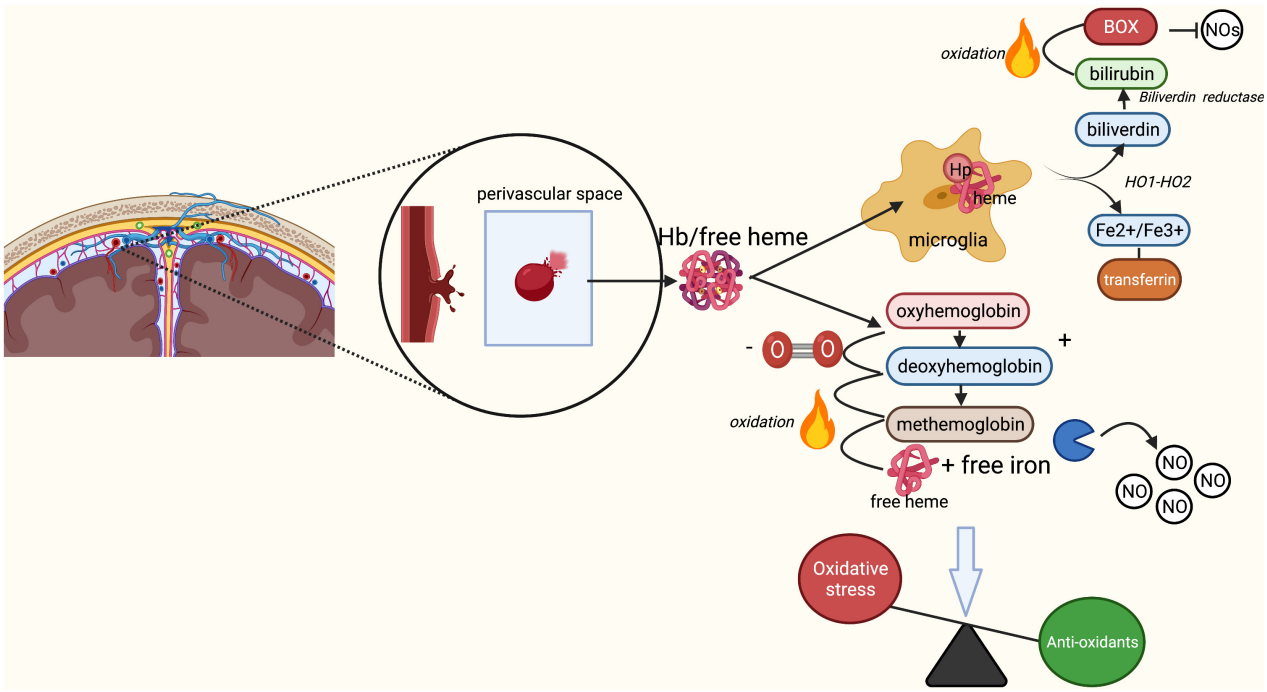


**FIGURE 2 |** Breakdown of red blood cells following aSAH leading to oxidative stress. Rupture of an intracranial aneurysm results in the extravasation of red blood cells (RBCs) into the subarachnoid space. Here, lysis of the RBCs starts within a few days after the rupture, peaking at 7 days post-rupture. Under physiological conditions, the released free heme and iron from RBCs bind to haptoglobin, forming a Hb-Hp complex. The Hb-Hp complex subsequently attracts microglia and macrophages by the membrane receptor CD163 leading to its phagocytosis and neutralization. End products of this phagocytosis are biliverdin and iron through the action of heme oxygenase 1 and 2. Biliverdin is converted into bilirubin through biliverdin reductase. In the presence of oxygen, biliverdin may turn into bilirubin oxidation products, which act as inhibitors of nitric oxide (NO). Iron may be present in its ferrous ($Fe^{2+}$) or ferric ($Fe^{3+}$) form. The ferrous form of iron participates in the Fenton reaction, causing formation of reactive oxygen species and subsequent lipid peroxidation (*oxidative stress)*. Under physiological circumstances, the transport protein transferritin and binding protein ferritin prevent iron from causing damage and transport iron back to neurons for later use. In SAH, Hp quickly becomes saturated due to the enormous increase in lysis of RBCs. Unbound Hb turns into oxyhemoglobin, which loses its oxygen and converts to deoxyhemoglobin. Deoxyhemoglobin spontaneously and non-enzymatically converts to methemoglobin, which converts to free heme and iron. Free heme and iron bind NO and contribute to an absolute reduction of NO, and thus a decrease in vasodilation and increase in endothelin-induced vasoconstriction. Finally, free heme and iron contribute to the production of free radicals and lipid peroxides, increasing the overall rate of oxidative stress. BOX, bilirubin oxidation product; $Fe^{2+}$, ferrous iron, $Fe^{3+}$, ferric iron; Hb, hemoglobin; Hp, haptoglobin; HO-1/HO-2, heme oxygenase 1/2; NO, nitric oxide; $O_2$, oxygen; ROS, reactive oxygen species. Image is created using BioRender.com.

cells (SMCs), neurons, microglia, pericytes and astrocytes; together these form the neurovascular unit (NVU) (Iadecola, 2004). Endothelial dysfunction and limited endothelial NO synthesis in aSAH result in an altered activation of SMCs via endothelium-released endothelin-1 and NO (Vergouwen et al., 2008; **Figure 3**). Moreover, astrocytic transformation due to increased BBB permeability affects intra- and extracellular water and electrolyte distributions, which in turn also affect the release of vasoactive substances such as potassium and prostacyclins (Iadecola, 2004; Koide et al., 2013b; van Dijk et al., 2016). In addition, experimentally induced inflammatory responses using lipopolysaccharide in rodents have been associated with changes in hemodynamic function and cerebrovascular dynamic, underlining the role of inflammation in dysfunction of the NVU (Brezzo et al., 2020).

The above-mentioned processes cumulatively result in dysfunction of NVC following aSAH. Preclinical and clinical studies have indeed revealed dysregulation of vasodilatation and even pathological vasoconstriction in response to different stimuli in experimental aSAH models and patients (Britz et al., 2007; Budohoski et al., 2012; Koide et al., 2013a; Balbi et al., 2017; Neumaier et al., 2021). Moreover, DCI has been associated with decreased vasoreactivity of the middle cerebral artery measured 4 to 10 days after ictus in a prospective clinical study including 34 patients with aSAH (Carrera et al., 2010). These findings are also in line with the observed increased vasoconstriction of small cortical vessels in SAH patients in response to increased levels of carbon dioxide during surgery (Pennings et al., 2004).

As a result of dysfunctional NVC, cortical spreading depolarization (CSD) may occur. This CSD is a phenomenon characterized by sudden electrical discharge due to a breakdown of ion gradients, followed by sustained neuronal and glial depolarization propagating throughout the cortex (Budohoski et al., 2012; Woitzik et al., 2012; Koide et al., 2013b). During CSD, a considerable amount of intracellular [$K^+$] efflux causes an increase in perivascular (extracellular) [$K^+$], which is compensated by a $Ca^{2+}$ and $Na^+$ influx into the cells (Koide et al., 2013b). As a consequence of such electrolyte

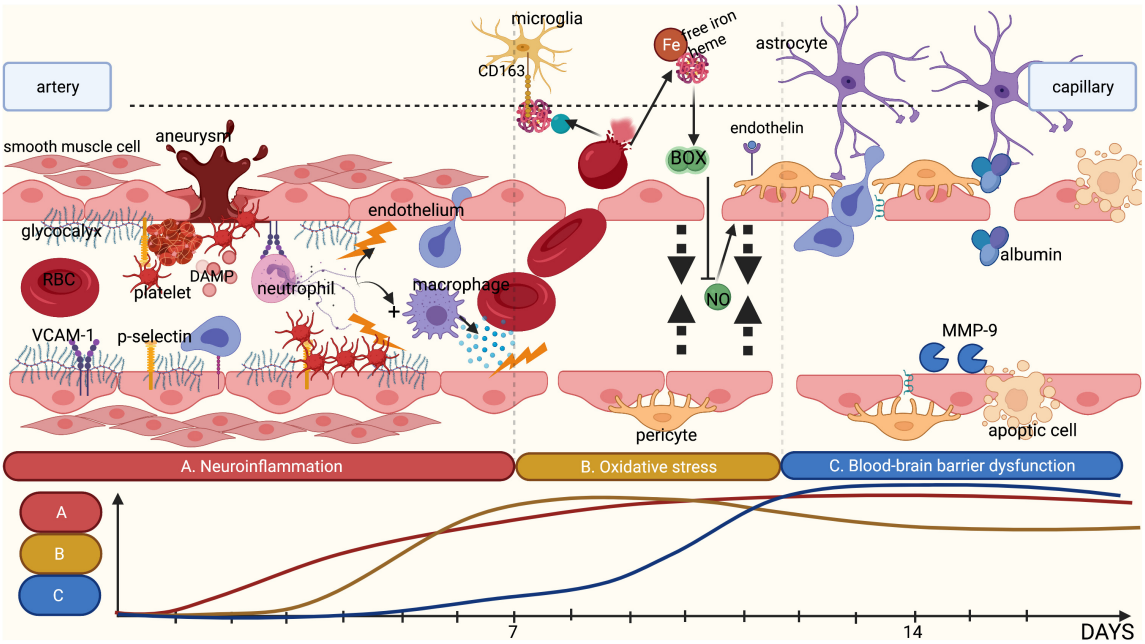


**FIGURE 3 |** Summary of the different pathophysiological phases contributing to DCI. **(A)** Rupture of an intracranial aneurysm is associated with tissue damage and subsequent tissue ischemia, releasing DAMPs. This release attracts leucocytes such as neutrophils, thereby initiating local neuroinflammation. Combined with an increase in shear stress, rupture of an intracranial aneurysm is likely to damage the glycocalyx. This loss of glycocalyx integrity promotes adhesion of platelets and neutrophils to the endothelium by cell-adhesion molecules and selectins, which are no longer covered by the glycocalyx. The adhered inflammatory cells release cytokines, further stimulating local neuroinflammation. **(B)** Following rupture of an intracranial aneurysm, red blood cells (RBCs) enter the subarachnoid space wherein they undergo lysis, resulting in the release of free iron and heme. Under physiological conditions, haptoglobin and hemoglobin form a complex that binds microglia and macrophages through the membrane receptor CD163 for phagocytosis. However, following the rupture of an aneurysm, the copious amounts of RBC lysis products quickly saturate haptoglobin, leaving free iron unbound. Following oxidation, free iron results in the synthesis of reactive oxygen species and subsequently in reduction of the availability of nitric oxide. Moreover, the disrupted glycocalyx has a reduced synthesis capacity for nitric oxide in response to shear stress. This leads to an absolute shortage in nitric oxide, limiting vasodilatory capacity. In addition, endothelin-1 is no longer inhibited by endothelial nitric oxide leading to increased vasoconstriction. **(C)** The above-mentioned processes promote blood-brain barrier (BBB) disruption. Products of RBC lysis activate microglia, which in turn release additional cytokines. Activated neutrophils and macrophages entering the subarachnoid space also release inflammatory cytokines and matrix metalloproteinases, disrupting the extracellular matrix and the basement membrane, leading to increased BBB permeability. This is further aggravated by the disruption of the glycocalyx that can no longer exert its barrier functions. Finally, this results in the formation of local oedema, inflammation and ischemia. Image is created using BioRender.com.

shift, an uncontrolled release of excitatory neurotransmitters is triggered. Neurotransmitters depolarize neighboring neurons and cause further propagation of the depolarization wave. This spreading depolarization is associated with an arrest of electrical activity due to complete membrane depolarization, thereby inhibiting action potentials. This phenomenon has been shown to persist in the presence of ischemia and leads to a sustained vasoconstriction of cerebral vessels (Dreier et al., 2006; Bosche et al., 2010). The presence of CSD has been shown to be a good predictor of DCI, and can occur in the absence of vasospasms (Petzold et al., 2003; Dreier et al., 2006; Woitzik et al., 2012). Triggers of CSD in aSAH are thought to involve increases in extracellular ($K^+$), decreased NO bioavailability, oxyhemoglobin, and endothelin-1 (Koide et al., 2013b; Østergaard et al., 2013; Geraghty and Testai, 2017). As an important regulator of NO bioavailability, and indirectly of endothelin-1, a damaged glycocalyx decreases the brain's reserve defense mechanisms and exposes aSAH patients to processes that increase the metabolic mismatch leading to DCI. This phenomenon is further amplified by the above-mentioned mechanisms that are also likely to involve disruption of the glycocalyx: neuroinflammation, procoagulation, increase in oxidative stress and increase in BBB permeability.

## CLINICAL FINDINGS ON THE GLYCOCALYX AND DELAYED CEREBRAL ISCHEMIA

The foregoing discussion on the pathomechanisms underlying DCI illustrates that disintegration of the glycocalyx may contribute to all consecutive pathophysiological processes (**Figure 3**). To the best of our knowledge, there is currently only one clinical study that reported glycocalyx assessment in association with DCI (Bell et al., 2017). In this small observational study, plasma markers of glycocalyx disruption such as Syndecan-1 and CD44, a glycoprotein receptor for hyaluronan, as well as the levels of ICAM-1 and VCAM-1 were assessed in three patients who developed DCI following their aSAH. When these were compared

to a healthy population, it was found that the occurrence of aSAH was associated with increased plasma levels of Syndecan-1 and CD44, as well as ICAM-1 and VCAM-1 (Bell et al., 2017). In addition, levels of Syndecan-1 increased significantly when DCI was observed (Bell et al., 2017). Since measurements of these markers were not compared to aSAH patients without DCI, it is unclear whether the increase in these markers reflects the natural course of endothelial damage following aSAH, or if it is specifically associated with endothelial damage in DCI.

Aside from this single study directly relating disruption of the glycocalyx to the development of DCI following aSAH, other studies have identified many risk factors for the development of DCI that are associated with glycocalyx disruption and dysfunction. In their review, de Rooij et al. found that, among others factors, smoking, hyperglycemia, history of diabetes mellitus, and early systemic inflammatory response syndrome were associated with the occurrence of DCI (De Rooij et al., 2013). Numerous studies have reported the destructive effects of smoking on the glycocalyx (Johnson et al., 2010; Ikonomidis et al., 2017). Similarly, hyperglycemia and diabetes mellitus have repeatedly been associated with decreased glycocalyx integrity (Lopez-Quintero et al., 2013; Kolářová et al., 2014; Yilmaz et al., 2019). These "risk factor"-based data suggest that aSAH patients who develop DCI may have a history of chronic degeneration of glycocalyx due to their generally poor vascular health, more often compared to patients who do not develop DCI. In other words, poor baseline-condition of the vasoprotective glycocalyx is a potential risk factor for aSAH-related DCI. Moreover, these vascular risk factors could explain the differences between aSAH patients. Lastly, various inflammatory conditions, including infectious diseases like Covid-19 (Yamaoka-Tojo, 2020b) and dengue fever (Puerta-Guardo et al., 2016), as well as sepsis (Rovas et al., 2018; Iba and Levy, 2019; Goligorsky and Sun, 2020) have been related to a disturbed glycocalyx integrity.

## DISCUSSION

This narrative review sheds light on the important contributions of the glycocalyx to various physiological properties of the endothelium. Destruction of the glycocalyx and associated implications stemming from its function as a barrier and a mediator of vascular homeostasis have been demonstrated extensively. However, the clinical relevance of the glycocalyx in pathological conditions remains to be elucidated. This also applies to the potential role of the glycocalyx in the pathophysiology of DCI. In this review, we have sought to connect the physiological roles of the glycocalyx to pathomechanisms leading to DCI. However, preclinical and clinical studies relating glycocalyx perturbation and restoration to the development of DCI are sparse. This is partly due to the lack of sensitivity and specificity of the available techniques to assess glycocalyx properties (Haeren et al., 2018; Valerio et al., 2019). Therefore, this discussion will firstly focus on the strengths and limitations of the techniques available for assessing the glycocalyx of the cerebral vasculature, and secondly explore the opportunities for prevention and restoration of glycocalyx shedding.

## TECHNIQUES FOR ASSESSING THE CEREBROVASCULAR GLYCOCALYX

Techniques for assessing the glycocalyx in *ex vivo* conditions should be discerned from those that are *in vivo*. Various microscopy techniques are available for the former techniques for assessing the cerebrovascular glycocalyx (**Table 1**). For example, the first images of the glycocalyx were made by Luft et al., using a ruthenium red stain with osmium tetroxide in combination with transmission electron microscopy (Luft, 1966). Although the glycocalyx can indeed be visualized with transmission electron microscopy (**Figure 4**), this technique warrants many preparation procedures that affect constituents of the glycocalyx, causing it to collapse (Haeren et al., 2016). This collapse can be partly overcome by rapid freezing and a freeze substation technique, but this is likely to underestimate the actual glycocalyx thickness, which complicates comparisons (Ebong et al., 2011). Other *ex vivo* microscopy techniques such as confocal and two-photon laser scanning microscopy are mainly used to visualize specific constituents of the glycocalyx using fluorescent markers like lycopersicon esculentum agglutinin or wheat germ agglutinin (Reitsma et al., 2007). This enables both a quantitative (i.e., glycocalyx thickness) and qualitative (i.e., constituent ratios) three-dimensional analysis of the glycocalyx (Reitsma et al., 2011). Furthermore, stochastic optical reconstruction microscopy was recently used to reveal specific glycocalyx components with very high resolution (Xia and Fu, 2018; Fan et al., 2019). However, these techniques are nevertheless limited by the frailty of the glycocalyx in *ex-vivo* conditions (Reitsma et al., 2007; Haeren et al., 2016). Recent advances in handheld multi-photon microscopy probes could potentially provide a novel *in vivo* technique to evaluate the glycocalyx (Khan et al., 2021).

Current *in vivo* techniques are mainly based on handheld videomicroscopy techniques, such as orthogonal polarization spectral (OPS) imaging and its successor, sidestream darkfield (SDF) imaging. In both techniques, light is emitted at a wavelength of 530nm, which is absorbed by (de-)oxyhemoglobin within erythrocytes (Nieuwdorp et al., 2008) that are observed as small discs flowing through the microcirculation. Based on the width variations of the intraluminal red blood cell column, the perfused boundary region – a validated marker for glycocalyx thickness – is calculated (Goedhart et al., 2007; Nieuwdorp et al., 2008; Lee et al., 2014). These techniques have been applied in cerebral microcirculation during intracranial surgery, including aneurysm surgery (Pennings et al., 2004; Pérez-Bárcena et al., 2011; Haeren et al., 2018). However, cerebral microcirculation is not accessible for follow-up measurements after surgery, limiting its clinical application. Assessment of the sublingual microcirculation is non-invasive and easily accessible, and therefore often used as a surrogate measurement for systemic glycocalyx evaluation (Nieuwdorp et al., 2008). This has indeed been applied successfully, and revealed that various vascular disease-related risk factors like hypertension and atherosclerosis,

**TABLE 1 |** Summary of the pros and cons of different methods for assessing the glycocalyx.

| | TEM | CLSM | TPLSM | SDF | OPS | Markers |
|---|---|---|---|---|---|---|
| | *Ex vivo* | *Ex vivo* | *Ex vivo* | *In vivo* | *In vivo* | *In vitro* |
| Advantages | Quantitative assessment | Quantitative and qualitative assessment | Quantitative and qualitative assessment | No collapse Quantitative assessment No dye | No collapse Quantitative assessment No dye | Quantitative assessment |
| Limitations | Time consuming Glycocalyx collapse | Use of lectins Glycocalyx collapse | Use of lectins Glycocalyx collapse | Motion and pressure artifacts | Motion and pressure artifacts | Non-specific Invasive |

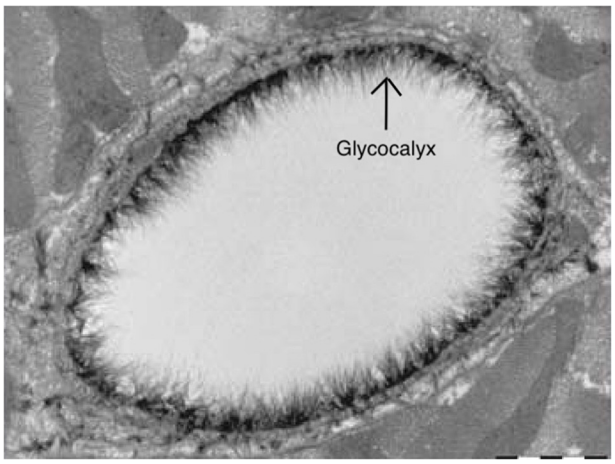


**FIGURE 4 |** Electron microscopy image of the endothelial glycocalyx from Reitsma et al. (2007), with permission. Endothelial glycocalyx (*arrow)* of a rat left ventricular myocardial capillary following staining with Alcian blue 8GX. Image is created using BioRender.com.

as well as specific diseases like renal failure, sepsis, infections and lacunar stroke, are associated with decreased glycocalyx thickness (Vlahu et al., 2012; Dane et al., 2013; Martens et al., 2013; Becker et al., 2015; DellaValle et al., 2019; Yamaoka-Tojo, 2020a; Weinbaum et al., 2021). With regards to assessment of cerebral microcirculation, recent studies have applied SDF imaging techniques to the conjunctiva of the eye, and related this to cerebral pathology (Tamosuitis et al., 2016). As conjunctival microcirculation is supplied by branches of the ophthalmic artery, this microcirculation may resemble the pathology of cerebral microcirculation seen in DCI. As such, evaluation of the glycocalyx of conjunctival microcirculation could provide a non-invasive surrogate measure of the glycocalyx of cerebral microcirculation.

Finally, another technique to evaluate glycocalyx integrity is the measurement of structural and specific constituents of the glycocalyx, such as Syndecan-1, Heparan sulfate and Hyaluronan, within blood plasma or CSF. Numerous studies have shown that these glycocalyx markers are increased in the presence of inflammation, sepsis, hypoperfusion, and ischemic stroke (Rehm et al., 2007; Ostrowski et al., 2015; DellaValle et al., 2019; Abassi et al., 2020). The major advantage of these analyses is their simplicity and safety. However, these analyses are limited by high inter-individual variability and lack of specificity (Haeren et al., 2016).

## PREVENTION AND RESTORATION OF GLYCOCALYX SHEDDING

If glycocalyx shedding precedes the occurrence of DCI, preventing this shedding could be a novel strategy for arresting the development of DCI. Similarly, considering disintegration of the glycocalyx as a pathomechanism of DCI, restoration of the glycocalyx could provide a potential therapeutic strategy for DCI. Multiple studies have explored the potential of prevention and restoration of glycocalyx shedding in laboratory and preclinical conditions. Among these, sphingosine-1 phosphate (S1P) is one of the most studied potential molecules. S1P is a sphingolipid in the blood plasma that is usually incorporated within serum albumin and high-density lipoproteins (Zeng et al., 2014). It inhibits the actions of MMPs, which results in a reduction of Syndecan-1 shedding (Curry et al., 2012; Zeng et al., 2014). Moreover, S1P induces glycocalyx synthesis on cultured endothelial cells (Zeng et al., 2015); in combination with heparan sulfate, S1P has the potential to regenerate the glycocalyx (Mensah et al., 2017). S1P mediates its actions via S1P receptors on the endothelial surface (Lee et al., 1998). In previous studies, S1P administration indeed preserved the glycocalyx in endothelial cell monolayers and in rats' microvessels, while concurrently maintaining normal vascular permeability (Zhang et al., 2016; Mensah et al., 2017). Furthermore, the infusion of 5% albumin – a major source of S1P – as fluid resuscitation following hemorrhagic shock restored glycocalyx thickness, reduced plasma syndecan-1 to baseline levels, and stabilized microvascular permeability and leucocyte adhesion in rats (Torres et al., 2017; Aldecoa et al., 2020). Since fluid therapy is central in the treatment of SAH and prevention of DCI (Tseng et al., 2008; Diringer et al., 2011), a comprehensive understanding of the effects of different kinds of fluid therapies on the glycocalyx could offer additional benefits.

Direct inhibitors of MMPs such as biphenylylsulfonylamino-3-phenylpropionic acid and batimastat have also been shown to be effective in restoring glycocalyx integrity after its breakdown (Ramnath et al., 2014, 2020). Furthermore, hydrocortisone and dexamethasone have succesfully been applied to reduce glycocalyx degradation, possibly by reducing local inflammation and indirectly inhibiting MMPs (Chappell et al., 2007; Cui et al., 2015; Zhu et al., 2018; Yu et al., 2019). For example, Zhu et al. described the protective effects of dexamethasone on the integrity of the cerebral endothelial glycocalyx in mice, thereby also reducing BBB leakage and the occurrence of cerebral edema (Zhu et al., 2018).

In addition to MMP inhibition, numerous pharmacological strategies have been applied to prevent glycocalyx shedding or restore glycocalyx integrity, with some promising – albeit preliminary – results. These include anti-diabetic medication like sulodexide, atrasentan and metformin (Boels et al., 2016; Haare et al., 2017), anticoagulant medication like antithrombin (Becker et al., 2010), and the stimulation of angiogenesis by growth factors (Desideri et al., 2019).

Although the above-mentioned results on strategies for preventing and restoring glycocalyx disruption seem promising, we did not find any clinical studies that evaluated their effects on the glycocalyx, or on disease conditions. Therefore, these findings should be considered as preliminary, and should be supported by further studies.

## FUTURE PERSPECTIVES

Based on our proposed model relating the glycocalyx to DCI, it remains to be determined whether glycocalyx shedding precedes or results from the pathophysiological processes of DCI. Shedding could be a result of the aforementioned pathophysiological mechanisms of DCI, making evaluation of glycocalyx integrity a potential biomarker of DCI. Alternatively, glycocalyx shedding could be a primary contributor to the development of DCI, which would imply that prevention and restoration of glycocalyx shedding are a potential novel preventive and therapeutic targets for DCI, respectively. Evaluation of the glycocalyx, or glycocalyx markers in preclinical models of aSAH could form a future direction for DCI studies. However, preclinical studies are lacking a standardized approach to mimic aSAH, and mainly evaluate acute or short-term changes following the induction of the subarachnoid hemorrhage, thus limiting their ability to evaluate changes related to DCI. Moreover, preclinical models may not be comparable to the pathophysiology of DCI in humans. In the absence of a standardized preclinical model mimicking human aSAH and the development of DCI, clinical studies may offer more potential to evaluate the glycocalyx in relation to the development of DCI. To date, only one small ($n$ = 3) clinical study has observed the relation between the glycocalyx and occurrence of DCI following aSAH (Bell et al., 2017). Hence, further and larger clinical studies evaluating glycocalyx integrity in aSAH patients are needed to determine a potential relation, and the preventive and/or therapeutic value of the glycocalyx as a biomarker for the development of DCI. Currently, one registered ongoing clinical study (NCT03706768) is analyzing glycocalyx changes in an aSAH cohort, however, the results have not been published yet. Considering the lack of sensitivity and specificity of the current glycocalyx analysis methods, we would recommend applying multiple glycocalyx assessment techniques simultaneously. Hence, a large observational study in which glycocalyx markers are frequently evaluated in serum and/or CSF of aSAH patients, of which around 30% will develop DCI, seems a reasonable approach to explore a role of the glycocalyx in the development of DCI. In addition, the assessment of the microcirculation and its glycocalyx using SDF-imaging could form an additional strategy in these patients. In this regard, one could consider intraoperative cerebral measurements, and pre- and postoperative sequential imaging of the sublingual and conjunctival microcirculation. Findings from such clinical studies could steer the direction of future studies. Such future studies could for example assess the potential of preventive measures of glycocalyx disruption and the therapeutic value of glycocalyx restoration in patients suffering from DCI. Importantly, further studies are needed to evaluate the actual therapeutic properties of the pharmacological substances regenerating or protecting the glycocalyx, as current evidence is limited.

### Limitations

This study has multiple limitations. Firstly, this review is not a systematic review, and the search strategy was based on multiple explorative search queries, thereby limiting reproducibility and introducing a selection bias. The explorative nature of this study, also resulted in a process of study selection that is subject to an inherent selection bias. Furthermore, only one small case study described original experiments relating glycocalyx markers to the development of DCI, whereas other studies included in this review mainly provided indirect evidence to support our hypothesis. This reduces the strength of our conclusion. Moreover, the complexity of this topic, i.e., pathomechanisms of DCI following aSAH, is further increased by the lack of standardized and reliable preclinical study models to mimic the effects of aSAH in humans. Consequently, the preclinical studies included in our review used multiple aSAH models in numerous animals, mainly rodents, which may not be comparable to the clinical situation. Lastly, definitions of DCI have evolved over time (from vasospasms to delayed ischemic neurological deficit), preventing accurate charting and comparative analysis of results of studies evaluating the pathophysiology of DCI after aSAH.

## CONCLUSION

We have reviewed the physiological roles of the glycocalyx with the aim of relating these to the pathomechanisms involved in DCI. Our results suggest that glycocalyx damage is associated with the development of DCI, however, current studies on this association are sparse. To explore this hypothesis, clinical studies assessing glycocalyx properties of the cerebral microcirculation in aSAH patients are warranted. Since the techniques that are currently available for evaluating the glycocalyx are lacking sensitivity and specificity, the inclusion of multiple assessment techniques would be indispensable for such studies.

## AUTHOR CONTRIBUTIONS

HS is the first author of this work. HS and RH wrote the manuscript. RH has senior authorship of this work. EN, OT, ID, JD, MN, YT, and GH have critically reviewed the manuscript. All authors contributed to the article and approved the submitted version.

## REFERENCES


Abassi, Z., Armaly, Z., and Heyman, S. N. (2020). Glycocalyx degradation in ischemia-reperfusion injury. *Am. J. Pathol.* 190, 752–767. doi: 10.1016/j.ajpath.2019.08.019

Abbott, N. J., Rönnbäck, L., and Hansson, E. (2006). Astrocyte-endothelial interactions at the blood-brain barrier. *Nat. Rev. Neurosci.* 7, 41–53. doi: 10.1038/nrn1824

Ahn, S. H., Savarraj, J. P. J., Parsha, K., Hergenroeder, G. W., Chang, T. R., Kim, D. H., et al. (2019). Inflammation in delayed ischemia and functional outcomes after subarachnoid hemorrhage. *J. Neuroinflammation* 16:213.

Aldecoa, C., Llau, J. V., Nuvials, X., and Artigas, A. (2020). Role of albumin in the preservation of endothelial glycocalyx integrity and the microcirculation: a review. *Ann. Intensive Care* 10:85. doi: 10.1186/s13613-020-00697-1

Alphonsus, C. S., and Rodseth, R. N. (2014). The endothelial glycocalyx: a review of the vascular barrier. *Anaesthesia* 69, 777–784. doi: 10.1111/anae.12661

Ando, Y., Okada, H., Takemura, G., Suzuki, K., Takada, C., Tomita, H., et al. (2018). Brain-specific ultrastructure of capillary endothelial glycocalyx and its possible contribution for blood brain barrier. *Sci. Rep.* 8:17523.

Appel, D., Seeberger, M., Schwedhelm, E., Czorlich, P., Goetz, A. E., Böger, R. H., et al. (2018). Asymmetric and symmetric dimethylarginines are markers of delayed cerebral ischemia and neurological outcome in patients with subarachnoid hemorrhage. *Neurocrit. Care* 29, 84–93. doi: 10.1007/s12028-018-0520-1

Atangana, E., Schneider, U. C., Blecharz, K., Magrini, S., Wagner, J., Nieminen-Kelhä, M., et al. (2017). Intravascular inflammation triggers intracerebral activated microglia and contributes to secondary brain injury after experimental subarachnoid hemorrhage (eSAH). *Transl. Stroke Res.* 8, 144–156. doi: 10.1007/s12975-016-0485-3

Balbi, M., Koide, M., Wellman, G. C., and Plesnila, N. (2017). Inversion of neurovascular coupling after subarachnoid hemorrhage in vivo. *J. Cereb. Blood Flow Metab.* 37, 3625–3634. doi: 10.1177/0271678x16686595

Becker, B. F., Chappell, D., Bruegger, D., Annecke, T., and Jacob, M. (2010). Therapeutic strategies targeting the endothelial glycocalyx: acute deficits, but great potential. *Cardiovasc. Res.* 87, 300–310. doi: 10.1093/cvr/cvq137

Becker, B. F., Jacob, M., Leipert, S., Salmon, A. H. J., and Chappell, D. (2015). Degradation of the endothelial glycocalyx in clinical settings: searching for the sheddases. *Br. J. Clin. Pharmacol.* 80, 389–402. doi: 10.1111/bcp.12629

Bell, J. D., Rhind, S. G., Di Battista, A. P., Macdonald, R. L., and Baker, A. J. (2017). Biomarkers of glycocalyx injury are associated with delayed cerebral ischemia following aneurysmal subarachnoid hemorrhage: a case series supporting a new hypothesis. *Neurocrit. Care* 26, 339–347. doi: 10.1007/s12028-016-0357-4

Blackburn, S. L., Kumar, P. T., McBride, D., Zeineddine, H. A., Leclerc, J., Choi, H. A., et al. (2018). Unique contribution of haptoglobin and haptoglobin genotype in aneurysmal subarachnoid hemorrhage. *Front. Physiol.* 9:592. doi: 10.3389/fphys.2018.00592

Boels, M. G. S., Avramut, M. C., Koudijs, A., Dane, M. J. C., Lee, D. H., Van Der Vlag, J., et al. (2016). Atrasentan reduces albuminuria by restoring the glomerular endothelial glycocalyx barrier in diabetic nephropathy. *Diabetes* 65, 2429–2439. doi: 10.2337/db15-1413

Bosche, B., Graf, R., Ernestus, R. I., Dohmen, C., Reithmeier, T., Brinker, G., et al. (2010). Recurrent spreading depolarizations after subarachnoid hemorrhage decreases oxygen availability in human cerebral cortex. *Ann. Neurol.* 67, 607–617. doi: 10.1002/ana.21943

Brezzo, G., Simpson, J., Ameen-Ali, K. E., Berwick, J., and Martin, C. (2020). Acute effects of systemic inflammation upon the neuro-glial-vascular unit and cerebrovascular function. *Brain Behav. Immun. Health* 5:100074. doi: 10.1016/j.bbih.2020.100074

Britz, G. W., Meno, J. R., Park, I. S., Abel, T. J., Chowdhary, A., Nguyen, T. S. K., et al. (2007). Time-dependent alterations in functional and pharmacological arteriolar reactivity after subarachnoid hemorrhage. *Stroke* 38, 1329–1335. doi: 10.1161/01.str.0000259853.43084.03

Budohoski, K. P., Czosnyka, M., Smielewski, P., Kasprowicz, M., Helmy, A., Bulters, D., et al. (2012). Impairment of cerebral autoregulation predicts delayed cerebral ischemia after subarachnoid hemorrhage: a prospective observational study. *Stroke* 43, 3230–3237. doi: 10.1161/strokeaha.112.669788

Budohoski, K. P., Guilfoyle, M., Helmy, A., Huuskonen, T., Czosnyka, M., Kirollos, R., et al. (2014). The pathophysiology and treatment of delayed cerebral ischaemia following subarachnoid haemorrhage. *J. Neurol. Neurosurg. Psychiatry* 85, 1343–1353.

Carrera, E., Kurtz, P., Badjatia, N., Fernandez, L., Claassen, J., Lee, K., et al. (2010). Cerebrovascular carbon dioxide reactivity and delayed cerebral ischemia after subarachnoid hemorrhage. *Arch. Neurol.* 67, 434–439.

Changyaleket, B., Chong, Z. Z., Dull, R. O., Nanegrungsunk, D., and Xu, H. (2017). Heparanase promotes neuroinflammatory response during subarachnoid hemorrhage in rats. *J. Neuroinflammation* 14:137.

Chappell, D., Jacob, M., Hofmann-Kiefer, K., Bruegger, D., Rehm, M., Conzen, P., et al. (2007). Hydrocortisone preserves the vascular barrier by protecting the endothelial glycocalyx. *Anesthesiology* 107, 776–784. doi: 10.1097/01.anes.0000286984.39328.96

Chaudhry, S. R., Hafez, A., Jahromi, B. R., Kinfe, T. M., Lamprecht, A., Niemelä, M., et al. (2018). Role of damage associated molecular pattern molecules (DAMPs) in aneurysmal subarachnoid hemorrhage (aSAH). *Int. J. Mol. Sci.* 19:2035. doi: 10.3390/ijms19072035

Choi, S. J., and Lillicrap, D. (2020). A sticky proposition: the endothelial glycocalyx and von willebrand factor. *J. Thromb. Haemost.* 18, 781–785. doi: 10.1111/jth.14743

Clarke, J. V., Suggs, J. M., Diwan, D., Lee, J. V., Lipsey, K., Vellimana, A. K., et al. (2020). Microvascular platelet aggregation and thrombosis after subarachnoid hemorrhage: a review and synthesis. *J. Cereb. Blood Flow Metab.* 40, 1565–1575. doi: 10.1177/0271678x20921974

Cosgun, Z. C., Fels, B., and Kusche-Vihrog, K. (2020). Nanomechanics of the endothelial glycocalyx: from structure to function. *Am. J. Pathol.* 190, 732–741. doi: 10.1016/j.ajpath.2019.07.021

Cui, N., Wang, H., Long, Y., Su, L., and Liu, D. (2015). Dexamethasone suppressed LPS-induced matrix metalloproteinase and its effect on endothelial glycocalyx shedding. *Mediators Inflamm.* 2015:912726.

Curry, F. E., Clark, J. F., and Adamson, R. H. (2012). Erythrocyte-derived sphingosine-1-phosphate stabilizes basal hydraulic conductivity and solute permeability in rat microvessels. *Am. J. Physiol.Heart Circ. Physiol.* 303, H825–H834.

Dane, M. J. C., Van Den Berg, B. M., Avramut, M. C., Faas, F. G. A., Van Der Vlag, J., Rops, A. L. W. M. M., et al. (2013). Glomerular endothelial surface layer acts as a barrier against albumin filtration. *Am. J. Pathol.* 182, 1532–1540. doi: 10.1016/j.ajpath.2013.01.049

de Oliveira Manoel, A. L., and Loch Macdonald, R. (2018). Neuroinflammation as a target for intervention in subarachnoid hemorrhage. *Front. Neurol.* 9:292. doi: 10.3389/fneur.2018.00292

De Rooij, N. K., Rinkel, G. J. E., Dankbaar, J. W., and Frijns, C. J. M. (2013). Delayed cerebral ischemia after subarachnoid hemorrhage: a systematic review of clinical, laboratory, and radiological predictors. *Stroke* 44, 43–54. doi: 10.1161/strokeaha.112.674291

DellaValle, B., Hasseldam, H., Johansen, F. F., Iversen, H. K., Rungby, J., and Hempel, C. (2019). Multiple soluble components of the glycocalyx are increased in patient plasma after ischemic stroke. *Stroke* 50, 2948–2951. doi: 10.1161/strokeaha.119.025953

Desideri, S., Onions, K. L., Baker, S. L., Gamez, M., El Hegni, E., Hussien, H., et al. (2019). Endothelial glycocalyx restoration by growth factors in diabetic nephropathy. *Biorheology* 56, 163–179. doi: 10.3233/bir-180199

Dhar, R., and Diringer, M. (2015). Relationship between angiographic vasospasm, cerebral blood flow, and cerebral infarction after subarachnoid hemorrhage. *Acta Neurochir. Suppl.* 20, 161–165. doi: 10.1007/978-3-319-04981-6_27

Di Wang, H., Rätsep, M. T., Chapman, A., and Boyd, R. (2010). Adventitial fibroblasts in vascular structure and function: the role of oxidative stress and beyond. *Can. J. Physiol. Pharmacol.* 88, 177–186. doi: 10.1139/y10-015

Diringer, M. N., Bleck, T. P., Hemphill, J. C., Menon, D., Shutter, L., Vespa, P., et al. (2011). Critical care management of patients following aneurysmal subarachnoid hemorrhage: recommendations from the neurocritical care society's multidisciplinary consensus conference. *Neurocrit. Care* 15, 211–240.

Dreier, J. P., Ebert, N., Priller, J., Megow, D., Lindauer, U., Klee, R., et al. (2000). Products of hemolysis in the subarachnoid space inducing spreading ischemia in the cortex and focal necrosis in rats: a model for delayed ischemic neurological deficits after subarachnoid hemorrhage? *J. Neurosurg.* 93, 658–666. doi: 10.3171/jns.2000.93.4.0658

Dreier, J. P., Woitzik, J., Fabricius, M., Bhatia, R., Major, S., Drenckhahn, C., et al. (2006). Delayed ischaemic neurological deficits after subarachnoid

haemorrhage are associated with clusters of spreading depolarizations. *Brain* 129, 3224–3237. doi: 10.1093/brain/awl297

Ebong, E. E., Lopez-Quintero, S. V., Rizzo, V., Spray, D. C., and Tarbell, J. M. (2014). Shear-induced endothelial NOS activation and remodeling via heparan sulfate, glypican-1, and syndecan-1. *Integr. Biol.* 6, 338–347. doi: 10.1039/c3ib40199e

Ebong, E. E., Macaluso, F. P., Spray, D. C., and Tarbell, J. M. (2011). Imaging the endothelial glycocalyx in vitro by rapid freezing/freeze substitution transmission electron microscopy. *Arter. Thromb. Vasc. Biol.* 31, 1908–1915. doi: 10.1161/atvbaha.111.225268

El Amki, M., Dubois, M., Lefevre-Scelles, A., Magne, N., Roussel, M., Clavier, T., et al. (2018). Long-lasting cerebral vasospasm, microthrombosis, apoptosis and paravascular alterations associated with neurological deficits in a mouse model of subarachnoid hemorrhage. *Mol. Neurobiol.* 55, 2763–2779. doi: 10.1007/s12035-017-0514-6

Fabriek, B. O., Dijkstra, C. D., and van den Berg, T. K. (2005). The macrophage scavenger receptor CD163. *Immunobiology* 210, 153–160. doi: 10.1016/j.imbio.2005.05.010

Fan, J., Sun, Y., Xia, Y., Tarbell, J. M., and Fu, B. M. (2019). Endothelial surface glycocalyx (ESG) components and ultra-structure revealed by stochastic optical reconstruction microscopy (STORM). *Biorheology* 56, 77–88. doi: 10.3233/bir-180204

Fischer, M., Dietmann, A., Beer, R., Broessner, G., Helbok, R., Pfausler, B., et al. (2013). Differential regulation of matrix-metalloproteinases and their tissue inhibitors in patients with aneurysmal subarachnoid hemorrhage. *PLoS One* 8:e59952. doi: 10.1371/journal.pone.0059952

Friedman, A., Kaufer, D., and Heinemann, U. (2009). Blood-brain barrier breakdown-inducing astrocytic transformation: novel targets for the prevention of epilepsy. *Epilepsy Res.* 85, 142–149.

Friedrich, V., Flores, R., Muller, A., Bi, W., Peerschke, E. I. B., and Sehba, F. A. (2011). Reduction of neutrophil activity decreases early microvascular injury after subarachnoid haemorrhage. *J. Neuroinflammation* 8:103. doi: 10.1186/1742-2094-8-103

Friedrich, V., Flores, R., Muller, A., and Sehba, F. A. (2010). Escape of intraluminal platelets into brain parenchyma after subarachnoid hemorrhage. *Neuroscience* 165, 968–975. doi: 10.1016/j.neuroscience.2009.10.038

Frijns, C. J. M., Fijnheer, R., Algra, A., Van Mourik, J. A., Van Gijn, J., and Rinkel, G. J. E. (2006). Early circulating levels of endothelial cell activation markers in aneurysmal subarachnoid haemorrhage: associations with cerebral ischaemic events and outcome. *J. Neurol. Neurosurg. Psychiatry.* 77, 77–83. doi: 10.1136/jnnp.2005.064956

Fumoto, T., Naraoka, M., Katagai, T., Li, Y., Shimamura, N., and Ohkuma, H. (2019). The role of oxidative stress in microvascular disturbances after experimental subarachnoid hemorrhage. *Transl. Stroke Res.* 10, 684–694. doi: 10.1007/s12975-018-0685-0

Geraghty, J. R., and Testai, F. D. (2017). Delayed cerebral ischemia after subarachnoid hemorrhage: beyond vasospasm and towards a multifactorial pathophysiology. *Curr. Atheroscler. Rep.* 19:50.

Goedhart, P. T., Khalilzada, M., Bezemer, R., Merza, J., and Ince, C. (2007). Sidestream dark field (SDF) imaging: a novel stroboscopic LED ring-based imaging modality for clinical assessment of the microcirculation. *Opt. Express.* 15:15101.

Goligorsky, M. S., and Sun, D. (2020). Glycocalyx in endotoxemia and sepsis. *Am. J. Pathol.* 190, 791–798. doi: 10.1016/j.ajpath.2019.06.017

Haare, J., Kooi, M. E., Teeffelen, J. W. G. E., Vink, H., Slenter, J., Cobelens, H., et al. (2017). Metformin and sulodexide restore cardiac microvascular perfusion capacity in diet-induced obese rats. *Cardiovasc. Diabetol.* 16:47.

Haeren, R. H., van de Ven, S. E., van Zandvoort, M. A., Vink, H., van Overbeeke, J. J., Hoogland, G., et al. (2016). Assessment and imaging of the cerebrovascular glycocalyx. *Curr. Neurovasc. Res.* 13, 249–260. doi: 10.2174/1567202613666160504104434

Haeren, R. H. L., Rijkers, K., Schijns, O. E. M. G., Dings, J., Hoogland, G., van Zandvoort, M. A. M. J., et al. (2018). In vivo assessment of the human cerebral microcirculation and its glycocalyx: a technical report. *J. Neurosci. Methods* 303, 114–125. doi: 10.1016/j.jneumeth.2018.03.009

Hamed, S., Brenner, B., Aharon, A., Daoud, D., and Roguin, A. (2009). Nitric oxide and superoxide dismutase modulate endothelial progenitor cell function in type 2 diabetes mellitus. *Cardiovasc. Diabetol.* 8:56. doi: 10.1186/1475-2840-8-56

He, L., He, T., Farrar, S., Ji, L., Liu, T., and Ma, X. (2017). Antioxidants maintain cellular redox homeostasis by elimination of reactive oxygen species. *Cell. Physiol. Biochem.* 44, 532–553. doi: 10.1159/000485089

Hiroshima, Y., Nakamura, S., Endo, S., Kuwayama, N., Naruse, Y., and Takaku, A. (1997). Elevation of platelet activating factor, inflammatory cytokines, and coagulation factors in the internal jugular vein of patients with subarachnoid hemorrhage. *Neurochem. Res.* 22, 1249–1255.

Iadecola, C. (2004). Neurovascular regulation in the normal brain and in Alzheimer's disease. *Nat. Rev. Neurosci.* 5, 347–360. doi: 10.1038/nrn1387

Iba, T. (2016). Glycocalyx regulates the intravascular hemostasis. *Juntendo Med. J.* 62, 330–335. doi: 10.14789/jmj.62.330

Iba, T., and Levy, J. H. (2019). Derangement of the endothelial glycocalyx in sepsis. *J. Thromb. Haemost.* 17, 283–294. doi: 10.1111/jth.14371

Ikonomidis, I., Marinou, M., Vlastos, D., Kourea, K., Andreadou, I., Liarakos, N., et al. (2017). Effects of varenicline and nicotine replacement therapy on arterial elasticity, endothelial glycocalyx and oxidative stress during a 3-month smoking cessation program. *Atherosclerosis* 262, 123–130. doi: 10.1016/j.atherosclerosis.2017.05.012

Ishikawa, M., Kusaka, G., Yamaguchi, N., Sekizuka, E., Nakadate, H., Minamitani, H., et al. (2009). Platelet and leukocyte adhesion in the microvasculature at the cerebral surface immediately after subarachnoid hemorrhage. *Neurosurgery* 64, 546–553. doi: 10.1227/01.neu.0000337579.05110.f4

Johnson, H. M., Gossett, L. K., Piper, M. E., Aeschlimann, S. E., Korcarz, C. E., Baker, T. B., et al. (2010). Effects of smoking and smoking cessation on endothelial function: 1-year outcomes from a randomized clinical trial. *J. Am. Coll. Cardiol.* 55, 1988–1995.

Jung, C. S., Lange, B., Zimmermann, M., and Seifert, V. (2012). The CSF concentration of ADMA, but not of ET-1, is correlated with the occurrence and severity of cerebral vasospasm after subarachnoid hemorrhage. *Neurosci. Lett.* 524, 20–24. doi: 10.1016/j.neulet.2012.06.076

Kalagara, T., Moutsis, T., Yang, Y., Pappelbaum, K. I., Farken, A., Cladder-Micus, L., et al. (2018). The endothelial glycocalyx anchors von willebrand factor fibers to the vascular endothelium. *Blood Adv.* 2, 2347–2357.

Kaplan, L., Chow, B. W., and Gu, C. (2020). Neuronal regulation of the blood–brain barrier and neurovascular coupling. *Nat. Rev. Neurosci.* 21, 416–432. doi: 10.1038/s41583-020-0322-2

Khan, L., van Lanen, R., Hoogland, G., Schijns, O., Rijkers, K., Kapsokalyvas, D., et al. (2021). Two-photon imaging to unravel the pathomechanisms associated with epileptic seizures: a review. *Appl. Sci.* 11, 2404–2427. doi: 10.3390/app11052404

Koide, M., Bonev, A. D., Nelson, M. T., and Wellman, G. C. (2013a). Subarachnoid blood converts neurally evoked vasodilation to vasoconstriction in rat brain cortex. *Acta Neurochir. Suppl.* 115, 167–171. doi: 10.1007/978-3-7091-1192-5_32

Koide, M., Sukhotinsky, I., Ayata, C., and Wellman, G. C. (2013b). Subarachnoid hemorrhage, spreading depolarizations and impaired neurovascular coupling. *Stroke Res. Treat.* 2013:819340.

Kolářová, H., Ambrůzová, B., Švihálková Šindlerová, L., Klinke, A., and Kubala, L. (2014). Modulation of endothelial glycocalyx structure under inflammatory conditions. *Mediators Inflamm.* 2014:694312.

Kumagai, R., Lu, X., and Kassab, G. S. (2009). Role of glycocalyx in flow-induced production of nitric oxide and reactive oxygen species. *Free Radic. Biol. Med.* 47, 600–607. doi: 10.1016/j.freeradbiomed.2009.05.034

Kutuzov, N., Flyvbjerg, H., and Lauritzen, M. (2018). Contributions of the glycocalyx, endothelium, and extravascular compartment to the blood–brain Barrier. *Proc. Natl. Acad. Sci. U.S.A.* 115, E9429–E9438.

Laight, D. W., Kaw, A. V., Carrier, M. J., and Änggård, E. E. (1998). Interaction between superoxide anion and nitric oxide in the regulation of vascular endothelial function. *Br. J. Pharmacol.* 124, 238–244. doi: 10.1038/sj.bjp.0701814

Lee, D. H., Dane, M. J. C., Van Den Berg, B. M., Boels, M. G. S., Van Teeffelen, J. W., De Mutsert, R., et al. (2014). Deeper penetration of erythrocytes into the endothelial glycocalyx is associated with impaired microvascular perfusion. *PLoS One* 9:e96477. doi: 10.1371/journal.pone.0096477

Lee, M. J., Van Brocklyn, J. R., Thangada, S., Liu, C. H., Hand, A. R., Menzeleev, R., et al. (1998). Sphingosine-1-phosphate as a ligand for the G protein-coupled receptor EDG-1. *Science* 279, 1552–1555. doi: 10.1126/science.279.5356.1552

Lipowsky, H. H. (2012). The endothelial glycocalyx as a barrier to leukocyte adhesion and its mediation by extracellular proteases. *Ann. Biomed. Eng.* 40, 840–848. doi: 10.1007/s10439-011-0427-x

Lopez-Quintero, S. V., Cancel, L. M., Pierides, A., Antonetti, D., Spray, D. C., and Tarbell, J. M. (2013). High glucose attenuates shear-induced changes in endothelial hydraulic conductivity by degrading the glycocalyx. *PLoS One* 8:e78954. doi: 10.1371/journal.pone.0078954

Luft, J. H. (1966). Fine structures of capillary and endocapillary layer as revealed by ruthenium red. *Fed. Proc.* 25, 1773–1783.

Macdonald, R. L., and Weir, B. K. A. (1991). A review of hemoglobin and the pathogenesis of cerebral vasospasm. *Stroke* 22, 971–982. doi: 10.1161/01.str.22.8.971

Manchanda, K., Kolarova, H., Kerkenpaß, C., Mollenhauer, M., Vitecek, J., Rudolph, V., et al. (2018). MPO (myeloperoxidase) reduces endothelial glycocalyx thickness dependent on its cationic charge. *Arterioscler. Thromb. Vasc. Biol.* 38, 1859–1867. doi: 10.1161/atvbaha.118.311143

Martens, R. J. H., Vink, H., Van Oostenbrugge, R. J., and Staals, J. (2013). Sublingual microvascular glycocalyx dimensions in lacunar stroke patients. *Cerebrovasc. Dis.* 35, 451–454. doi: 10.1159/000348854

Mastorakos, P., and McGavern, D. (2019). The anatomy and immunology of vasculature in the central nervous system. *Sci. Immunol.* 4:eaav0492. doi: 10.1126/sciimmunol.aav0492

Meguro, R., Asano, Y., Odagiri, S., Li, C., Iwatsuki, H. S. K., Meguro, R., et al. (2007). Nonheme-iron histochemistry for light and electron microscopy: a historical, theoretical and technical review. *Arch. Hist. Cytol.* 70, 1–19. doi: 10.1679/aohc.70.1

Mensah, S. A., Cheng, M. J., Homayoni, H., Plouffe, B. D., Coury, A. J., and Ebong, E. E. (2017). Regeneration of glycocalyx by heparan sulfate and sphingosine 1-phosphate restores interendothelial communication. *PLoS One* 12:e0186116. doi: 10.1371/journal.pone.0186116

Muhammad, S., Chaudhry, S. R., Kahlert, U. D., Lehecka, M., Korja, M., Niemelä, M., et al. (2020). Targeting high mobility group box 1 in subarachnoid hemorrhage: a systematic review. *Int. J. Mol. Sci.* 21:2709. doi: 10.3390/ijms21082709

Naraoka, M., Matsuda, N., Shimamura, N., Asano, K., and Ohkuma, H. (2014). The role of arterioles and the microcirculation in the development of vasospasm after aneurysmal SAH. *Biomed. Res. Int.* 2014:253746.

Neumaier, F., Kotliar, K., Haeren, R. H. L., Temel, Y., Lüke, J. N., Seyam, O., et al. (2021). Retinal vessel responses to flicker stimulation are impaired in cav2.3-deficient mice—an in-vivo evaluation using retinal vessel analysis (RVA). *Front. Neurol.* 12:659890. doi: 10.3389/fneur.2021.659890

Nian, K., Harding, I. C., Herman, I. M., and Ebong, E. E. (2020). Blood-brain barrier damage in ischemic stroke and its regulation by endothelial mechanotransduction. *Front. Physiol.* 11:605398. doi: 10.3389/fphys.2020.605398

Nieuwdorp, M., Meuwese, M. C., Mooij, H. L., Ince, C., Broekhuizen, L. N., Kastelein, J. J. P., et al. (2008). Measuring endothelial glycocalyx dimensions in humans: a potential novel tool to monitor vascular vulnerability. *J. Appl. Physiol.* 104, 845–852. doi: 10.1152/japplphysiol.00440.2007

Nissen, J. J., Mantle, D., Gregson, B., and Mendelow, A. D. (2001). Serum concentration of adhesion molecules in patients with delayed ischaemic neurological deficit after aneurysmal subarachnoid haemorrhage: the immunoglobulin and selectin superfamilies. *J. Neurol. Neurosurg. Psychiatry.* 71, 329–333. doi: 10.1136/jnnp.71.3.329

Oka, F., Chung, D. Y., Suzuki, M., and Ayata, C. (2020). Delayed cerebral ischemia after subarachnoid hemorrhage: experimental-clinical disconnect and the unmet need. *Neurocrit. Care* 32, 238–251. doi: 10.1007/s12028-018-0650-5

Østergaard, L., Aamand, R., Karabegovic, S., Tietze, A., Blicher, J. U., Mikkelsen, I. K., et al. (2013). The role of the microcirculation in delayed cerebral ischemia and chronic degenerative changes after subarachnoid hemorrhage. *J. Cereb. Blood Flow Metab.* 33, 1825–1837. doi: 10.1038/jcbfm.2013.173

Ostrowski, S. R., Gaïni, S., Pedersen, C., and Johansson, P. I. (2015). Sympathoadrenal activation and endothelial damage in patients with varying degrees of acute infectious disease: an observational study. *J. Crit. Care* 30, 90–96. doi: 10.1016/j.jcrc.2014.10.006

Osuka, K., Suzuki, Y., Tanazawa, T., Hattori, K., Yamamoto, N., Takayasu, M., et al. (1998). Interleukin-6 and development of vasospasm after subarachnoid haemorrhage. *Acta Neurochir.* 140, 943–951. doi: 10.1007/s007010050197

Palma, F. R., He, C., Danes, J. M., Paviani, V., Coelho, D. R., Gantner, B. N., et al. (2020). Mitochondrial superoxide dismutase: what the established, the intriguing, and the novel reveal about a key cellular redox switch. *Antioxid. Redox Signal.* 32, 701–714. doi: 10.1089/ars.2019.7962

Peeyush Kumar, T., McBride, D. W., Dash, P. K., Matsumura, K., Rubi, A., and Blackburn, S. L. (2019). Endothelial cell dysfunction and injury in subarachnoid hemorrhage. *Mol. Neurobiol.* 56, 1992–2006. doi: 10.1007/s12035-018-1213-7

Pennings, F. A., Bouma, G. J., and Ince, C. (2004). Direct observation of the human cerebral microcirculation during aneurysm surgery reveals increased arteriolar contractility. *Stroke* 35, 1284–1288. doi: 10.1161/01.str.0000126039.91400.cb

Pérez-Bárcena, J., Goedhart, P., Ibáñez, J., Brell, M., García, R., Llinás, P., et al. (2011). Direct observation of human microcirculation during decompressive craniectomy after stroke. *Crit. Care Med.* 39, 1126–1129. doi: 10.1097/ccm.0b013e31820ead5e

Petzold, G. C., Einhäupl, K. M., Dirnagl, U., and Dreier, J. P. (2003). Ischemia triggered by spreading neuronal activation is induced by endothelin-1 and hemoglobin in the subarachnoid space. *Ann. Neurol.* 54, 591–598. doi: 10.1002/ana.10723

Pluta, R. M., Afshar, J. K. B., Boock, R. J., and Oldfield, E. H. (1998). Temporal changes in perivascular concentrations of oxyhemoglobin, deoxyhemoglobin, and methemoglobin after subarachnoid hemorrhage. *J. Neurosurg.* 88, 557–561. doi: 10.3171/jns.1998.88.3.0557

Pradilla, G., Chaichana, K. L., Hoang, S., Huang, J., and Tamargo, R. J. (2010). Inflammation and cerebral vasospasm after subarachnoid hemorrhage. *Neurosurg. Clin. N. Am.* 21, 365–379. doi: 10.1016/j.nec.2009.10.008

Puerta-Guardo, H., Glasner, D. R., and Harris, E. (2016). Dengue virus NS1 disrupts the endothelial glycocalyx, leading to hyperpermeability. *PLoS Pathog.* 12:e1005738. doi: 10.1371/journal.ppat.1005738

Pyne-Geithman, G. J., Nair, S. G., Stamper, D. N., and Clark, J. F. (2013). Role of bilirubin oxidation products in the pathophysiology of DIND following SAH. *Acta Neurochir. Suppl.* 115, 267–273. doi: 10.1007/978-3-7091-1192-5_47

Ramnath, R., Foster, R. R., Qiu, Y., Cope, G., Butler, M. J., Salmon, A. H., et al. (2014). Matrix metalloproteinase 9-mediated shedding of syndecan 4 in response to tumor necrosis factor α: a contributor to endothelial cell glycocalyx dysfunction. *FASEB J.* 28, 4686–4699. doi: 10.1096/fj.14-252221

Ramnath, R. D., Butler, M. J., Newman, G., Desideri, S., Russell, A., Lay, A. C., et al. (2020). Blocking matrix metalloproteinase-mediated syndecan-4 shedding restores the endothelial glycocalyx and glomerular filtration barrier function in early diabetic kidney disease. *Kidney Int.* 97, 951–965. doi: 10.1016/j.kint.2019.09.035

Rapoport, R. M. (2018). Bilirubin oxidation products and cerebral vasoconstriction. *Front. Pharmacol.* 9:303. doi: 10.3389/fphar.2018.00303

Rehm, M., Bruegger, D., Christ, F., Conzen, P., Thiel, M., Jacob, M., et al. (2007). Shedding of the endothelial glycocalyx in patients undergoing major vascular surgery with global and regional ischemia. *Circulation* 116, 1896–1906. doi: 10.1161/circulationaha.106.684852

Reitsma, S., Oude Egbrink, M. G. A., Vink, H., Van Den Berg, B. M., Lima Passos, V., Engels, W., et al. (2011). Endothelial glycocalyx structure in the intact carotid artery: a two-photon laser scanning microscopy study. *J. Vasc. Res.* 48, 297–306. doi: 10.1159/000322176

Reitsma, S., Slaaf, D. W., Vink, H., Van Zandvoort, M. A. M. J., and Oude Egbrink, M. G. A. (2007). The endothelial glycocalyx: composition, functions, and visualization. *Pflugers Arch. Eur. J. Physiol.* 454, 345–359.

Rifkind, J. M., Mohanty, J. G., and Nagababu, E. (2015). The pathophysiology of extracellular hemoglobin associated with enhanced oxidative reactions. *Front. Physiol.* 6:500. doi: 10.3389/fphys.2014.00500

Rovas, A., Lukasz, A. H., Vink, H., Urban, M., Sackarnd, J., Pavenstädt, H., et al. (2018). Bedside analysis of the sublingual microvascular glycocalyx in the emergency room and intensive care unit - the GlycoNurse study. *Scand. J. Trauma. Resusc. Emerg. Med.* 26:16.

Rovas, A., Seidel, L. M., Vink, H., Pohlkötter, T., Pavenstädt, H., Ertmer, C., et al. (2019). Association of sublingual microcirculation parameters and endothelial glycocalyx dimensions in resuscitated sepsis. *Crit. Care* 23:260.

Rowland, M. J., Hadjipavlou, G., Kelly, M., Westbrook, J., and Pattinson, K. T. S. (2012). Delayed cerebral ischaemia after subarachnoid haemorrhage: looking beyond vasospasm. *Br. J. Anaesth.* 109, 315–329. doi: 10.1093/bja/aes264

Sabri, M., Ai, J., Knight, B., Tariq, A., Jeon, H., Shang, X., et al. (2011). Uncoupling of endothelial nitric oxide synthase after experimental

subarachnoid hemorrhage. *J. Cereb. Blood Flow Metab.* 31, 190–199. doi: 10.1038/jcbfm.2010.76

Sabri, M., Ai, J., Lakovic, K., D'abbondanza, J., Ilodigwe, D., and MacDonald, R. L. (2012). Mechanisms of microthrombi formation after experimental subarachnoid hemorrhage. *Neuroscience* 224, 26–37. doi: 10.1016/j.neuroscience.2012.08.002

Sabri, M., Jeon, H., Ai, J., Tariq, A., Shang, X., Chen, G., et al. (2009). Anterior circulation mouse model of subarachnoid hemorrhage. *Brain Res.* 1295, 179–185. doi: 10.1016/j.brainres.2009.08.021

Schneider, U. C., Xu, R., and Vajkoczy, P. (2018). Inflammatory events following subarachnoid hemorrhage (SAH). *Curr. Neuropharmacol.* 16, 1385–1395. doi: 10.2174/1570159x16666180412110919

Schoknecht, K., David, Y., and Heinemann, U. (2015). The blood-brain barrier-gatekeeper to neuronal homeostasis: clinical implications in the setting of stroke. *Semin. Cell Dev. Biol.* 38, 35–42. doi: 10.1016/j.semcdb.2014.10.004

Schöller, K., Trinkl, A., Klopotowski, M., Thal, S. C., Plesnila, N., Trabold, R., et al. (2007). Characterization of microvascular basal lamina damage and blood-brain barrier dysfunction following subarachnoid hemorrhage in rats. *Brain Res.* 1142, 237–246. doi: 10.1016/j.brainres.2007.01.034

Schött, U., Solomon, C., Fries, D., and Bentzer, P. (2016). The endothelial glycocalyx and its disruption, protection and regeneration: a narrative review. *Scand. J. Trauma Resusc. Emerg. Med.* 24:48. doi: 10.1186/s13049-016-0239-y

Sehba, F. A., and Friedrich, V. (2011). Early micro vascular changes after subarachnoid hemorrhage. *Acta Neurochir. Suppl.* 110, 49–55. doi: 10.1007/978-3-7091-0353-1_9

Sehba, F. A., Pluta, R. M., and Zhang, J. H. (2011). Metamorphosis of subarachnoid hemorrhage research: from delayed vasospasm to early brain injury. *Mol. Neurobiol.* 43, 27–40. doi: 10.1007/s12035-010-8155-z

Sehba, F. A., Schwartz, A. Y., Chereshnev, I., and Bederson, J. B. (2000). Acute decrease in cerebral nitric oxide levels after subarachnoid hemorrhage. *J. Cereb. Blood Flow Metab.* 20, 604–611. doi: 10.1097/00004647-200003000-00018

Sen, O., Caner, H., Aydin, M. V., Ozen, O., Atalay, B., Altinors, N., et al. (2006). The effect of mexiletine on the level of lipid peroxidation and apoptosis of endothelium following experimental subarachnoid hemorrhage. *Neurol. Res.* 28, 859–863. doi: 10.1179/016164106x115099

Sena, C. M., Leandro, A., Azul, L., Seiça, R., and Perry, G. (2018). Vascular oxidative stress: impact and therapeutic approaches. *Front. Physiol.* 9:1668. doi: 10.3389/fphys.2018.01668

Sercombe, R., Tran Dinh, Y. R., and Gomis, P. (2002). Cerebrovascular inflammation following subarachnoid hemorrhage. *Jpn. J. Pharmacol.* 88, 227–249. doi: 10.1254/jjp.88.227

Sharif, Y., Jumah, F., Coplan, L., Krosser, A., Sharif, K., and Tubbs, R. S. (2018). Blood brain barrier: a review of its anatomy and physiology in health and disease. *Clin. Anat.* 31, 812–823. doi: 10.1002/ca.23083

Stanimirovic, D. B., and Friedman, A. (2012). Pathophysiology of the neurovascular unit: disease cause or consequence. *J. Cereb. Blood Flow Metab.* 32, 1207–1221. doi: 10.1038/jcbfm.2012.25

Stein, S. C., Chen, X., Smith, D. H., Graham, D. I., Ph, D., and Al, E. T. (2006). Thromboebolism and delayed cerebral ischemia after subarachnoid hemorrhage: an autopsy study. *Neurosurgery* 59, 781–788. doi: 10.1227/01.neu.0000227519.27569.45

Suzuki, S., Suzuki, M., Iwabuchi, T., and Kamata, Y. (1983). Role of multiple cerebral microthrombosis in symptomatic cerebral vasospasm: with a case report. *Neurosurgery* 13, 199–203. doi: 10.1227/00006123-198308000-00018

Tamosuitis, T., Pranskunas, A., Balciuniene, N., Pilvinis, V., and Boerma, E. C. (2016). Conjunctival microcirculatory blood flow is altered but not abolished in brain dead patients: a prospective observational study. *BMC Neurol.* 16:95. doi: 10.1186/s12883-016-0618-z

Tarbell, J. M., and Pahakis, M. Y. (2006). Mechanotransduction and the glycocalyx. *J. Intern. Med.* 259, 339–350. doi: 10.1111/j.1365-2796.2006.01620.x

Terpolilli, N. A., Brem, C., Bühler, D., and Plesnila, N. (2015). Are we barking up the wrong vessels?: cerebral microcirculation after subarachnoid hemorrhage. *Stroke* 46, 3014–3019. doi: 10.1161/strokeaha.115.006353

Torres, L. N., Chung, K. K., Salgado, C. L., Dubick, M. A., and Torres Filho, I. P. (2017). Low-.ume resuscitation with normal saline is associated with microvascular endothelial dysfunction after hemorrhage in rats, compared to colloids and balanced crystalloids. *Crit. Care.* 21:160.

Triglia, T., Mezzapesa, A., Martin, J. C., Verdier, M., Lagier, D., Dufour, H., et al. (2016). Early matrix metalloproteinase-9 concentration in the first 48h after aneurysmal subarachnoid haemorrhage predicts delayed cerebral ischaemia. *Eur. J. Anaesthesiol.* 33, 662–669. doi: 10.1097/eja.0000000000000494

Tseng, M. Y., Hutchinson, P. J., and Kirkpatrick, P. J. (2008). Effects of fluid therapy following aneurysmal subarachnoid haemorrhage: a prospective clinical study. *Br. J. Neurosurg.* 22, 257–268. doi: 10.1080/02688690701832100

Valerio, L., Peters, R. J., Zwinderman, A. H., and Pinto-Sietsma, S. J. (2019). Reproducibility of sublingual microcirculation parameters obtained from sidestream darkfield imaging. *PLoS One* 14:e0213175. doi: 10.1371/journal.pone.0213175

van Dijk, B. J., Vergouwen, M. D. I., Kelfkens, M. M., Rinkel, G. J. E., and Hol, E. M. (2016). Glial cell response after aneurysmal subarachnoid hemorrhage - functional consequences and clinical implications. *Biochim. Biophys. Acta Mol. Basis Dis.* 1862, 492–505. doi: 10.1016/j.bbadis.2015.10.013

Vergouwen, M. D. I., Vermeulen, M., Coert, B. A., Stroes, E. S. G., and Roos, Y. B. W. E. M. (2008). Microthrombosis after aneurysmal subarachnoid hemorrhage: an additional explanation for delayed cerebral ischemia. *J. Cereb. Blood Flow Metab.* 28, 1761–1770. doi: 10.1038/jcbfm.2008.74

Vergouwen, M. D. I., Vermeulen, M., van Gijn, J., Rinkel, G. J. E., Wijdicks, E. F., Muizelaar, J. P., et al. (2010). Definition of delayed cerebral ischemia after aneurysmal subarachnoid hemorrhage as an outcome event in clinical trials and observational studies: proposal of a multidisciplinary research group. *Stroke* 41, 2391–2395. doi: 10.1161/strokeaha.110.589275

Vlahu, C. A., Lemkes, B. A., Struijk, D. G., Koopman, M. G., Krediet, R. T., and Vink, H. (2012). Damage of the endothelial glycocalyx in dialysis patients. *J. Am. Soc. Nephrol.* 23, 1900–1908.

Vlak, M. H. M., Algra, A., Brandenburg, R., and Rinkel, G. J. E. (2011). Prevalence of unruptured intracranial aneurysms, with emphasis on sex, age, comorbidity, country, and time period: a systematic review and meta-analysis. *Lancet Neurol.* 10, 626–636. doi: 10.1016/s1474-4422(11)70109-0

Wagner, K. R., Sharp, F. R., Ardizzone, T. D., Lu, A., and Clark, J. F. (2003). Heme and iron metabolism: role in cerebral hemorrhage. *J. Cereb. Blood Flow Metab.* 23, 629–652. doi: 10.1097/01.wcb.0000073905.87928.6d

Wang, Y., Branicky, R., Noë, A., and Hekimi, S. (2018). Superoxide dismutases: dual roles in controlling ROS damage and regulating ROS signaling. *J. Cell Biol.* 217, 1915–1928.

Weinbaum, S., Cancel, L. M., Fu, B. M., and Tarbell, J. M. (2021). The glycocalyx and its role in vascular physiology and vascular related diseases. *Cardiovasc. Eng. Technol.* 12, 37–71. doi: 10.1007/s13239-020-00485-9

Woitzik, J., Dreier, J. P., Hecht, N., Fiss, I., Sandow, N., Major, S., et al. (2012). Delayed cerebral ischemia and spreading depolarization in absence of angiographic vasospasm after subarachnoid hemorrhage. *J. Cereb. Blood Flow Metab.* 32, 203–212. doi: 10.1038/jcbfm.2011.169

Xia, Y., and Fu, B. M. (2018). Investigation of endothelial surface glycocalyx components and ultrastructure by single molecule localization microscopy: stochastic optical reconstruction microscopy (STORM). *Yale J. Biol. Med.* 91, 257–266.

Yamaoka-Tojo, M. (2020a). Vascular endothelial glycocalyx as a mechanism of vascular endothelial dysfunction and atherosclerosis. *World J. Cardiovasc. Dis.* 10, 731–749. doi: 10.4236/wjcd.2020.1010070

Yamaoka-Tojo, M. (2020b). Vascular endothelial glycocalyx damage in COVID-19. *Int. J. Mol. Sci.* 21:9712. doi: 10.3390/ijms21249712

Yen, W., Cai, B., Yang, J., Zhang, L., Zeng, M., Tarbell, J. M., et al. (2015). Endothelial surface glycocalyx can regulate flow-induced nitric oxide production in microvessels in vivo. *PLoS One* 10:e0117133. doi: 10.1371/journal.pone.0117133

Yilmaz, O., Afsar, B., Ortiz, A., and Kanbay, M. (2019). The role of endothelial glycocalyx in health and disease. *Clin. Kidney J.* 12, 611–619. doi: 10.1093/ckj/sfz042

Yin, W., Robyn, B., Alycia, N., and Siegfired, H. (2018). Superoxide dismutases: dual roles in controlling ROS damage and regulating ROS signaling. *J. Cell Biol.* 217, 1915–1928. doi: 10.1083/jcb.201708007

Yu, W. Q., Zhang, S. Y., Fu, S. Q., Fu, Q. H., Lu, W. N., Zhang, J., et al. (2019). Dexamethasone protects the glycocalyx on the kidney microvascular endothelium during severe acute pancreatitis. *J. Zhejiang Univ. Sci. B.* 20, 355–362. doi: 10.1631/jzus.b1900006

Zacharia, B. E., Hickman, Z. L., Grobelny, B. T., DeRosa, P., Kotchetkov, I., Ducruet, A. F., et al. (2010). Epidemiology of aneurysmal subarachnoid hemorrhage. *Neurosurg. Clin. N. Am.* 21, 221–233.

Zeng, Y. (2017). Endothelial glycocalyx as a critical signalling platform integrating the extracellular haemodynamic forces and chemical signalling. *J. Cell. Mol. Med.* 21, 1457–1462. doi: 10.1111/jcmm.13081

Zeng, Y., Adamson, R. H., Curry, F. R. E., and Tarbell, J. M. (2014). Sphingosine-1-phosphate protects endothelial glycocalyx by inhibiting syndecan-1 shedding. *Am. J. Physiol. Hear. Circ. Physiol.* 306, 363–372.

Zeng, Y., Liu, X. H., Tarbell, J., and Fu, B. (2015). Sphingosine 1-phosphate induced synthesis of glycocalyx on endothelial cells. *Exp. Cell. Res.* 339, 90–95. doi: 10.1016/j.yexcr.2015.08.013

Zhang, L., Zeng, M., Fan, J., Tarbell, J. M., Curry, F. R. E., and Fu, B. M. (2016). Sphingosine-1-phosphate maintains normal vascular permeability by preserving endothelial surface glycocalyx in intact microvessels. *Microcirculation* 23, 301–310.

Zhu, J., Li, X., Yin, J., Hu, Y., Gu, Y., and Pan, S. (2018). Glycocalyx degradation leads to blood–brain barrier dysfunction and brain edema after asphyxia cardiac arrest in rats. *J. Cereb. Blood Flow Metab.* 38, 1979–1992.

**Conflict of Interest:** The authors declare that the research was conducted in the absence of any commercial or financial relationships that could be construed as a potential conflict of interest.

**Publisher's Note:** All claims expressed in this article are solely those of the authors and do not necessarily represent those of their affiliated organizations, or those of the publisher, the editors and the reviewers. Any product that may be evaluated in this article, or claim that may be made by its manufacturer, is not guaranteed or endorsed by the publisher.

frontiers in Cell and Developmental Biology

ORIGINAL RESEARCH
published: 07 September 2021
doi: 10.3389/fcell.2021.724905

# Hydrogen Sulfide Is a Novel Protector of the Retinal Glycocalyx and Endothelial Permeability Barrier

*Claire L. Allen[1], Katarzyna Wolanska[2], Naseeb K. Malhi[1], Andrew V. Benest[1], Mark E. Wood[3], Winfried Amoaku[4], Roberta Torregrossa[2], Matthew Whiteman[2], David O. Bates[1]* and Jacqueline L. Whatmore[2]**

[1] Cancer Biology, Division of Cancer and Stem Cells, School of Medicine, Biodiscovery Institute, University of Nottingham, Nottingham, United Kingdom, [2] The Institute of Biomedical and Clinical Science, University of Exeter Medical School, St. Luke's Campus, University of Exeter, Exeter, United Kingdom, [3] Biosciences, College of Life and Environmental Science, University of Exeter, Exeter, United Kingdom, [4] Academic Ophthalmology, Division of Clinical Neuroscience, School of Medicine, University of Nottingham, Nottingham, United Kingdom

OPEN ACCESS

**Edited by:**
*Ye Zeng,*
*Sichuan University, China*

**Reviewed by:**
*Rocío Salceda,*
*National Autonomous University of Mexico, Mexico*
*Hongyan Kang,*
*Beihang University, China*

***Correspondence:**
*David O. Bates*
*David.Bates@nottingham.ac.uk*
*Jacqueline L. Whatmore*
*J.L.Whatmore@exeter.ac.uk*

**Specialty section:**
*This article was submitted to Signaling, a section of the journal Frontiers in Cell and Developmental Biology*

**Received:** *14 June 2021*
**Accepted:** *29 July 2021*
**Published:** *07 September 2021*

**Citation:**
*Allen CL, Wolanska K, Malhi NK, Benest AV, Wood ME, Amoaku W, Torregrossa R, Whiteman M, Bates DO and Whatmore JL (2021) Hydrogen Sulfide Is a Novel Protector of the Retinal Glycocalyx and Endothelial Permeability Barrier. Front. Cell Dev. Biol. 9:724905. doi: 10.3389/fcell.2021.724905*

Significantly reduced levels of the anti-inflammatory gaseous transmitter hydrogen sulfide ($H_2S$) are observed in diabetic patients and correlate with microvascular dysfunction. $H_2S$ may protect the microvasculature by preventing loss of the endothelial glycocalyx. We tested the hypothesis that $H_2S$ could prevent or treat retinal microvascular endothelial dysfunction in diabetes. Bovine retinal endothelial cells (BRECs) were exposed to normal (NG, 5.5 mmol/L) or high glucose (HG, 25 mmol/L) ± the slow-release $H_2S$ donor NaGYY4137 *in vitro*. Glycocalyx coverage (stained with WGA-FITC) and calcein-labeled monocyte adherence were measured. *In vivo,* fundus fluorescein angiography (FFA) was performed in normal and streptozotocin-induced (STZ) diabetic rats. Animals received intraocular injection of NaGYY4137 (1 μM) or the mitochondrial-targeted $H_2S$ donor AP39 (100 nM) simultaneously with STZ (prevention) or on day 6 after STZ (treatment), and the ratio of interstitial to vascular fluorescence was used to estimate apparent permeability. NaGYY4137 prevented HG-induced loss of BREC glycocalyx, increased monocyte binding to BRECs ($p \leq 0.001$), and increased overall glycocalyx coverage ($p \leq 0.001$). In rats, the STZ-induced increase in apparent retinal vascular permeability ($p \leq 0.01$) was significantly prevented by pre-treatment with NaGYY4137 and AP39 ($p < 0.05$) and stabilized by their post-STZ administration. NaGYY4137 also reduced the number of acellular capillaries (collagen IV + /IB4-) in the diabetic retina in both groups ($p \leq 0.05$). We conclude that NaGYY4137 and AP39 protected the retinal glycocalyx and endothelial permeability barrier from diabetes-associated loss of integrity and reduced the progression of diabetic retinopathy (DR). Hydrogen sulfide donors that target the glycocalyx may therefore be a therapeutic candidate for DR.

**Keywords: glycocalyx, retinal permeability, diabetes, hydrogen sulfide, inflammation, mitochondria, slow-release hydrogen sulfide donors**

## INTRODUCTION

Loss of integrity of the vascular permeability barrier is associated with a range of pathological conditions. In particular, increased permeability is observed in diabetes, and in hyperglycemic conditions (Gillies et al., 1997; Brownlee, 2001; Allen and Bayraktutan, 2009; Saker et al., 2014) where it is associated with the pathogenesis of life-altering diabetic microvascular complications such as retinopathy (Sander et al., 2007). The vascular permeability barrier is formed of endothelial cells (ECs), their underlying basement membrane, and the endothelial glycocalyx. The latter is now recognized as a key regulator of permeability as demonstrated by a range of studies showing that selective loss of specific glycocalyx components is associated with altered permeability properties in various vascular beds (Jeansson and Haraldsson, 2003; Singh et al., 2007; Landsverk et al., 2012; Betteridge et al., 2017; Onions et al., 2019).

A role for endothelial glycocalyx damage in diabetes-associated vascular changes has been described. Glycocalyx reduction is associated with increased vascular permeability and increased leucocyte and platelet adhesion in acute hyperglycemia and diabetes (Nieuwdorp et al., 2006a,b; Broekhuizen et al., 2010; Kumase et al., 2010), which were reversed by glycocalyx restoration experimentally in animals (Henry and Duling, 1999; Constantinescu et al., 2003). Strategies to reverse or reduce glycocalyx damage in diabetes have the potential to rescue some of the potentially damaging vascular changes that underlie the development of vascular complications such as retinopathy.

We hypothesized that exogenous application of hydrogen sulfide ($H_2S$) may protect the glycocalyx in diabetes, reversing or preventing the retinal vascular leakage observed in diabetic retinopathy (DR). Hydrogen sulfide has recently been identified as a seemingly ubiquitous "gaseous mediator" in mammals and humans where it is synthesized by multiple cell types by at least four distinct enzyme systems utilizing endogenous sulfur-containing amino acids. These systems include the cytosolic cystathionase (CSE), cystathionine-β-synthase (CBS), mitochondrial cysteine aminotransferase/3-mercaptopyruvate sulfurtransferase (CAT/3MST), and D-amino acid oxidase/3-mercaptopyruvate sulfurtransferase (DAO/3MST) (Whiteman et al., 2011; Szabo, 2012; Wang, 2012; Szabo et al., 2014). The first three, at least have been demonstrated in ECs (Wang, 2012; Tao et al., 2013; Mitidieri et al., 2020). Experimentally, manipulation of $H_2S$ level has been achieved by pharmacological inhibition or genetic removal of enzyme systems for $H_2S$ and the use of $H_2S$ delivery molecules, albeit generally limited to the use of simple inorganic sulfide salts [e.g., sodium hydrosulfide (NaSH) or disodium sulfide ($Na_2S$)]. These studies have revealed that $H_2S$ and/or physiologically derived species exert a wide variety of effects on different organ systems including regulation of vascular tone (Yang et al., 2008; Kanagy et al., 2017; Szabo, 2017), inflammation (Whiteman and Winyard, 2011), aging and health span (Ng et al., 2018; Zivanovic et al., 2019), and more recently as a regulator of retinal physiology (Du et al., 2017).

There is increasing evidence for impaired vascular EC synthesis and/or bioavailability of $H_2S$ in diabetes (Szabo, 2012). Lower vascular and/or tissue levels of "$H_2S$" have been observed in humans with diabetes (Whiteman et al., 2010a; Suzuki et al., 2017), and in several animal diabetic models, including streptozotocin (STZ)-treated rats (Yusuf et al., 2005; Si et al., 2013; Zhou et al., 2014) and mice (Suzuki et al., 2011) and in db/db (Peake et al., 2013; Sun et al., 2018), ob/ob (Zhao et al., 2017), Akita (Kundu et al., 2013; John et al., 2017), and NOD (Brancaleone et al., 2008) mice. Administration of often high doses of $H_2S$ *via* sulfide salts at least partially prevented the diabetic phenotype in some of these studies. In the STZ diabetes model specifically, retinal levels of $H_2S$ were lower in diabetic animals compared with controls (Si et al., 2013), and retinal capillary leakage, VEGF levels, and oxidative stress markers were partially normalized after NaSH treatment (Si et al., 2013). NaSH administration also partially restored mitochondrial function, e.g., increased ATP synthesis and complex II and III activity and prevented mitochondrial oxidant production and mitochondrial swelling, demonstrating a likely mitochondrial target for pharmacological $H_2S$ (Si et al., 2013). Collectively, these studies strongly suggest that diabetes and diabetic retinopathy (DR) result from "$H_2S$ deficiency," which could at least be partially overcome by pharmacological manipulation of mitochondrial $H_2S$ levels.

It is important to note that these previous studies on $H_2S$ and diabetes have exclusively relied on the use of sulfide salts to generate $H_2S$ (e.g., NaSH and $Na_2S$). While useful laboratory tools for $H_2S$ generation, they are not without severe limitations (Whiteman et al., 2011). These include generation of an instant, and unphysiological bolus of $H_2S$ by pH-dependent dissociation (and rapid decay), whereas endogenous organic enzymatic $H_2S$ synthesis produces low levels of $H_2S$ over prolonged periods of time (Li et al., 2008; Whiteman et al., 2010b, 2011; Kabil and Banerjee, 2014).

It is now recognized that mitochondrial oxidative stress may contribute to the pathogenesis of diabetic endothelial dysfunction (Brownlee, 2005) and that in diabetes, the primary target for $H_2S$ activity appears to be the mitochondria where it is used as an electron source for respiration to reduce oxidative stress (Módis et al., 2014; Szabo et al., 2014). This is supported by data indicating that mitochondrial-targeted slow-release $H_2S$ donors preserved cellular bioenergetics and increased levels of Nrf2 and peroxisome proliferator-activated receptor-gamma coactivator (PGC-1α), key regulators of mitochondrial antioxidant capacity, bioenergetics, and biogenesis, both *in vitro* and *in vivo* in response to UVA-induced photoaging (Lohakul et al., 2021).

However, $H_2S$ concentrations (derived from sulfide salts) that are required to reverse mitochondrial dysfunction in the vasculature (e.g., in diabetic rats) are unattainable (Suzuki et al., 2011; Montoya and Pluth, 2016). This is presumably because $H_2S$ from these tools is generated immediately, locally, and not targeted to mitochondria. With the development of the slow-release cytosolic donor sodium GYY4137 (Li et al., 2008) and the mitochondria-specific sulfide donor AP39 (Le Trionnaire et al., 2014) the limitations of NaSH/$Na_2S$ have been overcome. The effects on microvascular EC and in the kidney have been previously reported (Ahmad et al., 2016; Gerő et al., 2016), but to the best of our knowledge, no previous studies have reported on the effects of these molecules in DR.

In this current study, we investigated the effects of a single dose (administered by intravitreal injection) of two slow-release $H_2S$ donor molecules, the cytosolic sodium GYY4137 (Li et al., 2008) and the mitochondria-specific sulfide donor AP39 (Le Trionnaire et al., 2014), on retinal vascular permeability *in vivo* in the Norway Brown rat streptozotocin-induced DR model. In addition, the effects of these two $H_2S$ generators on *in vitro* EC glycocalyx thickness using bovine retinal endothelial cells (BRECs) were studied. Leucocyte adhesion to BRECs and the effects of the $H_2S$ modulation were also evaluated in normal and high-glucose conditions.

# MATERIALS AND METHODS

## $H_2S$ Donor Synthesis

The mitochondria-targeted $H_2S$ donor AP39 was synthesized in our laboratories as previously described by our team (Le Trionnaire et al., 2014). Commercially available GYY4137 is a morpholine salt that contains unstated quantities of dichloromethane residual from its initial synthesis and which forms part of the lattice structure (at least 2 dichloromethane:1 GYY4137 molecule) (Alexander et al., 2015), i.e., it is commercially available as $xCHCl_2$ or a dichloromethane complex. Dichloromethane is metabolized *in vivo* to carbon monoxide (Ratney et al., 1974; Takano and Miyazaki, 1988). Furthermore, the morpholinium counter ion (1 morpholine:1 GYY4137 molecule) is not biologically inert and has a half-life in rats of ∼90 min (Sohn et al., 1982). $LD_{50}$ values for morpholine in rats and mice, e.g., 100–400 mg/kg for i.p. administration (Kielhorn and Rosner, 1996), are well within the commonly used doses of commercial GYY4137, e.g., 50–300 mg/kg (Lee et al., 2011; Li et al., 2013). In the eye, morpholine and dichloromethane have been reported to cause keratoconjunctivitis, focal/diffuse cataract formation, keratitis, iritis, conjunctival epithelial edema and detachment, and denudation of corneal epithelium (Ballantyne et al., 1976; Brandt and Okamoto, 1988; Toxicology–cosmetic ingredient review, 1989). To avoid these clinical indications and associated toxicity, a cleaner dichloromethane and morpholine-free sodium salt synthesized as previously described was used in this study (Alexander et al., 2015).

## Cell Culture and Treatments

Primary cultures of BRECs were isolated from bovine retinae dissected from eyes of freshly slaughtered cattle, by homogenization and a series of filtration steps as previously described (Chibber et al., 2000). Briefly, excess fat and muscle tissue was removed from the eye globes and the retina were dissected, placed in 20 ml of minimal essential medium (MEM) and homogenized using a hand-held sterile glass homogenizer to dissociate the neural retina. The resulting homogenate was filtered through 80-μm nylon mesh, the material remaining on the mesh was collected, and the trapped microvessels were resuspended in serum free MEM with collagenase-dispase (2 mg/ml) and digested for 90 min at 37°C on a rotator shaker. Following further filtration through a 45-μm polypropylene net filter, the trapped microvessel fragments were vigorously pipetted in MEM with 10% (v/v) pooled human serum, 10% (v/v) tryptose phosphate broth (TPB), L-glutamine 2 mM, penicillin (100 U/ml), and streptomycin (100 μg/ml) and plated in fibronectin-coated tissue culture flasks. After 24 h, the flasks were rinsed once with MEM to remove debris and unattached cells and refilled with fresh growth medium [MEM supplemented with 10% (v/v) pooled human serum, 10% (v/v) tryptose phosphate broth (TPB), L-glutamine 2 mmol/L, and penicillin (100 U/ml) and streptomycin (100 μg/ml)]. From passage 1 onward, the BRECs were cultured on gelatin-coated tissue culture flasks and human serum was replaced with 10% (v/v) horse serum. Pericyte contamination was removed by differential trypsinization. Cultures were >90% pure as assessed by morphology and staining for von Willebrand factor. Preliminary studies confirmed that treatment with 25 mmol/L D-mannitol as osmotic control had no effect on either the glycocalyx or leukocyte adhesion compared with the normal glucose (NG) treatment. U937 cells (human leukemic monocyte lymphoma cell line) were cultured in RPMI-1640 with 10% (v/v) fetal bovine serum, 5.6 mmol/L D-glucose, 25 mmol/L HEPES, and antibiotics. Based on our preliminary results, a final concentration of 500 μmol/L of NaGYY4137 was used in the definitive experiment. NaGYY4137 (500 μmol/L) generates approximately 1 μmol/L or less of $H_2S$ during the incubation period (Szabo, 2017).

## Glycocalyx Assessment

A cell-based fluorescent assay, based on that described by Singh et al. (2007), was performed to quantify changes within the glycocalyx using fluorescein isothiocyanate-labeled wheat germ agglutinin (WGA-FITC). Bovine retinal endothelial cells were exposed to normal (NG, 5.5 mmol/L) or high glucose (HG, 25 mmol/L) ± GYY4137 (500 μmol/L) in MEM with 0.5% bovine serum albumin (BSA, w/v) for 24 h. Cells were washed 3× with phosphate buffered saline (PBS) and incubated with WGA-FITC [2 μg/ml in HEPES-buffered phenol red-free MEM containing 0.5% BSA (w/v)] for 30 min at 37°C. After washing with PBS (3×), fluorescence intensities were measured (Ex/Em, 485/520 nm) using a fluorescence microplate reader. Cells were lysed and the protein content of each well was measured using the bicinchoninic acid method. Results are presented as fluorescence unit/μg of protein.

## Leukocyte Adhesion Assay

Bovine retinal endothelial cells (BRECs) were cultured to confluency in commercially available μ-slide VI0.4 perfusion slides (Ibidi, München, Germany) coated first with 2% (w/v) bovine gelatin (2 h) and then overnight with bovine fibronectin (50 μg/ml). Cells were treated with NG or HG as above. Calcein acetoxymethyl ester labeled (0.5 μmol/L for 30 min) U937 cells ($1 \times 10^6$/ml) were then flowed over confluent BREC cultures at a laminar shear stress of 1 dyne/cm$^2$ generated by a peristaltic pump. This shear stress was chosen to mimic venular wall shear stresses that favor leucocyte adhesion *in vivo* (Jones et al., 1995; Sundd et al., 2011). After 6 min, slides were washed with PBS for 1 min to remove non-adherent cells, fixed in 4% (w/v) paraformaldehyde, and examined using a Nikon Eclipse

TS100 (Nikon UK Limited, Kingston upon Thames, Surrey, United Kingdom) fluorescence microscope to assess the number of adherent U937 cells (10 random fields of view/slide). All experiments were performed on at least three separate occasions. Statistical significance was tested using the Student *t*-test.

## Animal Ethics

Experimental animals were treated in accordance with ARVO Statement for the Use of Animals in Ophthalmic and Vision Research and under a UK Home Office license at the University of Nottingham Biological Services Unit.

## Streptozotocin-Induced Diabetes

A total of 12 male Norway Brown rats (250–300 g, Envigo, United States) were weighed and given a single intraperitoneal (i.p.) injection of STZ (50 mg/kg, Sigma–Aldrich, MO, United States). A total of six control rats were injected with 300 μl of saline i.p. On days 0 and 4 and prior to sacrifice (day 7), blood glucose levels were tested using a sample of blood taken from the tail vein and an Accuchek blood glucose monitor. Rats with blood glucose levels of 15 mmol/L and above were deemed diabetic. Streptozotocin-injected rats that did not become hyperglycemic on day 4 were re-injected with STZ the following morning and subsequently included if deemed diabetic following evaluation for diabetes as outlined above.

## Intravitreal Injections

Rats were anaesthetized with a single 10 mg/ml i.p. injection of Domitor (medetomidine hydrochloride, Pfizer, United Kingdom) and Ketaset (ketamine hydrochloride, Zoetis, NJ, United States). Pupils were dilated with topical applications of 5% (w/v) phenylephrine hydrochloride (Bausch and Lomb) and 0.8% (w/v) tropicamide (Bausch and Lomb), and eyes were coated with Lubrithal (*Dechra)* to prevent dehydration. A 1.5-cm 34-gauge hypodermic needle (Hamilton, NV, United States) attached to a 5-μl syringe (World Precision Instruments, FL, United States) was inserted through pars plana at 3 mm from the limbus into the vitreous of the left eye at a 45° angle. Rats received 5 μl of sterile PBS, 1 μmol/L NaGYY4137 [sodium 4-methoxyphenyl(morpholino)-phosphinodithioate], or 100 nmol/L AP39 [(10-oxo-10-(4-(3-thioxo-3H-1,2-dithiol-5yl)phenoxy)decyl) triphenylphosphonium bromide] on day 0 (prevention arm) or day 6 (treatment arm).

## Fundus Fluorescein Angiography

Angiography was performed as described (Allen et al., 2020). Sodium fluorescein (NaF) dye was prepared by dissolving in sterile PBS to give a final concentration of 100 mg/ml and sterile filtered (0.2 μm). Rats were anesthetized as previously described and fundus images of the retina were captured to check for any ocular abnormalities. Rats received a single 250 μl i.p. injection of sodium fluorescein (100 mg/ml), which was allowed to circulate for ∼60 s before imaging with a Micron IV Retinal Imaging Microscope (Phoenix Research Labs). The green filter was selected, and a 3-min video footage of the retina was recorded at 15 frames per second. This was carried out on days 0 and 7. Development of cataracts with resultant blurring of posterior segment view meant that some eyes ($n = 2$) were excluded from the consecutive fundus fluorescein angiography (FFA).

## Retinal Permeability Model

Angiograms were imported into ImageJ software and fluorescence was measured in the interstitium and a major retinal vessel every 200 frames up to 2,400 frames. The ratio of interstitial to vascular fluorescence was adjusted for background level and plotted against time and the slope used to determine an estimate of permeability (**Figure 1**). **Figure 1A** shows images taken from rats given NaF and recording started within 1 min of injection. The large vessels of the retina are clearly seen, and the retina becomes brighter over time. To estimate a measure of permeability, the fluorescence intensity in an area with no large vessels was measured. The solute flux (number of fluorescence molecules entering the interstitium per unit time) was calculated from the change in fluorescence intensity in the window outside the major vessel, as a proportion of the fluorescence intensity in the blood vessel in the same frame, to account for any changes in focus, excitation intensity, or noise, plotted against the time in seconds. The permeability surface area product was calculated from the solute flux, the concentration gradient between the intravascular and extravascular compartments (difference in fluorescence intensity), and the area of the extravascular sample measurement according to Fick's law. In healthy Norway Brown rats, the permeability was the same 7 days after intraocular injection with 2 μl saline ($7.47 \pm 1.74 \times 10^{-4}$ $s^{-1}$) as it was before injection ($6.57 \pm 2.13 \times 10^{-4}$ $s^{-1}$). Streptozotocin treatment resulted in a significant increase in blood glucose (29.73 ± 0.66 mmol/L) after 1 week (compared with 7.92 ± 0.37 mmol/L), which was accompanied by a significant increase in solute flux in the retina (**Figure 4**), which translated to an increase in estimated permeability from $8.19 \pm 0.95 \times 10^{-4}$ $s^{-1}$ before STZ to $13.32 \pm 1.65 \times 10^{-4}$ $s^{-1}$ after STZ induction (Allen et al., 2020).

## Immunofluorescence

After animal termination and ocular dissection (day 14), retinae were flat-mounted and blocked in 5% (v/v) goat serum, 3% (v/v) Triton X-100, 1% (w/v) BSA, and stained with isolectin-B4 (IB4) (Sigma Aldrich, biotin conjugated) 5 μg/ml and rabbit anti-collagen IV (Abcam) 5 μg/ml overnight at 4°C. Streptavidin conjugated Alexafluor 488 2 μg/ml and donkey anti-rabbit Alexafluor 555 4 μg/ml were used to detect IB4 and collagen IV staining, respectively. Coverslips were mounted with Fluoroshield with DAPI. Images were obtained using a Leica TCS SPE confocal microscope, and all settings were maintained between images.

## Statistics

All statistics and graphs were produced in GraphPad Prism 6 and statistical tests are shown in figure legends. Significant differences are indicated on graphs as asterisks, where: $^{*}p \leq 0.05$; $^{**}p \leq 0.01$; $^{***}p \leq 0.001$.

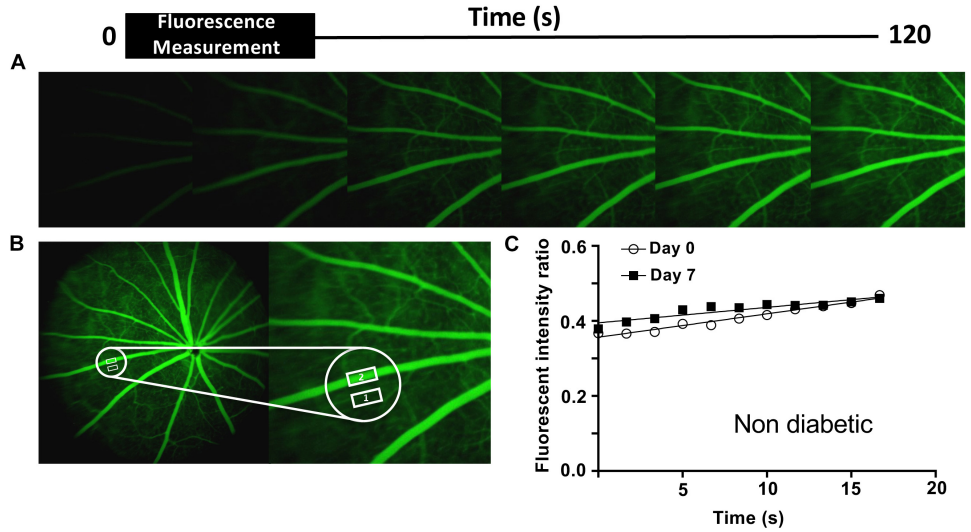


**FIGURE 1 |** Retinal permeability analysis model. **(A)** Fundus fluorescein angiography was performed in non- and diabetic Norway Brown rats treated ± $H_2S$ donors, on days 0 and 7. The angiograms shown are representative of a non-diabetic animal. **(B)** The mean intensity of NaF in the retinal tissue (Adamis and Berman, 2008) and a main retinal vessel (Ahmad et al., 2016) were measured every 200 frames for 3 min. **(C)** Apparent permeability (Permeability.Surface Area product, PA) was calculated from the rate of change of extravascular fluorescence (= $\Delta I_f/\Delta t$) per unit concentration difference ($\Delta C$) between blood and tissue. $P = \Delta I_f/\Delta t/(\Delta C \times A)$. $\Delta I_f/\Delta t \sim$ slope. $\Delta C$ = difference between intra- and extravascular intensity.

# RESULTS

## Glycocalyx Integrity

Two hydrogen sulfide generating molecules were investigated, NaGYY4137 and AP39. The former is a slow-releasing hydrogen sulfide donor (Alexander et al., 2015) that does not target any specific part of the cell, whereas AP39 is a mitochondrial targeted donor (Le Trionnaire et al., 2014).

HG significantly reduced BREC glycocalyx *in vitro* (assessed by FITC-WGA staining) to 89.67% ± 6.6% compared with NG control conditions (100%), $p \leq 0.001$, $n$ = 12–30 (**Figure 2**). Simultaneous treatment with the slow-release $H_2S$ donor NaGYY4137 completely reversed this loss and actually restored the glycocalyx to higher levels than observed in the NG control (107.49 ± 8.13% vs. 100%, $p \leq 0.001$, $n$ = 12–30). Interestingly, cells incubated in NG conditions in the presence of NaGYY4137 also had significantly higher glycocalyx staining than control NG-treated cells (106.7 ± 6.35 vs. 100%, $p \leq 0.001$, $n$ = 12–30).

Since the integrity of the glycocalyx may alter endothelial cell adhesion molecule exposure and thus influence leukocyte/endothelial binding, adhesion of U937 leukocytes to a BREC monolayer was examined under the same experimental conditions. HG significantly increased leukocyte adhesion to 348 ± 110% vs. NG control (100%), $p \leq 0.01$, $n$ = 4 (**Figure 3**). This increase was fully attenuated to control levels by incubation with NaGYY4137 (HG + NaGYY4137; 124 ± 47% vs. HG; 348 ± 110%, $p \leq 0.01$, $n$ = 4). NaGYY4137 had no significant effect on leukocyte binding in NG conditions.

## Retinal Permeability

To determine the effect of hydrogen sulfide donors on retinal permeability, fluorescein fundus angiography was carried out before and after induction of diabetes with STZ. NaF was injected intraperitoneally into Norway Brown rats and the fluorescence intensity inside a large vessel and in the tissue outside a large vessel was determined over time by video-microscopy.

Retinal vascular permeability was significantly increased in the diabetic Norway Brown rats (23.51 ± 4.59 × $10^{-4}$ $s^{-1}$, $n$ = 3) compared with normal control rats (9.38 ± 1.40 × $10^{-4}$ $s^{-1}$, $n$ = 6, **Figure 4**) on day 28 ($p \leq 0.001$) on day 28 and all other time points. In the $H_2S$ donor treatment study no changes

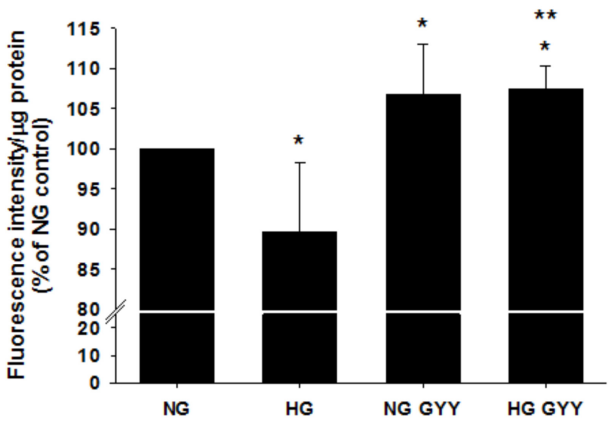


**FIGURE 2 |** Administration of the slow-release $H_2S$ donor NaGYY4137 completely reversed the loss of retinal EC glycocalyx integrity induced by hyperglycemia. Retinal ECs were incubated with normal (5.5 mmol/L, NG) or high glucose (25 mmol/L, HG) ± GYY4137 (500 µmol/L) for 24 h before assessment of glycocalyx integrity with fluorescently labeled lectin (WGA-FITC). Data are mean ± SD, presented as fluorescence intensity/µg protein. *$p \leq 0.01$ vs. control, **$p \leq 0.01$ vs. HG, $n$ = 12–30. One-way ANOVA.

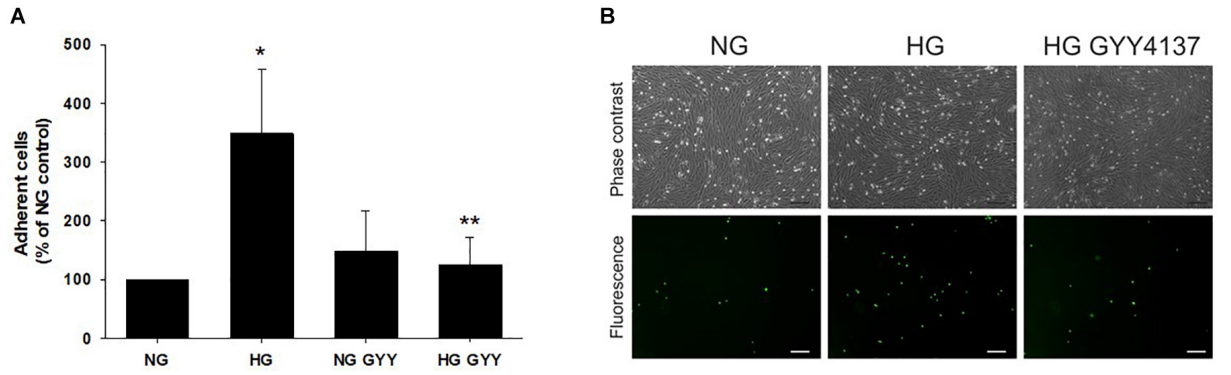


**FIGURE 3 |** Administration of the slow-release $H_2S$ donor NaGYY4137 completely attenuated the increased leukocyte adhesion to retinal ECs induced by hyperglycemia. Retinal ECs were incubated with normal (5.5 mmol/L, NG) or high glucose (25 mmol/L, HG) ± NaGYY4137 (500 μmol/L) for 24 h before examination of leukocyte adhesion under flow (1 dyne/cm$^2$). **(A)** Number of adherent U937 cells. Data are mean ± SD. *$p \leq 0.001$ vs. control, **$p \leq 0.001$ vs. HG, $n = 4$. One-way ANOVA. **(B)** Representative bright field, phase contrast (upper panel) and corresponding fluorescence images (lower panel) of adherent U937 cells stained with calcein acetoxymethyl ester adhering to a BREC monolayer. Scale bar, 75 μm; original magnification, ×100.

in retinal permeability were measured on day 7 compared to baseline in non-diabetic animals treated with vehicle control (saline) (**Figure 5A**). However, a significant ($p \leq 0.05$) increase in retinal permeability was measured in non-insulin treated diabetic animals on day 7 ($12.16 \pm 0.98 \times 10^{-4}$ s$^{-1}$) compared to baseline ($9.23 \pm 1.54 \times 10^{-4}$ s$^{-1}$) (**Figures 5B,C**). The slow-release hydrogen sulfide donor NaGYY4137 significantly reduced retinal vascular permeability in control, non-diabetic rats after 7 days ($3.24 \pm 0.66 \times 10^{-4}$ s$^{-1}$, $p \leq 0.05$, $n = 6$) vs. day 0 ($10.12 \pm 1.85 \times 10^{-4}$ s$^{-1}$) when administered as a single preventative intraocular dose pre-diabetes (**Figure 5D**). Similarly, NaGYY4137 given in diabetic rats significantly reduced retinal permeability on day 7 ($6.62 \pm 1.16 \times 10^{-4}$ s$^{-1}$, $p \leq 0.05$, $n = 6$) vs. day 0 ($13.08 \pm 2.61 \times 10^{-4}$ s$^{-1}$) when given as a preventative treatment (**Figure 5D**). When NaGYY4137 was administered therapeutically, retinal permeability was reduced in control, non-diabetic animals on day 7 ($5.31 \pm 1.24 \times 10^{-4}$ s$^{-1}$, $n = 6$) vs. day 0 ($8.90 \pm 1.19 \times 10^{-4}$ s$^{-1}$, $n = 6$). More importantly, in animals with pre-existing diabetes, retinal permeability stabilized on day 7 ($10.27 \pm 1.21 \times 10^{-4}$ s$^{-1}$, $n = 6$) compared to day 0 ($8.65 \pm 1.23 \times 10^{-4}$ s$^{-1}$, $n = 6$) (**Figure 5E**). Administering NaGYY4137 treatment prior to the onset of diabetes gave a 68% benefit in reducing retinal permeability compared with administration to animals with pre-existing diabetes (**Figure 5F**).

Similarly, the mitochondrial-targeted hydrogen sulfide donor AP39 significantly reduced retinal permeability in control, non-diabetic ($6.14 \pm 0.90 \times 10^{-4}$ s$^{-1}$, $p \leq 0.05$, $n = 6$) and diabetic rats ($9.84 \pm 1.48 \times 10^{-4}$ s$^{-1}$, $p \leq 0.05$, $n = 6$) compared with day 0 ($10.01 \pm 1.34 \times 10^{-4}$ s$^{-1}$ and $15.52 \pm 2.75 \times 10^{-4}$ s$^{-1}$, respectively) when administered as a single preventative dose (**Figure 5G**). In addition, AP39 reduced retinal permeability after a week ($5.93 \pm 2.25 \times 10^{-4}$ s$^{-1}$, $n = 6$) compared with baseline ($9.49 \pm 1.28 \times 10^{-4}$ s$^{-1}$, $p \leq 0.05$, $n = 6$) in control animals when administered therapeutically. However, in diabetic animals, AP39, when administered therapeutically, stabilized retinal permeability ($13.63 \pm 2.56 \times 10^{-4}$ s$^{-1}$, $n = 5$) on day 7 versus baseline ($8.99 \pm 1.31 \times 10^{-4}$ s$^{-1}$, $n = 5$) (**Figure 5H**). Similar to NaGYY4137, administering AP39 treatment prior to the onset of diabetes gave an 18% benefit in reducing retinal permeability when compared with animals with pre-existing diabetes (**Figure 5I**). Overall, both $H_2S$ donors were more effective in reducing retinal permeability when given to animals prior to the onset of diabetes. In addition, NaGYY4137 showed greater efficacy than a 10-fold lower dose of the mitochondrial targeted AP39 compound.

## Acellular Capillary Formation

One of the contributing factors to the pathogenesis of DR is the presence of acellular capillaries within the retina. These vessels maintain a basement membrane but have lost the supporting pericytes and EC cells and thus have no blood flow, promoting retinal ischemia. In order to assess the effects of NaGYY4137 on acellular capillary formation, retinae were collected at the end of the retinal permeability study and stained for isolectin B4, an EC marker, and collagen IV, a major constituent of the basement membrane. NaGYY4137 was found to reduce the number of acellular capillaries (collagen IV + /IB4-) in the diabetic retinae in both the prevention and treatment group to $80.2 \pm 13.9$ mm$^{-2}$ and $66.1 \pm 7.1$ mm$^{-2}$, respectively, compared with $113.6 \pm 11.7$ mm$^{-2}$ in the diabetic retinae ($p \leq 0.05$, $n = 3$, **Figure 6**). Despite the increased effectiveness of NaGYY4137 in reducing retinal permeability when administered prior to diabetes onset, the time of administration appeared to have no difference in acellular capillary formation.

# DISCUSSION

The data presented here indicate, for the first time, that (a) high glucose-driven glycocalyx loss, (b) high glucose-enhanced leukocyte adhesion to the endothelium, and (c) diabetes-associated increases in retinal permeability can all be reversed by administration of a slow-release $H_2S$ donor.

Hyperglycemia-related low-grade persistent inflammation is thought to contribute to the pathology of early DR (Adamis and Berman, 2008). Patients with DR have elevated ocular

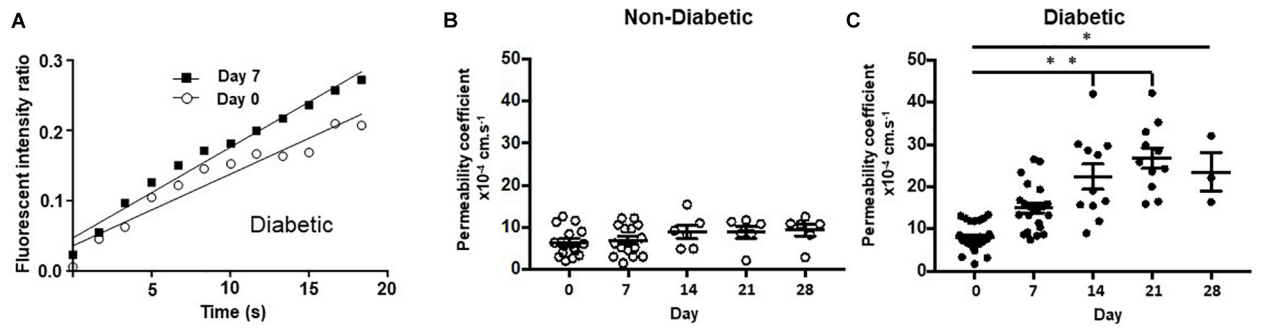


**FIGURE 4 |** Chemically induced diabetes significantly increased retinal vascular permeability in Norway Brown rats compared to non-diabetic controls. **(A)** Fundus fluorescein angiography measurements from a single rat carried out on day 0 (before STZ) and day 7 (1 week of STZ treatment). **(B)** Permeability was measured from control (blood glucose 7.99 ± 0.21 mmol/L), and **(C)** diabetic (blood glucose 29.75 ± 1.63 mmol/L) Norway Brown rats on days 0, 7, 14, 21, and 28. Apparent permeability was calculated as described in the methodology text and depicted in **Figure 1**. Data including mean ± SEM. *$p \leq 0.001$ vs. day 0, **$p \leq 0.0001$ vs. diabetic day 0. One-way ANOVA.

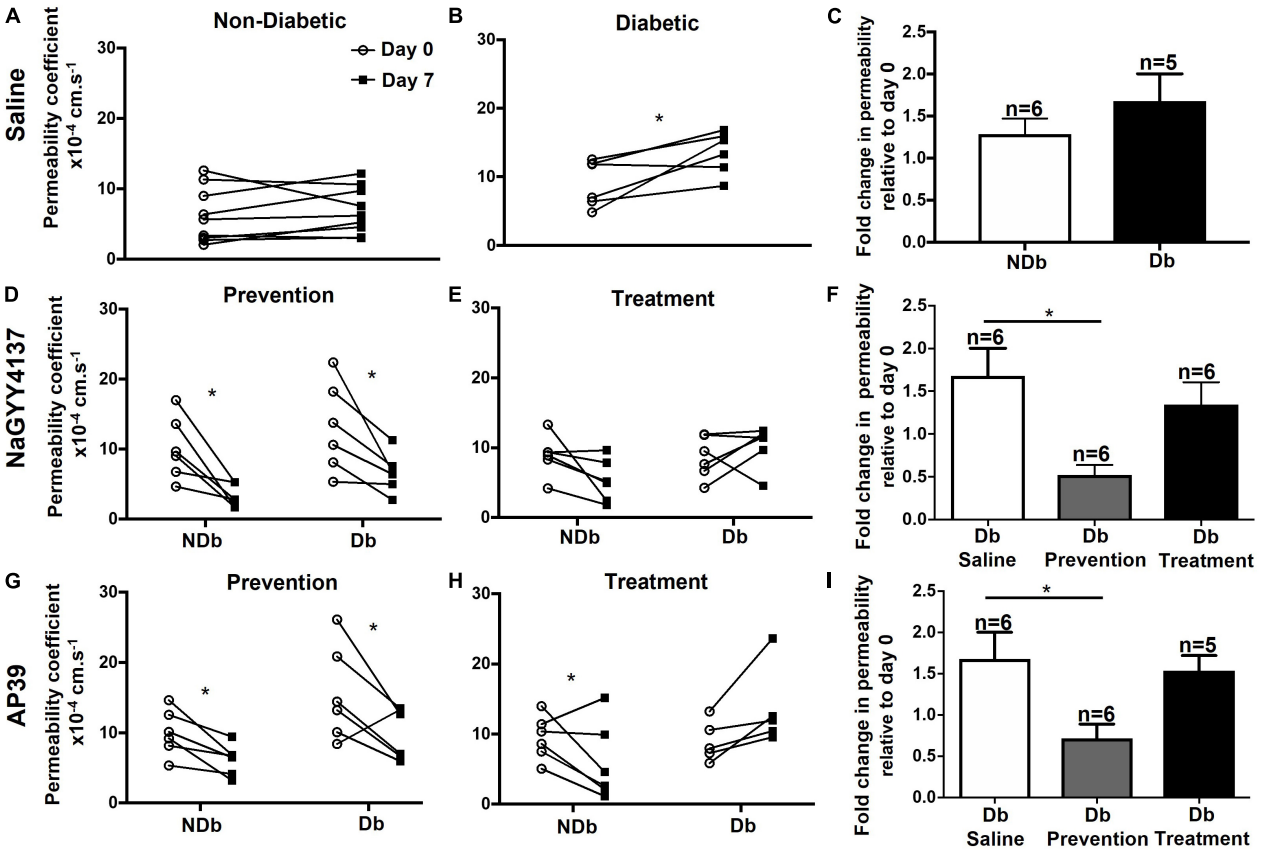


**FIGURE 5 |** Ocular administration of the slow-release $H_2S$ donors reduced retinal permeability in chemically induced diabetic rats. Type I diabetes was successfully induced in rats following a single dose of STZ and animals were maintained for 1 week without insulin supplementation. Retinal vascular leak was measured on day 0 and day 7 in non- and diabetic animals following treatment. No observed increases in retinal permeability were measured on day 7 in non-diabetic animals treated with saline **(A,C)**. In diabetic animals treated with saline a significant (*$p \leq 0.05$) increase in retinal permeability was measured on day 7 vs. day 0 **(B,C)**. NaGYY4137 and AP39 significantly (*$p < 0.05$, paired *t*-test) reduced retinal permeability in non- and diabetic rats **(D,G,F)** on day 7 when given as a single intraocular preventative dose, on day 0. In addition, NaGYY4137 and AP39 reduced retinal permeability in non-diabetic rats **(E,F,H,I)** when administered therapeutically (day 6). In diabetic rats, NaGYY4137 and AP39 stabilized retinal permeability on day 7 in rats with pre-existing diabetes **(E,F,H,I)**.

levels of inflammatory mediators and the diabetic retina displays characteristic features of inflammation including increased vascular permeability and leukocyte adhesion (Adamis and Berman, 2008). Since a healthy glycocalyx is critical to maintenance of both the anti-inflammatory and permeability characteristics of a healthy endothelium, our data highlight

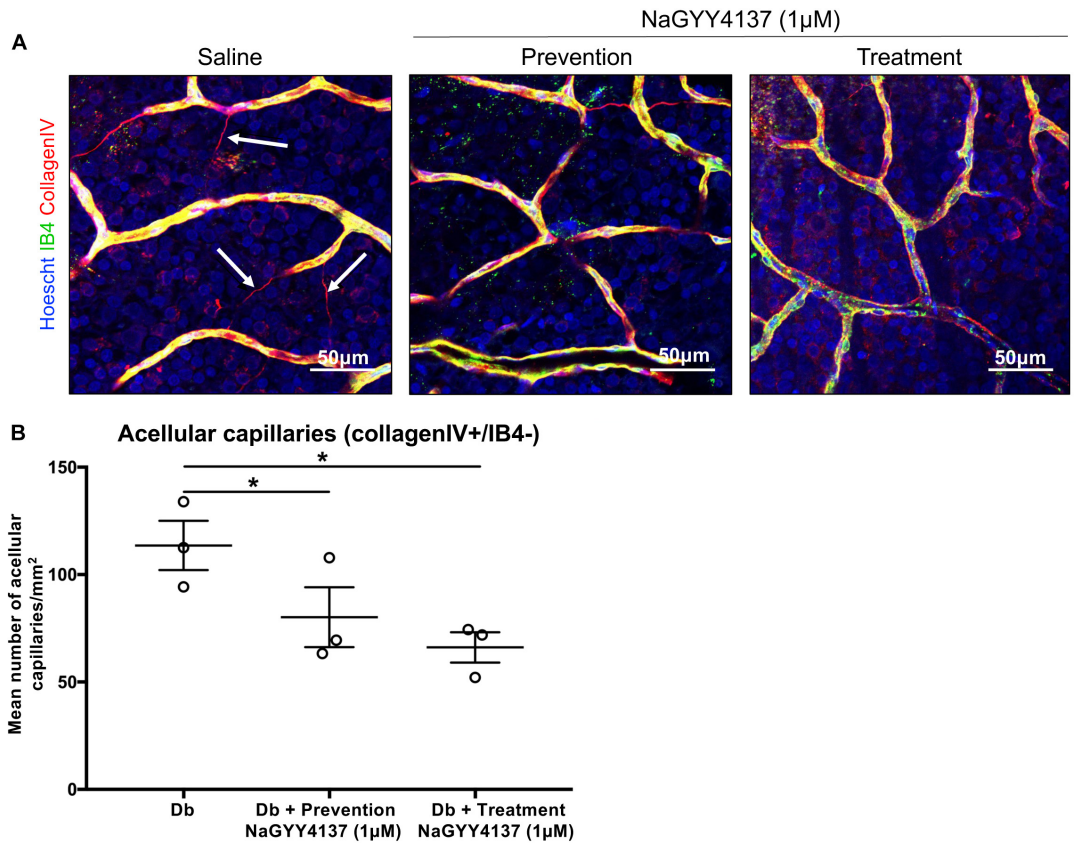


**FIGURE 6 |** NaGYY4137 protected against diabetes-induced increase in acellular capillaries. Norway Brown rats were given a single dose of streptozotocin (50 mg/kg) to induce Type I diabetes. Rats were treated with an intraocular injection of either saline or 1 μmol/L $H_2S$ donor NaGYY4137 at day 0 (prevention) or day 6 (treatment). **(A)** Rats were enucleated at day 7 and whole retinae were mounted and stained with Hoescht, IB4, and collagen IV. The tissue was imaged using 20 × lens. The number of capillaries positively stained for collagen IV but lacking IB4 (white arrows) were counted in three areas of the retina. **(B)** Acellular capillaries are expressed per $mm^2$. Error bars represent standard errors of the mean. Statistical analysis was performed using a one-way analysis of variance corrected for false discovery rate. *$p \leq 0.05$.

the potential of $H_2S$ donors as new therapeutic tools for the treatment of DR. Further investigations into optimal dosing and comparing other $H_2S$ delivery molecules are needed to further explore this potential.

The available literature describing other research in this area is scarce. However, glycocalyx loss and enhanced leukocyte adhesion have been reported in a rat model of diabetes (Kumase et al., 2010). Additionally, a clear link between *in vivo* retinal glycocalyx integrity and vascular permeability has been reported by Leskova et al. (2019), who demonstrated, in mice, that enzymatic degradation of the glycocalyx is associated with enhanced retinal permeability. These data support the hypothesis that maintaining glycocalyx integrity could be a viable therapeutic strategy for DR. EC glycocalyx thickness depends on the rate of shedding and circulatory levels of glycosaminoglycans (GAG)-degrading enzyme levels (Ikegami-Kawai et al., 2003; Maxhimer et al., 2005). The previously reported association of glycocalyx reduction with increased vascular permeability and leucocyte and platelet adhesion and subsequent reversal by glycocalyx restoration in experimental animals through increased GAG synthesis (Henry and Duling, 1999; Constantinescu et al., 2003) corroborate our findings. Furthermore, Ciszewicz et al. (2009), have shown that sulodexide attenuates hyperglycemia-associated EC permeability and inflammation. Similarly, Broekhuizen et al. (2010), demonstrated that sulodexide increased vascular EC glycocalyx and reversed the increased vascular permeability in type 2 diabetes. Additionally, Niu et al. (2019), using the STZ-induced diabetic rat model used here, showed that endomucin overexpression restored the diabetes-associated loss of retinal endothelial glycocalyx and that this restoration was associated with decreased leukocyte–endothelial adhesion and a reduction in vessel leakage in rats with DR.

The effects of $H_2S$ on the glycocalyx are still unknown. Although early studies showed potential antioxidant effects of $H_2S$, more recent work has shown that the reaction rate between $H_2S$ and oxidant species, e.g., peroxide and peroxynitrite, may be too slow for oxidant scavenging activity alone to be primarily responsible for glycocalyx- and vaso-protection, especially given the low *in vivo* concentrations of $H_2S$, which we have modeled using NaGYY4317 (Carballal et al., 2011). This strongly suggests that $H_2S$ is acting *via* other mechanisms to maintain the glycocalyx during hyperglycemic damage, e.g., enhancing synthesis of glycocalyx components or preventing

hyperglycemia-induced glycocalyx degradation. For instance, the glycocalyx component syndecan-1 is cleaved by matrix metalloproteinase-9 (MMP-9) and both activity and expression of the protease are known to be reduced by $H_2S$ administration (Du et al., 2017). It has also been reported that MMP-7 can cleave chondroitin sulfate (Lipowsky, 2011) and syndecans 1 and 4 (Manon-Jensen et al., 2013) and our unpublished data indicate that NaGYY4137 inhibits MMP-7 in *in vitro* assays at concentrations similar to those used in the studies described here. Interestingly, our additional preliminary data indicating that NaGYY4137 reduces shedding of hyaluronic acid from cultured ECs suggest another potential action of $H_2S$ since the significant reduction in EC glycocalyx observed in acute hyperglycemia (Nieuwdorp et al., 2006b) and in types 1 and type 2 diabetes (Nieuwdorp et al., 2006a; Broekhuizen et al., 2010) is thought to be related to increased hyaluronidase catabolism (Nieuwdorp et al., 2006a).

It is interesting to note that NaGYY4137 treatment in NG enhanced glycocalyx staining above the levels observed in NG alone (**Figure 2**), suggesting that $H_2S$ supplementation alone increased glycocalyx density. As mentioned previously, the glycocalyx is a dynamic structure and thus this observation could potentially be explained by the ability of $H_2S$ to modify glycocalyx-degrading enzymes to reduce their activity. Interestingly, $H_2S$ is the only molecule known to induce protein *S*-persulfidation (*S*-sulfhydration), a recently identified and unique post-translational protein modification. It is possible that the activity of glycocalyx-degrading enzymes such as heparinase might be altered by persulfidation of the cysteine residues of its active site. Additionally, cysteine residues in proteins have the potential to be redox modified by $H_2S$ in a non-S-persulfidation manner and several potential glycocalyx-degrading enzymes, including the proteinases MMP-1 (Lohakul et al., 2021), MMP-2, MMP-7, and MMP-9, have a cysteine in their active site. Thus, as has been shown with other zinc proteases including angiotensin-converting enzyme (Laggner et al., 2007) and TNF-α-converting enzyme (Li et al., 2013), $H_2S$ has the potential to modulate the glycocalyx-degrading enzyme activity of the proteinases, although further work is needed to confirm this hypothesis.

The effectiveness of our mitochondrial targeted $H_2S$ donor in decreasing retinal leakage *in vivo* raises the possibility of mitochondrial involvement in the observed effects. Modis et al. reported that endogenous mitochondrial $H_2S$ production was governed by MST (Módis et al., 2013). Additionally, Si et al. (2013) reported that DR was associated with significant decreases in retinal $H_2S$ levels and expression of the $H_2S$ synthesizing enzymes CSE, CBS, and 3MST (i.e., DR resulted in retinal $H_2S$ deficiency) and also with increased mitochondrial permeability and respiration (Si et al., 2013), strongly suggesting extensive mitochondrial dysfunction and $H_2S$ deficiency in the retina in DR. Vascular mitochondrial impairment induced by diabetes has previously been shown to be inhibited/reversed by sulfide administration albeit at high doses/concentrations (e.g., 300 μmol/L) (Módis et al., 2013; Coletta et al., 2015), suggesting that pharmacological sulfide could overcome impaired retinal bioenergetics in DR. Although NaSH administration has previously been shown to reduce retinal vascular abnormalities associated with DR and "correct" mitochondrial dysfunction (Si et al., 2013), this earlier study is intriguing for several reasons. Firstly, the NaSH was given as a daily intraperitoneal injection (over 14 weeks) at a dose equivalent to 280 mmol/kg. This was an exceptionally high and surprisingly non-lethal dose (although toxicity was not examined) given that 14 μmol/kg i.p. induces systemic inflammation and vascular collapse (Li et al., 2005) and the $LD_{50}$ for NaSH is 52.6 μmol/kg for the same route of administration (Strickland et al., 2003). Possible toxicological constraints aside, the half-life of bolus sulfide in blood is less than a minute as it is rapidly metabolized/removed (Wang, 2002, 2012), so the precise mechanisms by which a bolus of $H_2S$ (from NaSH), administered intraperitoneally survives intact to penetrate the blood–brain barrier and selectively increase sulfide levels in the retina *via* this route remain elusive. Given that plasma $H_2S$ levels have been measured at nanomolar to low micromolar concentrations, our approach to prevent/reverse DR-induced retinal vascular leakage using slow-release $H_2S$ donors (Wei et al., 2014; John et al., 2017; Qiu et al., 2018) or $H_2S$ delivery molecules that selectively target mitochondria (Le Trionnaire et al., 2014; Szczesny et al., 2014; Ikeda et al., 2015; Ahmad et al., 2016; Karwi et al., 2017) would overcome these concerns.

## CONCLUSION

The data presented here together with previous *in vivo* data (Whiteman et al., 2010a) suggest that, in health, $H_2S$ is vasculoprotective and that microvascular dysfunction in diabetes, including DR, is associated with reduced circulating and retinal $H_2S$ levels. Thus, diabetes may be a condition of $H_2S$ deficiency and $H_2S$ supplementation using slow-release and/or mitochondrial-targeted $H_2S$ delivery molecules may represent a novel, cost-effective alternative therapy for DR.

## DATA AVAILABILITY STATEMENT

The original contributions presented in the study are included in the article/supplementary material. The raw data supporting the conclusions of this article will be made available by the authors, without undue reservation.

## ETHICS STATEMENT

The animal study was reviewed and approved by University of Nottingham Biological Services Unit.

## AUTHOR CONTRIBUTIONS

JW, DB, and MWh conceived and planned the experiments. CA, JW, DB, and MWh took the lead in writing the manuscript. CA, KW, and NM carried out the experiments. RT and MWo synthesized the slow-release hydrogen sulfide donors. AB and WA contributed to the interpretation of the results. All authors provided critical feedback and helped shape the research, analysis, and manuscript.

## FUNDING

We wish to thank the Medical Research Council, UK (MR/M022706/1 to MWh and MWo; MR/L01985X/1 to JW, DB, and MWh), British Heart Foundation (PG/18/31/33759 to AB and DB), Royal Society (RGS\R1\191221 to AB) and the Brian Ridge Scholarship (RT), and the National Eye Research Centre and Masonic Charitable Foundation for funding this study.

## ACKNOWLEDGMENTS

We wish to thank Bridget Fox for her assistance with the preliminary studies.

## REFERENCES

Adamis, A. P., and Berman, A. J. (2008). Immunological mechanisms in the pathogenesis of diabetic retinopathy. *Semin. Immunopathol.* 30, 65–84. doi: 10.1007/s00281-008-0111-x

Ahmad, A., Olah, G., Szczesny, B., Wood, M. E., Whiteman, M., and Szabo, C. (2016). AP39, a mitochondrially targeted hydrogen sulfide donor, exerts protective effects in renal epithelial cells subjected to oxidative stress *in vitro* and in acute renal injury *in vivo*. *Shock* 45, 88–97. doi: 10.1097/shk.0000000000000478

Alexander, B. E., Coles, S. J., Fox, B. C., Khan, T. F., Maliszewski, J., Perry, A., et al. (2015). Investigating the generation of hydrogen sulfide from the phosphonamidodithioate slow-release donor GYY4137. *Med. Chem. Commun.* 6, 1649–1655. doi: 10.1039/c5md00170f

Allen, C. L., and Bayraktutan, U. (2009). Antioxidants attenuate hyperglycaemia-mediated brain endothelial cell dysfunction and blood-brain barrier hyperpermeability. *Diabetes Obes. Metab.* 11, 480–490. doi: 10.1111/j.1463-1326.2008.00987.x

Allen, C. L., Malhi, N. K., Whatmore, J. L., Bates, D. O., and Arkill, K. P. (2020). Non-invasive measurement of retinal permeability in a diabetic rat model. *Microcirculation.* 27:e12623.

Ballantyne, B., Gazzard, M. F., and Swanston, D. W. (1976). The opthalmic toxicology of dichloromethane. *Toxicology* 6, 173–187. doi: 10.1016/0300-483x(76)90019-6

Betteridge, K. B., Arkill, K. P., Neal, C. R., Harper, S. J., Foster, R. R., Satchell, S. C., et al. (2017). Sialic acids regulate microvessel permeability, revealed by novel *in vivo* studies of endothelial glycocalyx structure and function. *J. Physiol.* 595, 5015–5035. doi: 10.1113/JP274167

Brancaleone, V., Roviezzo, F., Vellecco, V., De Gruttola, L., Bucci, M., and Cirino, G. (2008). Biosynthesis of $H_2S$ is impaired in non-obese diabetic (n.d.) mice. *Br. J. Pharmacol.* 155, 673–680. doi: 10.1038/bjp.2008.296

Brandt, K. R., and Okamoto, M. Y. (1988). Final report on the safety assessment of methylene chloride. *J. Am. Coll. Toxicol.* 7, 741–835. doi: 10.3109/10915818809078710

Broekhuizen, L. N., Lemkes, B. A., Mooij, H. L., Meuwese, M. C., Verberne, H., Holleman, F., et al. (2010). Effect of sulodexide on endothelial glycocalyx and vascular permeability in patients with type 2 diabetes mellitus. *Diabetologia* 53, 2646–2655. doi: 10.1007/s00125-010-1910-x

Brownlee, M. (2001). Biochemistry and molecular cell biology of diabetic complications. *Nature* 414, 813–820. doi: 10.1038/414813a

Brownlee, M. (2005). The pathobiology of diabetic complications: a unifying mechanism. *Diabetes* 54, 1615–1625. doi: 10.2337/diabetes.54.6.1615

Carballal, S., Trujillo, M., Cuevasanta, E., Bartesaghi, S., Möller, M. N., Folkes, L. K., et al. (2011). Reactivity of hydrogen sulfide with peroxynitrite and other oxidants of biological interest. *Free Radic. Biol. Med.* 50, 196–205. doi: 10.1016/j.freeradbiomed.2010.10.705

Chibber, R., Ben-Mahmud, B. M., Coppini, D., Christ, E., and Kohner, E. M. (2000). Activity of the glycosylating enzyme, core 2 GlcNAc (beta1,6) transferase, is higher in polymorphonuclear leukocytes from diabetic patients compared with age-matched control subjects: relevance to capillary occlusion in diabetic retinopathy. *Diabetes* 49, 1724–1730. doi: 10.2337/diabetes.49.10.1724

Ciszewicz, M., Polubinska, A., Antoniewicz, A., Suminska-Jasinska, K., and Breborowicz, A. (2009). Sulodexide suppresses inflammation in human endothelial cells and prevents glucose cytotoxicity. *Transl. Res.* 153, 118–123. doi: 10.1016/j.trsl.2008.12.007

Coletta, C., Módis, K., Szczesny, B., Brunyánszki, A., Oláh, G., Rios, E. C., et al. (2015). Regulation of vascular tone, angiogenesis and cellular bioenergetics by the 3-mercaptopyruvate sulfurtransferase/H2S pathway: functional impairment by hyperglycemia and restoration by DL-α-lipoic acid. *Mol. Med.* 21, 1–14. doi: 10.2119/molmed.2015.00035

Constantinescu, A. A., Vink, H., and Spaan, J. A. (2003). Endothelial cell glycocalyx modulates immobilization of leukocytes at the endothelial surface. *Arterioscler. Thromb. Vasc. Biol.* 23, 1541–1547. doi: 10.1161/01.atv.0000085630.24353.3d

Du, J., Jin, H., and Yang, L. (2017). Role of hydrogen sulfide in retinal diseases. *Front. Pharmacol.* 8:588. doi: 10.3389/fphar.2017.00588

Gerő, D., Torregrossa, R., Perry, A., Waters, A., Le-Trionnaire, S., Whatmore, J. L., et al. (2016). The novel mitochondria-targeted hydrogen sulfide ($H_2S$) donors AP123 and AP39 protect against hyperglycemic injury in microvascular endothelial cells *in vitro*. *Pharmacol. Res.* 113, 186–198. doi: 10.1016/j.phrs.2016.08.019

Gillies, M. C., Su, T., Stayt, J., Simpson, J. M., Naidoo, D., and Salonikas, C. (1997). Effect of high glucose on permeability of retinal capillary endothelium *in vitro*. *Invest. Ophthalmol. Vis. Sci.* 38, 635–642.

Henry, C. B., and Duling, B. R. (1999). Permeation of the luminal capillary glycocalyx is determined by hyaluronan. *Am. J. Physiol.* 277, H508–H514.

Ikeda, K., Marutani, E., Hirai, S., Wood, M. E., Whiteman, M., and Ichinose, F. (2015). Mitochondria-targeted hydrogen sulfide donor AP39 improves neurological outcomes after cardiac arrest in mice. *Nitric Oxide* 49, 90–96. doi: 10.1016/j.niox.2015.05.001

Ikegami-Kawai, M., Suzuki, A., Karita, I., and Takahashi, T. (2003). Increased hyaluronidase activity in the kidney of streptozotocin-induced diabetic rats. *J. Biochem.* 134, 875–880. doi: 10.1093/jb/mvg214

Jeansson, M., and Haraldsson, B. (2003). Glomerular size and charge selectivity in the mouse after exposure to glucosaminoglycan-degrading enzymes. *J. Am. Soc. Nephrol.* 14, 1756–1765. doi: 10.1097/01.asn.0000072742.02714.6e

John, A., Kundu, S., Pushpakumar, S., Fordham, M., Weber, G., Mukhopadhyay, M., et al. (2017). GYY4137, a hydrogen sulfide donor modulates miR194-dependent collagen realignment in diabetic kidney. *Sci. Rep.* 7:10924.

Jones, D. A., Smith, C. W., and McIntire, L. V. (1995). *Effects of Fluid Shear Stress on Leukocyte Adhesion to Endothelial Cells. Physiology and Pathophysiology of Leukocyte Adhesion*. New York, NY: Oxford University Press, 148–168.

Kabil, O., and Banerjee, R. (2014). Enzymology of $H_2S$ biogenesis, decay and signaling. *Antioxid. Redox Signal.* 20, 770–782. doi: 10.1089/ars.2013.5339

Kanagy, N. L., Szabo, C., and Papapetropoulos, A. (2017). Vascular biology of hydrogen sulfide. *Am. J. Physiol. Cell Physiol.* 312, C537–C549.

Karwi, Q. G., Bornbaum, J., Boengler, K., Torregrossa, R., Whiteman, M., Wood, M. E., et al. (2017). AP39, a mitochondria-targeting hydrogen sulfide ($H_2S$) donor, protects against myocardial reperfusion injury independently of salvage kinase signalling. *Br. J. Pharmacol.* 174, 287–301. doi: 10.1111/bph.13688

Kielhorn, J., and Rosner, G. (1996). *Environmental Health Criteria: Morpholine. International Programme on Chemical Safety*. Geneva: World Health Organization.

Kumase, F., Morizane, Y., Mohri, S., Takasu, I., Ohtsuka, A., and Ohtsuki, H. (2010). Glycocalyx degradation in retinal and choroidal capillary endothelium in rats with diabetes and hypertension. *Acta Med. Okayama* 64, 277–283.

Kundu, S., Pushpakumar, S. B., Tyagi, A., Coley, D., and Sen, U. (2013). Hydrogen sulfide deficiency and diabetic renal remodeling: role of matrix metalloproteinase-9. *Am. J. Physiol. Endocrinol. Metab.* 304, E1365–E1378.

Laggner, H., Hermann, M., Esterbauer, H., Muellner, M. K., Exner, M., Gmeiner, B. M., et al. (2007). The novel gaseous vasorelaxant hydrogen sulfide inhibits angiotensin-converting enzyme activity of endothelial cells. *J. Hypertens.* 25, 2100–2104. doi: 10.1097/hjh.0b013e32829b8fd0

Landsverk, S. A., Tsai, A. G., Cabrales, P., and Intaglietta, M. (2012). Impact of enzymatic degradation of the endothelial glycocalyx on vascular permeability in an awake hamster model. *Crit. Care Res. Pract.* 2012:842545.

Le Trionnaire, S., Perry, A., Szczesny, B., Szabo, C., Winyard, P. G., Whatmore, J. L., et al. (2014). The synthesis and functional evaluation of a mitochondria-targeted hydrogen sulfide donor, (10-oxo-10-(4-(3-thioxo-3H-1,2-dithiol-5-yl)phenoxy)decyl)triphenylphosphonium bromide (AP39). *Med. Chem. Comm.* 5, 728–736. doi: 10.1039/c3md00323j

Lee, Z. W., Zhou, J., Chen, C. S., Zhao, Y., Tan, C. H., Li, L., et al. (2011). The slow-releasing hydrogen sulfide donor, GYY4137, exhibits novel anti-cancer effects *in vitro* and *in vivo*. *PloS One.* 6:e21077. doi: 10.1371/journal.pone.0021077

Leskova, W., Pickett, H., Eshaq, R. S., Shrestha, B., Pattillo, C. B., and Harris, N. R. (2019). Effect of diabetes and hyaluronidase on the retinal endothelial glycocalyx in mice. *Exp. Eye Res.* 179, 125–131. doi: 10.1016/j.exer.2018.11.012

Li, L., Bhatia, M., Zhu, Y. Z., Zhu, Y. C., Ramnath, R. D., Wang, Z. J., et al. (2005). Hydrogen sulfide is a novel mediator of lipopolysaccharide-induced inflammation in the mouse. *FASEB J.* 19, 1196–1198. doi: 10.1096/fj.04-3583fje

Li, L., Fox, B., Keeble, J., Salto-Tellez, M., Winyard, P. G., Wood, M. E., et al. (2013). The complex effects of the slow-releasing hydrogen sulfide donor GYY4137 in a model of acute joint inflammation and in human cartilage cells. *J. Cell Mol. Med.* 17, 365–376. doi: 10.1111/jcmm.12016

Li, L., Whiteman, M., Guan, Y. Y., Neo, K. L., Cheng, Y., Lee, S. W., et al. (2008). Characterization of a novel, water-soluble hydrogen sulfide-releasing molecule (GYY4137): new insights into the biology of hydrogen sulfide. *Circulation* 117, 2351–2360. doi: 10.1161/circulationaha.107.753467

Lipowsky, H. H. (2011). Protease activity and the role of the endothelial glycocalyx in inflammation. *Drug Discov. Today Dis. Models* 8, 57–62. doi: 10.1016/j.ddmod.2011.05.004

Lohakul, J., Jeayeng, S., Chaiprasongsuk, A., Torregrossa, R., Wood, M., Saelim, M., et al. (2021). Mitochondria-targeted hydrogen sulfide delivery molecules protect against UVA-induced photoimaging in dermal fibroblasts, and in mouse skin *in vivo*. *Antioxid. Redox Signal.* [Epub ahead of print].

Manon-Jensen, T., Multhaupt, H. A., and Couchman, J. R. (2013). Mapping of matrix metalloproteinase cleavage sites on syndecan-1 and syndecan-4 ectodomains. *FEBS J.* 280, 2320–2331. doi: 10.1111/febs.12174

Maxhimer, J. B., Somenek, M., Rao, G., Pesce, C. E., Baldwin, D. Jr., Gattuso, P., et al. (2005). Heparanase-1 gene expression and regulation by high glucose in renal epithelial cells: a potential role in the pathogenesis of proteinuria in diabetic patients. *Diabetes* 54, 2172–2178. doi: 10.2337/diabetes.54.7.2172

Mitidieri, E., Gurgone, D., Caiazzo, E., Tramontano, T., Cicala, C., Sorrentino, R., et al. (2020). L-cysteine/cystathionine-β-synthase-induced relaxation in mouse aorta involves a L-serine/sphingosine-1-phosphate/NO pathway. *Br. J. Pharmacol.* 177, 734–744. doi: 10.1111/bph.14654

Módis, K., Asimakopoulou, A., Coletta, C., Papapetropoulos, A., and Szabo, C. (2013). Oxidative stress suppresses the cellular bioenergetic effect of the 3-mercaptopyruvate sulfurtransferase/hydrogen sulfide pathway. *Biochem. Biophys. Res. Commun.* 433, 401–407. doi: 10.1016/j.bbrc.2013.02.131

Módis, K., Bos, E. M., Calzia, E., van Goor, H., Coletta, C., Papapetropoulos, A., et al. (2014). Regulation of mitochondrial bioenergetic function by hydrogen sulfide. Part II. Pathophysiological and therapeutic aspects. *Br. J. Pharmacol.* 171, 2123–2146. doi: 10.1111/bph.12368

Montoya, L. A., and Pluth, M. D. (2016). Organelle-targeted $H_2S$ probes enable visualization of the subcellular distribution of $H_2S$ donors. *Anal. Chem.* 88, 5769–5774. doi: 10.1021/acs.analchem.6b00087

Ng, L. T., Gruber, J., and Moore, P. K. (2018). Is there a role of $H_2S$ in mediating health span benefits of caloric restriction? *Biochem. Pharmacol.* 149, 91–100. doi: 10.1016/j.bcp.2018.01.030

Nieuwdorp, M., Mooij, H. L., Kroon, J., Atasever, B., Spaan, J. A., Ince, C., et al. (2006a). Endothelial glycocalyx damage coincides with microalbuminuria in type 1 diabetes. *Diabetes* 55, 1127–1132. doi: 10.2337/diabetes.55.04.06.db05-1619

Nieuwdorp, M., van Haeften, T. W., Gouverneur, M. C., Mooij, H. L., van Lieshout, M. H., Levi, M., et al. (2006b). Loss of endothelial glycocalyx during acute hyperglycemia coincides with endothelial dysfunction and coagulation activation *in vivo*. *Diabetes* 55, 480–486. doi: 10.2337/diabetes.55.02.06.db05-1103

Niu, T., Zhao, M., Jiang, Y., Xing, X., Shi, X., Cheng, L., et al. (2019). Endomucin restores depleted endothelial glycocalyx in the retinas of streptozotocin-induced diabetic rats. *FASEB J.* 33, 13346–13357. doi: 10.1096/fj.201901161r

Onions, K. L., Gamez, M., Buckner, N. R., Baker, S. L., Betteridge, K. B., Desideri, S., et al. (2019). VEGFC reduces glomerular albumin permeability and protects against alterations in VEGF receptor expression in diabetic nephropathy. *Diabetes* 68, 172–187. doi: 10.2337/db18-0045

Peake, B. F., Nicholson, C. K., Lambert, J. P., Hood, R. L., Amin, H., Amin, S., et al. (2013). Hydrogen sulfide preconditions the db/db diabetic mouse heart against ischemia-reperfusion injury by activating Nrf2 signaling in an Erk-dependent manner. *Am. J. Physiol. Heart Circ. Physiol.* 304, H1215–H1224.

Qiu, Y., Wu, Y., Meng, M., Luo, M., Zhao, H., Sun, H., et al. (2018). GYY4137 protects against myocardial ischemia/reperfusion injury via activation of the PHLPP-1/Akt/Nrf2 signaling pathway in diabetic mice. *J. Surg. Res.* 225, 29–39. doi: 10.1016/j.jss.2017.12.030

Ratney, R. S., Wegman, D. H., and Elkins, H. B. (1974). *In vivo* conversion of methylene chloride to carbon monoxide. *Arch. Environ. Health* 28, 223–226. doi: 10.1080/00039896.1974.10666472

Saker, S., Stewart, E. A., Browning, A. C., Allen, C. L., and Amoaku, W. M. (2014). The effect of hyperglycaemia on permeability and the expression of junctional complex molecules in human retinal and choroidal endothelial cells. *Exp. Eye Res.* 121, 161–167. doi: 10.1016/j.exer.2014.02.016

Sander, B., Thornit, D. N., Colmorn, L., Strøm, C., Girach, A., Hubbard, L. D., et al. (2007). Progression of diabetic macular edema: correlation with blood retinal barrier permeability, retinal thickness, and retinal vessel diameter. *Invest. Ophthalmol. Vis. Sci.* 48, 3983–3987. doi: 10.1167/iovs.06-1102

Si, Y. F., Wang, J., Guan, J., Zhou, L., Sheng, Y., and Zhao, J. (2013). Treatment with hydrogen sulfide alleviates streptozotocin-induced diabetic retinopathy in rats. *Br. J. Pharmacol.* 169, 619–631. doi: 10.1111/bph.12163

Singh, A., Satchell, S. C., Neal, C. R., McKenzie, E. A., Tooke, J. E., and Mathieson, P. W. (2007). Glomerular endothelial glycocalyx constitutes a barrier to protein permeability. *J. Am. Soc. Nephrol.* 18, 2885–2893. doi: 10.1681/asn.2007010119

Sohn, O. S., Fiala, E. S., Conaway, C. C., and Weisburger, J. H. (1982). Metabolism and disposition of morphine in the rat, hamster, and guinea pig. *Toxicol. Appl. Pharmacol.* 64, 486–491. doi: 10.1016/0041-008x(82)90246-0

Strickland, J., Cummings, A., Spinnato, J. A., and Liccione, J. J. (2003). *Toxicological Review of Hydrogen Sulfide (CAS No. 7783-06-4). In Support of Summary Information on the Integrated Risk Information System (IRIS)*. Washington, DC: U.S. Environmental Protection Agency.

Sun, Y., Tian, Z., Liu, N., Zhang, L., Gao, Z., Sun, X., et al. (2018). Exogenous $H_2S$ switches cardiac energy substrate metabolism by regulating SIRT3 expression in db/db mice. *J. Mol. Med. (Berl).* 96, 281–299. doi: 10.1007/s00109-017-1616-3

Sundd, P., Pospieszalska, M. K., Cheung, L. S., Konstantopoulos, K., and Ley, K. (2011). Biomechanics of leukocyte rolling. *Biorheology* 48, 1–35. doi: 10.3233/bir-2011-0579

Suzuki, K., Olah, G., Modis, K., Coletta, C., Kulp, G., Gerö, D., et al. (2011). Hydrogen sulfide replacement therapy protects the vascular endothelium in hyperglycemia by preserving mitochondrial function. *Proc. Natl. Acad. Sci. U.S.A.* 108, 13829–13834. doi: 10.1073/pnas.1105121108

Suzuki, K., Sagara, M., Aoki, C., Tanaka, S., and Aso, Y. (2017). Clinical implication of plasma hydrogen sulfide levels in Japanese patients with Type 2 diabetes. *Intern. Med.* 56, 17–21. doi: 10.2169/internalmedicine.56.7403

Szabo, C. (2012). Roles of hydrogen sulfide in the pathogenesis of diabetes mellitus and its complications. *Antioxid. Redox Signal.* 17, 68–80. doi: 10.1089/ars.2011.4451

Szabo, C. (2017). Hydrogen sulfide, an enhancer of vascular nitric oxide signaling: mechanisms and implications. *Am. J. Physiol. Cell Physiol.* 312, C3–C15.

Szabo, C., Ransy, C., Módis, K., Andriamihaja, M., Murghes, B., Coletta, C., et al. (2014). Regulation of mitochondrial bioenergetic function by hydrogen sulfide. Part I. Biochemical and physiological mechanisms. *Br. J. Pharmacol.* 171, 2099–2122. doi: 10.1111/bph.12369

Szczesny, B., Módis, K., Yanagi, K., Coletta, C., Le Trionnaire, S., Perry, A., et al. (2014). AP39, a novel mitochondria-targeted hydrogen sulfide donor, stimulates cellular bioenergetics, exerts cytoprotective effects and protects against the loss of mitochondrial DNA integrity in oxidatively stressed endothelial cells *in vitro*. *Nitric Oxide* 41, 120–130.

Takano, T., and Miyazaki, Y. (1988). Metabolism of dichloromethane and the subsequent binding of its product, carbon monoxide, to cytochrome P-450 in perfused rat liver. *Toxicol. Lett.* 40, 93–96. doi: 10.1016/0378-4274(88)90187-7

Tao, B. B., Liu, S. Y., Zhang, C. C., Fu, W., Cai, W. J., Wang, Y., et al. (2013). VEGFR2 functions as an $H_2S$-targeting receptor protein kinase with its novel Cys1045-Cys1024 disulfide bond serving as a specific molecular switch for hydrogen sulfide actions in vascular endothelial cells. *Antioxid. Redox Signal.* 19, 448–464. doi: 10.1089/ars.2012.4565

Toxicology–cosmetic ingredient review (1989). 6 Final report on the safety assessment of morpholine. *J. Am. Coll. Toxicol.* 8:707. doi: 10.3109/10915818909010528

Wang, R. (2002). Two's company, three's a crowd: can $H_2S$ be the third endogenous gaseous transmitter? *FASEB J.* 16, 1792–1798. doi: 10.1096/fj.02-0211hyp

Wang, R. (2012). Physiological implications of hydrogen sulfide: a whiff exploration that blossomed. *Physiol. Rev.* 92, 791–896. doi: 10.1152/physrev.00017.2011

Wei, W. B., Hu, X., Zhuang, X. D., Liao, L. Z., and Li, W. D. (2014). GYY4137, a novel hydrogen sulfide-releasing molecule, likely protects against high glucose-induced cytotoxicity by activation of the AMPK/mTOR signal pathway in H9c2 cells. *Mol. Cell Biochem.* 389, 249–256. doi: 10.1007/s11010-013-1946-6

Whiteman, M., Gooding, K. M., Whatmore, J. L., Ball, C. I., Mawson, D., Skinner, K., et al. (2010a). Adiposity is a major determinant of plasma levels of the novel vasodilator hydrogen sulphide. *Diabetologia* 53, 1722–1726. doi: 10.1007/s00125-010-1761-5

Whiteman, M., Le Trionnaire, S., Chopra, M., Fox, B., and Whatmore, J. (2011). Emerging role of hydrogen sulfide in health and disease: critical appraisal of biomarkers and pharmacological tools. *Clin. Sci. (Lond).* 121, 459–488. doi: 10.1042/cs20110267

Whiteman, M., Li, L., Rose, P., Tan, C. H., Parkinson, D. B., and Moore, P. K. (2010b). The effect of hydrogen sulfide donors on lipopolysaccharide-induced formation of inflammatory mediators in macrophages. *Antioxid. Redox Signal.* 12, 1147–1154. doi: 10.1089/ars.2009.2899

Whiteman, M., and Winyard, P. G. (2011). Hydrogen sulfide and inflammation: the good, the bad, the ugly and the promising. *Expert. Rev. Clin. Pharmacol.* 4, 13–32. doi: 10.1586/ecp.10.134

Yang, G., Wu, L., Jiang, B., Yang, W., Qi, J., Cao, K., et al. (2008). $H_2S$ as a physiologic vasorelaxant: hypertension in mice with deletion of cystathionine gamma-lyase. *Science* 322, 587–590. doi: 10.1126/science.1162667

Yusuf, M., Kwong Huat, B. T., Hsu, A., Whiteman, M., Bhatia, M., and Moore, P. K. (2005). Streptozotocin-induced diabetes in the rat is associated with enhanced tissue hydrogen sulfide biosynthesis. *Biochem. Biophys. Res. Commun.* 333, 1146–1152. doi: 10.1016/j.bbrc.2005.06.021

Zhao, H., Lu, S., Chai, J., Zhang, Y., Ma, X., Chen, J., et al. (2017). Hydrogen sulfide improves diabetic wound healing in ob/ob mice via attenuating inflammation. *J. Diabetes Complications* 31, 1363–1369. doi: 10.1016/j.jdiacomp.2017.06.011

Zhou, X., Feng, Y., Zhan, Z., and Chen, J. (2014). Hydrogen sulfide alleviates diabetic nephropathy in a streptozotocin-induced diabetic rat model. *J. Biol. Chem.* 289, 28827–28834. doi: 10.1074/jbc.m114.596593

Zivanovic, J., Kouroussis, E., Kohl, J. B., Adhikari, B., Bursac, B., Schott-Roux, S., et al. (2019). Selective persulfide detection reveals evolutionarily conserved antiaging effects of S-sulfhydration. *Cell Metab.* 30, 1152–1170.e13.

**Conflict of Interest:** MWh, RT, and MWo, and the University of Exeter have intellectual property (patent filings) related to hydrogen sulfide delivery molecules and their therapeutic use. MWh was a consultant to MitoRx Therapeutics (Oxford).

The remaining authors declare that the research was conducted in the absence of any commercial or financial relationships that could be construed as a potential conflict of interest.

**Publisher's Note:** All claims expressed in this article are solely those of the authors and do not necessarily represent those of their affiliated organizations, or those of the publisher, the editors and the reviewers. Any product that may be evaluated in this article, or claim that may be made by its manufacturer, is not guaranteed or endorsed by the publisher.

frontiers in Cell and Developmental Biology

MINI REVIEW
published: 13 September 2021
doi: 10.3389/fcell.2021.730621

# Glycocalyx Impairment in Vascular Disease: Focus on Inflammation

*Jing Qu[1†], Yue Cheng[2†], Wenchao Wu[1], Lixing Yuan[3*] and Xiaojing Liu[1,2*]*

*[1] Laboratory of Cardiovascular Diseases, Regenerative Medicine Research Center, West China Hospital, Sichuan University, Chengdu, China, [2] Department of Cardiology, West China Hospital, Sichuan University, Chengdu, China, [3] Public Laboratory of West China Second University Hospital, Sichuan University, Chengdu, China*

The glycocalyx is a complex polysaccharide-protein layer lining the lumen of vascular endothelial cells. Changes in the structure and function of the glycocalyx promote an inflammatory response in blood vessels and play an important role in the pathogenesis of many vascular diseases (e.g., diabetes, atherosclerosis, and sepsis). Vascular endothelial dysfunction is a hallmark of inflammation-related diseases. Endothelial dysfunction can lead to tissue swelling, chronic inflammation, and thrombosis. Therefore, elimination of endothelial inflammation could be a potential target for the treatment of vascular diseases. This review summarizes the key role of the glycocalyx in the inflammatory process and the possible mechanism by which it alleviates this process by interrupting the cycle of endothelial dysfunction and inflammation. Especially, we highlight the roles of different components of the glycocalyx in modulating the inflammatory process, including components that regulate leukocyte rolling, L-selectin binding, inflammasome activation and the signaling interactions between the glycocalyx components and the vascular cells. We discuss how the glycocalyx interferes with the development of inflammation and the importance of preventing glycocalyx impairment. Finally, drawing on current understanding of the role of the glycocalyx in inflammation, we consider a potential strategy for the treatment of vascular diseases.

**Keywords: glycocalyx, endothelial cell, endothelial dysfunction, inflammation, inflammasome**

OPEN ACCESS

***Edited by:***
*Bingmei M. Fu,*
*The City College of New York (CUNY), United States*

***Reviewed by:***
*Hans Vink,*
*Maastricht University, Netherlands*
*Hariharan Subramanian,*
*Michigan State University, United States*

****Correspondence:***
*Lixing Yuan*
*yuanlixing@scu.edu.cn*
*Xiaojing Liu*
*liuxq@scu.edu.cn*

*[†] These authors have contributed equally to this work*

***Specialty section:***
*This article was submitted to Signaling, a section of the journal Frontiers in Cell and Developmental Biology*

***Received:*** *25 June 2021*
***Accepted:*** *25 August 2021*
***Published:*** *13 September 2021*

***Citation:***
*Qu J, Cheng Y, Wu W, Yuan L and Liu X (2021) Glycocalyx Impairment in Vascular Disease: Focus on Inflammation. Front. Cell Dev. Biol. 9:730621. doi: 10.3389/fcell.2021.730621*

## INTRODUCTION

The glycocalyx is a general term for polysaccharide protein complexes covering the surface of vascular endothelial cells. As the skeletal structure of the endothelial cell surface, the glycocalyx is a key factor in the regulation of the fluid balance inside and outside of blood vessels and is closely related to vascular permeability (Jedlicka et al., 2020). Glycocalyx impairment is associated with many diseases, such as atherosclerosis, diabetes, and sepsis, all of which are related to chronic inflammation. **Table 1** lists the main diseases known to be related to glycocalyx impairment. In recent years, there have been major advances in anti-inflammatory drugs used to treat diabetes, atherosclerosis, and sepsis. Among these drugs, interleukin-1 (IL-1) receptor antagonists have attracted much attention (Jamilloux et al., 2018). Statins are now commonly used for the treatment

**TABLE 1 |** Main diseases to glycocalyx impairment.

| Diseases | References | Diseases | References |
|---|---|---|---|
| Systemic or local inflammation | Margraf et al., 2018 | Sepsis | Iba and Levy, 2019; Fernández-Sarmiento et al., 2020 |
| Diabetes mellitus | Dogné et al., 2018 | Ischemia-reperfusion injury | van Golen et al., 2012; Abassi et al., 2020 |
| Chronic and acute renal disease | Rabelink and de Zeeuw, 2015; Tarbell and Cancel, 2016 | Atherosclerosis | Tarbell and Cancel, 2016; Mitra et al., 2017 |
| Stroke | Zeng, 2017 | Hypertension and pulmonary oedema | Collins et al., 2013; Mendes et al., 2020 |
| Cancer | Kang et al., 2018; Buffone and Weaver, 2020 | COVID-19 | Yamaoka-Tojo, 2020a,b |

of atherosclerosis due to their cholesterol-lowering and anti-inflammatory effects (Horodinschi et al., 2019). Sepsis refers to a systemic inflammatory response syndrome caused by infection. The treatment of sepsis involves early circulatory resuscitation, as well as anti-inflammatory therapy (Huang et al., 2019). Although current anti-inflammatory treatments can alleviate the inflammatory response to some extent, they cannot restore endothelial dysfunction after glycocalyx impairment.

Endothelial cells consist of a single layer of cells covering the vascular cavity. The vascular endothelium serves as the first barrier, thereby providing protection against the effects of inflammation. Damage to the glycocalyx layer is thought to be initial stage in the development of inflammation (Lupu et al., 2020). The glycocalyx is connected to the endothelium by backbone molecules, including proteoglycans and glycoproteins. These interact to form a network structure, with various plasma-derived and endothelial cell-derived soluble biological macromolecules incorporated into this network to form the basic structure of the glycocalyx (Jedlicka et al., 2020). Due to the location of the glycocalyx, the entire structure provides a barrier to water and solute transmission and acts as a bridge for interactions between blood circulating cells and endothelial cells. The glycocalyx also functions as a sensor of mechanical forces, and it protects against overactivation of cell surface receptors (Pillinger and Kam, 2017). However, the structure of the glycocalyx is extremely vulnerable, and inflammation, ischemia/reperfusion, hypervolemia, and vascular surgery can cause endothelial glycocalyx impairment. Such impairment causes a decrease in anticoagulants, an increase in endothelial permeability, enhanced migration of proinflammatory cells, impaired mechanical conduction, and endothelial nitric oxide (NO) synthase activity (Sieve et al., 2018). Oxidative stress plays an important role in the progression of endothelial dysfunction. It serves as an intermediate trigger, activating the NOD-like receptor pyrin domain-containing 3(NLRP3) inflammasome and aggravating the subsequent inflammatory cascade and endothelial dysfunction (Incalza et al., 2018). Damage to the glycocalyx layer leads to endothelial cell dysfunction. Vascular endothelial dysfunction aggravates the inflammatory response, which leads to a cycle of inflammation and endothelial dysfunction, with the inflammatory response further aggravating glycocalyx impairment.

In this review, we summarize recent advances in understanding of the effects of glycocalyx impairment, focusing on inflammation development. We discuss components of the glycocalyx in modulating the inflammatory process. We conclude by discussing preventing glycocalyx impairment might provide a strategy to interrupt the cycle of endothelial dysfunction and inflammation.

## STRUCTURE AND FUNCTION OF THE GLYCOCALYX

The vascular endothelial glycocalyx comprises a layer of villous polyglycoproteins with a composite structure that are located on the apical membrane of endothelial cells between the tube wall and blood (**Figure 1**). The endothelial glycocalyx serves as a natural dynamic barrier on the surface of these cells (Jedlicka et al., 2020). The main components of the endothelial glycocalyx are glycoproteins with sialic acid residues at the ends and proteoglycans with glycosaminoglycan (GAG) side chains. GAGs are linear heteropolysaccharides, which contain one molecule of hexosamine and one molecule of hexuronic acid. They are huge family composed of specific combinations of hexosamine and hexuronic acids (Curry, 2018). GAGs found on the surface of endothelial cells include heparan sulfate (HS), chondroitin sulfate (CS), and hyaluronic acid (HA). Two families of cell surface molecules (syndecans and glypicans) make up the core protein skeleton of endothelial glycocalyx (Aldecoa et al., 2020). Syndecan-1 combines with HS and CS, playing an important role in signal transduction. Glypican-1 binds to HS, which is directly anchored to a lipid raft structure rich in cholesterol and sphingolipids via C-terminal phosphatidylinositol (**Figure 2**). This structure plays a role in vesicle transport and signal transduction. The glycocalyx covers the surface of all vascular endothelial cells and serves an important function in the pathophysiology

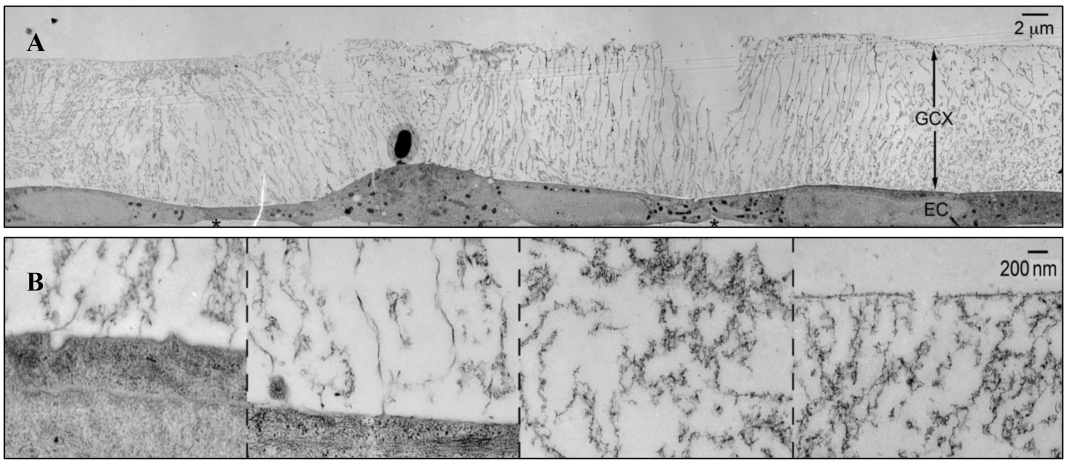


**FIGURE 1 |** The structure of glycocalyx (Tarbell and Cancel, 2016). **(A)** Transmission Electron Microscope of glycocalyx preserved by ruthenium red and osmium tetroxide. **(B)** High-magnification image of glycocalyx.

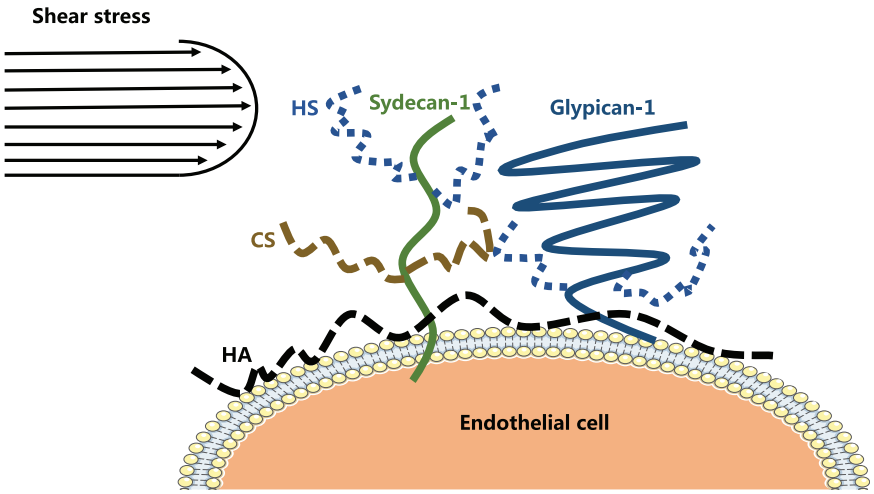


**FIGURE 2 |** The structure of endothelial glycocalyx.

of blood vessels (Cosgun et al., 2020). The glycocalyx has three main functions: (1) It acts as a bridge for interactions between blood circulating cells and endothelial cells, (2) it acts as a selective permeable barrier for the blood vessel wall, and (3) it acts as a mechanical sensor of blood shear force (Cosgun et al., 2020).

## THE ROLE OF THE ENDOTHELIAL GLYCOCALYX LAYER IN INFLAMMATION AND ENDOTHELIAL DYSFUNCTION

The vascular endothelial glycocalyx layer is a central player in the inflammatory response. Lipowsky (2018) observed rapid shedding of vascular endothelial glycocalyx layer in a murine inflammation model and the release of inflammation mediators, such as reactive oxygen species (ROS), reactive nitrogen species, and tumor necrosis factor-α (TNF-α), which impaired the structural integrity of the glycocalyx, thereby affecting its function (Lipowsky, 2018; Uchimido et al., 2019; Gallagher et al., 2020). After the structure of the vascular endothelial glycocalyx is damaged, vascular endothelial cell intercellular adhesion molecule 1 (ICAM-1) and vascular cell adhesion molecule 1 (VCAM-1) are exposed. As a result, leukocytes in the blood circulation can adhere more easily to vascular endothelial cells. This process promotes the development of inflammation and endothelial dysfunction (Mulivor and Lipowsky, 2004; Vestweber, 2015; Bui et al., 2020; Liew et al., 2021). Therefore, glycocalyx shedding is an important factor in vascular endothelial dysfunction.

Endothelial dysfunction results in a reduction in the level of NO in blood vessels, which, in turn, leads to abnormal vascular function. Evidence suggests that the characteristics of endothelial dysfunction include weakened endothelial-mediated

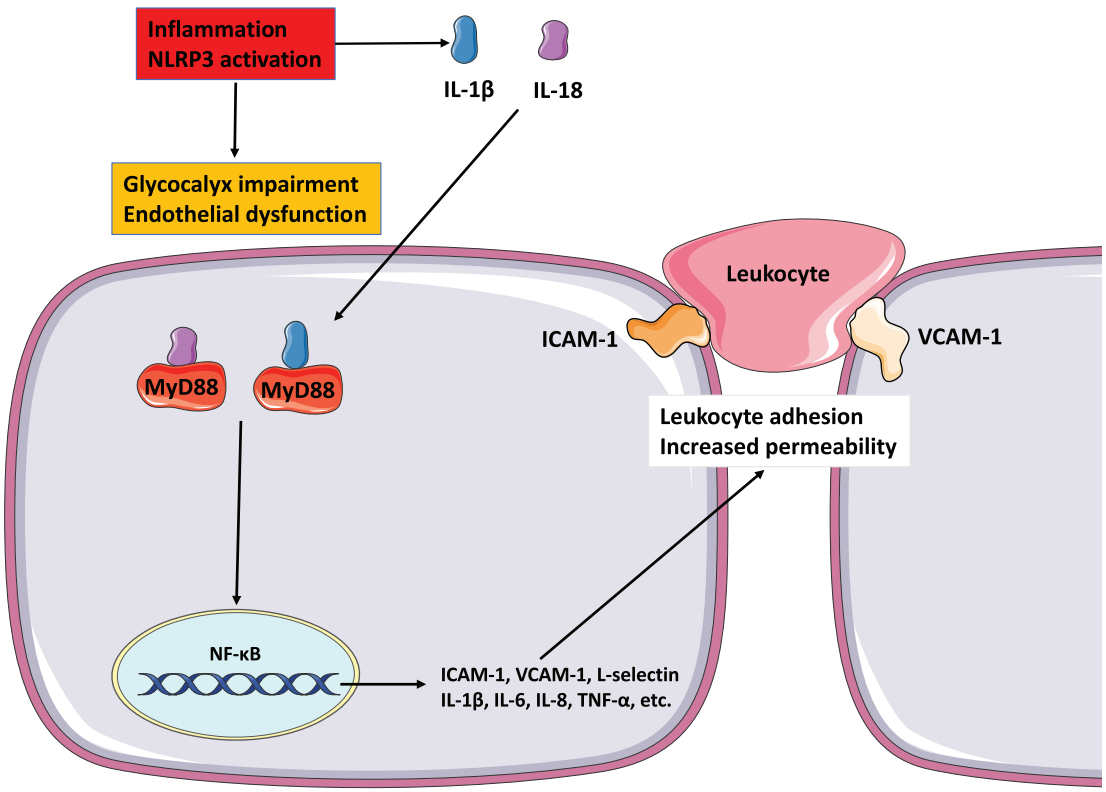


**FIGURE 3 |** The role of glycocalyx in endothelial dysfunction and inflammation NLRP3 inflammasome activates to release IL-1 1L-18, and destroys endothelial glycocalyx. These mediators possess properties of pro-inflammatory activation. IL-1 and IL-18 binding to its cell surface receptor to activate intracellular signaling molecules MyD88, which then causes NF-κB activation. The activation of NF-κB signaling pathway increases the secretion of pro-inflammatory mediators such as cytokines and chemokines to mediate the adhesion of leukocyte and promote leukocyte extravasation. All of these reactions increase endothelial dysfunction by altering cell contractility and disrupting intercellular connections.

vasodilation, disturbed hemodynamics, impaired fibrinolytic ability, and excessive generation of ROS and oxidative stress (Gimbrone and García-Cardeña, 2016; Incalza et al., 2018; Cyr et al., 2020; Zuchi et al., 2020).

The inflammatory response is an important mechanism underlying the development and progression of endothelial dysfunction, and it plays a pivotal role in the pathological process of vascular diseases. Soeki and Sata (2016) showed that high-sensitivity C-reactive protein, an inflammatory marker, is associated with metabolic risk factors for cardiovascular diseases (Li et al., 2018). C-reactive protein can damage the vascular endothelium, resulting in a decrease in NO production by the vascular endothelium (Sproston and Ashworth, 2018). When an inflammatory reaction occurs in blood vessels, B lymphocytes, T lymphocytes, and mononuclear are activated. This leads to an increase in the production of IL-6 and TNF-α. The activities of IL-6 and TNF-α are interlinked, with TNF-α inducing the production of IL-6 and IL-6 stimulating the liver to increase the production of C-reactive protein or vice versa. Macrophages in atherosclerotic plaques, neutrophils, and monocytes in the blood synthesize TNF-α, which induces the release of TNF-α in the presence of arterial injury. TNF-α rapidly upregulates endothelial cell adhesion factors, which activate endothelial cells and inflammatory cell aggregation and lead to the release of inflammatory mediators (Sahibzada et al., 2017; Ng et al., 2018; Wang and He, 2020). TNF-α also regulates endothelial cell damage and remodels through the nuclear factor-κB (NF-κB) signaling pathway (Hayden and Ghosh, 2014; Blaser et al., 2016).

Reactive oxygen species and RNS released in the inflammatory response degrade HA, HS, and CS. ROS and RNS cause degradation of vascular endothelial glycocalyx by activating matrix metalloproteins (MMPs) and inactivating endogenous protease inhibitors (Rubio-Gayosso et al., 2006; van Golen et al., 2014). Proteases result in structural damage to the vascular endothelial glycocalyx. This damage, with the associated loss of the activity of various enzymes, including superoxide dismutase, antithrombin III, and thrombomodulin, as well as that of signaling molecules, results in weakening or loss of the barrier function of the endothelial glycocalyx layer (Kolářová et al., 2014; Sieve et al., 2018; Moore et al., 2021). This eventually leads to an imbalance in the enzymatic system, with endothelial barrier coagulation and antioxidant dysfunction. Most importantly, damage to the structure of the vascular endothelial glycocalyx via an inflammation reaction disturbs the mechanical stress transduction function of the glycocalyx. The latter leads to a series of pathological changes, including increased vascular

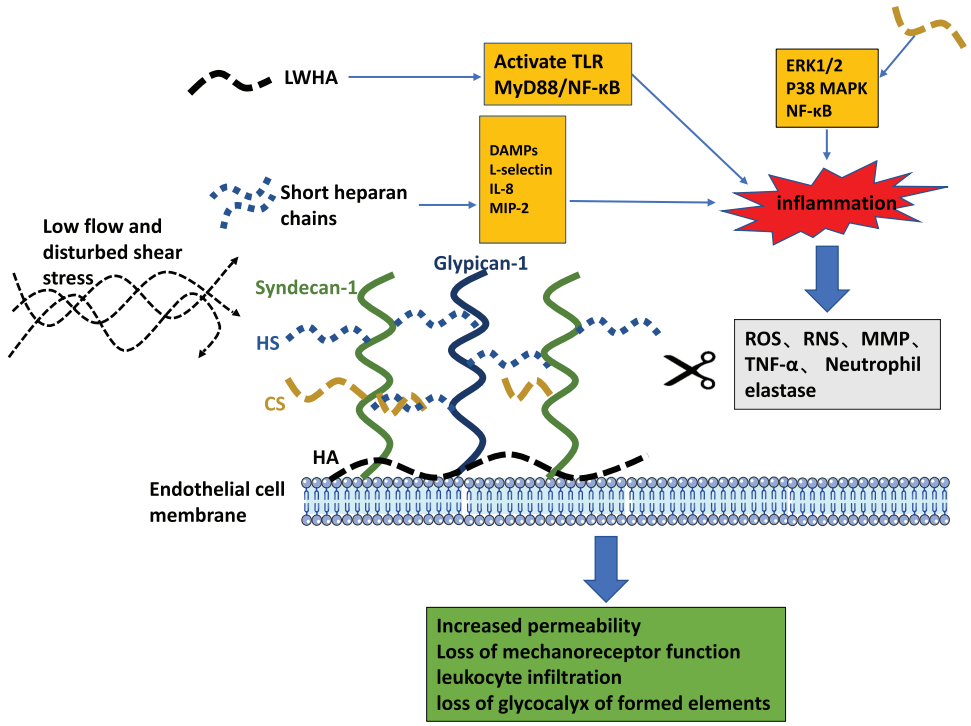


**FIGURE 4 |** The pathogenic role of glycocalyx liberated fragments and the pathophysiologic consequences of endothelial glycocalyx loss.

permeability, edema, changes in the interactions between endothelial cells and white blood cells, and an imbalance in the coagulation and antioxidant systems, and decreased vascular tone (Yao et al., 2007; Chappell and Jacob, 2014). These changes further exacerbate endothelial dysfunction. Therefore, endothelial glycocalyx impairment is a crucial factor in the cycle of inflammation and endothelial dysfunction.

## MECHANISM BY WHICH THE ENDOTHELIAL GLYCOCALYX LAYER REGULATES INFLAMMATION

In the cycle of inflammation and endothelial dysfunction, although the vascular endothelial glycocalyx layer is damaged and shed, it continues to play a critical role in regulating the development and progression of inflammation (**Figures 3**, **4**). HS is the main component of vascular endothelial glycocalyx GAGs, which are disseminated widely on the surface and matrix of vascular cells. Numerous studies have confirmed that through its protein binding properties, HS participates in various steps of inflammation. L-selectin is constitutively expressed by leukocytes and participates in the regulation of leukocyte rolling. Thus far, no natural ligand for L-selectin has been found. In the glycocalyx, HS is known to interact with L-selectin and to act as an L-selectin ligand, regulating the rolling of leukocytes in the vascular cavity in the initial stage of inflammation (Collins and Troeberg, 2019). In the inflammatory response, a variety of transmembrane glycoproteins in the immunoglobulin superfamily, including ICAM-1 and VCAM-1, and integrins are involved in inducing leukocytes to extend and adhere tightly to the side surface of the vessel lumen. Wang (2011) found that knocking out the HS gene significantly reduced the accumulation of the chemokine IL-8 on the luminal surface of endothelial cells, while inhibiting the tight adhesion of neutrophils caused by chemokines. However, the expression levels of ICAM-1 and VCAM-1 did not change. In the same study, in the absence of any difference in endothelial permeability, transcytosis of chemokines from the tissue to the vascular cavity was greatly weakened in the HS gene knockout mice (Middleton et al., 1997). Massena et al. (2010) reported that glycocalyx HS mediate the accumulation of the chemokine MIP-2 on the surface of the endothelial cell cavity and forms a concentration gradient, mediating the movement of leukocytes toward the transmembrane site. HS can combine with chemokines to form complexes (e.g., IL-8), which increases the affinity of chemokines for corresponding receptors on the cell membrane (Koenig et al., 1998). After enzyme digestion of HS, binding of chemokines to endothelial cells is reduced, and the effect of these chemokines on vascular endothelial cells is weakened. HS can regulate leukocyte chemotaxis in many ways during the inflammatory response. These include regulating neutrophil rolling, regulating the formation of inflammation-related chemokine concentration gradients, and regulating the transport of chemokines from the inflammation site to the vascular lumen (Kumar et al., 2015).

The CS is a type of sulfated GAG and the main component of the endothelial glycocalyx layer. It is a linear polysaccharide make up of repeated disaccharide units composed of glucuronic

acid and *N*-acetylhexosamine. CS is known to elicit a range of beneficial anti-inflammatory effects, including increasing type II collagen and proteoglycans, reducing bone resorption, and improving the anabolic/catabolic balance in chondrocytes (Martel-Pelletier et al., 2015). Therefore, CS is widely used in the study of osteoarthritis. Melgar-Lesmes et al. (2016) found that CS interferes with the proinflammatory activation of monocytes and endothelial cells driven by TNF-α, thus reducing the progression of inflammation and preventing the formation of atherosclerotic plaques. In this way, CS treatment might provide a new strategy for the clinical treatment of atherosclerosis. Moreover, *in vitro* studies showed that CS reduced inflammation mediators and the apoptotic process, in addition to reducing protein production of inflammatory cytokines, inducible NO synthase, and MMPs (Campo et al., 2009). The activation of NF-kB signaling is pivotal to the inflammatory response in the pathogenesis of numerous diseases. Vallières and du Souich (2010) reported benefits of CS in numerous inflammatory diseases and attributed these to a reduction in NF-kB nuclear translocation in chondrocytes and the synovial membrane. Loeser et al. (2005) reported that by reducing the phosphorylation of extracellular regulated protein kinase1/2 and p38 mitogen activated protein kinase, CS diminished the nuclear translocation of NF-kB triggered by heat shock proteins, glucose regulated proteins, fibronectin, extracellular matrix fragments, proinflammatory cytokines, IL-1β and TNF-α, Pathogen-associated molecular patterns, and lipopolysaccharides. In this way, CS reduced the expression of proinflammatory cytokines, NO synthase, cyclooxygenase 2, phospholipase A2, and MMPs and diminished the inflammatory reaction (Loeser et al., 2005). This mechanism of action of CS may explain its effect on diseases with a strong inflammatory component.

The HA belongs to a large family of GAGs and has been proven to display multiple biological functions, which depend on its molecular size (Litwiniuk et al., 2016). According to recent research, HA has anti-inflammatory properties. High-molecular weight (HMW) HA tends to be anti-inflammatory, whereas low-molecular weight (LMW) HA tends to be proinflammatory (Gall, 2010). LMW-HA can induce various proinflammatory responses, such as activation of murine alveolar macrophages (Noble et al., 1996). In addition, small HA fragments increase the expression of several cytokines, including MMP-12, plasmogen activator inhibitor-1, MIPs (MIP-1α and MIP-1β), monocyte chemoattractrant-1, keratinocyte chemoattractant, and IL-8 and IL-12 (Horton et al., 1999, 2000). Bourguignon et al. (2011) showed that LMW-HA stimulates TLR2, TLR4, and MyD88 to form a signaling complex with CD44, leading to NF-κB specific transcriptional activation and the expression of the proinflammatory cytokines IL-1β and IL-8 in a human breast cell line. Taken together, these reports suggest that LMW-HA induces inflammation via activation of TLRs and initiation of MyD88/NF-κB signaling, which leads to the production of proinflammatory cytokines and chemokines. Unlike small HA fragments, HMW-HA exhibits anti-inflammatory effects as it is a natural macromolecular polymer. Wang et al. (2006) analyzed the influence of HMW-HA on the expression of various inflammatory cytokines in patients with early-stage osteoarthritis. They reported downregulation of IL-8, inducible NO synthase, aggrecanase-2, and TNF-α gene expression in IL-1-stimulated fibroblast-like synoviocytes. Blocking the CD44 receptor with anti-CD44 antibody inhibited the downregulatory effects of HMW-HA on gene expression. Campo et al. (2011) reported that HMW-HA significantly diminished TLR4, TLR2, MyD88, and NF-kB expression and protein synthesis in synoviocytes in a murine model of osteoarthritis. They also observed reduced mRNA expression, TNFα, IL-1β, IL-17, and MMP-13 production, and inducible NO synthase gene expression in arthritic mice treated with HMW-HA (Campo et al., 2011). During inflammation, the endothelial glycocalyx is shed and degraded, and HA is degraded from a polymerized state to LMW-HA, thereby changing from an anti-inflammatory state to a proinflammatory state, which further promotes the development of inflammation. The aforementioned findings confirm the importance of protecting the integrity of the glycocalyx under inflammatory conditions.

The enzymatic degradation pathways of glycocalyx components are presented in the gray box. Pathogenic features of released fragments of short HS chains and LMWHA are depicted as orange boxes. The consequences of endothelial glycocalyx degradation are summarized in the green box.

## THE ROLE OF THE ENDOTHELIAL GLYCOCALYX LAYER IN REGULATING THE NLRP3 INFLAMMASOME

Inflammation is a protective immune response to external stimuli pathogen-associated molecular patterns and damage-associated molecular patterns released by body damage can activate various inflammasomes (Rathinam and Fitzgerald, 2016). The NLRP3 inflammasome is one of the most comprehensively studied and is known to be involved in the development and progression of various inflammation-related diseases, such as atherosclerosis and diabetes (Danielski et al., 2020). Recent studies confirmed that the glycocalyx plays an important role in regulating the activation of the NLRP3 inflammasome. Wang et al. (2018) reported that HS inhibits inflammation by downregulating the NLRP3 inflammasome and cleavage of IL-1β during wound healing in diabetic rats. In their study, rats treated with HS exhibited decreased activation of cleaved IL-1β, IL-18, and TNF-α, as well as decreased expression of NLRP3 (Wang et al., 2018). Rajan et al. (2010) found that in a cell-free system, NLRP3 directly interacts with intrinsic RNA and HA, which was followed by activation of the NLRP3 inflammasome. These studies illustrate the important role of the glycocalyx in regulating the activation of NLRP3 inflammasomes (Rajan et al., 2010). However, the specific mechanism underlying the activity of the glycocalyx remains unclear and requires further study. It is also not known whether the glycocalyx can regulate other inflammasomes (e.g., NLRP1, NLRC4, NLRP6, and AIM2). This may be a direction for further research.

## CONCLUSION

Recent evidence has accumulated that endothelial glycocalyx impairment promotes a cycle of endothelial dysfunction and inflammation. The findings presented herein highlight the important role of endothelial glycocalyx integrity in combating endothelial dysfunction and vascular inflammation. Stimulation by exogenous substances or endogenous mediators of endothelial cells induces an inflammatory response, leading to endothelial glycocalyx damage and impairment of its mechanical sensory function. This leads to increased vascular permeability and changes in interactions between endothelial cells and leukocytes, which results in endothelial dysfunction and further aggravates inflammation. These changes trigger signal transduction pathways and activation of the NLRP3 inflammasome, thereby exacerbating disease. We postulate that interrupting the cycle of endothelial dysfunction and inflammation may prevent endothelial glycocalyx impairment and lead the way toward new treatments for inflammatory diseases. It is worth noting that emerging studies point to a role for statins in improving vascular dysfunction by inhibiting the NLRP3 signaling pathway and combating glycocalyx impairment. Sulodexide, a common anticoagulant and antithrombotic drug used in the clinical setting, repairs vascular endothelial cell damage, including glycocalyx impairment. It also has anti-inflammatory effects. Drugs that can combat both glycocalyx impairment and exert anti-inflammatory effects may pave the way toward new treatments for cardiovascular diseases. Another potentially interesting area of research is the possible role of the endothelial glycocalyx layer as a target in COVID-19 therapy. It is well known that COVID-19 can cause a systemic inflammatory storm and endothelial cell injury (Rovas et al., 2021). Thus, characteristics of the glycocalyx seem to be a potential target for the treatment of COVID-19.

Although our understanding of the effect of the endothelial glycocalyx layer on inflammation is growing, the specific detailed mechanism of how the glycocalyx modulates inflammation, especially under disturbed oscillatory flow conditions, remains unclear. In addition, although the glycocalyx is known to regulate not only inflammation at multiple levels but also the activation of the NLRP3 inflammasome, whether the abnormal shear stress that occurs under vascular disease conditions regulates the NLRP3 inflammasome through the glycocalyx needs to be further studied. Furthermore, whether the glycocalyx can regulate NLRP1, NLRC4, NLRP6, and AIM2 inflammasomes is not yet clear. Finally, whether both syndecans and glypicans, the two main families of glycocalyx core protein skeletons, participate in regulating the inflammatory response remains to be determined.

## AUTHOR CONTRIBUTIONS

JQ and YC draft the manuscript. WW revised and polished the manuscript. XL and LY supervised the review and established the whole frame. All authors contributed to the article and approved the submitted version.

## FUNDING

This work was supported by the National Natural Science Foundation of China (Nos. 12072215 and 11672197) by XL.

## REFERENCES

Abassi, Z., Armaly, Z., and Heyman, S. N. (2020). Glycocalyx degradation in ischemia-reperfusion injury. *Am. J. Pathol.* 190, 752–767. doi: 10.1016/j.ajpath.2019.08.019

Aldecoa, C., Llau, J. V., Nuvials, X., and Artigas, A. (2020). Role of albumin in the preservation of endothelial glycocalyx integrity and the microcirculation: a review. *Ann. Intensive Care* 10:85.

Blaser, H., Dostert, C., Mak, T. W., and Brenner, D. (2016). TNF and ROS crosstalk in inflammation. *Trends Cell Biol.* 26, 249–261. doi: 10.1016/j.tcb.2015.12.002

Bourguignon, L. Y., Wong, G., Earle, C. A., and Xia, W. (2011). Interaction of low molecular weight hyaluronan with CD44 and toll-like receptors promotes the actin filament-associated protein 110-actin binding and MyD88-NFκB signaling leading to proinflammatory cytokine/chemokine production and breast tumor invasion. *Cytoskeleton* 68, 671–693. doi: 10.1002/cm.20544

Buffone, A., and Weaver, V. M. (2020). Don't sugarcoat it: how glycocalyx composition influences cancer progression. *J. Cell Biol.* 219:e201910070.

Bui, T. M., Wiesolek, H. L., and Sumagin, R. (2020). ICAM-1: a master regulator of cellular responses in inflammation, injury resolution, and tumorigenesis. *J. Leukoc. Biol.* 108, 787–799. doi: 10.1002/jlb.2mr0220-549r

Campo, G. M., Avenoso, A., Campo, S., D'Ascola, A., Traina, P., Samà, D., et al. (2009). Glycosaminoglycans modulate inflammation and apoptosis in LPS-treated chondrocytes. *J. Cell. Biochem.* 106, 83–92.

Campo, G. M., Avenoso, A., Nastasi, G., Micali, A., Prestipino, V., Vaccaro, M., et al. (2011). Hyaluronan reduces inflammation in experimental arthritis by modulating TLR-2 and TLR-4 cartilage expression. *Biochim. Biophys. Acta* 1812, 1170–1181. doi: 10.1016/j.bbadis.2011.06.006

Chappell, D., and Jacob, M. (2014). Role of the glycocalyx in fluid management: small things matter. *Best Pract. Res. Clin. Anaesthesiol.* 28, 227–234. doi: 10.1016/j.bpa.2014.06.003

Collins, L. E., and Troeberg, L. (2019). Heparan sulfate as a regulator of inflammation and immunity. *J. Leukoc. Biol.* 105, 81–92. doi: 10.1002/jlb.3ru0618-246r

Collins, S. R., Blank, R. S., Deatherage, L. S., and Dull, R. O. (2013). Special article: the endothelial glycocalyx: emerging concepts in pulmonary edema and acute lung injury. *Anesth. Analg.* 117, 664–674. doi: 10.1213/ane.0b013e3182975b85

Cosgun, Z. C., Fels, B., and Kusche-Vihrog, K. (2020). Nanomechanics of the endothelial glycocalyx: from structure to function. *Am. J. Pathol.* 190, 732–741. doi: 10.1016/j.ajpath.2019.07.021

Curry, F. E. (2018). The molecular structure of the endothelial glycocalyx layer (EGL) and surface layers (ESL) modulation of transvascular exchange. *Adv. Exp. Med. Biol.* 1097, 29–49. doi: 10.1007/978-3-319-96445-4_2

Cyr, A. R., Huckaby, L. V., Shiva, S. S., and Zuckerbraun, B. S. (2020). Nitric oxide and endothelial dysfunction. *Crit. Care Clin.* 36, 307–321.

Danielski, L. G., Giustina, A. D., Bonfante, S., Barichello, T., and Petronilho, F. (2020). The NLRP3 inflammasome and its role in sepsis development. *Inflammation* 43, 24–31. doi: 10.1007/s10753-019-01124-9

Dogné, S., Flamion, B., and Caron, N. (2018). Endothelial glycocalyx as a shield against diabetic vascular complications: involvement of hyaluronan and

hyaluronidases. *Arterioscler. Thromb. Vasc. Biol.* 38, 1427–1439. doi: 10.1161/atvbaha.118.310839

Fernández-Sarmiento, J., Salazar-Peláez, L. M., and Carcillo, J. A. (2020). The endothelial glycocalyx: a fundamental determinant of vascular permeability in sepsis. *Pediatr. Crit. Care Med.* 21, e291–e300.

Gall, Y. (2010). [Hyaluronic acid: structure, metabolism and implication in cicatrisation]. *Ann. Dermatol. Venereol.* 137, S30–S39.

Gallagher, P., Chan, K. R., Rivino, L., and Yacoub, S. (2020). The association of obesity and severe dengue: possible pathophysiological mechanisms. *J. Infect.* 81, 10–16. doi: 10.1016/j.jinf.2020.04.039

Gimbrone, M. A. and García-Cardeña, G. (2016). Endothelial cell dysfunction and the pathobiology of atherosclerosis. *Circ. Res.* 118, 620–636. doi: 10.1161/circresaha.115.306301

Hayden, M. S., and Ghosh, S. (2014). Regulation of NF-κB by TNF family cytokines. *Semin. Immunol.* 26, 253–266. doi: 10.1016/j.smim.2014.05.004

Horodinschi, R. N., Stanescu, A. M. A., Bratu, O. G., Pantea Stoian, A., Radavoi, D. G., and Diaconu, C. C. (2019). Treatment with statins in elderly patients. *Medicina* 55:721. doi: 10.3390/medicina55110721

Horton, M. R., Olman, M. A., Bao, C., White, K. E., Choi, A. M., Chin, B. Y., et al. (2000). Regulation of plasminogen activator inhibitor-1 and urokinase by hyaluronan fragments in mouse macrophages. *Am. J. Physiol. Lung Cell Mol. Physiol.* 279, L707–L715.

Horton, M. R., Shapiro, S., Bao, C., Lowenstein, C. J., and Noble, P. W. (1999). Induction and regulation of macrophage metalloelastase by hyaluronan fragments in mouse macrophages. *J. Immunol.* 162, 4171–4176.

Huang, M., Cai, S., and Su, J. (2019). The pathogenesis of sepsis and potential therapeutic targets. *Int. J. Mol. Sci.* 20:5376. doi: 10.3390/ijms20215376

Iba, T., and Levy, J. H. (2019). Derangement of the endothelial glycocalyx in sepsis. *J. Thromb. Haemost.* 17, 283–294. doi: 10.1111/jth.14371

Incalza, M. A., D'Oria, R., Natalicchio, A., Perrini, S., Laviola, L., and Giorgino, F. (2018). Oxidative stress and reactive oxygen species in endothelial dysfunction associated with cardiovascular and metabolic diseases. *Vasc. Pharmacol.* 100, 1–19. doi: 10.1016/j.vph.2017.05.005

Jamilloux, Y., Bourdonnay, E., Gerfaud-Valentin, M., Py, B. F., Lefeuvre, L., Barba, T., et al. (2018). [Interleukin-1, inflammasome and autoinflammatory diseases]. *Rev. Med. Interne* 39, 233–239.

Jedlicka, J., Becker, B. F., and Chappell, D. (2020). Endothelial glycocalyx. *Crit. Care Clin.* 36, 217–232.

Kang, H., Wu, Q., Sun, A., Liu, X., Fan, Y., and Deng, X. (2018). Cancer cell glycocalyx and its significance in cancer progression. *Int. J. Mol. Sci.* 19:2484. doi: 10.3390/ijms19092484

Koenig, A., Norgard-Sumnicht, K., Linhardt, R., and Varki, A. (1998). Differential interactions of heparin and heparan sulfate glycosaminoglycans with the selectins. Implications for the use of unfractionated and low molecular weight heparins as therapeutic agents. *J. Clin. Investig.* 101, 877–889. doi: 10.1172/jci1509

Kolářová, H., Ambrůzová, B., Svihálková, Šindlerová, L., Klinke, A., and Kubala, L. (2014). Modulation of endothelial glycocalyx structure under inflammatory conditions. *Mediators Inflamm.* 2014:694312.

Kumar, A. V., Katakam, S. K., Urbanowitz, A. K., and Gotte, M. (2015). Heparan sulphate as a regulator of leukocyte recruitment in inflammation. *Curr. Protein Pept. Sci.* 16, 77–86. doi: 10.2174/1573402111666150213165054

Li, H., Sun, K., Zhao, R., Hu, J., Hao, Z., Wang, F., et al. (2018). Inflammatory biomarkers of coronary heart disease. *Front. Biosci.* 10, 185–196. doi: 10.2741/s508

Liew, H., Roberts, M. A., Pope, A., and McMahon, L. P. (2021). Endothelial glycocalyx damage in kidney disease correlates with uraemic toxins and endothelial dysfunction. *BMC Nephrol.* 22:21. doi: 10.1186/s12882-020-02219-4

Lipowsky, H. H. (2018). Role of the glycocalyx as a barrier to leukocyte-endothelium adhesion. *Adv. Exp. Med. Biol.* 1097, 51–68. doi: 10.1007/978-3-319-96445-4_3

Litwiniuk, M., Krejner, A., Speyrer, M. S., Gauto, A. R., and Grzela, T. (2016). Hyaluronic acid in inflammation and tissue regeneration. *Wounds* 28, 78–88.

Loeser, R. F., Yammani, R. R., Carlson, C. S., Chen, H., Cole, A., Im, H. J., et al. (2005). Articular chondrocytes express the receptor for advanced glycation end products: potential role in osteoarthritis. *Arthritis Rheum.* 52, 2376–2385. doi: 10.1002/art.21199

Lupu, F., Kinasewitz, G., and Dormer, K. (2020). The role of endothelial shear stress on haemodynamics, inflammation, coagulation and glycocalyx during sepsis. *J. Cell. Mol. Med.* 24, 12258–12271. doi: 10.1111/jcmm.15895

Margraf, A., Herter, J. M., Kühne, K., Stadtmann, A., Ermert, T., Wenk, M., et al. (2018). 6% Hydroxyethyl starch (HES 130/0.4) diminishes glycocalyx degradation and decreases vascular permeability during systemic and pulmonary inflammation in mice. *Crit. Care* 22:111.

Martel-Pelletier, J., Farran, A., Montell, E., Vergés, J., and Pelletier, J. P. (2015). Discrepancies in composition and biological effects of different formulations of chondroitin sulfate. *Molecules* 20, 4277–4289. doi: 10.3390/molecules20034277

Massena, S., Christoffersson, G., Hjertström, E., Zcharia, E., Vlodavsky, I., Ausmees, N., et al. (2010). A chemotactic gradient sequestered on endothelial heparan sulfate induces directional intraluminal crawling of neutrophils. *Blood* 116, 1924–1931. doi: 10.1182/blood-2010-01-266072

Melgar-Lesmes, P., Garcia-Polite, F., Del-Rey-Puech, P., Rosas, E., Dreyfuss, J. L., Montell, E., et al. (2016). Treatment with chondroitin sulfate to modulate inflammation and atherogenesis in obesity. *Atherosclerosis* 245, 82–87. doi: 10.1016/j.atherosclerosis.2015.12.016

Mendes, R. S., Pelosi, P., Schultz, M. J., Rocco, P. R. M., and Silva, P. L. (2020). Fluids in ARDS: more pros than cons. *Intensive Care Med. Exp.* 8:32.

Middleton, J., Neil, S., Wintle, J., Clark-Lewis, I., Moore, H., Lam, C., et al. (1997). Transcytosis and surface presentation of IL-8 by venular endothelial cells. *Cell* 91, 385–395. doi: 10.1016/s0092-8674(00)80422-5

Mitra, R., O'Neil, G. L., Harding, I. C., Cheng, M. J., Mensah, S. A., and Ebong, E. E. (2017). Glycocalyx in atherosclerosis-relevant endothelium function and as a therapeutic target. *Curr. Atheroscler. Rep.* 19:63.

Moore, K. H., Murphy, H. A., and George, E. M. (2021). The glycocalyx: a central regulator of vascular function. *Am. J. Physiol. Regul. Integr. Comp. Physiol.* 320, R508–R518.

Mulivor, A. W., and Lipowsky, H. H. (2004). Inflammation- and ischemia-induced shedding of venular glycocalyx. *Am. J. Physiol. Heart Circ. Physiol.* 286, H1672–H1680.

Ng, A., Tam, W. W., Zhang, M. W., Ho, C. S., Husain, S. F., McIntyre, R. S., et al. (2018). IL-1β, IL-6, TNF- α and CRP in elderly patients with depression or Alzheimer's disease: systematic review and meta-analysis. *Sci. Rep.* 8:12050.

Noble, P. W., McKee, C. M., Cowman, M., and Shin, H. S. (1996). Hyaluronan fragments activate an NF-kappa B/I-kappa B alpha autoregulatory loop in murine macrophages. *J. Exp. Med.* 183, 2373–2378.

Pillinger, N. L., and Kam, P. (2017). Endothelial glycocalyx: basic science and clinical implications. *Anaesth. Intensive Care* 45, 295–307. doi: 10.1177/0310057x1704500305

Rabelink, T. J., and de Zeeuw, D. (2015). The glycocalyx–linking albuminuria with renal and cardiovascular disease. *Nat. Rev. Nephrol.* 11, 667–676. doi: 10.1038/nrneph.2015.162

Rajan, J. V., Warren, S. E., Miao, E. A., and Aderem, A. (2010). Activation of the NLRP3 inflammasome by intracellular poly I:C. *FEBS Lett.* 584, 4627–4632. doi: 10.1016/j.febslet.2010.10.036

Rathinam, V. A., and Fitzgerald, K. A. (2016). Inflammasome complexes: emerging mechanisms and effector functions. *Cell* 165, 792–800. doi: 10.1016/j.cell.2016.03.046

Rovas, A., Osiaevi, I., Buscher, K., Sackarnd, J., Tepasse, P. R., Fobker, M., et al. (2021). Microvascular dysfunction in COVID-19: the MYSTIC study. *Angiogenesis* 24, 145–157. doi: 10.1007/s10456-020-09753-7

Rubio-Gayosso, I., Platts, S. H., and Duling, B. R. (2006). Reactive oxygen species mediate modification of glycocalyx during ischemia-reperfusion injury. *Am. J. Physiol. Heart Circ. Physiol.* 290, H2247–H2256.

Sahibzada, H. A., Khurshid, Z., Khan, R. S., Naseem, M., Siddique, K. M., Mali, M., et al. (2017). Salivary IL-8, IL-6 and TNF-α as potential diagnostic biomarkers for oral cancer. *Diagnostics* 7:21. doi: 10.3390/diagnostics7020021

Sieve, I., Münster-Kühnel, A. K., and Hilfiker-Kleiner, D. (2018). Regulation and function of endothelial glycocalyx layer in vascular diseases. *Vasc. Pharmacol.* 100, 26–33. doi: 10.1016/j.vph.2017.09.002

Soeki, T., and Sata, M. (2016). Inflammatory biomarkers and atherosclerosis. *Int. Heart J.* 57, 134–139.

Sproston, N. R., and Ashworth, J. J. (2018). Role of C-reactive protein at sites of inflammation and infection. *Front. Immunol.* 9:754. doi: 10.3389/fimmu.2018.00754

Tarbell, J. M., and Cancel, L. M. (2016). The glycocalyx and its significance in human medicine. *J. Intern. Med.* 280, 97–113. doi: 10.1111/joim.12465

Uchimido, R., Schmidt, E. P., and Shapiro, N. I. (2019). The glycocalyx: a novel diagnostic and therapeutic target in sepsis. *Crit. Care* 23:16.

Vallières, M., and du Souich, P. (2010). Modulation of inflammation by chondroitin sulfate. *Osteoarthr. Cartil.* 18, S1–S6.

van Golen, R. F., Reiniers, M. J., Vrisekoop, N., Zuurbier, C. J., Olthof, P. B., van Rheenen, J., et al. (2014). The mechanisms and physiological relevance of glycocalyx degradation in hepatic ischemia/reperfusion injury. *Antioxid. Redox Signal* 21, 1098–1118. doi: 10.1089/ars.2013.5751

van Golen, R. F., van Gulik, T. M., and Heger, M. (2012). Mechanistic overview of reactive species-induced degradation of the endothelial glycocalyx during hepatic ischemia/reperfusion injury. *Free Radic. Biol. Med.* 52, 1382–1402. doi: 10.1016/j.freeradbiomed.2012.01.013

Vestweber, D. (2015). How leukocytes cross the vascular endothelium. *Nat. Rev. Immunol.* 15, 692–704. doi: 10.1038/nri3908

Wang, C. T., Lin, Y. T., Chiang, B. L., Lin, Y. H., and Hou, S. M. (2006). High molecular weight hyaluronic acid down-regulates the gene expression of osteoarthritis-associated cytokines and enzymes in fibroblast-like synoviocytes from patients with early osteoarthritis. *Osteoarthr. Cartil.* 14, 1237–1247. doi: 10.1016/j.joca.2006.05.009

Wang, L. (2011). "Heparan sulfate proteoglycan in inflammation and angiogenesis," in *Glycans in Diseases and Therapeutics*, eds Pavão and S. G. Mauro (New York, NY: Springer).

Wang, T., and He, C. (2020). TNF-α and IL-6: the link between immune and bone system. *Curr. Drug Targets* 21, 213–227. doi: 10.2174/1389450120666190821161259

Wang, T., Zhao, J., Zhang, J., Mei, J., Shao, M., Pan, Y., et al. (2018). Heparan sulfate inhibits inflammation and improves wound healing by downregulating the NLR family pyrin domain containing 3 (NLRP3) inflammasome in diabetic rats. *J. Diabetes* 10, 556–563. doi: 10.1111/1753-0407.12630

Yamaoka-Tojo, M. (2020a). Endothelial glycocalyx damage as a systemic inflammatory microvascular endotheliopathy in COVID-19. *Biomed. J.* 43, 399–413. doi: 10.1016/j.bj.2020.08.007

Yamaoka-Tojo, M. (2020b). Vascular endothelial glycocalyx damage in COVID-19. *Int. J. Mol. Sci.* 21:9712. doi: 10.3390/ijms21249712

Yao, Y., Rabodzey, A., and Dewey, C. F. Jr. (2007). Glycocalyx modulates the motility and proliferative response of vascular endothelium to fluid shear stress. *Am. J. Physiol. Heart Circ. Physiol.* 293, H1023–H1030.

Zeng, Y. (2017). Endothelial glycocalyx as a critical signalling platform integrating the extracellular haemodynamic forces and chemical signalling. *J. Cell. Mol. Med.* 21, 1457–1462. doi: 10.1111/jcmm.13081

Zuchi, C., Tritto, I., Carluccio, E., Mattei, C., Cattadori, G., and Ambrosio, G. (2020). Role of endothelial dysfunction in heart failure. *Heart Fail. Rev.* 25, 21–30. doi: 10.1007/s10741-019-09881-3

**Conflict of Interest:** The authors declare that the research was conducted in the absence of any commercial or financial relationships that could be construed as a potential conflict of interest.

**Publisher's Note:** All claims expressed in this article are solely those of the authors and do not necessarily represent those of their affiliated organizations, or those of the publisher, the editors and the reviewers. Any product that may be evaluated in this article, or claim that may be made by its manufacturer, is not guaranteed or endorsed by the publisher.

frontiers in Cell and Developmental Biology

ORIGINAL RESEARCH
published: 20 September 2021
doi: 10.3389/fcell.2021.734346

# Galectin-3 Enhances Vascular Endothelial Growth Factor-A Receptor 2 Activity in the Presence of Vascular Endothelial Growth Factor

*Issahy Cano[1,2], Zhengping Hu[1,2], Dina B. AbuSamra[1,2], Magali Saint-Geniez[1,2], Yin Shan Eric Ng[1,2], Pablo Argüeso[1,2] and Patricia A. D'Amore[1,2,3]**

[1] Schepens Eye Research Institute of Massachusetts Eye and Ear, Boston, MA, United States, [2] Department of Ophthalmology, Harvard Medical School, Boston, MA, United States, [3] Department of Pathology, Harvard Medical School, Boston, MA, United States

OPEN ACCESS

**Edited by:**
*Ye Zeng,*
*Sichuan University, China*

**Reviewed by:**
*Muhammad Nawaz,*
*University of Gothenburg, Sweden*
*Heiko Lemcke,*
*University Medical Center Rostock, Germany*

***Correspondence:**
*Patricia A. D'Amore*
*patricia_damore@meei.harvard.edu*

**Specialty section:**
*This article was submitted to Signaling, a section of the journal Frontiers in Cell and Developmental Biology*

**Received:** *01 July 2021*
**Accepted:** *30 August 2021*
**Published:** *20 September 2021*

**Citation:**
*Cano I, Hu Z, AbuSamra DB, Saint-Geniez M, Ng YSE, Argüeso P and D'Amore PA (2021) Galectin-3 Enhances Vascular Endothelial Growth Factor-A Receptor 2 Activity in the Presence of Vascular Endothelial Growth Factor. Front. Cell Dev. Biol. 9:734346. doi: 10.3389/fcell.2021.734346*

Galectin-3 (Gal3) is a carbohydrate-binding protein reported to promote angiogenesis by influencing vascular endothelial growth factor-A receptor 2 (VEGFR2) signal transduction. Here we evaluated whether the ability of Gal3 to function as an angiogenic factor involved vascular endothelial growth factor (VEGF). To address this possibility we used human retinal microvascular endothelial cells (HRECs) to determine whether exogenous Gal3 requires VEGF to activate VEGFR2 signaling and if Gal3 is required for VEGF to activate VEGFR2. VEGFR2 phosphorylation and HREC migration assays, following either VEGF neutralization with ranibizumab or Gal3 silencing, revealed that VEGF endogenously produced by the HRECs was essential for the effect of exogenous Gal3 on VEGFR2 activation and cell migration, and that VEGF-induced VEGFR2 activation was not dependent on Gal3 in HRECs. Gal3 depletion led to no reduction in VEGF-induced cell function. Since Gal3 has been suggested to be a potential therapeutic target for VEGFR2-mediated angiogenesis, it is crucial to define the possible Gal3-mediated VEGFR2 signal transduction mechanism to aid the development of efficacious therapeutic strategies.

**Keywords: endothelium, angiogenesis, ranibizumab, glycocalyx, migration**

## INTRODUCTION

Angiogenesis is the process by which blood vessels expand and remodel from existing vascular tissue. This mechanism is a critical element in embryonic development, wound healing, and disease progression (Folkman, 1995). Aberrant angiogenesis exacerbates disorders such as cancers and wet age-related macular degeneration by disturbing the well-organized vasculature and the associated vascular permeability leads to tissue dysfunction.

Vascular endothelial growth factor (VEGF), its isoforms, its receptors, and its functions have been well characterized with respect to angiogenesis. In particular, vascular endothelial growth factor-A receptor 2 (VEGFR2) mediates VEGF-induced endothelial cell (EC) survival, permeability, proliferation, tube formation, and cell migration (Koch et al., 2011; Peach et al., 2018).

VEGF activation of VEGFR2 induces receptor internalization, which is an integral aspect of its signaling (Simons et al., 2016). Cell surface proteins, such as neuropilin and endomucin have been shown to mediate VEGF binding and/or VEGFR2 trafficking, influencing angiogenic signaling (Olsson et al., 2006; Park-Windhol et al., 2017; LeBlanc et al., 2019).

Galectin-3 (Gal3) is a member of a family of lectins known as galectins. Galectins have a conserved carbohydrate-recognizing domain (CRD) that has an affinity for beta-galactosides, such as those found on the extracellular domain of membrane-bound receptors, including VEGFR2 (Funasaka et al., 2014). Gal3 is considered a chimera-type galectin due to its proline-rich N-terminal domain in conjunctions with its CRD, which provides it the ability to self-oligomerize and form lattice structures at the cell surface with other plasma membrane-bound molecules (Halimi et al., 2014).

Galectin-3 has been extensively studied in cancer biology and is considered a "pro-angiogenic" molecule (Halimi et al., 2014). Gal3, along with galectin 1, have been reported to mediate VEGFR2 activity at the cell surface by enhancing its signal transduction (Markowska et al., 2011; D'Haene et al., 2013). The binding of Gal3 to VEGFR2 is independent of activation by VEGF (Markowska et al., 2011). Previous studies have reported that exogenous Gal3 induces VEGFR2 activation in ECs, following serum starvation, leading to cell migration, proliferation, and tube formation (Nangia-Makker et al., 2000; Markowska et al., 2010, 2011). The suggested mechanisms for Gal3's activation of VEGFR2 correspond to its ability to cluster VEGFR2 at the EC surface, providing greater receptor availability to VEGF after cell starvation, as well as retention of the receptor at the cell surface. Most current anti-angiogenic treatments are focused on VEGF. However, due to challenges such as side effects seen with their use in cancer treatment and non-responder and/or resistance observed with anti-VEGF therapies in the eye, alternative and/or complementary therapies are being sought. Gal3's involvement in angiogenesis has led to the suggestion that it may provide an alternative anti-angiogenic target. This study aims to elucidate further the functional relationship between VEGF and Gal3 in VEGFR2 activation.

# MATERIALS AND METHODS

## Reagents and Antibodies

### Reagents

VEGF165 was purchased from Cell Signaling (#8065SC). Ranibizumab was obtained from Genentech. Mouse IgG (#sc-2025) was purchased from Santa Cruz. Goat (#005-000-003) and rabbit (#111-005-003) IgG was obtained from Jackson ImmunoResearch Laboratories. Phosphatase inhibitor cocktail tablet (#4906845001), protease inhibitor cocktail table (#5892970001), primaquine bisphosphate (PQB, #160393-1G), and Tween-20 (#X251-07) were purchased from Sigma-Aldrich. Sulfo-NHS-SS-Biotin (#1859385) and avidin agarose (#S1258122) were purchased from Life Technologies. Cell Lysis Buffer (#9803S) was from Cell Signaling. Gal3 was produced using vector as described previously (Mauris et al., 2013). Phosphate buffered saline (PBS, Sigma-Aldrich #D5652-10 × 1 L) and Tris-buffered saline (TBS, #170-6435) were obtained from Bio-Rad. Sodium orthovanadate was acquired from Sigma-Aldrich (#S6508-10G).

### Antibodies

Immunoblots were probed with rabbit anti-Gal3 (1:1,000, Abcam #ab209344), rabbit anti-VEGFR2 (1:1,000, Cell Signaling, #2479S) mouse anti-CD31 (1:1,000, Thermo Fisher, #14-0311-81), rabbit anti-phospho-Y1175-VEGFR2 (1:500, Cell Signaling, #2478S), mouse anti-α-tubulin (1:1,000, Millipore, #CP06-100UG), and goat anti-VEGFR2 (for immunocytochemistry, 1:100, R&D System, #AF357). Secondary antibodies used for immunoblots include goat anti-rabbit 800CW (1:20,000, LI-COR, #925-32211) and goat anti-mouse 680RD (1:20,000, LI-COR, #925-68070).

## Cell Culture

Human retinal microvascular endothelial cells (HRECs) were purchased from Cell Systems (#ACBRI 181) and cultured in Endothelial Basal Media-2 (EBM-2) BulletKit Medium (Lonza, #CC-3162) supplemented with 2% fetal bovine serum (FBS, Atlanta Biologicals) and 2 mM L-glutamine (Lonza, #CC-17-605E). Culture plates were coated in 0.2% gelatin from porcine skin (Sigma-Aldrich, #G1890) for 30 min at 37°C. Cells were used up to passage nine.

### siRNA Knockdown

Human retinal microvascular endothelial cells were seeded at 70–80% confluence 8 h before siRNA application. siControl (siCtrl) (50 nM, Ambion #4390844) or siGal3 (50 nM, Ambion #4392422) was incubated for 30 min at room temperature with Lipofectamine (Thermo Fisher, #L3000001) in OPTIMEM (Life Technologies, #51985034). The siRNA complex was added to the HRECs with 2% FBS complete EBM-2 media without penicillin–streptomycin overnight and removed with a change in medium.

## Cell Migration

Confluent HRECs were starved for 8 h in serum-free EBM-2 then mechanically scratched with a p200 pipette tip. Serum-free EBM-2 containing the Gal3 (50 ng/ml) with mouse IgG or ranibizumab (10 μg/ml) was applied to the cells. Images were taken right after scratching and 15 h after to obtain an area of the closure. Wound area was analyzed using the Image J MRI Wound Healing Tool plug-in.

## Biotin Cell Surface Isolation

Confluent HRECs were starved for 2 h in serum free EBM-2, cells were stimulated for 30 min with BSA (10 ng/ml), VEGF (10 ng/ml), or Gal3 (50 ng/ml) in the presence of mouse IgG or ranibizumab (10 μg/ml) in serum free EBM-2 with primaquine bisphosphate (0.6 μM). Sulfo-NHS-SS-Biotin (#1859385) in PBS was added for 30 min at 4°C. The cells were washed with 50 mM Tris (pH 8.0), followed by PBS (pH 8.0) for quenching. Cells were collected using TBS and centrifuged at 1,500 rcf for 10 min. The cell pellet was lysed and sonicated in cell lysis buffer then incubated with 100 μl of avidin agarose bead slurry

(#S1258122), rotating for 1 h at room temperature. The beads were then washed using a Wash Buffer (20 mM Tris–HCl, pH 6.8, 0.5% Tween-20) containing a protease inhibitor cocktail (#5871S) three times, centrifuged at 1,000 rcf for 1 min. Bound cell surface proteins were eluted using Laemmli SDS Sample Buffer with 100 mM DTT followed by a 10 min incubation at 95°C. Western blot analysis was performed on the samples with antibodies against rabbit anti-human VEGFR2 (1:1,000; #AF357) and mouse anti-human CD31 (1:1,000; #14-0311-81). The Dual Color Precision Plus Protein™ from Bio-Rad was used to identify the molecular weights of proteins (**Supplementary Figure 1**).

## Measurement of Kinase Activation

Human retinal microvascular endothelial cells grown to confluence were starved in serum-free EBM-2 for 2 h then stimulated with BSA (10 ng/ml), Gal3 (50 μg/ml), or VEGF (10 ng/ml) in serum-free EBM-2 with 200 mM sodium orthovanadate for 0, 5, 10, 30, and 60 min. After washing the cells in PBS, they were collected in lysis buffer and analyzed by western blot for tubulin, VEGFR2, and pVEGFR2.

## Analysis of Protein Expression

Following lysis in RIPA buffer (Cell Signaling, #9806S) with protease and phosphatase inhibitor cocktails (1:100, Sigma), samples were prepared with equal protein concentration determined using Peirce BCA assay kit (Thermo Scientific, #23227), run on SDS-PAGE, transferred onto nitrocellulose membranes (VWR, #27376-991), washed with 0.1–0.2% Tween-20 in PBS (PBST). Membranes were probed with antibodies for the proteins of interest. Corresponding secondary antibodies were used. SuperSignal™ West Pico Chemiluminescent Substrate (Thermo Scientific, #34077) or fluorescence LI-COR Odyssey (LI-COR) was utilized for final image development. Densitometric measurements were determined using ImageJ software. Final protein fluorescence was normalized to loading controls and represented as a fold-change.

## qPCR RNA Analysis

Immediately after treatment, cells were washed with PBS, collected and processed using the RNeasy Mini Kit provided by Qiagen. A measured amount of 1,000 ng of purified RNA was reverse transcribed into cDNA using the iScript cDNA synthesis kit (Bio-Rad). Using FastStart Universal SYBR Green master mix (Roche #A25743), gene expression was read with the Precision Plus Protein™ LightCycler® 480 II (Roche, Indianapolis, IN, United States) on 384 well plates containing a starting amount of 25 ng of cDNA. The primers used included:

E-selectin: Forward (5′-GCTGGAGAACTTGCGTTTAAG-3′)
Reverse (5′-GCTTTGCAGACTGGGATTTG-3′)

V-CAM1: Forward (5′-CCACGTGGACATCTACTCTTTC-3′)
Reverse (5′-CCAGCCTGTAAACTGGGTAAA-3′)

HPRT: Forward (5′-CCTGGCGTCGTGATTAGTGAT-3′)
Reverse (5′-AGACGTTCAGTCCTGTCCATAA-3′)

PrimePCR™ PCR primers for Gal3 were acquired from Bio-Rad (#qHsaCID0008552). Gene expression levels were normalized to HPRT. All samples were prepared with the same amount of starting reagents for qPCR analysis.

## Statistical Analysis

Data are presented as the mean ± SEM of at least three independent experiments. To evaluate for statistical significance, two-tail unpaired Student *T*-test or original one-way ANOVA were used (Prism 9 software package, GraphPad, San Diego, CA, United States). Values of $P < 0.05$ were considered statistically significant.

# RESULTS

## Galectin-3 Promotes Cell Function Through Vascular Endothelial Growth Factor-A Receptor 2

Galectin-3 has been reported to interact with VEGFR2 *via* *N*-glycans on its extracellular domain (Markowska et al., 2011). We confirmed this by examining Gal3 and VEGFR2 association using lysates of HREC and Gal3-conjugated agarose beads (**Figure 1A**). Bound materials eluted with lactose and analyzed by western blot revealed the binding of VEGFR2 by Gal3. These data suggest that Gal3 does in fact bind to VEGFR2 in a galactose-dependent manner.

In addition to its effects as an angiogenesis factor, VEGFR2 also mediates the pro-inflammatory signaling of VEGF (Kim et al., 2001; Shaik-Dasthagirisaheb et al., 2013). Thus, as an additional endpoint, we examined the expression of the leukocyte adhesion molecules, E-selectin and VCAM-1 (Chen et al., 2013). Gal3 stimulation of serum starved HRECs led to an increase in E-selectin ($7.46 \pm 0.745$ vs. $1.0 \pm 0.051$, $P < 0.001$) and VCAM-1 ($3.329 \pm 0.519$ vs. $1.0 \pm 0.140$, $P < 0.05$) mRNA, compared to untreated controls (**Figure 1B**). Sunitinib, a small molecule inhibitor that is selective for VEGFR2, was used to confirm the role of VEGFR2 in this effect. Serum starved HRECs treated with sunitinib had significantly reduced Gal3-induction of E-selectin by 91% ($0.676 \pm 0.0601$ vs. $7.46 \pm 0.745$, $P < 0.001$) and VCAM-1 by 67% ($1.158 \pm 0.0908$ vs. $3.329 \pm 0.519$, $P < 0.05$) mRNA expression (**Figure 1B**), providing strong evidence for the involvement of VEGFR2 in the effects of Gal3. EC migration, a component of angiogenesis, is induced by VEGF *via* activation of VEGFR2 (Santos et al., 2007).

## Galectin-3 Enhances, but Is Not Required for Vascular Endothelial Growth Factor-Induced Cell Function

After establishing the association between Gal3 and VEGFR2, we sought to determine if Gal3 was necessary for VEGF-induced VEGFR2 activity. Treatment of HRECs with siGal3 resulted in more than 90% reduction of Gal3 mRNA ($0.0643 \pm 0.00231$ vs. $1.0 \pm 0.247$, $P < 0.05$) (**Figure 2A**) and protein compared to the siCtrl group ($0.072 \pm 0.0233$ vs. $1.0 \pm 0.218$, $P < 0.05$) (**Figure 2B**). The depletion of Gal3 on the endothelial cell surface

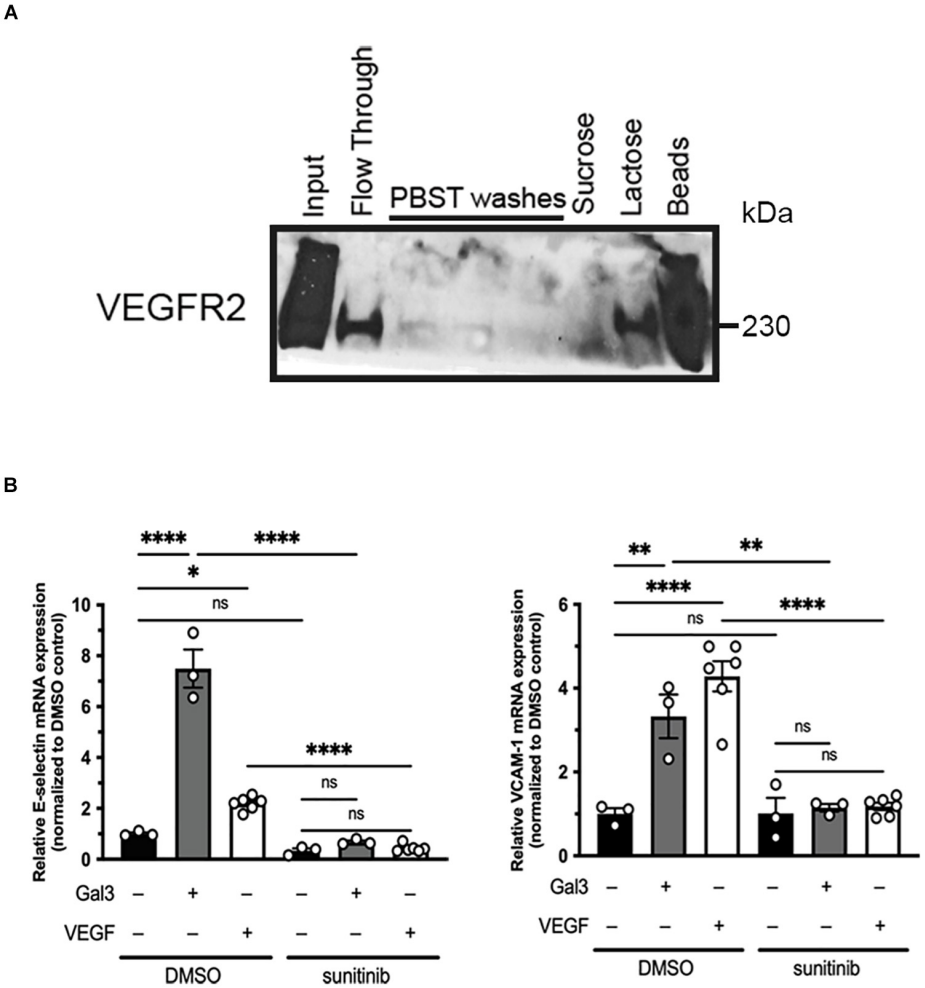


**FIGURE 1 |** Galectin-3 associates with and induces activation of VEGFR2. **(A)** Confluent HRECs were lysed using RIPA lysis buffer. HREC lysate was incubated with Gal3-conjugated beads, washed, and eluted either with a non-competitive sugar (0.1 mM sucrose) or a competitive sugar (0.5 mM lactose). Bound VEGFR2 was eluted once it was competed off of the beads by lactose **(B)** Serum-starved HRECS were stimulated with 50 μg/ml Gal3 or 10 ng/ml VEGF for 2 h with or without sunitinib then total RNA was isolated and reverse transcribed into cDNA. E-selectin, VCAM-1, and HPRT1 mRNA expression were analyzed using qPCR. One-way ANOVA analysis was applied, $*P < 0.05$, $**P < 0.01$, $****P < 0.0001$, $n = 3$.

was also observed using immunocytochemistry (**Supplementary Figure 2**). Stimulation of HRECs in which Gal3 had been knocked down with 10 ng/ml VEGF over a time course up to 30 min revealed no significant difference in the phosphorylation of VEGFR2. The phosphorylation of VEGFR2 at all time points was similar in both siCtrl and siGal3 conditions (**Figure 2C**). Consistent with that observation, Gal3 depletion did not prevent VEGF-stimulated HREC migration; VEGF-induced migration in Gal3 depleted cells was significantly compared to control cells ($4.85 \pm 0.474$ vs. $2.31 \pm 0.352$ $P < 0.01$) (**Figure 2D**).

Vascular endothelial growth factor activation of VEGFR2 leads to receptor internalization through clathrin-medicated endocytosis (LeBlanc et al., 2019). To assess whether Gal3 is necessary for this step, HRECs with depleted Gal3 were stimulated with VEGF at 10 ng/ml, all cell surface proteins were biotinylated and extracted from whole cell lysate with avidin agarose beads, then were analyzed for total VEGFR2 levels on the cell surface by western blot. There was no difference in VEGF-induced VEGFR2 internalization with or without Gal3 depletion ($0.0143 \pm 0.00373$ vs. $0.0146 \pm 0.00381$, $P > 0.05$) (**Figure 2E**).

## Vascular Endothelial Growth Factor Is Necessary for Gal3-Induced Vascular Endothelial Growth Factor-A Receptor 2 Activation

In light of our observation that Gal3 appears to enhance the activities of VEGFR2, we sought to determine the role of VEGF in Gal3's induction of VEGFR2 signaling. To accomplish this, we employed ranibizumab, a recombinant humanized antibody fragment (Fab) that neutralizes all VEGF-A isoforms. Serum-starved HRECs were stimulated with Gal3 in the presence of ranibizumab to neutralize VEGF in the system, and VEGFR2 phosphorylation (pVEGFR2 Y115) was examined over a time

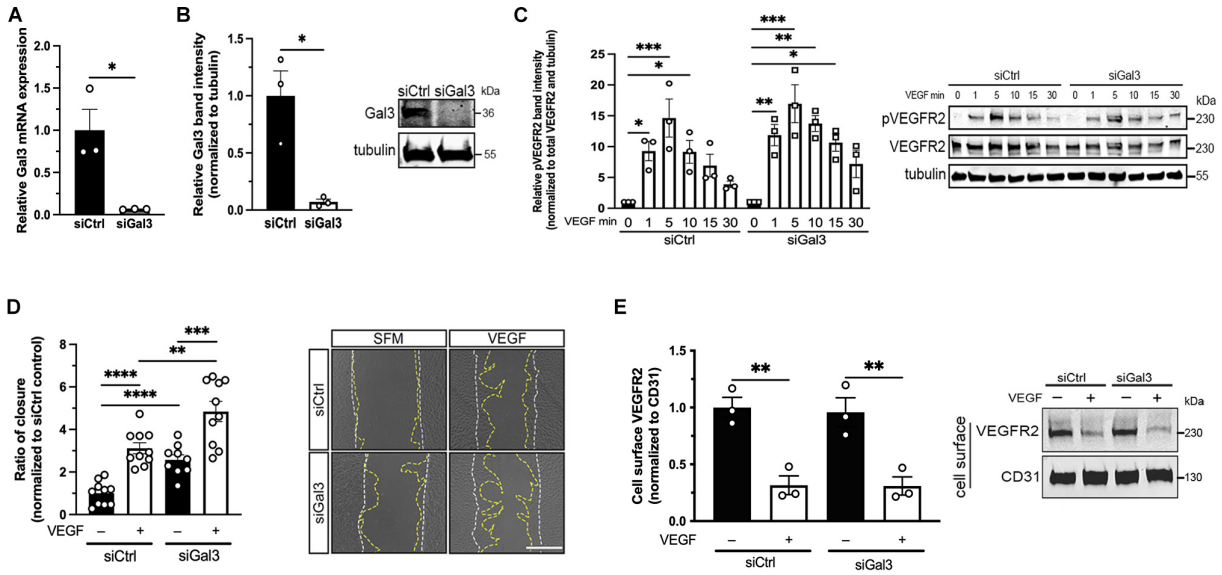


**FIGURE 2 |** Galectin-3 is not required for VEGF-induced VEGFR2 activity. **(A)** HRECs transfected with siRNA targeting Gal3 (siGal3) demonstrated over 90% mRNA knockdown of Gal3 compared to cells transfected with control siRNA (siCtrl), analyzed by reverse-transcription and qPCR assay. Student *T*-test was applied, $^{*}P < 0.05$, $n = 3$. **(B)** Lysate from HRECs transfected with siGal3 or siCtrl was analyzed by western blot and probed with an antibody against Gal3, which resulted in over 90% Gal3 protein reduction. Student *T*-test was applied, $^{*}P < 0.05$, $n = 3$. **(C)** siCtrl and siGal3 transfected HRECs were stimulated with 10 ng/ml of VEGF for 0, 1, 5, 10, 15, and 30 min. Cell lysates were collected and analyzed by western blot for tubulin, VEGFR2, and phospho-VEGFR2 (pVEGFR2 Y1175). Protein levels for pVEGFR2 were quantified using ImageJ and normalized to total VEGFR2 and α-tubulin. Ordinary one-way ANOVA was applied for comparisons within groups, $^{*}P < 0.05$, $^{**}P < 0.01$, $^{***}P < 0.001$, $n = 3$. **(D)** Confluent HRECs, transfected with siCtrl or siGal3, were scratched and stimulated with 10 ng/ml of VEGF. Images were taken immediately after scratching and 15 h later. Cell migration was quantified using ImageJ and normalized to the non-treatment control group. Scale bar represents 500 μm. Student *T*-test was applied, $^{**}P < 0.01$, $^{***}P < 0.001$, $^{****}P < 0.0001$, $n = 10$. **(E)** HRECs transfected with siCtrl and siGal3 were stimulated with 10 ng/ml VEGF. Cell surface proteins were labeled with NHS-SS-biotin and isolated from cell lysate using avidin agarose beads. Total VEGFR2 and CD31 protein levels were analyzed by western blot. Student *T*-test was applied, $^{*}P < 0.05$, $n = 3$.

course. Results showed that ranibizumab blocked the action of Gal3 as an inducer of VEGFR2 activation (**Figure 3A**). Gal3 induced significant VEGFR2 phosphorylation without ranibizumab in the control cells at the early time point ($1.59 \pm 0.202$ vs. 1.0, $P < 0.05$). Treatment with ranibizumab to neutralize VEGF completely inhibited Gal3-induced VEGFR2 phosphorylation, and ranibizumab alone had no effect on VEGFR2 activation ($0.764 \pm 0.249$ vs. $1.0 \pm 0.236$, $P > 0.05$).

To determine if VEGF is essential for the downstream effects of Gal3, we examined HREC migration. The scratch migration assay was conducted using Gal3 along with ranibizumab or mouse IgG as a control. HRECs treated with Gal3 in the presence of a control IgG migrated significantly more than the untreated control cells by about 17% ($1.167 \pm 0.0235$ vs. $1.0 \pm 0.310$, $P < 0.05$). VEGF neutralization by ranibizumab completely blocked the stimulatory effect of Gal3 on HREC migration ($0.968 \pm 0.207$ vs. $1.0 \pm 0.140$, $P > 0.05$) (**Figure 3B**).

Taken together these results reveal that Gal3 does not directly active VEGFR2 but depends on the presence of VEGF endogenously produced by the HREC.

## DISCUSSION

Galectin-3 has been previously shown to play an influential role in angiogenesis, in particularly in the context of VEGFR2 signaling. Surprisingly, Gal3 induced the activation of VEGFR2 even after the ECs were starved in serum-free media. As previously suggested, this phenomenon may be due to Gal3's ability to enhance VEGFR2 signaling in the presence of the suboptimal VEGF ligand rather than directly activating VEGFR2 itself (Markowska et al., 2011). The results of this study support the conclusion that while VEGF is necessary for the activation of VEGFR2-mediated signaling and functions, Gal3 facilitates that interaction but does not directly signal through VEGFR2.

Galectin-3 plays diverse roles in the physiology and function of cells, so not surprisingly, is implicated in a variety of pathologies. Elevated serum levels of Gal3 have been detected during the progression of various head and neck carcinomas, as well as in acute inflammation and renal failure (Nishiyama et al., 2000; Saussez et al., 2008; Henderson and Sethi, 2009). In contrast, downregulation of Gal3 in prostate cancer was shown to favor cancer progression (Pacis et al., 2000) and decreased expression of Gal3 in the context of breast cancer is speculated to contribute to metastasis (Castronovo et al., 1996). In addition, Gal3 knockdown has been previously shown to reduce VEGF- and basic fibroblast growth factor (FGF)-mediated angiogenesis (Markowska et al., 2010). In this work we determined that Gal3 depletion did not lead to a reduction in VEGF-mediated VEGFR2 phosphorylation at the Y1175 site, VEGF-induced HREC migration, or VEGF-induced VEGFR2 internalization. Thus, that while Gal3 is not necessary for VEGF-induced VEGFR2 activity,

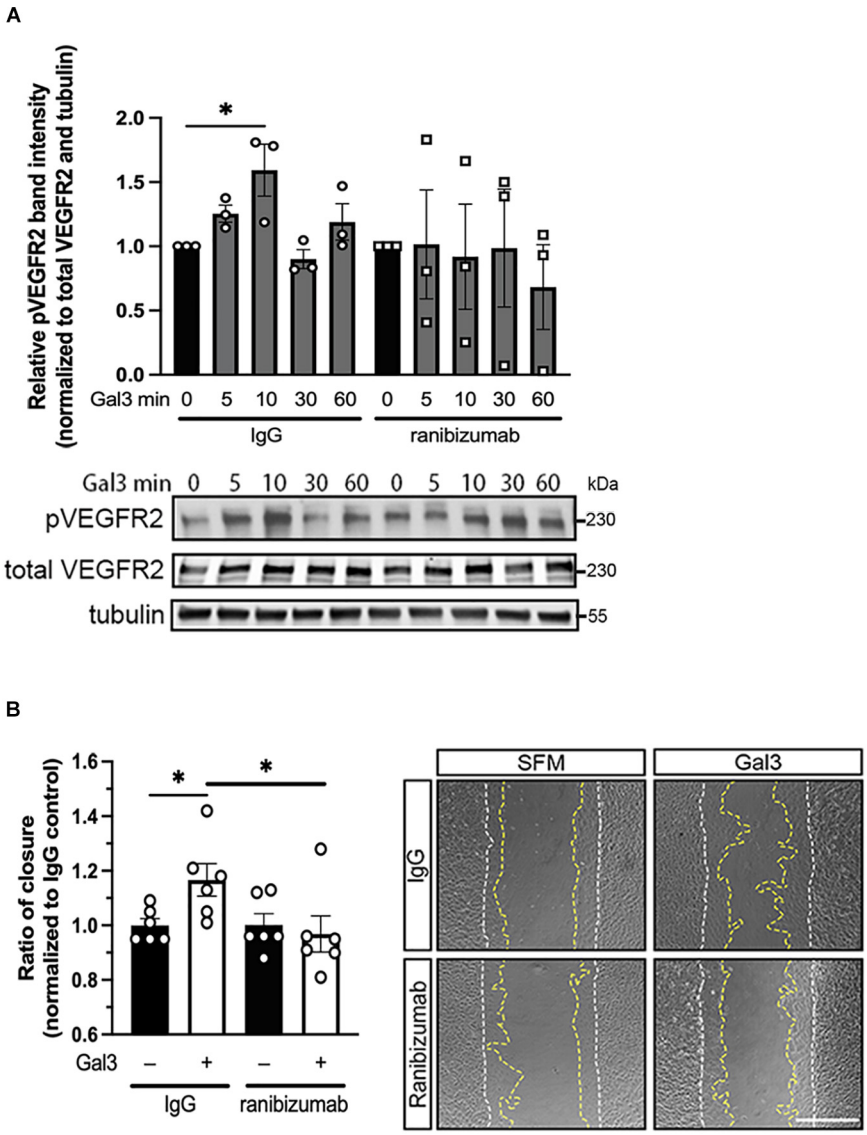


**FIGURE 3 |** Galectin-3 requires VEGF to induce VEGFR2 activity. **(A)** Ranibizumab (10 μg/ml) was added to neutralize endogenous VEGF and HRECs were stimulated with 50 μg/ml of Gal3 for 0, 5, 10, 30, and 60 min. Cell lysates were collected and pVEGFR2 Y1175 (pR2), VEGFR2 (TR2), and α-tubulin protein levels were analyzed by western blot. Ordinary one-way ANOVA was applied. $*P < 0.05$, $n = 3$. **(B)** Confluent HRECs were scratched and stimulated with 50 μg/ml of Gal3 with 10 μg/ml of ranibizumab or control IgG. Images were taken immediately after scratching and at 15 h later. Scale bar represents 500 μm. Cell migration was quantified using ImageJ. Student *T*-test was applied, $*P < 0.05$, $n = 6$.

it does appear to modulate it by enhancing it as it has been previously reported (Markowska et al., 2010). VEGFR2 is not the only tyrosine kinase receptor that Gal3 binds. FGF receptor 1 and epidermal growth factor receptor are N-glycosylated at the extracellular domain and, similar to VEGFR2, bind to Gal3 in a carbohydrate dependent manner (Duchesne et al., 2006; Azimzadeh Irani et al., 2017; Kucinska et al., 2019). In doing so, Gal3 has the potential to enhance their angiogenic signaling as well, potentially using the same or similar mechanism. FGF modulation by Gal3 was studied alongside VEGF and both were impacted similarly (Markowska et al., 2010).

Previous reports have examined the role of Gal3 in VEGFR2 signal transduction. Addition of Gal3 to human umbilical vein ECs resulted in the phosphorylation of VEGFR2 at the Y1175 (Markowska et al., 2011), which could lead to the conclusion that Gal3 functions as a ligand to directly activate VEGFR2 and downstream signal transduction. However, as suggested, any presence of VEGF, even post serum-starvation, may be amplified by the presence of Gal3, possibly *via* its effect on receptor clustering (Markowska et al., 2011). Our observation that neutralization of VEGF prevented the ability of exogenously added Gal3 to induce VEGFR2 signal transduction support this

notion and that Gal3 acts to amplify angiogenic signaling in an indirect manner.

Anti-VEGF therapies have transformed treatment strategies for pathologies involving aberrant angiogenesis. Ranibizumab along with bevacizumab and aflibercept are potent anti-VEGF treatments aimed at mitigating disease progression, such as in neovascular age-related macular degeneration. However, a significant number of patients show a variable response to conventional anti-VEGF therapy, and some are considered non-responders (Kitchens et al., 2013; Krebs et al., 2013; Bontzos et al., 2020). The findings in this study that Gal3 acts as an enhancer to VEGF activity suggest that blocking both VEGF and Gal3 might lead to a more robust inhibitory effect.

## DATA AVAILABILITY STATEMENT

The original contributions presented in the study are included in the article/**Supplementary Material**, further inquiries can be directed to the corresponding author.

## AUTHOR CONTRIBUTIONS

IC performed the research, analyzed the data, and wrote the first draft of the manuscript. ZH, DA, MS-G, YN, and PA provided critical discussion and technical help for the experiments and reviewed the manuscript. IC, ZH, MS-G, YN, and PD'A designed the research. PD'A directed the study, interpreted results with IC, and did the major editing of the manuscript. All authors contributed to the article and approved the submitted version.

## FUNDING

This work was supported by NIH/NEI R01 EY026539 (to PD'A). Supported by NIH National Eye Institute core grant P30EYE003790.

## SUPPLEMENTARY MATERIAL

The Supplementary Material for this article can be found online at: https://www.frontiersin.org/articles/10.3389/fcell.2021.734346/full#supplementary-material

**Supplementary Figure 1 |** Western blot with protein standard present. A representative western blot was chosen to demonstrate the positioning of the protein standard. The standard used is the Dual Color Precision Plus Protein™ Standards from Bio-Rad, which shows a maximum kDa of 250 and a minimum kDa of 10.

**Supplementary Figure 2 |** Immunofluorescence of cell surface Gal3. HRECs were grown to confluency on gelatin-coated coverslips. Prior to VEGF (10 ng/ml) stimulation, HRECs were starved in serum-free EBM-2 for 2 h. The HRECs were washed with PBS and fixed with 1% paraformaldehyde overnight at 4°C. The non-permeabilized cells were stained for DAPI, Gal3, and VEGFR2 followed by incubation with the appropriate fluorescent secondary antibodies [Alexa Fluor 594-labeled donkey anti-goat (1:1,000, #A-11058) and Alex Fluor 488-labeled donkey anti-rabbit (1:1,000, #A-21206)]. Images at 20× magnification were taken using the Zeiss Axioscope (Oberkochen, Germany). The scale bar represents 100 μm. Expression of Gal3 and VEGFR2 was confirmed on the cell surface, as well as the knockdown of Gal3 using siRNA.

## REFERENCES

Azimzadeh Irani, M., Kannan, S., and Verma, C. (2017). Role of N-glycosylation in EGFR ectodomain ligand binding. *Proteins* 85, 1529–1549. doi: 10.1002/prot.25314

Bontzos, G., Bagheri, S., Ioanidi, L., Kim, I., Datseris, I., Gragoudas, E., et al. (2020). Nonresponders to Ranibizumab Anti-VEGF treatment are actually short-term responders: a prospective spectral-domain oct study. *Ophthalmol. Retina* 4, 1138–1145. doi: 10.1016/j.oret.2019.11.004

Castronovo, V., Van Den Brule, F. A., Jackers, P., Clausse, N., Liu, F. T., Gillet, C., et al. (1996). Decreased expression of galectin-3 is associated with progression of human breast cancer. *J. Pathol.* 179, 43–48. doi: 10.1002/(SICI)1096-9896(199605)179:1<43::AID-PATH541<3.0.CO;2-N

Chen, C., Duckworth, C. A., Zhao, Q., Pritchard, D. M., Rhodes, J. M., and Yu, L. G. (2013). Increased circulation of galectin-3 in cancer induces secretion of metastasis-promoting cytokines from blood vascular endothelium. *Clin. Cancer Res.* 19, 1693–1704. doi: 10.1158/1078-0432.CCR-12-2940

D'Haene, N., Sauvage, S., Maris, C., Adanja, I., Le Mercier, M., Decaestecker, C., et al. (2013). VEGFR1 and VEGFR2 involvement in extracellular galectin-1- and galectin-3-induced angiogenesis. *PLoS One* 8:e67029. doi: 10.1371/journal.pone.0067029

Duchesne, L., Tissot, B., Rudd, T. R., Dell, A., and Fernig, D. G. (2006). N-glycosylation of fibroblast growth factor receptor 1 regulates ligand and heparan sulfate co-receptor binding. *J. Biol. Chem.* 281, 27178–27189. doi: 10.1074/jbc.M601248200

Folkman, J. (1995). Angiogenesis in cancer, vascular, rheumatoid and other disease. *Nat. Med.* 1, 27–31. doi: 10.1038/nm0195-27

Funasaka, T., Raz, A., and Nangia-Makker, P. (2014). Galectin-3 in angiogenesis and metastasis. *Glycobiology* 24, 886–891. doi: 10.1093/glycob/cwu086

Halimi, H., Rigato, A., Byrne, D., Ferracci, G., Sebban-Kreuzer, C., ElAntak, L., et al. (2014). Glycan dependence of Galectin-3 self-association properties. *PLoS One* 9:e111836. doi: 10.1371/journal.pone.0111836

Henderson, N. C., and Sethi, T. (2009). The regulation of inflammation by galectin-3. *Immunol. Rev.* 230, 160–171. doi: 10.1111/j.1600-065X.2009.00794.x

Kim, I., Moon, S. O., Kim, S. H., Kim, H. J., Koh, Y. S., and Koh, G. Y. (2001). Vascular endothelial growth factor expression of intercellular adhesion molecule 1 (ICAM-1), vascular cell adhesion molecule 1 (VCAM-1), and E-selectin through nuclear factor-kappa B activation in endothelial cells. *J. Biol. Chem.* 276, 7614–7620. doi: 10.1074/jbc.M009705200

Kitchens, J. W., Kassem, N., Wood, W., Stone, T. W., Isernhagen, R., Wood, E., et al. (2013). A pharmacogenetics study to predict outcome in patients receiving anti-VEGF therapy in age related macular degeneration. *Clin. Ophthalmol.* 7, 1987–1993. doi: 10.2147/OPTH.S39635

Koch, S., Tugues, S., Li, X., Gualandi, L., and Claesson-Welsh, L. (2011). Signal transduction by vascular endothelial growth factor receptors. *Biochem. J.* 437, 169–183. doi: 10.1042/BJ20110301

Krebs, I., Glittenberg, C., Ansari-Shahrezaei, S., Hagen, S., Steiner, I., and Binder, S. (2013). Non-responders to treatment with antagonists of vascular endothelial growth factor in age-related macular degeneration. *Br. J. Ophthalmol.* 97, 1443–1446. doi: 10.1136/bjophthalmol-2013-303513

Kucinska, M., Porebska, N., Lampart, A., Latko, M., Knapik, A., Zakrzewska, M., et al. (2019). Differential regulation of fibroblast growth factor receptor 1 trafficking and function by extracellular galectins. *Cell Commun. Signal.* 17:65. doi: 10.1186/s12964-019-0371-1

LeBlanc, M. E., Saez-Torres, K. L., Cano, I., Hu, Z., Saint-Geniez, M., Ng, Y. S., et al. (2019). Glycocalyx regulation of vascular endothelial growth factor receptor 2 activity. *FASEB J.* 33, 9362–9373. doi: 10.1096/fj.201900011R

Markowska, A. I., Jefferies, K. C., and Panjwani, N. (2011). Galectin-3 protein modulates cell surface expression and activation of vascular endothelial growth factor receptor 2 in human endothelial cells. *J. Biol. Chem.* 286, 29913–29921. doi: 10.1074/jbc.M111.226423

Markowska, A. I., Liu, F. T., and Panjwani, N. (2010). Galectin-3 is an important mediator of VEGF- and bFGF-mediated angiogenic response. *J. Exp. Med.* 207, 1981–1993. doi: 10.1084/jem.20090121

Mauris, J., Mantelli, F., Woodward, A. M., Cao, Z., Bertozzi, C. R., Panjwani, N., et al. (2013). Modulation of ocular surface glycocalyx barrier function by a galectin-3 N-terminal deletion mutant and membrane-anchored synthetic glycopolymers. *PLoS One* 8:e72304. doi: 10.1371/journal.pone.0072304

Nangia-Makker, P., Honjo, Y., Sarvis, R., Akahani, S., Hogan, V., Pienta, K. J., et al. (2000). Galectin-3 induces endothelial cell morphogenesis and angiogenesis. *Am. J. Pathol.* 156, 899–909. doi: 10.1016/S0002-9440(10)64959-0

Nishiyama, J., Kobayashi, S., Ishida, A., Nakabayashi, I., Tajima, O., Miura, S., et al. (2000). Up-regulation of galectin-3 in acute renal failure of the rat. *Am. J. Pathol.* 157, 815–823. doi: 10.1016/S0002-9440(10)64595-6

Olsson, A. K., Dimberg, A., Kreuger, J., and Claesson-Welsh, L. (2006). VEGF receptor signalling-in control of vascular function. *Nat. Rev. Mol. Cell Biol.* 7, 359–371. doi: 10.1038/nrm1911

Pacis, R. A., Pilat, M. J., Pienta, K. J., Wojno, K., Raz, A., Hogan, V., et al. (2000). Decreased galectin-3 expression in prostate cancer. *Prostate* 44, 118–123. doi: 10.1002/1097-0045(20000701)44:2<118::aid-pros4<3.0.co;2-u

Park-Windhol, C., Ng, Y. S., Yang, J., Primo, V., Saint-Geniez, M., and D'Amore, P. A. (2017). Endomucin inhibits VEGF-induced endothelial cell migration, growth, and morphogenesis by modulating VEGFR2 signaling. *Sci. Rep.* 7:17138. doi: 10.1038/s41598-017-16852-x

Peach, C. J., Mignone, V. W., Arruda, M. A., Alcobia, D. C., Hill, S. J., Kilpatrick, L. E., et al. (2018). Molecular pharmacology of VEGF-A isoforms: binding and signalling at VEGFR2. *Int. J. Mol. Sci.* 19:1264. doi: 10.3390/ijms19041264

Santos, S. C., Miguel, C., Domingues, I., Calado, A., Zhu, Z., Wu, Y., et al. (2007). VEGF and VEGFR-2 (KDR) internalization is required for endothelial recovery during wound healing. *Exp. Cell Res.* 313, 1561–1574. doi: 10.1016/j.yexcr.2007.02.020

Saussez, S., Decaestecker, C., Mahillon, V., Cludts, S., Capouillez, A., Chevalier, D., et al. (2008). Galectin-3 upregulation during tumor progression in head and neck cancer. *Laryngoscope* 118, 1583–1590. doi: 10.1097/MLG.0b013e31817b0718

Shaik-Dasthagirisaheb, Y. B., Varvara, G., Murmura, G., Saggini, A., Potalivo, G., Caraffa, A., et al. (2013). Vascular endothelial growth factor (VEGF), mast cells and inflammation. *Int. J. Immunopathol. Pharmacol.* 26, 327–335. doi: 10.1177/039463201302600206

Simons, M., Gordon, E., and Claesson-Welsh, L. (2016). Mechanisms and regulation of endothelial VEGF receptor signalling. *Nat. Rev. Mol. Cell Biol.* 17, 611–625. doi: 10.1038/nrm.2016.87

**Conflict of Interest:** The authors declare that the research was conducted in the absence of any commercial or financial relationships that could be construed as a potential conflict of interest.

**Publisher's Note:** All claims expressed in this article are solely those of the authors and do not necessarily represent those of their affiliated organizations, or those of the publisher, the editors and the reviewers. Any product that may be evaluated in this article, or claim that may be made by its manufacturer, is not guaranteed or endorsed by the publisher.

frontiers in Cell and Developmental Biology

ORIGINAL RESEARCH
published: 21 September 2021
doi: 10.3389/fcell.2021.733015

# Direct Evidence of Endothelial Dysfunction and Glycocalyx Loss in Dermal Biopsies of Patients With Chronic Kidney Disease and Their Association With Markers of Volume Overload

*Josephine Koch[1], Ryanne S. Hijmans[2], Manuela Ossa Builes[1], Wendy A. Dam[1], Robert A. Pol[2], Stephan J. L. Bakker[1], Hendri H. Pas[3], Casper F. M. Franssen[1] and Jacob van den Born[1]**

[1] Division of Nephrology, University Medical Center Groningen, University of Groningen, Groningen, Netherlands,
[2] Department of Surgery, University Medical Center Groningen, University of Groningen, Groningen, Netherlands,
[3] Department of Dermatology, University Medical Center Groningen, University of Groningen, Groningen, Netherlands

OPEN ACCESS

**Edited by:**
*Ye Zeng,*
*Sichuan University, China*

**Reviewed by:**
*Raffaele Strippoli,*
*Sapienza University of Rome, Italy*
*Xiaoming Fan,*
*University of Toledo, United States*

***Correspondence:**
*Jacob van den Born*
*j.van.den.born@umcg.nl*

**Specialty section:**
*This article was submitted to Signaling, a section of the journal Frontiers in Cell and Developmental Biology*

**Received:** *29 June 2021*
**Accepted:** *30 August 2021*
**Published:** *21 September 2021*

**Citation:**
*Koch J, Hijmans RS, Ossa Builes M, Dam WA, Pol RA, Bakker SJL, Pas HH, Franssen CFM and van den Born J (2021) Direct Evidence of Endothelial Dysfunction and Glycocalyx Loss in Dermal Biopsies of Patients With Chronic Kidney Disease and Their Association With Markers of Volume Overload. Front. Cell Dev. Biol. 9:733015. doi: 10.3389/fcell.2021.733015*

Cardiovascular morbidity is a major problem in patients with chronic kidney disease (CKD) and endothelial dysfunction (ED) is involved in its development. The luminal side of the vascular endothelium is covered by a protective endothelial glycocalyx (eGC) and indirect evidence indicates eGC loss in CKD patients. We aimed to investigate potential eGC loss and ED in skin biopsies of CKD patients and their association with inflammation and volume overload. During living kidney transplantation procedure, abdominal skin biopsies were taken from 11 patients with chronic kidney disease stage 5 of whom 4 were treated with hemodialysis and 7 did not receive dialysis treatment. Nine healthy kidney donors served as controls. Biopsies were stained and quantified for the eGC marker Ulex europaeus agglutinin-1 (UEA1) and the endothelial markers vascular endothelial growth factor-2 (VEGFR2) and von Willebrand factor (vWF) after double staining and normalization for the pan-endothelial marker cluster of differentiation 31. We also studied associations between quantified log-transformed dermal endothelial markers and plasma markers of inflammation and hydration status. Compared to healthy subjects, there was severe loss of the eGC marker UEA1 ($P < 0.01$) while VEGFR2 was increased in CKD patients, especially in those on dialysis ($P = 0.01$). For vWF, results were comparable between CKD patients and controls. Skin water content was identical in the three groups, which excluded dermal edema as an underlying cause in patients with CKD. The dermal eGC/ED markers UEA1, VEGFR2, and vWF all associated with plasma levels of NT-proBNP and sodium (all $R^2 > 0.29$ and $P < 0.01$), except for vWF that only associated with plasma NT-proBNP. This study is the first to show direct histopathological evidence of dermal glycocalyx loss and ED in patients with CKD. In line with previous research, our results show that ED associates with markers of volume overload arguing for strict volume control in CKD patients.

**Keywords: CKD, endothelial dysfunction, NT-proBNP, inflammation, sodium, glycocalyx**

## INTRODUCTION

Cardiovascular (CV) disease is the leading cause of morbidity and mortality in patients with chronic kidney disease (CKD) (Baigent et al., 2000; Matsushita et al., 2010; Mahmoodi et al., 2012; Cozzolino et al., 2017). Patients with CKD present with traditional CV risk factors, including hypertension, diabetes or dyslipidemia (Herzog et al., 2011; Gansevoort et al., 2013), but also with non-traditional CV risk factors (Go et al., 2004; El Nahas and Bello, 2005; Fox et al., 2012; Mahmoodi et al., 2012) of which endothelial dysfunction (ED) is established as a prominent one (Schächinger et al., 2000; Bonetti et al., 2003; Nagy et al., 2010).

A normally functioning endothelium modulates vascular permeability (Henry and Duling, 1999), controls vascular tone, and maintains blood flow [reviewed by Sandoo et al. (2015)]. Many of these endothelial functions are orchestrated by a properly functioning endothelial glycocalyx (eGC), which covers the luminal side of vascular endothelium. The eGC is a carbohydrate-rich mesh of glycoproteins, proteoglycans and glycosaminoglycans that interact with absorbed plasma proteins (Weinbaum et al., 2007). The highly sulfated and negatively charged properties of the eGC protect the endothelium and control cell migration (Constantinescu et al., 2003), and leakage of albumin (Ueda et al., 2004) and fluid (Van den Berg et al., 2003). Several studies indicated that damaged eGC in renal disease is associated with ED (Singh et al., 2007; Salmon et al., 2012; Vlahu et al., 2012; Padberg et al., 2014). For example, Vlahu et al. (2012) reported a diminished eGC thickness in hemodialysis patients by sidestream dark film imaging that was associated with elevated plasma markers of ED. For the development of ED, several interacting components seem to be involved. Next to oxidative stress and uremic toxins, the destructive effects of inflammation and volume overload on the vascular endothelium are increasingly receiving attention (Mitsides et al., 2018).

Patients with CKD often have elevated plasma markers of inflammation (Westphalen et al., 2020) which can have multiple underlying causes, including higher rates of various infections (De Jager et al., 2009). Additionally, accumulation of uremic toxins in patients with CKD promotes oxidative activity of leukocytes, which in turn leads to increased leukocyte-endothelial interactions, facilitating higher infiltration of macrophages and monocytes (Cozzolino et al., 2017; Liew et al., 2021). Importantly, the kidneys are a major source of antioxidants against reactive oxygen species causing diminished production of antioxidants to automatically translate in increased oxidative stress in CKD (Cozzolino et al., 2017). Next to directly inducing ED (Annuk et al., 2005), free radicals have been shown to contribute to inflammation (Kröller-Schön et al., 2014).

Overhydration, commonly seen in patients with end stage renal failure (Wizemann and Schilling, 1995; Wizemann et al., 1995), has been reported to associate with ED and microinflammation (Mitsides et al., 2017) contributing to arterial stiffness (Akdam et al., 2014), atherosclerosis, left ventricular hypertrophy (Bock and Gottlieb, 2010) and more CV events (Hung et al., 2014; Tsai et al., 2015). Interestingly, the interpretation of this association differs between authors with some concluding that ED leads to volume overload due to its role in water homeostasis (Levick and Michel, 2010; MacHnik et al., 2010; Paar et al., 2014; Dekker et al., 2017) whereas Colombo et al. posed that volume overload contributes to ED due to vascular stretch (Colombo et al., 2009, 2014). In fact, the damaging effect of overhydration on the endothelium may be due to increased shear stress as has been suggested by studies in patients with hypertension (Panza et al., 1990; Muiesan et al., 2001). Notably, endothelial cells can sense shear stress, hydrostatic pressure and stretch of the vessel wall through mechanosensors which can then be transferred into signaling pathways. Subsequently, gene and protein expression can be modified and endothelial function can deteriorate (Mammoto et al., 2012). The eGC functions as a mechanosensor of shear stress but at the same time pathologic shear stress might directly lead to eGC changes (Weinbaum et al., 2007) such as breakdown and shedding of eGC components (Zeng and Tarbell, 2014).

Clinical studies previously used indirect methods to demonstrate ED in CKD and its association with inflammation and volume overload (i.e., association analyses and imaging of the perfused boundary region) leaving open questions about possible targets for patient intervention. With the current work we aimed to investigate possible eGC loss and ED in skin biopsies of CKD patients by direct tissue staining and its association with inflammation and volume overload.

## PATIENTS AND METHODS

### Study Population

During living kidney transplantation procedure, abdominal skin biopsies were taken from 11 patients with chronic kidney disease stage 5 (CKD5) of whom 4 were treated with hemodialysis (CKD5D) and 7 did not receive dialysis treatment (CKD5ND). Nine healthy kidney donors served as controls as described before (Hijmans et al., 2019). For all individuals, clinical data were obtained from electronic patient files and urine and plasma were collected on the day of the operation or 1 day before. All study participants provided written informed consent prior to study and are enrolled in the Transplantlines Biobank and Cohort study (TXLINES01). The cohort is registered at clinicaltrials.gov as NCT03272841. The study protocol is in accordance with the Dutch Medical Research Involving Human Subjects Act (WMO), and approved by the Medical Ethics Committee of the University Medical Center Groningen (METc 2014/077). All procedures were conducted in accordance with the declarations of Helsinki and Istanbul. Details on the study protocol have been described (Hijmans et al., 2019).

**Abbreviations:** BSA, bovine serum albumin; ED, endothelial dysfunction; eGC, endothelial glycocalyx; CD31, cluster of differentiation 31; CCL2, C-C Motif Chemokine Ligand 2; CKD, chronic kidney disease; CKD5, chronic kidney disease stage 5; CKD5D, chronic kidney disease stage 5 on dialysis; CKD5ND, chronic kidney disease stage 5 not on dialysis; CV, cardiovascular; HES, hydroxyethyl starch; NT-proBNP, N-terminal prohormone of brain natriuretic peptide; PBS, phosphate-buffered saline; UEA1, Ulex europaeus agglutinin-1; VCAM-1, vascular cell adhesion protein 1; VEGFR2, vascular endothelial growth factor receptor-2; vWF, von Willebrand factor.

## Measurement of Dermal Fluid Content

The skin samples for determination of fluid content were weighed immediately after taking the biopsy, which delivered wet weight. Biopsies were then dried overnight in an oven at 80°C after which their dry weight was measured. Water content was calculated as ([wet weight – dry weight] / wet weight) × 100%. Biopsies with macroscopically visible subcutaneous fat deposits were excluded from this analysis due to disturbance of water content determination by fat deposits.

## Immunofluorescence

Immunofluorescence staining was performed on 4-μm-thick cryo sections cut from full thickness skin biopsies with a Leica CM1950 cryostat (Leica Biosystems, Wetzlar, Germany) followed by acetone fixation for 10 min. Endogenous peroxidase activity was blocked by incubating with 0.03% hydrogen peroxide (in phosphate buffered saline; PBS). Skin cryo sections were incubated for 1 h with the following primary antibodies/reagents: Rhodamine-labeled Ulex Europaeus Agglutinin I (UEA1-Rhodamine, Vector Laboratories #RL-1062), rabbit anti-human vWF (DAKO, #A0081, Santa Clara, CA, United States) and rabbit anti-human vascular endothelial growth factor receptor 2 (VEGFR2; clone D5B1, Cell Signaling Technology #9698, Danvers, MA, United States) diluted in PBS/1% Bovine Serum Albumin (BSA). Binding of primary antibodies was detected by incubating the sections for 30 min with a secondary antibody diluted in PBS/1% BSA. We used goat anti-rabbit IgG horseradish peroxidase (HRP, from DAKO) in PBS/1% BSA. Subsequently, Alexa488-conjugated mouse anti-human CD31 antibody (Abcam, ab215911, Cambridge, United Kingdom) diluted in 1% BSA was applied for 60 min. Horseradish peroxidase conjugated antibodies were visualized by the TSA TM tetramethylrhodamine system (PerkinElmer Life Sciences Inc., Waltham, MA, United States) (10 min). DAPI solution (Vector laboratories, Burlingame, CA, United States) was applied to the sections and incubated for 10 min for nuclear staining and subsequently mounted in Citifluor mounting medium (fluorescence; Sigma-Aldrich, Burlington, VT, United States). The whole staining procedure was carried out at room temperature. As negative controls, the primary antibody or lectin were replaced by PBS/1% BSA and were all found to be negative.

## Quantification of Immunofluorescence

Stainings were evaluated on a Leica DM4000B microscope (Leica Biosystems Wetzlar, Germany) equipped for immunofluorescence, and with a DFX345FX camera using a LAS software package. Five images at 20 × magnification per skin sample were taken followed by digital quantification using ImageJ 1.46r (Rasband, W.S., US National Institutes of Health). We used the pan-endothelial marker CD31 to identify vascular endothelium. To normalize for differences in vascular density and to differentiate endothelia from other cell types, the markers of interest (UEA1, VEGFR2, and vWF) were double stained with CD31. Only CD31-positive areas were quantified, and markers were expressed as a percentage/ proportion of CD31-positive pixels. Subsequently, the average percentages of five images were taken to receive a single value for each patient/ skin sample.

## Statistics

Data are shown as mean ± standard deviation (SD) if normally distributed and as median (interquartile range) if not normally distributed. Comparisons between groups were performed by Mann–Whitney *U* test, or Kruskal-Wallis-test if more than two groups were compared. Parameters were log-transformed for association studies using Spearman Rank correlation coefficient. Statistical analyses were performed using SPSS 25.0 (SPSS Inc., Chicago, IL, United States). *P*-values below 0.05 were considered to be statistically significant.

# RESULTS

## Clinical Characteristics

Baseline characteristics before surgery are presented in **Table 1**. Among CKD patients, those with CKD5D and CKD5ND were age- and sex-matched, whereas healthy donors were ∼10 years older and comprised a higher proportion of female participants than the CKD patient group. Body mass index (BMI) and blood pressure did not differ (significantly) between the donors and patients with CKD5D or CKD5ND. The most common diseases in both CKD patient groups were IgA nephropathy, focal segmental glomerulosclerosis, autosomal-dominant polycystic kidney disease and glomerulonephritis. As expected, CKD patients had more co-morbidities compared to the donor control group, especially hypertension (36% vs. 11%), coronary heart disease (9% vs. 0%) and diabetes mellitus (9% vs. 0%). Overhydration in CKD patients was evidenced by increased values of NT-proBNP compared to controls ($P < 0.01$), both in CKD5D ($P < 0.01$) and CKD5ND patients ($P < 0.01$). In addition, fluid overload was demonstrated by decreased plasma sodium levels in CKD patients ($P = 0.03$), especially in patients with CKD5D compared to controls ($P = 0.03$). Increased CRP levels in CKD5D ($P = 0.03$) and decreased levels of plasma lymphocyte counts in CKD patients ($P < 0.01$) were seen compared to healthy subjects, especially in patients CKD5D ($P < 0.01$). This reflects an increased inflammatory status of CKD patients.

## Endothelial Dysfunction in Dermal Biopsies of Patients With Renal Failure

The analysis of vessel number, vessel area/vessel number and total vessel area (CD31) revealed no significant differences between the three groups (**Figures 1A–C**), indicating neither dermal angiogenesis nor hyperaemia in CKD patients. Values of dermal water content were comparable between groups, showing no dermal edema in CKD patients (**Table 1**).

To correct for apparent differences in vascular surface area between samples and to distinguish endothelia from other cell types, we exclusively evaluated the endothelial markers

**TABLE 1 |** Baseline characteristics of donors and all CKD patients (CKD5D and CKD5ND) just before surgery.

| | Healthy donors(*N* = 9) | CKD patients(*N* = 11) | | |
|---|---|---|---|---|
| **Variables** | | **All(*N* = 11)** | **CKD5D patients(*N* = 4)** | **CKD5ND patients(*N* = 7)** |
| **Age (years)** | 60 ± 8 | 51 ± 10 | 49 ± 10 | 52 ± 11 |
| **Women, n (%)** | 6 (67) | 5 (46) | 2 (50) | 3 (43) |
| **BMI (kg/m$^2$)** | 27.1 ± 4.6 | 25.4 ± 3.9 | 28.6 ± 3.9 | 23.6 ± 2.7 |
| **Blood pressure (mmHg)** | | | | |
| Systolic | 135 ± 16 | 146 ± 17 | 144 ± 11 | 147 ± 21 |
| Diastolic | 76 ± 11 | 82 ± 15 | 76 ± 18 | 86 ± 14 |
| **Time on dialysis (months)** | – | – | 14 (12–19) | – |
| **Underlying disease (%)** | | | | |
| IgA nephropathy | 0 | 18 | 25 | 14 |
| Focal segmental glomerulosclerosis | 0 | 9 | 25 | 0 |
| Autosomal-dominant polycystic kidney disease | 0 | 27 | 25 | 29 |
| Glomerulonephritis | 0 | 27 | 25 | 29 |
| Other | 0 | 19 | 0 | 28 |
| **Known comorbidities (%)** | | | | |
| Hypertension | 11 | 36 | 50 | 29 |
| Malignancy | 11 | 9 | 0 | 14 |
| Coronary heart disease | 0 | 9 | 0 | 14 |
| Diabetes mellitus | 0 | 9 | 25 | 0 |
| Other | 11 | 19 | 25 | 14 |
| No relevant comorbidities | 67 | 18 | 0 | 29 |
| **Laboratory parameters** | | | | |
| Serum creatinine (μmol/L) | 68 (63–83) | 516 (460–655)** | 811 (6045–1096)** | 462 (442–516)** |
| eGFR (mL/min/1.73 m$^2$) | 91 (81–94) | 11 (8–14)** | – | 11 (10–14)** |
| Serum albumin (g/L) | 44 (43–45) | 43 (42–46) | 43 (40–45) | 43 (42–50) |
| Urine creatinine (mmol/L) | 4 (4–16) | 6 (4–9) | 11 (6–11) | 5 (3–8) |
| Proteinuria (g/L) | 0.4 (0.3–0.6) | 1.9 (0.3–3.4)** | 2.3 (1.9–2.3)* | 0.4 (0.3–6.6) |
| **Volume markers** | | | | |
| Plasma NT-proBNP (pg/mL) | 80 (28–99) | 512 (282–861)** | 666 (318–1481)* | 399 (242–701)* |
| Plasma sodium (mmol/L) | 141 (140–143) | 139 (137–140)* | 138 (137–140)* | 139 (138–142) |
| Tissue fluid content (%) | 62 (60–66) | 61 (60–62) | 62 (59–63) | 61 (61–62) |
| **Inflammatory plasma markers** | | | | |
| CRP (mg/l) | 1.2 (0.6–1.8) | 2.3 (0.5–9.0) | 8.5 (4.3–9.8)* | 0.6 (0.3–3.5) |
| Leukocytes (× 10$^E$9/mL) | 6.6 (6.1–7.8) | 6.8 (5.5–10,0) | 8.9 (6.1–10.2) | 5.9 (5.4–9.6) |
| Monocytes (× 10$^E$9/mL) | 0.5 (0.5–0.6) | 0.5 (0.4–0.7) | 0.7 (0.4–0.9) | 0.4 (0.3–0.6) |
| Lymphocytes (× 10$^E$9/mL) | 1.8 (1.8–2.2) | 1.3 (1.1–1.6)** | 1.5 (1.3–1.6)** | 1.2 (0.9–1.4)* |

**Significantly different compared to healthy donors (*P < 0.05; **P < 0.01).*

in a double staining with CD31. The endothelium in skin biopsies of CKD patients showed severe loss of the eGC marker UEA1 as compared to healthy controls ($P < 0.01$). Upon separation of the CKD patients, CKD5D patients ($P < 0.01$) as well as CKD5ND patients ($P < 0.01$) showed a severe decline in UEA1 compared to controls. Representative photomicrographs and results of quantitative analyses are shown in **Figure 2**.

Quantification of endothelial VEGFR2 expression showed a small increase in CKD patients compared to healthy individuals, although not statistically significant for the whole CKD group ($P = 0.65$). When looking closer, only CKD5D patients appeared to have this rise with a borderline significance compared to controls ($P = 0.05$). CKD5D patients had significantly higher VEGFR2 expression than CKD5ND patients, indicating endothelial activation ($P < 0.05$) (**Figure 3**).

For the endothelial marker vWF, only one patient showed very high levels whereas all other CKD patients had rather similar values in comparison to controls ($P = 0.82$; **Figure 4**).

## Endothelial Dysfunction Associates With Volume Overload Rather Than Inflammation

As presented in **Table 2** and **Figure 5**, the tissue markers of ED UEA1, VEGFR2, and vWF were associated with plasma markers of overhydration. The volume marker NT-proBNP inversely associated with UEA1 ($R = -0.50$; $P < 0.01$; **Figure 5A**). NT-proBNP also correlated significantly with VEGFR2 ($R = 0.29$; $P = 0.03$; **Figure 5B**) and with vWF ($R = 0.29$; $P = 0.03$). Plasma levels of sodium (with lower levels suggesting volume overload) significantly associated with the endothelial tissue

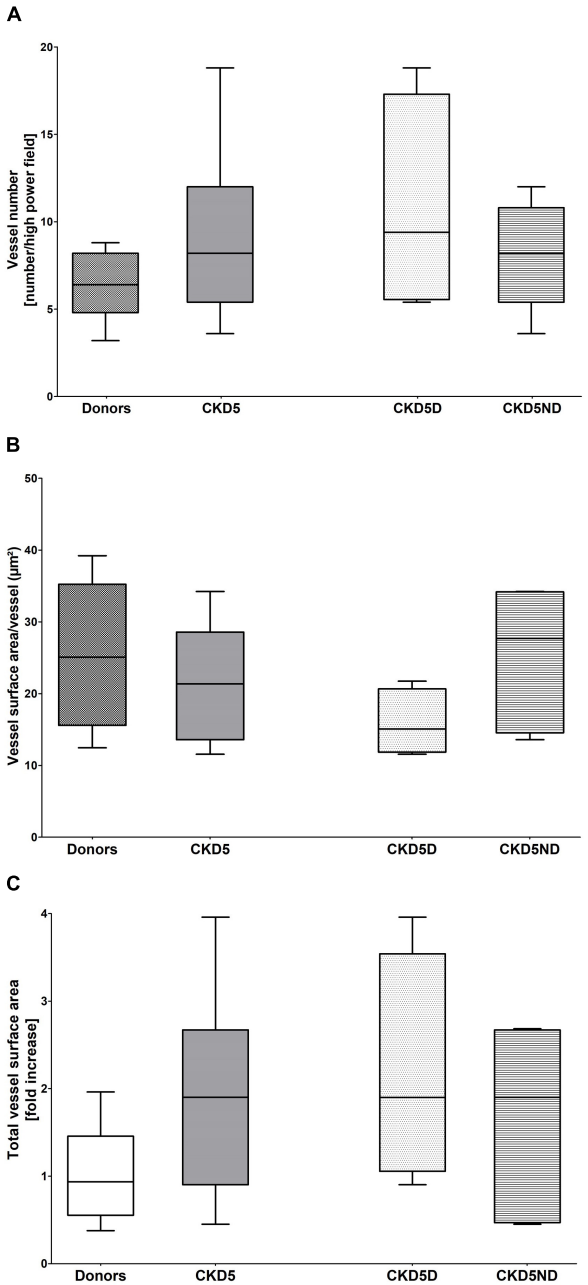


**FIGURE 1 |** Vessel quantification based on CD31 immunofluorescence in healthy donors vs. CKD patients including CKD5ND and CKD5D patients. **(A)** Number of CD31+ vessels per group. **(B)** CD31+ vessel surface area per vessel (total CD31+ vessel surface area / vessel number) in $\mu m^2$. **(C)** Total surface area of CD31 expression in fold increase. Differences are not statistically significant.

marker UEA1 ($R = 0.69$; $P < 0.01$; **Figure 5C**) and showed an inverse relationship with tissue VEGFR2 ($R = -0.54$; $P = 0.01$; **Figure 5D**).

Plasma markers of inflammation did barely associate with endothelial tissue markers (**Table 2**), except for plasma lymphocytes correlating with UEA1 ($R = 0.69$; $P < 0.01$). Additionally, we found significant associations between NT-proBNP and CRP ($R = 0.31$; $P = 0.01$), NT-proBNP and blood lymphocytes ($R = -0.60$; $P < 0.01$) and between plasma sodium and blood lymphocyte number ($R = 0.64$; $P < 0.01$) showing a link between volume and inflammation parameters.

## DISCUSSION

This study is the first to show direct evidence of dermal glycocalyx loss and ED in patients with CKD. In line with previous research, our results show that ED associates with volume overload rather than inflammation, emphasizing the importance of strict volume control in patients with CKD5. In fact, ED was associated with severe loss of the eGC marker UEA1 in endothelial cells of the dermal microcirculation of patients with CKD stage 5. Moreover, we found increased dermal endothelial expression levels of VEGFR2 in hemodialysis patients. A clear association between ED and volume overload was evidenced by elevated plasma levels of NT-proBNP and reduced plasma levels of sodium in CKD5 patients that significantly correlated with the tissue endothelial markers UEA1 and VEGFR2; and tissue vWF associating with plasma levels of NT-proBNP. We hardly found associations between plasma markers of inflammation and markers of ED in dermal biopsies. Together, these results suggest that dermal ED in CKD patients is associated with overhydration rather than with inflammation.

Chronic kidney disease stage 5 patients in our cohort clearly showed ED as evidenced by decreased UEA1 expression, and increased tissue VEGFR2 and vWF compared to healthy subjects. In this study, especially the breakdown of the eGC in CKD5 patients was striking as indicated by severe loss of the UEA1 glyco-epitope. Breakdown of eGC was significantly present in both CKD patient groups, but showed a tendency to be higher in patients with CKD5D than in those with CKD5ND. Breakdown of the eGC in CKD patients has been shown before by several indirect methods. Vlahu et al. (2012) used sidestream darkfield imaging to visualize the sublingual microcirculation. Other study groups showed similar results using the same technique in CKD patients (Dane et al., 2014; Mitsides et al., 2018). Several more publications reported glycocalyx components such as hyaluronan and syndecan-1 in plasma to be associated with eGC breakdown in CKD patients (Padberg et al., 2014; Liew et al., 2021). Moreover, Padberg et al. (2014) used atomic force microscopy to directly measure eGC in a CKD rat model. Here, they found decreased eGC thickness and stiffness which correlated with plasma biomarkers of ED such as vWF (Padberg et al., 2014).

In this study, we found strong associations between ED and volume overload in CKD patients. Increased plasma levels of NT-proBNP were present in all CKD patients as well as reduced sodium values, most outspoken in patients with CKD5D. NT-proBNP significantly associated with the tissue endothelial markers UEA1, VEGFR2, and vWF whereas plasma sodium associated with UEA1 and VEGFR2. The association between ED and volume overload has been shown before by several other groups that reported breakdown of the endothelial glycocalyx (Chappell et al., 2014; Mitsides et al., 2017) and elevated plasma

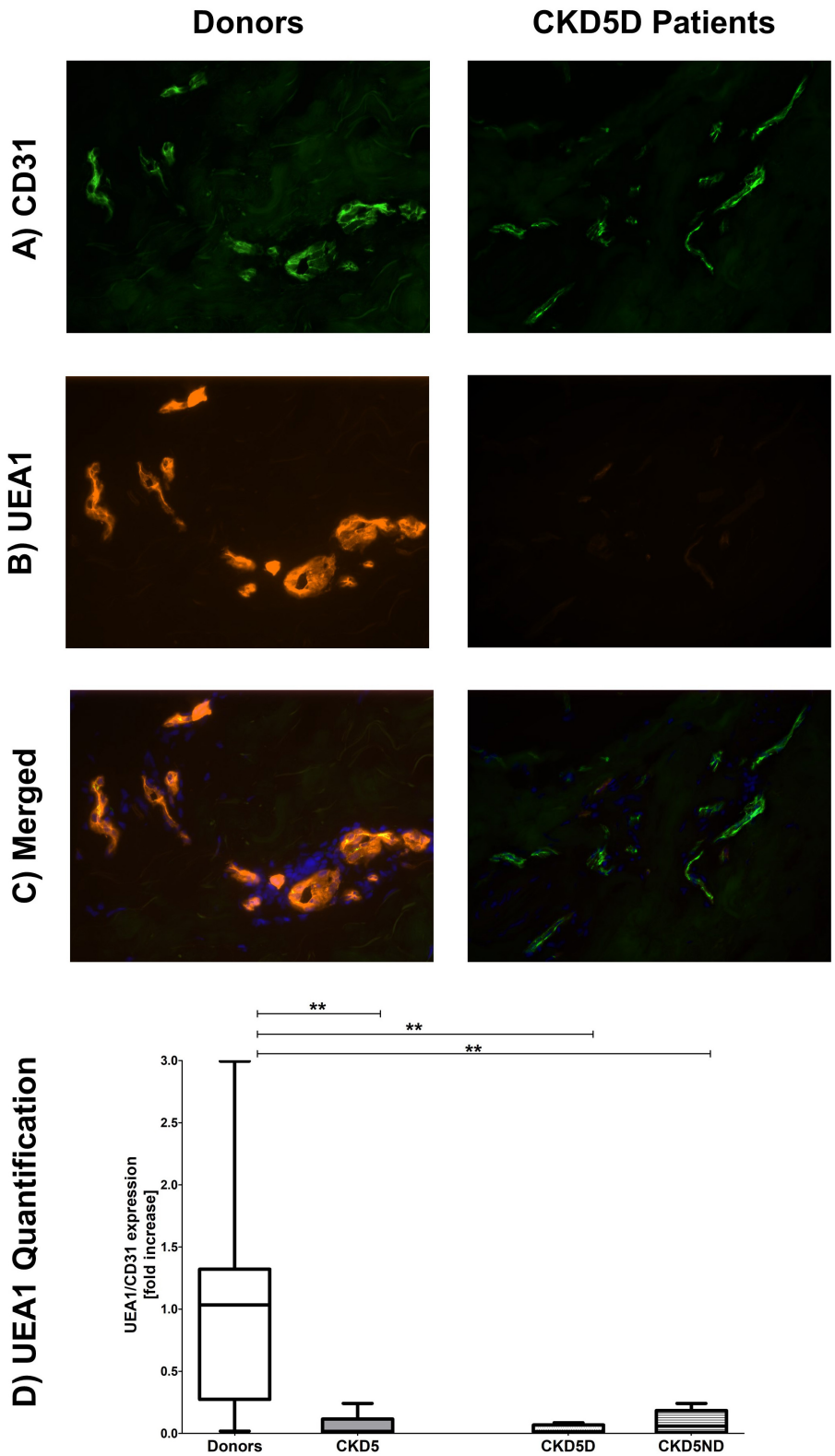


**FIGURE 2 |** Expression of UEA1 in the microvasculature of dermal biopsies patients with CKD. **(A)** Expression of CD31 in donors (left image) and CKD5D patients (right image). **(B)** Expression of UEA1 in donors (left image) and CKD5D patients (right image). **(C)** Merged expression of UEA1 and CD31 in donors (left image) and CKD5D patients (right image). **(D)** UEA1 quantification relative to CD31. Colors in images: green = CD31; red = UEA1; blue = DAPI. Statistical significance: $^{**}P < 0.01$.

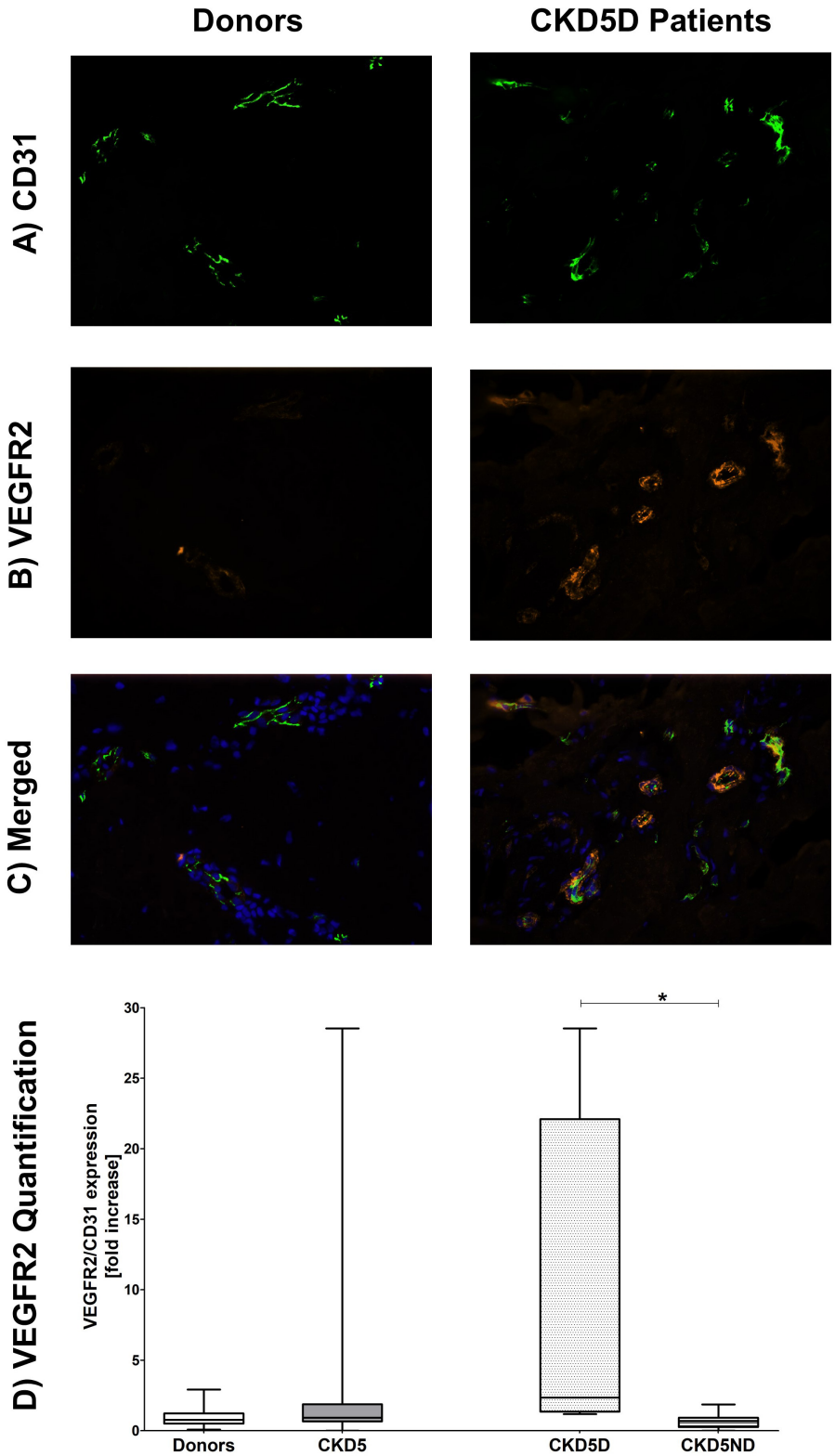


**FIGURE 3 |** Expression of VEGFR2 in the microvasculature of dermal biopsies in patients with CKD. **(A)** Expression of CD31 in donors (left image) and CKD5D patients (right image). **(B)** Expression of VEGFR2 in donors (left image) and CKD5D patients (right image). **(C)** Merged expression of VEGFR2 and CD31 in donors (left image) and CKD5D patients (right image). **(D)** VEGFR2 quantification with VEGFR2 expression relative to CD31. Colors in images: green = CD31; red = VEGFR2; blue = DAPI. Statistical significance: $^*P < 0.05$.

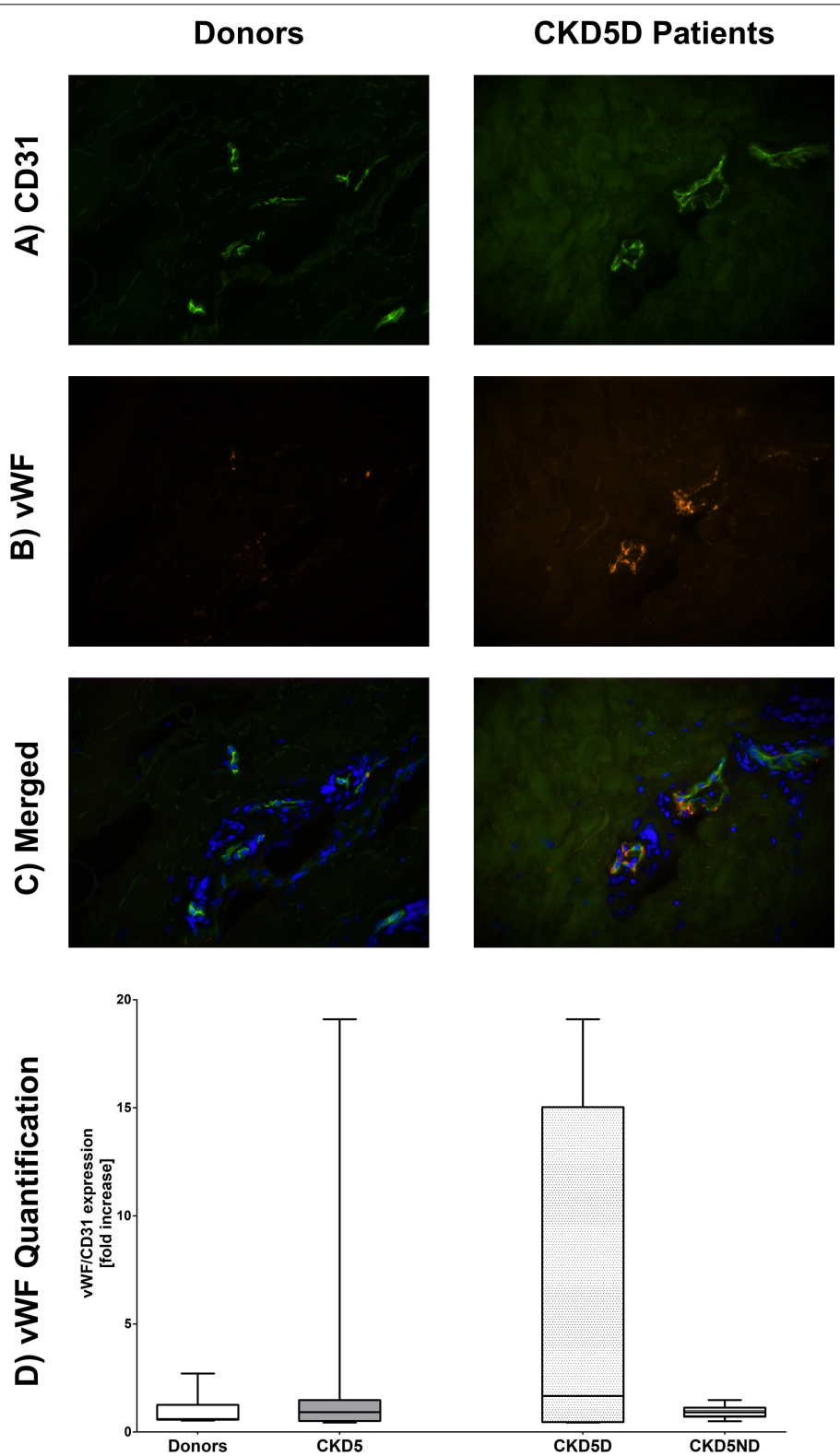


**FIGURE 4 |** Expression of vWF in the microvasculature of dermal biopsies in patients with CKD. **(A)** Expression of CD31 in donors (left image) and CKD5D patients (right image). **(B)** Expression of vWF in donors (left image) and CKD5D patients (right image). **(C)** Merged expression of vWF and CD31 in donors (left image) and CKD5D patients (right image). **(D)** vWF quantification with vWF expression relative to CD31. Colors in images: green = CD31; red = vWF; blue = DAPI. Differences between groups are not statistically significant.

**TABLE 2 |** Linear regression analysis of quantified tissue endothelial markers and laboratory parameters with plasma markers for volume and inflammation.

| | Plasma markers of volume overload | | Plasma markers of inflammation | |
|---|---|---|---|---|
| | **NT-proBNP (↑)** | **Sodium (↓)** | **CRP (↑)** | **Lymphocytes (↓)** |
| **Tissue endothelial markers** | | | | |
| UEA1 (↓) | ***R = −0.50; P < 0.01*** | ***R = 0.69; P < 0.001*** | ***R = −0.44; P = 0.07*** | ***R = 0.69;P = 0.002*** |
| VEGFR2 (↑) | ***R = 0.29; P = 0.03*** | ***R = −0.54; P < = 0.05*** | *R* = 0.11; *P* = 0.24 | ***R = 0.34;P = 0.61*** |
| vWF (↑) | ***R = 0.29; P = 0.03*** | *R* = 0.28; *P* = 0.54 | *R* = 0.11; *P* = 0.90 | *R* = 0.26;*P* = 0.18 |
| **Patient characteristics** | | | | |
| Age | *R* = −0.38;*P* = 0.16 | *R* = 0.11;*P* = 0.66 | *R* = 0.15;*P* = 0.56 | *R* = 0.04;*P* = 0.89 |
| BMI | *R* = 0.05;*P* = 0.86 | *R* = −0.36;*P* = 0.14 | *R* = −0.29;*P* = 0.26 | *R* = −0.39;*P* = 0.14 |
| Systolic blood pressure | *R* = 0.18;*P* = 0.53 | *R* = −0.17;*P* = 0.50 | *R* = −0.25;*P* = 0.33 | *R* = −0.47;*P* = 0.06 |
| Diastolic blood pressure | *R* = 0.20;*P* = 0.48 | *R* = 0.07;*P* = 0.79 | *R* = 0.10;*P* = 0.72 | *R* = 0.07;*P* = 0.80 |
| **Laboratory parameters** | | | | |
| Serum creatinine | ***R = 0.68P < 0.01*** | *R* = −0.27*P* = 0.27 | *R* = −0.25*P* = 0.34 | ***R = −0.71P < 0.01*** |
| eGFR | ***R = −0.63P = 0.02*** | *R* = 0.09*P* = 0.73 | *R* = −0.04*P* = 0.99 | ***R = 0.58P = 0.03*** |
| Serum albumin | *R* = −0.15*P* = 0.60 | *R* = 0.32*P* = 0.20 | *R* = −0.16*P* = 0.56 | *R* = −0.27*P* = 0.33 |
| Urine creatinine | ***R = −0.68P < 0.01*** | *R* = −0.71*P* = 0.27 | ***R = −0.25P < 0.01*** | ***R = −0.71P < 0.01*** |
| Proteinuria | *R* = 0.42*P* = 0.16 | ***R = −0.71P < 0.01*** | *R* = −0.20*P* = 0.50 | ***R = −0.70P = 0.01*** |
| **Markers of volume overload** | | | | |
| Plasma NT-proBNP | – | ***R = −0.45;P = 0.04*** | ***R = 0.56;P = 0.01*** | ***R = −0.60;P < 0.01*** |
| Plasma sodium | – | – | *R* = −0.33;*P* = 0.14 | ***R = 0.64;P < 0.01*** |
| Tissue fluid content | *R* = 0.35*P* = 0.17 | *R* = −0.06*P* = 0.81 | *R* = 0.43*P* = 0.07 | *R* = 0.07*P* = 0.79 |
| **Plasma markers of inflammation** | | | | |
| CRP | ***R = 0.56P = 0.01*** | *R* = −0.33*P* = 0.14 | – | *R* = −0.19*P* = 0.42 |
| Leukocytes | *R* = 0.13*P* = 0.59 | *R* = 0.26*P* = 0.22 | *R* = 0.26*P* = 0.25 | *R* = 0.36*P* = 0.12 |
| Monocytes | *R* = 0.05*P* = 0.83 | *R* = 0.07*P* = 0.78 | *R* = −0.13*P* = 0.60 | *R* = 0.26*P* = 0.27 |
| Lymphocytes | ***R = −0.61P < 0.01*** | ***R = 0.64P < 0.01*** | *R* = −0.19*P* = 0.42 | – |

*Arrows next to parameters indicate the direction of value change in CKD patients. Significant results are shown in bold italics.*

levels of the endothelial markers vascular cell adhesion protein 1 (VCAM-1) and thrombomodulin (Mitsides et al., 2017). Indeed, Chappell et al. observed that inducing acute hypervolemia by infusing 20 mL/kg body weight of an iso-oncotic hydroxyethyl starch (HES) colloid solution (6% HES 130/0.4, Volulyte) led to shedding of the endothelial glycocalyx as evidenced by a significant increase in plasma levels of atrial natriuretic peptide and a rise in serum hyaluronan and serum and urine syndecan-1 (Chappell et al., 2014). In our study, we did not find differences between CKD patients and healthy controls with regard to dermal fluid content. Thus, we can only assume that volume overload was predominantly intravascular. We speculate that this could have led to vascular stretch and, subsequently, to ED. Previous research showed endothelial cell activation after vascular stretch from acute volume loading (central venous pressure ≥20 mmHg). After that, the vascular endothelium of healthy dogs showed increased mRNA levels of cyclooxygenase 2 and induced nitric oxide synthase which resulted from activation of the inflammatory/oxidative and hemostatic programs, similar to dogs suffering from heart failure (Colombo et al., 2009). More studies indicated ED and subsequent atherosclerosis after excessive vascular stretch (Hatami et al., 2013) as it is seen in hypertension, heart and kidney failure. Here, vascular remodeling took place after pathologic stretch with subsequent cell apoptosis, inflammation and the production of reactive oxygen species (Okada et al., 1998; Lemarié et al., 2010) and [reviewed by Jufri et al. (2015)]. In addition, cell differentiation from endothelial cell to smooth muscle cell has been observed after application of vascular stretch (Cevallos et al., 2006). In our cohort, endothelial VEGFR2 expression was significantly upregulated in dialysis patients. It has been demonstrated that VEGFR2 can get activated upon binding with its ligands VEGFA, VEGFC or VEGFD leading to endothelial cell proliferation, angiogenesis, cell survival but also to vascular permeability [reviewed by Lohela et al. (2009)]. Our study could neither show signs of angiogenesis nor of dermal edema. Nevertheless, higher values of VEGFR2 were only seen in CKD5D patients and a direct association between NT-proBNP and VEGFR2 was observed. It has been shown that stretching of the vasculature might directly induce VEGFR2 expression which can be interpreted as an endothelial stress response (Smith et al., 2001; Tian et al., 2016).

According to our data, dialysis patients showing eGC damage had significantly increased CRP values. In a previous publication on this cohort, we showed increased inflammation in dermal biopsies of CKD5D patients with increased levels of tissue macrophages and T-cells. Besides, dermal endothelial stainings of the chemokine C-C Motif Chemokine Ligand 2 (CCL2) and hyaluronan were performed. Moreover, we performed quantitative RT-PCR on CCL2, VCAM-1, and three hyaluronan enzymes. These data showed significant loss of hyaluronan

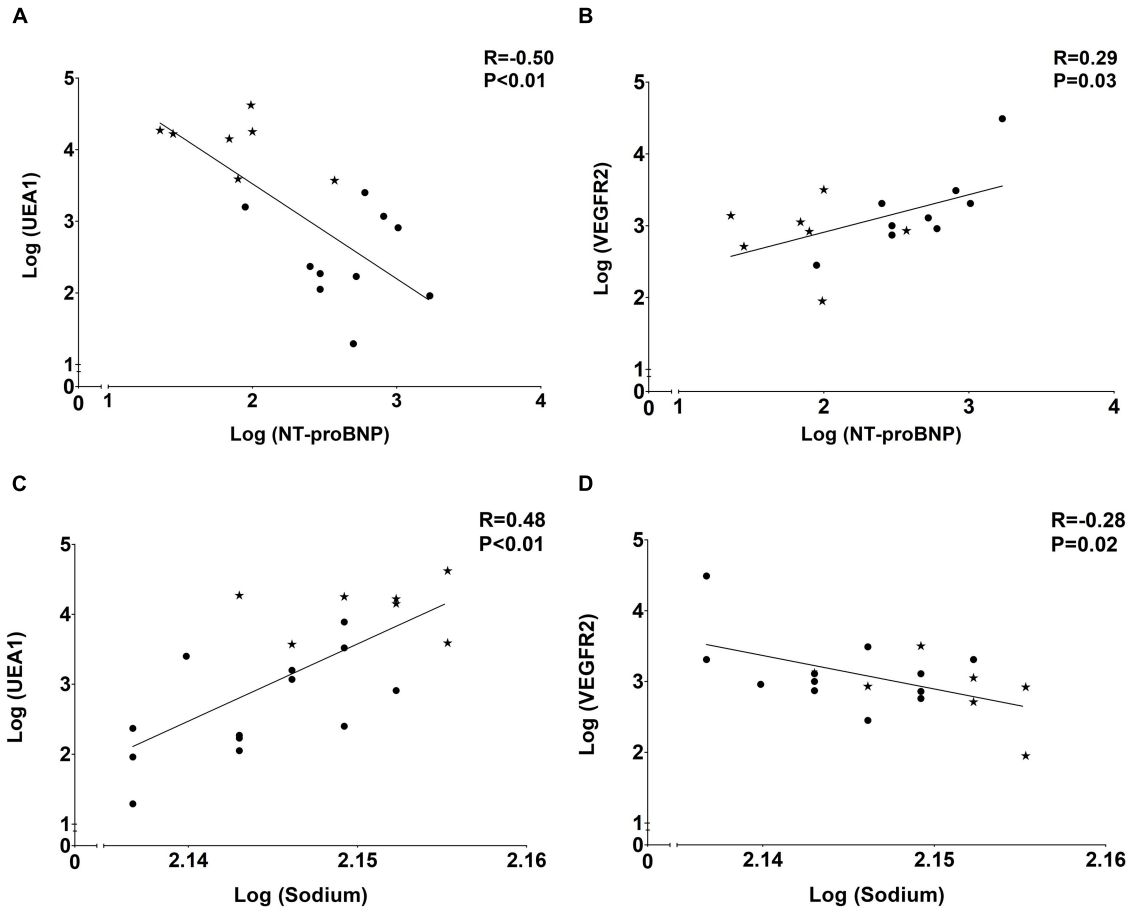


**FIGURE 5 |** Associations of plasma volume markerswith tissue endothelial markers. **(A)** Negative association of eGC marker UEA1 and volume marker NT-proBNP. **(B)** Positive association of endothelial marker VEGFR2 and volume marker NT-proBNP. **(C)** Positive association of eGC marker UEA1 and volume marker sodium. **(D)** Negative association of endothelial marker VEGFR2 and volume marker sodium. Dots represent CKD5 patients and stars indicate controls.

staining, which is in full agreement with our data on UEA1 in the current report. Moreover, we showed a significant inverse association of quantitative mRNA expression of hyaluronan synthase 2 with the quantitative mRNA expression of CCL2. These data suggest that dermal inflammation in CKD5 patients is quantitatively associated with loss of hyaluronan (Hijmans et al., 2019). In the present study we found an association between plasma lymphocytes and tissue UEA1 suggesting an association between glycocalyx breakdown and lymphocytopenia, thus with inflammation which is in accordance with published research (Moseley et al., 1997; Vigetti et al., 2010; Oberleithner et al., 2011; Vlahu et al., 2012). In the (above-mentioned) study of Vlahu et al. (2012), the eGC breakdown was indeed related to inflammation in dialysis patients with elevated CRP values (>10 mg/L) having significantly increased perfused boundary regions. Besides, Kusche-Vihrog et al. (2011) have directly measured eGC stiffness of human endothelial cells (Eahy.924) by atomic force microscopy and demonstrated an increase in eGC stiffness after incubation with CRP. Subsequently, fluid permeability increased (Kusche-Vihrog et al., 2011). More *in vitro* studies reported reactive oxygen species and inflammatory cytokines such as tumor necrosis factor-α to lead to hyaluronan degradation in the glycocalyx of endothelial cells and polymorphonuclear leukocytes (Moseley et al., 1997; Vigetti et al., 2010). Importantly, inflammation might also be linked to (and probably induced by) overhydration as has been shown by this work and other researchers [reviewed by Colombo et al. (2008)]. Our study showed signs of generalized inflammation with increased CRP and lymphocytopenia, with the latter being associated with eGC breakdown. Thus, although the associations of increased vascular volume with ED are much stronger, we cannot exclude the potential contribution of a chronic inflammatory state to ED in patients with CKD.

This study has several limitations. Firstly, as we observed more co-morbidities such as hypertension, coronary heart disease or diabetes in CKD patients compared to healthy controls, we cannot exclude that our results were influenced by a difference in comorbidity burden. Nevertheless, high blood pressure seemed to be treated quite well considering the comparable blood pressure between CKD patients and healthy donors. Moreover, there was only one diabetic CKD patient in the CKD study group. Secondly, we observed variability within each group which can reflect

biological variability in microvascular density and/or sampling error. Lastly, we only had access to a small number of patients which limits the validity of our results.

To conclude, this study is the first to show direct evidence of dermal glycocalyx loss and ED in patients with CKD. Moreover, plasma markers of volume overload were associated with tissue markers of endothelial breakdown (i.e., glycocalyx) and endothelial activation (i.e., VEGFR2 and vWF). Although our results argue for strict volume control in CKD patients, future studies should address whether such an approach is capable of attenuating the eGC loss and ED in these patients.

## DATA AVAILABILITY STATEMENT

The original contributions presented in the study are included in the article/supplementary material, further inquiries can be directed to the corresponding author.

## ETHICS STATEMENT

The studies involving human participants were reviewed and approved by the study protocol is in accordance with the Dutch Medical Research Involving Human Subjects Act (WMO), and approved by the Medical Ethics Committee of the University Medical Center Groningen (METc 2014/077). All procedures were conducted in accordance with the declarations of Helsinki and Istanbul. Details on the study protocol have been described (Hijmans et al., 2019). The patients/participants provided their written informed consent to participate in this study.

## AUTHOR CONTRIBUTIONS

JB, CF, RP, SB, and HP conceived and designed the study and made the skin biopsies and clinical data available. JK, RH, MO, and WD performed the laboratory measurements. JK, JB, and CF analyzed and interpreted the data and drafted the manuscript. All authors approved the final version of the manuscript.

## FUNDING

This study was supported by the Jan Kornelis de Cock Foundation (project code O/661264) and the Graduate School of Medical Sciences of the University Medical Center Groningen.

## REFERENCES

Akdam, H., Öğünç, H., Alp, A., Özbek, Ö, Ömürlü, I. K., Yeniçerioğlu, Y., et al. (2014). Assessment of volume status and arterial stiffness in chronic kidney disease. *Ren. Fail.* 36, 28–34. doi: 10.3109/0886022X.2013.830224

Annuk, M., Soveri, I., Zilmer, M., Lind, L., Hulthe, J., and Fellström, B. (2005). Endothelial function, CRP and oxidative stress in chronic kidney disease. *J. Nephrol.* 18, 721–726.

Baigent, C., Burbury, K., and Wheeler, D. (2000). Premature cardiovascular disease in chronic renal failure. *Lancet* 356, 147–152. doi: 10.1016/S0140-6736(00)02456-9

Bock, J. S., and Gottlieb, S. S. (2010). Cardiorenal syndrome: new perspectives. *Circulation* 121, 2592–2600. doi: 10.1161/CIRCULATIONAHA.109.886473

Bonetti, P. O., Lerman, L. O., and Lerman, A. (2003). Endothelial dysfunction: a marker of atherosclerotic risk. *Arterioscler. Thromb. Vasc. Biol.* 23, 168–175. doi: 10.1161/01.ATV.0000051384.43104.FC

Cevallos, M., Riha, G. M., Wang, X., Yang, H., Yan, S., Li, M., et al. (2006). Cyclic strain induces expression of specific smooth muscle cell markers in human endothelial cells. *Differentiation* 74, 552–561. doi: 10.1111/j.1432-0436.2006.00089.x

Chappell, D., Bruegger, D., Potzel, J., Jacob, M., Brettner, F., Vogeser, M., et al. (2014). Hypervolemia increases release of atrial natriuretic peptide and shedding of the endothelial glycocalyx. *Crit. Care* 18:538. doi: 10.1186/s13054-014-0538-5

Colombo, P. C., Onat, D., Harxhi, A., Demmer, R. T., Hayashi, Y., Jelic, S., et al. (2014). Peripheral venous congestion causes inflammation, neurohormonal, and endothelial cell activation. *Eur. Heart J.* 35, 448–454. doi: 10.1093/eurheartj/eht456

Colombo, P. C., Onat, D., and Sabbah, H. N. (2008). Acute heart failure as "acute endothelitis" – interaction of fluid overload and endothelial dysfunction. *Eur. J. Heart Fail.* 10, 170–175. doi: 10.1016/j.ejheart.2007.12.007

Colombo, P. C., Rastogi, S., Onat, D., Zacà, V., Gupta, R. C., Jorde, U. P., et al. (2009). Activation of endothelial cells in conduit veins of dogs with heart failure and veins of normal dogs after vascular stretch by acute volume loading. *J. Card. Fail.* 15, 457–463. doi: 10.1016/j.cardfail.2008.12.006

Constantinescu, A. A., Vink, H., and Spaan, J. A. E. (2003). Endothelial cell glycocalyx modulates immobilization of leukocytes at the endothelial surface. *Arterioscler. Thromb. Vasc. Biol.* 23, 1541–1547. doi: 10.1161/01.ATV.0000085630.24353.3D

Cozzolino, M., Galassi, A., Pivari, F., Ciceri, P., and Conte, F. (2017). The cardiovascular burden in end-stage renal disease. *Contrib. Nephrol.* 191, 44–57. doi: 10.1159/000479250

Dane, M. J. C., Khairoun, M. R., Hyun Lee, D., van den Berg, B. M., Eskens, B. J. M., Boels, M. G. S., et al. (2014). Association of kidney function with changes in the endothelial surface layer. *Clin. J. Am. Soc. Nephrol.* 9, 698–704. doi: 10.2215/CJN.08160813

De Jager, D. J., Grootendorst, D. C., Jager, K. J., Van Dijk, P. C., Tomas, L. M. J., Ansell, D., et al. (2009). Cardiovascular and noncardiovascular mortality among patients starting dialysis. *JAMA J. Am. Med. Assoc.* 302, 1782–1789. doi: 10.1001/jama.2009.1488

Dekker, M. J. E., Marcelli, D., Canaud, B. J., Carioni, P., Wang, Y., Grassmann, A., et al. (2017). Impact of fluid status and inflammation and their interaction on survival: a study in an international hemodialysis patient cohort. *Kidney Int.* 91, 1214–1223. doi: 10.1016/j.kint.2016.12.008

El Nahas, A. M., and Bello, A. K. (2005). Chronic kidney disease: the global challenge. *Lancet* 365, 331–340. doi: 10.1016/S0140-6736(05)17789-7

Fox, C. S., Matsushita, K., Woodward, M., Bilo, H. J. G., Chalmers, J., Lambers Heerspink, H. J., et al. (2012). Associations of kidney disease measures with mortality and end-stage renal disease in individuals with and without diabetes: a meta-analysis. *Lancet* 380, 1662–1673. doi: 10.1016/S0140-6736(12)61350-6

Gansevoort, R. T., Correa-Rotter, R., Hemmelgarn, B. R., Jafar, T. H., Heerspink, H. J. L., Mann, J. F., et al. (2013). Chronic kidney disease and cardiovascular risk: epidemiology, mechanisms, and prevention. *Lancet* 382, 339–352. doi: 10.1016/S0140-6736(13)60595-4

Go, A. S., Chertow, G. M., Fan, D., McCulloch, C. E., and Hsu, C. (2004). Chronic kidney disease and the risks of death, cardiovascular events, and hospitalization. *N. Engl. J. Med.* 351, 1296–1305. doi: 10.1056/NEJMoa041031

Hatami, J., Tafazzoli-Shadpour, M., Haghighipour, N., Shokrgozar, M. A., and Janmaleki, M. (2013). Influence of cyclic stretch on mechanical properties of endothelial cells. *Exp. Mech.* 53, 1291–1298. doi: 10.1007/s11340-013-9744-3

Henry, C. B. S., and Duling, B. R. (1999). Permeation of the luminal capillary glycocalyx is determined by hyaluronan. *Am. J. Physiol. Hear. Circ. Physiol.* 277, H508–H514. doi: 10.1152/ajpheart.1999.277.2.h508

Herzog, C. A., Asinger, R. W., Berger, A. K., Charytan, D. M., Díez, J., Hart, R. G., et al. (2011). Cardiovascular disease in chronic kidney disease. a clinical update

from kidney disease: improving global outcomes (KDIGO). *Kidney Int.* 80, 572–586. doi: 10.1038/ki.2011.223

Hijmans, R. S., Van Londen, M., Sarpong, K. A., Bakker, S. J. L., Navis, G. J., Storteboom, T. T. R., et al. (2019). Dermal tissue remodeling and non-osmotic sodium storage in kidney patients. *J. Transl. Med.* 17:88. doi: 10.1186/s12967-019-1815-5

Hung, S. C., Kuo, K. L., Peng, C. H., Wu, C. H., Lien, Y. C., Wang, Y. C., et al. (2014). Volume overload correlates with cardiovascular risk factors in patients with chronic kidney disease. *Kidney Int.* 85, 703–709. doi: 10.1038/ki.2013.336

Jufri, N. F., Mohamedali, A., Avolio, A., and Baker, M. S. (2015). Mechanical stretch: physiological and pathological implications for human vascular endothelial cells. *Vasc. Cell* 7:8. doi: 10.1186/s13221-015-0033-z

Kröller-Schön, S., Steven, S., Kossmann, S., Scholz, A., Daub, S., Oelze, M., et al. (2014). Molecular mechanisms of the crosstalk between mitochondria and NADPH oxidase through reactive oxygen species – studies in white blood cells and in animal models. *Antioxid. Redox Signal.* 20, 247–266. doi: 10.1089/ars.2012.4953

Kusche-Vihrog, K., Urbanova, K., Blanqué, A., Wilhelmi, M., Schillers, H., Kliche, K., et al. (2011). C-reactive protein makes human endothelium stiff and tight. *Hypertension* 57, 231–237. doi: 10.1161/HYPERTENSIONAHA.110.163444

Lemarié, C. A., Tharaux, P. L., and Lehoux, S. (2010). Extracellular matrix alterations in hypertensive vascular remodeling. *J. Mol. Cell. Cardiol.* 48, 433–439. doi: 10.1016/j.yjmcc.2009.09.018

Levick, J. R., and Michel, C. C. (2010). Microvascular fluid exchange and the revised Starling principle. *Cardiovasc. Res.* 87, 198–210. doi: 10.1093/cvr/cvq062

Liew, H., Roberts, M. A., Pope, A., and McMahon, L. P. (2021). Endothelial glycocalyx damage in kidney disease correlates with uraemic toxins and endothelial dysfunction. *BMC Nephrol.* 22:21. doi: 10.1186/s12882-020-02219-4

Lohela, M., Bry, M., Tammela, T., and Alitalo, K. (2009). VEGFs and receptors involved in angiogenesis versus lymphangiogenesis. *Curr. Opin. Cell Biol.* 21, 154–165. doi: 10.1016/j.ceb.2008.12.012

MacHnik, A., Dahlmann, A., Kopp, C., Goss, J., Wagner, H., Van Rooijen, N., et al. (2010). Mononuclear phagocyte system depletion blocks interstitial tonicity-responsive enhancer binding protein/vascular endothelial growth factor c expression and induces salt-sensitive hypertension in rats. *Hypertension* 55, 755–761. doi: 10.1161/HYPERTENSIONAHA.109.143339

Mahmoodi, B. K., Matsushita, K., Woodward, M., Blankestijn, P. J., Cirillo, M., Ohkubo, T., et al. (2012). Associations of kidney disease measures with mortality and end-stage renal disease in individuals with and without hypertension: a meta-analysis. *Lancet* 380, 1649–1661. doi: 10.1016/S0140-6736(12)61272-0

Mammoto, A., Mammoto, T., and Ingber, D. E. (2012). Mechanosensitive mechanisms in transcriptional regulation. *J. Cell Sci.* 125, 3061–3073. doi: 10.1242/jcs.093005

Matsushita, K., van der Velde, M., Astor, B. C., Woodward, M., Levey, A. S., de Jong, P. E., et al. (2010). Association of estimated glomerular filtration rate and albuminuria with all-cause and cardiovascular mortality in general population cohorts: a collaborative meta-analysis. *Lancet* 375, 2073–2081. doi: 10.1016/S0140-6736(10)60674-5

Mitsides, N., Cornelis, T., Broers, N. J. H., Diederen, N. M. P., Brenchley, P., Heitink-Ter Braak, N., et al. (2018). Inflammatory and angiogenic factors linked to longitudinal microvascular changes in hemodialysis patients irrespective of treatment dose intensity. *Kidney Blood Press. Res.* 42, 905–918. doi: 10.1159/000485048

Mitsides, N., Cornelis, T., Broers, N. J. H., Diederen, N. M. P., Brenchley, P., Van Der Sande, F. M., et al. (2017). Extracellular overhydration linked with endothelial dysfunction in the context of inflammation in haemodialysis dependent chronic kidney disease. *PLoS One* 12:e0183281. doi: 10.1371/journal.pone.0183281

Moseley, R., Waddington, R. J., and Embery, G. (1997). Degradation of glycosaminoglycans by reactive oxygen species derived from stimulated polymorphonuclear leukocytes. *Biochim. Biophys. Acta Mol. Basis Dis.* 1362, 221–231. doi: 10.1016/S0925-4439(97)00083-5

Muiesan, M. L., Salvetti, M., Monteduro, C., Corbellini, C., Guelfi, D., Rizzoni, D., et al. (2001). Flow-mediated dilatation of the brachial artery and left ventricular geometry in hypertensive patients. *J. Hypertens.* 19(3 Pt 2), 641–647. doi: 10.1097/00004872-200103001-00018

Nagy, N., Freudenberger, T., Melchior-Becker, A., Röck, K., Ter Braak, M., Jastrow, H., et al. (2010). Inhibition of hyaluronan synthesis accelerates murine atherosclerosis: novel insights into the role of hyaluronan synthesis. *Circulation* 122, 2313–2322. doi: 10.1161/CIRCULATIONAHA.110.972653

Oberleithner, H., Peters, W., Kusche-Vihrog, K., Korte, S., Schillers, H., Kliche, K., et al. (2011). Salt overload damages the glycocalyx sodium barrier of vascular endothelium. *Pflugers Arch. Eur. J. Physiol.* 462, 519–528. doi: 10.1007/s00424-011-0999-1

Okada, M., Matsumori, A., Ono, K., Furukawa, Y., Shioi, T., Iwasaki, A., et al. (1998). Cyclic stretch upregulates production of interleukin-8 and monocyte chemotactic and activating factor/monocyte chemoattractant protein-1 in human endothelial cells. *Arterioscler. Thromb. Vasc. Biol.* 18, 894–901. doi: 10.1161/01.ATV.18.6.894

Paar, M., Pavenstädt, H., Kusche-Vihrog, K., Drüppel, V., Oberleithner, H., and Kliche, K. (2014). Endothelial sodium channels trigger endothelial salt sensitivity with aging. *Hypertension* 64, 391–396. doi: 10.1161/HYPERTENSIONAHA.114.03348

Padberg, J. S., Wiesinger, A., di Marco, G. S., Reuter, S., Grabner, A., Kentrup, D., et al. (2014). Damage of the endothelial glycocalyx in chronic kidney disease. *Atherosclerosis* 234, 335–343. doi: 10.1016/j.atherosclerosis.2014.03.016

Panza, J. A., Quyyumi, A. A., Brush, J. E., and Epstein, S. E. (1990). Abnormal endothelium-dependent vascular relaxation in patients with essential hypertension. *N. Engl. J. Med.* 323, 22–27. doi: 10.1056/nejm199007053230105

Salmon, A. H. J., Ferguson, J. K., Burford, J. L., Gevorgyan, H., Nakano, D., Harper, S. J., et al. (2012). Loss of the endothelial glycocalyx links albuminuria and vascular dysfunction. *J. Am. Soc. Nephrol.* 23, 1339–1350. doi: 10.1681/ASN.2012010017

Sandoo, A., Veldhuijzen van Zanten, J. J. C., Metsios, G. S., Carroll, D., and Kitas, G. D. (2015). The endothelium and its role in regulating vascular tone. *Open Cardiovasc. Med. J.* 4, 302–312. doi: 10.2174/1874192401004010302

Schächinger, V., Britten, M. B., and Zeiher, A. M. (2000). Prognostic impact of coronary vasodilator dysfunction on adverse long- term outcome of coronary heart disease. *Circulation* 101, 1899–1906. doi: 10.1161/01.CIR.101.16.1899

Singh, A., Satchell, S. C., Neal, C. R., McKenzie, E. A., Tooke, J. E., and Mathieson, P. W. (2007). Glomerular endothelial glycocalyx constitutes a barrier to protein permeability. *J. Am. Soc. Nephrol.* 18, 2885–2893. doi: 10.1681/ASN.2007010119

Smith, J. D., Davies, N., Willis, A. I., Sumpio, B. E., and Zilla, P. (2001). Cyclic stretch induces the expression of vascular endothelial growth factor in vascular smooth muscle cells. *Endothelium* 8, 41–48. doi: 10.3109/10623320109063156

Tian, Y., Gawlak, G., O'Donnell, J. J., Birukova, A. A., and Birukov, K. G. (2016). Activation of vascular endothelial growth factor (VEGF) receptor 2 mediates endothelial permeability caused by cyclic stretch. *J. Biol. Chem.* 291, 10032–10045. doi: 10.1074/jbc.M115.690487

Tsai, Y. C., Chiu, Y. W., Tsai, J. C., Kuo, H. T., Hung, C. C., Hwang, S. J., et al. (2015). Association of fluid overload with cardiovascular morbidity and all-cause mortality in stages 4 and 5 CKD. *Clin. J. Am. Soc. Nephrol.* 10, 39–46. doi: 10.2215/CJN.03610414

Ueda, A., Shimomura, M., Ikeda, M., Yamaguchi, R., and Tanishita, K. (2004). Effect of glycocalyx on shear-dependent albumin uptake in endothelial cells. *Am. J. Physiol. Hear. Circ. Physiol.* 287, H2287–H2294. doi: 10.1152/ajpheart.00808.2003

Van den Berg, B. M., Vink, H., and Spaan, J. A. E. (2003). The endothelial glycocalyx protects against myocardial edema. *Circ. Res.* 92, 592–594. doi: 10.1161/01.RES.0000065917.53950.75

Vigetti, D., Genasetti, A., Karousou, E., Viola, M., Moretto, P., Clerici, M., et al. (2010). Proinflammatory cytokines induce hyaluronan synthesis and monocyte adhesion in human endothelial cells through hyaluronan synthase 2 (HAS2) and the nuclear factor-κB (NF-κB) pathway. *J. Biol. Chem.* 285, 24639–24645. doi: 10.1074/jbc.M110.134536

Vlahu, C. A., Lemkes, B. A., Struijk, D. G., Koopman, M. G., Krediet, R. T., and Vink, H. (2012). Damage of the endothelial glycocalyx in dialysis patients. *J. Am. Soc. Nephrol.* 23, 1900–1908. doi: 10.1681/ASN.2011121181

Weinbaum, S., Tarbell, J. M., and Damiano, E. R. (2007). The structure and function of the endothelial glycocalyx layer. *Annu. Rev. Biomed. Eng.* 9, 121–167. doi: 10.1146/annurev.bioeng.9.060906.151959

Westphalen, H., Saadati, S., Eduok, U., Abdelrasoul, A., Shoker, A., Choi, P., et al. (2020). Case studies of clinical hemodialysis membranes: influences of membrane morphology and biocompatibility on uremic blood-membrane interactions and inflammatory biomarkers. *Sci. Rep.* 10:14808. doi: 10.1038/s41598-020-71755-8

Wizemann, V., Leibinger, A., Mueller, K., and Nilson, A. (1995). Influence of hydration state on plasma volume changes during ultrafiltration. *Artif. Organs* 19, 416–419. doi: 10.1111/j.1525-1594.1995.tb02352.x

Wizemann, V., and Schilling, M. (1995). Dilemma of assessing volume state—the use and the limitations of a clinical score. *Nephrol. Dial. Transplant.* 10, 2114–2117. doi: 10.1093/oxfordjournals.ndt.a090948

Zeng, Y., and Tarbell, J. M. (2014). The adaptive remodeling of endothelial glycocalyx in response to fluid shear stress. *PLoS One* 9:86249. doi: 10.1371/journal.pone.0086249

**Conflict of Interest:** The authors declare that the research was conducted in the absence of any commercial or financial relationships that could be construed as a potential conflict of interest.

**Publisher's Note:** All claims expressed in this article are solely those of the authors and do not necessarily represent those of their affiliated organizations, or those of the publisher, the editors and the reviewers. Any product that may be evaluated in this article, or claim that may be made by its manufacturer, is not guaranteed or endorsed by the publisher.

frontiers in Cell and Developmental Biology

ORIGINAL RESEARCH
published: 28 September 2021
doi: 10.3389/fcell.2021.731028

# Direct Current Stimulation Disrupts Endothelial Glycocalyx and Tight Junctions of the Blood-Brain Barrier *in vitro*

*Yifan Xia, Yunfei Li, Wasem Khalid, Marom Bikson and Bingmei M. Fu**

*Department of Biomedical Engineering, The City College of the City University of New York, New York, NY, United States*

Transcranial direct current stimulation (tDCS) is a non-invasive physical therapy to treat many psychiatric disorders and to enhance memory and cognition in healthy individuals. Our recent studies showed that tDCS with the proper dosage and duration can transiently enhance the permeability (P) of the blood-brain barrier (BBB) in rat brain to various sized solutes. Based on the *in vivo* permeability data, a transport model for the paracellular pathway of the BBB also predicted that tDCS can transiently disrupt the endothelial glycocalyx (EG) and the tight junction between endothelial cells. To confirm these predictions and to investigate the structural mechanisms by which tDCS modulates P of the BBB, we directly quantified the EG and tight junctions of *in vitro* BBB models after DCS treatment. Human cerebral microvascular endothelial cells (hCMECs) and mouse brain microvascular endothelial cells (bEnd3) were cultured on the Transwell filter with 3 μm pores to generate *in vitro* BBBs. After confluence, 0.1–1 mA/cm$^2$ DCS was applied for 5 and 10 min. TEER and P to dextran-70k of the *in vitro* BBB were measured, HS (heparan sulfate) and hyaluronic acid (HA) of EG was immuno-stained and quantified, as well as the tight junction ZO-1. We found disrupted EG and ZO-1 when P to dextran-70k was increased and TEER was decreased by the DCS. To further investigate the cellular signaling mechanism of DCS on the BBB permeability, we pretreated the *in vitro* BBB with a nitric oxide synthase (NOS) inhibitor, L-NMMA. L-NMMA diminished the effect of DCS on the BBB permeability by protecting the EG and reinforcing tight junctions. These *in vitro* results conform to the *in vivo* observations and confirm the model prediction that DCS can disrupt the EG and tight junction of the BBB. Nevertheless, the *in vivo* effects of DCS are transient which backup its safety in the clinical application. In conclusion, our current study directly elucidates the structural and signaling mechanisms by which DCS modulates the BBB permeability.

**Keywords: solute permeability, trans-endothelial electrical resistance (TEER), heparan sulfate, ZO-1, inhibition of endothelial nitric oxide synthase (eNOS), human cerebral microvascular endothelial cells, mouse brain microvascular endothelial cells, hyaluronic acid**

OPEN ACCESS

***Edited by:***
*Arie Horowitz,*
*Université de Rouen, France*

***Reviewed by:***
*Anuska V. Andjelkovic,*
*University of Michigan, United States*
*Aric Flint Logsdon,*
*University of Washington,*
*United States*

****Correspondence:***
*Bingmei M. Fu*
*fu@ccny.cuny.edu*
*orcid.org/0000-0001-9343-5895*

***Specialty section:***
*This article was submitted to Signaling, a section of the journal Frontiers in Cell and Developmental Biology*

***Received:*** *25 June 2021*
***Accepted:*** *08 September 2021*
***Published:*** *28 September 2021*

***Citation:***
*Xia Y, Li Y, Khalid W, Bikson M and Fu BM (2021) Direct Current Stimulation Disrupts Endothelial Glycocalyx and Tight Junctions of the Blood-Brain Barrier in vitro. Front. Cell Dev. Biol. 9:731028. doi: 10.3389/fcell.2021.731028*

## INTRODUCTION

As a non-invasive neuromodulation technique, transcranial direct current stimulation (tDCS) has been used to treat various neurological and psychiatric disorders since nineteenth century (Steinberg, 2013; Kekic et al., 2016; Palm et al., 2016; Truong and Bikson, 2018). Weak direct currents across the human brain are introduced via electrodes distributed on the skull, the electric

current can alter the brain function by modulating neuron firing rates and changing neuron membrane potentials (Nitsche and Paulus, 2000; Jackson et al., 2016; Woods et al., 2016; Antal et al., 2017; Giordano et al., 2017; Kenney-Jung et al., 2019). In addition to priming neuronal capacity, tDCS has been found to enhance blood perfusion in humans (Stagg et al., 2013; Wang et al., 2015) and in animals (Mielke et al., 2013), and to increase blood nitric oxide (NO) levels (Marceglia et al., 2016).

To safeguard the brain from the blood-borne toxins in the circulating blood, the wall of the cerebral microvessels is specified as the blood-brain barrier (BBB) due to its very low permeability compared to the wall of peripheral microvessels in non-brain tissues. In addition to the endothelium, the BBB consists of basement membrane (BM) filled with extracellular matrix (ECM) and wrapped by the pericytes and astrocyte foot processes (Farkas and Luiten, 2001; Abbott et al., 2006; Fu, 2018). The BBB permeability to water and hydrophilic solutes is determined by its structural components in the paracellular pathway: the endothelial glycocalyx (EG) (Yoon et al., 2017; Kutuzov et al., 2018), the gap space and tight junctions between adjacent endothelial cells (ECs), the width of the BM, the ECM and the gap between astrocyte foot processes (Li et al., 2010b; Li and Fu, 2011; Fu, 2018). Recent study by Shin et al. (2020) showed that tDCS transiently increases the BBB solute permeability in rat brain through activation of nitric oxide synthase (NOS). By employing a transport model for the paracellular pathway of the BBB (Li et al., 2010b), Shin et al. (2020) also predicted that the structural mechanisms by which the tDCS transiently enhances the BBB permeability are temporarily disrupting the EG and the ECM of the BM, disrupting the tight junctions between ECs, as well as increasing the gap width between ECs and that of BM.

The first objective of this study is to confirm the above prediction for the structural mechanisms of tDCS *in vivo*. Since in the BBB, only EG and ECM carry charge, if they are disrupted by the tDCS, the BBB permeability to the same sized solutes with opposite charge should become identical. We thus used the same method and under tDCS with the same strength as in Shin et al. (2020) to determine the rat BBB permeability to FITC-ribonuclease and FITC-α-lactalbumin, which have almost the same size (Stokes radius ≈ 2 nm) but opposite charge (net charge of +4 and −10, respectively) (Yuan et al., 2010b).

Because it is very challenging to directly observe the transiently disrupted EG and tight junctions of the BBB *in vivo*, the second objective is thus to generate *in vitro* BBB models and determine the changes in the EG and tight junctions after tDCS treatments. Human cerebral microvascular endothelial cells (hCMECs) and mouse brain microvascular endothelial cells (bEnd3) were cultured on the Transwell filter with 3 μm pores to generate the *in vitro* BBB. We used similar set up and DCS strength as in Cancel et al. (2018) to treat the *in vitro* BBB. The BBB permeability to ions, the transendothelial electrical resistance (TEER), was measured before and after DCS treatments. Disruption of tight junctions of ECs would significantly affect TEER which is an indicator for permeability to ions or small molecules (Fu et al., 1994; Sugihara-Seki and Fu, 2005). The EG of the *in vitro* BBB formed by hCMEC/bEnd3 cells and the tight junction ZO-1 of that formed by bEnd3 were quantified under control and after DCS treatment. We also quantified *in vitro* BBB permeability to Dex-70k since disruption of EG would significantly affect the BBB permeability to large solutes such as Dex-70k (Fu and Shen, 2003; Sugihara-Seki and Fu, 2005; Yuan et al., 2010a; Kutuzov et al., 2018).

As shown in Shin et al. (2020), tDCS-increased BBB permeability is NO dependent but how is unanswered. Therefore, the third objective of this study is to directly demonstrate how the EG and tight junction ZO-1 of *in vitro* BBB are affected by a NO inhibitor, L-NMMA, a NO donor, SNP, and pretreatment of L-NMMA before DCS. Correspondingly, we also quantified the changes in the BBB TEER and permeability to Dex-70k by these factors. Taken together, our results directly elucidate the structural and signaling mechanisms by which DCS modulates the BBB permeability.

# MATERIALS AND METHODS

## Solutions and Fluorescent Test Solutes

### Mammalian Ringer's Solution and Reagents

Mammalian Ringer's solution was used for all the permeability measurement, which is composed of (in mM) NaCl 132, KCl 4.6, $MgSO_4$ 1.2, $CaCl_2$ 2.0, $NaHCO_3$ 5.0, glucose 5.5, and HEPES 20. These chemicals were from Sigma-Aldrich. The pH was adjusted to 7.4–7.45 by adjusting the ratio of HEPES acid to base. In addition, the florescent dye solution contained 10 mg/mL BSA (A4378; Sigma-Aldrich, United States) or 1% BSA to maintain the same oncotic pressure as in the plasma (Fu and Shen, 2004). $N^G$-monomethyl-L-arginine (L-NMMA) and sodium nitroprusside (SNP) were purchased from Sigma (Sigma-Aldrich). L-NMMA (1 mM) and SNP (300 μM) used in the experiments were achieved by dilutions of the stock with 1% BSA-Ringer solution (Zhang et al., 2016). The solutions were made fresh on the day of use to avoid binding to the serum albumin (Adamson et al., 1994; Fu et al., 1998).

### FITC-Ribonuclease, FITC-a-Lactalbumin and FITC-Dextran-70k

Ribonuclease A (R5500, MW = 13, 683, Sigma-Aldrich) and α-lactalbumin (L6010, MW = 14,176, Sigma-Aldrich) were labeled with fluorescein isothiocyanate isomer I (FITC, F7250, MW = 389.4, Sigma-Aldrich) as described in Adamson et al. (1994); Fu et al. (1998), and Yuan et al. (2010a). The intensity of free dye is less than 1% compared to that of the solution prepared by using this protocol (Yuan et al., 2010a). The influence of the free dye on measured permeability to a labeled protein was discussed by Fu et al. (1998) and contributed less than 0.5% to the BBB permeability for the understudied solutes (Yuan et al., 2010a,b; Shi et al., 2014b). After FITC labeling, the final charge of FITC-ribonuclease is +4 and FITC-α-lactalbumin is −10 (Yuan et al., 2010b; Li and Fu, 2011). The final concentrations FITC-ribonuclease and FITC-α-lactalbumin used in the *in vivo* experiment were 1 mg/mL in the Ringer solution containing 10 mg/mL BSA. In the *in vitro* permeability measurement, the concentration of FITC-ribonuclease, FITC-α-lactalbumin, and FITC-Dextran-70k (FD70s, Sigma-Aldrich) was 10 μM. The

concentration of the solution for each solute was chosen to be in the linear range of the concentration vs. fluorescence intensity calibrated in Li et al. (2010b) and Shi et al. (2014b). All dye solutions described above were made fresh on the day of use and discarded at the end of the day.

## *In vivo* Experiments

### Animal Preparation

All animal care and preparation procedures were approved by the Animal Care and Use Committee at the City College of the City University of New York and all experiments were performed in accordance with relevant guidelines and regulations. All experiments were performed on adult female SD rats (250–300g, Hilltop, Scottdale, PA). The preparation of the rat skull observation area was the same as previously described (Yuan et al., 2009; Shi et al., 2014b; Shin et al., 2020). Briefly, after anesthesia, a section of ∼6 mm by ∼4 mm area (ROI) on the frontoparietal bone was carefully ground with a high-speed micro-grinder (DLT 50KBU, Brasseler, Savannah, GA) until soft and translucent. After grinding, the carotid artery on the same side of the ROI was cannulated with a PE50 tubing (BD Medical, NJ). The rat was then fixed on a stereotaxic alignment system (SAS 597, David Kopf Instruments, Tujunga, CA). After tDCS treatment, the rat head was quickly placed to the objective lens of the multiphoton system for the permeability measurement. It took about 5 min to find the ROI with proper microvessels in the rat brain parenchyma. The images of a cerebral microvessel and its surrounding brain tissue were observed and collected under the objective lens of a multiphoton microscope through the thinned part of the skull.

### Transcranial Direct Current Stimulation

tDCS was administered using a constant current stimulator (1x1 tDCS, Soterix Medical Inc., New York, United States) to deliver a 1 mA current (the current density 8.0 mA/cm$^2$) for 20 min. This dose and duration were the optimal and also safe for the *in vivo* tDCS treatment on rats (Jackson et al., 2017; Shin et al., 2020; Xia et al., 2020). Current was applied transcranially to the frontal cortex of a rat head (approximately 2 mm anterior to Bregma and 2 mm right to Sagittal suture) to obtain similar physiological outcomes as in the human tDCS application studies (Marceglia et al., 2016; Jackson et al., 2017; Shin et al., 2020; Xia et al., 2020). Specifically, an epi-cranial anode (1 mm diameter, Ag/AgCl) in a plastic cannula (4 mm inner diameter) filled with conductive electrolyte gel (Signa, Parker Laboratory, NJ) was positioned onto the rat skull with the location described above. The returning electrode (5 × 5 cm adhesive conductive fabric electrode, AxelGaard, Fallbrook, CA) was placed onto the ventral thoracic region of the anesthetized rat (Shin et al., 2020).

### Multiphoton Microscopy and Image Analysis

The 12-bit images were collected *in vivo* by a two-photon microscopic system (Ultima, Prarie Technologies Inc., Middleton, WI) with a 40 × lens (NA = 0.8, water immersion, Olympus). The excitation wavelength was set to 820 nm to observe the cerebral microvessels 100–200 μm below the pia mater. The images were taken simultaneously while the fluorescence solution was introduced into the cerebral circulation via the ipsilateral carotid artery at 3 mL/min. We selected a brain region containing post-capillary venules of 20–40 μm diameter and collected images for a ROI of ∼240 μm × 240 μm at a rate of ∼1 frame/s for ∼1 min every 5 min for 20 min (Shin et al., 2020). The images were analyzed off-line using the Image J (National Institutes of Health) to determine the BBB permeability to solutes.

### Determination of the Blood-Brain Barrier Solute Permeability *in vivo*

The same method as in our previous studies (Shi et al., 2014a; Shin et al., 2020) was used to determine the permeability (P) of the cerebral microvessels in rat brain. P was determined by using the following equation:

$$P = \frac{1}{\Delta I_0} \times \left(\frac{dI}{dt}\right)_0 \times \frac{r}{2}$$

Here $\Delta I_0$ is the step increase of the florescence intensity in the measuring window when the dye just fills up the vessel lumen, $(dI/dt)_0$ is the slope of the increasing curve of the total intensity I of the measuring window vs. time t when the solute further diffuses into the surrounding tissue, and r is the vessel radius.

## *In vitro* Experiments

### Cell Culture and Trans-Endothelial Electrical Resistance Measurement

Two cell lines were used to generate *in vitro* BBB, human brain microvascular endothelial cells (hCMEC/D3 or hCMEC) from Millipore Sigma (Burlington, MA) and mouse brain microvascular endothelial cells (bEnd3) from ATCC (Manassas, VA). hCMECs were cultured in EBM-2 MV endothelial cell growth basal Medium (Lonza, Basel, Switzerland), supplemented with 100 U/mL Penicillin-Streptomycin streptomycin (Gibco, Thermo Fisher Scientific, Waltham, MA). bEnd3 was cultured in Dulbecco's Modified Eagle's Medium/Nutrient Mixture F-12 Ham (DMEM/F-12), 2 mM L-glutamine,10% fetal bovine serum (FBS, Gibco, Thermo Fisher Scientific, Waltham, MA), and supplemented with 100 U/mL Penicillin-Streptomycin streptomycin (Gibco, Thermo Fisher Scientific, Waltham, MA). Both cell lines were incubated in the humidified atmosphere with 5% $CO_2$ at 37°C. To form an *in vitro* human BBB, hCMECs were seeded at 60 k/cm$^2$ to a Transwell filter (PET 3.0 μm pore size, Corning, NY) precoated with 50 μg/mL collagen I (Sigma-Aldrich, St. Louis, MO) and cultured for 5–7 days until confluent. To form an *in vitro* mouse BBB, bEnd3 cells were seeded at 60k/cm$^2$ to the same type of the Transwell filter precoated with 30 μg/mL fibronectin (Sigma-Aldrich, St. Louis, MO) and cultured for 4–5 days until confluent. Tran-endothelial electrical resistance (TEER) was monitored 3 days after seeding to check the confluency and barrier formation. TEER was measured by EVOM2 epithelial Volt/Ohm meter with the electrode (STX2) (World Precision Instruments, Sarasota, FL). For each sample, the

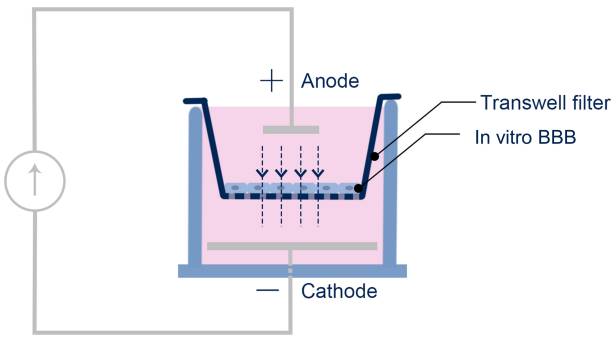


**FIGURE 1 |** Schematic of the setup for the DCS application to the *in vitro* BBB. The *in vitro* BBB was formed by hCMEC or bEnd3 monolayer on the Transwell filter.

TEER was measured three times. The average of the three measurements is the TEER for that sample. The TEER of a blank Transwell filter with the same cell culture medium was also measured and subtracted from the TEER of the total system to determine the TEER of the *in vitro* BBB (Li et al., 2010a).

## Direct Current Stimulation on *in vitro* Blood-Brain Barrier

Similar to Cancel et al. (2018), DCS was applied to the *in vitro* BBB generated on the Transwell filter by a pair of Ag/AgCl electrodes. The anode, a 4 mm × 1 mm disk (A-M systems, Sequim, WA), was placed on the upper chamber positioned 7 mm above the *in vitro* BBB. The cathode, a 15 mm x 1 mm disk, was placed in the bottom chamber positioned 7 mm below the *in vitro* BBB (**Figure 1**). A direct current stimulator (model 1300-A, Soterix Medical Inc., New York) was used to deliver a constant 0.1–1 mA/cm$^2$ across the *in vitro* BBB for 5 or 10 min. The current level ramped up in ∼30 s to the treatment level and ramped down to zero in ∼ 30 s. This ramping up/down time was excluded from the duration time. The dosage/duration for the *in vitro* experiment was designed to match the typical dosage/duration for the tDCS application in patients with neuronal disorders as well as in the *in vivo* rat experiments (Brunoni et al., 2012; Marceglia et al., 2016; Jackson et al., 2017; Cancel et al., 2018; Shin et al., 2020).

## Determination of the Blood-Brain Barrier Solute Permeability *in vitro*

The solvent for the permeability measurement was Ringer solution containing 10 mg/mL BSA (Yuan et al., 2010a). At the beginning of the permeability measurement, the upper chamber of the Transwell filter was added with 0.5 mL 10 μM fluorescence solution in 10 mg/mL BSA Ringer while the lower chamber was filled with 1.5 mL blank 10 mg/mL BSA Ringer. The samples of 50 μL were collected every 10 min for 90 min from the lower chamber and were then replaced with the same amount of blank 10 mg/mL BSA Ringer. The fluorescence concentration (intensity) in the samples was determined by SpectraMax M5 microplate reader (Molecule devices, San Jose, CA). The fluorescently labeled solute permeability of the *in vitro* BBB generated on the Transwell filter was calculated by:

$$P = \frac{\frac{\triangle C_L}{\triangle t} \times V_L}{C_U \times S}$$

where $(\Delta C_L)/\Delta t$ is the increase rate of the fluorescence concentration in the lower chamber, $C_U$ is the fluorescence concentration in the upper chamber, $V_L$ is the solution volume in the lower chamber, and S is the surface area of the filter. The permeability P of the blank filter was measured separately and subtracted from the measurement of the total system to obtain the P of the *in vitro* BBB. Since it takes 90 min for the solute permeability measurement, to prevent the change or recovery of the BBB permeability post DCS, we fixed the monolayer right after DCS before measuring its permeability. We tested that the fixation does not affect the monolayer permeability (**Supplementary Figure 1**).

## Immunostaining for Endothelial Glycocalyx and Tight Junction ZO-1

EG: Since heparan sulfate (HS) is the most abundant glycosaminoglycan (GAG) of the EG (Sarrazin et al., 2011; Fu and Tarbell, 2013; Zeng et al., 2018), we quantified HS to represent the EG by using the method in Li et al. (2010b); Fan and Fu (2016), Zullo et al. (2016), and Fan et al. (2019). We also labeled another EG component, hyaluronic acid (HA) at hCMEC monolayer (Fan et al., 2019). The hCMEC/bEnd3 monolayer was first washed three times with 10 mg/mL BSA in Dulbecco's Phosphate-Buffered Saline (DPBS, Corning, Corning, NY) and then fixed with 2% paraformaldehyde (Polyscience, Warrington, PA) and 0.1% glutaraldehyde (Sigma-Aldrich) for 20 min at RT. It was blocked with 2% NGS for 30 min at RT, and incubated with a monoclonal primary antibody to HS (1:100; 10E4 epitope; Amsbio, Cambridge, MA) or biotinylated hyaluronic acid binding protein (50 μg/mL, Amsbio) for hCMEC only at 4 C overnight. After washing three times with DPBS, the cells were incubated for 1 h at RT with AF488 conjugated secondary antibody to HS (1:200, Invitrogen, Thermo Fisher Scientific, Waltham, MA) or AF488 conjugated anti-biotin (1:200, Jackson ImmunoResearch, West Grove, PA) for hCMEC only. The hCMEC/bEnd3 monolayer was washed three times with DPBS, followed with DAPI staining and made into slides for later observation.

Tight junction (ZO-1): The method for labeling ZO-1 of bEnd3 monolayer was described in Li et al. (2010a); Yuan et al. (2010a), and Fan and Fu (2016). The monolayer was washed three times with DPBS, fixed with 1% paraformaldehyde for 10 min, permeabilized with 0.2% Triton X-100 (Sigma-Aldrich, St. Louis, MO) in DPBS for 10 min and blocked with 10% BSA and 0.1% Triton X-100 in DPBS for 1 h in RT. After washing with DPBS, the monolayer was incubated with a primary ZO-1 polyclonal antibody (1:100, 40–2200, Invitrogen, Thermo Fisher Scientific, Waltham, MA) at 4$^o$C overnight. After three times washed with DPBS, the monolayer was incubated in Alexa Fluor 488 conjugated goat anti-rabbit antibody (1:200, Invitrogen, Thermo

Fisher Scientific, Waltham, MA) for 1 h at RT. The monolayer was then washed three times with DPBS, followed with the DAPI staining and made into slides for later observation.

### Confocal Microscopy and Quantification of Endothelial Glycocalyx and ZO-1

All the samples were imaged by Zeiss LSM 800 confocal laser scanning microscope with 40x oil immersion objective lens (NA = 1.30). For imaging ZO-1, three fields of 160 μm x 160 μm (2,048 × 2,048) were randomly chosen for each sample, and captured as a z-stack of 50–60 images with a z-step of 0.2 μm for two channels (AF488 and DAPI). For EG imaging, three fields of 320 μm by 320 μm (2,048 × 2,048) for each sample were captured as a z-stack of 30–40 images with a z-step of 0.32 μm. Image projection and intensity quantification for EG and ZO-1 were performed by Zeiss ZEN and NIH ImageJ (Fan and Fu, 2016).

### Data Analysis and Statistics

Data were presented as means ± SE (standard error) unless otherwise specified. Statistical analysis was performed by a two-way (time and different treatment) ANOVA in Prism 8.0. Kurtosis analysis was used to compare the ZO-1 distribution profiles under various conditions. Significance was assumed for probability level $p < 0.05$. For *in vivo* experiments, sample size $n = 6$ at each time point for each treatment, while for *in vitro* experiments, $n \geq 6$ samples for permeability and TEER, $n = 3$ samples for EG and ZO-1, correspondingly.

## RESULTS

### Effects of Direct Current Stimulation on the Blood-Brain Barrier Permeability (P) to Charged Solutes *in vivo* and *in vitro*

Since in the structural components of the BBB, only EG and ECM carry negative charge (Yuan et al., 2010b; Li and Fu, 2011; Alphonsus and Rodseth, 2014; Yoon et al., 2017; Kutuzov et al., 2018), we measured the BBB permeability (P) to FITC-ribonuclease and FITC-α-lactalbumin with the same size (Stokes radius ≈ 2.0 nm) but opposite charge *in vivo* after tDCS treatment. If EG and ECM are disrupted by tDCS, the P to these solutes would become the same. **Figure 2A** demonstrates that under control, the P to the positively charged FITC-ribonuclease (+4) is ∼4-fold that to FITC-α-lactalbumin (−10), indicating that the BBB carrying negative charge under control condition. However, at 5, 10,15 min post tDCS, the P to both solutes significantly increase from their respective controls, but no difference between P to positively charged FITC-ribonuclease and that to negatively charged FITC-α-lactalbumin ($p > 0.3$). The results imply that the charged components of the BBB, EG and ECM, are disrupted by tDCS. At 20 min post tDCS, P to both charged solutes return to their control values, indicating the recovery of EG and ECM and other structural components of the BBB. This is the same as for the P to the neutral solutes reported in Shin et al. (2020).

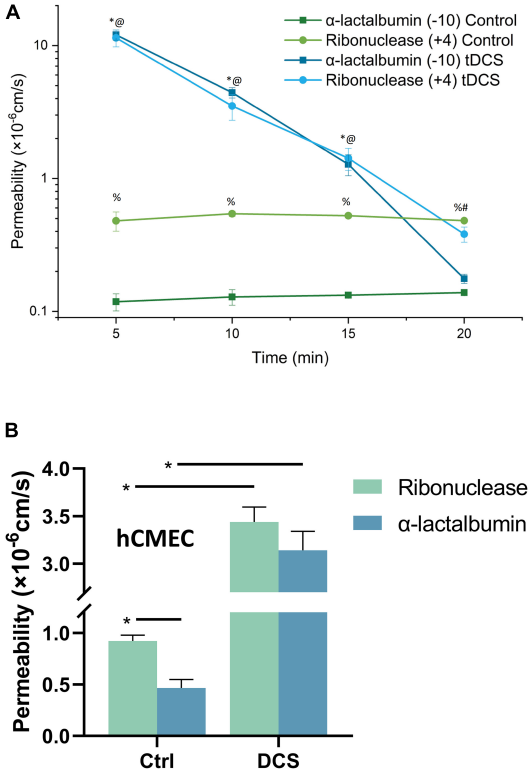


**FIGURE 2 |** Effects of DCS on the BBB permeability (P) to charged solutes with similar size but opposite charge. **(A)** Comparison of *in vivo* BBB P to FITC-ribonuclease (+4) and that to FITC-α-lactalbumin (–10) under control and 5, 10, 15, 20 min after 20 min 1 mA (8 mA/cm$^2$) -tDCS treatment. $^{*,@}p < 0.05$, compared with the corresponding controls at the same time; $^{\%}p < 0.05$ comparing P to FITC-ribonuclease with that to FITC-α-lactalbumin under control; $^{\#}p < 0.05$ comparing P to FITC-ribonuclease and that to FITC-α-lactalbumin 20 min post tDCS; $n = 6$ for each case. **(B)** Comparison of *in vitro* BBB P to FITC-ribonuclease and that to FITC-α-lactalbumin under control and after 10 min 1 mA/cm$^2$-DCS treatment. $^{*}p < 0.05$. The *in vitro* BBB was formed by hCMEC monolayer. $n = 7$ for the control of ribonuclease, $n = 6$ for all other cases.

The above *in vivo* BBB P data to the charged solutes with the same size, and the prediction from a mathematical model for the BBB (Li et al., 2010b; Shin et al., 2020), all suggest that the EG and ECM are temporally disrupted by tDCS, but it is very hard to detect this transient disruption *in vivo*. To directly show that DCS can disrupt EG, we generated an *in vitro* BBB model by culturing a hCMEC monolayer on a Transwell filter with 3 μm pores. For validation, we measured P of this *in vitro* BBB to FITC-ribonuclease and FITC-α-lactalbumin under control and after 10 min treatment with 1 mA/cm$^2$ DCS, equivalent dose/duration as those for *in vivo* tDCS (Cancel et al., 2018; Shin et al., 2020). **Figure 2B** shows that P of *in vitro* BBB to FITC-ribonuclease is ∼2-fold that to FITC-α-lactalbumin, half of the fold as *in vivo*. This is reasonable since no astrocytes in the *in vitro* BBB and ECM is negligible. After DCS treatment, P to these oppositely charged solutes increase from their respective controls but there is no difference between their P right after DCS treatment ($p = 0.32$). The *in vitro* results conform to

the *in vivo* data. We thus used this *in vitro* BBB for the effects of DCS on EG.

## Dose Effects of Direct Current Stimulation on *in vitro* Blood-Brain Barrier Transendothelial Electrical Resistance and Permeability to Dextran-70k

The DCS dosage and duration are important factors in controlling the BBB-disruption levels, we applied 0.1, 0.5 and 1 mA/cm$^2$ DCS with duration 5 and 10 min to the *in vitro* BBB to test their effects on the BBB TEER and P to Dex-70k. These dosages and durations were based on the prior studies in rats and humans (Marceglia et al., 2016; Jackson et al., 2017; Cancel et al., 2018; Shin et al., 2020). **Figure 3A** shows that TEER significantly decreased to 0.46 ± 0.06, 0.67 ± 0.02, 0.75 ± 0.05, 0.83 ± 0.01 of the control, after 1 mA/cm$^2$–10 min, 1 mA/cm$^2$–5 min, 0.5 mA/cm$^2$–10 min and 0.5 mA/cm$^2$–5 min DCS treatments, respectively. There were no significant changes in TEER after treatments with 0.1 mA/cm$^2$–10 min and 0.1 mA/cm$^2$–5 min. The control TEER of hCMEC monolayers is 123.2 ± 2.6 (range 96–134) Ωcm$^2$. Correspondingly, **Figure 3B** demonstrates that P to Dex-70k significantly increased to 7.78 ± 0.78, 1.81 ± 0.23, 1.35 ± 0.11 of the control after 1 mA/cm$^2$–10 min, 1 mA/cm$^2$–5 min, 0.5 mA/cm$^2$–10 min DCS treatments, but no significant change after 0.5 mA/cm$^2$–5 min treatment. The control P to Dex-70k is 2.2 ± 0.26 (range 1.4–3.6) × $10^{-7}$ cm/s. Interestingly, much larger increase in P to Dex-70k occurs at 1 mA/cm$^2$-10 min treatment. This is likely due to the significant disruption in the EG of the *in vitro* BBB since EG provides much larger resistance to large solutes such as Dex-70k (Fu and Shen, 2003; Fu et al., 2005; Yuan et al., 2010a; Kutuzov et al., 2018).

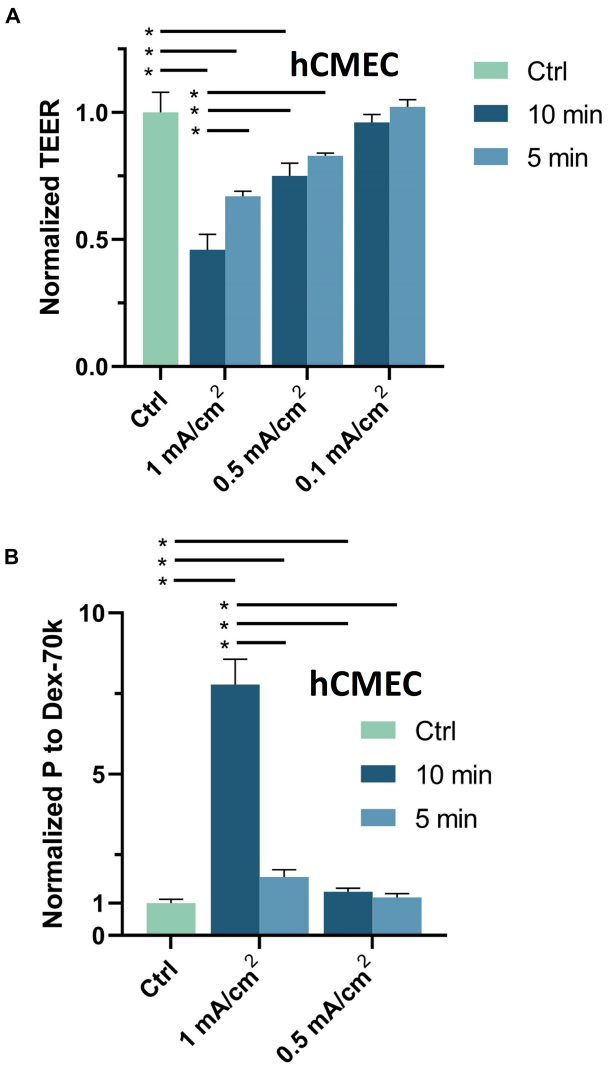


**FIGURE 3 |** Effects of DCS strength on *in vitro* BBB TEER and permeability. **(A)** Normalized TEER and **(B)** normalized permeability to Dex-70K under control and after 5 min or 10 min treatments with 0.1, 0.5, or 1 mA/cm$^2$ DCS. *$p < 0.05$. The *in vitro* BBB was formed by hCMEC monolayer.

## Disruption of Endothelial Glycocalyx on *in vitro* Blood-Brain Barrier by Direct Current Stimulation

To investigate the structural mechanism by which DCS decreases BBB TEER but increases P to Dex-70k, we first quantified EG, or heparan sulfate (HS), the most abundant GAG in EG, before and after DCS treatments. **Figure 4A** demonstrates the confocal images of HS (green) on the hCMEC monolayer under control and after 1 mA/cm$^2$–10 min, 1 mA/cm$^2$–5 min, 0.5 mA/cm$^2$–10 min, 0.5 mA/cm$^2$–5 min, 0.1 mA/cm$^2$–10 min and 0.1 mA/cm$^2$–5 min DCS treatments. Correspondingly, **Figure 4B** shows that the total intensity of HS decreased significantly to 0.31 ± 0.03, 0.56 ± 0.06, 0.59 ± 0.01 of the control after 1 mA/cm$^2$–10 min, 1 mA/cm$^2$–5 min and 0.5 mA/cm$^2$–10 min treatments; but insignificantly to 0.73 ± 0.14, 1.06 ± 0.1, and 1.11 ± 0.03 of the control after 0.5 mA/cm$^2$–5 min, 0.1 mA/cm$^2$–10 min and 0.1 mA/cm$^2$–5 min DCS treatments, respectively. The effect of DCS on another EG component, hyaluronic acid (HA) of hCMEC monolayers is shown in **Figure 5**. The intensity of HA decreased to 0.35 ± 0.03 after treatment of 1 mA/cm$^2$ DCS for 10 min, similar to the effect of DCS on HS. DCS disrupts EG of the BBB at the dose/duration which can significantly increase P to Dex-70k and decrease TEER.

To examine the effect of DCS on the EG of bEnd3 monolayers, we quantified the HS intensity of bEnd3 after the treatment of DCS with the same levels as for hCMEC monolayers. **Figure 6A** demonstrates the confocal images of HS on the bEnd3 monolayer under control and after 1 mA/cm$^2$–10 min, 1 mA/cm$^2$–5 min, 0.5 mA/cm$^2$–10 min, 0.5 mA/cm$^2$–5 min, 0.1 mA/cm$^2$–10 min and 0.1 mA/cm$^2$–5 min DCS treatments. **Figure 6B** shows that the total intensity of HS decreased significantly to 0.35 ± 0.04, 0.59 ± 0.05, 0.65 ± 0.06 of the control after 1 mA/cm$^2$–10 min, 1 mA/cm$^2$–5 min and 0.5 mA/cm$^2$–10 min treatments; but insignificantly to 0.77 ± 0.04, 0.92 ± 0.06, and 1.13 ± 0.08 of the control after

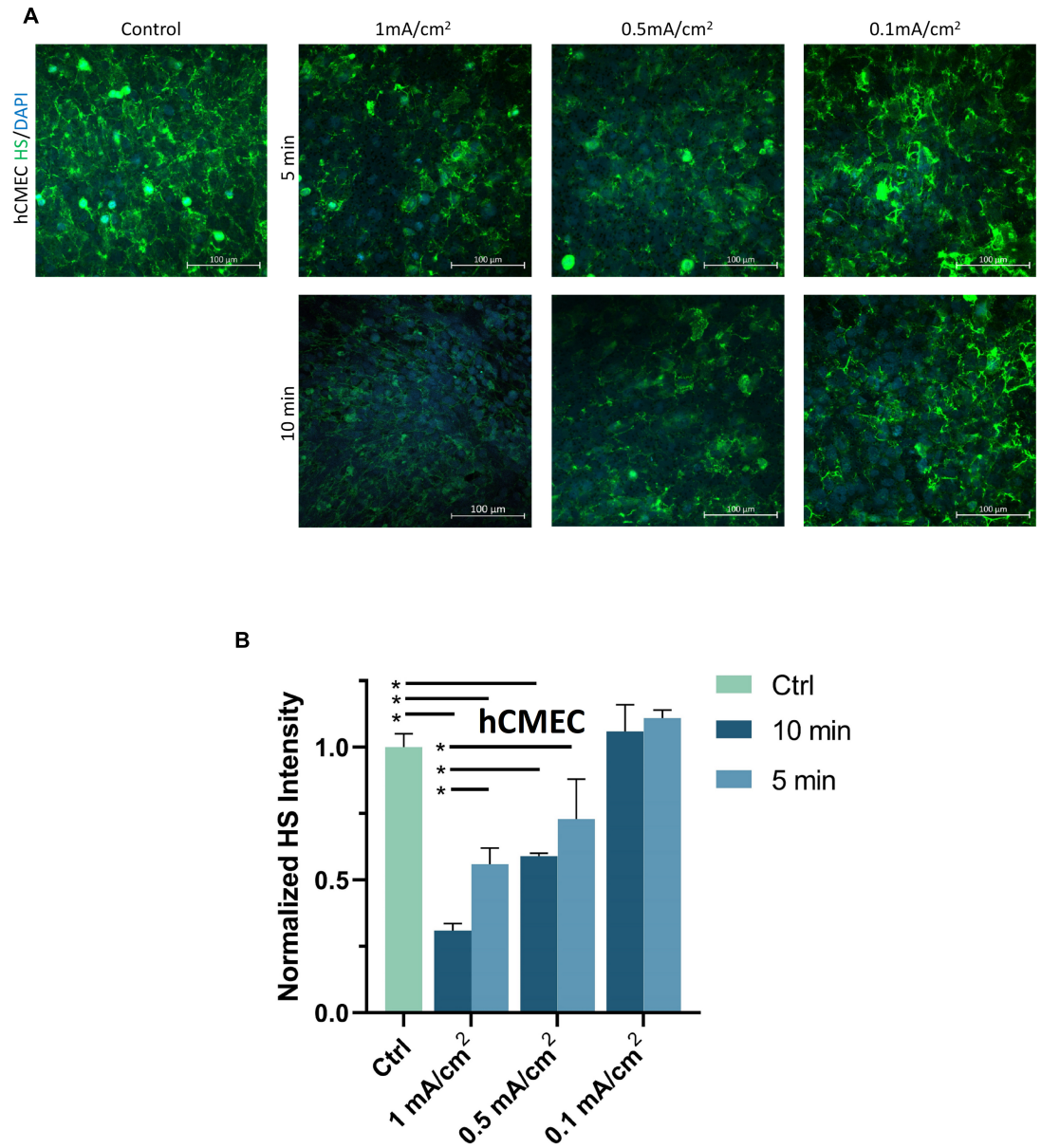


**FIGURE 4 |** Effects of DCS strength on HS of endothelial glycocalyx (EG) of *in vitro* BBB formed by hCMEC monolayer. **(A)** Confocal images of heparan sulfate (HS) of EG on *in vitro* BBB and **(B)** comparison of HS intensity under control and after 5 min or 10 min treatments with 0.1, 0.5, or 1 mA/cm$^2$ DCS. *$p < 0.05$.

0.5 mA/cm$^2$–5 min, 0.1 mA/cm$^2$–10 min and 0.1 mA/cm$^2$–5 min DCS treatments, respectively. The pattern of DCS effects on HS of bEnd3 monolayers is the same as that on HS of hCMEC monolayers.

## Disruption of Tight Junctions of *in vitro* Blood-Brain Barrier by Direct Current Stimulation

To investigate another structural change, the junction proteins between ECs, by the DCS to increase BBB permeability, we quantified the tight junction, ZO-1 of the *in vitro* BBB formed by bEnd3 monolayer since no good labeling was found for the junction proteins of hCMEC monolayer (**Supplementary Figure 2**). We first measured the effect of DCS on the TEER of bEnd3 monolayers. **Figure 7A** shows that after 1 mA/cm$^2$–10 min DCS treatment, TEER of bEnd3 monolayers significantly decreased to 0.65 ± 0.04. The control TEER of bEnd3 monolayer is 140.3 ± 3.5 (range 127–160) Ωcm$^2$. **Figure 7B** demonstrates the confocal images of ZO-1 (green) of bEnd3 monolayer under control and after 1 mA/cm$^2$–10 min DCS treatment. Correspondingly, **Figure 7C** compares the ZO-1 concentration (intensity) distribution under control and after DCS treatment. **Figure 7C** shows

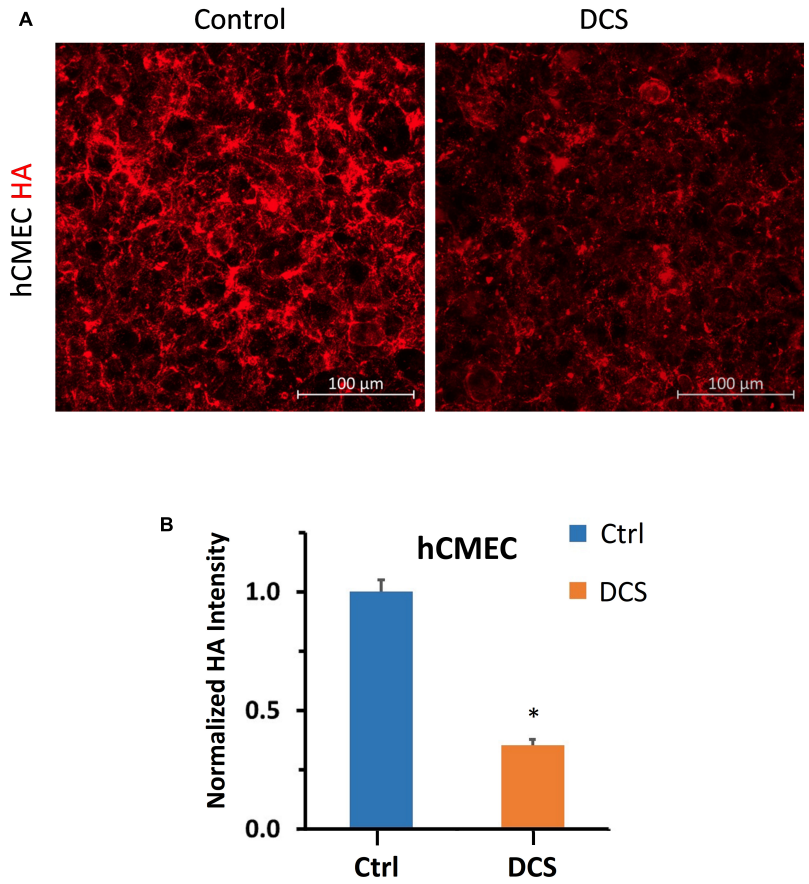


**FIGURE 5 |** Effects of DCS on HA of endothelial glycocalyx (EG) of *in vitro* BBB formed by hCMEC monolayer. **(A)** Confocal images of hyaluronic acid (HA) of EG on *in vitro* BBB and **(B)** comparison of HA intensity under control and after 10 min treatment with 1 mA/cm$^2$ DCS. *$p < 0.05$.

that ZO-1 was significantly disrupted after 1 mA/cm$^2$–10 min DCS treatment.

## Effects of Nitric Oxide Synthase Inhibition, Nitric Oxide and Combined Effects of Nitric Oxide Synthase Inhibition and Direct Current Stimulation on *in vitro* Blood-Brain Barrier Permeability

Prior studies have reported that activation of NOS by cytokines or inflammatory agents enhances endothelial NO release to increase microvascular permeability (Duran et al., 2010; Shi et al., 2014a). Our recent *in vivo* study also showed that tDCS-induced BBB permeability increase is NO dependent (Shin et al., 2020). To test if DCS-induced BBB permeability increase is also NO dependent in the *in vitro* BBB, we measured TEER and P to Dex-70k of hCMEC monolayers after treatment of 1 mA/cm$^2$ DCS for 10 min, after treatment of a NOS inhibitor, L-NMMA, for 60 min, and pretreatment with L-NMMA before 1 mA/cm$^2$-10 min DCS treatment. Inhibition of NOS by 1 mA L-NMMA for 60 min significantly increased TEER to 1.29-fold (or 129%) that of the control (**Figure 8A**), and decreased P to Dex-70k to 0.58 (**Figure 8B**) of the control, respectively. Pretreatment of 1 mM L-NMMA for 60 min significantly diminished the effects of DCS on both TEER and P to Dex-70k, like what observed in the *in vivo* study (Shin et al., 2020). We also tested the effect of a NO donor, SNP, on the permeability of the *in vitro* BBB. Treatment of 300 µM SNP for 30 min significantly decreased TEER to 0.47 (**Figure 8A**) and increased P to Dex-70k to 5.67-fold (**Figure 8B**) that of the corresponding controls. Treatment with 300 µM SNP for 30 min has a similar effect on the TEER compared to the treatment of 1 mA/cm$^2$ DCS for 10 min but its effect on P to Dex-70k is smaller than that of DCS.

## Disruption of Endothelial Glycocalyx by Direct Current Stimulation Is Nitric Oxide Dependent

To investigate if EG disruption by DCS is NO dependent, we quantified the EG of hCMEC monolayers under treatments of NO inhibition, NO and pretreatment of NOS inhibitor before DCS. The doses and durations of the treatments are the same as in **Figure 8**. **Figure 9A** demonstrates the confocal images of HS (green) on the hCMEC monolayer

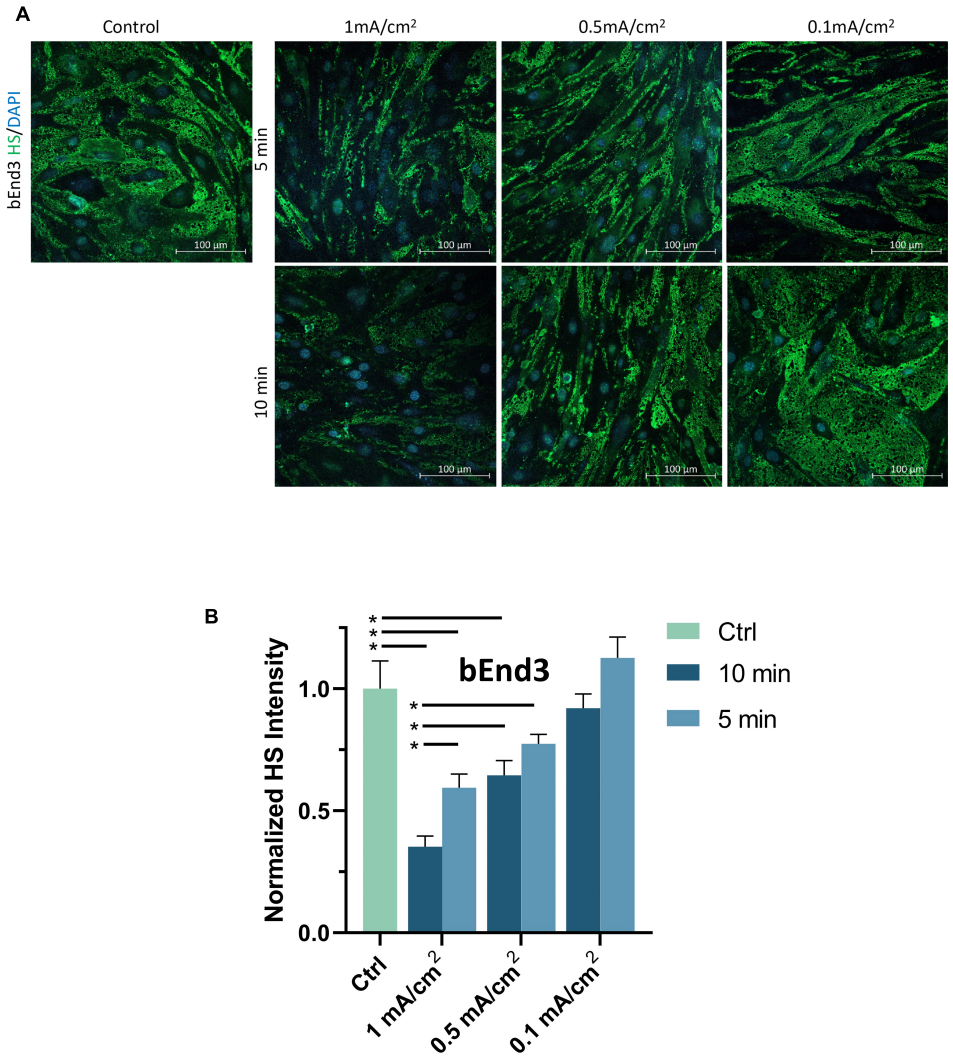


**FIGURE 6 |** Effects of DCS strength on HS of endothelial glycocalyx (EG) of *in vitro* BBB formed by bEnd3 monolayer. **(A)** Confocal images of heparan sulfate (HS) of EG on *in vitro* BBB and **(B)** comparison of HS intensity under control and after 5 min or 10 min treatments with 0.1, 0.5, or 1 mA/cm$^2$ DCS. *$p < 0.05$.

under control, DCS, SNP, NO inhibition by L-NMMA, and pretreatment with L-NMMA before DCS. **Figure 9B** compares the HS intensity under various treatments. L-NMMA alone has no influence on EG of *in vitro* BBB. Pretreatment with L-NMMA before DCS seems to protect the EG from DCS disruption. SNP greatly degrades the HS to 0.52 of the control, which has slightly smaller effect than that by DCS (0.31). The results indicate that disruption of EG by DCS is NO dependent.

## Disruption of Tight Junctions by Direct Current Stimulation Is Nitric Oxide Dependent

To further investigate if tight junction disruption by DCS is NO dependent, we quantified ZO-1 of bEnd3 monolayers under treatments of NO inhibition, NO and pretreatment of NOS inhibitor before DCS. The doses and durations of the treatments are the same as in **Figure 8**. Like what in **Figure 8A**, we measured the TEER of bEnd3 monolayer under these treatments, which are shown in **Figure 10A**. The effects of these treatments on TEER of bEnd3 monolayer are the same as those on TEER of hCMEC monolayer. **Figure 10** demonstrates the confocal images of ZO-1 (green) on the bEnd3 monolayer under control, DCS, SNP, NO inhibition by L-NMMA, and pretreatment with L-NMMA before DCS. **Figure 10C** compares the ZO-1 intensity distribution profiles under various treatments. In contrast to that on EG, L-NMMA alone significantly enhances the ZO-1 intensity to ∼2-fold that of the control. Pretreatment with L-NMMA before DCS partially abolishes the ZO-1 disruption by DCS. SNP greatly disrupts ZO-1 to 0.64 of the control, the same as that by DCS (0.69). The results indicate that disruption of ZO-1 by DCS is NO dependent.

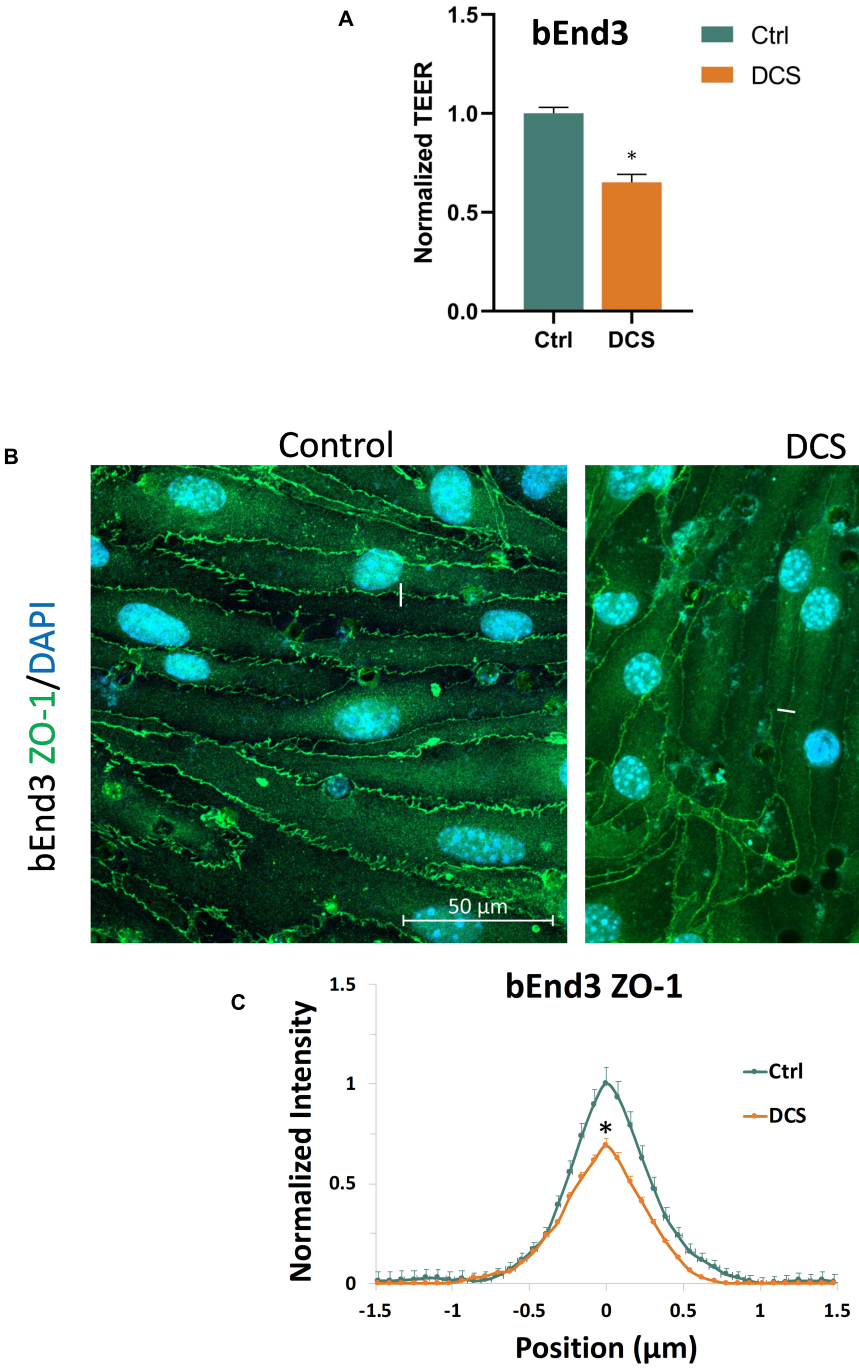


**FIGURE 7 |** Effects of DCS on TEER and tight junction protein ZO-1 of *in vitro* BBB formed by bEnd3 monolayer. **(A)** Normalized TEER, **(B)** confocal images of ZO-1 of *in vitro* BBB, and **(C)** comparison of the intensity profiles of ZO-1 along a ~3 μm line perpendicular to the EC junctions (white lines in the confocal images) under control and after 10 min treatment with 1 mA/cm$^2$ DCS. The peak intensity of ZO-1 from the control was used for the normalization. $n$ = 120 profiles for junctions between 30 ECs were averaged for each plot. *$p < 0.05$.

## DISCUSSION

Prior studies have shown the direct effects of electrical stimulation on endothelial cells (ECs), including re-orientation and secretion of vascular endothelial growth factors (VEGFs) (Bai et al., 2011) and NO (Trivedi et al., 2013). Our current study shows the direct effects of electrical stimulation (or DCS) on the *in vitro* BBB formed by the confluent EC monolayer with the comparable permeability to that of cerebral microvessels in rats (Shi et al., 2014b; Shin et al., 2020). The decreased

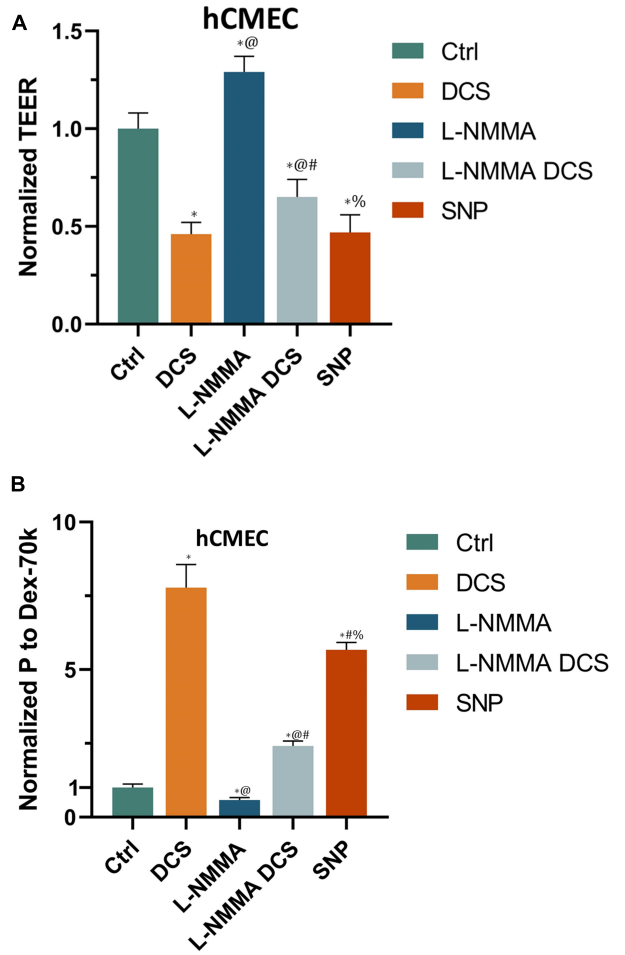


**FIGURE 8 |** Effects of a NOS inhibitor (L-NMMA) and a NO donor, sodium nitroprusside (SNP) on *in vitro* BBB TEER and permeability. **(A)** Normalized TEER and **(B)** normalized permeability to Dex-70K under control and after treatment of 10 min 1 mA/cm$^2$ DCS (DCS), or treatment of 60 min 1 mM L-NMMA, or pretreatment of 60 min 1 mM L-NMMA and treatment of 10 min 1 mA/cm$^2$ DCS (L-NMMA DCS), or treatment of 30 min 300 μM SNP (SNP). $n = 6$ samples for each case in **(A,B)**. $^{*}p < 0.05$, compared with the control, $^{@}p < 0.05$, compared with DCS, $^{\#}p < 0.05$, comparing L-NMMA DCS and SNP with L-NMMA, $^{\%}p < 0.05$, comparing SNP with L-NMMA DCS. The *in vitro* BBB was formed by hCMEC monolayer.

TEER and increased P to Dex-70k by DCS found in the current study are consistent with those prior findings *in vitro* since VEGF can enhance BBB permeability *in vivo* and *in vitro* (Shi et al., 2014a; Fan and Fu, 2016), and NO (by a NO donor, SNP) can decrease TEER and increase P to Dex-70k of *in vitro* BBB. Our *in vitro* results are also consistent with those from the prior *in vivo* study that tDCS can increase BBB permeability and this increase is NO dependent. Inhibition of NOS by pretreatment of L-NMMA reduced the BBB permeability increase by tDCS in rats (Shin et al., 2020). Nevertheless, in the *in vivo* setting, it is unclear if L-NMMA inhibits NOS of ECs, or NOS from other types of cells in the brain, or both. The current study on the *in vitro* BBB with only ECs showed that L-NMMA can inhibit NOS of ECs to diminish the increased BBB permeability by DCS, indicating that DCS can directly activate NOS of ECs in the BBB. The released NO from ECs by the DCS can modulate the blood vessel dilation and enhance blood perfusion to the brain, which were reported in humans (Stagg et al., 2013; Wang et al., 2015) and in animals (Mielke et al., 2013).

To investigate the structural mechanisms by which DCS altered BBB permeability, based on their *in vivo* permeability data for small and large solutes, by employing a transport model for the paracellular pathway of the BBB (Li et al., 2010b), Shin et al. (2020) predicted that tDCS increases the BBB permeability by altering the barrier structural components of the BBB, i.e., disrupting the EG, ECM, and tight junctions of ECs, as well as enlarging the width of the inter-endothelial cleft and the width of the BM. In the *in vivo* experiment of the current study, the finding that after tDCS treatment, the BBB permeability to the same sized solutes with opposite charge became identical although their permeability has 4-fold difference in the absence of tDCS, also suggests that the EG and ECM are temporally disrupted by tDCS because only the EG and ECM carry charge in the BBB.

However, it seems very challenging to detect the above structural changes *in vivo* due to transient behavior and nano-scale structures. We thus generated two *in vitro* BBB models, one formed by human cerebral microvascular endothelial cells (hCMEC) monolayer and another by mouse brain microvascular endothelial cells (bEnd3) monolayer. The generated *in vitro* BBB by both types of ECs has comparable solute permeability to that of rat cerebral microvessels (Yuan et al., 2010a,b; Shi et al., 2014b; Shin et al., 2020). The reason for using two types of ECs is that there was no good labeling for any junction formed on the hCMEC monolayer (**Supplementary Figure 2**) but good labeling for the tight and adherens junctions especially ZO-1 formed on bEnd3 monolayer (Li et al., 2010a; Yuan et al., 2010a; Fan and Fu, 2016).

The baseline TEER for hCMEC monolayers is 123.2 ± 2.6 Ωcm$^2$ and that for bEnd3 monolayers is 140.3 ± 3.5 Ωcm$^2$. The higher TEER of bEnd3 monolayers reflects a better tight junction at bEnd3 monolayers than that at hCMEC monolayers (Fu et al., 1994; Sugihara-Seki and Fu, 2005). But the higher permeability of bEnd3 monolayers to Dex-70k, $4.4 \times 10^{-7}$ cm/s (Yuan et al., 2010a), compared to $2.2 \times 10^{-7}$ cm/s of hCMEC monolayers (current study), suggests a fewer EG on bEnd3 monolayers (Fu and Shen, 2003; Sugihara-Seki and Fu, 2005; Yuan et al., 2010a; Kutuzov et al., 2018). By immunostaining the EG of the hCMEC/bEnd3 monolayer formed *in vitro* BBB and the tight junction ZO-1 of the bEnd3 monolayer formed *in vitro* BBB, we found that DCS disrupts the EG and ZO-1 when it is at a strength which significantly decreases the TEER and increases permeability to Dex-70k.

In the *in vivo* study on rats, the increased BBB permeability by the tDCS returned to the control level in 20 min. The recovery of the BBB permeability by the proper strength of tDCS guarantees its safety in clinical applications. Although in the *in vitro* study, we used the equivalent or smaller strength of DCS compared to that used *in vivo*, we did not see the recovery of the BBB permeability after 60 min (**Supplementary Figure 3**).

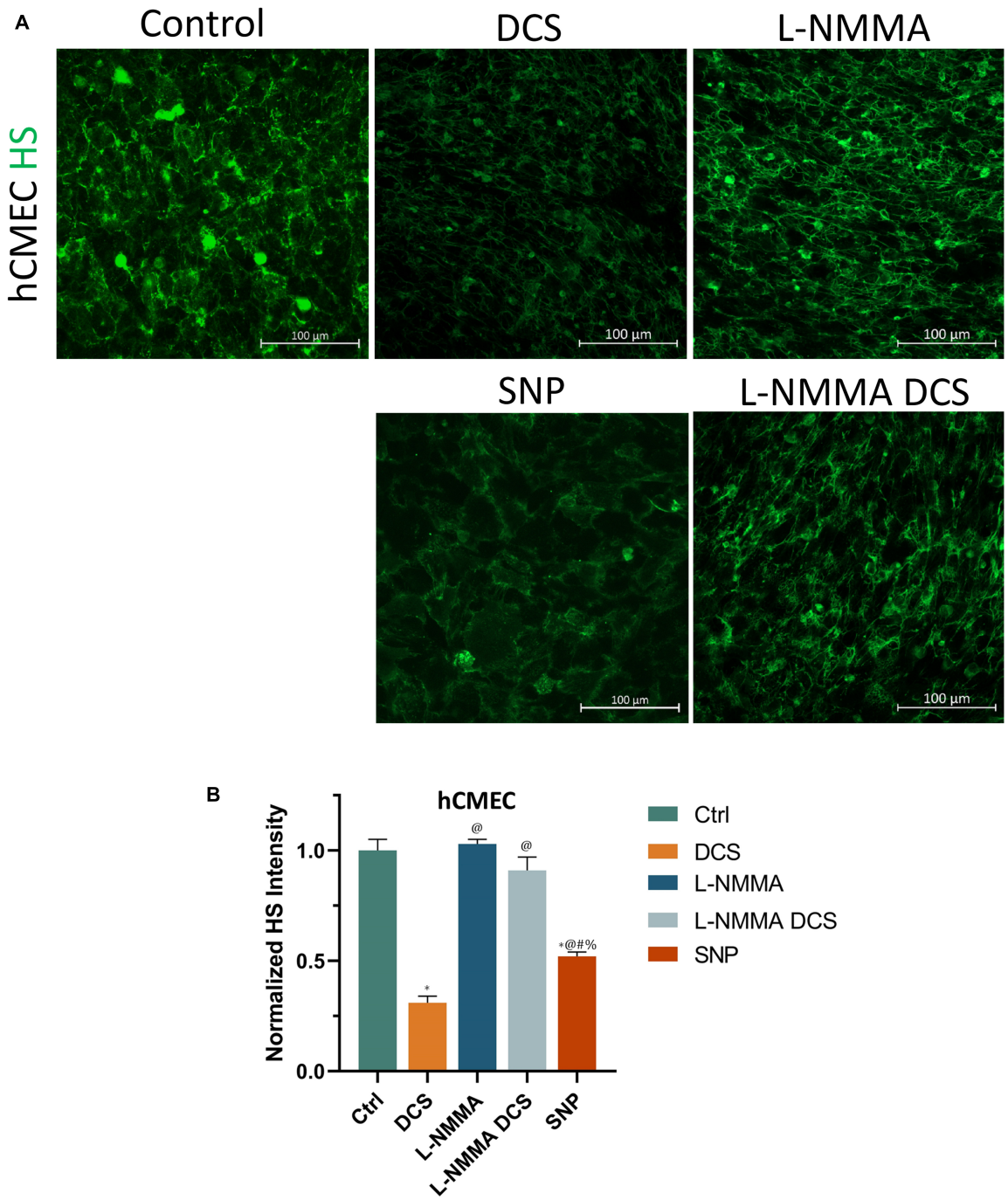


**FIGURE 9 |** Effects of a NOS inhibitor (L-NMMA) and a NO donor, sodium nitroprusside (SNP) on endothelial glycocalyx (EG) of *in vitro* BBB formed by hCMEC monolayer. **(A)** Confocal images of heparan sulfate (HS) of EG on *in vitro* BBB and **(B)** comparison of HS intensity under control and after treatment of 10 min 1 mA/cm$^2$ DCS (DCS), or treatment of 60 min 1 mM L-NMMA, or pretreatment of 60 min 1 mM L-NMMA and treatment of 10 min 1 mA/cm$^2$ DCS (L-NMMA DCS), or treatment of 30 min 300 μM SNP (SNP). $n = 3$ samples for each case in **(B)**. $^{*}p < 0.05$, compared with the control, $^{@}p < 0.05$, compared with DCS, $^{\#}p < 0.05$, comparing L-NMMA DCS and SNP with L-NMMA, $^{\%}p < 0.05$, comparing SNP with L-NMMA DCS.

Under this strength of DCS, there were no visible changes in the monolayer before and after treatment (**Supplementary Figure 4**). The possible reason is that in the brain, the BBB is a 3-D tube structure formed by ECs and surrounding pericytes and astrocyte foot processes. The tDCS- enlarged inter-cellular gaps by EC contractions can go back to the baseline when the tDCS triggered $Ca^{2+}$ and NO release (Marceglia et al., 2016; Monai et al., 2016) is over. The EG can be reconstructed

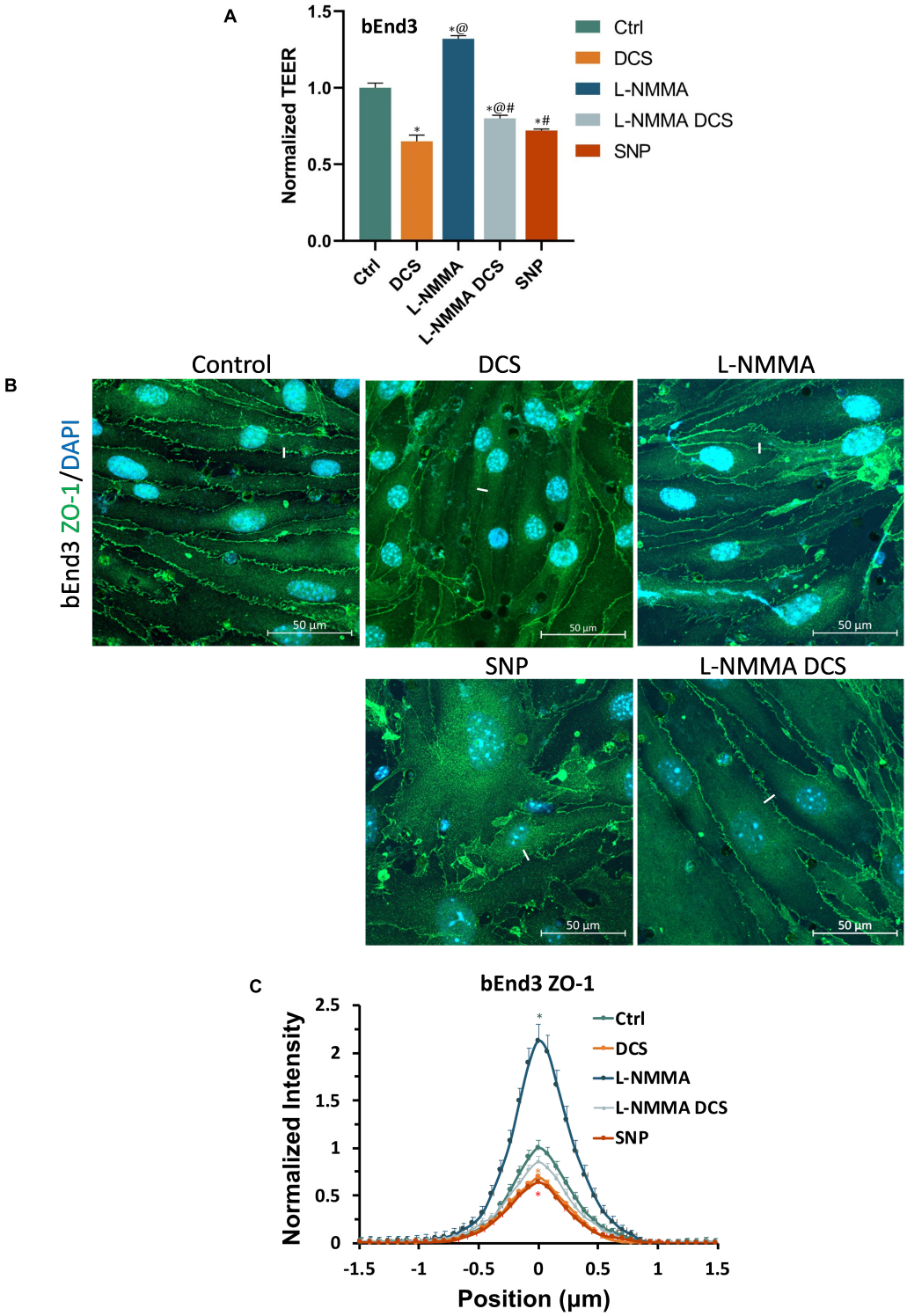


**FIGURE 10 |** Effects of a NOS inhibitor (L-NMMA) and a NO donor, sodium nitroprusside (SNP) on TEER and tight junction protein ZO-1 of *in vitro* BBB formed by bEnd3 monolayer. **(A)** Normalized TEER, **(B)** confocal images of ZO-1 of *in vitro* BBB, and **(C)** comparison of the intensity profiles of ZO-1 along a ~3 μm line perpendicular to the EC junctions (white lines in the confocal images) under control and after treatment of 10 min 1 mA/cm$^2$ DCS (DCS), or treatment of 60 min 1 mM L-NMMA, or pretreatment of 60 min 1 mM L-NMMA and treatment of 10 min 1 mA/cm$^2$ DCS (L-NMMA DCS), or treatment of 30 min 300 μM SNP (SNP). $n = 6$ samples for each case in **(A)** and $n = 3$ samples for each case in **(C)**. $^{*}p < 0.05$, compared with the control, $^{@}p < 0.05$, compared with DCS, $^{\#}p < 0.05$, comparing L-NMMA DCS and SNP with L-NMMA, $^{\%}p < 0.05$, comparing SNP with L-NMMA DCS.

by the components existing in the circulating blood (Zeng et al., 2018; Weinbaum et al., 2021). The disrupted EG and tight junctions can also be resynthesized by ECs (Zihni et al., 2016; Komarova et al., 2017) in the proper environment. In contrast, the *in vitro* BBB under study is formed by the EC monolayer cultured on a Transwell filter, which is a 2-D structure. When its ECs contract under DCS, the inter-endothelial cleft may not be able to go back to the original due to the attachment of the ECs and the filter membrane. The disrupted EG and tight junctions are also not able to recover due to lack of enough building components in the cell culture medium or lack of the proper environment for the re-synthesization. Although the *in vitro* 2-D BBB model cannot completely mimic the *in vivo* effects of tDCS on the BBB, it provides a convenient and direct measurement (snapshot) on the changes in the structural components of the BBB by DCS.

Cancel et al. (2018) used bEnd3 cells to generate an *in vitro* BBB. They showed that DCS can modulate water permeability of this *in vitro* BBB through electroosmosis but they did not observe the EC tight junction disruption by the DCS with the similar strength as we used. The discrepancy is that they used the Transwell filter with 0.4 μm pores which only accounts for 0.5% of the surface area of the filter, 99.5% of the area is not electrically conductive due to the material used to make the filter. In their set-up, only 0.5% of the EC monolayer received the DCS. Instead, we used the Transwell filter with 3 μm pores which accounts for 14.1% of surface area of the filter, 28.2-fold that of the pore area in the filter used in Cancel et al. (2018).

To further investigate the cellular signaling mechanisms by which DCS disrupts the EG and tight junction to increase the BBB permeability, we treated the *in vitro* BBB with a NOS inhibitor, L-NMMA, and a NO donor, SNP, as well as pretreatment with L-NMMA before DCS. We found that exogenous NO (by SNP) disrupts the EG and ZO-1, the same as DCS behaves. Although inhibition of NOS (to reduce NO release by ECs) by L-NMMA has no effects on the EG under control conditions, it can prevent the EG disruption from the DCS. On the other hand, L-NMMA can stimulate the formation of tight junction ZO-1 under control conditions and the reinforced tight junctions can diminish the tight junction disruption by the DCS. Our current results are consistent with previous studies. A prior study reported that NOS inhibition for 35 min or longer by 1 mM L-NMMA reduced the microvascular permeability of rat mesenteric microvessels to below the baseline value *in vivo* (Zhang et al., 2016). The reduced NO production by NOS inhibition was found to elevate intracellular cAMP levels by inhibiting phosphodiesterase 3 (Surapisitchat et al., 2007). cAMP has been reported to decrease permeability by strengthening the tight junction integrity (Adamson et al., 1998; Spindler et al., 2011; Fu et al., 2015; Fan and Fu, 2016).

Although hCMEC/bEnd3 monolayers may not be the best *in vitro* BBB model, their permeability to Dex-70k, $2.2 \times 10^{-7}$ cm/s for hCMEC (in current study) and $4.4 \times 10^{-7}$ cm/s for bEnd3 (Yuan et al., 2010a) are comparable to the permeability of rat cerebral microvessels measured *in vivo*, $1.1\text{-}1.3 \times 10^{-7}$ cm/s (Shi et al., 2014b; Shin et al., 2020). In addition, both monolayers have significant EG (HS) and bEnd3 has a very good tight junction protein ZO-1 expression. Furthermore, the TEER of both monolayers (123.2 $\Omega cm^2$ for hCMEC and 140.3 $\Omega cm^2$ for bEnd3) is much higher than the best TEER ($\sim$75 $\Omega cm^2$) of the mono-culture and co-culture *in vitro* BBB models formed from primary human cells including brain microvascular endothelial cells, astrocytes, pericytes and neurons (Stone et al., 2019). The permeability of hCMEC and bEnd3 monolayers to Dex-70k (2.2 and $4.4 \times 10^{-7}$ cm/s) is much smaller than that of the *in vitro* BBB formed from rat primary brain microvascular endothelial cells (Romero et al., 2003), which is $6.3 \times 10^{-7}$ cm/s. Therefore, the *in vitro* BBB models formed by hCMEC and bEnd3 cell lines are suitable for our purpose to directly visualize the structural changes in the BBB by the DCS, which can only be predicted by a mathematical model from the measured permeability data *in vivo*. Certainly, a better *in vitro* BBB model by using primary cells and co-coculture with the astrocytes/pericytes to achieve better barrier property should be utilized in the future study. In addition, a 3-D circular shaped *in vitro* BBB surrounded by a proper brain tissue mimicking hydrogel with a continuous perfusion system can be generated to simulate the real physiological conditions. Furthermore, to directly measure the effect of tDCS on the BBB ultra-structures, it is expected to develop an *in vivo* detecting technique by utilizing high-resolution multiphoton microscopy (Shi et al., 2014b; Kutuzov et al., 2018) and specific biomarkers for the junction proteins and glycocalyx/ECM, or transgenic animal models with optically detectable junction proteins and glycocalyx/ECM.

## CONCLUSION

In conclusion, our current study reveals that DCS increases the BBB permeability by disrupting the endothelial glycocalyx and tight junctions of the BBB and the disruption is NO dependent.

## DATA AVAILABILITY STATEMENT

The raw data supporting the conclusions of this article will be made available by the authors, without undue reservation.

## ETHICS STATEMENT

The animal study was reviewed and approved by the Animal Care and Use Committee at the City College of The City University of New York.

## AUTHOR CONTRIBUTIONS

The experiments described here were performed in the Microcirculation Laboratory at The City College of the City University of New York. BF and YX contributed

to the conception and design of the work. YX, YL, WK, and BF contributed to acquisition, analysis, and interpretation of data for the work. YX, MB, and BF contributed to drafting and revising the work. All authors approved the final version of the manuscript, agreed to be accountable for all aspects of the work in ensuring that questions related to the accuracy or integrity of any part of the work are appropriately investigated and resolved, designated as authors qualify for authorship, and all those who qualify for authorship are listed.

## FUNDING

This work was supported by the U.S. National Institutes of Health grants R01 NS101362 (BF and MB) and 1UG3UH3TR002151 (BF).

## SUPPLEMENTARY MATERIAL

The Supplementary Material for this article can be found online at: https://www.frontiersin.org/articles/10.3389/fcell.2021.731028/full#supplementary-material

**Supplementary Figure 1 |** Comparison of *in vitro* BBB permeability to Dex-70k measured with and without fixation. The *in vitro* BBB was formed by hCMEC monolayer.

**Supplementary Figure 2 |** Confocal images of ZO-1, claudin-5, occludin and VE-Cadherin at the *in vitro* BBB formed by hCMEC monolayer.

**Supplementary Figure 3 |** Comparison of normalized *in vitro* BBB permeability to Dex-70k under control and 0, 10, 30 and 60 min post 10 min 1 mA/cm$^2$ DCS treatment. *$p < 0.05$. The *in vitro* BBB was formed by hCMEC monolayer.

**Supplementary Figure 4 |** Bright-field images of the bEnd3 monolayer before and after 10 min–1 mA/cm$^2$ DCS.

## REFERENCES


Abbott, N. J., Rönnbäck, L., and Hansson, E. (2006). Astrocyte–endothelial interactions at the blood–brain barrier. *Nat. Rev. Neurosci.* 7, 41–53. doi: 10.1038/nrn1824

Adamson, R., Liu, B., Fry, G. N., Rubin, L., and Curry, F. (1998). Microvascular permeability and number of tight junctions are modulated by cAMP. *Am. J. Physiol. Heart Circ. Physiol.* 274, H1885–H1894. doi: 10.1152/ajpheart.1998.274.6.H1885

Adamson, R. H., Lenz, J. F., and Curry, F. E. (1994). Quantitative laser scanning confocal microscopy on single capillaries: permeability measurement. *Microcirculation* 1, 251–265. doi: 10.3109/10739689409146752

Alphonsus, C., and Rodseth, R. (2014). The endothelial glycocalyx: a review of the vascular barrier. *Anaesthesia* 69, 777–784. doi: 10.1111/anae.12661

Antal, A., Alekseichuk, I., Bikson, M., Brockmöller, J., Brunoni, A. R., Chen, R., et al. (2017). Low intensity transcranial electric stimulation: safety, ethical, legal regulatory and application guidelines. *Clin. Neurophysiol.* 128, 1774–1809. doi: 10.1016/j.clinph.2017.06.001

Bai, H., Forrester, J. V., and Zhao, M. (2011). DC electric stimulation upregulates angiogenic factors in endothelial cells through activation of VEGF receptors. *Cytokine* 55, 110–115. doi: 10.1016/j.cyto.2011.03.003

Brunoni, A. R., Nitsche, M. A., Bolognini, N., Bikson, M., Wagner, T., Merabet, L., et al. (2012). Clinical research with transcranial direct current stimulation (tDCS): challenges and future directions. *Brain Stimul.* 5, 175–195. doi: 10.1016/j.brs.2011.03.002

Cancel, L. M., Arias, K., Bikson, M., and Tarbell, J. M. (2018). Direct current stimulation of endothelial monolayers induces a transient and reversible increase in transport due to the electroosmotic effect. *Sci. Rep.* 8:9265. doi: 10.1038/s41598-018-27524-9

Duran, W. N., Breslin, J. W., and Sanchez, F. A. (2010). The NO cascade, eNOS location, and microvascular permeability. *Cardiovasc. Res.* 87, 254–261. doi: 10.1093/cvr/cvq139

Fan, J., and Fu, B. M. (2016). Quantification of malignant breast cancer cell MDA-MB-231 transmigration across brain and lung microvascular endothelium. *Ann. biomed. Eng.* 44, 2189–2201. doi: 10.1007/s10439-015-1517-y

Fan, J., Sun, Y., Xia, Y., Tarbell, J. M., and Fu, B. M. (2019). Endothelial surface glycocalyx (ESG) components and ultra-structure revealed by stochastic optical reconstruction microscopy (STORM). *Biorheology* 56, 77–88. doi: 10.3233/BIR-180204

Farkas, E., and Luiten, P. G. (2001). Cerebral microvascular pathology in aging and Alzheimer's disease. *Prog. Neurobiol.* 64, 575–611. doi: 10.1016/S0301-0082(00)00068-X

Fu, B., Weinbaum, S., Tsay, R., and Curry, F. (1994). A junction-orifice-fiber entrance layer model for capillary permeability: application to frog mesenteric capillaries. *J. Biomech. Eng.* 116, 502–513. doi: 10.1115/1.2895802

Fu, B. M. (2018). Transport across the blood-brain barrier. *Adv. Exp. Med. Biol.* 1097, 235–259. doi: 10.1007/978-3-319-96445-4_13

Fu, B. M., Adamson, R. H., and Curry, F. E. (1998). Test of a two-pathway model for small-solute exchange across the capillary wall. *Am. J. Physiol.* 274, H2062–H2073. doi: 10.1152/ajpheart.1998.274.6.H2062

Fu, B. M., Adamson, R. H., and Curry, F.-R. E. (2005). Determination of microvessel permeability and tissue diffusion coefficient of solutes by laser scanning confocal microscopy. *J. Biomech. Eng.* 127, 270–278. doi: 10.1115/1.1865186

Fu, B. M., and Shen, S. (2003). Structural mechanisms of acute VEGF effect on microvessel permeability. *Am. J. Physiol. Heart Circ. Physiol.* 284, H2124–H2135. doi: 10.1152/ajpheart.00894.2002

Fu, B. M., and Shen, S. (2004). Acute VEGF effect on solute permeability of mammalian microvessels in vivo. *Microvasc. Res.* 68, 51–62. doi: 10.1016/j.mvr.2004.03.004

Fu, B. M., and Tarbell, J. M. (2013). Mechano-sensing and transduction by endothelial surface glycocalyx: composition, structure, and function. *Wiley Interdiscip. Rev. Syst. Biol. Med.* 5, 381–390. doi: 10.1002/wsbm.1211

Fu, B. M., Yang, J., Cai, B., Fan, J., Zhang, L., and Zeng, M. (2015). Reinforcing endothelial junctions prevents microvessel permeability increase and tumor cell adhesion in microvessels in vivo. *Sci. Rep.* 5:15697. doi: 10.1038/srep15697

Giordano, J., Bikson, M., Kappenman, E. S., Clark, V. P., Coslett, H. B., Hamblin, M. R., et al. (2017). Mechanisms and effects of transcranial direct current stimulation. *Dose Response* 15:1559325816685467. doi: 10.1177/1559325816685467

Jackson, M. P., Rahman, A., Lafon, B., Kronberg, G., Ling, D., Parra, L. C., et al. (2016). Animal models of transcranial direct current stimulation: methods and mechanisms. *Clin. Neurophysiol.* 127, 3425–3454. doi: 10.1016/j.clinph.2016.08.016

Jackson, M. P., Truong, D., Brownlow, M. L., Wagner, J. A., Mckinley, R. A., Bikson, M., et al. (2017). Safety parameter considerations of anodal transcranial direct current stimulation in rats. *Brain Behav. Immun.* 64, 152–161. doi: 10.1016/j.bbi.2017.04.008

Kekic, M., Boysen, E., Campbell, I. C., and Schmidt, U. (2016). A systematic review of the clinical efficacy of transcranial direct current stimulation (tDCS) in psychiatric disorders. *J. Psychiatr. Res.* 74, 70–86. doi: 10.1016/j.jpsychires.2015.12.018

Kenney-Jung, D. L., Blacker, C. J., Camsari, D. D., Lee, J. C., and Lewis, C. P. (2019). Transcranial direct current stimulation: mechanisms and psychiatric applications. *Child Adolesc. Psychiatr. Clin. N. Am.* 28, 53–60. doi: 10.1016/j.chc.2018.07.008

Komarova, Y. A., Kruse, K., Mehta, D., and Malik, A. B. (2017). Protein interactions at endothelial junctions and signaling mechanisms regulating endothelial permeability. *Circ. Res.* 120, 179–206. doi: 10.1161/CIRCRESAHA.116.306534

Kutuzov, N., Flyvbjerg, H., and Lauritzen, M. (2018). Contributions of the glycocalyx, endothelium, and extravascular compartment to the blood–brain barrier. *Proc. Natl. Acad. Sci. U.S.A.* 115, E9429–E9438. doi: 10.1073/pnas.1802155115

Li, G., and Fu, B. M. (2011). An electrodiffusion model for the blood-brain barrier permeability to charged molecules. *J. Biomech. Eng.* 133:021002. doi: 10.1115/1.4003309

Li, G., Yuan, W., and Fu, B. M. (2010b). A model for the blood–brain barrier permeability to water and small solutes. *J. Biomech.* 43, 2133–2140. doi: 10.1016/j.jbiomech.2010.03.047

Li, G., Simon, M. J., Cancel, L. M., Shi, Z.-D., Ji, X., Tarbell, J. M., et al. (2010a). Permeability of endothelial and astrocyte cocultures: in vitro blood–brain barrier models for drug delivery studies. *Ann. Biomed. Eng.* 38, 2499–2511. doi: 10.1007/s10439-010-0023-5

Marceglia, S., Mrakic-Sposta, S., Rosa, M., Ferrucci, R., Mameli, F., Vergari, M., et al. (2016). Transcranial direct current stimulation modulates cortical neuronal activity in Alzheimer's disease. *Front. Neurosci.* 10:134. doi: 10.3389/fnins.2016.00134

Mielke, D., Wrede, A., Schulz-Schaeffer, W., Taghizadeh-Waghefi, A., Nitsche, M. A., Rohde, V., et al. (2013). Cathodal transcranial direct current stimulation induces regional, long-lasting reductions of cortical blood flow in rats. *Neurol. Res.* 35, 1029–1037. doi: 10.1179/1743132813Y.0000000248

Monai, H., Ohkura, M., Tanaka, M., Oe, Y., Konno, A., Hirai, H., et al. (2016). Calcium imaging reveals glial involvement in transcranial direct current stimulation-induced plasticity in mouse brain. *Nat. Commun.* 7:11100. doi: 10.1038/ncomms11100

Nitsche, M. A., and Paulus, W. (2000). Excitability changes induced in the human motor cortex by weak transcranial direct current stimulation. *J. Physiol.* 527(Pt 3), 633–639. doi: 10.1111/j.1469-7793.2000.t01-1-00633.x

Palm, U., Hasan, A., Strube, W., and Padberg, F. (2016). tDCS for the treatment of depression: a comprehensive review. *Eur. Arch. Psychiatry Clin. Neurosci.* 266, 681–694. doi: 10.1007/s00406-016-0674-9

Romero, I. A., Radewicz, K., Jubin, E., Michel, C. C., Greenwood, J., Couraud, P.-O., et al. (2003). Changes in cytoskeletal and tight junctional proteins correlate with decreased permeability induced by dexamethasone in cultured rat brain endothelial cells. *Neurosci. Lett.* 344, 112–116. doi: 10.1016/S0304-3940(03)00348-3

Sarrazin, S., Lamanna, W. C., and Esko, J. D. (2011). Heparan sulfate proteoglycans. *Cold Spring Harb. Perspect. Biol.* 3:a004952. doi: 10.1101/cshperspect.a004952

Shi, L., Zeng, M., Sun, Y., and Fu, B. M. (2014b). Quantification of blood-brain barrier solute permeability and brain transport by multiphoton microscopy. *J. Biomech. Eng.* 136:031005. doi: 10.1115/1.4025892

Shi, L., Zeng, M., and Fu, B. M. (2014a). Temporal effects of vascular endothelial growth factor and 3, 5-cyclic monophosphate on blood–brain barrier solute permeability in vivo. *J. Neurosci. Res.* 92, 1678–1689. doi: 10.1002/jnr.23457

Shin, D. W., Fan, J., Luu, E., Khalid, W., Xia, Y., Khadka, N., et al. (2020). In vivo modulation of the blood–brain barrier permeability by transcranial direct current stimulation (tDCS). *Ann. Biomed. Eng.* 48, 1256–1270. doi: 10.1007/s10439-020-02447-7

Spindler, V., Peter, D., Harms, G. S., Asan, E., and Waschke, J. (2011). Ultrastructural analysis reveals cAMP-dependent enhancement of microvascular endothelial barrier functions via Rac1-mediated reorganization of intercellular junctions. *Am. J. Pathol.* 178, 2424–2436. doi: 10.1016/j.ajpath.2011.01.014

Stagg, C. J., Lin, R. L., Mezue, M., Segerdahl, A., Kong, Y., Xie, J., et al. (2013). Widespread modulation of cerebral perfusion induced during and after transcranial direct current stimulation applied to the left dorsolateral prefrontal cortex. *J. Neurosci.* 33, 11425–11431. doi: 10.1523/JNEUROSCI.3887-12.2013

Steinberg, H. (2013). Letter to the editor: transcranial direct current stimulation (tDCS) has a history reaching back to the 19th century. *Psychol. Med.* 43, 669–671. doi: 10.1017/S0033291712002929

Stone, N. L., England, T. J., and O'sullivan, S. E. (2019). A novel transwell blood brain barrier model using primary human cells. *Front. Cell. Neurosci.* 13:230. doi: 10.3389/fncel.2019.00230

Sugihara-Seki, M., and Fu, B. M. M. (2005). Blood flow and permeability in microvessels. *Fluid Dyn. Res.* 37, 82–132. doi: 10.1016/j.fluiddyn.2004.03.006

Surapisitchat, J., Jeon, K.-I., Yan, C., and Beavo, J. A. (2007). Differential regulation of endothelial cell permeability by cGMP via phosphodiesterases 2 and 3. *Circ. Res.* 101, 811–818. doi: 10.1161/CIRCRESAHA.107.154229

Trivedi, D. P., Hallock, K. J., and Bergethon, P. R. (2013). Electric fields caused by blood flow modulate vascular endothelial electrophysiology and nitric oxide production. *Bioelectromagnetics* 34, 22–30. doi: 10.1002/bem.21741

Truong, D. Q., and Bikson, M. (2018). Physics of transcranial direct current stimulation devices and their history. *J. ECT* 34, 137–143. doi: 10.1097/YCT.0000000000000531

Wang, Y., Hao, Y., Zhou, J., Fried, P. J., Wang, X., Zhang, J., et al. (2015). Direct current stimulation over the human sensorimotor cortex modulates the brain's hemodynamic response to tactile stimulation. *Eur. J. Neurosci.* 42, 1933–1940. doi: 10.1111/ejn.12953

Weinbaum, S., Cancel, L. M., Fu, B. M., and Tarbell, J. M. (2021). The glycocalyx and its role in vascular physiology and vascular related diseases. *Cardiovasc. Eng. Technol.* 12, 37–71. doi: 10.1007/s13239-020-00485-9

Woods, A. J., Antal, A., Bikson, M., Boggio, P. S., Brunoni, A. R., Celnik, P., et al. (2016). A technical guide to tDCS, and related non-invasive brain stimulation tools. *Clin. Neurophysiol.* 127, 1031–1048. doi: 10.1016/j.clinph.2015.11.012

Xia, Y., Khalid, W., Yin, Z., Huang, G., Bikson, M., and Fu, B. M. (2020). Modulation of solute diffusivity in brain tissue as a novel mechanism of transcranial direct current stimulation (tDCS). *Sci. Rep.* 10:18488. doi: 10.1038/s41598-020-75460-4

Yoon, J.-H., Lee, E.-S., and Jeong, Y. (2017). In vivo imaging of the cerebral endothelial glycocalyx in mice. *J. Vasc. Res.* 54, 59–67. doi: 10.1159/000457799

Yuan, W., Li, G., Zeng, M., and Fu, B. M. (2010b). Modulation of the blood–brain barrier permeability by plasma glycoprotein orosomucoid. *Microvasc. Res.* 80, 148–157. doi: 10.1016/j.mvr.2010.03.011

Yuan, W., Li, G., and Fu, B. M. (2010a). Effect of surface charge of immortalized mouse cerebral endothelial cell monolayer on transport of charged solutes. *Ann. Biomed. Eng.* 38, 1463–1472. doi: 10.1007/s10439-010-9920-x

Yuan, W., Lv, Y., Zeng, M., and Fu, B. M. (2009). Non-invasive measurement of solute permeability in cerebral microvessels of the rat. *Microvasc. Res.* 77, 166–173. doi: 10.1016/j.mvr.2008.08.004

Zeng, Y., Zhang, X. F., Fu, B. M., and Tarbell, J. M. (2018). "The role of endothelial surface glycocalyx in mechanosensing and transduction," in *Molecular, Cellular, and Tissue Engineering of the Vascular System*, eds B. Fu and N. Wright (Cham: Springer), 1–27. doi: 10.1007/978-3-319-96445-4_1

Zhang, L., Zeng, M., and Fu, B. M. (2016). Inhibition of endothelial nitric oxide synthase decreases breast cancer cell MDA-MB-231 adhesion to intact microvessels under physiological flows. *Am. J. Physiol. Heart Circ. Physiol.* 310, H1735–H1747. doi: 10.1152/ajpheart.00109.2016

Zihni, C., Mills, C., Matter, K., and Balda, M. S. (2016). Tight junctions: from simple barriers to multifunctional molecular gates. *Nat. Rev. Mol. Cell Biol.* 17:564. doi: 10.1038/nrm.2016.80

Zullo, J. A., Fan, J., Azar, T. T., Yen, W., Zeng, M., Chen, J., et al. (2016). Exocytosis of endothelial lysosome-related organelles hair-triggers a patchy loss of glycocalyx at the onset of sepsis. *Am. J. Pathol.* 186, 248–258. doi: 10.1016/j.ajpath.2015.10.001

**Conflict of Interest:** The authors declare that the research was conducted in the absence of any commercial or financial relationships that could be construed as a potential conflict of interest.

**Publisher's Note:** All claims expressed in this article are solely those of the authors and do not necessarily represent those of their affiliated organizations, or those of the publisher, the editors and the reviewers. Any product that may be evaluated in this article, or claim that may be made by its manufacturer, is not guaranteed or endorsed by the publisher.

frontiers in Cell and Developmental Biology

ORIGINAL RESEARCH
published: 07 October 2021
doi: 10.3389/fcell.2021.731666

# Matrix Stiffness Affects Glycocalyx Expression in Cultured Endothelial Cells

*Marwa Mahmoud*, Limary Cancel and John M. Tarbell**

*Tarbell Lab, Department of Biomedical Engineering, The City University of New York, New York, NY, United States*

**Rationale:** The endothelial cell glycocalyx (GCX) is a mechanosensor that plays a key role in protecting against vascular diseases. We have previously shown that age/disease mediated matrix stiffness inhibits the glycocalyx glycosaminoglycan heparan sulfate and its core protein Glypican 1 in human umbilical vein endothelial cells, rat fat pad endothelial cells and in a mouse model of age-mediated stiffness. Glypican 1 inhibition resulted in enhanced endothelial cell dysfunction. Endothelial cell culture typically occurs on stiff matrices such as plastic or glass. For the study of the endothelial GCX specifically it is important to culture cells on soft matrices to preserve GCX expression. To test the generality of this statement, we hypothesized that stiff matrices inhibit GCX expression and consequently endothelial cell function in additional cell types: bovine aortic endothelial cells, mouse aortic endothelial cell and mouse brain endothelial cells.

**Methods and Results:** All cell types cultured on glass showed reduced GCX heparan sulfate expression compared to cells cultured on either soft polyacrylamide (PA) gels of a substrate stiffness of 2.5 kPa (mimicking the stiffness of young, healthy arteries) or on either stiff gels 10 kPa (mimicking the stiffness of old, diseased arteries). Specific cell types showed reduced expression of GCX protein Glypican 1 (4 of 5 cell types) and hyaluronic acid (2 of 5 cell types) on glass vs soft gels.

**Conclusion:** Matrix stiffness affects GCX expression in endothelial cells. Therefore, the study of the endothelial glycocalyx on stiff matrices (glass/plastic) is not recommended for specific cell types.

**Keywords: endothelial cells, matrix stiffness, glycocalyx, heparan sulfate, glypican 1**

OPEN ACCESS

***Edited by:***
*Ye Zeng,*
*Sichuan University, China*

***Reviewed by:***
*Fitzroy Curry,*
*University of California, Davis, United States*
*Hongyan Kang,*
*Beihang University, China*

****Correspondence:***
*Marwa Mahmoud*
*mmahmoud@ccny.cuny.edu*
*John M. Tarbell*
*jtarbell@ccny.cuny.edu*

***Specialty section:***
*This article was submitted to Signaling, a section of the journal Frontiers in Cell and Developmental Biology*

***Received:*** *27 June 2021*
***Accepted:*** *15 September 2021*
***Published:*** *07 October 2021*

***Citation:***
*Mahmoud M, Cancel L and Tarbell JM (2021) Matrix Stiffness Affects Glycocalyx Expression in Cultured Endothelial Cells. Front. Cell Dev. Biol. 9:731666. doi: 10.3389/fcell.2021.731666*

## INTRODUCTION

Endothelial cells (ECs) are highly sensitive to mechanical forces and respond to these forces by altering gene expression and downstream signaling pathways (Davies, 2009; Baeyens et al., 2016; Chistiakov et al., 2017). Age/disease related arterial stiffness along with blood flow shear stress are prominent mechanical forces controlling endothelial cell function and vascular disease (Duprez, 2010; Mitchell et al., 2010; Maruhashi et al., 2018).

Endothelial cells lining the vasculature are covered by a multifunctional surface layer of glycans that is referred to as the endothelial glycocalyx (GCX). The common classes of glycans found in the GCX are glycoproteins and proteoglycans. Heparan sulfate proteoglycans (HSPG) are composed

of core proteins, including Glypicans that are bound to the plasma membrane by GPI anchors and Syndecans that are transmembrane, with covalently bound glycosaminoglycan (GAG) chains. Heparan sulfate (HS, GAG associated with Glypicans and Syndecans), chondroitin sulfate (CS, GAG associated with Syndecans) and Hyaluronic acid (HA, non-sulfated GAG that binds to surface receptors, e.g., CD44) are the prevalent GAGs on EC surfaces (Weinbaum et al., 2007; Tarbell and Cancel, 2016).

The endothelial GCX is mechanosensor that translates external forces into genetic and functional changes in cells. In addition, the GCX plays an essential role in maintaining EC integrity and vascular homeostasis by preserving barrier function, suppressing inflammation, and cell turnover and mediating flow-induced nitric oxide release (Ebong et al., 2010; Cancel et al., 2016; Tarbell and Cancel, 2016; Bartosch et al., 2017; Mitra et al., 2017; Russell-Puleri et al., 2017). The expression of the endothelial glycocalyx is suppressed under pathological conditions such as hypertension, aging, and disturbed blood flow (Mitra et al., 2017; Harding et al., 2018; Machin et al., 2018; Nelson et al., 2018). We have previously shown using human umbilical vein endothelial cells (HUVECs) and rat fat pad endothelial cells (RFPECs) grown on polyacrylamide (PA) gels of varying stiffnesses representative of healthy or aged/diseased vessels, that age/disease related stiffness promotes endothelial cell inflammation and vascular disease through the suppression of the proteoglycan Glypican 1 and its associated GAG, HS. Glypican 1 in turn plays a protective role in preventing EC dysfunction in response to stiffness (Mahmoud et al., 2021).

We have not considered Perlecan or other matrix proteoglycans that are not bound directly to the EC by a GPI anchor (glypican) or a transmembrane anchor (syndecan) as discussed in Varki et al. (2009). We are only looking at cell bound molecules that might be involved in mechanotransduction. HS and HA were the only GAGs studied in Mahmoud et al. (2021) because in Pahakis et al. (2007) in RFPECs, it was shown that CS was not involved in mechanotransduction to produce nitric oxide (NO) or prostacyclin ($PGI_2$). In Zeng et al. (2012) it was shown that CS had much lower surface concentration than either HS or HA. In addition, Syndecan 1 and CD44 were not affected by stiffness on HUVECs and RFPECs in Mahmoud et al. (2021) so they were not included in the present study.

Matrix stiffness is defined as the rigidity of the substrate on which cells grow as typically characterized by the Young's modulus. Most endothelial cell culture studies involve the seeding of cells on stiff surfaces such as plastic cell culture surfaces or glass. The stiff matrices may have an influence on the expression of the endothelial glycocalyx and thus may impact the study of the glycocalyx *in vitro*. As a follow up to our previous study that utilized HUVECs and RFPECs (Mahmoud et al., 2021), here we examine additional common EC types (BAECs, MAECs, and bEnd3) to examine whether the expression of the glycocalyx protein Glypican 1, and GAG HS are affected by matrix stiffness in different endothelial cell types. Our previous study concluded that reduction of Glypican 1 and HS with increased stiffness were associated with endothelial dysfunction. For that reason, we will focus on studying the expression of Glypican 1 and HS in different commonly used cell types and not on endothelial function. Here we show that matrix stiffness inhibits glycocalyx expression in multiple types of endothelial cells widely used in cell culture studies, suggesting that studies of the glycocalyx on glass and plastic should be interpreted with caution and that softer substrates are encouraged to be employed for studies involving glycocalyx biology.

# MATERIALS AND METHODS

## Culture of Cells on to Polyacrylamide Gels

Bovine Arterial Endothelial Cells (BAECs), Mouse Aortic Endothelial Cells (MAECs), and Brain-derived endothelial cells 3 (bEnd3) cells were maintained and cultured as previously described (Cancel et al., 2007, 2021; Nikmanesh et al., 2019). BAECs and MAECs were used at passages P5–7, and bEnd3 at P 24–26. Cells were cultured on Polyacrylamide gels as described previously (Mahmoud et al., 2021). Briefly, PA gels were synthesized using different percentages of 30% Acrylamide (Sigma) and Bis-Acrylamide (Sigma) solutions to give a substrate stiffness of either 2.5 or 10 kPa. Cells were seeded on to glass coverslips covered with Fibronectin (Sigma) (60 μg/ml)-coated Polyacrylamide gels and placed into 6-well plate cell culture dishes (Corning). Alternatively, Cells were seeded directly onto Fibronectin-coated glass coverslips for the glass control. Following 48 h of seeding, the cells were processed for immunostaining or for lysis followed by mRNA isolation as previously described (Mahmoud et al., 2021).

## Quantitative Polymerase Chain Reaction

Following mRNA isolation, reverse transcription was carried out using High-Capacity cDNA Reverse Transcription Kit (ThermoScientific), following the manufacturer's instructions. The reaction took place using a thermal cycler (DNA Engine, Biorad) and thermal profile was determined following the manufacturer's recommendations. Gene expression was assessed by quantitative polymerase chain reaction (qPCR) on an ABI Prism 7000 Sequence detection system, using gene-specific primers for Glypican 1 and housekeeping gene HPRT (Mahmoud et al., 2021). Data was analyzed using the comparative Ct ($2^{-\Delta\Delta CT}$) method.

## Immunostaining

The expression of GAGs was assessed in ECs by immunostaining. Heparan Sulfate and Hyaluronic Acid expression were assessed as described previously (Mahmoud et al., 2021). The cells were briefly washed with 1 × Dulbecco's phosphate-buffered saline (DPBS) and fixed with 2% paraformaldehyde/0.1% glutaraldehyde for 30 min at RT, then blocked with 2% Goat serum (GS, Invitrogen, United States) for 30 min. This was followed by an overnight incubation at 4°C with mouse monoclonal primary antibody (For HS;1:100; 10E4 epitope, AMS Biotechnology, United States; or HepSS-1, US Biological, United States or for HA; biotinylated hyaluronic acid binding protein (HABP; 50 μg/mL; EMD Chemicals, United States). Cells were then washed three times in

1 × DPBS, and finally incubated with Alexa Fluor 488 goat anti-mouse secondary antibody for HS (1:400; Molecular Probes, United States) or for HA (Alexa Fluor 488 anti-Biotin (1:100; Jackson ImmunoResearch Lab, United States) for 30 min at RT followed by three washes in 1 × DPBS. The cells were visualized by confocal laser imaging using a ZEISS LSM 800 microscope. Image collection and analysis were carried out as in Zeng et al. (2012). Briefly, Z stacks were obtained with interval slices of 0.4 μm. Images were analyzed using Image J software (1.47 V). The maximum intensity Z-projection of the green Z-series stack (Alexa Fluor 488 channel) was created from which intensity and coverage were calculated.

## Statistical Analysis

All results were generated from at least three independent experiments. Differences between samples were analyzed using a One-way ANOVA for comparison among more than two groups ($^{*}p < 0.05$, $^{**}p < 0.01$, $^{***}p < 0.001$). The mean + Standard Error of mean (SEM) was plotted in all graphs.

# RESULTS

We assessed the effects of matrix stiffness on GCX expression by culturing multiple cell types; BAECs, MAECs, and bEnd3 on polyacrylamide gels at a substrate stiffness of either 2.5 kPa (mimicking the subendothelial layer stiffness of young/healthy arteries) or 10 kPa (mimicking the subendothelial layer stiffness of aged/unhealthy arteries), or on glass (Mahmoud et al., 2021).

Glycocalyx expression was assessed by immunostaining for the most abundant glycocalyx GAG side chain, heparan sulfate (HS). HS expression was inhibited on glass vs on soft, 2.5 kPa, gels for BAECS, MAECS, and bEnd3 cells (**Figures 1A,B**). These

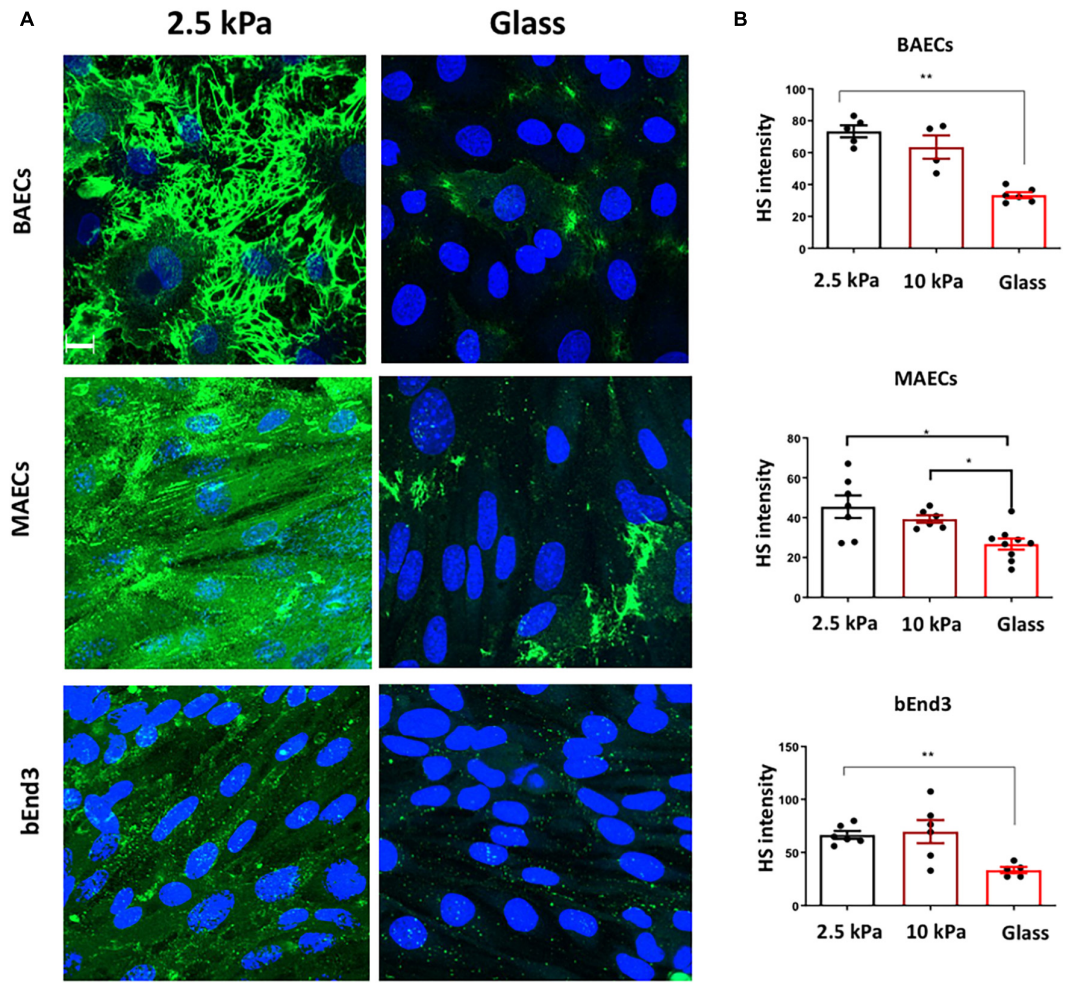


**FIGURE 1 |** Stiffness inhibits Heparan Sulfate GAG expression on the surface of endothelial cells. **(A)** Bovine aortic endothelial cells (BAECs), Mouse aortic endothelial cells (MAECs) and brain-derived endothelial cells 3 (BEND3) were cultured onto polyacrylamide gels at stiffness of 2.5 kPa (soft gel), 10 kPa (stiff gel) or on glass until confluent. Heparan Sulfate (HS) (green) expression was assessed by immunostaining. Cell nuclei were identified using DAPI 4′,6-diamidino-2-phenylindole (DAPI) (blue). Scale bar = 10 μm. **(B)** Heparan sulfate expression was quantified as fluorescent intensity. Mean values ± SEM are shown. $N = 6$. $^{*}P < 0.05$ and $^{**}P < 0.01$ and using a One-way ANOVA test. N.S indicates no statistically significant difference.

data revealed that similar to HUVECs and RFPECs (Mahmoud et al., 2021) these endothelial cells types also showed reduced HS expression on stiff matrices.

We next assessed the expression of Hyaluronic Acid (HA) GAG on the surface of endothelial cells. Immunostaining showed that the expression of HA was significantly inhibited on the surface of BAECs, but not on MAECs and bEnd3 cells cultured on glass vs. on soft 2.5 kPa PA gels (**Figures 2A,B**). These data show that HA expression is not consistently affected in different cell types in response to stiffness. This data is consistent with our previously published data showing that HA expression was not affected by stiffness in HUVECs, whereas in RFPECs HA expression was inhibited by stiff matrices (Mahmoud et al., 2021).

We have previously shown that matrix stiffness promoted EC dysfunction through inhibiting the GCX proteoglycan Glypican 1 (Mahmoud et al., 2021). Thus, to assess if stiffness also inhibited Glypican 1 in other endothelial cell types we assessed Glypican 1 mRNA expression by qPCR in BAECs, MAECs and bEnd3 cells. The results showed that Glypican 1 expression was inhibited in MAECs and bEnd3 cultured on stiff matrices (glass/10 kPa gels) vs. on soft gels (**Figures 3A–C**), whereas Glypican 1 expression was not significantly changed in BAECs.

The results of these new experiments with BAECs, MAECs, and bEnd3 cells along with previous results for HUVECs and RFPECs are summarized in **Figures 4**, **5**. The data reveal that HS was inhibited in response to matrix stiffness in all cell types tested, however, HA and Glypican 1 expression were affected differently in different cell types. Glypican 1 expression was reduced in all tested cell types except BAECs. The expression of HA was affected in RFPECs and BAECs cultured on stiff matrices

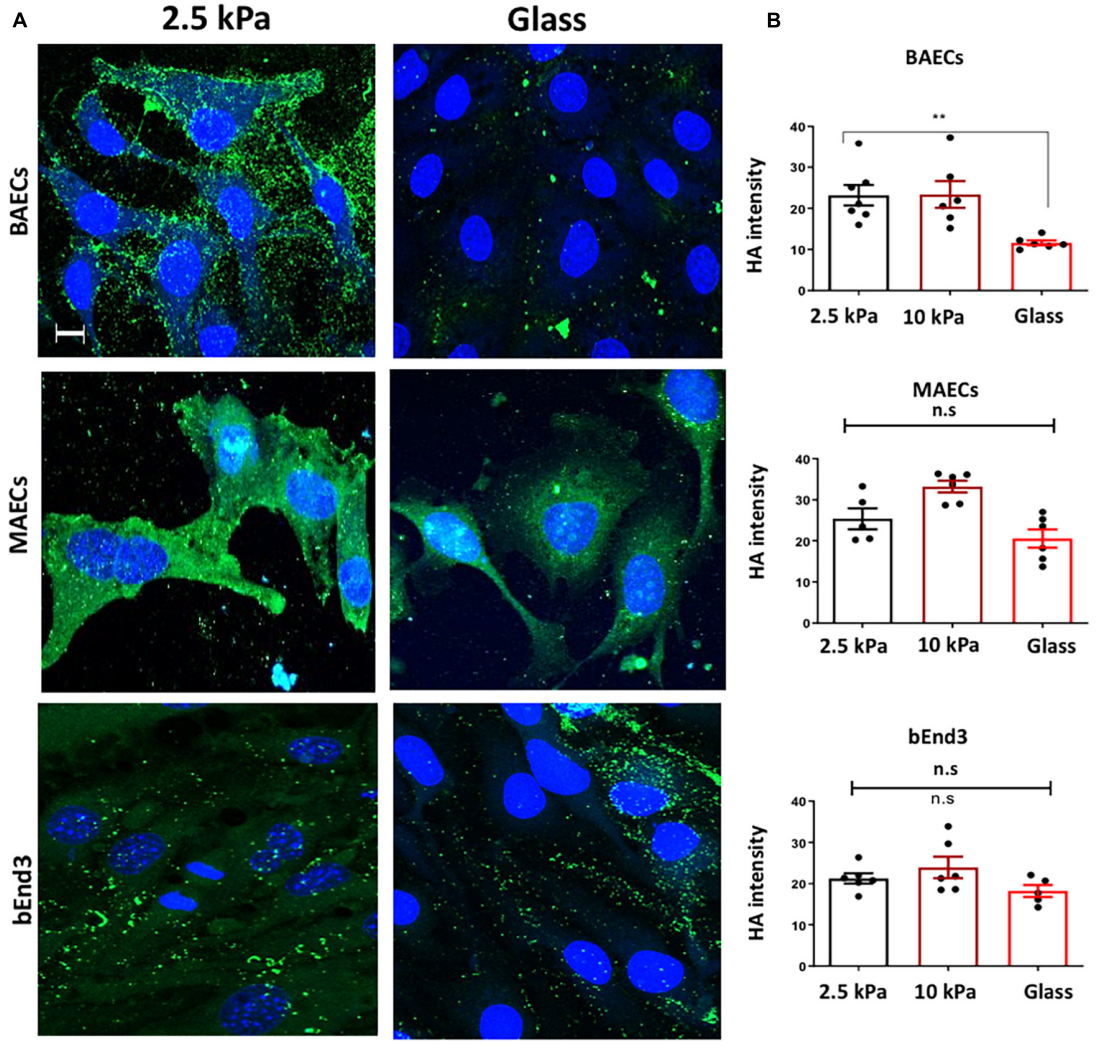


**FIGURE 2 |** Stiffness inhibits Hyaluronic Acid GAG expression on the surface of BAECs, but not MAECs and BEND3 cells. **(A)** BAECs, MAECs, and BEND3 were cultured onto polyacrylamide gels at stiffness of 2.5 kPa (soft gel), 10 kPa (stiff gel) or on glass until confluent. Hyaluronic Acid (HA) (green) expression was assessed by immunostaining. Cell nuclei were identified using DAPI 4′,6-diamidino-2-phenylindole (DAPI) (blue). Scale bar = 10 μm. **(B)** Hyaluronic Acid expression was quantified as fluorescent intensity. Mean values ± SEM are shown. $N = 6$. $^{*}P < 0.05$ and $^{**}P < 0.01$ using a One-way ANOVA test. N.S indicates no statistically significant difference was found.

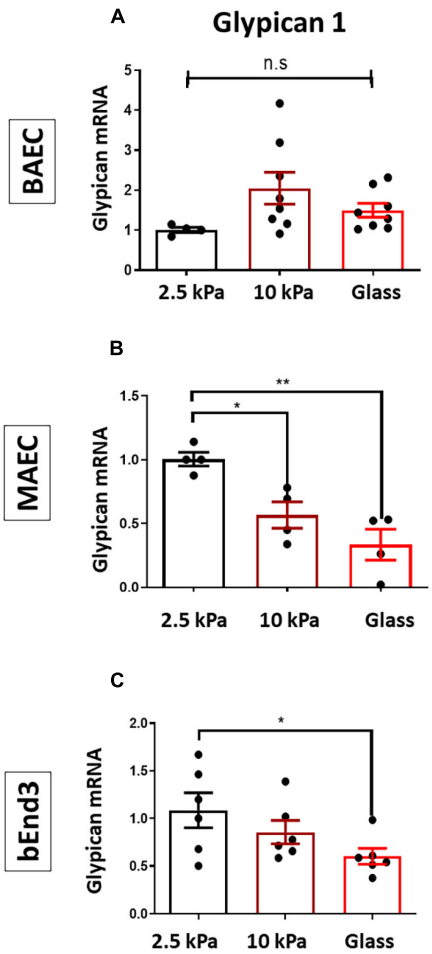


**FIGURE 3 |** Stiffness inhibits the expression of Glypican 1 in endothelial cells. **(A)** BAECs, **(B)** MAECs, and **(C)** bEnd3 were cultured onto polyacrylamide gels at stiffness of 2.5 kPa (soft gel), 10 kPa (stiff gel) or on glass until confluent. The expression of Glypican 1 mRNA was assessed by qPCR from cells cultured on either 2.5,10 kPa gels or on glass. Hypoxanthine phosphor-ribosyl transferase (HPRT) was used as a housekeeping gene. Mean values ± SEM are shown. $N = 5–8$, $^{*}P < 0.05$ and $^{**}P < 0.01$ using a One-way ANOVA test. N.S indicates no statistically significant difference was found.

(glass/10 kPa gel), but not the other 3 cell types. The data suggest that depending on the endothelial cell origin the endothelial GCX components (HS, HA, and Glypican 1) are inhibited by matrix stiffness. Matrix stiffness inhibition of the endothelial glycocalyx potentially leads to changes in EC function (**Figure 4**).

## DISCUSSION

With increased age and hypertension, arteries lose elasticity and become thicker, giving rise to arterial stiffness. Arterial stiffness is an underlying risk factor for cardiovascular diseases including atherosclerosis and stroke (Mitchell et al., 2010). Arterial stiffness promotes endothelial cell dysfunction (enhanced inflammation, proliferation, and permeability) driving the progression of cardiovascular diseases (Duprez, 2010; Maruhashi et al., 2018). Although the glycocalyx has not been studied directly in the context of arterial stiffness *in vivo*, our lab has recently shown that age-mediated stiffness directly inhibits the GCX core protein Glypican 1 in a mouse model (Mahmoud et al., 2021). Several studies have indirectly linked the expression of the GCX with arterial stiffness; atheroprone shear stress promotes stiffness and suppresses GCX expression in ECs and is associated with the development of atherosclerosis (Pahakis et al., 2007). GCX expression, including Glypican 1, is inhibited in hypertension (Nelson et al., 2018). Furthermore, in the context of age-mediated stiffness, studies have shown that the expression of GCX was reduced in aged mouse and human subjects vs younger subjects (Machin et al., 2018; Osuka et al., 2018).

Here we showed that the expression of glycocalyx GAGs and core protein Glypican 1 are affected by matrix stiffness in different cell types commonly used in glycocalyx and cell biology research including: HUVECs, BAECs, MAECs, RFPECs, and bEnd3 (**Figure 5**). We have shown that the expression of HS GAG was inhibited on stiff culture matrices in HUVECs, RFPECs (Mahmoud et al., 2021), BAECs, MAECs, and bEnd3 cells. The expression of HS was consistently inhibited in cells cultured on glass as opposed to stiff gels (10 kPa) which may indicate that the threshold of stiffness that inhibits HS expression is at a value higher than 10 kPa. Interestingly, the expression of HS was inhibited in RFPECs cultured on stiff gels as opposite to glass where the expression of HS was not altered. Fortuitously our lab has frequently studied the glycocalyx in RFPECs cultured on glass (Thi et al., 2004; Cancel et al., 2007; Ebong et al., 2011; Zeng et al., 2012, 2013, 2014; Zeng and Tarbell, 2014; Bartosch et al., 2017, 2021; Mahmoud et al., 2021). In contrast, the expression of HA did not show a consistent change in expression in cells cultured on stiff matrices (10 kPa gel/glass). Of the cell types

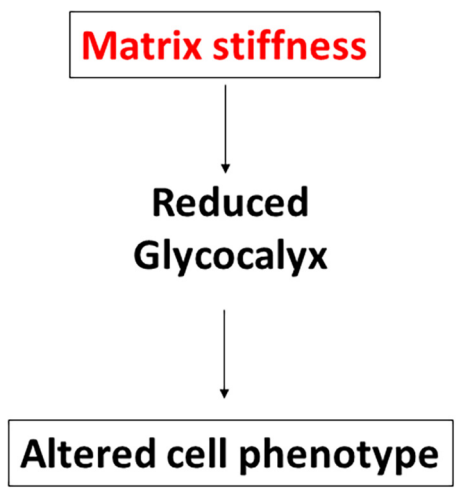


**FIGURE 4 |** Stiffness inhibits GCX expression in different cell types. Schematic to show that enhanced stiffness inhibits GCX expression through suppressing HS or HA glycosaminoglycan (GAG) expression. Stiffness inhibits the expression of the GCX core protein Glypican 1. The reduction of GCX expression subsequently alters endothelial cell phenotype.

| | Glycocalyx expression | | |
|---|---|---|---|
| | Heparan Sulfate | Hyaluronic Acid | Glypican 1 |
| Cell type | Affected by stiffness? ( stiff gel/glass) | Affected by stiffness? ( stiff gel/glass) | Affected by stiffness? ( stiff gel/glass) |
| BAEC | Reduced (glass) | Reduced (glass) | Uncertain |
| MAEC | Reduced (glass) | Unchanged | Reduced (glass+ stiff gel) |
| bEnd3 | Reduced (glass) | Unchanged | Reduced (glass) |
| HUVEC | Reduced (glass+ stiff gel) | Unchanged | Reduced (glass+ stiff gel) |
| RFPEC | Reduced (stiff gel) | Reduced (stiff gel) | Reduced (stiff gel) |

**FIGURE 5 |** Stiffness inhibits GCX expression in different cell types differently. Summary table to show how matrix stiffness inhibits HS, HA, and Glypican 1 differently for cells cultured on soft, stiff gels or on glass.

investigated only BAECs in this study showed a reduction in HA in cells cultured on stiff matrices; this also includes RFPECs as tested previously (Mahmoud et al., 2021). In summary, HS was reduced by stiffness in all five cell types; glypican 1 was reduced in 4 out of 5 cell types tested; and HA was reduced in only 2 of 5 cell types. These observations suggest that HS and glypican 1 that covalently binds HS are most clearly affected by stiffness.

The mRNA expression of the glycocalyx core protein Glypican 1 was suppressed on stiff matrices in MAECs and bEnd3 as shown before in HUVECs and RFPECs (Mahmoud et al., 2021). In addition, the expression of Glypican 1 was also reduced in MAECs *in vivo* in a mouse model of age-mediated stiffness (Mahmoud et al., 2021). Consistent with this, using Glypican 1 gene silencing and gene over expression *in vitro*, along with Glypican 1 KO endothelial cells *in vivo* revealed that the loss of Glypican 1 correlated with enhanced characteristics of endothelial cell dysfunction such as inflammation, endothelial mesenchymal transition (EndMT), and proliferation, along with reduced protective nitric oxide signaling (Mahmoud et al., 2021). Although Syndecan 1 and CD44 were not affected by stiffness in HUVECs and RFPECs, we can't draw strong conclusions about Syndecan 1 and CD44 in the additional cell types since they were not studied directly.

The observation that expression of different glycocalyx components (HS, HA, and Glypican 1) is affected by substrate stiffness differently depending on the cell type is intriguing. To understand this observation, it will be important to conduct a gene microarray study using different endothelial cell types and to assess a wide array of glycocalyx genes and genes responsible for endothelial dysfunction (inflammation, proliferation, and EndMT). This will determine which subset of genes of the glycocalyx are affected by matrix stiffness and whether they correlate with enhanced expression of genes involved in EC dysfunction.

It could well be that other glycocalyx core proteins such as Syndecans that support HS, along with the CD44 receptor that supports HA are also affected by stiff matrices in certain cell types. However, based on our previous work we have shown in RFPECs and HUVECs that Glypican 1 was the only significantly suppressed protein in response to matrix stiffness out of a group of genes encoding GAG synthesis, core proteins and glycocalyx degradation proteins (Mahmoud et al., 2021). Syndecan1 and CD44 expression were not altered by matrix stiffness in HUVECs and RFPECs (Mahmoud et al., 2021).

There have been reports of a reduced glycocalyx layer in *in vitro* studies which rendered the study of the glycocalyx difficult in some cells (Barker et al., 2004; Potter and Damiano, 2008; Chappell et al., 2009; Janczyk et al., 2010). Our work here provides insight into the optimal conditions to study the endothelial glycocalyx – on soft matrices as opposed to tissue culture plastic or glass. Most *in vitro* studies of the glycocalyx have been carried out under static conditions as we have done in our previous manuscript (Mahmoud et al., 2021). We have also shown that the *in vitro* effects are reciprocated *in vivo* in mouse aortic endothelial cells which have been exposed to flow (Mahmoud et al., 2021). This observation suggests that the effects of stiffness, whether with or without flow, on the reduction of GCX expression is consistent.

The mechanism by which stiffness inhibits the glycocalyx in endothelial cells is not fully known. In our previous work we ruled out the possibility of a degradation mechanism, specifically with regard to Glypican 1, but not HS (Mahmoud et al., 2021). The mechanism could potentially involve the action of miRNAs. Glypican 1 has been shown to be a target of miR-149 in cell types including melanoma cells and endothelial cells (Jin et al., 2011; Chamorro-Jorganes et al., 2014; Lai et al., 2017). In addition, the mechanism could involve signal mechanotransduction from upstream mechanosensing pathways

such as integrins and stretch activated ion channels such as Piezo 1. These pathways may result in the suppression of Glypican 1 and GAGs in response to matrix stiffness. Future work will be required to determine the mechanisms by which stiffness inhibits the glycocalyx and whether these mechanisms are conserved in different endothelial cells.

In conclusion, this work revealed that commonly used cell types in cell biology studies are sensitive to substrate stiffness in regard to expression of their cell surface glycocalyx. These observations have implications for our understanding of endothelial cell biology as demonstrated by studies showing that a reduction in glycocalyx expression correlates with changes in EC function (Baeyens et al., 2016; Cancel et al., 2016; Mitra et al., 2017; Bar et al., 2019; Mahmoud et al., 2021). Our previous work has shown that a reduction in Glypican 1 along with its GAG heparan sulfate resulted in enhanced inflammation, proliferation, EndMT and reduced protective nitric oxide signaling in endothelial cells, all characteristics of endothelial cell dysfunction. There have been numerous studies which show that the reduction of the endothelial glycocalyx layer thickness/expression occurs in disease conditions including atherosclerosis, hypertension and in aging (Machin et al., 2018; Nelson et al., 2018; Osuka et al., 2018; Bar et al., 2019). All of these conditions have a common element of enhanced matrix stiffness. An important question to address is whether glycocalyx protection or restoration can rescue endothelial cell integrity and prevent disease progression.

The observations from this work reveal that the culture of endothelial cells on stiff matrices such as glass or tissue culture plastic may give rise to reduced glycocalyx expression and consequential changes in cell function triggering endothelial cell dysfunction. Thus, for the *in vitro* study of the glycocalyx in cultured cells, in order to generate a rich glycocalyx layer, it would be optimal to study the glycocalyx in cells cultured on soft matrices as opposed to tissue culture plastic and glass. Although the use of softer substrates such as polyacrylamide gels (2.5 kPa) may be the most obvious recommendation to be drawn from our study, we did observe that the immortalized RFPEC cell line expressed abundant glycocalyx on glass. Other immortalized cell lines may also preserve the glycocalyx on glass? We hope that our findings allow labs to optimize their methods for studying the endothelial GCX *in vitro*.

## DATA AVAILABILITY STATEMENT

The original contributions presented in the study are included in the article/supplementary material, further inquiries can be directed to the corresponding authors.

## AUTHOR CONTRIBUTIONS

MM conducted all experiments, gathered the data, interpreted the results, and wrote the manuscript. LC gave useful advice during the experiment discussion. JT interpreted the results, supervised the research, and reviewed the manuscript. All authors contributed to the article and approved the submitted version.

## FUNDING

This research was supported by the National Heart, Lung and Blood Institute of the National Institutes of Health under Award Number F32HL145913.

## REFERENCES

Baeyens, N., Bandyopadhyay, C., Coon, B. G., Yun, S., and Schwartz, M. A. (2016). Endothelial fluid shear stress sensing in vascular health and disease. *J. Clin. Invest.* 126, 821–828. doi: 10.1172/jci83083

Bar, A., Targosz-Korecka, M., Suraj, J., Proniewski, B., Jasztal, A., Marczyk, B., et al. (2019). Degradation of Glycocalyx and multiple manifestations of endothelial dysfunction coincide in the early phase of endothelial dysfunction before atherosclerotic plaque development in apolipoprotein E/low-density lipoprotein receptor-deficient mice. *J. Am. Heart Assoc.* 8:e011171.

Barker, A. L., Konopatskaya, O., Neal, C. R., Macpherson, J. V., Whatmore, J. L., Winlove, C. P., et al. (2004). Observation and characterisation of the glycocalyx of viable human endothelial cells using confocal laser scanning microscopy. *Phys. Chem. Chem. Phys.* 6, 1006–1011. doi: 10.1039/b312189e

Bartosch, A. M. W., Mathews, R., Mahmoud, M. M., Cancel, L. M., Haq, Z. S., and Tarbell, J. M. (2021). Heparan sulfate proteoglycan glypican-1 and PECAM-1 cooperate in shear-induced endothelial nitric oxide production. *Sci. Rep.* 11:11386.

Bartosch, A. M. W., Mathews, R., and Tarbell, J. M. (2017). Endothelial glycocalyx-mediated nitric oxide production in response to selective AFM pulling. *Biophys. J.* 113, 101–108. doi: 10.1016/j.bpj.2017.05.033

Cancel, L., Silas, D., Bikson, M., and Tarbell, J. (2021). Direct current stimulation modulates gene expression in endothelial cells and astrocytes. *FASEB J.* 35. doi: 10.1096/fasebj.2021.35.S1.05090

Cancel, L. M., Ebong, E. E., Mensah, S., Hirshberg, C., and Tarbell, J. M. (2016). Endothelial glycocalyx, apoptosis and inflammation in an atherosclerotic mouse model. *Atherosclerosis.* 252, 136–146. doi: 10.1016/j.atherosclerosis.2016.07.930

Cancel, L. M., Fitting, A., and Tarbell, J. M. (2007). *In vitro* study of LDL transport under pressurized (convective) conditions. *Am. J. Physiol. Heart Circ. Physiol.* 293, H126–H132.

Chamorro-Jorganes, A., Araldi, E., Rotllan, N., Cirera-Salinas, D., and Suárez, Y. (2014). Autoregulation of glypican-1 by intronic microRNA-149 fine tunes the angiogenic response to FGF2 in human endothelial cells. *J. Cell Sci.* 127, 1169–1178.

Chappell, D., Jacob, M., Paul, O., Rehm, M., Welsch, U., Stoeckelhuber, M., et al. (2009). The glycocalyx of the human umbilical vein endothelial cell: an impressive structure *ex vivo* but not in culture. *Circ. Res.* 104, 1313–1317. doi: 10.1161/circresaha.108.187831

Chistiakov, D. A., Orekhov, A. N., and Bobryshev, Y. V. (2017). Effects of shear stress on endothelial cells: go with the flow. *Acta Physiol.* 219, 382–408. doi: 10.1111/apha.12725

Davies, P. F. (2009). Hemodynamic shear stress and the endothelium in cardiovascular pathophysiology. *Nat. Clin. Pract. Cardiovasc. Med.* 6, 16–26. doi: 10.1038/ncpcardio1397

Duprez, D. A. (2010). Arterial stiffness and endothelial function. *Hypertension* 55, 612–613. doi: 10.1161/hypertensionaha.109.144725

Ebong, E. E., Macaluso, F. P., Spray, D. C., and Tarbell, J. M. (2011). Imaging the endothelial glycocalyx *in vitro* by rapid freezing/freeze substitution transmission electron microscopy. *Arterioscler. Thromb. Vasc. Biol.* 31, 1908–1915. doi: 10.1161/atvbaha.111.225268

Ebong, E. E., Spray, D. C., and Tarbell, J. M. (2010). The endothelial glycocalyx *in vitro:* its structure and the role of heparan sulfate and glypican-1 in eNOS activation by flow. *FASEB J.* 24:784.

Harding, I. C., Mitra, R., Mensah, S. A., Herman, I. M., and Ebong, E. E. (2018). Pro-atherosclerotic disturbed flow disrupts caveolin-1 expression, localization, and function via glycocalyx degradation. *J. Transl. Med.* 16:364.

Janczyk, P., Hansen, S., Bahramsoltani, M., and Plendl, J. (2010). The glycocalyx of human, bovine and murine microvascular endothelial cells cultured *in vitro*. *J. Electron Microsc. (Tokyo)* 59, 291–298. doi: 10.1093/jmicro/dfq007

Jin, L., Hu, W. L., Jiang, C. C., Wang, J. X., Han, C. C., Chu, P., et al. (2011). MicroRNA-149*, a p53-responsive microRNA, functions as an oncogenic regulator in human melanoma. *Proc. Natl. Acad. Sci. U. S. A.* 108, 15840–15845. doi: 10.1073/pnas.1019312108

Lai, X., Wang, M., McElyea, S. D., Sherman, S., House, M., and Korc, M. (2017). A microRNA signature in circulating exosomes is superior to exosomal glypican-1 levels for diagnosing pancreatic cancer. *Cancer Lett.* 393, 86–93. doi: 10.1016/j.canlet.2017.02.019

Machin, D. R., Bloom, S. I., Campbell, R. A., Phuong, T. T. T., Gates, P. E., Lesniewski, L. A., et al. (2018). Advanced age results in a diminished endothelial glycocalyx. *Am. J. Physiol. Heart Circ. Physiol.* 315, H531–H539.

Mahmoud, M., Mayer, M., Cancel, L. M., Bartosch, A. M., Mathews, R., and Tarbell, J. M. (2021). The glycocalyx core protein Glypican 1 protects vessel wall endothelial cells from stiffness-mediated dysfunction and disease. *Cardiovasc. Res.* 117, 1592–1605. doi: 10.1093/cvr/cvaa201

Maruhashi, T., Soga, J., Fujimura, N., Idei, N., Mikami, S., Iwamoto, Y., et al. (2018). Endothelial dysfunction, increased arterial stiffness, and cardiovascular risk prediction in patients with coronary artery disease: FMD-J (flow-mediated dilation Japan) study A. *J. Am. Heart Assoc.* 7:e008588.

Mitchell, G. F., Hwang, S. J., Vasan, R. S., Larson, M. G., Pencina, M. J., Hamburg, N. M., et al. (2010). Arterial stiffness and cardiovascular events: the Framingham heart study. *Circulation* 121, 505–511. doi: 10.1161/circulationaha.109.886655

Mitra, R., O'Neil, G. L., Harding, I. C., Cheng, M. J., Mensah, S. A., and Ebong, E. E. (2017). Glycocalyx in atherosclerosis-relevant endothelium function and as a therapeutic target. *Curr. Atheroscler. Rep.* 19, 63–63.

Nelson, J. W., Ferdaus, M. Z., McCormick, J. A., Minnier, J., Kaul, S., Ellison, D. H., et al. (2018). Endothelial transcriptomics reveals activation of fibrosis-related pathways in hypertension. *Physiol. Genom.* 50, 104–116. doi: 10.1152/physiolgenomics.00111.2017

Nikmanesh, M., Cancel, L. M., Shi, Z.-D., and Tarbell, J. M. (2019). Heparan sulfate proteoglycan, integrin, and syndecan-4 are mechanosensors mediating cyclic strain-modulated endothelial gene expression in mouse embryonic stem cell-derived endothelial cells. *Biotechnol. Bioeng.* 116, 2730–2741. doi: 10.1002/bit.27104

Osuka, A., Kusuki, H., Yoneda, K., Matsuura, H., Matsumoto, H., Ogura, H., et al. (2018). Glycocalyx shedding is enhanced by age and correlates with increased fluid requirement in patients with major burns. *Shock* 50, 60–65. doi: 10.1097/shk.0000000000001028

Pahakis, M. Y., Kosky, J. R., Dull, R. O., and Tarbell, J. M. (2007). The role of endothelial glycocalyx components in mechanotransduction of fluid shear stress. *Biochem. Biophys. Res. Commun.* 355, 228–233. doi: 10.1016/j.bbrc.2007.01.137

Potter, D. R., and Damiano, E. R. (2008). The hydrodynamically relevant endothelial cell glycocalyx observed in vivo is absent *in vitro*. *Circ. Res.* 102, 770–776. doi: 10.1161/circresaha.107.160226

Russell-Puleri, S., Dela Paz, N. G., Adams, D., Chattopadhyay, M., Cancel, L., Ebong, E., et al. (2017). Fluid shear stress induces upregulation of COX-2 and PGI2 release in endothelial cells via a pathway involving PECAM-1, PI3K, FAK, and p38. *Am. J. Physiol. Heart Circ. Physiol.* 312, H485–H500.

Tarbell, J. M., and Cancel, L. M. (2016). The glycocalyx and its significance in human medicine. *J. Int. Med.* 280, 97–113. doi: 10.1111/joim.12465

Thi, M. M., Tarbell, J. M., Weinbaum, S., and Spray, D. C. (2004). The role of the glycocalyx in reorganization of the actin cytoskeleton under fluid shear stress: a "bumper-car" model. *Proc. Natl. Acad. Sci. U. S. A.* 101, 16483–16488. doi: 10.1073/pnas.0407474101

Varki, A., Cummings, R., Esko, J., Freeze, H., Stanley, P., Bertozzi, C., et al. (eds) (2009). *Essentials of Glycobiology*, 2nd Edn. New York, NY: Cold Spring Harbor Laboratory Press.

Weinbaum, S., Tarbell, J. M., and Damiano, E. R. (2007). The structure and function of the endothelial glycocalyx layer. *Annu. Rev. Biomed. Eng.* 9, 121–167. doi: 10.1146/annurev.bioeng.9.060906.151959

Zeng, Y., Adamson, R. H., Curry, F. R., and Tarbell, J. M. (2014). Sphingosine-1-phosphate protects endothelial glycocalyx by inhibiting syndecan-1 shedding. *Am. J. Physiol. Heart Circ. Physiol.* 306, H363–H372.

Zeng, Y., Ebong, E. E., Fu, B. M., and Tarbell, J. M. (2012). The structural stability of the endothelial glycocalyx after enzymatic removal of glycosaminoglycans. *PLoS One* 7:e43168.

Zeng, Y., and Tarbell, J. M. (2014). The adaptive remodeling of endothelial glycocalyx in response to fluid shear stress. *PLoS One* 9:e86249. doi: 10.1371/journal.pone.0043168

Zeng, Y., Waters, M., Andrews, A., Honarmandi, P., Ebong, E. E., Rizzo, V., et al. (2013). Fluid shear stress induces the clustering of heparan sulfate via mobility of glypican-1 in lipid rafts. *Am. J. Physiol. Heart Circ. Physiol.* 305, H811–H820.

**Conflict of Interest:** The authors declare that the research was conducted in the absence of any commercial or financial relationships that could be construed as a potential conflict of interest.

**Publisher's Note:** All claims expressed in this article are solely those of the authors and do not necessarily represent those of their affiliated organizations, or those of the publisher, the editors and the reviewers. Any product that may be evaluated in this article, or claim that may be made by its manufacturer, is not guaranteed or endorsed by the publisher.

frontiers in Cell and Developmental Biology

MINI REVIEW
published: 10 November 2021
doi: 10.3389/fcell.2021.751251

# Vascular Dysfunction in Malaria: Understanding the Role of the Endothelial Glycocalyx

*Margaret A. Bush[1], Nicholas M. Anstey[2], Tsin W. Yeo[2,3,4], Salvatore M. Florence[5], Donald L. Granger[6], Esther D. Mwaikambo[5] and J. Brice Weinberg[7]**

[1] Duke University School of Nursing and Durham VA Medical Centers, Durham, NC, United States, [2] Menzies School of Health Research, Charles Darwin University, Darwin, NT, Australia, [3] Lee Kong Chian School of Medicine, Nanyang Technological University, Singapore, Singapore, [4] National Centre for Infectious Diseases, Tan Tock Seng Hospital, Singapore, Singapore, [5] Hubert Kairuki Memorial University, Dar es Salaam, Tanzania, [6] School of Medicine, University of Utah and Salt Lake City VA Medical Centers, Salt Lake City, UT, United States, [7] Duke University School of Medicine and Durham VA Medical Centers, Durham, NC, United States

Malaria caused by *Plasmodium falciparum* results in over 400,000 deaths annually, predominantly affecting African children. In addition, non-falciparum species including vivax and knowlesi cause significant morbidity and mortality. Vascular dysfunction is a key feature in malaria pathogenesis leading to impaired blood perfusion, vascular obstruction, and tissue hypoxia. Contributing factors include adhesion of infected RBC to endothelium, endothelial activation, and reduced nitric oxide formation. Endothelial glycocalyx (eGC) protects the vasculature by maintaining vessel integrity and regulating cellular adhesion and nitric oxide signaling pathways. Breakdown of eGC is known to occur in infectious diseases such as bacterial sepsis and dengue and is associated with adverse outcomes. Emerging studies using biochemical markers and *in vivo* imaging suggest that eGC breakdown occurs during *Plasmodium* infection and is associated with markers of malaria disease severity, endothelial activation, and vascular function. In this review, we describe characteristics of eGC breakdown in malaria and discuss how these relate to vascular dysfunction and adverse outcomes. Further understanding of this process may lead to adjunctive therapy to preserve or restore damaged eGC and reduce microvascular dysfunction and the morbidity/mortality of malaria.

**Keywords: glycocalyx, malaria, glycosaminoglycans, endothelium, vascular dysfunction**

OPEN ACCESS

***Edited by:***
*Ye Zeng,*
*Sichuan University, China*

***Reviewed by:***
*Leonardo Jose de Moura Carvalho,*
*Oswaldo Cruz Foundation (Fiocruz), Brazil*
*Casper Hempel,*
*Technical University of Denmark, Denmark*

****Correspondence:***
*J. Brice Weinberg*
*brice@duke.edu*

***Specialty section:***
*This article was submitted to Signaling, a section of the journal Frontiers in Cell and Developmental Biology*

***Received:*** *31 July 2021*
***Accepted:*** *27 September 2021*
***Published:*** *10 November 2021*

***Citation:***
*Bush MA, Anstey NM, Yeo TW, Florence SM, Granger DL, Mwaikambo ED and Weinberg JB (2021) Vascular Dysfunction in Malaria: Understanding the Role of the Endothelial Glycocalyx. Front. Cell Dev. Biol. 9:751251. doi: 10.3389/fcell.2021.751251*

## INTRODUCTION

In 2019 there were 229 million cases of malaria and 409,000 deaths despite effective anti-parasitic drug therapy (WHO, 2020). The highest malaria disease burden is in Africa, (94% of cases and deaths), followed by South and South-East Asia (WHO, 2020). Children < 5 years account for ∼2/3 of deaths (WHO, 2020). *Plasmodium falciparum* is the malaria responsible for the vast majority of severe illness and deaths globally (WHO, 2020). *Plasmodium vivax* causes significant morbidity

**Abbreviations:** ADMA, asymmetric dimethylarginine; Ang-2, angiopoietin-2; BDNF, brain-derived neurotrophic factor; CM, cerebral malaria; CS, chondroitin sulfate; eGC, endothelial glycocalyx; eNOS, endothelial nitric oxide synthase; GAG, glycosaminoglycan; HS, heparan sulfate; HA, hyaluronic acid; iRBC, infected red blood cell; NO, nitric oxide; OPG, osteoprotegerin; PfEMP1, *P. falciparum* erythrocyte membrane protein 1; RBC, red blood cell; S1P, sphingosine-1-phosphate.

outside of sub-Saharan Africa, and is recognized as causing delayed severe disease and death (Price et al., 2020). Although less common, the simian parasite *Plasmodium knowlesi* causes zoonotic malaria in Southeast Asia, which is frequently severe and sometimes fatal (Grigg et al., 2018).

The malaria life cycle in humans starts with the bite of an infected female *Anopheles* mosquito. Injected sporozoites quickly pass into the liver, multiply asexually within hepatocytes, and develop into merozoites over ∼7 days. After this asymptomatic period, merozoites rupture from the hepatocytes and invade red blood cells (RBC) where they multiply. Rupture of infected RBC (iRBC) causes fever and release of new merozoites which invade other RBC. This erythrocytic/asexual cycle then repeats (Miller et al., 2013).

Interaction between the iRBC and the vascular endothelium results in key features of pathogenesis (Miller et al., 2013). In *P. falciparum* infections, iRBC express binding proteins on the RBC membrane (e.g., PfEMP1) and develop knobs that facilitate adherence to vascular endothelium resulting in parasite sequestration in microvessels (Miller et al., 2013). Vascular dysfunction is associated with endothelial activation, impaired perfusion/oxygenation, as well as organ dysfunction. Endothelial activation, microvascular dysfunction, and reduced availability of the endogenous vasodilator nitric oxide (NO) are related to disease severity and outcome (Anstey et al., 1996; Yeo et al., 2007, 2014, 2017). Microvascular sequestration and endothelial activation are independent predictors of impaired perfusion, severe disease, and death (Hanson et al., 2015), but the precise mechanisms of vascular dysfunction in malaria remain unclear.

The endothelial glycocalyx (eGC) serves protective and homeostatic roles in the vasculature (Villalba et al., 2021). Major structural components of the eGC are glycosaminoglycans (GAG), including chondroitin sulfate (CS), heparan sulfate (HS), and hyaluronic acid (HA), and proteoglycans such as syndecans and glypicans (Weinbaum et al., 2021). Of particular interest in malaria, the eGC can modulate cellular adhesion of platelets and iRBC to endothelial cells (Chappell et al., 2014; Hempel et al., 2017; Introini et al., 2018). In placental malaria, CS and syndecan-1 support cytoadhesion/sequestration after syncytiotrophoblast denudation (Hromatka et al., 2013; Ayres Pereira et al., 2016; Fried and Duffy, 2017). eGC regulates blood flow-mediated NO production by endothelial NO synthase (eNOS) (Florian et al., 2003; Yen et al., 2015; Weinbaum et al., 2021). Shear stress generated by flowing blood can activate eNOS through a mechano-transduction pathway mediated by eGG (specifically HS and the proteoglycan glypican-1). Downstream effects of this pathway include phosphorylation of PECAM-1 and eNOS, which ultimately results in synthesis of NO (Weinbaum et al., 2021).

Breakdown of eGC occurs in certain infectious diseases in which blood borne pathogens (and host factors they induce) come into contact with eGC. Loss of eGC reported in these diseases relates to pathology, disease severity, and adverse outcomes. In sepsis, blood and urine levels of eGC breakdown products are associated with adverse outcomes including organ dysfunction and mortality (Schmidt et al., 2016; Uchimido et al., 2019). In dengue infection, eGC breakdown is related to increased vascular permeability and disease severity (Tang et al., 2017). More recently, injury to eGC has been reported in patients with severe COVID-19 infection (Stahl et al., 2020; Queisser et al., 2021).

Given the close overlap of eGC functions with key pathophysiological characteristics of malaria, including cytoadhesion and reduced NO bioavailability, it is logical to suspect potential involvement of the eGC in malaria (**Figure 1**). The purpose of this review is to summarize evidence for eGC breakdown in malaria and describe how this may relate to pathogenesis of microvascular dysfunction and adverse clinical outcomes. Pre-clinical and clinical studies in malaria are listed in **Table 1**.

## EXPERIMENTAL ANIMAL STUDIES OF THE ENDOTHELIAL GLYCOCALYX IN MALARIA

Hempel et al. (2014) first reported loss of eGC in malaria using a mouse model of cerebral malaria (CM). Plasma GAG levels were significantly increased, and transmission electron microscopy showed complete or partial loss of eGC in mice with CM (Hempel et al., 2014). Daily plasma GAG levels suggested that shedding of eGC begins early in the infection (Hempel et al., 2014). Follow-up studies with the murine experimental CM model demonstrated loss of GAG (HA, HS, CS) and proteoglycans (syndecan-1 and 4) in the brain with corresponding increases in plasma concentrations of these eGC constituents, as well as an increase in vascular permeability (Hempel et al., 2019). The authors showed that dexamethasone or antithrombin-3 prevent the eGC loss and certain disease manifestations (Hempel et al., 2019). While the murine cerebral malaria model is commonly used in malaria research, questions have been raised about suitability of the model for translation of results to clinical disease in humans (White et al., 2010; Craig et al., 2012). Challenges with the model include use of different species of parasite and innate differences between mice and humans in disease manifestations and pathophysiology (notably characteristics of adherence of iRBC to endothelial cells and degree of sequestration) (White et al., 2010; Craig et al., 2012). While certain treatments have shown to be effective in the mouse CM model, thus far the findings in mice have not proven helpful in identifying beneficial therapeutics for adjunctive treatment in humans.

## CYTOADHESION STUDIES

Several *in vitro* studies have demonstrated that cytoadhesion is increased upon loss of eGC. Hempel et al. (2017) studied *in vitro* binding to Chinese hamster ovary cells expressing CD36, a known binding receptor for falciparum-infected RBCs. They found that cytoadhesion was inhibited by presence of eGC, suggesting that loss of eGC may have a role in cellular adhesion process by facilitating the ability to interact with binding receptors such as CD36.

Using a "microfluidic organ-on-chip" model designed to mimic human microvessels, adhesion of iRBC to human

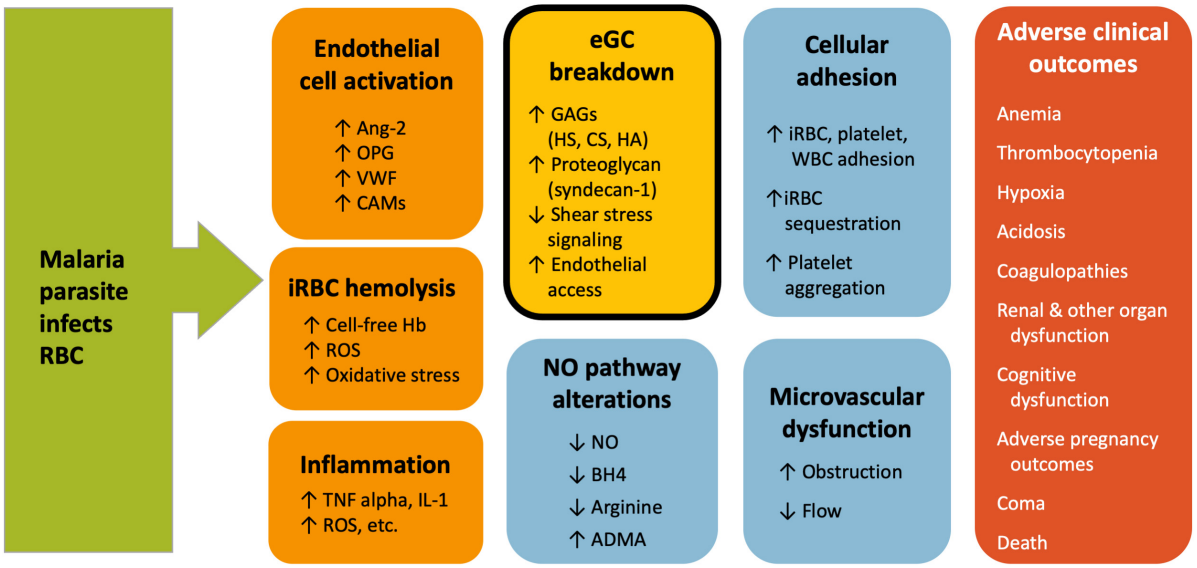


**FIGURE 1 |** Vascular dysfunction in Malaria. Multiple vascular events contribute to malaria pathogenesis and lead to adverse clinical outcomes. The exact mechanism and sequence of events is not known, but early events include endothelial cell activation and rupture of infected RBC. These lead to endothelial glycocalyx breakdown, reduced NO, cellular adhesion and microvascular dysfunction. Endothelial glycocalyx breakdown (shown in the gold, bolded box) is associated with multiple markers of malaria disease severity and may play a central role in different aspects of malaria pathogenesis. ADMA, asymmetric dimethylarginine; Ang-2, angiopoietin-2; BH4, tetrahydrobiopterin; CAMs, cell adhesion molecules; CS, chondroitin sulfate; eGC, endothelial glycocalyx; GAG, glycosaminoglycan; Hb, hemoglobin; HA, hyaluronic acid; HS, heparan sulfate; iRBC, infected red blood cell; NO, nitric oxide; OPG, osteoprotegerin; ROS, reactive oxygen species; S1P, sphingosine-1-phosphate; VWF, von Willebrand factor.

umbilical vein endothelial cells (HUVEC) was enhanced following enzymatic degradation of the eGC, compared to adhesion of healthy RBC (Introini et al., 2018). Altered dynamics of the iRBC, including flipping and decreased flow velocity, were also reported, consistent with altered hemodynamics that contribute to cytoadhesion of iRBC to endothelium (Introini et al., 2018). These cytoadhesion studies suggest that the eGC is integral in regulating cytoadhesion of iRBC.

## CLINICAL STUDIES IN HUMAN MALARIA

The eGC is required for induction of NO formation by blood flow over endothelial cells (Florian et al., 2003; Yen et al., 2015; Weinbaum et al., 2021). Our prior studies have documented that host NO production is associated with protection against severe disease in falciparum malaria (Anstey et al., 1996; Yeo et al., 2007, 2014), vivax malaria (Barber et al., 2016), and knowlesi malaria (Barber et al., 2018). Thus, we performed studies to determine if eGC is damaged in humans with malaria from each of *Plasmodium* species known to cause severe disease.

We initially reported evidence of degradation of the eGC in falciparum malaria in 129 Indonesian adults (Yeo et al., 2019b) and 100 Tanzanian children (Yeo et al., 2019a); and subsequently in 146 Tanzanian children (Bush et al., 2021). In both children and adults, there were significant increases in total sulfated GAG in urine. We further characterized the elevated urinary GAG constituents by mass spectrometry and found predominantly HS and CS (but not dermatan sulfate) to be elevated in malaria patients (Yeo et al., 2019a,b), consistent with the composition of GC from the endothelium (Weinbaum et al., 2007). In children, longitudinal analyses showed that urine total GAG levels decreased daily with treatment and normalized by Day 3 (Yeo et al., 2019a). Total GAG were significantly associated with markers of malaria disease severity including parasitemia, parasite biomass, cell-free hemoglobin, and plasma TNF (Yeo et al., 2019a,b). Markers of endothelial activation such as ICAM-1, E-selectin, and Ang-2 were also associated with eGC breakdown products (Yeo et al., 2019b). Breakdown of eGC may expose ICAM-1 and E-selectin, endothelial adhesion molecules implicated in cytoadherence of *P. falciparum*, and exacerbate microvascular sequestration (Hempel et al., 2017; Introini et al., 2018). In both adults and children, measures of NO bioavailability and vascular function were inversely related to the eGC breakdown products (Yeo et al., 2019a,b). In adults, degradation of eGC was associated with mortality (Yeo et al., 2019b). The plasma core protein syndecan-1 was also significantly elevated in adult patients and associated with various markers of disease severity (Yeo et al., 2019b). Degradation of eGC has been implicated in the pathogenesis of acute kidney injury in sepsis (Schmidt et al., 2016). The greater magnitude of eGC degradation in acute kidney injury seen in severe falciparum malaria (Yeo et al., 2019b) supports a role for glomerular eGC degradation in the pathogenesis of acute kidney injury in malaria.

Lyimo et al. (2020) used incident dark field imaging of the microvasculature in the buccal region of the mouth along with biochemical measures including GAG and syndecan-1 to demonstrate eGC loss in African children with malaria. Imaging

**TABLE 1 |** Studies of eGC in malaria.

| Pre-clinical | Clinical |
|---|---|
| Mouse cerebral malaria (Hempel et al., 2014) | *P. falciparum* in Indonesian adults (Yeo et al., 2019b) |
| Mouse cerebral malaria (Hempel et al., 2019) | *P. falciparum* in Tanzanian children (Yeo et al., 2019a) |
| CD36 binding *in vitro* (Hempel et al., 2017) | *P. falciparum* in Tanzanian children (Lyimo et al., 2020) |
| iRBC cytoadhesion and flow characteristics (Introini et al., 2018) | *P. falciparum* or *P. vivax*, experimentally induced in human volunteers (Woodford et al., 2020) |
| | *P. vivax* and *P. knowlesi* in Malaysian adults (Barber et al., 2021) |
| | *P. falciparum* in Tanzanian children (Bush et al., 2021) |

was used to calculate the perfused boundary region (PBR), a measure used to assess the ability of perfused RBC to penetrate the eGC. The PBR measurement for children with either uncomplicated or severe malaria was significantly increased compared with healthy children, supporting breakdown of the eGC barrier (Lyimo et al., 2020). Additional findings detected on imaging in the malaria patients included impaired vascular integrity, stagnant erythrocytes external to blood vessels, perivascular hemorrhages, and sequestration of late-stage parasites within vessels (Lyimo et al., 2020). Similar to other clinical studies, biochemical markers of eGC loss were elevated in the malaria patients. However in these studies, measures of eGC degradation were slower to recover, with eGC integrity remaining impaired for at least 2 weeks. Biomarkers of endothelial activation in plasma (i.e., angiopoietin-1/2 and thrombomodulin) were also significantly altered in malaria patients (Lyimo et al., 2020).

While most studies to date have focused on breakdown of eGC in falciparum malaria, there is also evidence for breakdown of eGC in vivax and knowlesi malaria (Barber et al., 2021). In Malaysian adults with either vivax or knowlesi infection, levels of eGC breakdown products were significantly increased compared to healthy controls and in knowlesi malaria, were significantly correlated with disease severity (Barber et al., 2021). In knowlesi malaria, there is also significant correlation with biomarkers of endothelial activation [angiopoietin-2 and osteoprotegerin (OPG)] and measures of microvascular function. In the patients with knowlesi malaria, the eGC breakdown marker syndecan-1 was also significantly related to acute kidney injury, supporting the notion that glomerular glycocalyx degradation is a key mechanism of acute kidney injury in malaria and other acute infections.

## CLINICAL EVIDENCE IN EXPERIMENTALLY INDUCED HUMAN MALARIA

The study of healthy volunteers inoculated with malaria parasites presents a unique opportunity to observe events early in infection, compared with clinical trials in which patients have had infection for some time prior to diagnosis. Subjects are inoculated with infected RBC following which parasitemia develops. At onset of clinical signs or ∼7 days after inoculation, the patients receive antimalarial drug treatment. In 45 healthy subjects inoculated with *P. falciparum* or *P. vivax*, biomarkers of endothelial activation, including von Willebrand factor and OPG, increased from baseline to the start of antimalarial treatment, after which levels declined back to baseline (Woodford et al., 2020). In the *P. falciparum* group, Ang-2 increased significantly. However at these earlier timepoints of infection, there were no changes observed in biochemical markers of eGC breakdown, abnormalities using sidestream dark field microscopy of sublingual vessels, or microvascular function as assessed by peripheral arterial tonometry or near-infrared spectroscopy (Woodford et al., 2020). Our study suggests that endothelial activation precedes eGC breakdown and vascular dysfunction, and it also supports potential involvement of Ang-2 as a mediator of eGC breakdown.

## MECHANISMS OF ENDOTHELIAL GLYCOCALYX DEGRADATION IN MALARIA

While the mechanisms of eGC loss in malaria are not certain, a number of mediators are implicated. There is evidence that angiopoietin-2 contributes to eGC degradation. Elevated plasma levels of Ang-2 have been demonstrated in malaria and are associated with endothelial activation and disease severity (Yeo et al., 2008; Conroy et al., 2009). In falciparum malaria (Yeo et al., 2019b), vivax malaria (Barber et al., 2021), knowlesi malaria (Barber et al., 2021), and other disease settings including sepsis (Beurskens et al., 2020), Ang-2 has been associated with eGC loss, independent of other potential mediators. And in cultured endothelial cells, Ang-2 induces a heparanase-dependent degradation of eGC (Lukasz et al., 2017). Loss of eGC results when the breakdown predominates over new eGC synthesis. Heparanase as well as other substances (e.g., membrane or matrix metalloproteases, thrombin, plasmin, and hyaluronidases) have been implicated as potential "sheddases" that are responsible for eGC breakdown clinically (Becker et al., 2015; Iba and Levy, 2019). Endothelial NOS (eNOS) can prevent the induction of heparanases, with heparanase induced by the eNOS inhibitor asymetric dimethylarginine (ADMA) (Garsen et al., 2016). The eNOS-inhibitors OPG and ADMA are elevated in both falciparum and knowlesi malaria (Yeo et al., 2010; Barber et al., 2021), and both are associated with eGC degradation in malaria (Barber et al., 2021). ADMA and OPG may therefore contribute to induction of heparanase in malaria and to eGC degradation. Oxidative stress is elevated in severe malaria (Rubach et al., 2015; Yeo et al., 2015), and can also mediate glycocalyx breakdown (Pillinger and Kam, 2017). Hemolysis in malaria results in circulating, cell-free plasma hemoglobin that is associated with oxidative stress (Plewes et al., 2017) and eGC breakdown, independent of disease severity (Yeo et al., 2019b). Heme-mediated oxidative stress

likely also contributes to glycocalyx breakdown in malaria. The lipid mediator, sphingosine-1-phosphate (S1P), protects against eGC damage by inhibiting syndecan-1 shedding and increasing glycocalyx synthesis (Zeng et al., 2014). S1P is decreased in malaria (Finney et al., 2011; Punsawad and Viriyavejakul, 2017; Yeo et al., 2019b; Barber et al., 2021), and in falciparum malaria is inversely associated with eGC degradation (Yeo et al., 2019b). This suggests that reduced S1P may also contribute toward loss of glycocalyx integrity in malaria. Since erythrocytes are a major source of S1P, malaria-associated anemia could enhance deficiencies in S1P signaling pathways.

Further understanding of which sheddases are involved in malaria could identify potential pharmacologic targets leading to new adjunctive treatments. Better understanding of the mechanisms will also help determine how eGC loss affects factors related to both eGC function and malaria pathogenesis (including NO formation in response to shear stress of flowing blood and the processes of cellular adhesion to endothelium by leukocytes, platelets and iRBC).

An interesting question is whether the eGC breakdown products could themselves have detrimental effects and contribute to pathogenesis, rather than being simply being inert, circulating GAGs and proteoglycans. This concept has been reported in sepsis in which GAG are linked to cognitive sequelae. In a mouse model, circulating GAG fragments were shown to cross the blood brain barrier, bind to brain-derived neurotrophic factor (BDNF), and inhibit BDNF-mediated long-term potentiation in the hippocampus, a mechanism underlying memory (Hippensteel et al., 2019). Particular sulfation patterns of HS were associated with better binding to BDNF (Hippensteel et al., 2019). Interestingly, in patients with sepsis in the intensive care unit, these same sulfation patterns in plasma HS predicted cognitive impairment lasting up to 2 weeks after discharge (Hippensteel et al., 2019). Lyimo et al. showed that in children with cerebral malaria, plasma concentrations of HS were significantly higher in those with deeper coma (Lyimo et al., 2020). It is possible that eGC degradation not only exacerbates parasite sequestration and microvascular dysfunction in cerebral malaria, but through elevated circulating HS, may compound coma severity in cerebral malaria. Another example of pathological changes related to breakdown products themselves is in COVID-19 in which endothelial barrier dysfunction can be induced by HA fragments (Queisser et al., 2021).

A therapeutic that could prevent loss or promote formation of eGC could potentially be used as adjunctive therapy in patients with malaria. There are a number of proposed therapeutics to ameliorate eGC loss by mechanisms such as preventing shedding, inhibiting putative sheddases, or regenerating eGC (e.g., albumin, sulodexide, sevoflurane, rhamnan sulfate) (Iba and Levy, 2019; Weinbaum et al., 2021). Data regarding these agents are mainly based on experimental animal studies, and there is no clinical evidence to support their clinical use currently. Of relevance to malaria, sevuparin is a modified low molecular weight heparin-like molecule without anticoagulant properties and with close similarity to the glycosaminoglycan HS. Sevuparin and other heparin analogs inhibit rosetting (binding of iRBCs and RBCs) and cytoadhesion of iRBC to endothelium *in vitro* (Vogt et al., 2006; Leitgeb et al., 2011; Saiwaew et al., 2017). In a Phase I/II clinical trial in patients with uncomplicated malaria, sevuparin inhibited parasite invasion of RBC and reversed sequestration of iRBC (Leitgeb et al., 2017).

## CONCLUSION

There is growing evidence that loss of eGC is associated with vascular dysfunction and disease severity in malaria. This loss may lead to multiple vascular events and adverse clinical outcomes in malaria (Hempel et al., 2016; Georgiadou and Cunnington, 2019). Many questions remain including the need for further understanding of the mechanisms underlying eGC breakdown in malaria. We need to identify pathways responsible for eGC breakdown, e.g., the initial steps and role of the parasite or host factors as triggers; whether the breakdown products themselves are detrimental contributors to pathology; and the relation and kinetics of eGC synthesis vs. breakdown in malaria. Clinically, it will be important to determine if rapid assays of eGC breakdown products (e.g., urine total GAG) can provide helpful prognostic and treatment insights, and whether adjunctive agents that prevent loss or replace eGC can ameliorate or prevent severe disease.

## AUTHOR CONTRIBUTIONS

All authors listed have made a substantial, direct and intellectual contribution to the work, and approved it for publication.

## FUNDING

This work was supported by the US National Institutes of Health, National Heart, Lung, and Blood Institute Grant R01 HL130763-01 and the VA Research Service (JW). NA was supported by the National Health and Medical Research Council (1135820).

## REFERENCES

Anstey, N. M., Weinberg, J. B., Hassanali, M. Y., Mwaikambo, E. D., Manyenga, D., Misukonis, M. A., et al. (1996). Nitric oxide in Tanzanian children with malaria: inverse relationship between malaria severity and nitric oxide production/nitric oxide synthase type 2 expression. *J. Exp. Med.* 184, 557–567.

Ayres Pereira, M., Mandel Clausen, T., Pehrson, C., Mao, Y., Resende, M., Daugaard, M., et al. (2016). Placental sequestration of plasmodium falciparum malaria parasites is mediated by the interaction between VAR2CSA and chondroitin sulfate a on syndecan-1. *PLoS Pathog.* 12:e1005831. doi: 10.1371/journal.ppat.1005831

Barber, B. E., Grigg, M. J., Piera, K. A., Chen, Y., William, T., Weinberg, J. B., et al. (2021). Endothelial glycocalyx degradation and disease severity in *Plasmodium vivax* and *Plasmodium knowlesi* malaria. *Sci. Rep.* 11:9741.

Barber, B. E., Grigg, M. J., Piera, K. A., William, T., Cooper, D. J., Plewes, K., et al. (2018). Intravascular haemolysis in severe *Plasmodium knowlesi* malaria:

association with endothelial activation, microvascular dysfunction, and acute kidney injury. *Emerg. Microbes Infect.* 7:106. doi: 10.1038/s41426-018-0105-2

Barber, B. E., William, T., Grigg, M. J., Piera, K. A., Chen, Y., Wang, H., et al. (2016). Nitric oxide-dependent endothelial dysfunction and reduced arginine bioavailability in *Plasmodium vivax* malaria but no greater increase in intravascular hemolysis in severe disease. *J. Infect. Dis.* 214, 1557–1564. doi: 10.1093/infdis/jiw427

Becker, B. F., Jacob, M., Leipert, S., Salmon, A. H., and Chappell, D. (2015). Degradation of the endothelial glycocalyx in clinical settings: searching for the sheddases. *Br. J. Clin. Pharmacol.* 80, 389–402. doi: 10.1111/bcp.12629

Beurskens, D. M., Bol, M. E., Delhaas, T., van de Poll, M. C., Reutelingsperger, C. P., Nicolaes, G. A., et al. (2020). Decreased endothelial glycocalyx thickness is an early predictor of mortality in sepsis. *Anaesth. Intensive Care* 48, 221–228. doi: 10.1177/0310057X20916471

Bush, M. A., Florence, S. M., Yeo, T. W., Kalingonji, A. R., Chen, Y., Granger, D. L., et al. (2021). Degradation of endothelial glycocalyx in Tanzanian children with falciparum malaria. *FASEB J.* 35:e21805. doi: 10.1096/fj.202100277RR

Chappell, D., Brettner, F., Doerfler, N., Jacob, M., Rehm, M., Bruegger, D., et al. (2014). Protection of glycocalyx decreases platelet adhesion after ischaemia/reperfusion: an animal study. *Eur. J. Anaesthesiol.* 31, 474–481. doi: 10.1097/EJA.0000000000000085

Conroy, A. L., Lafferty, E. I., Lovegrove, F. E., Krudsood, S., Tangpukdee, N., Liles, W. C., et al. (2009). Whole blood angiopoietin-1 and -2 levels discriminate cerebral and severe (non-cerebral) malaria from uncomplicated malaria. *Malar. J.* 8:295. doi: 10.1186/1475-2875-8-295

Craig, A. G., Grau, G. E., Janse, C., Kazura, J. W., Milner, D., Barnwell, J. W., et al. (2012). The role of animal models for research on severe malaria. *PLoS Pathog.* 8:e1002401. doi: 10.1371/journal.ppat.1002401

Finney, C. A., Hawkes, C. A., Kain, D. C., Dhabangi, A., Musoke, C., Cserti-Gazdewich, C., et al. (2011). S1P is associated with protection in human and experimental cerebral malaria. *Mol. Med.* 17, 717–725. doi: 10.2119/molmed.2010.00214

Florian, J. A., Kosky, J. R., Ainslie, K., Pang, Z., Dull, R. O., and Tarbell, J. M. (2003). Heparan sulfate proteoglycan is a mechanosensor on endothelial cells. *Circ. Res.* 93, e136–e142. doi: 10.1161/01.RES.0000101744.47866.D5

Fried, M., and Duffy, P. E. (2017). Malaria during pregnancy. *Cold Spring Harb. Perspect. Med.* 7:a025551. doi: 10.1101/cshperspect.a025551

Garsen, M., Rops, A. L., Li, J., van Beneden, K., van den Branden, C., Berden, J. H., et al. (2016). Endothelial nitric oxide synthase prevents heparanase induction and the development of proteinuria. *PLoS One* 11:e0160894. doi: 10.1371/journal.pone.0160894

Georgiadou, A., and Cunnington, A. J. (2019). Shedding of the vascular endothelial glycocalyx: a common pathway to severe malaria? *Clin. Infect. Dis.* 69, 1721–1723. doi: 10.1093/cid/ciz043

Grigg, M. J., William, T., Barber, B. E., Rajahram, G. S., Menon, J., Schimann, E., et al. (2018). Age-related clinical spectrum of plasmodium knowlesi malaria and predictors of severity. *Clin. Infect. Dis.* 67, 350–359. doi: 10.1093/cid/ciy065

Hanson, J., Lee, S. J., Hossain, M. A., Anstey, N. M., Charunwatthana, P., Maude, R. J., et al. (2015). Microvascular obstruction and endothelial activation are independently associated with the clinical manifestations of severe falciparum malaria in adults: an observational study. *BMC Med.* 13:122. doi: 10.1186/s12916-015-0365-9

Hempel, C., Hyttel, P., and Kurtzhals, J. A. (2014). Endothelial glycocalyx on brain endothelial cells is lost in experimental cerebral malaria. *J. Cereb. Blood Flow Metab.* 34, 1107–1110. doi: 10.1038/jcbfm.2014.79

Hempel, C., Pasini, E. M., and Kurtzhals, J. A. (2016). Endothelial glycocalyx: shedding light on malaria pathogenesis. *Trends Mol. Med.* 22, 453–457. doi: 10.1016/j.molmed.2016.04.004

Hempel, C., Sporring, J., and Kurtzhals, J. A. L. (2019). Experimental cerebral malaria is associated with profound loss of both glycan and protein components of the endothelial glycocalyx. *FASEB J.* 33, 2058–2071. doi: 10.1096/fj.201800657R

Hempel, C., Wang, C. W., Kurtzhals, J. A. L., and Staalso, T. (2017). Binding of plasmodium falciparum to CD36 can be shielded by the glycocalyx. *Malar. J.* 16:193. doi: 10.1186/s12936-017-1844-6

Hippensteel, J. A., Anderson, B. J., Orfila, J. E., McMurtry, S. A., Dietz, R. M., Su, G., et al. (2019). Circulating heparan sulfate fragments mediate septic cognitive dysfunction. *J. Clin. Invest.* 129, 1779–1784. doi: 10.1172/JCI124485

Hromatka, B. S., Ngeleza, S., Adibi, J. J., Niles, R. K., Tshefu, A. K., and Fisher, S. J. (2013). Histopathologies, immunolocalization, and a glycan binding screen provide insights into Plasmodium falciparum interactions with the human placenta. *Biol. Reprod.* 88:154. doi: 10.1095/biolreprod.112.106195

Iba, T., and Levy, J. H. (2019). Derangement of the endothelial glycocalyx in sepsis. *J. Thromb. Haemost.* 17, 283–294. doi: 10.1111/jth.14371

Introini, V., Carciati, A., Tomaiuolo, G., Cicuta, P., and Guido, S. (2018). Endothelial glycocalyx regulates cytoadherence in *Plasmodium falciparum* malaria. *J. R. Soc. Interface* 15:20180773. doi: 10.1098/rsif.2018.0773

Leitgeb, A. M., Blomqvist, K., Cho-Ngwa, F., Samje, M., Nde, P., Titanji, V., et al. (2011). Low anticoagulant heparin disrupts *Plasmodium falciparum* rosettes in fresh clinical isolates. *Am. J. Trop. Med. Hyg.* 84, 390–396. doi: 10.4269/ajtmh.2011.10-0256

Leitgeb, A. M., Charunwatthana, P., Rueangveerayut, R., Uthaisin, C., Silamut, K., Chotivanich, K., et al. (2017). Inhibition of merozoite invasion and transient de-sequestration by sevuparin in humans with Plasmodium falciparum malaria. *PLoS One* 12:e0188754. doi: 10.1371/journal.pone.0188754

Lukasz, A., Hillgruber, C., Oberleithner, H., Kusche-Vihrog, K., Pavenstadt, H., Rovas, A., et al. (2017). Endothelial glycocalyx breakdown is mediated by angiopoietin-2. *Cardiovasc. Res.* 113, 671–680. doi: 10.1093/cvr/cvx023

Lyimo, E., Haslund, L. E., Ramsing, T., Wang, C. W., Efunshile, A. M., Manjurano, A., et al. (2020). In vivo imaging of the buccal mucosa shows loss of the endothelial glycocalyx and perivascular hemorrhages in pediatric *Plasmodium falciparum* Malaria. *Infect. Immun.* 88, e679–e619. doi: 10.1128/IAI.00679-19

Miller, L. H., Ackerman, H. C., Su, X. Z., and Wellems, T. E. (2013). Malaria biology and disease pathogenesis: insights for new treatments. *Nat. Med.* 19, 156–167. doi: 10.1038/nm.3073

Pillinger, N. L., and Kam, P. (2017). Endothelial glycocalyx: basic science and clinical implications. *Anaesth. Intensive Care* 45, 295–307. doi: 10.1177/0310057X1704500305

Plewes, K., Kingston, H. W. F., Ghose, A., Maude, R. J., Herdman, M. T., Leopold, S. J., et al. (2017). Cell-free hemoglobin mediated oxidative stress is associated with acute kidney injury and renal replacement therapy in severe falciparum malaria: an observational study. *BMC Infect. Dis.* 17:313. doi: 10.1186/s12879-017-2373-1

Price, R. N., Commons, R. J., Battle, K. E., Thriemer, K., and Mendis, K. (2020). Plasmodium vivax in the Era of the Shrinking *P. falciparum* Map. *Trends Parasitol.* 36, 560–570. doi: 10.1016/j.pt.2020.03.009

Punsawad, C., and Viriyavejakul, P. (2017). Reduction in serum sphingosine 1-phosphate concentration in malaria. *PLoS One* 12:e0180631. doi: 10.1371/journal.pone.0180631

Queisser, K. A., Mellema, R. A., Middleton, E. A., Portier, I., Manne, B. K., Denorme, F., et al. (2021). COVID-19 generates hyaluronan fragments that directly induce endothelial barrier dysfunction. *JCI Insight* 6:147472. doi: 10.1172/jci.insight.147472

Rubach, M. P., Mukemba, J., Florence, S., Lopansri, B. K., Hyland, K., Volkheimer, A. D., et al. (2015). Impaired systemic tetrahydrobiopterin bioavailability and increased oxidized biopterins in pediatric falciparum malaria: association with disease severity. *PLoS Pathog.* 11:e1004655. doi: 10.1371/journal.ppat.1004655

Saiwaew, S., Sritabal, J., Piaraksa, N., Keayarsa, S., Ruengweerayut, R., Utaisin, C., et al. (2017). Effects of sevuparin on rosette formation and cytoadherence of *Plasmodium falciparum* infected erythrocytes. *PLoS One* 12:e0172718. doi: 10.1371/journal.pone.0172718

Schmidt, E. P., Overdier, K. H., Sun, X., Lin, L., Liu, X., Yang, Y., et al. (2016). Urinary glycosaminoglycans predict outcomes in septic shock and acute respiratory distress syndrome. *Am. J. Respir. Crit. Care Med.* 194, 439–449. doi: 10.1164/rccm.201511-2281OC

Stahl, K., Gronski, P. A., Kiyan, Y., Seeliger, B., Bertram, A., Pape, T., et al. (2020). Injury to the endothelial glycocalyx in critically ill patients with COVID-19. *Am. J. Respir. Crit. Care Med.* 202, 1178–1181. doi: 10.1164/rccm.202007-2676LE

Tang, T. H., Alonso, S., Ng, L. F., Thein, T. L., Pang, V. J., Leo, Y. S., et al. (2017). Increased serum hyaluronic acid and heparan sulfate in dengue fever: association with plasma leakage and disease severity. *Sci. Rep.* 7:46191. doi: 10.1038/srep46191

Uchimido, R., Schmidt, E. P., and Shapiro, N. I. (2019). The glycocalyx: a novel diagnostic and therapeutic target in sepsis. *Crit. Care* 23:16. doi: 10.1186/s13054-018-2292-6

Villalba, N., Baby, S., and Yuan, S. Y. (2021). The endothelial glycocalyx as a double-edged sword in microvascular homeostasis and pathogenesis. *Front. Cell Dev. Biol.* 9:711003. doi: 10.3389/fcell.2021.711003

Vogt, A. M., Pettersson, F., Moll, K., Jonsson, C., Normark, J., Ribacke, U., et al. (2006). Release of sequestered malaria parasites upon injection of a glycosaminoglycan. *PLoS Pathog.* 2:e100. doi: 10.1371/journal.ppat.0020100

Weinbaum, S., Cancel, L. M., Fu, B. M., and Tarbell, J. M. (2021). The glycocalyx and its role in vascular physiology and vascular related diseases. *Cardiovasc. Eng. Technol.* 12, 37–71. doi: 10.1007/s13239-020-00485-9

Weinbaum, S., Tarbell, J. M., and Damiano, E. R. (2007). The structure and function of the endothelial glycocalyx layer. *Annu. Rev. Biomed. Eng.* 9, 121–167. doi: 10.1146/annurev.bioeng.9.060906.151959

White, N. J., Turner, G. D. I, Medana, M., Dondorp, A. M., and Day, N. P. (2010). The murine cerebral malaria phenomenon. *Trends Parasitol.* 26, 11–15. doi: 10.1016/j.pt.2009.10.007

WHO (2020). *World Malaria Report 2020*. Geneva: World Health Organization.

Woodford, J., Yeo, T. W., Piera, K. A., Butler, K., Weinberg, J. B., McCarthy, J. S., et al. (2020). Early endothelial activation precedes glycocalyx degradation and microvascular dysfunction in experimentally induced plasmodium falciparum and plasmodium vivax infection. *Infect. Immun.* 88, e895–e819. doi: 10.1128/IAI.00895-19

Yen, W., Cai, B., Yang, J., Zhang, L., Zeng, M., Tarbell, J. M., et al. (2015). Endothelial surface glycocalyx can regulate flow-induced nitric oxide production in microvessels in vivo. *PLoS One* 10:e0117133. doi: 10.1371/journal.pone.0117133

Yeo, T. W., Florence, S. M., Kalingonji, A. R., Chen, Y., Granger, D. L., Anstey, N. M., et al. (2017). Decreased microvascular function in tanzanian children with severe and uncomplicated falciparum malaria. *Open Forum Infect. Dis.* 4:ofx079. doi: 10.1093/ofid/ofx079

Yeo, T. W., Lampah, D. A., Gitawati, R., Tjitra, E., Kenangalem, E., McNeil, Y. R., et al. (2007). Impaired nitric oxide bioavailability and L-arginine reversible endothelial dysfunction in adults with falciparum malaria. *J. Exp. Med.* 204, 2693–2704. doi: 10.1084/jem.20070819

Yeo, T. W., Lampah, D. A., Gitawati, R., Tjitra, E., Kenangalem, E., Piera, K., et al. (2008). Angiopoietin-2 is associated with decreased endothelial nitric oxide and poor clinical outcome in severe falciparum malaria. *Proc. Natl. Acad. Sci. U.S.A* 105, 17097–17102. doi: 10.1073/pnas.0805782105

Yeo, T. W., Lampah, D. A., Kenangalem, E., Tjitra, E., Price, R. N., Weinberg, J. B., et al. (2015). Impaired systemic tetrahydrobiopterin bioavailability and increased dihydrobiopterin in adult falciparum malaria: association with disease severity, impaired microvascular function and increased endothelial activation. *PLoS Pathog.* 11:e1004667. doi: 10.1371/journal.ppat.1004667

Yeo, T. W., Lampah, D. A., Kenangalem, E., Tjitra, E., Weinberg, J. B., Granger, D. L., et al. (2014). Decreased endothelial nitric oxide bioavailability, impaired microvascular function, and increased tissue oxygen consumption in children with falciparum malaria. *J. Infect. Dis.* 210, 1627–1632. doi: 10.1093/infdis/jiu308

Yeo, T. W., Lampah, D. A., Tjitra, E., Gitawati, R., Darcy, C. J., Jones, C., et al. (2010). Increased asymmetric dimethylarginine in severe falciparum malaria: association with impaired nitric oxide bioavailability and fatal outcome. *PLoS Pathog.* 6:e1000868. doi: 10.1371/journal.ppat.1000868

Yeo, T. W., Weinberg, J. B., Lampah, D. A., Kenangalem, E., Bush, P., Chen, Y., et al. (2019b). Glycocalyx breakdown is associated with severe disease and fatal outcome in *Plasmodium falciparum* malaria. *Clin. Infect. Dis.* 69, 1712–1720. doi: 10.1093/cid/ciz038

Yeo, T. W., Bush, P. A., Chen, Y., Young, S. P., Zhang, H., Millington, D. S., et al. (2019a). Glycocalyx breakdown is increased in African children with cerebral and uncomplicated falciparum malaria. *FASEB J.* 33, 14185–14193. doi: 10.1096/fj.201901048RR

Zeng, Y., Adamson, R. H., Curry, F. R., and Tarbell, J. M. (2014). Sphingosine-1-phosphate protects endothelial glycocalyx by inhibiting syndecan-1 shedding. *Am. J. Physiol. Heart Circ. Physiol.* 306, H363–H372. doi: 10.1152/ajpheart.00687.2013

**Conflict of Interest:** The authors declare that the research was conducted in the absence of any commercial or financial relationships that could be construed as a potential conflict of interest.

**Publisher's Note:** All claims expressed in this article are solely those of the authors and do not necessarily represent those of their affiliated organizations, or those of the publisher, the editors and the reviewers. Any product that may be evaluated in this article, or claim that may be made by its manufacturer, is not guaranteed or endorsed by the publisher.

# Advantages of publishing in Frontiers

**OPEN ACCESS**
Articles are free to read for greatest visibility and readership

**FAST PUBLICATION**
Around 90 days from submission to decision

**HIGH QUALITY PEER-REVIEW**
Rigorous, collaborative, and constructive peer-review

**TRANSPARENT PEER-REVIEW**
Editors and reviewers acknowledged by name on published articles

**Frontiers**
Avenue du Tribunal-Fédéral 34
1005 Lausanne | Switzerland

**Visit us:** www.frontiersin.org
**Contact us:** frontiersin.org/about/contact

**REPRODUCIBILITY OF RESEARCH**
Support open data and methods to enhance research reproducibility

**DIGITAL PUBLISHING**
Articles designed for optimal readership across devices

**FOLLOW US**
@frontiersin

**IMPACT METRICS**
Advanced article metrics track visibility across digital media

**EXTENSIVE PROMOTION**
Marketing and promotion of impactful research

**LOOP RESEARCH NETWORK**
Our network increases your article's readership